Physics Lib.
Sayers

THE JOURNAL
OF
CHEMICAL PHYSICS

VOLUME 21, NUMBER 1 JANUARY, 1953

Editorial

THE editorship of *The Journal of Chemical Physics* changes hands with this issue.

The Journal started in January, 1933, with Harold C. Urey as editor. In 1941 Joseph E. Mayer became editor, and after twelve years has submitted his resignation. It was suggested that the Executive Committee of the Division of Chemical Physics nominate the new editor, the appointment being made by the Governing Board of the American Institute of Physics. Clyde A. Hutchison, Jr., was nominated and appointed, and takes office with the first issue of this year, although many of the papers for the next few issues have been handled by his predecessor.

The character of a Journal is determined by the contributors. It is not anticipated that the change of editorship will usher in any change of policy or character.

The retiring editor wishes to take this opportunity to thank the many able contributors whose articles have given *The Journal of Chemical Physics* its outstanding reputation. He is particularly grateful to the many reviewers who have done the real work of editing in the past twelve years. These reviewers, only partly chosen from the Associate Editors listed on the back of the front cover, have conscientiously and anonymously contributed their time and skill, and have frequently greatly improved the quality of the articles appearing in the Journal. Their efforts and patience are hereby thankfully acknowledged.

In the future, manuscripts should be addressed to:

Clyde A. Hutchison, Jr., Editor
The Journal of Chemical Physics
Institute of Nuclear Studies
University of Chicago
Chicago 37, Illinois

JOSEPH E. MAYER

THE JOURNAL OF CHEMICAL PHYSICS VOLUME 21, NUMBER 1 JANUARY, 1953

Conditions for the Formation of Hydrogen Bonds

W. S. FYFE
Chemistry Department, University of Otago, Dunedin, New Zealand
(Received June 27, 1952)

The conditions necessary for the formation of hydrogen bonds are suggested to be asymmetry of nonbonding electron pairs and small size of hydrogen bonded atoms. Conditions for symmetry of such bonds are discussed.

ALTHOUGH a large amount of descriptive data has accumulated on the subject of hydrogen bonding, this linkage has received slight theoretical consideration, and a number of problems regarding conditions for its formation remain only partially answered. The major problems which appear to exist are, firstly, should the bonding be considered as purely electrostatic in origin arising between ion-dipole or dipole-dipole interaction; secondly, is the hydrogen atom to be considered as being symmetrically placed in the bond? Also an explanation of why the bond is restricted almost entirely to the elements nitrogen, oxygen and fluorine must be given. When the importance of substances associated through hydrogen bonds is considered it is surprising that these questions still remain unanswered in the majority of cases.

Several workers have considered the energy of hydrogen bonds from consideration of the dipole-dipole interaction of the bonded components. Some of the most successful cases to be treated in this fashion are the bifluoride ion $(HF_2)^-$ and carboxylic acid dimers considered by Davies.[1] Using a model based on ion-dipole interaction Davies calculated a bond energy for the hydrogen bond in $(HF_2)^-$ of 47.3 kcal/mole in reasonable agreement with experimental data. The dipole moment of the HF molecule was considered to arise entirely from ionic-covalent resonance in the molecule. There is little doubt that this treatment is not entirely free from objection as it is becoming increasingly recognized that large contributions to the dipole moments of such molecules arise from hybridization of bonding orbitals which in turn leaves the nonbonding electrons asymmetrically distributed. However, Davies also obtained reasonable values for acid dimers but in these cases there must be considerable uncertainty in assigning formal charges to dipoles of groups in molecules. If the interaction between water molecules is considered in the same manner as being dipole-dipole interaction the bond energies calculated are too small (e.g., about 1.5 kcal/mole). Also such treatments place too much emphasis on ionic character of bonds and do not explain why HCl is not associated while water is when the bonds in each would have similar polarities.

More recently Coulson[2] and others have emphasized the importance of lone pair distribution in making contributions to dipole moments. If the bonding in say water or ammonia was pure "*s*" or "*p*" then lone pairs in nonbonding orbitals would maintain their ground state symmetry and contribute nothing to the moment. However, it is now widely recognized that to obtain a condition of maximum overlapping of bonding orbitals some hybridization nearly always occurs and lone pair orbitals do not remain symmetrically distributed. Coulson[2] considered the water molecule hybridized in a trigonal fashion and with this model demonstrated that a large amount of the resultant dipole moment was to be attributed to the lone pair. More recently Pople[3] in a molecular orbital treatment of water with emphasis on equivalent orbitals obtained results suggesting an almost tetrahedral distribution of bonding and lone pair electrons about the oxygen atom. The model provides excellent confirmation of the original Bernal Fowler postulates. Pople evaluated all possible contributions to the moment of the water molecule. These results led Lennard-Jones and Pople[4] to suggest that a better model for calculating the hydrogen bond energy would be as shown in Fig. 1. With this model and the distances between electrons and nuclei adjusted to give the correct dipole component in the direction of the bond Pople[5] calculated a hydrogen bond energy of about 6 kcal/mole in reasonable agreement with experimental values.

In the type of model suggested by Pople, the largest part of the attractive force responsible for association arises from the interaction of the proton and the lone pair electrons. It thus appears reasonable to assume that one of the necessary conditions for this type of bonding is asymmetry of lone pairs. It was thought that it might be of considerable interest to carry out analogous calculations for the H_2S molecule where association appears to be practically nonexistent. The most significant differences between H_2O and H_2S is the X−H−X bond angle which is 105° for H_2O and approximately 90° for H_2S. This suggests that a smaller amount of hybridization might be present in H_2S for the bond angle deviates little from that expected for pure "*p*" bonding.

[1] M. Davies, J. Chem. Phys. **15**, 739 (1947); Trans. Faraday Soc. **36**, 341 (1940).
[2] C. A. Coulson, Proc. Roy. Soc. (London) **207**, 63 (1951).
[3] J. A. Pople, Proc. Roy. Soc. (London) **202**, 323 (1950).
[4] J. Lennard-Jones and J. A. Pople, Proc. Roy. Soc. (London) **205**, 155 (1951).
[5] J. A. Pople, Proc. Roy. Soc. (London) **205**, 163 (1951).

In performing calculations for H_2S the same method used by Pople[3] was employed, the only significant differences being the alteration of the wave functions. For these, Slater nodeless functions were used with the form

$$\phi(H, 1s)=\left(\frac{1}{\pi}\right)^{\frac{1}{2}} e^{-r},$$

$$\phi(S, 3s)=\frac{1}{24}\left(\frac{2^7Z^7}{3^75\pi}\right)^{\frac{1}{2}} r^2e^{-Zr/3},$$

$$\phi(S, 3p)=\frac{1}{24}\left(\frac{2^73Z^7}{5\pi3^7}\right)^{\frac{1}{2}} r^2\cos\theta e^{-Zr/3},$$

where Z is the effective nuclear charge evaluated by the method of Slater.[6] For this system the dipole moment of a directed hybrid orbital is given by

$$\int r_1\cos\theta\phi_1^2dr_1=\frac{7\sqrt{3}}{Z}\cos\epsilon\sin\epsilon,$$

$$\phi_1=\cos\epsilon\phi(S, 3s)+\sin\epsilon\phi(S, 3p),$$

where ϵ is the bond hybridization parameter. The cal-

TABLE I. Dipole moments of H_2S and H_2O.

	$M\times10^{-18}$ esu						
	M_1	M_b	M	α	β	ϵ_b	ϵ_1
H_2O	3.15	− 6.91	1.84	105	104.3	63	63.5
H_2S	5.1	−13.2	0.95	90	123.5	90	53.5

culated moments angles and hybridization parameters compared with those of Pople[3] for H_2O are given in Table I, where M_1=lone pair resultant moment, M_b=bond resultant moment, M=resultant moment for molecule, α=H−X−H angle, β=angle between lone pairs, ϵ_b=bond hybridization parameter, and ϵ_1=lone pair hybridization parameter.

The total moment for the molecule $M=M_1+M_b+2\rho\cos\frac{1}{2}\alpha$, where ρ equals the X−H bond length (0.97A for water, 1.34A for H_2S).

It will be noted that as with water the lone pair electrons are making a marked contribution to the dipole moment. The most significant difference between the two sets of results is the much wider angle between the lone pairs in H_2S which follows the smaller H−S−H bond angle. We may now proceed to calculate what the hydrogen bond energy would be in H_2S if it possessed a similar structure to water. Following the method of Pople[5] we resolve the dipole so that each part of the molecule has the correct dipole component in the direction of the bond. The principal uncertainty in the calculations is the value to be assigned to a hypothetical S−H−S bond. A reasonable value for such bonds

[6] J. C. Slater, Phys. Rev. 36, 57 (1930).

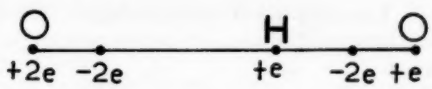

FIG. 1. Lennard-Jones and Pople model for electrostatic system in the hydrogen bond in water.

appears to be given by summing the normal bond length of an X−H bond, the covalent radius of hydrogen and the van der Waals radius of X. For example, the calculated distance in F−H−F is 2.5 (obs. 2.26–2.55) for O−H−O 2.7 (obs. 2.5–2.7) and for N−H−N 2.8 (obs. 2.9–3.4). On this basis a reasonable value for H_2S will be 3.7–4.0A. Using a value of 3.7A for the bond length and a similar model to that of Pople for the charge distribution, the hydrogen bond energy calculated is 1.82 kcal/mole. This energy is probably less than the van der Waals energy of a close packed structure, and such a small additional bond energy would probably not account for H_2S taking up an open structure such as ice.

By using similar models we may also calculate the hydrogen bond energy in ammonia and hydrofluoric acid assuming long pair asymmetry. If this is done the reasonable values of 5.1 and 10.9 kcal/mole, respectively, are obtained. In these calculations HF was assumed to have a zig-zag chain structure with an angle of 134°.

From the results obtained it appears most probable that the critical factor governing hydrogen bond formation is the X−X distance in X−H−X. If we consider reasonable bond lengths calculated as outlined, it will be seen that marked changes occur between first and second row elements of the periodic table (Table II). It thus appears that the principle factors involved in hydrogen bond formation are firstly the presence of asymmetric lone pairs and secondly the interatomic distance which must be reasonably short. It must be emphasized that there will be no sharp transition between elements forming or not forming hydrogen bonds. There is only a marked difference in bond energy. It should be remembered that van der Waals forces between molecules such as O_2, CH_4, etc., reach 3 kcal/mole and that these forces increase with size or polarizability of a molecule so will increase in the orders HF, HCl, HBr, HI. The van der Waals interaction in a close packed HCl structure is 5 kcal/mole and for hydrogen bonding to occur the bond would need an energy comparable with this figure.

The question of symmetry of X−H−X bonds is more complicated. If such a linkage is to be symmetrical the bond energy of this form must be greater than that in the short-long bond form. The bond energy will

TABLE II. Calculated X−H−X bond lengths.

F	O	N
2.5	2.7	2.8
Cl	*S*	*P*
3.4	3.5	3.6

TABLE III. F—H overlap integrals.

Bond length A	S_{ss}	S_{sp}	S_{tet}
0.92	0.47	0.30	0.49
1.34	0.27	0.19	0.30
1.13	0.36	0.22	0.37
1.34[a]	0.28	0.21	
1.13[a]	0.39	0.27	

[a] u value used in these cases for F^- not F.

depend mainly on the sum of the electrostatic interactions and the covalent bond energy which will in turn depend on the overlap of bonding orbitals. One of the most suitable cases to consider in this fashion is the F_2H^- ion. If we consider electrostatic interaction and use the results of Davies,[1] we obtain for the total interaction in the unsymmetrical form an energy of approximately 158 kcal/mole. In the model used by Davies a formal charge of 2.7×10^{-10} esu is placed on each atom in the F—H short bond and 4.8×10^{-10} esu on the fluoride ion. If we now lengthen the F—H bond until a symmetrical structure is reached the actual polarity of the bond will increase for the overlap decreases with increasing bond length. However, we may consider as a first approximation that the hydrogen atom maintains a charge of $+2.7$ and place -3.75 on each fluorine to give a resultant charge of $-e$ to the whole ion. With this type of model an energy of 168 kcal/mole is obtained.

The charge distribution pictured can only be considered very approximate but should be reasonable when the overlap integrals are considered. It thus appears that on electrostatic grounds, either configuration may be possible with the symmetrical form slightly favored.

The overlap of atomic orbitals in this case provides some interesting information. The overlap integrals for some F—H bonds are given in Table III. It will be noticed that even for the long bonds the overlap is still very appreciable. As the covalent bond energy is a function of S we may get approximate indications of the magnitude of the total covalent bond energies by summing in the case of the unsymmetrical structure the overlap integrals for $R=0.92$ and 1.34 and the symmetrical case by doubling the integrals for $R=1.13$.

It will be noticed from Table IV that in all cases the overlap sum is approximately equal for either structure. It does, however, reach a maximum for the symmetrical case when we calculate the "u" values for F^- ion. This appears reasonable when we consider that in the unsymmetrical case one fluorine is negatively charged while in the symmetrical case both approach nearly to this state. The sum of these two factors indicates that either configuration gives similar energies and probably the symmetrical is favored. This conclusion is in agreement with that of Westrum and Pitzer[7] who discussed the thermodynamic and spectroscopic data. The overlap integrals were calculated from the formulas and tables of Mulliken, Riecke, Orloff, and Orloff.[8]

If similar overlap integral sums are evaluated for the systems O—H—O and N—H—N or for F—H—F at the distances in the gas phase distinct minima are obtained for the symmetrical cases, this minima being the greatest for N—H—N.

It must be noted that some uncertainty exists in such overlap calculations as the type of orbitals to be used is a matter of some doubt. It must also be assumed that the formation of a bond in one direction does not alter the possibility of overlap in another. It may also be possible that in unsymmetrical cases atoms at either end may use different orbitals.

TABLE IV. Overlap integral sums for F—H—F bonds.

	A (unsymmetrical) $S_{(R=0.92)}+S_{(R=1.34)}$	B (symmetrical) $2\times S_{(R=1.13)}$
$S_{(ss)}$	0.74	0.72
$S_{(sp)}$	0.49	0.44
$S_{(tet)}$	0.79	0.74
$S_{(ss)}^*$	0.75	0.78
$S_{(sp)}^*$	0.51	0.54

Use of the sum of the two overlap integrals is not entirely satisfactory but is considered only as an indication of the covalent energy contribution. It has been demonstrated by Mulliken[9] that at large distances Slater atomic orbitals are not satisfactory for calculating overlap integrals, and the arguments probably could be improved by using self-consistent field overlaps in discussing the long bonds.

The author wishes to thank Professor C. A. Coulson, F.R.S. (Oxford) for helpful communication on some aspects of the problem and Dr. A. G. McLellan of the Department of Physics of this University for much helpful discussion.

[7] E. F. Westrum and K. S. Pitzer, J. Am. Chem. Soc. **71**, 1940 (1949).
[8] Mulliken, Rieke, Orloff, and Orloff, J. Chem. Phys. **17**, 1248 (1949).
[9] R. S. Mulliken, J. Am. Chem. Soc. **72**, 4493 (1950).

Luminescence and Trapping in Phosphors Containing Gallium

RICHARD H. BUBE AND SIMON LARACH
Radio Corporation of America, RCA Laboratories Division, Princeton, New Jersey
(Received July 21, 1952)

A study was made of the effects of gallium impurity on the luminescence emission and trapping in phosphors with oxygen-dominated host crystals and in phosphors with zinc sulfide host crystal. Gallium acts (1) as an intensifier for host-crystal emissions in zinc silicate, magnesium silicate, and zinc sulfide phosphors; (2) as an originative activator in zinc germanate phosphor; (3) as a poison for emissions resulting from manganese activator in silicate and germanate phosphors, and for emissions caused by copper and manganese in zinc sulfide phosphors for cathode-ray excitation; (4) as a sensitizer for emissions resulting from copper and manganese in zinc sulfide phosphors for ultraviolet excitation; (5) as a trapping agent in zinc silicate, magnesium silicate, zinc germanate, and zinc sulfide; (6) as a trapping poison in beryllium silicate phosphors.

Evidence is found for a correlation between types of emission centers and trapping centers in silicate and germanate phosphors.

Results on intensification indicate that intensifier activators are effective in increasing the intensity of host-crystal emissions by introducing crystal defects of the same type as those formed by random thermal processes in the preparation of the phosphor.

I. OXYGEN-DOMINATED HOST CRYSTALS WITH GALLIUM IMPURITY

THE choice of gallium as an impurity in preparing phosphors was made for several reasons. (1) There have been few reports on the use of gallium as an activator. (2) Gallium, a liquid metal near room temperature, has only recently become available in pure form. (3) Gallium ion has an ionic radius near to that of zinc and magnesium, major cations in many phosphor systems, but has a charge of +3 rather than +2.

Tiede and Lueders[1] reported a weak red luminescence emission for Al_2O_3:Ga, and Leverenz[2] described the luminescence of "self-activated" Ga_2O_3.

The present study concerns the effect of gallium impurity on the host-crystal luminescence of rbhdl.-Zn_2SiO_4, rbhdl.-$ZnO \cdot SiO_2$, rhomb.-Mg_2SiO_4, rbhdl.-Zn_2GeO_4, and rbhdl.-Be_2SiO_4; and the effect of gallium impurity on the emission associated with manganese activator in these same host crystals. Both gallium and manganese have an effect on the distribution of traps in these host crystals, and glow curves are used to study these effects.

Experimental Procedure

The silicate phosphors were prepared using special "bulky" silica (Mallinckrodt), "ultra-pure" ZnO (Mallinckrodt), "ultra-pure" MgO (Mallinckrodt), and "purest" $Be(NO_3)_2$ (Schering-Kallbaum). The germanate phosphors were prepared using "purest" GeO_2 (Eagle-Picher).

Pure (99.99 percent) gallium metal (Aluminum Corporation of America) was dissolved in silica-distilled nitric acid by heating to 80°C. A standard solution of gallium nitrate was prepared, and portions of this solution were used in the synthesis of the materials to be described.

In preparing phosphors with manganese activator, manganese was added as the nitrate in proportions to give 0.3 percent by weight. Except where otherwise specified, gallium activator was used in proportions of 0.5 percent by weight.

Spectral distributions and peak intensities of cathodoluminescence emission were measured with an automatic recording spectroradiometer.[3] The phosphors were excited by 6-kv cathode rays at a current density of about 1.0 $\mu a/cm^2$.

Measurements of glow curves were obtained with the specially constructed apparatus used in previous work by one of the authors.[4] A heating rate of 0.082 degree/sec was used over the temperature range from 23° to 270°C. The phosphor was excited at room temperature by a high frequency spark discharge in vacuum, was allowed to remain for a fixed period of time at room temperature (about 10 min), and was then heated at a linear rate. The thermostimulated emission was detected with a 1P21 phototube.

None of the phosphors tested was appreciably excited by 3650A ultraviolet. The effect of 3650A ultraviolet on the glow curve was tested by illuminating the phosphor with ultraviolet for the final 5-minute interval before starting the glow measurement. The source of ultraviolet was a 100-watt, C-H4 mercury spot projector lamp with appropriate filters.

Results

(1) *Luminescence Emission*

The spectral distributions of the host-crystal luminescence emissions of the phosphors of this study have been reported.[5] The spectra for rbhdl.-Zn_2SiO_4, rbhdl.-$ZnO \cdot SiO_2$, and rhomb.-Mg_2SiO_4 are practically identical, with peak at 4100A. The fact that the emission is essentially independent of host-crystal cation and crystal structure has led to the conclusion that the emission centers are perturbed SiO_4 groups.[6] The emission of rbhdl.-Zn_2GeO_4, in which emission centers are pre-

[1] E. Tiede and H. Lueders, Ber. deut. chem. Ges. **66**, 1681 (1933).
[2] H. W. Leverenz, *An Introduction to Luminescence of Solids* (John Wiley and Sons, Inc., New York, 1950), p. 222.
[3] V. K. Zworykin, J. Opt. Soc. Am. **29**, 84 (1939).
[4] R. H. Bube, Phys. Rev. **80**, 655 (1950).
[5] See reference 2, p. 221.
[6] See reference 2, p. 222.

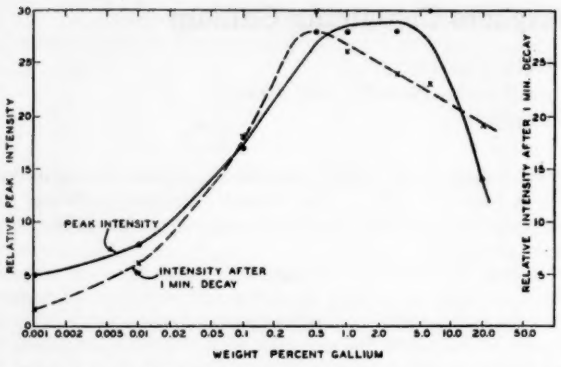

FIG. 1. The relative cathodoluminescence emission peak intensity, and the relative cathodophosphorescence emission intensity after one minute decay, (in arbitrary units), for rbhdl.-Zn_2SiO_4:Ga, 1200°C, as a function of gallium proportion.

sumably perturbed GeO_4 groups,[6] is located at shorter wavelengths with peak at 3650A. The emission of the rbhdl.-Be_2SiO_4 has a peak at 3000A; the discrepancy between this wavelength and the peak wavelength for the other silicate phosphors has led to the hypothesis that the active luminescence centers in Be_2SiO_4 are associated with BeO_4 groups.[7]

The effect of gallium impurity on the luminescence emission of the zinc silicates and magnesium silicate is different from its effect on the emission of zinc germanate or of beryllium silicate. Gallium acts as an intensifier activator for the host-crystal emission of rbhdl.-Zn_2SiO_4, rbhdl.-$ZnO \cdot SiO_2$, and rhomb.-Mg_2SiO_4, but it acts as an originative activator in rbhdl.-Zn_2GeO_4, and has no detectable effect on the emission of rbhdl.-Be_2SiO_4. Gallium acts as a poison for the emission associated with manganese activator in all of these host crystals.

Figure 1 shows the detailed dependence of peak intensity and afterglow at room temperature for rbhdl.-Zn_2SiO_4 as a function of the gallium proportion. An intensification by a factor of six is obtained for proportions of gallium between 0.5 and 5.0 percent. The action of gallium as an intensifier activator is similar for rbhdl.-$ZnO \cdot SiO_2$ and rhomb.-Mg_2SiO_4.

In the case of rbhdl.-Zn_2GeO_4, gallium acts as an originative activator, producing a broad emission band with peak at 5300A, as shown in Fig. 2.

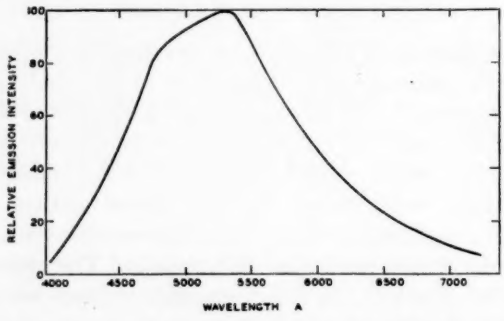

FIG. 2. The spectral distribution of the cathodoluminescence emission of rbhdl.-Zn_2GeO_4:Ga(0.5) phosphor.

[7] H. W. Leverenz, RCA Rev. 5, 131 (1940).

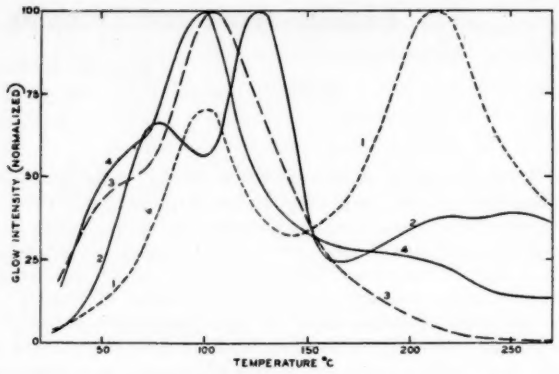

FIG. 3. Glow curves for the rbhdl.-Zn_2SiO_4 family of phosphors. (1) Without added impurity, (2) with 0.3 percent Mn, (3) with 0.5 percent Ga, (4) with 0.3 percent Mn and 0.5 percent Ga.

The effect of gallium impurity on the emission intensity of the phosphors with manganese activator may be described using rbhdl.-Zn_2SiO_4:Mn(0.3) as an example. The emission intensity was progressively decreased by the incorporation of increasing proportions of gallium, although the afterglow intensity was increased. At 5.0 percent gallium, the emission intensity during excitation was 14 percent of its value for the phosphor without gallium. The poisoning effect of gallium on the other manganese-activated phosphors studied was similar.

(2) *Trapping*

Normalized glow curves for the five families of this section of the study are given in Figs. 3 through 7. These glow curves show only the deepest traps with corresponding glow peaks above room temperature. Each figure gives the glow curves for the phosphor (1) without added impurity, (2) with 0.3 percent Mn, (3) with 0.5 percent Ga, and (4) with 0.3 percent Mn and 0.5 percent Ga. Table I lists the maximum glow intensity, uncorrected for phototube sensitivity.

Gallium increases the glow intensity in all of the

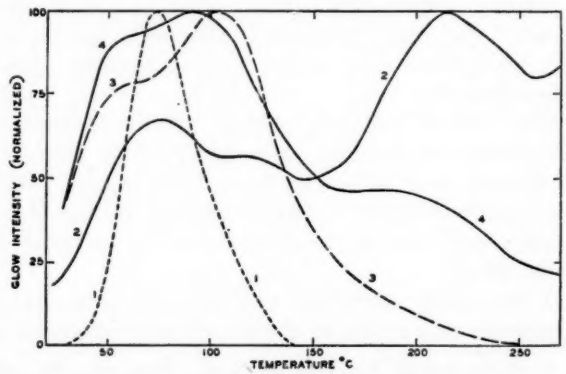

FIG. 4. Glow curves for the rbhdl.-$ZnO \cdot SiO_2$ family of phosphors. (1) Without added impurity, (2) with 0.3 percent Mn, (3) with 0.5 percent Ga, (4) with 0.3 percent Mn and 0.5 percent Ga.

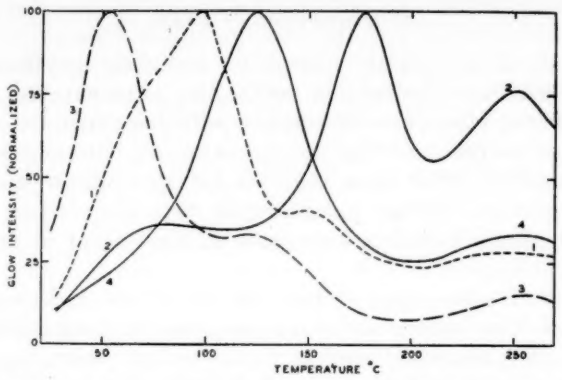

FIG. 5. Glow curves for the rhomb.-Mg_2SiO_4 family of phosphors. (1) Without added impurity, (2) with 0.3 percent Mn, (3) with 0.5 percent Ga, (4) with 0.3 percent Mn and 0.5 percent Ga.

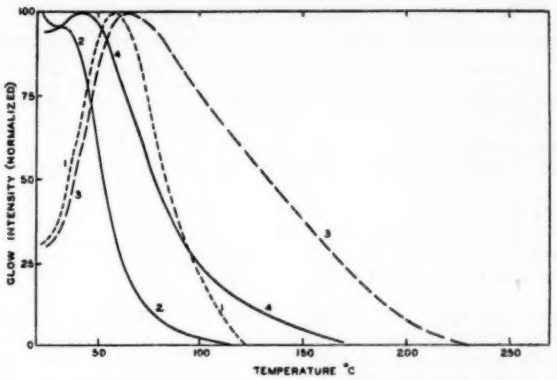

FIG. 7. Glow curves for the rbhdl.-Be_2SiO_4 family of phosphors. (1) Without added impurity, (2) with 0.3 percent Mn, (3) with 0.5 percent Ga, (4) with 0.3 percent Mn and 0.5 percent Ga.

phosphors, with or without Mn activator, except for the beryllium silicate phosphors.

A summary of the glow peaks found is given in Table II. As is indicated in the table, it is found that a small number of glow peaks seem to occur throughout all the glow curves of these five families of phosphors, with the probable exception of the zinc germanate phosphors. Because of the large variation of glow intensity among different phosphors, the absence of a glow peak from Table II for any particular phosphor does not mean that the glow peak may not be present.

It was found that 3650A ultraviolet was able to empty traps originally filled by cathode-ray excitation. This appears to be a general property of traps with glow peaks above room temperature, in silicates and germanates. The process, however, is a complicated one, and the extent of the trap-emptying varies with host crystal, activator, and trap depth. An example of the emptying of traps by ultraviolet is given for the rbhdl.-Zn_2SiO_4 family of phosphors in Fig. 8. The percent of the glow intensity remaining after 5 minutes of ultraviolet illumination before measuring the glow curve (as compared with the glow curve obtained without previous ultraviolet illumination) is plotted as a function of temperature, and hence also of trap depth.

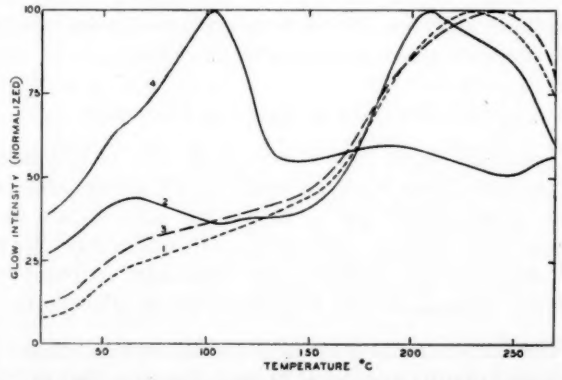

FIG. 6. Glow curves for the rbhdl.-Zn_2GeO_4 family of phosphors. (1) Without added impurity, (2) with 0.3 percent Mn, (3) with 0.5 percent Ga, (4), with 0.3 percent Mn and 0.5 percent Ga.

The glow peak at 210°C is relatively little affected by ultraviolet irradiation. Table III gives a summary of the extent of trap-emptying for all the phosphors tested. The glow curves were divided into two arbitrary equal temperature ranges, and the percent of originally trapped electrons (as measured from glow curve areas) that remained in traps after illumination by ultraviolet was determined separately between 30° and 150°C, and between 150° and 270°C. In all cases, a higher percentage of electrons was freed from traps in the lower temperature range. The incorporation of gallium increases the efficiency of trap emptying by ultraviolet.

Emission Centers and Trapping Centers

The experimental results described above provide a number of criteria which classify rbhdl.-Zn_2SiO_4,

TABLE I. Maximum glow intensity.
(Not corrected for phototube sensitivity.)

Phosphor	Glow intensity, arbitrary units	Approximate emission peak wavelength, A
rbhdl.-Zn_2SiO_4	12	4100
rbhdl.-Zn_2SiO_4:Mn(0.3)	150	5250
rbhdl.-Zn_2SiO_4:Ga(0.5)	1800	4100
rbhdl.-Zn_2SiO_4:Mn(0.3):Ga(0.5)	300	5250
rbhdl.-$ZnO \cdot SiO_2$	0.12	4100
rbhdl.-$ZnO \cdot SiO_2$:Mn(0.3)	18	5250
rbhdl.-$ZnO \cdot SiO_2$:Ga(0.5)	135	4100
rbhdl.-$ZnO \cdot SiO_2$:Mn(0.3):Ga(0.5)	47	5250
rhomb.-Mg_2SiO_4	5	4100
rhomb.-Mg_2SiO_4:Mn(0.3)	15	6450, 7350
rhomb.-Mg_2SiO_4:Ga(0.5)	57	4100
rhomb.-Mg_2SiO_4:Mn(0.3):Ga(0.5)	28	6450, 7350
rbhdl.-Zn_2GeO_4	3.5	3500
rbhdl.-Zn_2GeO_4:Mn(0.3)	4	5370
rbhdl.-Zn_2GeO_4:Ga(0.5)	37	3500
rbhdl.-Zn_2GeO_4:Mn(0.3):Ga(0.5)	10	5370
rbhdl.-Be_2SiO_4	29	3100
rbhdl.-Be_2SiO_4:Mn(0.3)	4.5	6300
rbhdl.-Be_2SiO_4:Ga(0.5)	16	3100
rbhdl.-Be_2SiO_4:Mn(0.3):Ga(0.5)	1.8	6300

TABLE II. Summary of glow peaks, °C.

Average values	57°	75°	100°	125°	150°	177°	210°	250°
rbhdl.-Zn_2SiO_4			98				211	
rbhdl.-Zn_2SiO_4:Mn		77		126			220	249
rbhdl.-Zn_2SiO_4:Ga	55		103					
rbhdl.-Zn_2SiO_4:Mn:Ga	55		98				200	
rbhdl.-ZnO·SiO_2		73						
rbhdl.-ZnO·SiO_2:Mn		74		122			215	
rbhdl.-ZnO·SiO_2:Ga	57		102					
rbhdl.-ZnO·SiO_2:Mn:Ga	55		95				200	
rhomb.-Mg_2SiO_4	60		98		150			250
rhomb.-Mg_2SiO_4:Mn		75				177		250
rhomb.-Mg_2SiO_4:Ga	52			123				255
rhomb.-Mg_2SiO_4:Mn:Ga	57			125				247
rbhdl.-Be_2SiO_4	60			130			200	250
rbhdl.-Be_2SiO_4:Mn	63			125			207	250
rbhdl.-Be_2SiO_4:Ga	60			120			200	250
rbhdl.-Be_2SiO_4:Mn:Ga	60		103				190	260
rbhdl.-Zn_2GeO_4	58							
rbhdl.-Zn_2GeO_4:Mn	(33)							
rbhdl.-Zn_2GeO_4:Ga	65							
rbhdl.-Zn_2GeO_4:Mn:Ga	(42)							

rbhdl.-ZnO·SiO_2, and rhomb.-Mg_2SiO_4 phosphors as a group, and which classify rbhdl.-Zn_2GeO_4 and rbhdl.-Be_2SiO_4 phosphors as separate groups.

(1) *Host-Crystal Emission*

The zinc silicates and magnesium silicate have practically identical emission spectra (associated with SiO_4 groups). Zinc germanate and beryllium silicate each have a unique emission spectrum (associated with GeO_4 and BeO_4 groups, respectively).

(2) *Effect of Gallium on Host-Crystal Emission*

Gallium impurity acts as an intensifier activator in the zinc silicates and magnesium silicate, but as an originative activator in zinc germanate. Evidence thus far indicates that gallium is probably inert in beryllium silicate.

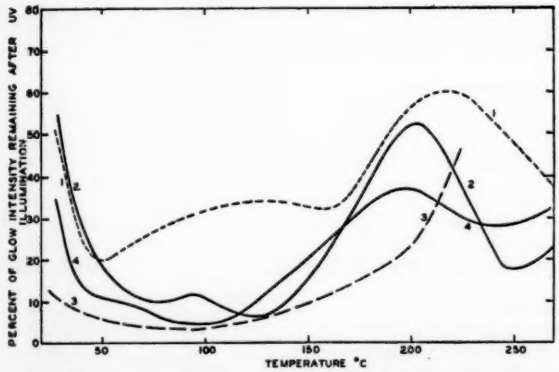

FIG. 8. The percent of glow intensity remaining after 5 minutes of 3650A-ultraviolet irradiation as compared to the glow intensity obtained without the ultraviolet irradiation for the rbhdl.-Zn_2SiO_4 family of phosphors. (1) Without added impurity, (2) with 0.3 percent Mn, (3) with 0.5 percent Ga, and (4) with 0.3 percent Mn and 0.5 percent Ga.

(3) *Distribution of Traps*

All of the silicate phosphors, including beryllium silicate, have similar glow peaks. Zinc germanate has a different glow peak distribution with few traps above room temperature. The glow peaks for beryllium silicate phosphors differ from those of the zinc silicate and magnesium silicate phosphors in that their relative magnitude is rather insensitive to the nature of the impurity.

If the glow peaks at 150° and 177°C are neglected, since they appear only once each (in the magnesium silicate phosphors), each of the other forty-seven glow peaks listed in Table II for the silicate phosphors may be identified with one of only six different glow peaks at 57°, 75°, 100°, 125°, 210°, and 250°C. Each of these six different glow peaks occurs at least once in a host crystal without added impurity; it may therefore be concluded that all glow peaks are associated with host-crystal defects.

TABLE III. Summary of trap emptying by 3650A ultraviolet.

	Percent of originally trapped electrons remaining after uv. 30°–150°C	150°–270°C	Total percent of originally trapped electrons remaining after uv.
rbhdl.-Zn_2SiO_4	32	51	44
rbhdl.-Zn_2SiO_4:Mn	10	33	19
rbhdl.-Zn_2SiO_4:Ga	5	17	7
rbhdl.-Zn_2SiO_4:Mn:Ga	9	29	14
rhomb.-Mg_2SiO_4	27	85	45
rhomb.-Mg_2SiO_4:Mn	31	42	38
rhomb.-Mg_2SiO_4:Ga	6	29	10
rhomb.-Mg_2SiO_4:Mn:Ga	6	28	14
rbhdl.-ZnO·SiO_2:Ga	37	89	43
rbhdl.-Zn_2GeO_4:Ga	73	83	74
rbhdl.-Be_2SiO_4:Ga	57	71	67

(4) *Effect of Gallium on Traps*

The glow intensity is increased by the incorporation of gallium impurity in all the phosphors except the beryllium silicates; for these phosphors the incorporation of gallium reduces the glow intensity.

(5) *Emptying of Traps by Ultraviolet*

Table III shows that the total percent of originally trapped electrons wich are freed by ultraviolet irradiation is practically the same for the zinc silicate and magnesium silicate phosphors. Considerably lower efficiency of trap emptying by ultraviolet is found for the zinc germanate and beryllium silicate phosphors.

The fact that the same host-crystal emission spectra and trap depths are found in both the zinc silicate and magnesium silicate phosphors, in spite of changes in host-crystal cation and crystal structure, suggests that

both host-crystal emission centers and trapping centers in these phosphors are associated with perturbed SiO_4 tetrahedral groups.

The same set of silicate trap depths is found also for the beryllium silicate phosphors, but the trapping process in these phosphors differs from that in the zinc silicates and magnesium silicates in that (1) the trap distribution is practically independent of incorporated impurity, (2) gallium impurity decreases the number of traps, (3) ultraviolet is much less efficient in emptying traps filled by cathode-ray excitation. These results indicate that trapping centers in beryllium silicate phosphors are associated with perturbed SiO_4 groups, but that the whole system is altered by the fact that the host-crystal emission centers are associated with perturbed BeO_4 groups.

Both host-crystal emission spectra and trap depths of zinc germanate phosphors are different from those of the silicate phosphors. In germanate phosphors it is probable that both host-crystal emission centers and

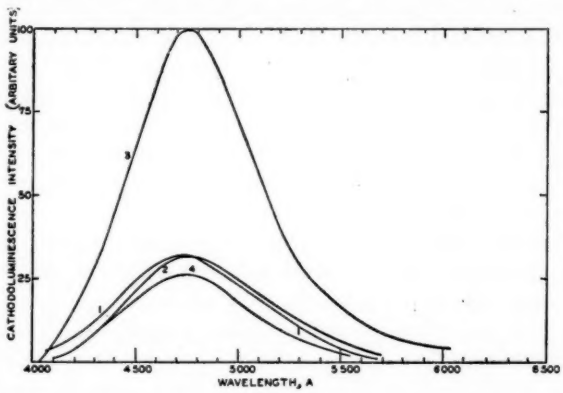

FIG. 9. Cathodoluminescence emission spectra for cub.-ZnS:Ga phosphors. (1) Without added Ga, (2) 0.001 percent Ga, (3) 0.1 percent Ga, (4) 1.0 percent Ga.

trapping centers are associated with perturbed GeO_4 tetrahedral groups.

II. ZINC SULFIDE PHOSPHORS WITH GALLIUM IMPURITY

The effects of gallium impurity in zinc sulfide phosphors have been reported as part of a general program of Kroeger and Dikhoff[8] on the effect of trivalent cations in zinc sulfide. Most of the detailed data given in their report was concerned with the effects of aluminum as an example. The present study confirms the finding that gallium acts as an intensifier for the emissions of certain zinc sulfide phosphors, and adds additional information about the effect of gallium in ZnS:Mn phosphors.

The effect of the incorporation of gallium in activator proportions in zinc sulfide phosphors without other added impurity, and with silver, copper, and manganese activators was studied. The results reported here are concerned only with variations in emission

[8] F. A. Kroeger and J. Dikhoff, Physica **16**, 297 (1950).

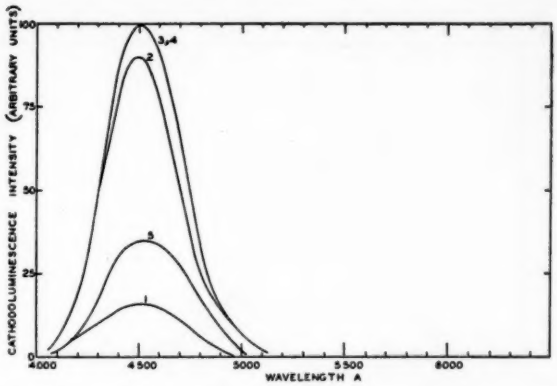

FIG. 10. Cathodoluminescence emission spectra for cub.-ZnS:Ag(0.005):Ga phosphors. (1) Without added Ga, (2) 0.0001 percent Ga, (3) 0.001 percent Ga, (4) 0.1 percent Ga, (5) 1.0 percent Ga.

spectra and intensity. Gallium acts as a trapping agent in all zinc sulfide phosphors, as evidenced by an increase in the afterglow intensity at room temperature. Hoogenstraaten[9] has reported that a characteristic glow peak at about room temperature is introduced in zinc sulfide phosphors by the incorporation of gallium.

Preparation of Phosphors

Triple-purified ZnS (RCA LM476), spectrographically free of impurities, was used to prepare all the phosphors. Additions of gallium, silver, copper, and manganese were made as solutions of their nitrates. The individual phosphors were synthesized by adding the appropriate activator solutions to water slurries of ZnS, drying at 150°C, heating for 15 minutes at 850°C in an atmosphere of H_2S, and cooling in an H_2S stream.

Results

The emission spectra for the cubic zinc sulfide phosphors, for varying gallium proportion, are given in

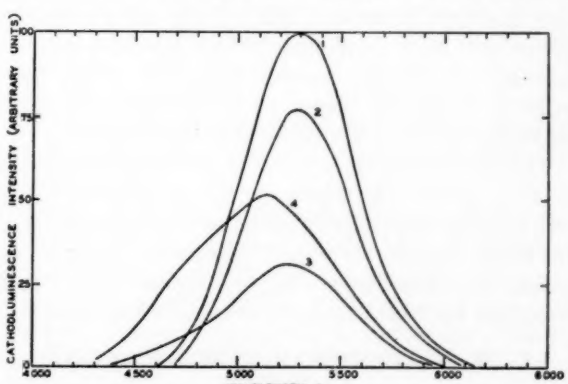

FIG. 11. Cathodoluminescence emission spectra for cub.-ZnS:Cu(0.01):Ga phosphors. (1) Without added Ga, (2) 0.0001 percent Ga, (3) 0.01 percent Ga, (4) 1.0 percent Ga.

[9] W. Hoogenstraaten, as cited by H. A. Klasens, Luminescence Symposium of Electrochemical Society, Philadelphia, May 5, 1952.

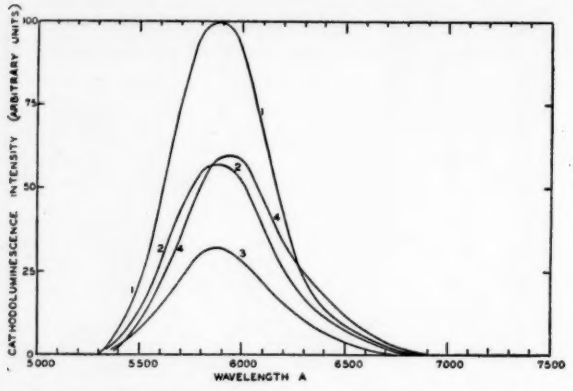

FIG. 12. Cathodoluminescence emission spectra for cub.-ZnS:Mn(0.5):Ga phosphors. (1) Without added Ga, (2) 0.0001 percent Ga, (3) 0.01 percent Ga, (4) 1.0 percent Ga.

Figs. 9 through 12. All of these curves were obtained for cathode-ray excitation.

Gallium in proportions less than 1.0 percent produces intensification for ZnS phosphor without added impurity and for ZnS:Ag phosphor. Higher proportions of gallium decrease the emission intensity.

For ZnS:Cu and ZnS:Mn, however, gallium in proportions less than 1.0 percent acts as a poison. Higher proportions of gallium increase the emission intensity but produce slight shifts in the spectral peak. Evidence that the blue band of the ZnS phosphor is being intensified at high gallium proportions is shown in the curves of Fig. 11 for the ZnS:Cu phosphors.

The ultraviolet-excited emission of the ZnS:Cu and ZnS:Mn phosphors, however, is affected quite differently by the incorporation of gallium. Figure 13 shows the dependence of the emission of the ZnS:Mn phosphor for 3650A-ultraviolet excitation on the gallium proportion. The emission intensity increases continuously with the gallium proportion, at least up to 1.0 percent gallium. A subsidiary band of ZnS:Mn phosphors at about 6700A, found only for ultraviolet excitation, is shown in curves 3 and 4 of Fig. 13. The emission intensity of ZnS:Cu phosphors for ultraviolet excitation increases in similar manner with the proportion of gallium. These are cases in which the gallium is a sensitizer activator for ultraviolet excitation.

The effect of the incorporation of 0.01 percent gallium in zinc sulfide phosphors activated with silver and copper, and with copper and manganese was also tested. In these doubly activated phosphors, gallium is a poison for cathode-ray excited luminescence, and a sensitizer for 3650A-ultraviolet excited luminescence.

III. DISCUSSION OF INTENSIFICATION

There seems to be sufficient evidence that effects of simple intensification (increase of efficiency without change of spectral distribution), occur in a number of different phosphors, and that these effects can be considered to be fundamentally different from effects due to originative activators.

The following reported examples of intensification may be cited:

(1) Halides in ZnS phosphors.[10–12]

(2) Al, Gd, Y, Pr, La, Sc, Yb, Si, and Ga in ZnS phosphors.[8]

(3) Ag, Cu, Ti, V, and Ga in silicates without added impurity.[13]

(4) Ag in (Zn:Cd)S and Zn(S:Se) phosphors.[14]

(5) Pb in tetr.-$CaWO_4$, tetr.-$CaMoO_4$, rhomb.-$BaSO_4$, and $Ba_2Si_3O_8$.[14]

(6) Nb in tetr.-ZnF_2.[15]

(7) Effect of increasing preparation temperature for the host-crystal emission of ZnS.[12]

(8) Li, Be, Si, Sc, Ti, Zn, Ga, Ge, Zr, Nb, Ru, Ag, Cd, In, Sn, Sb, Ta, W, Tl, Pb, Bi, and La in MgO.[16]

(9) Cu in ZnSe.[17]

In examining the known cases of intensification, one finds that most of them occur for emissions associated with host-crystals without added impurity. The luminescence centers in these phosphors are associated with imperfections in the crystal which can occur as a result of random thermal effects in the preparation of the phosphor. The intensifier activator, by its very nature, cannot be an intimate part of the luminescence center, but must be considered to cause imperfections in the crystal of such a type as is responsible for producing active luminescence centers.

Application of the principle of charge compensation, as developed by Kroeger and Dikhoff,[10] to the intensification effects reported in this paper for gallium impurity in silicates and sulfides, suggests a possible mechanism by which intensifier activators may, in some cases, introduce crystal defects. The incorporation of gallium in zinc or magnesium silicate or in zinc sulfide may result either in the formation of monovalent zinc or magnesium cations or in the formation of zinc or magnesium omission defects. These defects may be the perturbing agents in rendering particular SiO_4 or SZn_4 groups luminescently active.

For a ZnS phosphor[14] qualitatively similar intensification effects are caused by increasing the preparation temperature without additives in the preparation as by adding halide in the preparation at a fixed temperature. Increasing the preparation temperature, however, is much more effective in increasing the glow intensity than in increasing the emission intensity, whereas adding halide is much more effective in increasing the

[10] W. P. Jorissen and W. E. Ringer, Chem. Centralblatt. **1**, 644 (1906).
[11] F. A. Kroeger and J. E. Hellingman, J. Electrochem. Soc. **95**, 68 (1949).
[12] R. H. Bube, J. Chem. Phys. **20**, 708 (1952).
[13] See reference 2, p. 222, U. S. Patents 2,110,161 and 2,110,162 (1938).
[14] See reference 2, p. 239.
[15] F. E. Williams, cited by H. W. Leverenz, PB25481, Office Pub. Board, Washington, D. C. (1945).
[16] R. H. Bube and K. F. Stripp, J. Chem. Phys. **20**, 193 (1952).
[17] See reference 2, p. 207.

emission intensity than in increasing the glow intensity. These effects can be explained if it is assumed that halide produces primarily zinc omission defects either by charge compensation or by formation of volatile zinc chloride, and that increasing the temperature produces primarily sulfur omission defects by thermal diffusion or formation of volatile SO_2. Emission centers would be identified with sulfide ions perturbed by neighboring or near-by zinc omission defects; trapping centers would be identified with sulfur omission defects.

Activators which intensify the host-crystal emission of a particular material act in general as poisons for the emissions due to originative activators in the same material. For cathode-ray excitation, the effect of the incorporation of gallium is to poison the emission of ZnS:Cu, ZnS:Mn, Zn_2SiO_4:Mn, $ZnO \cdot SiO_2$:Mn, Mg_2SiO_4:Mn, and Be_2SiO_4:Mn phosphors. The incorporation of halide has a similar effect on the emission of ZnS:Mn.

The explanation for these effects may be associated with the different characteristics of originative-activator luminescence centers and host-crystal luminescence centers. An essential part of the luminescence center in the host crystal without added impurity in these phosphors is a perturbing imperfection of some type, such as an omission defect. Imperfections of this type are characteristic of the host crystal. The luminescence center for an originative activator, however, is associated with an imperfection which that activator itself has caused in a local region of the crystal which was otherwise relatively perfect, such as tetrahedral MnO_4 groups in Zn_2SiO_4:Mn or tetrahedral MnS_4 groups in ZnS:Mn. When the impurity which intensifies the host-crystal emission is incorporated, the originative activator centers, which are in the neighborhood of the additional imperfections formed by the presence of the incorporated impurity, are poisoned.

Exceptions to the statements of the last paragraph are the intensifying effects of halides and of some trivalent cations on the emissions due to Ag and Cu in ZnS. The role of the intensifier activators in these cases is apparently to aid the incorporation of the originative activator in the crystal. It has been reported that the proportion of incorporated halide is proportional to the proportion of Cu in the phosphor,[18,19] and that the efficiency of ZnS:Ag phosphor is continuously increased by the addition of increasing proportions of aluminum in the preparation.[10] In the case of ZnS:Ag phosphors, however, the proportion of halide incorporated is not a function of the Ag proportion of halide incorporated is not a function of the Ag proportion. The presence of the halide in the preparation is apparently able to produce enough zinc omission defects by formation of volatile zinc chloride to allow incorporation of Ag ions without corresponding one-to-one incorporation of halide ions.

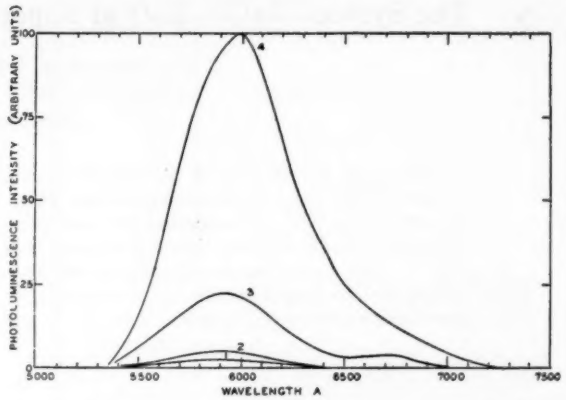

FIG. 13. Photoluminescence emission spectra for cub.-ZnS:Mn(0.5):Ga phosphors. (1) Without added Ga, (2) 0.0001 percent Ga, (3) 0.01 percent Ga, (4) 1.0 percent Ga.

The effects of gallium and halide are alike in the poisoning of the emission of ZnS:Mn phosphors for cathode-ray excitation, and in the sensitizing of the emission of ZnS:Mn phosphors for 3650A-ultraviolet excitation. Gallium and halide differ in their effects on ZnS:Cu phosphors, however, since halide acts as an intensifier for both cathode-rays and ultraviolet excitation, whereas gallium is a poison for cathode-ray excitation and a sensitizer for ultraviolet excitation.

Summary

Gallium, like many other elements, acts in a wide variety of ways according to the phosphor in which it is incorporated and the nature of the excitation. Examples are presented for the action of gallium impurity as originative activator, intensifier activator, sensitizer activator, poison, trapping agent, and trapping poison.

The effects of gallium on the traps of silicate and germanate phosphors indicate that host-crystal emission centers and trapping centers in these phosphors are associated with particular perturbed tetrahedral groups: SiO_4 for centers and traps in zinc and magnesium silicates, BeO_4 for centers and SiO_4 for traps in beryllium silicate, and GeO_4 for centers and traps in zinc germanate.

A review of intensification effects show that most cases of intensification occur for host-crystal emissions, and that the same activators which intensify the host-crystal emission poison the emission due to originative activators in the same phosphor. Examples are given to demonstrate that such effects could be the result of the intensifier activator causing the formation of crystal defects of the same type as are formed to a much less extent by processes of thermal disorder in the preparation of the phosphor.

[18] Kroeger, Hellingman, and Smit, Physica **15**, 990 (1949).
[19] R. H. Bube, J. Chem. Phys. **19**, 985 (1951).

The System $NaCl-H_2O$ at Supercritical Temperatures and Pressures*†

C. S. COPELAND, J. SILVERMAN,‡ AND S. W. BENSON
Department of Chemistry, University of Southern California, Los Angeles 7, California
(Received June 25, 1952)

Apparatus and techniques are described for the sampling of one phase of a liquid-vapor equilibrium system at high temperatures and pressures. These have been applied to the system $NaCl-H_2O$ in the supercritical region. Where the experimental ranges overlap, the present data are in reasonable agreement with that of previous workers. From the data obtained it has been possible to construct partial phase diagrams of the $NaCl-H_2O$ system and to calculate partial molal volumes of NaCl. The partial molal volumes of NaCl in steam are the largest partial molal volumes ever reported (order of magnitude of -2 liters) and indicate extensive solvation of the solute molecules in the vapor solution.

THAT sodium chloride is appreciably soluble in steam at high temperatures and pressures has been shown by Spillner,[1] Straub,[2] and Ölander and Liander.[3] In particular, Ölander and Liander measured over a wide range of temperatures and pressures the equilibrium distribution of sodium chloride between the aqueous liquid and vapor phases. None of the above investigators, however, determined the densities of either the liquid or vapor phases. The present paper gives the results of a series of density-composition-pressure measurements made by us at 385, 390, and 396°C for both vapor and liquid sodium chloride—water phases.

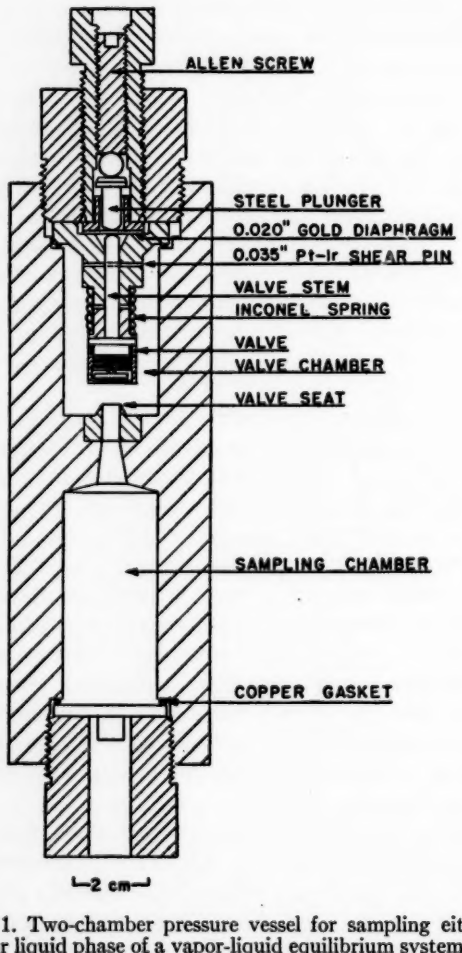

FIG. 1. Two-chamber pressure vessel for sampling either the vapor or liquid phase of a vapor-liquid equilibrium system at high temperatures and pressures. Material stainless steel unless otherwise noted.

EXPERIMENTAL

Density-Composition Measurements

To determine the density and composition of either the vapor or liquid phase of a liquid-vapor equilibrium system the pressure vessel shown in Fig. 1 was used. This vessel contains two chambers, a sampling chamber and a valve chamber, which can be sealed one from the other by means of a spring valve. The valve is held in its open position, under approximately 60 pounds tension, by a 0.035-in. platinum-iridium shear pin inserted through the valve stem. To close the valve, the Allen screw is turned. This causes a steel plunger to depress a deformable 0.020-in. annealed gold diaphragm. The resultant thrust against the valve stem, which is in contact with the gold diaphragm, shears the pin, and the valve is driven forcibly against the lapped steel valve seat. After expansion, the spring still exerts enough force, about 30 pounds, to hold the valve firmly in place. The sealing surface of the valve is a 0.040-in. annealed gold disk.

For vapor phase measurements such a volume of sodium chloride solution of appropriate composition was introduced into the pressure vessel that at the desired temperature the sampling chamber contained only vapor when this chamber was uppermost. For liquid phase measurements the volume and composition of the solution used were such that, with the pressure vessel vertical and the sampling chamber below, this chamber was filled with liquid. After the pressure vessel was charged, it was brought to temperature in an electrically heated air oven equipped with a fan to

* Presented in part at the XIIth International Congress of Pure and Applied Chemistry, New York, September 10–13, 1951.
† Supported in part by the ONR, Project No. NR 058-146.
‡ Present address, Physical and Nuclear Chemistry Section, U. S. Naval Radiological Defense Laboratory, San Francisco 24, California.
[1] F. Spillner, Chem. Fabrik. 13, 405 (1940).
[2] F. G. Straub, Univ. of Illinois Bull. 43, 59 (1946).
[3] A. Ölander and H. Liander, Acta Chem. Scandinavica 4, 1437 (1950).

provide adequate air circulation. In every case, before the valve was closed, the pressure vessel was kept in the oven for 3½ hours after the oven had reached the desired temperature and during the entire time the pressure vessel was continuously rotated at 3 rpm to insure thorough stirring of its contents. Previous tests showed that it took about 2½ hours to establish temperature equilibrium in the interior of the pressure vessel. The air temperature of the oven was measured with a Leeds and Northrup potentiometer and an iron-Constantan thermocouple with its cold junction immersed in an ice bath. The thermocouple was calibrated against a platinum resistance thermometer certified by the National Bureau of Standards.

When it was desired to sample the vapor or liquid phase,[4] the pressure vessel was set in the appropriate vertical position; an Allen wrench was inserted through a hole in the top or bottom of the oven, and the valve was closed. The pressure vessel was then immediately removed from the oven and quenched in water. The sampling chamber was opened, and its contents were drawn into a specially calibrated pipette whose tip reached to the bottom of the small well in the sampling chamber. The composition of this residual solution was determined by titration of a known volume, generally 5 cc, with standard silver nitrate solution. The density of the high temperature phase was readily calculated from the volume of the residual liquid, the known densities of sodium chloride solutions, and the volume of the sampling chamber (29.4 cc at 400°C).

Before the density-composition determinations were made for the sodium chloride-water system, three tests were made to determine that the valve operated effectively. In the first two tests the pressure vessel contained 10.0 cc of water and was heated in each case to 380°C. In the third test the pressure vessel contained 12.0 cc of 0.25 percent sodium chloride solution and was heated to 400°C. In each case all of the liquid was vaporized, and accordingly, the mean density of material in the sampling chamber must have been the same as the original mean density of material in the pressure vessel. In the first two tests the original mean density of water was 0.21_4 g/cc and the determined mean densities of water in the sampling chamber were 0.21_3 and 0.20_6 g/cc. In the third test the original mean density of salt solution was 0.25_6 g/cc and the mean density of solution in the sampling chamber was found to be 0.25_1 g/cc. The agreement is quite good and shows that the valve operated effectively.[5]

[4] Both phases could not be simultaneously sampled with the present apparatus. This arises from the fact that while the sampling chamber will contain only a single phase, the valve chamber will contain both phases and there is no way of obtaining the individual volumes of the phases present in this chamber.

[5] In earlier forms of the pressure vessel we attempted to use magnetically operated ball type and conical type valves held seated by their own weight. These values were found to be quite unreliable, and they could not, as the spring valve can, be closed with the pressure vessel in any position.

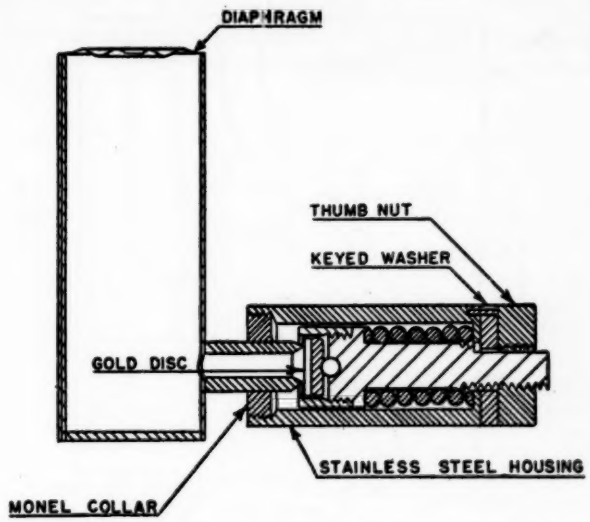

FIG. 2. Pressure cell. The cell body, diaphragm (0.004 in.), and side arm are constructed from platinum-iridium alloy (80 Pt-20 Ir). The spring is stainless steel.

Pressure Measurements

A pressure counterbalancing method[6] was used to measure the pressures of sodium chloride—water systems at different mean densities and temperatures. Briefly, the apparatus and procedure were as follows. A small, lightly constructed platinum-iridium cell (Fig. 2) contained the sodium chloride—water solution. This cell was mounted inside a steel pressure vessel which in turn was mounted in an electrically heated, cylindrical oven. The entire assembly could be oscillated through a 180° angle to stir the cell contents. The pressure developed in the cell as it was heated was continuously counterbalanced by admission of nitrogen into the pressure vessel. The direction and magnitude of the pressure differential between the interior of the cell and the surrounding nitrogen was indicated by a meter circuit which measured the potential drop of a radiofrequency current across a variable condenser operated by the aneroid diaphragm of the cell. The nitrogen pressure was read on a 6-inch dial 0–5000 psi test gauge.

The side arm, through which the cell was filled and drained, is a platinum-iridium tube sealed by a spring actuated plunger which holds an annealed gold disk firmly against the sharp lapped seat of the tube.

Because the cell was light enough to be weighed on an analytical balance, its internal volume and the mean density of any solution introduced into the cell could be determined with good precision. The internal volume, corrected for the thermal expansion of the cell, was estimated to be 12.64 cc in the temperature range 360–400°C.

To determine the pressure-temperature relationship for a sodium chloride—water system, sodium chloride solution of known composition was introduced into

[6] Fogo, Copeland, and Benson, Rev. Sci. Instr. 22, 765 (1951).

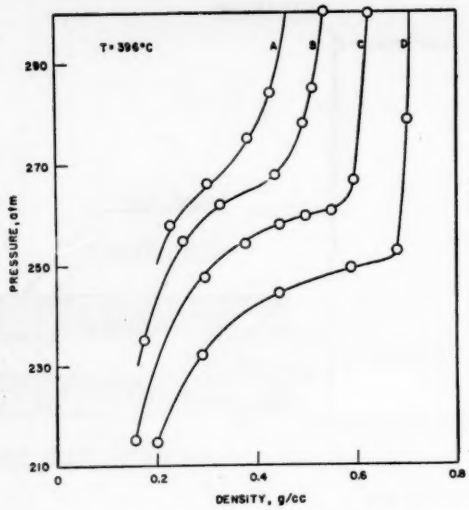

FIG. 3. Pressure-density isotherms for the NaCl-H_2O system at 396°C. *A*, 1.00; *B*, 3.00; *C*, 6.74; *D*, 11.96 weight percent NaCl.

the cell to give the desired mean density of the system. The cell was then heated as described to a desired temperature. The temperature was then held constant, and the cell contents were stirred by intermittent oscillation of the heating oven until the pressure became constant. The time required to reach equilibrium was generally about fifteen minutes. After the pressure was read, the temperature was raised a few degrees and the new equilibrium pressure determined. This process was repeated until an adequate temperature range had been covered. A reweighing of the cell after each run showed that the loss in weight of the cell never exceeded 0.05 percent of the weight of the solution in the cell.

To check the accuracy of the method, the first pressure-temperature measurements were made with pure water in the cell at known mean densities. The experimentally determined values were compared with steam table data.[7] This comparison indicated that in the temperature range 380–400°C the method could be relied upon to give results good to one percent.

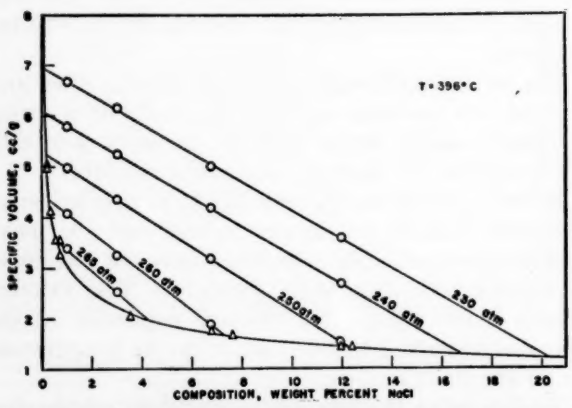

FIG. 4. Specific volume-composition diagram for the NaCl-H_2O system at 396°C showing typical tie lines.

[7] J. H. Keenan and F. G. Keyes, *Thermodynamic Properties of Steam* (John Wiley and Sons, Inc., New York, 1936).

EXPERIMENTAL RESULTS

Table I gives measured densities and compositions of a number of vapor and liquid solutions which were independently investigated.[8] The liquid densities marked *b* were estimated from pressure-density isotherms such as those of Fig. 3.

The pressure-temperature measurements gave directly, at different temperatures, the pressures of various sodium chloride—water systems at constant mean densities and compositions. These data were plotted, and from their curves were obtained the isothermal pressures corresponding to various mean densities of sodium chloride—water systems of constant mean composition. These results were plotted to give pressure-density isotherms such as those shown in Fig. 3. From these and similar curves at 385 and 390°C were obtained the pressure-density-composition values given in Table II.

TABLE I. Densities and compositions of some vapor and liquid sodium chloride—water solutions.[a]

	Vapor Solution		Liquid Solution	
T (°C)	C (%NaCl)	ρ (g/cc)	C (%NaCl)	ρ (g/cc)
385	0.12	0.22	3.00	0.50[b]
	0.15	0.24	6.74	0.60[b]
	0.19	0.26	11.96	0.70[b]
	0.44	0.32		
390	0.21	0.22	3.00	0.50[b]
	0.34	0.26	11.96	0.69[b]
	0.62	0.34		
396	0.21	0.20	3.5	0.49
	0.23	0.20	7.6	0.61
	0.30	0.24	12.4	0.69
	0.51	0.28	6.74	0.58[b]
	0.69	0.29	11.96	0.68[b]
	0.68	0.31		

[a] See references 4 and 8.
[b] Estimated from pressure-density isotherms.

To obtain the densities, compositions, and pressures of vapor and liquid solutions in equilibrium with each other at a given temperature, reciprocals of the densities of Table I were plotted against the weight percent of sodium chloride. On such a diagram, the isobars which are the tie lines connecting corresponding equilibrium vapor and liquid solutions must be linear.

This relation arises from application of the phase rule to the solution of the following mass and volume balance equations:

$$V_t = V_l + V_g,$$
$$V_t\rho_t = V_l \cdot \rho_l + V_g\rho_g,$$
$$C_t \cdot V_t \cdot \rho_t = C_l \cdot V_l \cdot \rho_l + C_g \cdot V_g \cdot \rho_g,$$

[8] The reader should note that the vapor and liquid solutions are not in equilibrium with each other but rather each is in equilibrium with a solution phase whose composition was not determined (see reference 4).

TABLE II. Pressures and mean densities at different temperatures of sodium chloride—water systems of various mean compositions.

P (atmos)	ρ(g/cc)														
C(%NaCl) =	0[a]			1.00			3.00			6.74			11.96[b]		
T (°C) =	385	390	396	385	390	396	385	390	396	385	390	396	385	390	396
210	0.132	0.124	0.118			0.121	0.154		0.130	0.193		0.148	0.301		0.183
220	0.152	0.140	0.129			0.134		0.161	0.144	0.246	0.199	0.169	0.467	0.297	0.224
230	0.181	0.160	0.144			0.150	0.246	0.189	0.163	0.467	0.248	0.200	0.711	0.433	0.278
235	0.202	0.172	0.153	0.237		0.161	0.313	0.212	0.175	0.619	0.293	0.218		0.605	0.317
240	0.231	0.187	0.163	0.300		0.173	0.422	0.244	0.191	0.625	0.384	0.239		0.700	0.372
245	0.272	0.206	0.175	0.401	0.228	0.186	0.517	0.292	0.209	0.629	0.567	0.272		0.702	0.463
250	0.353	0.231	0.188	0.422	0.275	0.201	0.535	0.371	0.230	0.632	0.605	0.315		0.704	0.642
255	0.397	0.263	0.204	0.466	0.347	0.220	0.541	0.483	0.259	0.634	0.615	0.387		0.707	0.682
260	0.422	0.305	0.222	0.483	0.403	0.246	0.547	0.515	0.307	0.637	0.623	0.526		0.709	0.687
265		0.357	0.244		0.430	0.296		0.524	0.396		0.629	0.591		0.711	0.691
270		0.386	0.270		0.449	0.348		0.531	0.456		0.632	0.596		0.713	0.695
275		0.407	0.300		0.464	0.387		0.537	0.481		0.635	0.600			0.698
280		0.424	0.335		0.476	0.410		0.543	0.498		0.638	0.605			0.700
285			0.363			0.428			0.511			0.609			0.702
290			0.383			0.441			0.519			0.613			
295			0.400			0.452			0.527			0.619			
300			0.415			0.459			0.535			0.622			

[a] See reference 7.
[b] We are indebted to Mr. J. K. Fogo, of this laboratory, for these data.

where V is volume, ρ is density, and C is percent composition, the subscripts t, l, and g referring to the total system, liquid phase, and gas phase, respectively. For the total system of two phases and two components there are two degrees of freedom. On fixing the pressure and temperature (as for the tie lines) the system becomes invariant, and a change in total composition cannot change the composition of the individual phases but only their relative extent. Thus, along the tie lines P_l, P_g, C_l, and C_g are constants, and it then turns out that C_t is a linear function of $1/\rho_t$:

$$(\rho_l-\rho_g)C_t=C_l\rho_l-C_g\rho_g-(C_l-C_g)\rho_g\rho_l(1/\rho_t).$$

Table II furnished the necessary data to construct the tie-lines. Figure 4 shows the diagram obtained at 396°C. Table III gives the pressures, compositions, and densities so obtained for vapor and liquid solutions in equilibrium with each other at 385, 390, and 396°C.

PHASE DIAGRAMS

The density-composition diagram at 396°C is shown in Fig. 5. Similar diagrams are obtained at 385 and 390°C. From the origin to point E, points on the curve give the densities and compositions of vapor solutions which can be in equilibrium with solid sodium chloride. Between E and the critical point C,[9] a point on the curve gives the density and composition of a vapor solution which can be in equilibrium with an undersaturated liquid solution represented by the appropriate point on the curve between C and S. Several tie lines are shown. The region bounded by the curve ECS and the tie line connecting E and S shows the range of densities and compositions at 396°C which a sodium chloride—water system may have and exist as an equilibrium vapor-liquid system. Points in the region above and to the left of the curve OECS give the densities and compositions of undersaturated, one-phase fluid systems. Such a fluid phase might be designated as a vapor solution if its composition is less than the critical composition and as a liquid solution if its composition is greater than the critical composition.

Typical pressure-composition and temperature-com-

TABLE III. Pressures, compositions and densities of some equilibrium vapor and liquid sodium chloride—water solutions.

	385°C				390°C				396°C			
	vapor		liquid		vapor		liquid		vapor		liquid	
P (atmos)	C (%NaCl)	ρ (g/cc)	C	ρ	C	ρ	C	ρ	C	ρ	C	ρ
210	0.03	0.13	17.8	0.80								
220	0.04	0.15	14.0	0.73	0.06	0.14	18.6	0.79				
225	0.06	0.17	10.8	0.68	0.07	0.15	16.7	0.77				
230	0.07	0.18	7.8	0.63	0.08	0.16	14.8	0.74	0.09	0.14	20.5	0.81
235	0.11	0.21	5.9	0.58	0.10	0.18	12.6	0.69	0.10	0.15	18.6	0.78
240	0.25	0.27	4.0	0.54	0.12	0.19	9.5	0.65	0.12	0.16	16.7	0.77
245					0.18	0.22	7.0	0.60	0.14	0.18	14.6	0.73
250					0.28	0.25	4.8	0.54	0.17	0.19	12.3	0.69
255					0.59	0.32	2.5	0.46	0.22	0.21	9.8	0.65
260									0.30	0.23	7.4	0.60
265									0.56	0.28	4.4	0.51

[9] Estimated from data of E. Schroer, Z. Physik. Chem. 129, 79 (1927).

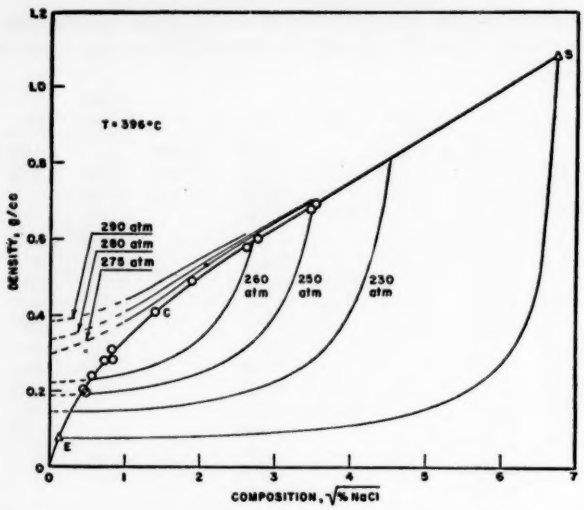

FIG. 5. Density-composition diagram for the NaCl-H_2O system at 396°C. Point *C*, after Schroer (see reference 9). △, Mr. D. Fisher, unpublished data, this laboratory.

position diagrams are shown in Figs. 6 and 7. The general characteristics and explanations of these diagrams are given on the inserts. The pressures, compositions, and temperatures of the saturated liquid solutions were obtained from data reported by Keevil.[10] The critical curve of Fig. 7 is based on the critical temperature-composition data of Schroer.[9] The points of intersection of the isobars with this curve were obtained from a plot of the critical pressures, from Fig. 6, against temperature. It will be noted from Figs. 6 and 7 that our results and those of Ölander and Liander[3] are in reasonably good agreement, particularly if one considers that the temperature coefficient of pressure is about 3 atm/°C in this region.

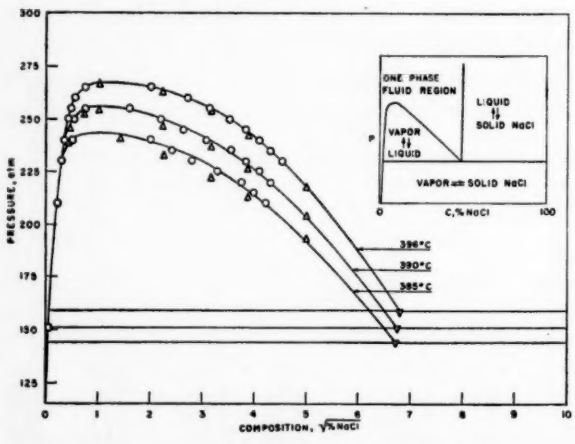

FIG. 6. Pressure-composition diagram for the NaCl-H_2O system at supercritical temperatures. △, after Ölander and Liander (see reference 3). ▽, after Keevil (see reference 10). □, after Straub (see reference 2).

[10] N. B. Keevil, J. Am. Chem. Soc. 64, 841 (1942).

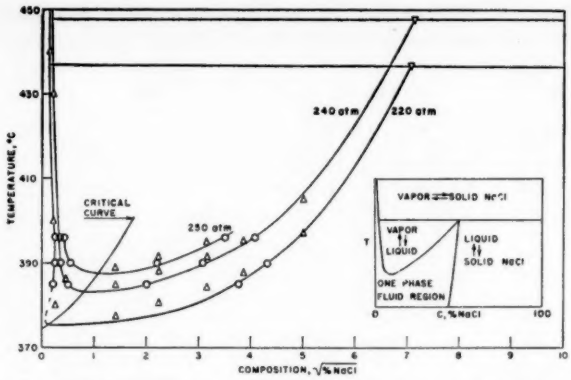

FIG. 7. Temperature-composition diagram for the NaCl-H_2O system at supercritical temperatures. △, after Ölander and Liander (see reference 3). ▽, after Keevil (see reference 10).

THE PARTIAL MOLAL VOLUME OF SODIUM CHLORIDE IN STEAM

The apparent molal volumes of sodium chloride in steam are readily calculated from densities and compositions read directly from isobars in the homogeneous, fluid region of a density-composition diagram such as that shown in Fig. 5. From such apparent molal volumes we have obtained, in the usual way, the partial molal volumes given in Table IV.

TABLE IV. Partial molal volumes ($\bar{V}_2$) of sodium chloride in steam.

P(atmos)	$-\bar{V}_2$(cc) ×10⁻³								
T(°C) =		385			390			396	
C(%NaCl) =	1.00	3.00	6.74	1.00	3.00	6.74	1.00	3.00	6.74
250	1.78	0.62	0.2						
255	1.36	0.45	0.2						
260	1.04	0.36	0.2						
265				1.77	0.61	0.29			
270				1.37	0.54	0.24			
275				1.14	0.48	0.21	2.33	0.88	0.41
280				0.96	0.44	0.20	1.74	0.80	0.35
285							1.62	0.62	0.28
290							1.34	0.60	0.22

The variation of the partial molal volume as the percent of sodium chloride approaches zero cannot be determined from our present data since the exact course of any isobar in the fluid region below one percent sodium chloride is not accurately known.

The absolute magnitudes of the partial molal volumes of sodium chloride are extraordinarily high and are, to the best of our knowledge, the largest ever observed. While a quantitative explanation of these large values has not been made, the data do indicate that there must be a quite extensive solvation of the solvent by the solute particles. Further investigations are being made of these systems, and we hope to publish soon some data on the other thermodynamic properties of this system. Measurements have also been made of the electrical conductivities in these systems[6] and will be reported on in the near future.

It is a pleasure to acknowledge the generous support of this project by the Office of Naval Research, without whose help this work could not have been done.

Dielectric and Ultrasonic Relaxation in Glycerol*

THEODORE A. LITOVITZ, *Physics Department, Catholic University of America, Washington D. C.*

AND

DANIELE SETTE, *Istituto Nazionale di Ultracustica "O. M. Corbino" Rome, Italy*

(Received June 26, 1952)

Measurements of dielectric and ultrasonic relaxation in glycerol are compared over a frequency range of 7.5 to 37.5 megacycles and over a temperature range from 20°C to −25°C. Reduced dielectric and ultrasonic constants when plotted against viscosity at a constant frequency of 30 megacycles appeared quite similar. The imaginary (or loss) part of the reduced constants exhibited a peak at the same viscosity. Both phenomena exhibited a departure from a single relaxation time theory. This deviation of the dielectric phenomena from the simple theory was attributed in the usual manner to a distribution of relaxation times. The striking similarities in the behavior of the dielectric and ultrasonic phenomena suggests an intimate relation between the two. Thus, if a distribution of relaxation times exists for the dielectric, it should in all probability exist in the ultrasonic process.

Both shear and compressional viscous processes are associated with the acoustic phenomena. It was concluded that if any difference exists in the shear and compressional viscous relaxation times, its effect is masked by a probable distribution in relaxation times for each process.

Calculations indicated that the natural "rotational jump" time in glycerol is between ½ and 4 times the "translational (or viscous) jump" time.

INTRODUCTION

IT has been pointed out that a similarity exists in the dielectric and viscous behavior of a liquid. It would appear that the molecular motions performed by rotating dipoles as they jump from one equilibrium position to another are closely related to the processes occurring in viscous flow when a molecule jumps between different positions of equilibrium in a liquid quasi-crystalline lattice.

That a relation exists between viscosity and dielectric relaxation is shown by the fact that the dielectric relaxation time has the same temperature dependence as the viscosity in many liquids.[1]

A correspondence between dielectric relaxation time and viscosity is predicted by Debye[2] who, using a hydrodynamic model, arrived at the following expression: $\tau_d = 3\eta V/KT$, where τ_d is the dielectric relaxation time, η is the shear viscosity coefficient, and V is the volume of the molecule.

Relaxation theories of dielectric behavior picture a rotational jump rate as a factor controlling the dielectric constant and losses at a given temperature.

Eyring's[3] picture of viscous flow involves the translational jump of molecules from one liquid lattice position to another. The magnitude of the flow and thus the viscosity of the liquid are determined by the factors controlling the jump rate.

It has been demonstrated that ultrasonic propagation in glycerol is associated with a viscous relaxation process.[4,5]

The compressibility or elasticity of a liquid is dependent upon its structure (and viscosity) because a change in volume following an applied pressure indicates some change in liquid structure. But change in structure involves motions of the molecules in two possible ways. First, a simple displacement of the molecules could occur about some equilibrium (as in a solid or crystalline lattice under compression). This contribution of the compressibility would have extremely small time lag associated with it (of the order of 10^{-13} second).

A second type of structural change would be due to the flow of molecules past each other into a position of closer packing which could account for some of the change in volume resulting from a compression. This latter contribution to the compressibility would have associated with it a time lag for rearrangement that is connected with the "translational" jump rate of the molecular units in the liquid. This latter time lag would be usually much larger than the first. Thus, we find the compressibility made up of two parts, one time dependent and the other essentially independent of the time measurement. If one were to measure the compressibility in a time comparable to this flow or rearrangement time, it would be possible to study the relaxation time associated with this part of the compressibility.

By measuring the acoustic properties of glycerol as a function of the temperature, it was possible to cover the relaxation region at a frequency of 30 Mc.

It is of interest to compare this acoustic relaxation effect with the analogous phenomena, dielectric relaxation in the same liquid. Because the acoustic effect is determined by a "translational" viscosity, whereas dielectric relaxation can be ascribed to a "rotational" viscosity, a comparison of these two phenomena should show just how similar are the two relaxation times in-

* Supported by the ONR.

[1] W. Kauzmann, Revs. Modern Phys. **14**, 12 (1942).

[2] P. Debye, *Polar Molecules* (Dover Publications, New York, 1929).

[3] H. Eyring, J. Chem. Phys. **4**, 283 (1936).

[4] T. A. Litovitz, J. Acoust. Soc. Am. **23**, 75 (1951).

[5] F. E. Fox and T. A. Litovitz, International Colloquium on Ultrasonic Vibrations, June, 1951, p. 38.

TABLE I. Dielectric constant (real and imaginary part) of glycerol (5 percent water) at various temperatures measured at a frequency of 30 Mc.

T°C	ϵ'	ϵ''	$\epsilon_0-\epsilon_\infty$[a]	$\frac{\epsilon''}{\epsilon_0-\epsilon_\infty}$	$\frac{\epsilon'-\epsilon_\infty}{\epsilon_0-\epsilon_\infty}$
20	43.5	...	38.5	...	1.0
14.8	43.5	9.0	39.7	0.226	0.97
10.4	43.2	12.2	41.6	0.293	0.92
5.0	38.9	14.7	42.0	0.350	0.81
2.6	35.9	15.8	42.5	0.370	0.73
0.5	34.6	16.3	43.1	0.378	0.69
−3.1	28.7	16.8	43.7	0.383	0.54
−5.4	29.4	16.8	44.4	0.379	0.55
−7.4	27.0	16.6	45.0	0.369	0.49
−9.8	24.2	15.8	45.8	0.345	0.42
−13.5	20.5	14.0	46.8	0.299	0.33
−18.3	17.3	12.1	48.0	0.252	0.26
−22.1	14.0	9.4	49.5	0.190	0.18
−26.5	12.3	7.7	50.8	0.151	0.14
−29.5	10.6	5.8	52.0	0.110	0.11

[a] The value of ϵ_∞ used here is 5.

volved. The acoustic data are available over a large temperature range, but there are no dielectric data on glycerol in the literature, with the same water content (5 percent) as that used in the ultrasonic work. Since 5 percent water changes the viscosity markedly, the dielectric measurements are repeated here.

EXPERIMENTAL METHOD

The capacitance and resistance of a dielectric cell were measured over a frequency range from 8 to 37.5 Mc using a General Radio Type 1061-*A* VHF bridge in conjunction with a suitable signal generator and receiver. The dielectric cell consisted of a small variable plane parallel plate capacitor enclosed in a shielded container. The cell was immersed in a thermal bath, the temperature of which was controlled to ±0.1C, and measurements were made over a temperature range from 20°C to −29°C. The absolute value of the dielectric constant was determined by measuring the change in capacity of the cell due to a change in the setting of the capacitor both with the liquid as dielectric and then with just air. The accuracy of this absolute value is estimated at ±5 percent, after making appropriate corrections for residual parameters. The sample of glycerol used contained 5 percent water and came from the same bottle as the glycerol used in the acoustic experiments.

RESULTS AND DISCUSSION

The real part of the dielectric constant ϵ' measured at 20°C was found to be 43.5±5 percent which agrees well with the static value for 100 percent glycerol. The variation of the complex dielectric constant with temperature is tabulated in Table I, where ϵ'' is the coefficient of the imaginary part. The frequency used for this temperature study was 30 Mc, because of the availability of ultrasonic data at that frequency. Actually, the ultrasonic absorption data were taken at 31 Mc, but this 3 percent difference in frequency will be neglected in the comparison.

It can be noted from Table I that typical relaxation behavior is occurring. ϵ' falls as the liquid becomes more viscous and the loss factor reaches a peak and declines.

In Table II the complex dielectric constant is tabulated as a function of the frequency at −28°C. It can be noted that both ϵ' and ϵ'' are decreasing in this frequency range at this temperature.

In order to compare the dielectric and ultrasonic data, one must consider the relaxation equations for each phenomena.

Kauzmann,[1] considering dielectric relaxation as a chemical rate process, has derived an expression for the complex dielectric constant. He finds that

$$\epsilon=\epsilon'-i\epsilon'', \tag{1}$$

where

$$\epsilon'=\frac{\epsilon_0-\epsilon_\infty}{1+x^2}+\epsilon_\infty \tag{2}$$

and

$$\epsilon''=\frac{(\epsilon_0-\epsilon_\infty)x}{1+x^2}. \tag{3}$$

ϵ_0 is the static or low frequency value of the dielectric constant, and ϵ_∞ is the high frequency or optical value;

$$x=\omega\tau_d=\omega\left(\frac{\epsilon_0+2}{\epsilon_\infty+2}\right)\tau_d', \tag{4}$$

where τ_d' is the relaxation time (time between rotational jumps) of the dipoles in the absence of an electric field;

$$\tau_d=\tau_d'\left(\frac{\epsilon_0+2}{\epsilon_\infty+2}\right), \tag{5}$$

where τ_d is the relaxation time in the presence of a field. This "effective" relaxation time is larger than τ_d' due to the tendency of the field to maintain itself. However, the correction $(\epsilon_0+2)/(\epsilon_\infty+2)$ overemphasizes this effect and should be considered only as an upper limit to the ratio of τ_d to τ_d'.

The theoretical maximum in ϵ'' occurs when

$$x^2=1$$

or

$$\tau_d=\frac{1}{\omega}.$$

Thus, here

$$\tau_d'\geqq\frac{1}{\omega}\frac{\epsilon_\infty+2}{\epsilon_0+2}. \tag{6}$$

Turning attention to the ultrasonic relaxation theory, it is first important to note the presence of two viscous effects which contribute to the loss and velocity dispersion. The absorption in glycerol (in the nondispersion region-high temperature) is approximately twice that which one calculates considering a shear viscosity

process only. This "excess" absorption has been explained by assuming that a compressional viscosity exists and that the absorption α is made up of the sum of these effects. Thus,

$$\alpha_{\text{total}}=\alpha_{\text{shear}}+\alpha_{\text{compressional}}.$$

Frenkel,[6] considering both of these effects, has derived an expression for the complex velocity squared in a visco-elastic medium. It has been suggested[4] that the relaxation times associated with the two viscous processes are the same or very nearly the same in glycerol. Applying this assumption of equal relaxation times to the Frenkel expression for the complex velocity squared, one gets

$$\rho V_c^2=K_1+\frac{(K_2+\frac{4}{3}G)\omega\tau_A'}{1+i\omega\tau_A'}, \tag{7}$$

where V_c is the complex velocity, ρ is the density, G is the shear rigidity modulus, K_1 is the static bulk modulus of compressibility, and K_1+K_2 is the high frequency bulk modulus. τ_A' is the viscous relaxation time associated with "translational" jumps in the liquid.

The quantity analogous to the complex dielectric constant is $1/V_c^2$ or the complex ultrasonic propagation constant squared. We shall define a complex elastic constant (β_c) for a longitudinal sonic wave, where

$$\beta_c=1/\rho V_c^2.$$

From Eq. (7) we get

$$\beta_c=\beta'+i\beta''=\beta_\infty+\frac{\beta_0-\beta_\infty}{1+\omega^2\tau_A^2}+i\frac{(\beta_0-\beta_\infty)\omega\tau_A}{1+\omega^2\tau_A^2}, \tag{8}$$

where β' and β'' are the real and imaginary part of the complex elastic constant, $\beta_\infty=1/(K_1+K_2+\frac{4}{3}G)$ is high frequency elastic constant for a longitudinal wave, $\beta_0=1/K_1$ is the static compressibility, and

$$\tau_A=(\beta_0/\beta_\infty)\tau_A'. \tag{9}$$

β' and β'' are related to the measured quantities velocity (V) and absorption coefficient per cm (α) in the following manner. The amplitude (A) of a traveling sonic wave can be written

$$A=A_0\exp i[\omega t-(\rho\beta)^{\frac{1}{2}}x]=A_0\exp i\left[\omega t-\frac{x}{V}+i\frac{\alpha x}{\omega}\right]. \tag{10}$$

From this relation it can be shown that

$$\beta''=2\alpha/\omega\rho V \tag{11}$$

and

$$\beta'=\frac{1}{\rho V^2}-\frac{1}{\rho}\left(\frac{\alpha}{\omega}\right)^2. \tag{12}$$

The second term is less than 3 percent of $1/\rho V^2$ for even the highest α measured; thus β' is calculated from the approximate relation

$$\beta'\cong 1/\rho V^2. \tag{13}$$

It is of interest to compare, respectively, the real and imaginary parts of the elastic and dielectric constants. It can be noted that each phenomenon has associated with it a relaxation time. To compare these times, we reduce Eqs. (2), (3), and (8) to the following:

$$\frac{\epsilon'-\epsilon_\infty}{\epsilon_0-\epsilon_\infty}=\frac{1}{1+\omega^2\tau_d^2}=D', \tag{14}$$

$$\frac{\epsilon''}{\epsilon_0-\epsilon_\infty}=\frac{\omega\tau_d}{1+\omega^2\tau_d^2}=D'', \tag{15}$$

$$\frac{\beta'-\beta_\infty}{\beta_0-\beta_\infty}=\frac{1}{1+\omega^2\tau_A^2}=B', \tag{16}$$

$$\frac{\beta''}{\beta_0-\beta_\infty}=\frac{\omega\tau_A}{1+\omega^2\tau_A^2}=B''. \tag{17}$$

B and D are called the "reduced" elastic and dielectric constants. These reduced constants are tabulated in Tables I–IV.

In Fig. 1 the imaginary (or loss) part of the reduced constants at different temperatures are plotted as a function of the viscosity. Assuming that the relaxation time in both phenomena is proportional to the viscosity, Fig. 1 becomes essentially a plot of Eq. (15) and Eq. (17) *vs* τ_d and τ_A.

The striking feature is that both phenomena exhibit a maximum at about the same viscosity. The uncertainty in locating the maxima as a function of viscosity is about 20 percent. Also in Fig. 1 is plotted the function $\omega\tau/(1+\omega^2\tau^2)$ *vs* the viscosity. It is assumed here that τ is proportional to viscosity, and τ is obtained by setting $\omega\tau=1$ at the viscosity value for which the experimental curves exhibit a maximum. τ is the effective relaxation time in each phenomenon and is affected by changes with temperature of β_0, β_∞, and ϵ_0 and ϵ_∞. This is neglected in the theoretical plot since the deviations from theory are much larger than this correction. From the theoretical curve in Fig. 1, it can be seen that although the data plotted qualitatively obey the simple single relaxation time expression, they do differ quantitatively from the theory. Both the elastic and dielectric

TABLE II. Dielectric data at −28°C as a function of frequency.

f Mc	ϵ'	ϵ''	$\frac{\epsilon'-\epsilon_\infty}{\epsilon_0-\epsilon_\infty}$	$\frac{\epsilon''}{\epsilon_0-\epsilon_\infty}$
8	19.2	11.0	0.275	0.22
15	14.9	9.3	0.192	0.18
25	12.5	7.7	0.145	0.15
30	11.6	6.7	0.128	0.13
37.5	11.1	6.2	0.118	0.12

[6] J. Frenkel, *Kinetic Theory of Liquids* (Clarendon Press, Oxford, 1946).
[7] T. A. Litovitz, J. Chem. Phys. **20**, 1088 (1952).
[8] Litovitz, Peselnick, and Fox (to be published).

TABLE III. Viscosity and ultrasonic data of glycerol at 30 Mc (31 Mc for absorption) as a function of temperature.

T°C	η centipoise	α[b] cm^{-1}	V[c] cm/sec $\times 10^{-5}$	β'' dyne/sec $\times 10^{12}$	β' dyne/sec $\times 10^{12}$	β_0[+] dyne/sec $\times 10^{12}$	β_∞[++] dyne/sec $\times 10^{12}$	$\frac{\beta''}{\beta_0-\beta_\infty}$	$\frac{\beta'-\beta_\infty}{\beta_0-\beta_\infty}$
20	5.5	28	1.92	1.19	22.1	22.1	12.1	0.122	1.0
10	12.5	60	1.96	2.47	21.1	21.3	11.5	0.260	0.98
5	24	80.5	2.02	3.21	19.7	20.8	10.9	0.325	0.89
0	34	102	2.09	3.94	18.4	20.5	10.3	0.386	0.80
−5	64[a]	110	2.21	4.0	16.1	20.2	10.0	0.392	0.60
−10	120[a]	105	2.37	3.55	13.6	19.9	9.5	0.341	0.39
−20	480[a]	61	2.68	1.81	10.7	19.2	8.6	0.171	0.20
−25	1100[a]	42	2.82	1.19	9.8	18.9	8.4	0.113	0.11
−30	2400[a]	···	2.98	···	8.8	18.6	8.1	···	0.07

α = ultrasonic absorption coefficient per cm. V = ultrasonic velocity of longitidunal wave. β' = real part of elastic constant. β'' = imaginary part of elastic constant. β_0 = low frequency or static value of compressibility. β_∞ = high frequency value of elastic constant.
[a] Extrapolated from data at room temperature (see reference 7 for method).
[b] Data from reference 4.
[c] Data from reference 5.

phenomena exhibit a broader and lower maximum than the theory predicts.

Two differences in the behavior of the constants can be noted in Fig. 1. One is that the acoustic phenomena appear to deviate from the theory to a smaller extent than the dielectric. This is especially noticeable in the low viscosity region where the acoustic data are in rather fair agreement with the theory. This points up the second difference between the acoustic and dielectric behavior, and that is the rather asymmetrical deviation from theory exhibited by the acoustic constant as a function of viscosity. It is felt by the authors that this is not absolutely certain because of the uncertainty in the values of β_∞ at low viscosities combined with the experimental error in the measurements. The values for β_∞ were extrapolated from the high viscosity region.

In Fig. 2, which shows the real part of the reduced constants, the same general deviations from theory are exhibited. Again the acoustic data appear to be in fair agreement with theory at low viscosity values.

In Figs. 3 and 4 the imaginary and real parts are given as function of the frequency at −28°C. The lack of a wide range in frequencies in the acoustic data makes the comparisons in Figs. 3 and 4 rather incomplete. In Fig. 3 it can be noted that at −28°C the losses in both phenomena are beyond the peak in the frequency range measured and are decreasing with frequency. The elastic constant appears to be falling somewhat faster with frequency than the dielectric constant.

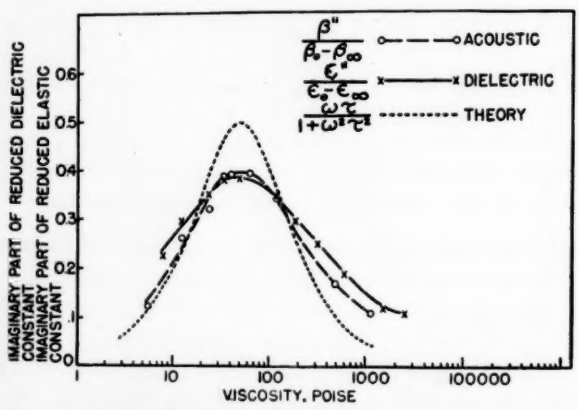

FIG. 1. Plot of the imaginary part of the reduced dielectric and elastic constants of glycerol (5 percent water) *vs* viscosity at a frequency of 30 Mc. Curve with short dashes is theoretical plot assuming a single relaxation time.

In Fig. 4 the real parts of the elastic and dielectric constant are compared. Here the general behavior with frequency follows that shown in Fig. 2 at high viscosities, the acoustic constant approaching zero somewhat faster than the dielectric constant.

The departure of the dielectric phenomena from theoretical behavior has been explained by the suggestion that a distribution of relaxation times exists. This would be due in a simple liquid to thermal fluctuations of the neighboring molecules such that the activation energy for rotation of a dipole might vary from molecule to molecule.

In considering the deviation of the acoustic data from the single relaxation theory, we have a complicating factor. This factor is the presence of the two viscous processes—the shear and compressional viscosity. Should one attempt to explain the acoustic data by the existence of two separate relaxation times or by a distribution as is considered in the dielectric phenomena? It would appear that the answer is in the striking similarities of the behavior of the dielectric and elastic constant as exhibited in Figs. 1 and 2. Although the elastic case has possibly a smaller deviation from theory,

TABLE IV. Ultrasonic data measured as a function of the frequency at −28°C.

f Mc	α[a] cm^{-1}	V[a] cm/sec	β' dyne/sec $\times 10^{12}$	$\beta'-\beta_\infty$ $\times 10^{12}$	β'' $\times 10^{12}$	$\frac{\beta''}{\beta_0-\beta_\infty}$	$\frac{\beta'-\beta_\infty}{\beta_0-\beta_\infty}$
5	···	2590	12.3	4.0	···	···	0.39
8	24.1	[2680]	···	···	2.77	0.266	···
15	···	2910	9.2	1.0	···	···	0.10
22.5	41.3	[2965]	···	···	1.54	0.148	···
25	···	2990	8.7	0.5	···	···	0.05
37.5	33.7	(3000)	8.7	0.5	0.74	0.071	···

α = ultrasonic absorption coefficient. V = velocity of longitidinal wave. [ ] = interpolated data. ( ) = extrapolated data. β' = real part of elastic constant. β'' = imaginary part of elastic constant. β_0 = low frequency compressibility (from Table III). β_∞ = high frequency compressibility (from Table III).
[a] Data from reference 8.

the fact that they both exhibit a maxima at about the same viscosity values would seem to indicate an intimate relation exists between the acoustic and dielectric relaxation times. It therefore seems improbable that the local thermal fluctuations which would cause a distribution of dielectric relaxations times would not cause (to some extent) a distribution in the acoustic or viscous relaxation times. With the data at hand it seems possible to conclude only that any difference which might exist between compressional and shear relaxation times is masked by the very probable existence of a distribution of relaxation times for both types of viscous flow.

Davidson and Cole[9] have proposed a useful empirical expression, which they have shown to be adequate in describing the relaxation behavior of water-free glycerol. Their expression for the complex dielectric constant is

$$\epsilon'-i\epsilon''=\epsilon_\infty+\frac{\epsilon_0-\epsilon_\infty}{(1+i\omega\tau_0)^\gamma}, \tag{18}$$

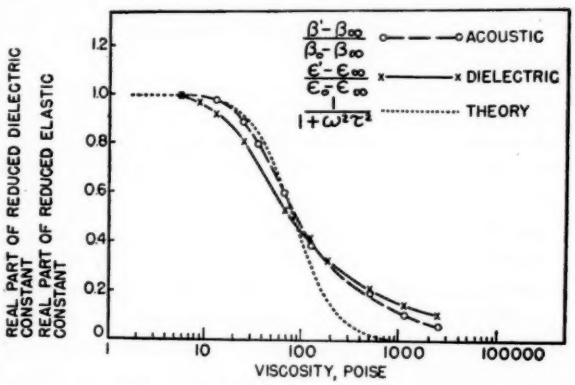

FIG. 2. Plot of the real part of the reduced dielectric and elastic constants of glycerol (5 percent water) *vs* viscosity at a frequency of 30 Mc. Curve with short dashes is theoretical plot and based on a single relaxation time.

where τ_0 is a relaxation time, and γ is a parameter which may take values between zero and one. They have derived analytical expressions showing how the value of γ is indicative of the breadth of the distribution of relaxation times away from τ_0 the maximum relaxation time. Thus, when $\gamma=1$, only a single relaxation time τ_0 is present and Eq. (18) reverts to Eq. (2). The smaller the value of γ, the broader is the distribution of relaxation times.

The real and imaginary parts of Eq. (18) can be expressed in terms of the reduced constants and are given by

$$D'=\frac{\epsilon'-\epsilon_\infty}{\epsilon_0-\epsilon_\infty}=(\cos\varphi)^\gamma\cos\gamma\varphi, \tag{19}$$

$$D''=\frac{\epsilon''}{\epsilon_0-\epsilon_\infty}=(\cos\varphi)^\gamma\sin\gamma\varphi, \tag{20}$$

where $\tan\varphi=\omega\tau_0$.

[9] D. W. Davidson and R. H. Cole, J. Chem. Phys. **19**, 1484 (1951).

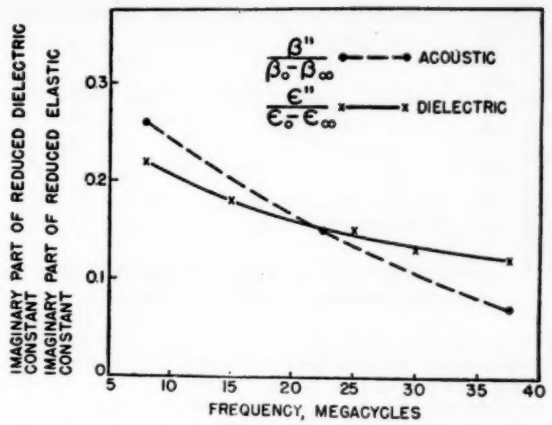

FIG. 3. Plot of imaginary part of reduced dielectric and elastic constants of glycerol (5 percent water) *vs* frequency at a temperature of −28°C.

Applying this same empirical approach to the acoustic equations, one finds that the reduced elastic constants are given by

$$B'=\frac{\beta'-\beta_\infty}{\beta_0-\beta_\infty}=(\cos\varphi)^\gamma\cos\gamma\varphi, \tag{21}$$

$$B''=\frac{\beta''}{\beta_0-\beta_\infty}=(\cos\varphi)^\gamma\sin\gamma\varphi. \tag{22}$$

A complex plane plot of the real *vs* the imaginary part of the reduced constants is useful in analyzing the data.

In Fig. 5, each dashed line represents the locus of points in the complex plane for a given value of γ. The sparseness of the acoustic data as a function of frequency does not allow any real analysis of it by this method. Thus, Fig. 5 contains only the data on temperature dependence of the reduced constants.

One can note that the acoustic and dielectric data appear, within experimental error, to lie on the same curve in the complex plane. But it is apparent that the

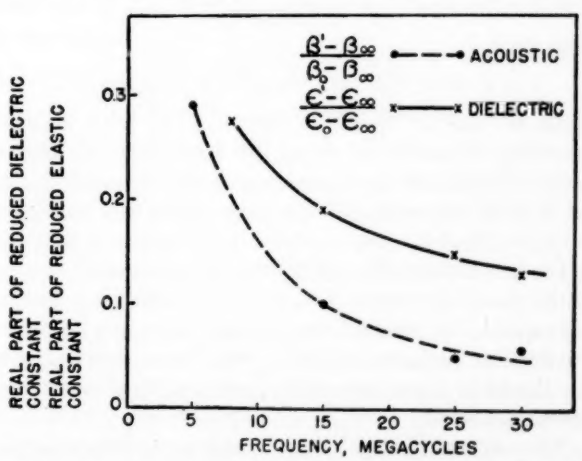

FIG. 4. Plot of real part of the reduced dielectric and elastic constants of glycerol (5 percent water) *vs* frequency at a temperature of −28°C.

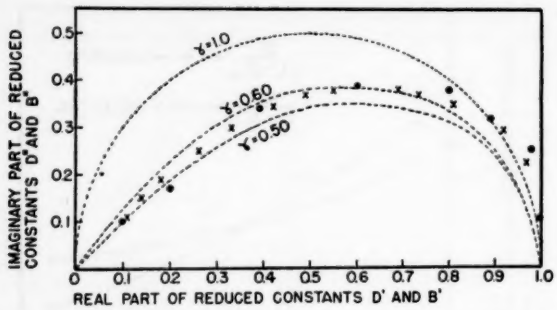

FIG. 5. Complex plane plot of imaginary *vs* real parts of the reduced constants. Dashed lines are theoretical curves obtained by use of Eqs. (19) and (20) for different values of γ. The × marks are for the dielectric and the ○ points are for the acoustic data. The data are taken from Tables I and III for the values of the reduced constants at various temperatures.

experimental points do not lie on a curve of constant γ. This would indicate that the distribution of relaxation times changes with temperature. From the low temperatures of about −30°C ($D'\sim0.1$) to about 0°C ($D'\sim0.6$), γ slowly increases from 0.5 to 0.6. Between 0°C and 25°C the experimental values for the imaginary part of reduced constants seems to be unaccountably high.

An increase in γ with temperature has been noted by Davidson and Cole for water-free glycerol. Over a range from −75°C to −40°C, a change in γ from 0.55 to about 0.61 was found. The values of γ found in this present work are reasonable in comparison with the values reported for pure glycerol.

It is evident that analysis of the data on temperature dependence of the reduced constants has limitations due to the variation of γ. A similar study at a constant temperature over a wide frequency range should be fruitful. However, it does not seem unreasonable to consider the significance of the fact that both B'' and D'' peak at the same temperature (within experimental error). Considering Eqs. (20) and (22), it can easily be shown that B'' and D'' as functions of $\omega\tau_0$ (or φ) would peak when

$$\varphi=\pi/[2(1+\gamma)].$$

And thus,

$$\omega\tau_0=\tan\pi/[2(1+\gamma)].$$

Both B'' and D'' peak at about −5°C with a corresponding B' and D' of about 0.6. From Fig. 5 it can be estimated that at this temperature and value of B' and D', a γ of 0.6 would fit the data. Thus, $\omega\tau_0$ would be equal to about 1.5, and τ_0 at the temperature of the peak in the loss factors B'' and D'' can be calculated. τ_0 is τ_D in the dielectric case and τ_A in the acoustic phenomena.

It should be recalled that neither τ_D nor τ_A are the "molecular" relaxation times which are descriptive of the liquid in the absence of an electric field or a compressional wave.

The natural "jump" time between re-orientations is given by Eq. (5). Equation (9) gives the relaxation time associated with "translational" change in the lattice position of a molecule. In Table V these are tabulated for the viscosity at which the loss factors are maximum using the assumptions that $\omega\tau_D=1.5$ and $\omega\tau_A=1.5$ at this point.

In computing the "rotational" relaxation time, a large uncertainty exists due to the recognized fact that the $(\epsilon_0+2)/(\epsilon_\infty+2)$ correction overemphasizes the effect of the dipole tending to stay oriented. No estimate can be given as to how much this is in error. $(\epsilon_0+2)/(\epsilon_\infty+2)$ is about 8; therefore, the "rotational" relaxation time lies somewhere between 8.1×10^{-9} and 65×10^{-9} sec. The "translational" relaxation time is 16.2×10^{-9} sec. Thus, we may conclude only that the "rotational" relaxation is somewhere between $\frac{1}{2}$ and 4 times the "translational" relaxation time.

This conclusion appears valid, even though the absolute value of the relaxation times as calculated above may be in error. The assumption that $\omega\tau=1.5$ at the peak may not be valid, but since both peaks appear at the same viscosity (within experimental error) τ_0 is most probably equal to τ_A.

TABLE V. Dielectric and ultrasonic relaxation times in glycerol (5 percent water) calculated from maxima in loss curves.

	τ[a]	τ'[b]
Dielectric	8.1×10^{-9}	$\leqq64.8\times10^{-9}$
Acoustic	8.1×10^{-9}	16.2×10^{-9}

[a] τ is effective relaxation time as determined directly from peak in loss curves.
[b] τ' is the molecular or natural relaxation or jump time in absence of electric field or acoustic wave.

One cannot assume from the above that the observed similarities between viscous and dielectric relaxation times in glycerol will occur in all liquids. It seems probable that this correlation will exist only in simple liquids made of relatively small molecules.

CONCLUSIONS

A comparison of the dielectric and ultrasonic relaxation properties of glycerol has demonstrated that these two phenomena are closely related. The results indicate that the "effective" relaxation time for dipole rotation and viscous flow are equal within experimental error. It was concluded that in both phenomena the existence of a distribution of relaxation times must be assumed. From the limited data available it appears that the distribution is similar in the two processes.

It has previously been shown that ultrasonic propagation in glycerol is connected with both a shear and compressional viscous process. The results of this present work indicate that if there is any difference in the values of the shear and compressional relaxation times, it is masked by the existence of a distribution of relaxation times for both viscous processes.

Study of the Structure of Quartz, Cristobalite, and Vitreous Silica by Reflection in Infrared*

I. ŠIMON AND H. O. MCMAHON
Arthur D. Little, Inc., Cambridge 42, Massachusetts

(Received June 30, 1952)

Infrared spectra of α- and β-quartz, α- and β-cristobalite, and vitreous silica were studied by the reflection method using natural and polarized radiation in the 700 to 1400 cm^{-1} wave number interval. By measuring the reflecting powers at two different angles of incidence, the indices of refraction and extinction were obtained and the absorption bands could be correctly located, sometimes at variance with the existing data, based on reflection maxima alone. The strong band at 1055 cm^{-1} in α-quartz and at 1095 cm^{-1} in α-cristobalite and vitreous silica can be assigned as a valence stretching $\overleftarrow{Si}-\overrightarrow{O}-\overleftarrow{Si}$ vibration. Other observed bands are consistent with the already existing assignments. The effect of temperature on the total intensity and width of the bands was studied in a temperature interval between 4°K and 880°K.

I. INTRODUCTION

THE vibration bands in the infrared and Raman spectra of various forms of silicon dioxide have been a subject of numerous investigations. Some of the more recent contributions containing complete references to the previous work are listed below.[1-4] In spite of the amount of published data, the assignment of many of the observed vibration bands is not yet satisfactory. Also, experimental data obtained previously in the infrared by reflection have not been always interpreted correctly. Finally, infrared data on some of the crystalline modifications of SiO_2 were still lacking.

The purpose of this study was to fill the gap in the existing experimental data, in particular in relation with the problem of the transition from the crystalline to the vitreous state. Vitreous silica and many silicate glasses exhibit a very strong infrared band at approximately 1100 cm^{-1}. A similar strong band has been observed[5,6] in the infrared spectra of certain organosilicon compounds, containing the siloxy group. This leads to the assumption that the corresponding band is caused by a bond-stretching vibration of the oxygen shared between two silicons of the adjacent SiO_4 groups. It remained to be investigated whether any of the vibrational modes of quartz or cristobalite unit cells correspond to this type of vibration, and how the transition from the crystalline to the vitreous state manifests itself in the spectra.

Group-theoretical analyses of the vibrational modes in the unit cells of the α- and β-modifications of quartz have been performed by Saksena[1] and Barriol,[3] respectively. Some of the modes described in these papers can be identified with the observed infrared vibrations directly, using the polarization properties in infrared alone. Concerning the α- and β-forms of cristobalite, no theoretical analysis has been yet made, although the unit cell is simpler and possesses higher (cubic) symmetry than that of quartz. The experimental data for cristobalite obtained in our work are less complete than those for quartz, because of impossibility of obtaining large single crystals of cristobalite. However, the spectra are very similar to those of quartz so that some conclusions may be reached by analogy.

The β-forms of quartz and cristobalite exist only at elevated temperatures above quite definite inversion temperatures. Some of the infrared bands exhibit systematic changes in intensity with temperature which allow some conclusions to be made concerning the nature of the $\alpha-\beta$ transition. Other bands increase in width steadily with increasing temperature as a result of the interaction between the vibrational modes of the lattice and its incoherent thermal agitation. It was quite natural to study the effect of temperature on the width of the bands in the crystalline and vitreous samples of silica in a more detailed way. By investigation of the infrared spectra of the samples of silica in a wide temperature interval, including the lowest temperature (4.2°K), we have attempted to ascertain to what extent the thermal band broadening is responsible for the actually observed band widths in crystals at ordinary temperatures.

II. REFLECTION SPECTRA AND LOCATION OF THE VIBRATION BANDS

The maxima occurring in a reflection spectrum of a substance possessing several dispersion bands result from the combined effects of the changes of both refractive and absorption indices and, therefore, do not locate the position of the proper vibrations directly. For instance, a high reflecting power may result from a high value of the absorption index κ or from a value of the refractive index n largely different from unity ($n \gg 1$ or $n \ll 1$). It can be shown from electromagnetic theory that the proper vibration frequencies are located by the maxima of the imaginary part of the complex polarizability (n'^2-1), which is $n^2\kappa$. Here, $n'=n(1-i\kappa)$ denotes the complex refractive index. Actually, the quantity

* This research was sponsored by the Owens-Illinois Glass Company, Toledo, Ohio.

[1] B. D. Saksena, Proc. Indian Acad. Sci. **12A**, 93 (1940).
[2] R. S. Krishnan, Nature **155**, 452 (1945).
[3] J. Barriol, J. phys. et radium **7** (8), 209 (1946).
[4] F. Matossi, J. Chem. Phys. **17**, 679 (1949).
[5] N. Wright and M. J. Hunter, J. Am. Chem. Soc. **69**, 803 (1947).
[6] R. E. Richards and H. W. Thompson, J. Chem. Soc. (London), p. 124 (1949).

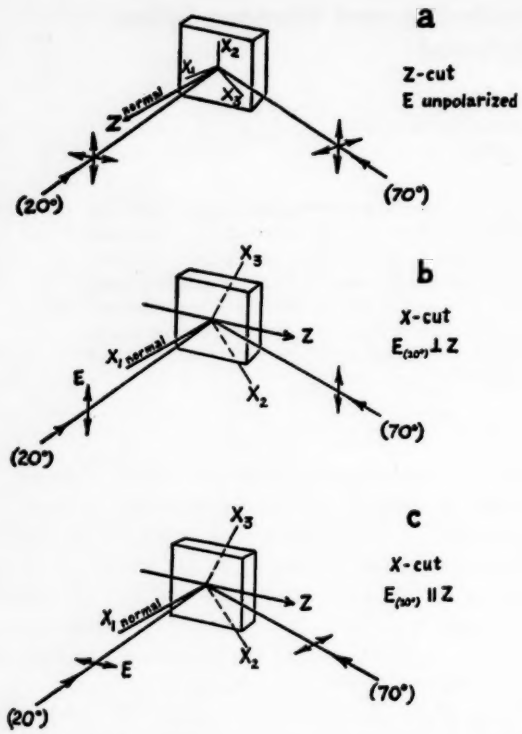

FIG. 1. Orientation of the quartz plates with respect to the incident beam in the 20° and 70° positions. Direction of the electric vector **E** in the polarized radiation is indicated by the double arrows across the incident ray. X_1, X_2, X_3 are the twofold axes.

$n^2\kappa$ has to be corrected for the polarization of the medium, as will be explained later.

The two indices n and κ can be obtained by measuring the reflecting powers at two different angles of incidence, e.g., 20° and 70°, by means of a method described in reference.[7] From the resulting plots n *vs* ν and κ *vs* ν (ν= wave number), the product $n^2\kappa$ can be formed point by point and replotted *vs* ν. At the same time, the correction for the dielectric polarization within the medium is applied, multiplying by the factor $3/(n^2+2)$. For a homogeneous, isotropic medium, this factor results from a consideration usual in the derivation of the Clausius-Mosotti formula. The final quantity

$$\epsilon''=3n^2\kappa/(n^2+2) \qquad (1)$$

is essentially the imaginary part of the complex dielectric constant $\epsilon=\epsilon'-i\epsilon''$ and, accordingly, closely related to the absorption coefficient as measured, e.g., by direct transmission.

The plot of ϵ'' *vs* ν represents a corrected or "true" infrared spectrum in which each maximum locates exactly the resonance frequency of the vibration causing each particular dispersion band. An absorption spectrum, obtained by the usual transmission method, could be corrected in a similar way.[7]

In an anisotropic medium, the Clausius-Mosotti correction should be computed for each vibrational mode from the actual field configuration within the unit cell of the given crystal. In the case of quartz, this would be a very difficult task. Moreover, our method of analysis of the reflection data is rigorously applicable only to isotropic media. While crystalline quartz may be considered as fairly "isotropic" far enough from strong dispersion bands, this is not the case within the bands. In fact, strong dichroism is usually observed there and the method of analysis fails to yield consistent results near the very centers of these bands. However, the quantities n, κ can be secured there by means of the impedance method,[7] in which the use of oblique incidence is avoided.

III. EXPERIMENTAL TECHNIQUE

The measurements were performed by means of a Perkin-Elmer spectrometer, Type 12-B, with rocksalt prism, equipped with a recording system. A detailed description of the experimental arrangement was given earlier.[7]

The samples of quartz and vitreous silica were in the form of plates of various dimensions, approximately one millimeter thick, polished on one side. The sample of cristobalite was formed as a layer (approximately 0.02 mm thick) on a polished plate of vitreous silica by devitrification at 1400°C.

The following samples have been used:

(1) Crystalline quartz cut perpendicularly to the optic axis (Z-cut).

(2) Crystalline quartz cut perpendicularly to one of the twofold axes of symmetry and parallel to the optic axis (X-cut).

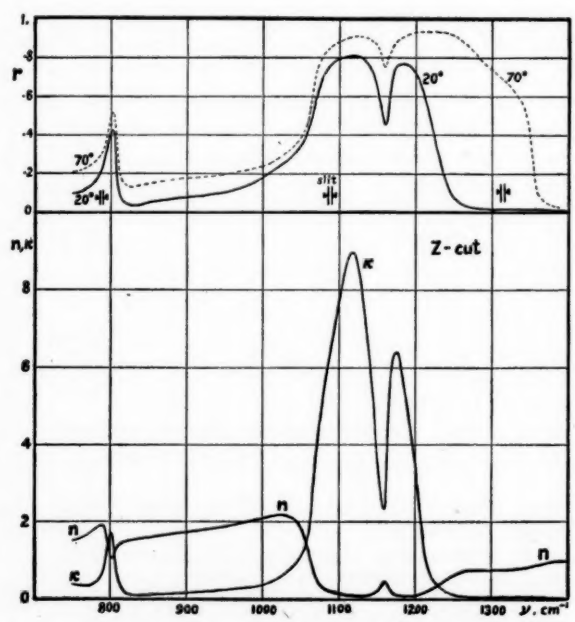

FIG. 2. Reflecting powers and the optical constants (indices of refraction and extinction n, κ) of a quartz plate cut perpendicularly to the optic axis.

[7] I. Šimon, J. Opt. Soc. Am. **41**, 336 (1951).

(3) Crystalline quartz cut parallel to one of the twofold axes and parallel to the optic axis (Y-cut).

(4) Samples of polycrystalline cristobalite layer on vitreous silica base. The x-ray diffraction has shown an almost complete orientation with the (100) plane parallel to the surface.

(5) Plate of vitreous silica (fused quartz).

The direction of the optic axis within the plane of the X- and Y-cut samples of quartz has been determined by inspection in polarized light. The directions of the X- or Y-axes within the plane of the Z-cut sample have not been established. For reflection measurements, the samples were mounted on a holder in which they could be rotated around the normal to their surface. The notation used in the following description is explained in Fig. 1.

For studying the β-modifications of quartz and cristobalite by reflection, the samples had to be heated above approximately 575°C and 250°C, respectively. A small heater placed behind the flat sample and a simple insulating envelope made of transite and asbestos cardboard proved to be quite satisfactory for the moderate temperatures required in the experiments. Although the quartz crystals developed cracks on passing through the β-transition temperature, the fragments usually adhered together, and it was possible to complete the reflection measurements.

For the low temperature measurements, a vacuum cell with rocksalt windows was designed in such a way as to fit in place of the usual sample holder. The sample was kept at the desired temperature by thermal contact with an internal metallic container filled with liquid nitrogen (~80°K) or liquid helium (~4°K).

Measurements at room temperature have been performed both with natural and polarized radiation. A polarizer[8] made of six silver chloride sheets, 0.5 mm thick each, inclined at 70°, was placed in front of the entrance slit of the spectrometer.

IV. RESULTS OF MEASUREMENTS

1. α-Quartz, Z-Cut

The measured reflecting powers (in unpolarized radiation) and the derived quantities n, κ for a Z-cut sample are plotted *vs* frequency in Fig. 2. The maxima of ϵ'' derived from n, κ by means of formula (1) locate four strong vibration bands at 795 cm^{-1}, 802 cm^{-1}, 1065 cm^{-1}, and 1162 cm^{-1} (see Fig. 7a). A comparison with the curves of the reflecting powers reveals that the centers of the bands do not coincide with maxima of reflection, as directly observed. In particular, the conspicuous region of high reflection between 1050 to 1250 cm^{-1} is resolved in two sharp bands located at 1065 and 1162 cm^{-1}. Accordingly, the dip in the broad reflection maximum cannot be considered as a gap between two partially overlapping bands, but rather a manifestation of an individual, sharp absorption band (see also reference 7).

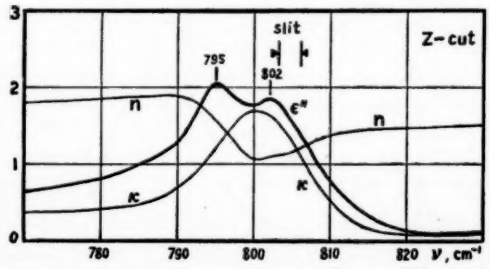

FIG. 3. Optical constants n, κ and the imaginary part of the dielectric constant ϵ'' of a Z-cut quartz plate in the region around 800 cm^{-1}.

[8] R. Newman and R. S. Halford, Rev. Sci. Instr. **19**, 270 (1948).

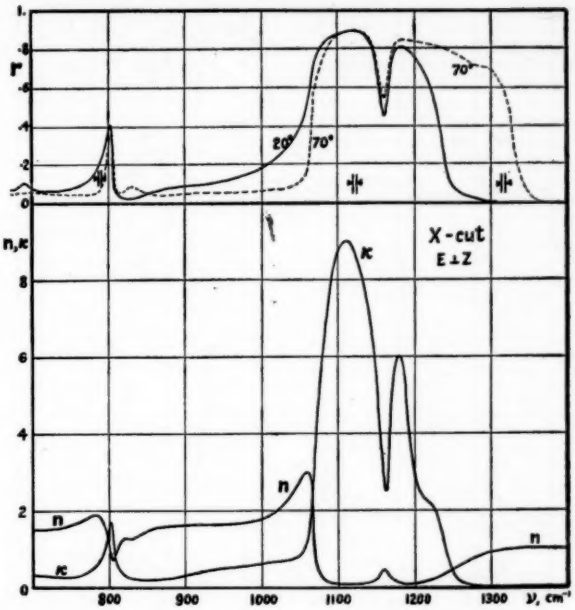

FIG. 4. Reflecting powers and the optical constants of a quartz plate cut parallel to the optic axis, in radiation polarized perpendicularly to the direction of the optic axis (case b in Fig. 1).

The band at 800 cm^{-1} is a doublet with components 795 and 802 cm^{-1}. This is borne out by a detailed investigation (Fig. 3), in agreement with the observations in Raman effect. For instance, Krishnan[2] reports a doublet at 794 and 805 cm^{-1}. The spectrum remains unchanged when polarized radiation is used, and the Z-cut sample is examined in different orientations by rotation around the optic axis. A weak band is observed in the reflection spectrum at 695 cm^{-1} (Fig. 14).

2. α-Quartz, X- and Y-Cuts

Significant results are obtained in this case with polarized radiation. The reflecting powers and the quantities n, κ for polarizations perpendicular and parallel to the optic axis are plotted in Figs. 4 and 5, respectively.

A comparison of the diagrams indicates that the direction of the effective dipole associated with the vibration at 1162 cm^{-1} is perpendicular to the optic

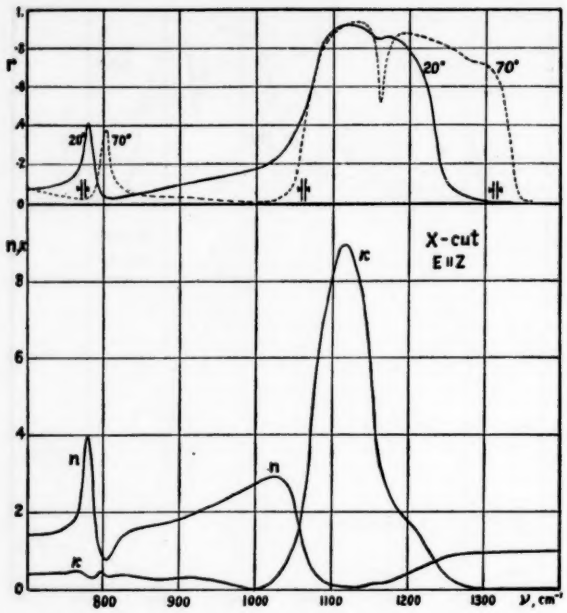

FIG. 5. Reflecting powers and optical constants of a quartz plate cut parallel to the optic axis, in radiation polarized parallel to the direction of the optic axis (case c in Fig. 1).

axis (Fig. 7b, c). Accordingly, the corresponding band (dip) should not be expected to appear in the reflection measurements taken with polarization parallel to the optic axis. The reason for which the band is observed there at 70° incidence becomes obvious on considering the diagram in Fig. 1c. Although the electric vector is almost parallel to the Z axis at 20° incidence, it has a very large perpendicular component at 70° incidence.

A new vibration, parallel to the optic axis, appears at 780 cm^{-1}. A closer examination of the 780 and 800 cm^{-1} bands shows that the two vibrations are mutually perpendicular. A similar effect is observed with a Y-cut sample. This is demonstrated in Fig. 6, where reflecting powers measured at 780 and 800 cm^{-1} are plotted as a function of angle of rotation around the normal of the plate with respect to the direction of the electric vector in the incident radiation. It can be concluded from these observations that the 780 cm^{-1} vibration is parallel to the optic axis, whereas the 800 cm^{-1} vibration lies in a plane perpendicular to the optic axis.

The actual determination of the vibration frequencies was made from the plots of ϵ'' *vs* ν, which are presented in Fig. 7. The polarization properties of the bands at

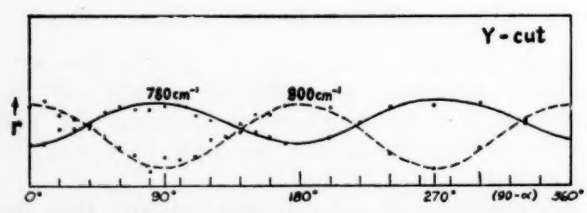

FIG. 6. Variation of the reflecting powers of the 780 cm^{-1} and 800 cm^{-1} bands in a Y-cut quartz plate rotated around its normal, in polarized radiation.

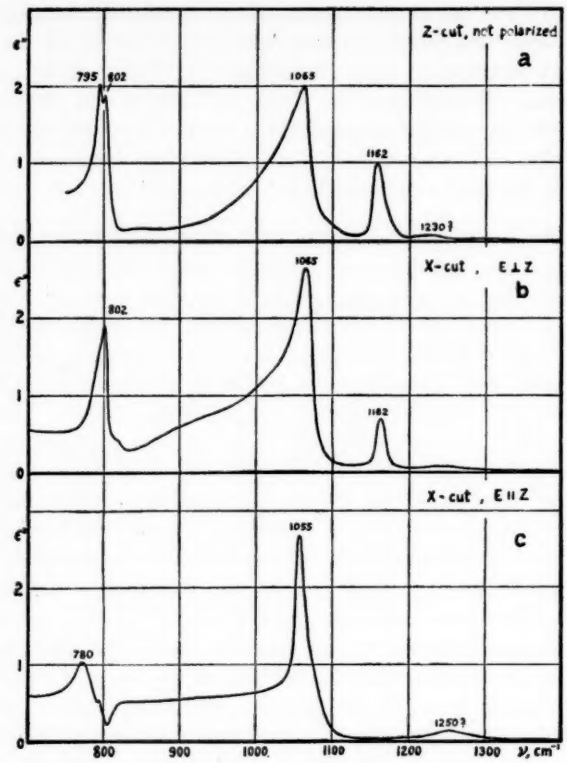

FIG. 7. Plots of the imaginary part of the complex dielectric constant, ϵ'', for Z- and Y-cut quartz plates. Cases a, b, c correspond to those of Fig. 1.

780, 800, and 1162 cm^{-1} as described above are clearly visible. The strong band at approximately 1060 cm^{-1} appears to have two components at 1055 and 1065 cm^{-1}. However, the evidence for their real existence is not quite conclusive because the resolving power of the

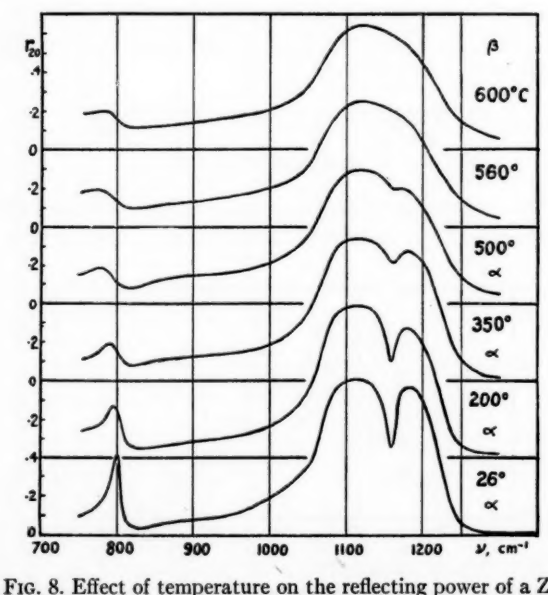

FIG. 8. Effect of temperature on the reflecting power of a Z-cut quartz plate (20° incidence, radiation not polarized). The $\alpha-\beta$ inversion, indicated by fracture of the plate, occurred somewhere between 560° and 580°C.

graphical method of evaluation of the reflection spectra is of the same order of magnitude as the observed difference.

3. β-Quartz, Z-Cut

Reflecting powers for a sample of quartz cut perpendicularly to the optic axis have been measured for a series of temperatures up to 600°C. The data obtained at 20° incidence are presented in Fig. 8. From a similar set of data taken at 70° incidence, the optical constants n, κ were obtained and finally the curves ϵ'' *vs* ν plotted (Fig. 9). In addition to the general broadening of the bands and shifts to lower frequencies, a gradual disappearance of the band at 1162 cm^{-1} is observed, beginning long before the transition temperature

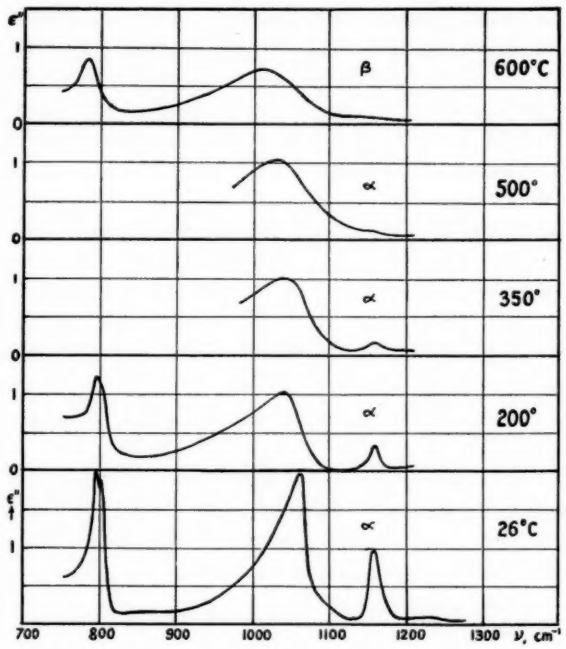

FIG. 9. Plots of ϵ'' for the same quartz plate as in Fig. 8 at elevated temperatures.

(575°C) is reached. No trace of the 1162 cm^{-1} vibration persists above 575°C.

4. α- and β-Cristobalite

The measured reflecting powers and the optical constants n, κ for the sample of oriented layer of α-cristobalite are presented in Fig. 10. The curves resemble those for quartz (Fig. 2) except for a conspicuous shift toward higher frequencies. This is clearly visible from the plots of ϵ'' *vs* ν in Fig. 11. The band at 800 cm^{-1} remains unchanged, the 1060 and 1162 cm^{-1} bands are shifted to 1085 and 1192 cm^{-1}. Although the unit cells of α-quartz and α-cristobalite are closely related and the average silicon-to-oxygen distances are very nearly the same,[9] there is obviously a difference in

[9] R. W. G. Wyckoff, *Crystal Structures* (Interscience Publishers, Inc., New York, 1951), Vol. 1, Chap. IV, pp. 25–29.

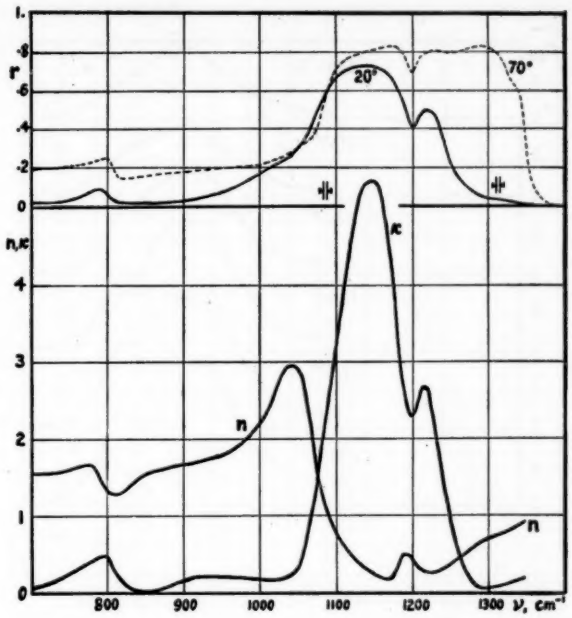

FIG. 10. Reflecting powers and optical constants of a layer of polycrystalline cristobalite formed on the surface of vitreous silica (radiation not polarized).

force constants determining the frequency of some of the strong bands.

The transition of α-cristobalite to the β-form was studied only by reflection at 20° incidence, without completing the analysis in terms of n, κ, and ϵ''. A behavior very similar to that of quartz is observed (Fig.

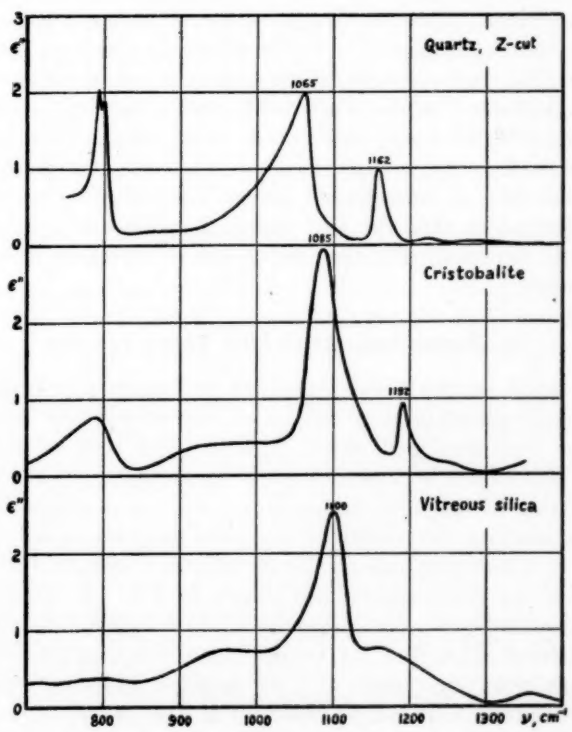

FIG. 11. Comparison of plots of ϵ'' *vs* ν for quartz, cristobalite and vitreous silica.

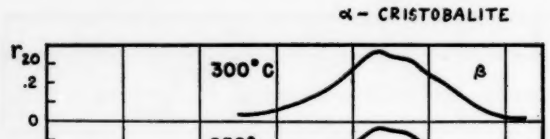

FIG. 12. Effect of temperature on the reflecting power of cristobalite (20° incidence, radiation not polarized).

12), namely, a gradual disappearance of the band at 1192 cm^{-1} and its complete absence in the β-form.

5. Vitreous Silica

The reflecting powers and optical constants n, κ for vitreous silica are shown in Fig. 13. The ϵ'' *vs* ν curve was already plotted in Fig. 11, together with corresponding curves for quartz and cristobalite. A comparison of these curves indicates that the force constants in vitreous silica are closer to those of cristobalite than to those of quartz. The bands at 800 cm^{-1} and at 1162 or 1192 cm^{-1} are very diffuse or absent, while the band at 1100 cm^{-1} is practically unchanged in intensity. The fact that the latter band persists even after destruction of the long-range order, indicates that it is caused by a vibration of immediately neighboring Si—O ions. In contrast to this, the two vanished bands are possible only in periodic lattices with well-developed long-range order.

6. Measurements at Low Temperatures

Most of the bands observed in quartz and other modifications of silica exhibit widths surprisingly large for well-developed single crystals. The part of this width, which is caused by the thermal agitation of the lattice at ordinary temperature, can be removed by performing the measurements with samples cooled to a very low temperature. Results of measurements of this kind on Z-cut quartz are shown in Fig. 14. Similar measurements were performed also on cristobalite and vitreous silica. At 4.2°K (temperature of boiling helium) only reflecting powers at a 20° angle of incidence were measured. As it can be observed in Fig. 14, the curves for the reflecting power at 20° incidence measured at 4.2°K and at 80°K are practically indistinguishable, indicating that there is no measurable decrease of the band width below approximately 80°K. Accordingly, it was felt that there is no need for measuring the reflecting powers at 70° incidence and performing the complete analysis in terms of n, κ, and ϵ'' for the lowest temperature (4.2°K).

In fact, it can be estimated theoretically on general grounds that the effect of thermal broadening becomes entirely negligible below a temperature equal to approximately one-fourth of the characteristic Debye temperature of the given solid. In quartz, the Debye temperature is of the order of 200°K. Therefore, at 80°K the effect of thermal agitation is largely removed, and the measured curves may be taken as a result of other remaining band-broadening effects. This is shown in Fig. 15 for the three modifications of silica at 80°K.

All bands appear considerably narrower, and the finite resolving power of the spectrometer (approximately 5 cm^{-1}) becomes definitely a limiting factor for the quite narrow bands, such as the 800 cm^{-1} doublet in quartz. Some of the observed changes in intensities of the bands, as compared with those of Fig. 11, may not be necessarily real because the graphical computing procedures become less accurate when the slopes of the curves become very steep. Comparing the widths of the strongest band in the three modifications of silica in Fig. 15, it can be observed that in quartz and cristobalite the widths are identical within the limits of experimental accuracy (approximately ± 5 cm^{-1}), while in vitreous silica the band width is only slightly larger (27 as compared with 22 cm^{-1}). Since on transition from the crystalline lattice to the random (vitreous) state, the band width increases only by 5 cm^{-1} (approx 20 percent), this vibration must be associated with a feature of the silica structure which persists even when the long-range order is destroyed.

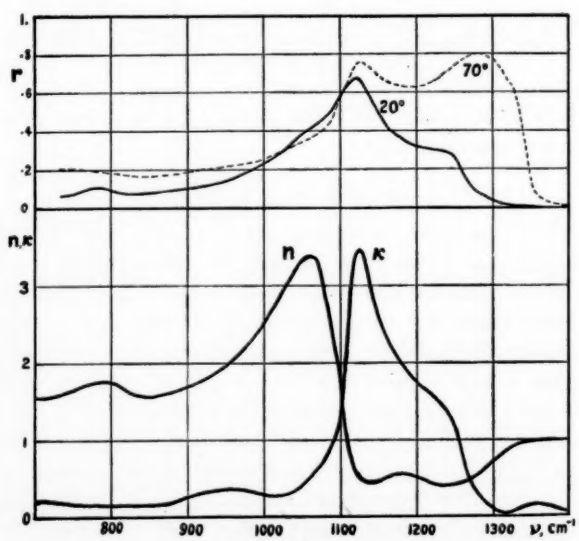

FIG. 13. Reflecting powers and optical constants of vitreous silica (radiation not polarized).

V. DISCUSSION OF THE RESULTS AND CONCLUSIONS

It is convenient to start the discussion of the infrared spectra of various forms of silicon dioxide with the case of α-quartz, for which the data are most complete, and comprehensive theoretical analyses are available.[1,3] The fundamental unit in quartz is a group of three silicons and six oxygens constituting one-half of the crystallographic unit cell. This group possesses sixteen fundamental vibrational modes which may be divided in three classes, A (Raman-active only), B (infrared-active only), and E (Raman- and infrared-active), as indicated in the three first columns of Table I. In the remaining columns are listed observed frequencies as assigned by several investigators. Obviously the assignment of the four Raman-active fundamentals, Class A, is established without dispute. This is not the case in Class B, where the assignments of different investigators vary, undoubtedly because of lack of consistent experimental data. Most of the infrared data on quartz were obtained by reflection, which, if not followed by a complete analysis in terms of optical constants, may lead to misleading interpretations. Although only infrared spectra were studied in the present work, the observed polarization properties enable us to extend the classification also to Class E.

In general, our assignments are in agreement with those of Saksena with the only exception that the frequency at 1149 cm^{-1} (assigned as Class B) is nonexistent, originating obviously from uncorrected reflection data. A correct frequency is observed at 1162 cm^{-1} (Fig. 7) in close coincidence with the Raman band observed at 1159 cm^{-1}. The Raman-activity and the polarization of this band places it now in Class E.

The band observed at 1065 cm^{-1} is both Raman- and infrared-active and has polarization properties (Fig. 7a, b) which place it in Class E, in agreement with Saksena. If the other band observed at 1055 cm^{-1} is real, which is not beyond doubt in view of the limitations mentioned in Sec. IV, 2, it would belong to the Class B, among the infrared active fundamentals. If, however, it is assumed that the 1055–1065 vibrations are actually a single band, its assignment to the Class E would violate the selection rules because it has a component polarized parallel to the optic axis (Fig. 7c). The band at 780 cm^{-1} belongs among the fundamentals of Class B, in agreement with the selection rules and having the required polarization. The band reported at 805 or 800 cm^{-1} cannot be counted in Class B (Krishnan,[2] Barriol[3]) because of its Raman activity (Saksena,[1] Narayanaswamy[10]).

The description of the vibration modes corresponding to the observed and classified bands is not quite satisfactory. None of the available theoretical analyses is performed in terms of actual normal modes. However, the results of Saksena and Barriol yield qualitative descriptions of the vibration modes which are useful for further discussion. In particular, the fundamental vibration of Class B, tentatively assigned by us to the frequency observed at 1055 cm^{-1}, is described as a valence vibration of the oxygen atom.

It is quite possible that a more satisfactory descrip-

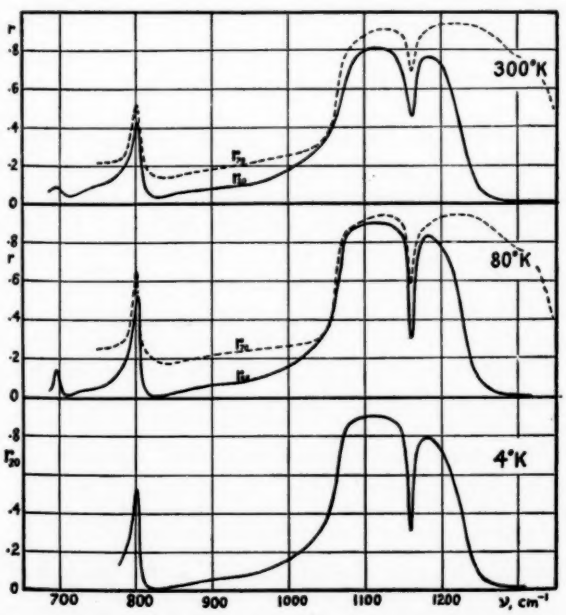

FIG. 14. Reflecting powers of a Z-cut quartz plate at temperatures of liquid oxygen and liquid helium.

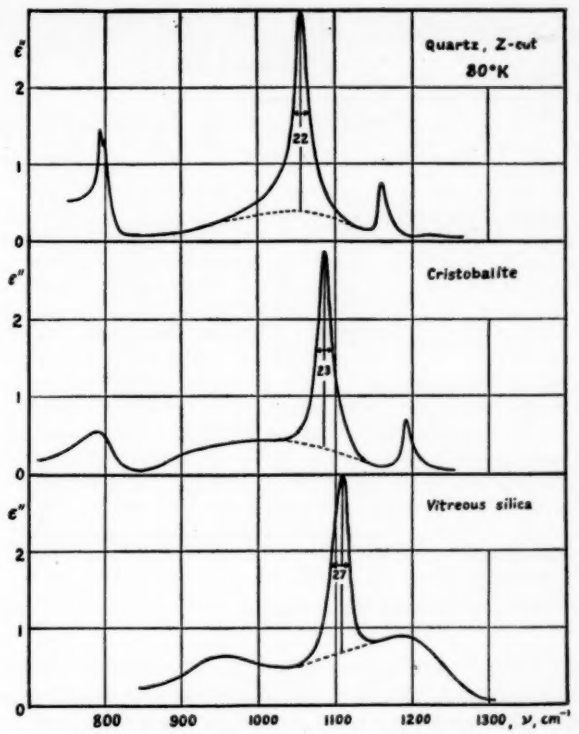

FIG. 15. Band width of the ϵ'' *vs* ν curves for quartz, cristobalite and vitreous silica at the temperature of liquid nitrogen. Compare with Fig. 11.

[10] P. K. Narayanaswamy, Proc. Indian Acad. Sci. A28, 417 (1948).

TABLE I. Classification of fundamental frequencies in α-quartz.

Class	Selection rules: Raman	Selection rules: Infrared	Fundamental frequencies: Saksena[a]	Fundamental frequencies: Krishnan[b]	Fundamental frequencies: Barriol[c]	Fundamental frequencies: This work
A	Permitted	Forbidden	207	207	207	...
			356	358	356	...
			466	467	466	...
			1082	1082	1082	...
B	Forbidden	Permitted, with no dipole $\perp Z$[d]	364	378	385	...
			508	480	488	...
			777	805	800	780
			1149 (approx.)	...	1190, 1227	(1055)
E	Permitted	Permitted, with no dipole $\parallel Z$[d]	128	127	127	...
			392–403	404	Type V 394	...
			695	696	696	695
			1159	1160	1163	1162
			265	267	268	...
			479	...	...	...
			795–807	794	Type VI 798	795–802
			1063	1065	...	1065
			...	1228	1248	...

[a] See reference 1.
[b] See reference 2.
[c] See reference 3.
[d] Z denotes the direction of the optic axis.

tion could be found, in which both bands would appear as two components of a doublet possessing an effective dipole inclined with respect to the optic axis as well as to the binary axes, presumably in a screw arrangement. At least this is strongly suggested by considering the three spectra in Fig. 7 and taking the 1055–1065 bands as one doublet. The fact that at least one of its components is observed in all three orientations would then be interpreted as a presence of a valence-stretching vibration with an effective dipole in a skew direction.

Let us discuss now the infrared spectra of β-quartz. Considering the spectra plotted in Fig. 9, the only major change observed on increasing the temperature is a gradual disappearance of the band at 1162 cm^{-1} and its final absence in the β-modification. A similar study of the $\alpha-\beta$ transition in the Raman spectra of quartz was undertaken by Narayanaswamy.[10] His results show that the Raman-active band observed at 1160 cm^{-1} is only slightly attenuated at elevated temperatures and persists also in the β-modification. The corresponding mode must be, therefore, of such a kind as to allow a gradual transition from the Class E in α-quartz to the Class A in β-quartz.

The same effect is observed also on transition from α- to β-cristobalite (Fig. 12), only at lower temperatures. There is, unfortunately, no theoretical analysis available of the vibration modes of the cristobalite lattice, and therefore we can limit ourselves only to drawing conclusions by analogy. A comparison of Fig. 10 with Figs. 2, 4, and 5 shows that the analogy with quartz is a very close one. In particular, it may be inferred fairly safely that the strongest band observed in α-cristobalite at approximately 1090 cm^{-1} corresponds to the valence-stretching vibration observed in α-quartz at 1055–1065 cm^{-1}. The same remains true of the 1100 cm^{-1} band observed in vitreous silica (Fig. 11).

Although the present results are adequate to the purpose of providing a necessary basis for further studies of silicate glasses[11] by means of the reflection method in the 10-micron region, it is realized that for a complete study of the spectra of silica, the wave number interval covered was too narrow, and that an extension of the measurements into the far infrared region would be highly desirable.

VI. ACKNOWLEDGMENTS

In conclusion, we wish to thank Mr. O. G. Burch, Director of Research of the Owens-Illinois Glass Company, for permission to publish this paper. The cooperation of the staff of the General Research Division, notably H. H. Holscher, C. L. Babcock, S. W. Barber, and L. F. Gleysteen, in preparing the samples and in many fruitful discussions, is greatly appreciated. Also, the discussions with Gilbert W. King and A. G. Emslie of Arthur D. Little, Inc., contributed to the elucidation of many aspects of the problem.

[11] Paper submitted for publication in the J. Am. Ceram. Soc.

THE JOURNAL OF CHEMICAL PHYSICS VOLUME 21, NUMBER 1 JANUARY, 1953

Quantitative Studies of Apparent Rotational Temperatures of OH in Emission and Absorption (Spectral Lines with Doppler Contour)*

S. S. PENNER
Guggenheim Jet Propulsion Center, California Institute of Technology, Pasadena, California
(Received July 28, 1952)

Even if a Boltzmann distribution exists for the population of molecules in various energy levels, it is not possible to obtain a satisfactory interpretation of experimental data by the use of conventional procedures unless the product of maximum spectral absorption coefficient P_{max} and optical density X is sufficiently small. Detailed calculations are presented which show that the experimental results, which suggest an anomalous rotational temperature for the $^2\Sigma$ state of OH in low pressure combustion flames, can be accounted for by using sufficiently large values for $P_{max}X$ (Sec. II). Whether or not experimental data should be interpreted in this manner must be determined by auxiliary studies.

Representative absorption studies for the determination of rotational temperatures in isothermal systems have been analyzed for the P_1 branch, (0,0) band, $^2\Pi \rightarrow {}^2\Sigma$ transitions of OH at 3000°K. The calculations show that erroneous interpretation of experimental results occurs if the product $P_{max}X$ is not small compared to unity. Sample calculations for a blackbody light source show that the customary procedure for treating experimental results will permit adequate correlation of the data by straight lines up to relatively large values for $P_{max}X$. It is remarkable that the preceding statement remains true even under conditions in which emission data clearly indicate that $P_{max}X$ is no longer small compared to unity (Sec. III).

Representative calculations to determine observable peak and total intensity ratios in emission for spectral lines with Doppler contour have been carried out for $^2\Sigma \rightarrow {}^2\Pi$ transitions, (0,0) band, P_1 branch of OH at 3000°K. The calculations show that the ratios of peak and total intensities are functions of the products of maximum absorption coefficients (P_{max}) and optical density (X) for the lines under study (Sec. IV).

Quantitative calculations have been carried out of apparent rotational temperatures in systems containing nonequilibrium distributions of OH at 3000°K and at 6000°K. The calculations on the P_1 branch, $^2\Sigma \rightarrow {}^2\Pi$ transitions, indicate that, in the absence of self-absorption, conventional plots showing discontinuities necessarily overestimate one and underestimate the other of the known temperatures of 3000°K and 6000°K (Sec. V).

Quantitative calculations on the nature of distortions produced when an isothermal region at 3000°K is viewed through an isothermal region at 1500°K show that the presence of a nonisothermal field of view magnifies the distortion produced by self-absorption alone (Sec. VI).

On the basis of the noncontroversial quantitative calculations described in Secs. II to VI for idealized systems, some speculations regarding the significance of reported flame temperature anomalies for OH are presented in Sec. VII.

I. INTRODUCTION

EXPERIMENTAL studies of population temperatures in flames have been reported, by different investigators, for the $^2\Sigma \rightarrow {}^2\Pi$ transitions of OH in flames at low pressures[1,2] and at atmospheric pressures.[1,3,4] When the experimental data are treated according to conventional techniques,[1,2,4] the plots that are used for the determination of rotational temperatures are sometimes found to exhibit discontinuities or curvatures both in the regions of small and of large values of the rotational energy $E(K)$ of the initial (upper) state. The "discontinuities" observed for small values of K have been variously attributed to the formation of OH in the excited electronic state by different chemical reactions leading to a bimodal distribution of population densities,[1,4] to falsification of experimental data by absorption of emitted radiation by cooler gas layers through which the flame is viewed,[5] and to self-absorption.[5] Some of the curvatures observed for large values of K have been interpreted[1] to indicate predissociation according to the process

$$OH(^2\Sigma^+) \rightarrow OH(^2\Sigma^-) \rightarrow O(^3P) + H(^2S).$$

In a previous publication[6] we have called attention to the fact that the best available intensity estimates[7] on OH indicate that the product of the maximum absorption coefficient P_{max} and of the optical density of the emitters X is not small compared to unity for the more intense spectral lines of OH in representative low pressure flames. In order to obtain reliable quantitative data upon which a rational interpretation of flame spectra can be based, we shall investigate theoretically, as an essential step in the interpretation of flame spectra, the radiation characteristics of various idealized systems both in emission and in absorption.

In Sec. II we examine quantitatively the effect of the size of $P_{max}X$ on apparent population temperatures in isothermal systems for emission experiments. This study leads us to the conclusion that most of the experimental data *could be* accounted for by a population temperature which is close to the adiabatic flame temperature. Thus, the quantitative calculations are in agreement with Dieke's remarks that the observed discontinuities or curvatures for small values of E_k *may be* the result of self-absorption. Furthermore, an apparent falling off in

* Supported by the ONR under Contract Nonr-220(03), NR 015 210.

[1] A. G. Gaydon and H. G. Wolfhard, Proc. Roy. Soc. (London) **A194**, 169 (1948); **A199**, 89 (1949); **A201**, 561 (1950); **A201**, 570 (1950); **A205**, 118 (1951); **A208**, 63 (1951).

[2] Penner, Gilbert, and Weber, J. Chem. Phys. **20**, 522 (1952). For a detailed description of the low pressure flame apparatus see M. Gilbert, "The Investigation of Low Pressure Flames," Report No. 4-54 (Jet Propulsion Laboratory, Pasadena, August 30, 1949).

[3] H. P. Broida and K. E. Shuler, J. Chem. Phys. **20**, 168 (1952).

[4] H. P. Broida, J. Chem. Phys. **19**, 1383 (1951).

[5] G. H. Dieke and H. M. Crosswhite, "The Ultraviolet Bands of OH," The Johns Hopkins University, Bumblebee Series Report No. 87, 1948.

[6] S. S. Penner, J. Chem. Phys. **20**, 507 (1952).

[7] R. J. Dwyer and O. Oldenberg, J. Chem. Phys. **12**, 351 (1944); O. Oldenberg and F. F. Rieke, J. Chem. Phys. **6**, 439 (1938).

intensity for large values of E_K also *could be* the result, in part, of falsification of experimental data by self-absorption.

In Sec. III we indicate briefly possible effects of large values of $P_{max}X$ on apparent population temperatures T_l' obtained in absorption experiments for spectral lines with Doppler contour. The results of calculations for $^2\Pi \rightarrow {}^2\Sigma$ transitions of OH and the (0,0) band show that the apparent population temperature is strongly dependent on the numerical value of $P_{max}X$ and relatively insensitive to the temperature of the light source, as long as the source is appreciably hotter than the flame.

In Sec. IV quantitative calculations are described on the influence of absolute values of spectral emissivities on the use of the isointensity methods.[5,8] Representative calculations have been carried out for $^2\Sigma \rightarrow {}^2\Pi$ transitions of OH at 3000°K for the (0,0) band and the P_1 branch. The results of the present analysis show that temperature anomalies, obtained by use of the isointensity method, *could be* the result of failure to allow for the effect of values of the spectral emissivity on the peak and total intensities of spectral lines with Doppler contour.

In Sec. V the radiation characteristics of a nonequilibrium mixture of OH are investigated in terms of conventional and isointensity methods for the interpretation of emission experiments. These calculations show that even for systems without self-absorption the interpretation of experimental data is not unambiguous as long as conventional plots show any deviations from linearity. Furthermore, at least for the P_1 branch, linear isointensity plots of the Shuler type are no assurance for thermal equilibrium of the emitter.

In Sec. VI a simplified model is used to study the simultaneous distortion of experimental data by the combined effects of self-absorption and temperature gradients. These studies show that observation of a hot isothermal region through a cooler gas layer accentuates the distortion produced in conventional plots for the interpretation of emission data.

The material presented in Secs. II to VI rests on accepted procedures for the analysis of radiating systems and spectral lines with Doppler contour. The results obtained are not applicable to real flames without conjectures. However, on the basis of the quantitative studies described in Secs. II to VI, some words of caution regarding the acceptance of anomalous population temperatures for OH appear to be justified (Sec. VII).

II. THE EFFECT OF SELF-ABSORPTION ON APPARENT POPULATION TEMPERATURES IN EMISSION EXPERIMENTS

The effect of instrumental distortion on experimental data will be neglected in the present discussion. For the sake of simplicity, a complete analysis will be carried out only for studies involving peak intensities. It is shown in Appendix I that the results obtained for total intensities, for representative calculations, are similar to those obtained for peak intensities.† Hence, the applicability of the principal conclusions reached in the following discussion depends only on the experimental determination of valid relative peak or integrated intensities for different spectral lines.

A. Equations for the Determination of Apparent Population Temperatures

For spectral lines with Doppler contour the maximum observable intensity in emission I_{max} is given by the relation

$$I_{max}=R^0(\nu_{lu})[1-\exp(-P_{max}X)], \quad (1)$$

where $R^0(\nu_{lu})$ denotes the intensity of radiation emitted by a blackbody, which is at the same temperature T_u as the gaseous emitters under study, and X is the optical density of the emitter. The frequency ν_{lu} is obtained from the values of the upper (E_u) and lower (E_l) energy levels by use of the Bohr frequency relation. For spectral lines with Doppler contour it is well known that

$$P_{max}=S_{lu}(mc^2/2\pi kT_t\nu_{lu}^2)^{\frac{1}{2}},$$

where S_{lu} is the integrated intensity for the transition under study, m equals the mass of the radiator, c is the velocity of light, k represents the Boltzmann constant, and T_t is the translational temperature.[6] Let

$$\epsilon'=I_{max}/R^0(\nu_{lu}) \quad (2)$$

and $x=-P_{max}X$, whence it follows that $-\epsilon'=\exp(x)-1$. It is evident that ϵ' represents the maximum value of the spectral emissivity for the emitted spectral lines.‡ If the population temperature of the emitter is defined in the usual way, then $\epsilon' \leqslant 1$.

For very small values of ϵ' the well-known result $-x=\epsilon'$ is obtained. From an appropriate expression for S_{lu} it is readily shown that[6]

$$\frac{\partial \ln[I_{max}/(\nu_{lu})^3 g_u(q_{lu})^2]}{\partial E_u}=-\frac{1}{kT_u} \text{ for } \epsilon' \ll 1, \quad (3)$$

where g_u is the statistical weight of the upper (initial) energy state, q_{lu} is the matrix element for the transition under study, and T_u is the apparent temperature of the upper state involved in the given transition.

If ϵ' is not small compared to unity then it is no longer possible to obtain the value of T_u in a simple manner unless numerical values of ϵ' are available.

[8] K. E. Shuler, J. Chem. Phys. 18, 1466 (1950).

† In general, peak intensity ratios are obtained if the instrumental slit width is small compared to the line width, whereas total intensity ratios are measured when the instrumental slit width is large compared to the line width.

‡ Representative values of $\epsilon'(1)$ for low pressure flames lie between 0.3 and 0.90. In order to utilize the data given in Table II of reference 6 for the calculation of $\epsilon'(1)$, care must be taken to use for X the optical density of emitter in the ground level involved in a given transition.

B. A Method for Demonstrating the Effect of Self-Absorption on Apparent Population Temperatures of OH ($^2\Sigma \rightarrow {}^2\Pi$ Transitions)

We proceed now to examine quantitatively the effect of the absolute values of ϵ' on apparent population temperatures determined according to Eq. (3).

Plots of $\log[I_{\max}/(\nu_{lu})^3 g_u(q_{lu})^2]$ as a function of E_u can be constructed for various assumed values of ϵ' by proceeding according to the scheme outlined below.

(1) Assume a value of ϵ', for example, for the P_1 branch, (0,0) band, for the transition identified by the index $K=1$, using the notation of Dieke and Crosswhite.[5] It is then evident from Eqs. (1) and (2) that

$$(P_{\max}X)_{K=1} = -2.303 \log[1-\epsilon'(K=1)]. \quad (4)$$

(2) Calculate the ratio $S_{lu}(K)/S_{lu}(K=1)$ from the expression

$$\frac{S_{lu}(K)}{S_{lu}(K=1)} = \frac{g_u(K)[q_{lu}(K)^2]}{g_u(K=1)[q_{lu}(K=1)^2]} \frac{\nu_{lu}(K)}{\nu_{lu}(K=1)} \times\{\exp-[E_u(K)-E_u(K=1)]/kT\} \times\{\exp[h\nu_{lu}(K)/kT]-1\} \times\{\exp[h\nu_{lu}(K=1)/kT]-1\}^{-1}. \quad (5)$$

The first fraction appearing on the right-hand side of Eq. (5) is given by results obtained by Hill and Van Vleck[9] as written in convenient form by Earls[10] and tabulated by Dieke and Crosswhite.[5] The quantities $\nu_{lu}(K)$ and $E_u(K)$ have also been tabulated.[5]

(3) Determine $(P_{\max}X)_K$ from the relation

$$(P_{\max}X)_K = (P_{\max}X)_{K-1} \cdot \frac{S_{lu}(K)}{S_{lu}(K=1)} \cdot \frac{\nu_{lu}(K=1)}{\nu_{lu}(K)}, \quad (6)$$

and evaluate

$$\epsilon'(K) = 1-\exp-(P_{\max}X)_K. \quad (7)$$

(4) Calculate

$$(I_{\max})_K = \epsilon'(K)[R^0(\nu_{lu})]_K. \quad (8)$$

TABLE I. Apparent population temperatures T_u' obtained from lines with $10 \leqslant K \leqslant 18$ for the P_1 branch, (0,0) band, and $^2\Sigma \rightarrow {}^2\Pi$ transitions of OH at 3000°K, as a function of assumed values of $\epsilon'(1)$.[a]

$\epsilon'(1)$	T_u', °K
0.1	3 000
0.3	~3 200
0.5	~3 500
0.7	~5 000
0.9	~6 500
0.95	~10 000
0.999	~19 000

[a] For representative flames: $0.3 \leqslant \epsilon'(1) \leqslant 0.90$.

[9] E. Hill and J. H. Van Vleck, Phys. Rev. 32, 250 (1928).
[10] L. T. Earls, Phys. Rev. 48, 423 (1935).

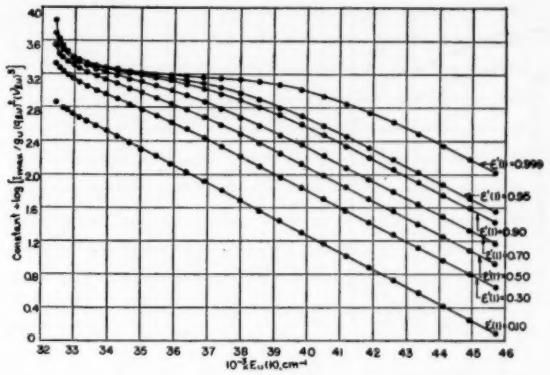

FIG. 1. Conventional plots for the determination of rotational temperatures of OH in emission for various assumed values of $\epsilon'(1)$ for the P_1 branch, $^2\Sigma \rightarrow {}^2\Pi$ transitions, (0,0) band, $T=3000$°K.

(5) Finally calculate $\log(I_{\max})_K - \log\{g_u(K)[q_{lu}(K)]^2 \times[\nu_{lu}(K)]^3\}$, and plot this quantity as a function of $E_u(K)$. From the slope of this plot determine the apparent population temperature T_u' in the usual way by applying Eq. (3).

The results of calculations carried out according to the scheme outlined above are summarized in Fig. 1 for the P_1 branch for various assumed values of $\epsilon'(1)$.

C. Discussion of Results

Analysis of the data listed in Fig. 1 leads to the conclusions enumerated below.

(1) For sufficiently small values of $\epsilon'(1)$, the apparent and true values of the population temperatures are identical since Eq. (3) applies in good approximation. This result is, of course, well known.

(2) As the value of $\epsilon'(1)$ is increased, the plots constructed according to Eq. (3) show increasing curvature for the more intense rotational lines until for $\epsilon'(1)=0.5$ and greater the constructed curves simulate population temperatures which are of the same order of magnitude as the anomalous values reported for flames. It is easy to see how a limited number of experimental points between $K=3$ and $K=20$ *could be* correlated by two intersecting straight lines. Apparent population temperatures T_u' obtained for lines with $10 \leqslant K \leqslant 18$ for the P_1 branch, (0,0) band, and $^2\Sigma \rightarrow {}^2\Pi$ transitions of OH at 3000°K are listed in Table I as a function of the assumed value of $\epsilon'(1)$.

(3) For sufficiently large values of K, all of the curves become parallel independently of the assumed values of $\epsilon'(1)$. Thus, all of the experimental data yield apparent population temperatures which are in agreement with the true value of the population temperature. Hence, by extending experimental studies to sufficiently large values of K, it is always possible to obtain unambiguous estimates of the true population temperature.

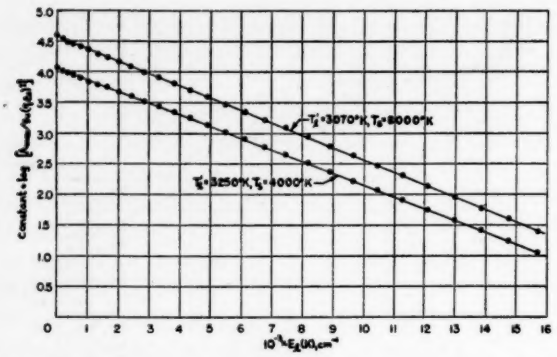

FIG. 2. Conventional plots for the determination of apparent population temperatures T_l' of the ground electronic state from absorption experiments for different temperatures of the light source T_S[$^2\Pi \rightarrow {}^2\Sigma$ transitions of OH, (0,0) band, P_1 branch, $T=3000°K$, $\alpha'(1)=0.10$; the ordinate for the plot at $T_S=8000°K$ has been reduced by 2.00 relative to the plot for $T_S=4000°K$].

III. THE EFFECT OF SELF-ABSORPTION ON APPARENT POPULATION TEMPERATURES IN ABSORPTION EXPERIMENTS

At thermodynamic equilibrium the spectral emissivities and absorptivities arising from a given transition are identical. Hence, it is to be expected that falsification of experimental data in absorption experiments needs to be considered whenever self-absorption is known to be of importance in emission. The following analysis is restricted to the use of peak intensities for the calculation of population temperatures.§ Instrumental distortion will be neglected as in Sec. II.

A. Equations for the Determination of Apparent Population Temperatures

In an absorption experiment with a source which is much brighter than the emission lines and which emits the spectral radiant intensity $R_S(\nu)$, the maximum value of the fractional absorbed intensity, $\alpha'=A_{\max}/R_S(\nu_{lu})$, is given by the expression

$$\alpha'=1-\exp(-P_{\max}X), \tag{9}$$

and

$$-x=\alpha'[1+\tfrac{1}{2}\alpha'+(1/3)(\alpha')^2+(1/4)(\alpha')^3+\cdots]. \tag{10}$$

For $\alpha'\ll 1$, Eq. (10) reduces to the expression $-x=\alpha'$, where[6]

$$S_{lu}X\simeq(8\pi^3N/3hcQ)\nu_{lu}g_u q_{lu}{}^2[\exp(-E_l/kT_l)]. \tag{11}$$

Here T_l is the population temperature of the ground (initial) state in an absorption experiment. From Eq. (11) it is readily shown[6] that for graybody emitters, with the effective temperature of the source, T_S, large compared to T_l,

$$\frac{\partial \ln[A_{\max}/g_u q_{lu}{}^2]}{\partial E_l}=-\frac{1}{kT_l}. \tag{12}$$

It is evident that T_l can, in general, be determined only if absolute values of α' are known.

§ The use of apparent total absorption measurements is discussed briefly in Appendix II.

B. A Method for Demonstrating the Effect of Self-Absorption on Apparent Population Temperatures of OH ($^2\Pi \rightarrow {}^2\Sigma$ Transitions)

We proceed to examine quantitatively the effect of absolute values of α' on apparent population temperatures determined according to Eq. (12). Plots of $\log[A_{\max}/g_u(q_{lu})^2]$ as a function of E_l can be constructed by using the following scheme.

(1) Assume a value of α', for example, for the P_1 branch, (0,0) band, for the transition identified by the index $K=1$, using the notation of Dieke and Crosswhite.[5] Next calculate $\alpha'(K)$ by using the same procedure as was used to obtain the maximum values of the spectral emissivity for the line with index K (see Sec. II).

(2) Calculate

$$A_{\max}=\alpha'(K)R_S(\nu_{lu}), \tag{13}$$

assuming a blackbody distribution curve for the source

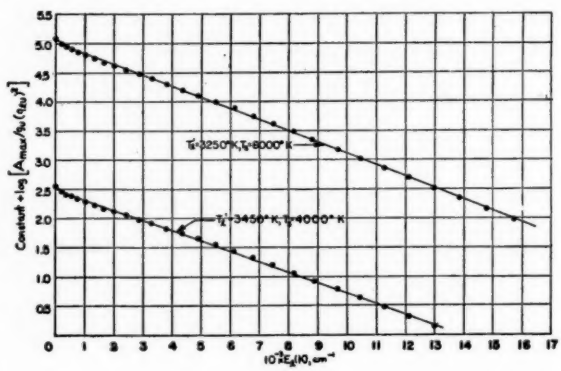

FIG. 3. Conventional plots for the determination of apparent population temperatures T_l' of the ground electronic state from absorption experiments for different temperatures of the light source T_S[$^2\Pi \rightarrow {}^2\Sigma$ transitions of OH, (0,0) band, P_1 branch, $T=3000°K$, $\alpha'(1)=0.30$].

at the temperature T_S.

(3) Calculate

$$\log\{(A_{\max})_K/g_u(K)[q_{lu}(K)]^2\}$$

and plot this quantity as a function of $E_l(K)$. From the slope of this plot determine the apparent population temperature T_l' in the usual way by applying Eq. (12).

The results of calculations carried out according to the scheme outlined above are summarized in Figs. 2–5 for $\alpha'(K=1)$ of P_1 branch=0.1, 0.3, 0.7, and 0.9, respectively, for two or more values of the source temperature T_S. Apparent population temperatures for the relevant assumed conditions are indicated in Figs. 2–5.

C. Discussion of Results

Analysis of the data presented in Figs. 2–5 leads to the conclusions enumerated below.

(1) Experimental data treated according to conventional procedures permit correlation of results by

linear plots even for values of $\alpha'(K=1)$ of the P_1 branch which are so large that T_l' differs appreciably from T_l. Hence, absolute values obtained for T_l' cannot be considered to be meaningful without convincing proof that $P_{\max}X$ is sufficiently small for the spectral lines under study to justify conventional treatment of data.

(2) Apparent population temperatures T_l' are always larger than T_l. The difference between T_l' and T_l decreases somewhat as the temperature of the light source is increased for fixed values of $P_{\max}X$. However, the apparent temperatures are relatively insensitive to the numerical values of T_S, decreasing by only a few hundred degrees as T_S is raised from 3500°K to 8000°K.

(3) For sufficiently large values of $\alpha'(K=1)$ for the P_1 branch, discontinuities or curvatures are observed in the conventional plots which are reminiscent of the results obtained in emission experiments (Sec. II).

Adequate care in the interpretation of absorption studies, as well as of emission studies, permits the determination of both the true rotational temperature and of the concentration of the absorbing or emitting species,

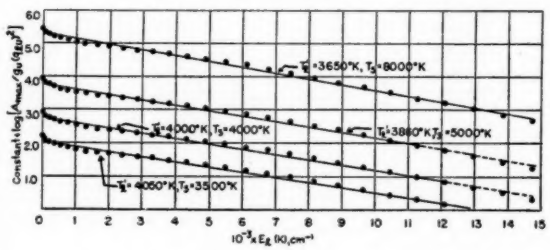

FIG. 4. Conventional plots for the determination of apparent population temperatures T_l' of the ground electronic state from absorption experiments for different temperatures of the light source $T_S[^2\Pi\rightarrow{}^2\Sigma$ transitions of OH, (0,0) band, P_1 branch, $T=3000°K$, $\alpha'(1)=0.70]$.

provided the population of molecules in the rotational energy levels obeys the Maxwell-Boltzmann distribution law. Thus data on spectral lines with large K can be used to obtain T_l. Next, a family of curves for the known values of T_l and T_S, is constructed, for example, for different values of $\alpha'(K=1)$ for the P_1 branch (compare Figs. 2–5). The data obtained by using Eq. (12) for the lower values of K can then be employed to determine $\alpha'(K=1)$, whence the optical density X is determined since S_{lu} is known.[7]

IV. THE EFFECT OF SELF-ABSORPTION ON THE USE OF ISOINTENSITY METHODS

Serious attempts to correct for the distortion of experimental data produced by self-absorption have been made by Dieke[5] and his collaborators and also by Shuler.[8] The limitations of the isointensity method and the care required in its use have been clearly stated by Dieke and Crosswhite.[5] The quantitative calculations presented here emphasize the fact that it is easy to

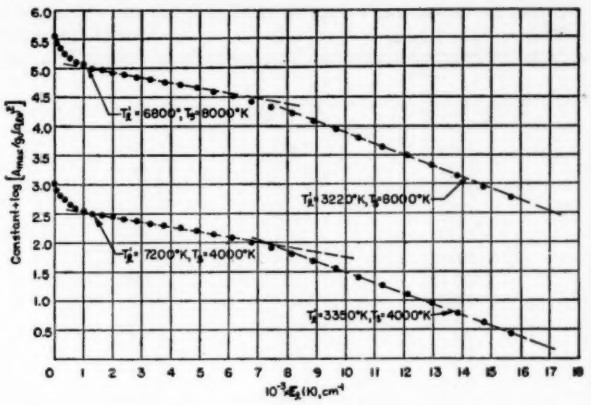

FIG. 5. Conventional plots for the determination of apparent population temperatures T_l' of the ground electronic state from absorption experiments for different temperatures of the light source $T_S[^2\Pi\rightarrow{}^2\Sigma$ transitions of OH, (0,0) band, P_1 branch, $T=3000°K$, $\alpha'(1)=0.90]$.

obtain erroneous results if isointensity methods are used for the P_1 branch. It is clear that the errors will be smaller but not negligible if the isointensity methods are used for the R_2 branch, as originally proposed by Dieke and Crosswhite.[5]

A. Outline of Calculations

Two spectral lines, which are differentiated by the indices K and K', appear to have equal peak intensities $I_{\max}$ in an emission experiment, if

$$I_{\max}(K)=I_{\max}(K'), \tag{14}$$

where $I_{\max}$ is given by Eq. (1). For various assumed values of $\epsilon'(K=1)$ of the P_1 branch at 3000°K, it is a simple matter to calculate the ratios $I_{\max}(K)/I_{\max}(K=1)$ by following the procedure described in Sec. II. The results of these calculations are summarized in Table II, and representative values are plotted in Fig. 6.

The spectral lines, which are identified by the indices K and K', appear to have equal total intensities in emission if

$$A(K)=A(K'), \tag{15}$$

where

$$A(K)=[R\nu_{lu}{}^0(mc^2/2\pi kT_l)^{-\frac{1}{2}}\nu_{lu}(K)][P_{\max}(K)X]$$
$$\times\sum_{n=0}^{\infty}[(n+1)^{\frac{1}{2}}(n+1)!]^{-1}[-P_{\max}(K)X]^n. \tag{16}$$

By proceeding according to the method described in Appendix I, it is readily shown that

$$A(K)/A(K')=[I_{\max}(K)/I_{\max}(K')]$$
$$\times[\nu_{lu}(K)/\nu_{lu}(K')][\xi(K')/\xi(K)]. \tag{17}$$

Representative numerical values of $A(K)/A(K')$ are listed in Table III and plotted in Fig. 7 for $^2\Sigma\rightarrow{}^2\Pi$ transitions of OH at 3000°K for the (0,0) band and the P_1 branch.

TABLE II. Numerical values of $S_{lu}(K)/S_{lu}(1)$ and of $I_{max}(K)/I_{max}(1)$ as a function of $\epsilon'(K=1)$ for the P_1 branch, (0,0) band, $^2\Sigma \rightarrow {}^2\Pi$ transitions of OH at 3000°K.

		$I_{max}(K)/I_{max}(1)$ for						
K	$S_{lu}(K)/S_{lu}(1)$	$\epsilon'(1)=0.1$	$\epsilon'(1)=0.3$	$\epsilon'(1)=0.5$	$\epsilon'(1)=0.7$	$\epsilon'(1)=0.9$	$\epsilon'(1)=0.95$	$\epsilon'(1)=0.99$
1	1.00	1.00	1.00	1.00	1.00	1.00	1.00	1.00
2	1.29	1.30	1.26	1.21	1.15	1.08	1.05	1.03
3	1.59	1.60	1.50	1.39	1.27	1.13	1.08	1.05
4	1.83	1.86	1.70	1.53	1.35	1.16	1.11	1.07
5	2.00	2.05	1.85	1.63	1.41	1.19	1.14	1.09
6	2.09	2.18	1.95	1.70	1.45	1.22	1.16	1.11
7	2.11[a]	2.25[a]	2.00	1.74	1.49	1.25	1.19	1.14
8	2.05	2.25[a]	2.02[a]	1.77[a]	1.52	1.27	1.22	1.17
9	1.94	2.20	1.99	1.77[a]	1.53	1.30	1.24	1.19
10	1.79	2.09	1.93	1.74	1.54[a]	1.33	1.27	1.22
11	1.61	1.94	1.84	1.69	1.53	1.35	1.30	1.26
12	1.41	1.77	1.72	1.62	1.51	1.37	1.33	1.29
13	1.21	1.58	1.57	1.52	1.46	1.38[a]	1.35	1.32
14	1.02	1.38	1.41	1.40	1.39	1.37	1.37[a]	1.36
15	0.842	1.19	1.24	1.26	1.29	1.34	1.36	1.38
16	0.681	1.00	1.06	1.11	1.17	1.28	1.33	1.40[a]
17	0.541	0.824	0.896	0.956	1.04	1.20	1.27	1.39
18	0.421	0.664	0.740	0.804	0.899	1.08	1.18	1.34
19	0.323	0.534	0.600	0.662	0.757	0.954	1.06	1.26
20	0.244	0.419	0.477	0.533	0.621	0.812	0.926	1.15
21	0.181	0.323	0.373	0.421	0.498	0.672	0.780	1.00
22	0.132	0.246	0.286	0.326	0.391	0.540	0.637	0.847
23	0.0954	0.185	0.217	0.249	0.301	0.424	0.506	0.690
24	0.0678	0.137	0.162	0.186	0.227	0.325	0.391	0.545
25	0.0475	0.1004	0.119	0.138	0.169	0.244	0.296	0.419
26	0.0328	0.0723	0.0868	0.100	0.123	0.180	0.219	0.314
27	0.0224	0.0517	0.0618	0.0721	0.0889	0.131	0.160	0.231
28	0.0151	0.0364	0.0442	0.0511	0.0632	0.0933	0.115	0.166
29	0.0101	0.0257	0.0312	0.0359	0.0447	0.0623	0.0814	0.119
30	0.0067	0.0177	0.0219	0.0252	0.0312	0.0462	0.0568	0.0831

[a] Maximum intensity ratios.

B. Discussion of Results

Reference to the data listed in Tables II and III and plotted in Figs. 6 and 7 shows that the ratios $I_{max}(K)/I_{max}(K')$ and $A(K)/A(K')$ are functions of the values of

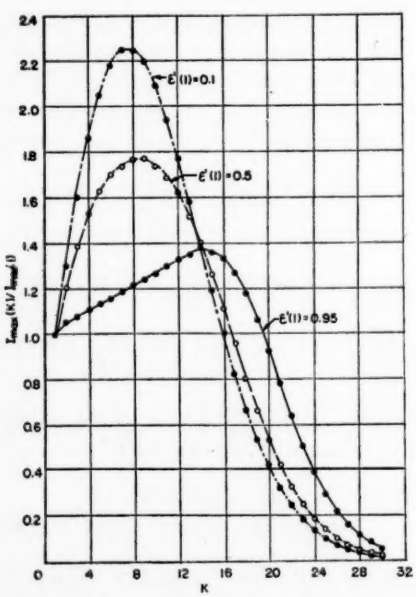

FIG. 6. The ratio $I_{max}(K)/I_{max}(1)$ as a function of K for the P_1 branch, (0,0) band, $^2\Sigma \rightarrow {}^2\Pi$ transitions of OH at 3000°K for different values of $\epsilon'(1)$.

TABLE III. Representative numerical values of $A(K)/A(1)$ as a function of $\epsilon'(K=1)$ for the P_1 branch, (0,0) band, $^2\Sigma \rightarrow {}^2\Pi$ transitions of OH at 3000°K.

	$A(K)/A(1)$ for			
K	$\epsilon'(1)=0.1$	$\epsilon'(1)=0.5$	$\epsilon'(1)=0.9$	$\epsilon'(1)=0.95$
1	1.00	1.00	1.00	1.00
2	1.31	1.24	1.15	1.11
3	1.61	1.47	1.25	1.20
4	1.88	1.64	1.34	1.27
5	2.07	1.77	1.39	1.32
6	2.21	1.86	1.43	1.36
7	2.27	1.90	1.47	1.39
8	2.26	1.91	1.49	1.41
9	2.20	1.90	1.50	1.43
10	2.08	1.84	1.51	1.43
11	1.93	1.76	1.50	1.43
12	1.75	1.65	1.47	1.42
13	1.55	1.52	1.42	1.39
14	1.35	1.37	1.35	1.35
15	1.15	1.21	1.27	1.28
16	0.968	1.05	1.16	1.19
17	0.793	0.888	1.04	1.08
18	0.636	0.736	0.902	0.959
19	0.509	0.599	0.772	0.828
20	0.397	0.477	0.635	0.696
21	0.305	0.373	0.515	0.569
22	0.232	0.286	0.405	0.454
23	0.173	0.217	0.313	0.352
24	0.128	0.161	0.237	0.269
25	0.0935	0.119	0.176	0.201
26	0.0671	0.0859	0.129	0.147
27	0.0478	0.0615	0.0927	0.107
28	0.0335	0.0433	0.0657	0.0757
29	0.0236	0.0304	0.0463	0.0536
30	0.0161	0.0212	0.0321	0.0372

$\epsilon'(K=1)$ for the P_1 branch, the dependence on $\epsilon'(K=1)$ becoming stronger as $\epsilon'(K=1)$ approaches unity, i.e., as the extent of self-absorption increases. This observation is emphasized by noting, for example, that the line having absolute peak intensity closest to the line with $K=3$, has $K=13$ for $\epsilon'(1)=0.1$, $K=13$ for $\epsilon'(1)=0.3$, $K=14$ for $\epsilon'(1)=0.5$, $K=15$ for $\epsilon'(1)=0.7$, $K=18$ for $\epsilon'(1)=0.9$, $K=19$ for $\epsilon'(1)=0.95$, and $K=21$ for $\epsilon'(1)=0.99$. Comparison of the data given in Tables II and III and plotted in Figs. 6 and 7, respectively, also shows that the effect of self-absorption in falsifying the data obtained by use of the isointensity method is more pronounced for peak emitted intensities than for total intensities.

The effect of self-absorption on population temperatures determined from the isointensity method can be demonstrated graphically by using the procedure de-

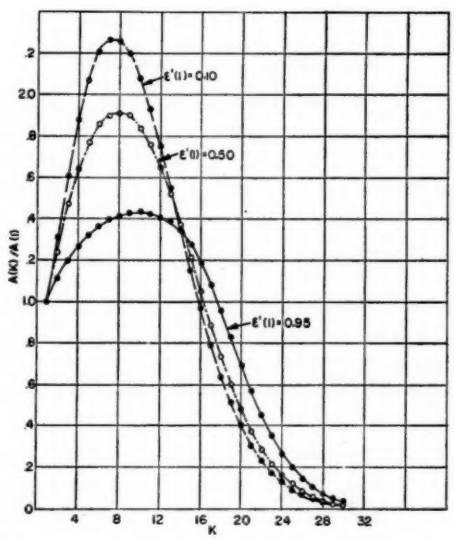

FIG. 7. The ratio $A(K)/A(1)$ as a function of K for the P_1 branch, (0,0) band, $^2\Sigma \rightarrow {}^2\Pi$ transitions of OH at 3000°K for different values of $\epsilon'(1)$.

veloped by Shuler[8] whose method is equivalent to the assumption that total intensity ratios $A(K)/A(K')$ can be replaced by the product of transition probability ratios $g_u(K)[q_{lu}(K)]^2/g_u(K')[q_{lu}(K')]^2$ and appropriate exponential factors for spectral lines which are close together. Plots of $E(K)-E(K')$ *vs* $\log\{g_u(K)[q_{lu}(K)]^2/g_u(K')[q_{lu}(K')]^2\}$ are shown in Fig. 8 as a function of $\epsilon'(1)$ for pairs of spectral lines for which $I_{\max}(K)/I_{\max}(K')$ is nearly equal to unity. Similarly, plots of $E(K)-E(K')$ *vs* $\log\{g_u(K)[q_{lu}(K)]^2/g_u(K')[q_{lu}(K')]^2\}$ are shown in Fig. 9 as a function of $\epsilon'(1)$ for pairs of spectral lines for which $A(K)/A(K')$ is nearly equal to unity.

Reference to Figs. 8 and 9 shows that the plots deviate progressively more from straight lines as $\epsilon'(1)$ is increased. Apparent population temperatures T_u' are noted on the curves given in Figs. 8 and 9. The results are seen to be an immediate consequence of the de-

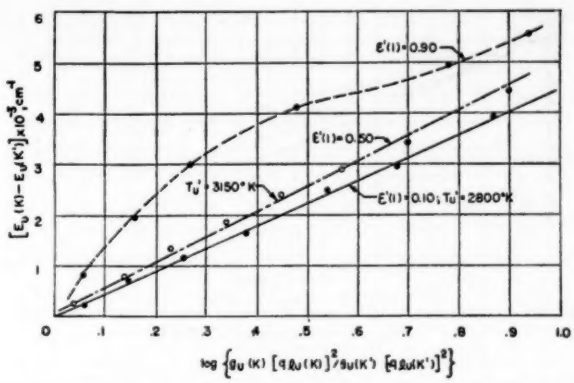

FIG. 8. Plot of $[E_u(K)-E_u(K')]$ *vs* $\log\{g_u(K)[q_{lu}(K)]^2/g_u(K')\times[q_{lu}(K')]^2\}$ for lines with equal peak intensities at 3000°K as a function of $\epsilon'(1)$ for the P_1 branch, (0,0) band, $^2\Sigma \rightarrow {}^2\Pi$ transitions of OH.

pendence of the K values for lines with equal peak or total intensities on $\epsilon'(1)$. Hence, the conclusion is reached that the effects of self-absorption in distorting experimental data do not necessarily cancel in first order for the isointensity methods. A simple physical explanation for failure of the isointensity methods at large values of the spectral emissivity is obtained by noting that the quantities $R^0(\nu_{lu})$ influence the observable intensities and that $R^0(\nu_{lu})$, which is a function of temperature, is not the same for any distinguishable pair of spectral lines. Furthermore, equally intense spectral lines, for which $S_{lu}(K)=S_{lu}(K')$, have slightly different widths since the Doppler width is proportional to the frequency of the line center. Thus, the obvious conclusion is reached that the effects of self-absorption will cancel exactly only for equally intense spectral lines with line centers occurring at identical frequencies.

V. ERRORS IN CONVENTIONAL PROCEDURES FOR ISOTHERMAL SYSTEMS IN THE ABSENCE OF SELF-ABSORPTION

Whereas the effect of self-absorption in producing distortion of emission data has been amply discussed, relatively little analytical work has been done on the meaning of discontinuous curves *for a mixture of*

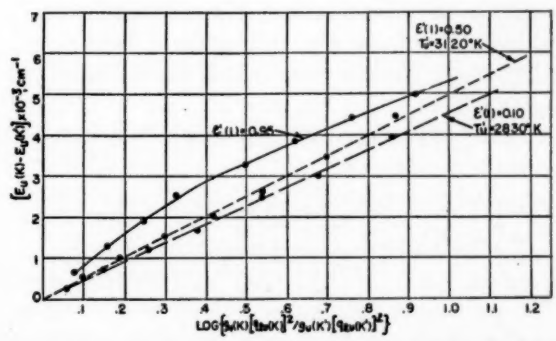

FIG. 9. Plot of $[E_u(K)-E_u(K')]$ *vs* $\log\{g_u(K)[q_{lu}(K)]^2/g_u(K')\times[q_{lu}(K')]^2\}$ for lines with equal total intensities at 3000°K as a function of $\epsilon'(1)$ for the P_1 branch, (0,0) band, $^2\Sigma \rightarrow {}^2\Pi$ transitions of OH.

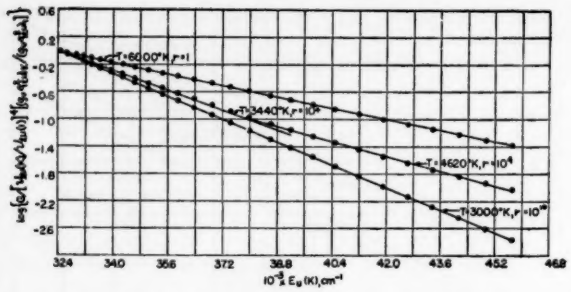

FIG. 10. Conventional plots and apparent temperatures for various bimodal distributions of OH.

isothermal systems in the absence of self-absorption. Although the methods of calculation that we employ are well-known and the conclusions to which they lead are almost obvious, it is somewhat surprising to note that errors in interpretation can be made even for the often-postulated nonequilibrium distribution of OH. Aside from emphasizing the need for care in dealing with anything other than a linear plot, the present analysis also serves to give examples of linear isointensity plots of the Shuler type[8] for the P_1 branch with meaningless temperatures for a nonequilibrium distribution of OH. Whether or not the R_2 branch is quite as bad can be said with assurance only after quantitative calculations have been carried out; however, we expect the errors to be less pronounced. In this connection reference should be made also to the discussion of the isointensity method given by Dieke and Crosswhite,[5] who indicate very clearly under what conditions the method is usable.

A. Outline of Theory

For a nonequilibrium mixture of gases containing OH at 3000°K and at 6000°K, the total observable intensity $A(K)$ emitted from the spectral line identified by the index K with line center at $\nu_{lu}(K)$ is given by the expression

$$A(K)/(c/4)=\{\rho^0[\nu_{lu}(K)]S_{lu}(K)X\}_{T=3000°K}+\{\rho^0[\nu_{lu}(K)]S_{lu}(K)X\}_{T=6000°K}, \quad (18)$$

where $\rho^0[\nu_{lu}(K)]$ is the volume density of radiation emitted by a blackbody at $\nu_{lu}(K)$ and the effects of self-absorption have been assumed to be negligible. The total intensity of the line with index K divided by the total intensity of the line with index $K=1$ is

$$G=A(K)/A(1)=[B(T=6000)+B(T=3000)C]/(1+C), \quad (19)$$

where

$$B(T)=\{\rho^0[\nu_{lu}(K)]S_{lu}(K)/\rho^0[\nu_{lu}(1)]S_{lu}(1)\}_T=[\nu_{lu}(K)/\nu_{lu}(1)]^4[(g_uq_{lu}^2)_K/(g_uq_{lu}^2)_1]\times\exp\{-[E_u(K)-E_u(1)]/kT\} \quad (20)$$

and

$$C=\{\rho^0[\nu_{lu}(1)]S_{lu}(1)X\}_{T=3000}/\{\rho^0[\nu_{lu}(1)]S_{lu}(1)X\}_{T=6000}=(X_{3000}/X_{6000})\times[\exp-\{[E_u(1)/k][(1/3000)-(1/6000)]\}]. \quad (21)$$

The nonequilibrium character of the OH distribution is expressed by

$$r=X_{3000}/X_{6000}. \quad (22)$$

For $r=0$ the present discussion reduces to the analysis of an isothermal system at 6000°K, whereas for $1/r=0$, the radiation becomes that characteristic of an isothermal system at 3000°K. It is apparent that r must be considerably greater than unity before the OH with rotational temperature at 3000°K will influence the observed radiation from the nonequilibrium mixture.

The apparent temperatures which would be obtained from observations of the mixture if conventional treatment of emission data were employed is obtained by plotting $\log\{G/[\nu_{lu}(K)/\nu_{lu}(1)]^4[(g_uq_{lu}^2)_K/(g_uq_{lu}^2)_1]\}$ as a function of $E_u(K)$. Similarly, isointensity plots may be constructed according to the method of Shuler[8] by noting that for equally intense lines with indexes K and K', respectively, $G(K)=G(K')$.

B. Discussion of Results

Interpretation of measurable intensities according to conventional procedures for analysis of emission data is illustrated in Figs. 10 and 11. In accord with expectations, we find for $r\leqslant 10^2$ that the observable intensity ratios are practically those characteristic of an isothermal system at 6000°K. On the other hand, for $r\geqslant 10^6$, the nonequilibrium mixture radiates almost like an isothermal system at 3000°K. For intermediate values of r, numerical values are obtained in the usual logarithmic plots (see Figs. 10 and 11) which can be represented, in adequate approximation, by two intersecting straight lines. For low values of K temperatures greater than 3000°K are obtained, whereas for high values of K temperatures lower than 6000°K are obtained. Of particular interest is the fact that data calculated according to Shuler's isointensity method (see Figs. 12 and 13) can be correlated by linear plots even under conditions in which conventional procedures clearly show discontinuities.‖ Of course, the slopes

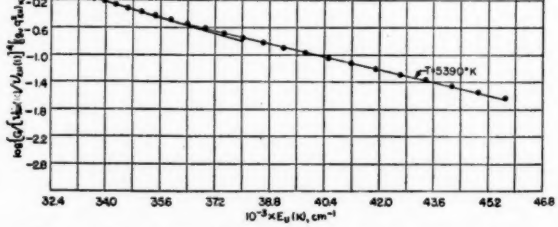

FIG. 11. Conventional plot and apparent temperatures for $r=2\times10^3$.

‖ There are several obvious reasons for this result. Thus, without applying a suitable frequency correction or using interpolation between listed values of K, there is considerable intrinsic scatter in the isointensity plots. Furthermore, the number of points which can be used to draw the final plot is reduced to one-half. Hence, it is quite possible to obtain isointensity plots which do not show the finer details of conventional plots.

derived from Shuler's isointensity plots are meaningless in these cases. These results certainly indicate that as long as nonlinear plots are obtained a simple interpretation of observable data is inadmissible even for a mixture of isothermal systems in the absence of self-absorption. Thus, two intersecting straight lines with apparent temperatures T_1 and T_2 can be obtained only by nonequilibrium mixtures at temperatures other than T_1 and T_2.

VI. APPARENT TEMPERATURES FOR TWO ADJACENT ISOTHERMAL REGIONS

The observable radiation from real flames is always produced from a nonisothermal field of view. Without a detailed prescription of temperature and concentration gradients along the line of sight, it is not possible to incorporate quantitative corrections in the interpretation of experimental data. However, it is apparent that the falsification of data in conventional plots will be similar to the falsification produced by self-absorption as long as a hot region is viewed through a cooler gas layer. We shall demonstrate this conclusion by representative calculations on the observable emitted radiation for spectral lines with Doppler contour when an isothermal region at 3000°K is viewed through an isothermal region at 1500°K. The concentrations of emitter in the two regions will be treated as variable parameters. Although we present theoretical results only for the P_1 branch, it is clear from a study of the factors responsible for distortions produced by observations through cooler gas layers that, for example, the R_2 branch will be modified in roughly the same manner as the P_1 branch. Hence, although the use of isointensity methods is advantageous in minimizing the effects of self-absorption for the R_2 branch, the use of the R_2 branch becomes less significant if distortion by temperature gradients is also of importance. It is gratifying to note, however, that the distortions resulting from temperature gradients are reduced if the extent of self-absorption is diminished.

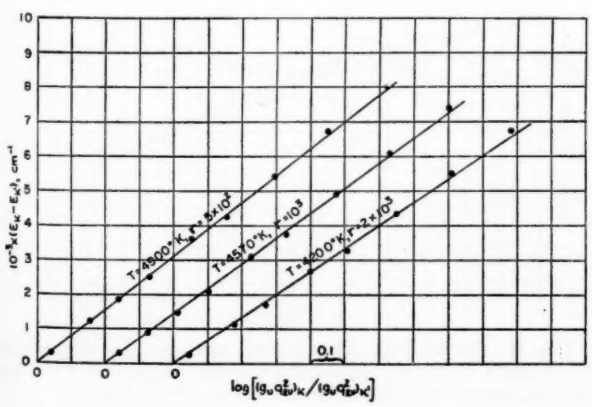

FIG. 12. Isointensity plots and apparent temperatures for $r=5\times10^2$, 1×10^3, and 2×10^3.

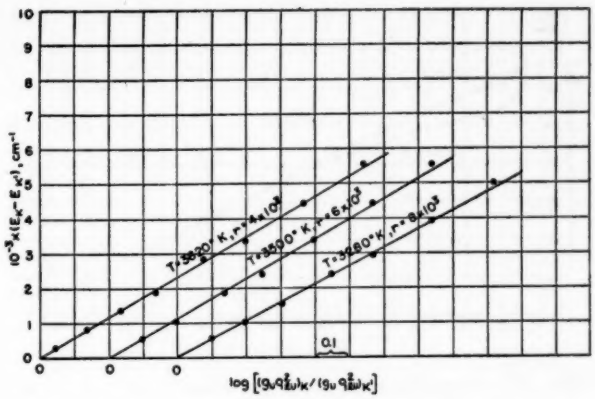

FIG. 13. Isointensity plots and apparent temperatures for $r=4\times10^3$, 6×10^3, and 8×10^3.

A. Outline of Theory for Peak Intensities

Consider an isothermal region at temperature T with properties X, $P_{\max}$, $R(\nu_{lu})$, and $\epsilon=1-\exp(-P_{\max}X)$ which is observed through an isothermal region at temperature T' with properties X', $P_{\max}'$, $R'(\nu_{lu})$, and $\epsilon'=1-\exp(-P_{\max}'X')$. The maximum observable intensity for the spectral line whose center lies at the frequency ν_{lu} is

$$I_{\max}=R(\nu_{lu})\{\epsilon+[\epsilon'/(1-\epsilon')]\times\exp(-h\nu_{lu}/k)[(1/T')-(1/T)]\}(1-\epsilon'). \quad (23)$$

A conventional plot for the study of emission experiments can be constructed according to the scheme outlined below.

(1) For $T=3000$°K and $T'=1500$°K and fixed values of $\epsilon(K=1)$ and $\epsilon'(K=1)$ for the P_1 branch calculate $(P_{\max}X)_{K=1}$ and $(P_{\max}'X')_{K=1}$.

(2) Calculate the ratios $S_{lu}(K,T)/S_{lu}(K=1,T)$ and $S_{lu}'(K,T')/S_{lu}'(K=1,T')$.

(3) Calculate $(P_{\max}X)_K$ and $(P_{\max}'X')_K$ and hence $\epsilon(K)$ and $\epsilon'(K)$.

(4) Determine $I_{\max}$ from Eq. (23) and plot $\log[I_{\max}/(g_uq_{lu}^2)(\nu_{lu})^3]$ as a function of $E_u(K)$.

B. Discussion of Results for Peak Intensities

The results of numerical calculations are summarized in Figs. 14 and 15 for $\epsilon(K=1)=0.3$ and 0.9, respectively, for varying values of $\epsilon'(K=1)$ with $\epsilon'(K=1)\leqslant\epsilon(K=1)$. Reference to Figs. 14 and 15 clearly shows that observations through a cool isothermal region accentuate the distortion observed for self-absorption alone. For example, for $\epsilon(K=1)=\epsilon'(K=1)=0.3$ a definite curvature is observed (see Fig. 14), whereas for $\epsilon(K=1)=0.3$ and $\epsilon'(K=1)=0$ a linear plot with a nearly "normal" temperature obtains (see Fig. 1). For strong self-absorption both in the hotter and cooler gas layers, extensive self-reversal may occur,[11] leading to no real values for the "temperature" (see Fig. 15).

[11] R. D. Cowan and G. H. Dieke, Revs. Modern Phys. **20**, 418 (1948).

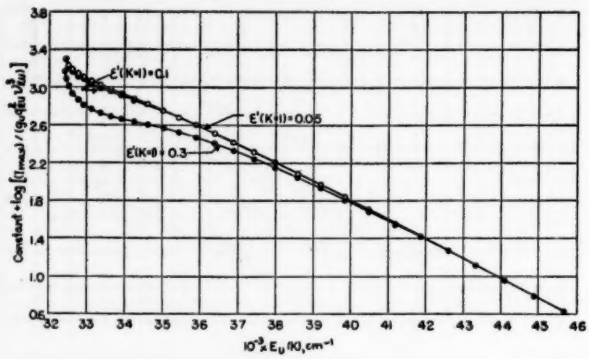

FIG. 14. Conventional plots for the interpretation of emission experiments with two adjacent isothermal regions at 1500 and 3000°K, respectively, for $\epsilon(K=1)=0.3$ for the P_1 branch.

It should perhaps be emphasized that the data shown in Figs. 14 and 15 are only of qualitative significance in so far as application to real flames is concerned. Furthermore, the results are, of course, modified if appropriate plots for total intensities are used instead of plots for peak intensities. In general, one would expect the extent of distortion to be somewhat diminished for total intensity measurements. Detailed calculations will not be presented here since the precise evaluation of the integrals involved is somewhat laborious and since the results would add little to the qualitative conclusions stated above.

VII. APPLICATION TO FLAMES

It is evident that none of the quantitative results presented for idealized systems in Secs. II to VI apply to real flames. Nevertheless, it is perhaps justifiable to perform some extrapolation to real systems.

To begin with, it is clear that observed "anomalies" *can be* explained by distortion of experimental data through self-absorption and/or temperature gradients. In order to make observable anomalies appear real, it is therefore necessary to perform experiments proving that distortion of data does not play a significant role. The proof should be direct and not inferential.

In order to emphasize the fact that inferential proof may be no proof at all, we consider, for example, an isothermal system at 3000°K with $\epsilon'(1)=0.70$ for the P_1 branch. Conventional interpretation of emission experiments (see Fig. 1) will then show experimental data which can be correlated by intersecting straight lines leading to a value of $T_u'\simeq 5000$°K for the $^2\Sigma$ state for $10\leqslant K\leqslant 18$ (see Table I). Next, absorption experiments are performed with a light source at 8000°K, and considering the inevitable scatter of experimental data, the observed results are well correlated by a single straight line with $T_l'\simeq 3650$°K (see Fig. 3). On the basis of these experimental results, one could argue with vigor for a nearly "normal" distribution of OH in the ground ($^2\Pi$) state and for abnormal excitation of OH in the excited ($^2\Sigma$) state. For the case under discussion, in spite of the seemingly convincing inferential evidence, the conclusion would obviously be erroneous.

We have presented previously[12] a critical review of available experimental evidence for anomalous population temperatures in flames in which we emphasized the lack of unequivocal evidence either for or against the reality of the anomalies, noting, however, the wealth of inferential evidence, in favor of a nonequilibrium distribution of OH, presented by Gaydon and Wolfhard.[1] We did not necessarily intend to replace a temperature anomaly by a concentration anomaly. Rather we were primarily interested in showing that as yet the experimental evidence is not sufficiently clear to warrant quantitative interpretation. We have proposed a two-path method which eliminates all errors arising from self-absorption in *isothermal* systems for spectral lines with Doppler contour.[13] However, we do not consider the method to be exactly valid for the study of regions of active combustion. The only conclusion which we feel justified in stating at the present time is that the spectroscopic study of regions of active combustion is useful for species identification and may, in time, lead to a valid quantitative picture, for example, of OH rotational temperatures and OH concentrations. The final analysis may prove or disprove the reality of anomalies. However, we shall find such proof convincing only if every precaution has been taken to eliminate instrumental errors and if all necessary corrections for distortions have been made by a realistic study of temperature gradients and of the extent of self-absorption. In this connection we wish to emphasize again the fact that the use of the isointensity method for the R_2 branch, with proper consideration for all of the precautions mentioned by Dieke,[5] will minimize self-absorption errors. However, the use of the R_2 branch is not sufficient to eliminate the coupled effects of self-absorption and temperature gradients (compare with Sec. VI).

The question of the reality or fiction of anomalous rotational, vibrational, and electronic temperatures for OH in flames is of practical importance in connection

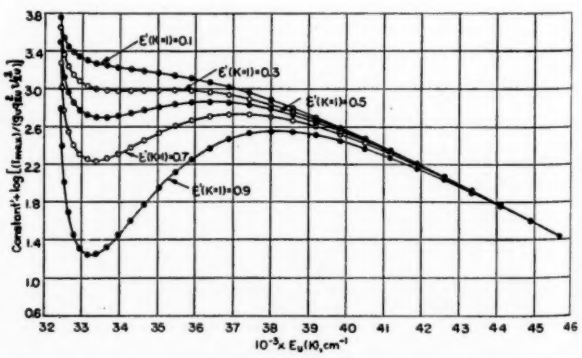

FIG. 15. Conventional plots for the interpretation of emission experiments with two adjacent isothermal regions at 1500 and 3000°K, respectively, for $\epsilon(K=1)=0.9$ for the P_1 branch.

[12] S. S. Penner, J. Chem. Phys. **20**, 1334 (1952).
[13] S. S. Penner, J. Chem. Phys. **20**, 1341 (1952).

with the development of rigorous theories of one-dimensional laminar flame propagation.[14] A review of observed anomalies shows uniformly high population temperatures not only for OH but also for other chemical species. On the other hand, theoretical studies by Golden and Peiser show a low rotational temperature for newly formed HBr.[15] If nonequilibrium distributions persist in flames, the attempts at a rigorous calculation of burning velocities for one-dimensional flame propagation are enormously complicated because of our completely inadequate knowledge of detailed reaction mechanisms, particularly between molecules and radicals in excited states. The hypothesis that spectroscopic investigations yield information about side reactions and can therefore be ignored in a realistic formulation of the detailed reaction steps in flames is not altogether satisfying, since energy must be conserved and we have as yet no detailed knowledge concerning energy-deficient chemical species in the reaction zones of flames. For this reason, continued spectroscopic studies of flames are of interest not only in ascertaining details concerning the particular reaction steps which can be studied conveniently, but they also have a bearing on a parameter such as the linear burning velocity.

In conclusion, the author takes pleasure in expressing his appreciation to Dr. O. R. Wulf and Dr. H. S. Tsien for helpful comments. The numerical work was performed by E. K. Björnerud and R. W. Kavanagh.

APPENDIX I. BASIC RELATIONS IN TERMS OF TOTAL EMITTED INTENSITIES

The expressions given in Sec. II require slight modifications when total intensity ratios rather than peak intensity ratios are available. If the apparent integrated intensity of the spectral line with center at the frequency ν_{lu} is denoted by the symbol $A(\nu_{lu})$, then, as is well known,[16]

$$A(\nu_{lu})\simeq R^0(\nu_{lu})(mc^2/2\pi kT_t\nu_{lu}^2)^{-\frac{1}{2}}(P_{\max}X)\times\{\sum_{n=0}^{\infty}[(n+1)^{\frac{1}{2}}(n+1)!]^{-1}(-P_{\max}X)^n\}. \quad \text{(A1)}$$

From Eqs. (1) and (A1) it follows that

$$I_{\max}=[A(\nu_{lu})/\nu_{lu}](mc^2/2\pi kT_t)^{\frac{1}{2}}\xi, \quad \text{(A2)}$$

where

$$\xi=\{(P_{\max}X)\sum_{n=0}^{\infty}[(n+1)^{\frac{1}{2}}(n+1)!]^{-1}\times(-P_{\max}X)^n\}^{-1}[1-\exp(-P_{\max}X)]. \quad \text{(A3)}$$

[14] J. O. Hirschfelder and C. F. Curtiss, J. Chem. Phys. **17**, 1076 (1949).
[15] S. Golden and A. M. Peiser, J. Chem. Phys. **17**, 630 (1949).
[16] R. Ladenburg, Z. Physik **65**, 200 (1930).

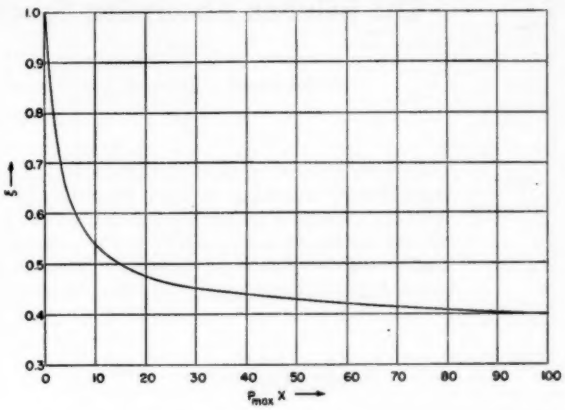

FIG. 16. The quantity ξ as a function of $P_{\max}X$.

Since $\xi=1$ for $P_{\max}X\ll 1$, it is apparent from Eqs. (7) and (A2) that

$$\frac{\partial \ln[A(\nu_{lu})/\nu_{lu}^4 g_u(q_{lu})^2]}{\partial E_u}=-\frac{1}{kT_u}$$

for $\epsilon'\ll 1$ for all lines. (A4)

Equation (A4) is the expression which is usually employed for the interpretation of experimental data. The value of ξ is plotted as a function of $P_{\max}X$ in Fig. 16.

When conventional plots for the determination of population temperatures are constructed according to Eq. (A4) for arbitrary values of $\epsilon'(1)$, results substantially equivalent to those shown in Fig. 1 are obtained. In this case the quantity $A(\nu_{lu})$ can be calculated from Eq. (A2) after obtaining $I_{\max}$ by use of the procedure described in Sec. IIB.

APPENDIX II. POPULATION TEMPERATURES BASED ON APPARENT TOTAL ABSORPTION MEASUREMENTS FOR SPECTRAL LINES WITH DOPPLER CONTOUR

It is readily shown that the apparent total absorption A_T is related to the peak absorption $A_{\max}$ through the expression

$$A_{\max}=A_T\cdot\xi\cdot(\nu_{lu})^{-1}(mc^2/2\pi kT_t)^{\frac{1}{2}}, \quad \text{(A5)}$$

where ξ is given by Eq. (A3). By the use of Eqs. (A3) and (A5) it is a simple matter to convert the data given in Figs. 4 to 7 to the corresponding plots involving A_T. The values of ξ as a function of $P_{\max}X$ have been given in Fig. 16. Conclusions derived from conventional plots in terms of A_T for estimating population temperatures do not differ significantly from the material given in Sec. III, for the range of spectral emissivities considered in the present analysis.

The Solution Absorption Spectra of Americium(III), (V), and (VI)*

S. E. Stephanou, J. P. Nigon, and R. A. Penneman
University of California, Los Alamos Scientific Laboratory, Los Alamos, New Mexico
(Received May 9, 1952)

Detailed absorption spectra of Am(III), (V), (VI), and Eu(III) in perchloric acid were obtained over the range 200–800 mμ using the Cary Recording Spectrophotometer. Molecular extinction coefficients obtained from the average of several determinations are given for each absorption peak of the americium species. No vibrational fine structure similar to that reported for U(VI), Np(V), Np(VI), and Pu(VI) was found in the visible and ultraviolet spectra of Am(V) and (VI). This fine structure has been interpreted as arising from symmetrical metal-oxygen vibration in ions of the type MO_2^+ and MO_2^{++}.

INTRODUCTION

THE very narrow absorption bands found in the ultraviolet and visible region for various valence states of uranium, neptunium, and plutonium have been reported by several investigators.[1–3] The spectra of the (III), (V), and (VI) oxidation states of americium in solution also exhibit very prominent absorption bands which have been found to obey the Beer-Lambert law.[4] These early measurements on americium spectra were made using the Beckman (Model DU) quartz spectrophotometer with matched 1 cm microcells. The dispersion of this instrument per mm slit ranges from 8 A/mm at 200 millimicrons to 640 A/mm at 800 millimicrons.[5]

Recently, the spectrum of Am(III) in perchloric acid solutions has been measured using a Baird Spectrograph with a dispersion of 5.6 A/mm in the first order.[6] However, the relative intensities of the spectral lines were not reported.

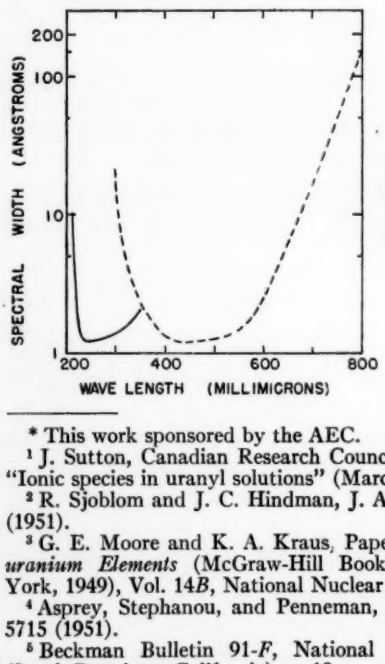

FIG. 1. Dispersion *vs* wavelength plot for Cary Recording Spectrophotometer. Solid line, hydrogen lamp; dotted line, tungsten lamp.

The purpose of the present investigation was threefold: first, to obtain better data on the absorption spectra of Am(V) and (VI) using an automatic recording instrument; second, to determine accurately the molecular extinction coefficients of the americium absorption band maxima; and third, to search for vibrational fine structure in Am(V) and (VI) similar to that reported for U(VI),[7] Np(V),[2] Np(VI),[2] and Pu(VI).[7,8] This fine structure has been interpreted as arising from symmetrical metal-oxygen vibration in ions of the type MO_2^+ and MO_2^{++}.

The spectrum of Eu(III), both in crystals at low temperature and in solution, has been examined in great detail by a number of investigators. Since Am(III) in the 5 f series is considered to be the analog of Eu(III) in the 4 f series, it was of interest to measure the spectrum of Eu(III) for the purpose of comparison, using the same instrument and technique.

EXPERIMENTAL

The absorption spectrum measurements were made with the excellent Cary Recording Spectrophotometer (Model 11) using quartz cells 5 cm in length. In each experiment, the cell was first filled with the perchloric acid at the concentration to be used in the sample and inserted in the upper light beam of the Cary. The instrument was adjusted to read zero optical density (*versus* air in the lower light path) for the complete ultraviolet and visible range. In our experiments, the dispersion varied in the manner shown in

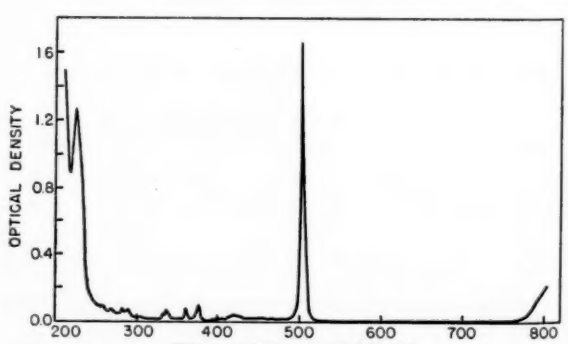

FIG. 2. Absorption spectrum of 0.854×10^{-3} f Am(III) in 0.1 f $HClO_4$.

* This work sponsored by the AEC.

[1] J. Sutton, Canadian Research Council Document, CRC-325, "Ionic species in uranyl solutions" (March 21, 1947).

[2] R. Sjoblom and J. C. Hindman, J. Am. Chem. Soc. **73**, 1744 (1951).

[3] G. E. Moore and K. A. Kraus, Paper No. 4–22, *The Transuranium Elements* (McGraw-Hill Book Company, Inc., New York, 1949), Vol. 14*B*, National Nuclear Energy Series.

[4] Asprey, Stephanou, and Penneman, J. Am. Chem. Soc. **73**, 5715 (1951).

[5] Beckman Bulletin 91-*F*, National Technical Laboratories (South Pasadena, California), p. 10.

[6] Stover, Conway, and Cunningham, J. Am. Chem. Soc. **73**, 491 (1951).

[7] M. Kasha, J. Chem. Phys. **17**, 349 (1949).

[8] R. H. Betts and B. G. Harvey, J. Chem. Phys. **16**, 1089 (1948).

Fig. 1. The cell was then emptied, refilled with the sample solution, and the spectrum measured with the cell in the upper chamber of the Cary, as before. After each determination, the absorption of "air *versus* air" in the two light paths was run as a check on instrument drift. This technique eliminates the errors which might be introduced by the use of two cells, one for the sample and one for the solvent.

Experiments by Newton and Brickwedde[9] have shown that the analyzing beam of the Cary is not spectrally pure but is contaminated with a trace of light of other wavelengths. The center of the beam was found to be the least contaminated. To lessen this source of error, masks of 9-mm aperture were used at both ends of the cell. However, for extremely narrow absorption bands, such as the 503 mμ absorption of Am(III), apparent Beer-Lambert Law failure was observed at *OD* of 1.7 and higher (corresponding to ~3/1000 of I_0 excess transmission).

Because of the intense alpha-activity from Am^{241}, a quartz 19/22 standard taper joint was sealed around the stopper of the cell. Using this double seal, no alpha-activity was detected on the outer surface of the cell after repeated fillings. The cell was mounted in a sealed brass compartment, machined to accurately position the cell. This also served as an additional safety measure in case of

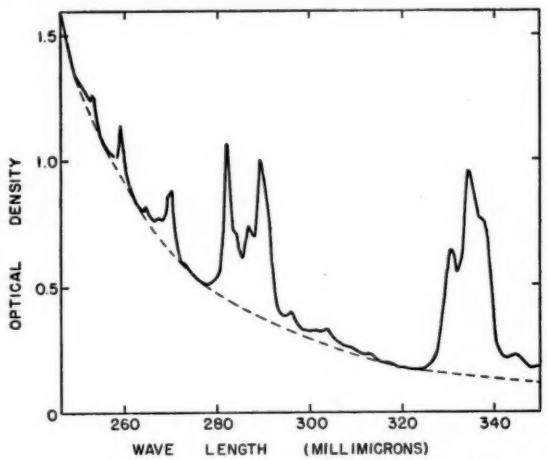

FIG. 3. Ultraviolet absorption spectrum (246–350 mμ) of 0.0124 f Am(III) in 0.1 f $HClO_4$.

cell breakage. After insertion in the Cary, two shutters were opened so that the cell was exposed to the analyzing beam.

Americium(III) hydroxide was precipitated with gaseous NH_3, washed thoroughly with water, and dissolved in 0.1 f $HClO_4$ from a stock solution used throughout these experiments. Americium(V) was prepared by oxidation of Am(III) in carbonate solution with ammonium peroxydisulfate or ozone. The precipitate was washed thoroughly and dissolved in 0.1 f $HClO_4$. Americium(VI) was obtained by oxidizing a 0.1 f $HClO_4$ solution of Am(V) to Am(VI) with ozone. Americium concentrations were determined by radiometric methods.

The Eu(III) solution at two concentrations was prepared in the same manner as the Am(III) solution. It was spectroscopically free from other rare earths, and contained sodium as the only detectable impurity. The europium concentration was determined by precipitation of the oxalate, and ignition to the oxide.

The purity of the americium(III) was checked spectroscopically and found to be >98 percent pure, with sodium as the principal impurity. The Am(V) and (VI) solutions contained some potassium, since it was not possible to wash the Am(V) precipitate completely free from potassium without peptization.

The spectrophotometric measurements were taken at room temperature, 23±2°C.

[9] T. W. Newton and L. H. Brickwedde, unpublished work, Los Alamos.

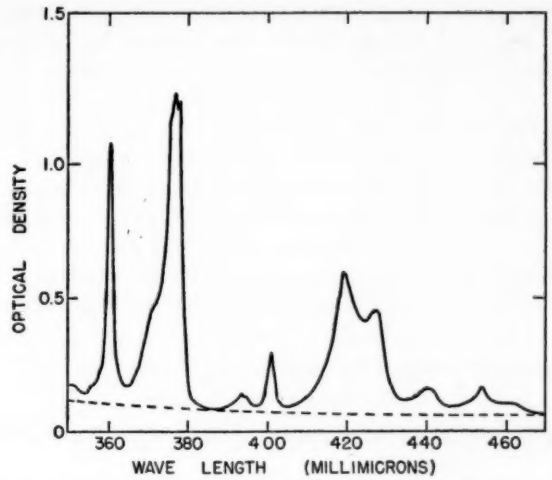

FIG. 4. Ultraviolet absorption spectrum (350–470 mμ) of 0.0124 f Am(III) in 0.1 f $HClO_4$.

The Am(VI) spectrum was determined on two preparations, 2.77×10^{-2} and 4.31×10^{-3} f; the Am(V) was prepared and measured separately at 1.01×10^{-3} and 4.62×10^{-3} f, and also determined from the two Am(VI) solutions after reduction to Am(V); the Am(III) spectrum was the result of seven determinations at concentrations ranging from 0.181×10^{-3} to 12.4×10^{-3} f.

RESULTS AND DISCUSSION

Figure 2 shows the complete spectrum of 0.854×10^{-3} f Am(III) solution in 0.1 f $HClO_4$. A prominent absorption band was found at 224.6 mμ which was not reported by Stover, Conway, and Cunningham.[6] In order to determine the fine structure present in the ultraviolet region, a 12.4×10^{-3} f Am(III) solution was examined. The results of this latter measurement are shown in Figs. 3 and 4. The absorption spectra of Am(V) and (VI) are shown in Figs. 5 and 6.

The wavelengths and molecular extinction coefficients for the absorption band maxima of Am(III), (V), and (VI) are tabulated in Table I. The wavelength data for Am(III) are in good agreement with those of Stover, Conway, and Cunningham[6] which are enclosed in parentheses in the table. Ten additional weak absorption bands were observed.

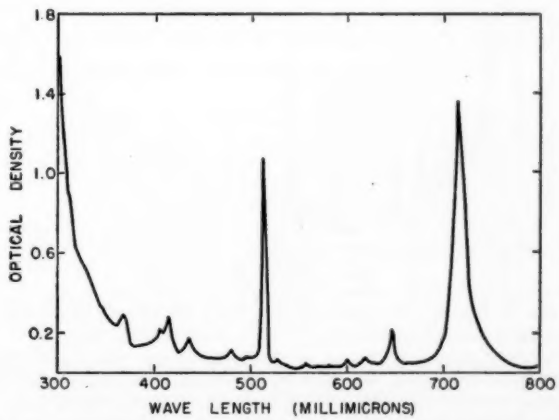

FIG. 5. Absorption spectrum of 4.62×10^{-3} f Am(V) in 0.1 f $HClO_4$.

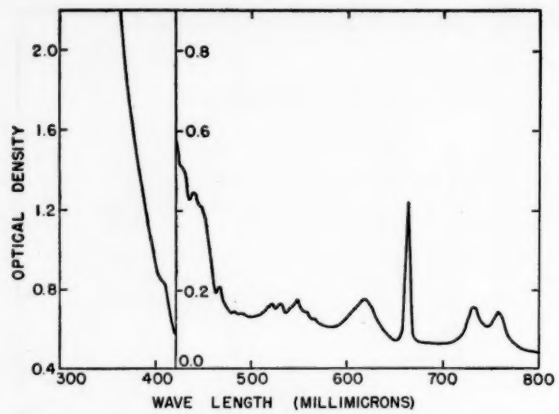

FIG. 6. Absorption spectrum of 2.77×10^{-3} f Am(VI) in 0.1 f $HClO_4$.

The molecular extinction coefficients for Am(III) were calculated after subtracting the continuous ultraviolet absorption present (indicated by a dotted line in Figs. 3 and 4). The ultraviolet absorption in the spectrum of Am(III) was found to gradually increase when the solution was allowed to stand for several days. The absorption peaks in the visible region, however, did not change in intensity. This effect can be accounted for by the growth of hydrogen peroxide, which is formed in a solution of Am(III) due to the reaction of alpha particles with water.[10] A measurement of the spectrum of hydrogen peroxide showed that the magnitude and general features of the ultraviolet absorption were similar to the continuous ultraviolet absorption found in Am(III) solutions. For this reason, the general ultraviolet absorption was not taken into account in calculating the molecular extinction coefficients for Am(III).

With Am(V) and (VI), however, the ultraviolet absorption does vary regularly with the concentration of

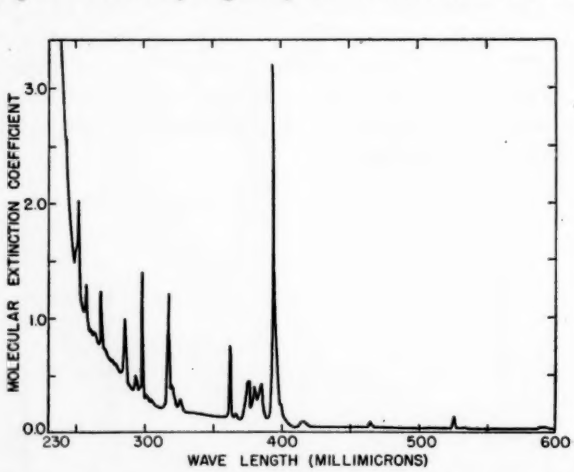

FIG. 7. Absorption spectrum of 0.123 f Eu(III) in 1 f $HClO_4$.

[10] (a) Llewellyn H. Jones, at this Laboratory, has observed the growth of hydrogen peroxide in an Am(III) solution using the peroxy complex of titanium. (b) E. Onstott, unpublished work on the polarographic determination of hydrogen peroxide in americium solutions.

Am(V) or Am(VI), and therefore, in the calculation of the molecular extinction coefficients for these species, the general ultraviolet absorption was included. Furthermore, since Am(V) and Am(VI) are strong oxidizing agents, it would be expected that the concentration of peroxide present would be considerably smaller than that existing in an Am(III) solution. The ultraviolet absorption of Am(V) and Am(VI) was found to

TABLE I. Americium solution absorption spectra. Wavelengths and molecular extinction coefficients of band maxima.

Am(III) ($HClO_4$) = 0.1*M*			Am(V) ($HClO_4$) = 0.1*M*		Am(VI) ($HClO_4$) = 0.1*M*	
mμ		ε[c]	mμ	ε	mμ	ε
224.6[a]		171	312	37.7	408.5	60.2
243.0[a]	(243.3)[b]	1.73	327	22.9	428.2	36.3
	(243.6)					
			346	14.2	438.8	32.3
253.5	(253.7)	1.29	368.1	12.4	448.3	29.0
259.4	(259.7)	3.14	405.1	9.5	466.6	14.9
264.9	(265.1)	0.58	415.3	12.0	481.6	10.5
267.7		1.10	435.7	7.0	488.9	10.3
269.8	(269.9)	3.52	479.7	4.6	517.2	10.0
270.2	(270.5)	3.94	513.1	45.6	521.0	11.7
273.0		0.21	530.0	2.4	529.3	11.8
	(275.4)		559.2	2.0	548.0	12.8
282.3	(282.6)	9.81	601.2	2.6	556.6	10.3
284.2	(284.7)	4.24	620.8	3.0	565.9	9.2
287.0	(286.1)	5.08	646.8	9.5	619.0	12.6
289.4	(289.3)	9.48	715.1	59.3	663.0	30.5
296.0		0.74			731.8	11.4
303.6		0.55			757.8	10.4
312.9		0.27				
331.0	(331.2)	7.74				
334.8	(335.3)	12.95				
337.8	(339.1)	9.86				
344.6		1.08				
351.2		0.87				
356.2		0.97				
360.1	(360.5)	15.5				
371.3		5.82				
375.5	(375.6)	17.3				
376.6	(377.1)	18.74				
377.7	(378.4)	18.2				
393.3		0.97				
394.8		0.81				
401.2	(401.8)	34.2				
419.2	(419.8)	8.24				
427.2	(428.7)	6.05				
440.2		1.44				
453.6	(454.3)	1.61				
502.7[a]	(503.0)	391				
506[a]	(507.8)					
510.3[a]	(510.4)					
516.0[a]	(516.6)	3.85				
	(813.3)					

[a] These absorption band maxima were obtained by using more dilute solutions of Am(III).
[b] Wavelengths in parentheses are those obtained by Stover, Conway, and Cunningham (J. Am. Chem. Soc. 73, 491 (1951)).
[c] Molecular extinction coefficients were calculated from net optical densities (subtracting the general ultraviolet background).

gradually decrease with time, with corresponding decrease in the height of the Am(V) and (VI) peaks. This can be attributed to the autoreduction of Am(V) and (VI).[11] Agreement between experiments at different

[11] L. B. Asprey and S. E. Stephanou, AECU-924, November 10, 1950.

concentrations showed that the prominent peaks of Am(III), (V), and (VI) obey the Beer-Lambert Law (with the exception of Am(III) at high optical density as mentioned above).

The spectrum of 0.123 f Eu(III) in 1 f $HClO_4$ is shown in Fig. 7. The general features of the Eu(III) and Am(III) spectra are similar in that the absorption bands are extremely sharp. However, the molecular extinction coefficients of Am(III) are greater than those of Eu(III) by approximately a factor of 100. For example, the 393 mμ peak of Eu(III) has a molecular extinction coefficient of 3.2 as compared with 390 for the 503 mμ peak of Am(III). This can be interpreted as signifying that the transitions within the 5 f shell have greater probability than those involving the 4 f shell, since the origin of the lines in these spectra is generally accepted as being due to electronic transitions of f electrons.

A careful examination of the near-ultraviolet spectra of Am(V) and (VI) has revealed no regular vibrational frequency intervals of the type reported for U(VI),[7] Np(V)[2] and (VI),[2] and Pu(VI).[7,8] However, infrared measurements in progress at this Laboratory[12] have definitely established that the uranyl structure is repeated in Np(VI), Pu(VI), and Am(VI).

We wish to express our thanks to C. F. Metz of the analytical group of the Chemistry-Metallurgy Division for the use of the Cary Recording Spectrophotometer and also to O. R. Simi for the spectroscopic analyses of the americium and europium samples.

[12] Llewellyn H. Jones (to be published).

THE JOURNAL OF CHEMICAL PHYSICS VOLUME 21, NUMBER 1 JANUARY, 1953

Atomic Excitation in Beta-Decay*

H. M. SCHWARTZ
Department of Physics, University of Arkansas, Fayetteville, Arkansas
(Received September 2, 1952)

The excitation and ionization of the daughter atom coming from a beta-decay, which is of interest in connection with some hot atom studies and possibly also in connection with beta-recoil experiments, is the subject of an introductory discussion (Secs. 1, 3, 4, and 5) with explicit calculations given only in the case of one-electron hydrogenlike wave function representation of atomic states (Sec. 2). The latter correct results in the literature, the only ones so far published on this subject. The present discussion is confined to direct effects of the beta-process itself and does not evaluate those resulting from Auger processes (Sec. 5).

1. INTRODUCTION

THE mean ionization of the daughter atom resulting from beta-decay[1] is of interest in hot atom studies[2] involving molecular dissociation which accompanies the beta-decay of a constituent atom.[3] Quantitative information concerning such ionization might also prove useful in connection with beta-recoil experiments,[4] when the relevant measuring techniques are sufficiently refined.[5]

A general perturbation scheme for the calculation of the probabilities of beta-induced atomic excitation has been suggested by Feinberg.[6] This general approach will not be discussed here;[7] rather, our starting point will be the conclusion that follows from the published discussion to the effect that the beta-induced excitation can be considered as arising essentially from three (approximately) independent effects: (a) nuclear recoil, (b) direct interaction between the atomic electrons and the emitted beta-particle, and (c) change of nuclear charge. The effect (a) can be shown to be relatively unimportant in the atomic case.[8] According to Feinberg's analysis,[6] also effect (b) is generally negligible. This point requires, however, further study.[9]

* This work is supported in part by the AEC.

[1] This will be referred to for the sake of brevity as "beta-induced ionization." Similarly, we shall speak of beta-induced excitation. By state of "excitation" we will understand also any state of ionization.

[2] R. R. Edwards and T. H. Davies, Nucleonics 2, No. 6, 44 (1948); H. M. Schwartz and R. R. Edwards, J. Chem. Phys. 19, 385 (1951). The statement made in these references regarding the possible utilization of the excess atomic binding energy which is set free in the negative beta-decay of a heavy atom appears to be misleading in the light of an extension, which will be presented elsewhere, of the discussion given by the present author in Phys. Rev. 86, 195 (1952).

[3] It is intended to present in a succeeding note a discussion of the theoretical deduction of probabilities of such molecular dissociations.

[4] See, for instance, O. Kofoed-Hansen, Kgl. Danske Mat. fys. Medd. 26, No. 8 (1951) and references therein; G. W. Rodeback and J. S. Allen, Phys. Rev. 86, 446 (1952); Raymond Davis, Jr., Phys. Rev. 86, 976 (1952.)

[5] The measurement by Miskel and Perlman, which has just been published, [Phys. Rev. 87, 543 (1952)], of the average charge produced by electron capture in A^{37} and continuing similar work on other nuclides at Brookhaven and at Argonne, present an incentive for the calculation of beta-induced mean ionizations in atoms for which reliable measurements will be forthcoming.

[6] E. L. Feinberg, J. Phys. (U.S.S.R.) 4, 423 (1941). See also A. Migdal, J. Phys. (U.S.S.R) 4, 449 (1941); and A. Winther, Kgl. Danske. Mat. fys. Medd. 27, No. 2 (1952). (The discussion in the latter paper relating to very light atoms as illustrated by calculations for He^6 is especially interesting).

[7] It is intended to present such a discussion for publication elsewhere (see footnote 2).

[8] It is more significant in the studies of beta-induced molecular dissociation.

[9] J. A. Bruner reports (Phys. Rev. 84, 282 (1951)) the detection of a considerable proportion of a negative electrons in the β^+ decay of Sc^{44} (about 4 per hundred disintegrations), presumably due to direct interaction between the beta-particle and the atomic

When the effect (b) is negligible, it is permissible to consider the change in nuclear charge as transpiring sufficiently rapidly in terms of characteristic atomic times, so that sudden perturbation theory can be applied.[10] It follows then that the probability $P_\alpha(\pm)$ of finding the daughter atom in the excited state α subsequent to a β-decay resulting in the change of Z into $Z\pm1$, is given by the expression

$$P_\alpha(\pm)=\left|\int\cdots\int\psi_\alpha^*(q_1,\cdots,q_N;Z\pm1)\times\psi_0(q_1,\cdots,q_N;Z)d\tau_1\cdots d\tau_N\right|^2, \quad (1)$$

where q_i symbolize the spatial and spin coordinates of electron i, ψ_0 is the wave function of the ground state, and the other notation is obvious from the context. The difficulty of the problem of calculating probabilities of beta-induced excitation, even if only effect (c) alone needs to be considered, stems from the requirement of employment of sufficiently accurate atomic wave functions in Eq. (1) corresponding to various states of atomic excitation. Published calculations of such wave functions are at present quite scarce.[11] A few general remarks relating to (1) are given in Secs. 3 and 4. These are, however, of only limited scope. A more complete discussion could be given more profitably in connection with calculations pertaining to a specific case.

There is one type of approximation in which it is possible to compute all expressions (1) explicitly without undue labor; namely, that involving one-electron hydrogenlike wave functions. With this approximation, one has for the beta-induced excitation probability corresponding to a transition of an atomic electron from the original state μ to the state ν in the daughter atom:

$$p_{\mu,\nu}(\pm)=\left|\int\varphi_\nu^*(q;Z\pm1)\varphi_\mu(q;Z)d\tau\right|^2, \quad (2)$$

where the φ_ν are hydrogenlike wave functions corresponding to the indicated Z value and set of quantum numbers characterized by ν. Although the scope of validity of the probabilities given by (2) appears to be quite limited, nevertheless, these have been the only ones available and use has been made of them in the literature. Unfortunately, the published calculations[12] of beta-induced ionization probabilities given by (2) are all in error except that referring to ionization in the K shell. For that reason, it was deemed advisable to present a sketch of the evaluation of the integrals entering in (2). This is done in Sec. 2, which contains a tabulation of a few beta-induced excitation and ionization probabilities computed by means of (2). These probabilities are expressible as an inverse Z_{eff} expansion

$$p_{nl,n'l}(\pm)=\frac{a_{nn',l}}{Z_{\text{eff}}^2(nl)}+\frac{b_{nn',l}(\pm)}{Z_{\text{eff}}^3(nl)}+\cdots \quad (n\neq n'), \quad (3)$$

and only the coefficients $a_{nn',l}$ have been computed. Here nl and $n'l$ represent the quantum number sets μ, ν of (2) and l' is taken equal to l in accordance with a selection rule operative in this case (Sec. 4). Z_{eff} is a suitable effective Z which depends on the quantum set (nl).

A major difficulty in this method which is briefly discussed in Sec. 2, is the formulation of a suitable criterion for the choosing of Z_{eff}. Lacking this, it is hardly possible to assess the range of validity of the approximation. Because of this limitation, it was not considered worth while to evaluate the second coefficient in the expansion (3) although it presents some interest in showing, as is indicated by the notation, a dependence of the type of Z change involved in the beta-transition. This is not true of the first coefficient. Another question which should be considered in a more complete discussion of the present topic is the behavior of the sequence of coefficients in the series (3) for only then would it be possible to determine how large Z must be for the leading term to be adequate for the problem at hand. A similar question arises in the general discussion given in Sec. 3 in connection with an expansion similar to (3), and it is there also left open, this time because the context is too general. As stated above, a complete discussion relating to expression (1) would appear warranted at the present time only in connection with a specific calculation.

In addition to "direct" beta-induced ionization, a significant contribution to the measurable mean ionization following beta-decay arises from the Auger effect. Aside from brief mention in Sec. 5, this effect is not discussed in the present note. This effect is obviously of particular importance in the case of K capture. Although the present discussion is limited to ordinary negative and positive beta-decay, Sec. 5 contains a brief and largely qualitative discussion of the mean ionization following electron capture in A^{37}, for which a measured value has appeared recently[5] (after the present investigation was already completed).

2. THE ONE-ELECTRON HYDROGENLIKE WAVE-FUNCTION APPROXIMATION

As stated earlier in connection with formula (3), and as will be proved in Sec. 4, the expression (2) is different from zero only if all quantum numbers with the exception of the principal quantum number remain un-

electrons. This large proportion of the negative electrons and particularly their reported energy spectrum, appear surprising. Further measurements of the type reported by Bruner are obviously desirable for the clarification of secondary atomic effects associated with beta-decay.

[10] This theory is explained in L. I. Schiff, *Quantum Mechanics* (McGraw-Hill Book Company, Inc., New York, 1949), pp. 211–212. It has been applied in the present connection by A. Migdal (reference 6). See also H. M. Schwartz, Phys. Rev. 86, 195 (1952), for an indication of another, but in this case essentially equivalent, approach.

[11] See, for instance, the review article by D. R. Hartree on "The calculation of atomic structures" in Reports on Progress in Physics [Proc. Phys. Soc. (London) 11, 113 (1946–1947)].

[12] A. Migdal, J. Phys. (U.S.S.R.) 4, 449 (1949).

changed. Consequently, if the angular and spin wave functions entering in the one-electron hydrogenlike wave functions are separately normalized, (2) reduces to

$$p_{nn',l}(\pm)=\left(\int_0^\infty R_{nl}(r;Z)R_{n'l}(r;Z\pm1)r^2dr\right)^2$$
$$=\frac{2^{4(l+1)}}{a^{6+4}}\frac{(n-l-1)!(n'-l-1)![Z(Z\pm1)]^{3+2l}}{[(n+l)!(n'+l)!]^3(nn')^{4+2l}}$$
$$\times\left[\int_0^\infty r^{2l+2}\exp\left[-\frac{r}{a}\left(\frac{Z}{n}+\frac{Z\pm1}{n'}\right)\right]\right.$$
$$\left.\times L_{n+l}^{2l+1}\left(\frac{2Z}{na}r\right)L_{n'+l}^{2l+1}\left(\frac{2Z\pm2}{n'a}r\right)dr\right]^2, \quad (4)$$

where a is the Bohr radius. We can evaluate the integral in (4) by means of two formulas given by Schrödinger,[13] which yield

$$p_{nn',l}(\pm)=2^{4s}\frac{(n-s)!(n'-s)!(nn')^{2s}}{(n+s-1)!(n'+s-1)!}$$
$$\times\left[\frac{Z(Z\pm1)}{(n'Z+nZ\pm n)^2}\right]^{2s+1}\left[\sum_{\lambda=0}^{n-s}\sum_{\mu=0}^{n'-s}\sum_{\nu=0}^{<n-s-\lambda,\,n'-s-\mu>}\right.$$
$$\times(-1)^{\mu+\nu}\frac{(2s+\lambda+\mu)!}{\lambda!\mu!}\binom{\mu+1}{n-s-\lambda-\nu}$$
$$\times\binom{\lambda+1}{n'-s-\mu-\nu}\binom{-2s-1-\lambda-\mu}{\nu}$$
$$\left.\times\left(\frac{n'Z-nZ\mp n}{n'Z+nZ\pm n}\right)^{\lambda+\mu}\right]^2$$
$$s\equiv l+1, \quad \langle a,b\rangle\equiv\text{minimum }(a,b). \quad (5)$$

After completing the numerical calculations with the use of Eq. (5), the following simpler one was obtained:

$$p_{nn',l}(\pm)=2^{2(2s+1)}\frac{(nn')^{2(s+1)}(n'-s)!(n'+s-1)!}{(n'-n)!^2(n-s)!(n+s-1)!}$$
$$\times\frac{1}{Z^2}\left(1\pm\frac{1}{Z}\right)^{2s+1}\frac{[n'-n\mp(n/Z)]^{2(n'-n-1)}}{[n'+n\pm(n/Z)]^{2(2s+1+n'-n)}}$$
$$\times\left[\sum_{\lambda=0}^{n-s}(-1)^\lambda\frac{\binom{-n'-s}{\lambda}\binom{n-s}{\lambda}}{\binom{-n'+n-1}{\lambda}}\right.$$
$$\left.\times\left(\frac{n'-n\mp(n/Z)}{n'+n\pm(n/Z)}\right)^{2\lambda}\right]^2. \quad (6)$$

[13] E. Schrödinger, *Collected Papers on Wave Mechanics* (Blackie & Son, Limited, London and Glasgow, 1928), p. 99, formula (115), and p. 100, (120). (The factor $e^{-\nu}$ should be inserted in the integrand of the latter formula.)

This formula was deduced from a relationship given by Bateman,[14] and makes use of the following identity obtainable from the atomic wave equation with the help of Green's lemma,

$$\int\cdots\int\psi_\alpha^*(q_1,\cdots q_N;Z')\psi_\beta(q_1,\cdots q_N;Z)d\tau_1\cdots d\tau_N$$
$$=-\frac{Z'-Z}{E_\alpha(Z')-E_\beta(Z)}\int\cdots\int\sum_{i=1}^N\frac{1}{r_i}\psi_\alpha^*(q_1\cdots q_N;Z')$$
$$\times\psi_\beta(q_1\cdots q_N;Z)d\tau_1\cdots d\tau_N. \quad (7)$$

The derivation of this identity, which for later possible use we have written out in its general form, involves the assumptions that at least one of the states α, β belongs to the discrete spectrum and that the wave equation is of the form

$$\left(-\frac{\hbar^2}{2m}\sum_{i=1}^n\Delta_i+\sum_{i<j}^{1,n}\frac{e^2}{r_{ij}}-\sum_{i=1}^n\frac{Ze^2}{r_i}-E\right)\psi=0. \quad (8)$$

Equation (6) was subsequently found to be the same as given by L. Goldstein[15] without proof.

The numerical calculations were repeated using (6), and the agreement with the corresponding results obtained with (5) served as an adequate check of the accuracy of the numerical work. It was further possible to develop an analytic proof of the complete equivalence of Eqs. (5) and (6).

Expanding (5) or (6) in inverse powers of Z, one finds

$$p_{nn',l}(\pm)=a_{nn',l}Z^{-2}+0(Z^{-3}) \quad (n\neq n'),$$
$$p_{nn,l}(\pm)=1-a_{nn,l}Z^{-2}+0(Z^{-3}). \quad (9)$$

The algebraic expressions of the a coefficients simplify considerably in a number of special cases, substantially reducing the arithmetical labor. Numerical evaluations of these coefficients are collected in Table I.

It must be remembered that in applying formula (9), it is necessary to replace Z by a suitable effective Z depending on (nl) [see Eq. (3)]. As explained in Sec. 1, it was not thought worth while to compute here the coefficients of Z^{-3} in (9) or to investigate the order of magnitude of the neglected terms with respect to the leading term. However, this can be done without essential difficulties if required.

Of more immediate interest than the discrete excitation probabilities are the ionization probabilities from the various shells. Inasmuch as the actual energy spectrum of the beta-induced ionization electrons cannot

[14] H. Bateman, *Partial Differential Equations of Mathematical Physics* (Cambridge University Press, London and New York, 1932), Sec. 9.22, p. 453.

[15] L. Goldstein, J. phys. radium 8, 316 (1937), p. 319, formula (24). [This contains a misprint which can be corrected by comparing with formula (6) given here].

TABLE I. Numerical values of some $a_{nn',l}$ [Eq. (9)].

nl \ n'	1	2	3	4	5	6	7	8
1 0	3/4	0.312	0.0593	0.0217	0.0105	0.00585	0.00387	0.00239
2 0	0.312	9/4	1.082	0.189	0.0621	0.0377	0.0285	0.0143
2 1	0	5/4	0.783	0.137	0.0629	0.0243	0.0138	0.00873
3 0	0.0593	1.082	19/4	2.238	0.422	0.161	0.0808	0.0472
3 1	0	0.783	15/4	1.947	0.348	0.129	0.064	0.0369
3 2	0	0	7/4	1.272	0.196	0.0674	0.0320	0.0181

present much practical interest at the present time,[16] it is advantageous to avoid the employment of continuum wave functions by using the completeness theorem and thus writing for the probability $p_{nl}(\pm)$ of beta-induced ionization from the (nl) subshell in the beta-transition $Z\rightarrow Z\pm1$:

$$p_{nl}(\pm)=\int_0^\infty p_{nl,\,lE}(\pm)dE=1$$

$$-\sum_{n'=1}^{\infty} p_{nn',l}(\pm)=(a_{nn,\,l}-\sum_{\substack{1\\ n'\neq n}}^{\infty} a_{nn',l})Z^{-2}$$

$$+0(Z^{-3})\equiv q_{nl}Z^{-2}+0(Z^{-3}). \quad (10)$$

By summing over the $a_{nn',l}$ given in Table I and then finding a rough estimate of the contribution of the remaining terms in the infinite sum in (10), the results given in Table II were obtained. It was possible to check most of these results with corresponding calculations of spectral intensities,[17] owing to the expressibility of the q in terms of linear combinations of corresponding integrals occurring in the expressions for spectral intensities.

It has been indicated in Sec. 1, that apart from the question of the adequacy in general of the one-electron hydrogenlike wave function approximation, there is encountered also a difficulty in the choice of suitable $Z_{eff}(nl)$. Even if we can discover a suitable criterion for determining these effective Z values, it is clear that in all strictness we have to employ in (4) or in the first part of (10) two separate Z_{eff}, one for (nl) and another for $(n'l)$ or (El), respectively. Whether it is nevertheless possible to a certain degree of approximation to employ only one Z_{eff} cannot be asserted without further investigation.[18]

[16] An indication of the energy dependence of the ionization electron from the K shell is given by Migdal, reference 6. We can also obtain an estimate of the upper bound of the mean energy of the ionization electrons by employing the Fermi-Thomas atomic model, as done, e.g., by R. Serber and H. S. Snyder, Phys. Rev. **87**, 152 (1952). They find for the beta-induced mean excitation energy the approximate expression 22.85 $Z^{2/5}$ ev, which is seen to be of the order of at most some 100 ev.

[17] V. Sugiura, J. phys. et radium **8**, 113 (1927); H. Bethe, *Handbuch der Physik*, 24/1, second edition (Verlag von Julius Springer, Berlin, 1933), Table 15, p. 442. The L shell ionization coefficients have also been computed by J. Levinger, private communication. His results are in agreement with those in Table II.

[18] See discussion of a similar question in connection with inner shell ionization of atoms by electron impact: E. H. S. Burhop, Proc. Cambridge Phil. Soc. **36**, 43 (1940), discussion by H. S. W. Massey in the Appendix.

3. SOME GENERAL REMARKS REGARDING THE PROBABILITY INTEGRAL (1)

It was pointed out in Sec. 1 that under the assumption that we may disregard the direct interaction between the beta-particle and the atomic electrons, the probability of finding the daughter atom in the state α in a beta-decay $Z\rightarrow Z\pm1$, is given essentially by the squared modulus (1) of the integral

$$I_\alpha(\pm)\equiv\int\cdots\int\psi_\alpha^*(q_1,\cdots,q_N;Z\pm1)$$

$$\times\psi_0(q_1,\cdots,q_N;Z)d\tau_1\cdots d\tau_N$$

$$\equiv(\psi_\alpha(Z\pm1),\psi_0(Z)). \quad (11)$$

We have introduced here the inner product notation that will be useful to us presently. It is also to be borne in mind that the integration symbols represent in accordance with common usage both integration with respect to the spatial coordinates and summation with respect to the spin variables.

In general, it is to be expected that the accuracy of an integral such as (11) depends in a sensitive manner on the accuracy of the wave functions that enter in it, at least in certain appropriate integration ranges. This is known to be true of similar overlap integrals that occur for instance in the calculation of spectral intensities or of atomic photo-ionization cross sections.[19] In this connection, it is to be recalled that many of the ionization probability coefficients q_{nl} discussed in Sec. 2 could be expressed linearly in terms of appropriate integrals that occur in corresponding expressions of spectral intensities. This suggests the possibility of bringing (11) into a form bearing more direct resemblance to known integrals, by an expansion in falling powers of Z.

A Taylor expansion of $\psi_\alpha(Z\pm1)$ considered as a function of Z yields

$$I_\alpha(\pm)=(\psi_\alpha(Z),\psi_0(Z))$$

$$\pm\left(\frac{\partial\psi_\alpha}{\partial Z},\psi_0(Z)\right)+\frac{1}{2}\left(\frac{\partial^2\psi_\alpha}{\partial Z^2},\psi_0(Z)\right)$$

$$+\cdots\equiv A_{\alpha0}\pm B_{\alpha0}+\tfrac{1}{2}C_{\alpha0}+\cdots. \quad (12)$$

We suppose the aggregate of all $\psi_\alpha(Z)$ to constitute an orthonormal complete set. Thus

$$(\psi_\alpha,\psi_\beta)=\delta(\alpha,\beta), \quad (13)$$

where $\delta(\alpha,\beta)$ represents a product of Kronecker deltas or of Dirac delta symbols according to the character of the states symbolized by α and β. Repeated differentiation of (13) with respect to Z yields a sequence of relations from which we readily obtain, making use of the completeness theorem and remembering the rule of

[19] See, for instance, D. R. Bates, Proc. Roy. Soc. (London) **188**, 350 (1946–1947).

product formation of matrices,

$$\left(\frac{\partial\psi_\alpha}{\partial Z},\psi_\beta\right)\equiv B_{\alpha\beta}=-B_{\beta\alpha}{}^*,$$
$$\left(\frac{\partial^2\psi_\alpha}{\partial Z^2},\psi_\beta\right)\equiv C_{\alpha\beta}=(B^2)_{\alpha\beta}+\frac{\partial B_{\alpha\beta}}{\partial Z},\ \cdots. \tag{14}$$

Here B^2 is the square of the matrix $B_{\alpha\beta}$. In obtaining the second set of relations (14), we have made use of the first set:

$$C_{\alpha\beta}-C_{\beta\alpha}{}^*=\frac{1}{2}\frac{\partial}{\partial Z}\left[\left(\frac{\partial\psi_\alpha}{\partial Z},\psi_\beta\right)-\left(\psi_\alpha,\frac{\partial\psi_\beta}{\partial Z}\right)\right]=\frac{\partial}{\partial Z}B_{\alpha\beta}.$$

We can proceed similarly with the other terms in (12) and thus obtain an expression involving the $B_{\alpha\beta}$ and their derivatives with respect to Z.

In order to determine $B_{\alpha\beta}$ in terms of the ψ_α, we differentiate with respect to Z the Schrödinger equation of our atomic system:

$$[H(Z)-E_\alpha(Z)]\psi_\alpha(Z)=0.$$

After multiplying the resulting equation scalarly by $\psi_\beta(Z)$ and making use of the fact that the energy operator H is Hermitian, one finds

$$B_{\alpha\beta}=\frac{1}{E_\alpha-E_\beta}\left(\psi_\alpha,\frac{\partial H}{\partial Z}\psi_\beta\right)\quad(E_\alpha\neq E_\beta).$$

Referring to the expression (8) which involves our Hamiltonian H and considering the number N of electrons as fixed (and not dependent on Z), we get

$$B_{\alpha\beta}=-\frac{Ne^2}{E_\alpha-E_\beta}\left(\psi_\alpha,\sum_{i=1}^{N}\frac{1}{r_i}\psi_\beta\right)\quad(E_\alpha\neq E_\beta). \tag{15}$$

An alternative derivation can be developed with formula (7) as the starting point.

Expression (15) is clearly of the desired form. The integral entering in it differs from those entering, say, in the expressions for photo-ionization cross sections, by involving the radial variables r_i in the minus first rather than the first powers, so that the region near the nucleus is of relatively greater importance for the former than for the latter. In case of degeneracy ($E_\alpha=E_\beta$ and $\psi_\alpha\not\equiv\psi_\beta$) the above discussion requires of course further refinement.

What was stated above is of course significant only if we can establish the nature of the expansion (12), and in particular, if we can establish the type of Z dependence of the $B_{\alpha\beta}$. Whether this can be done readily in a general way does not appear too evident. Since the present discussion has no pretensions at any completeness and is intended to be only of an introductory character, it will suffice to show that if we specialize the ψ_α to be built up from hydrogenlike one-electron wave functions, then (12) is in fact an expansion in inverse powers of Z.

By writing $E_\alpha=Z^2(e^2/2a)W_\alpha$ ($a\equiv$Bohr radius) in (15), we have

$$B_{\alpha\beta}=\frac{2}{Z^2(W_\beta-W_\alpha)}Q_{\alpha\beta},\quad Q_{\alpha\beta}\equiv\left(\psi_\alpha,\sum_{i=1}^{N}\frac{a}{r_i}\psi_\beta\right). \tag{16}$$

In the aforementioned approximation, it can be shown[20] that

$$Q_{\alpha\beta}=\pm\left(\varphi_k,\frac{a}{r}\varphi_s\right)\quad(k\neq s), \tag{17}$$

where the φ_k are the one-electron hydrogenlike wave functions and the indices k, s refer to the constituent wave functions of ψ_α, ψ_β which (and the only ones which) do not have all quantum numbers equal. Expression (17) reduces to an integral involving only the radial variable r and an examination of the resulting integrand discloses at once that $Q_{\alpha\beta}$ is proportional to Z. Since the W are, of course, independent of Z, it is seen that the $B_{\alpha\beta}$ are proportional to $1/Z$. It then follows by (14) that the C's in (12) are proportional to $1/Z^2$,

TABLE II. Numerical values of the q_{nl} [Eq. (10)] corresponding to K, L, and M shells.

l \ n	1	2	3
0	0.33	0.47	0.52
1		0.22	0.34
2			0.12
Total for all electrons in each shell	0.66	2.26	4.28

and similarly for the other terms. We have then indeed in this case an expansion in inverse powers of Z.

Inasmuch as the evaluation of (11), in those cases when the approximation discussed in Sec. 2 is inadequate, must involve at present a considerable amount of computation, since wave functions for excited states and states in the continuum obtained by some type of self-consistent field approximation exist only for a very few atoms,[11] one may content oneself in some applications with knowing only an upper bound to any of the probabilities of beta-induced excitation. This is provided *a fortiori* by the total probability for all possible states of excitation. This quantity P_{tot}, in the notation of (1) and (11), obviously satisfies the following relation:

$$P_{\text{tot}}(\pm)=1-P_0(\pm)=1-|I_0(\pm)|^2. \tag{18}$$

This expression involves only the ground state wave functions $\psi_0(Z)$ and $\psi_0(Z\pm1)$ for which calculations exist for a considerable number of atoms.[11]

Since ψ_0 can be taken to be a real function, it follows from the first of (14) that $B_{00}=0$ and thence from the

[20] E. V. Condon and G. H. Shortley, *The Theory of Atomic Spectra* (The Macmillan Company, New York, 1935), p. 171.

second of (14) that $C_{00}=(B^2)_{00}$. Thus,

$$I_0=1+\tfrac{1}{2}C_{00}+\cdots, \quad I_0^2=1+C_{00}+\cdots=1+(B^2)_{00}+\cdots.$$

But $(B^2)_{00}=S_\alpha B_{\alpha 0}^2$ (S_α represents summation or integration, depending on the character of the state α). Hence

$$P_{\text{tot}}=S_\alpha B_{\alpha 0}^2+\cdots, \tag{19}$$

which is consistent with our probability definitions (remembering that $B_{00}=0$) as was of course to be expected. It is seen that the first term in (19) is proportional to $1/Z^2$ under conditions in which (12) is an expansion in inverse powers of Z.

It needs hardly to be remarked that all considerations pertaining to expansions in Z can be practically useful only in those cases when the method of approximating to the atomic wave functions involves an explicit dependence on Z, such as one encounters with Fermi-Thomas potentials, for example.

4. SELECTION RULES

If we make no specialization whatever on the wave functions entering in the expression (1), we can still state the following selection rule:

A. The probability (1) vanishes unless the parity and total angular momentum of the atomic system are preserved in the transition. In the case of Russell-Saunders coupling approximation, the same rule applies also to the total orbital angular momentum and total spin operators, respectively.

This result follows at once from the following more general proposition:

If T is an Hermitian operator which commutes with the Hamiltonian H of the atomic system and if S is an operator acting on some parameters in ψ_α (it need not be Hermitian), then if S commutes with T, we have

$$(\psi_\alpha, S\psi_\beta)=0$$

if $T_\alpha \neq T_\beta$. This result is immediate:

$$0=(\psi_\alpha, TS\psi_\beta)-(T\psi_\alpha, S\psi_\beta)=(\psi_\alpha, ST\psi_\beta)-(\text{id.})$$
$$=(T_\beta-T_\alpha)(\psi_\alpha, S\psi_\beta).$$

The rule A follows from this when we take

$$S\psi(Z)=\psi(Z\pm 1). \tag{20}$$

Specializing ψ_α to wave functions properly built up from one-electron central field wave functions ("central field approximation"), as would in any case be necessary at present for all but very small Z, if one is to use available results in atomic structure, we have also the following selection rule:

B. In the central field approximation it is necessary for the nonvanishing of (1) that the initial and final wave functions comprise the same group of individual angular momentum and spin quantum number sets ("angular quantum number sets").

To simplify, we shall sketch the proof for the special case when the atomic wave functions are represented by single determinants, and we shall further suppose that the individual angular quantum number sets in one of these wave functions are all distinct. The general proof presents no essential difficulties but would lengthen our discussion.

Again, we can proceed more generally by introducing the operator S, of which in the present instance it has to be assumed that it commutes with the operators of angular momentum and of spin of an individual electron. It will be convenient to employ the ϵ-notation of determinants[21] and the summation convention for repeated indices. The summations extend over the fixed number N of electrons. Remembering also our function-inner product notation [see Eq. (11)], we find (with some modification of notation for the sake of simplifying the printing of symbols)

$$(\psi_\alpha, S\psi_\beta)=\frac{1}{N!}(\epsilon_{i_1\cdots i_N}\varphi_{i_1}(1;\alpha)\cdots\varphi_{i_N}(N;\alpha),$$

$$\times\epsilon_{j_1\cdots j_N}S\psi_{j_1}(1;\beta)\cdots S\psi_{j_N}(N;\beta))=\frac{1}{N!}\epsilon_{i_1\cdots i_N}$$

$$\times\epsilon_{j_1\cdots j_N}(\varphi_{i_1}(1;\alpha), S\varphi_{j_1}(1;\beta))\cdots(\varphi_{i_N}(N;\alpha),$$

$$S\varphi_{j_N}(N;\beta))=\epsilon_{i_1\cdots i_N}\delta(i_1,1)f(\alpha_{i_1},\beta_1)\cdots$$

$$\times\delta(i_N,N)f(\alpha_{i_N},\beta_N),$$

where $\delta(\alpha,\beta)$ equals unity if φ_α and φ_β have the same angular quantum number sets and equals zero otherwise, and

$$f(\alpha,\beta)=(R_\alpha, SR_\beta), \tag{21}$$

where R_α is the normalized radial wave function entering in φ_α. The truth of statement B in the special case considered is now apparent. In addition, we have also obtained the following result, which we state in the more general form involving the operator S: *B'. In the central field approximation with determinantal wave functions, the nonvanishing matrix elements of S are given by*

$$(\psi_\alpha, S\psi_\beta)=\pm f(\alpha_{r_1},\beta_1)\cdots f(\alpha_{r_N},\beta_N). \tag{22}$$

Here $\alpha_{r_1},\cdots,\alpha_{r_N}$ is a rearrangement of $\alpha_1,\cdots\alpha_N$ such that $\varphi_{r_i}(\ ;\alpha)$ and $\varphi_i(\ ;\beta)$ have the same angular quantum number sets and the f's are defined in (21).

[21] See, for instance, D. R. Hartree, reference 11. All we require here is merely the definition

$$\begin{vmatrix} a_{11}\cdots a_{1N} \\ \cdots\cdots \\ a_{N1}\cdots a_{NN}\end{vmatrix}\equiv\epsilon_{i_1\cdots i_N}a_{i_1 1}\cdots a_{i_N N}\equiv\sum_{i_1=1}^{N}\cdots\sum_{i_N=1}^{N}\epsilon_{i_1\cdots i_N}a_{i_1}\cdots a_{i_N N},$$

$$\epsilon_{i_1\cdots i_N}=\begin{cases}1, & \text{if } i_1,\cdots,i_N \text{ is an even permutation of the natural sequence } 1,\cdots,N\\ -1, & \text{if } i_1,\cdots,i_N \text{ is an odd permutation of this natural sequence}\\ 0, & \text{otherwise.}\end{cases}$$

We obtain a still more drastic selection rule, if we consider an expansion (12) ($\alpha \neq 0$) and suppose that we can stop with the first term. The relation (15) then yields, according to a known result in atomic theory,[20] the following proposition:

C. In the central field approximation, the first term in expansion (12) ($\alpha \neq 0$) does not vanish only if all but one of the individual quantum number sets in ψ_0 and ψ_α are identical.

One can develop similar selection rules for the succeeding coefficients in the expansion (12), but whether these can present any interest at present appears doubtful. We can, however, see very simply the behavior of such selection rules by referring to (22) and assuming that an expansion in descending powers of Z exists for the factors (21) [with S given by (20)]. It is then only necessary to consider the expansion of (22) in descending powers of Z to find that, for the coefficient of Z^{-p} in (12), we have a selection rule similar to C with p being the maximum number of sets of individual quantum numbers that are allowed to change in the transition.

5. CONCLUDING REMARKS

The discussion in this note has been directed largely toward applications to the heavier atoms. It has been based entirely on the assumption of a completely nonrelativistic treatment of the atomic system involved in the beta-induced transition. Should experimental techniques in which this information is needed become sufficiently refined, then it would no doubt become desirable to examine for the innermost shells of the very heavy atoms also some relativistic corrections;[22] and possibly also some corrections that arise from using a central field approximation for the atomic wave functions.[23] At present such corrections appear to lie entirely outside the scope of experimental requirements.

Of much more immediate importance in questions concerned with the average ionization appearing in the daughter atom after a beta-decay, is the determination of the secondary Auger type ionization which accompanies the primary beta-induced excitation. Two difficulties are encountered here at present. Auger coefficients are fairly well known for the K shell, but the available information regarding the higher shells is largely incomplete.[24] Auger type transitions can occur not only from ionized states but also from some quasi-bound states (known also as "virtual" states) with energies overlapping the continuum levels[25] and the corresponding contribution to the resulting average ionization may be important in some instances, especially in the case of the lighter atoms.[26]

We have in preceding sections adduced some arguments which cast doubt on the general adequacy of the one-electron hydrogenlike wave function approximation. It is of some interest, however, pending more precise calculations, to apply it for finding an estimate of the mean beta-induced ionization in A^{37}, for which there now exists a measured value.[5] This will now be done using Slater's suggestions for Z_{eff}.[27]

Consulting Table II, we find that the probability of ionization of the single remaining K electron subsequent to K capture[28] is of order of 10^{-3}, and the total probability of ionization from the L and M shells is of the order of 10^{-2} and 5×10^{-2}, respectively. It follows that if the hydrogenlike wave function approximation and the use of (1) in the present case are adequate at least as far as order of magnitude of the mean ionization is concerned, then the principal contribution to this mean ionization must come from the Auger cascade in the filling of the K shell vacancy. It is difficult to see how this can lead to the published value of 3.85 charge units.[29] It is thus seen that a more thorough investigation of this case would be desirable, especially as there exist calculations of wave functions for both argon and chlorine.[11]

---

[22] For the corresponding question in the case of the Auger effect, see H. S. W. Massey and E. H. S. Burhop, Proc. Roy. Soc. (London) **153**, 661 (1936).

[23] A discussion of the limitations inherent in the central field approximation is given in V. Fock and M. Petrashen, Physik. Z. Sowjetunion **8**, 359 (1935).

[24] See B. B. Kinsey, Can. J. Research **26A**, 404 (1948), and references given therein.

[25] See, for instance, Condon and Shortley, reference 20, chapter 15, Sec. 3

[26] This point is strikingly illustrated in the case of He^6: A. Winther, reference 6.

[27] J. C. Slater, Phys. Rev. **36**, 57 (1930). This is done here for lack of any other known appropriate method of fixing Z_{eff} (although it must be observed, that the wave functions that enter in Slater's analysis are *not* hydrogenlike, and he in fact employs in addition to an effective Z also an effective principal quantum number). This procedure has been followed also in other similar connections. See reference 18 as well as the following theoretical papers on the Auger effect: E. H. S. Burhop, Proc. Roy. Soc. (London) **148**, 272 (1935); L. Pincherle, Nuovo cimento **12**, 81 (1935); E. P. Cooper, Phys. Rev. **61**, 1 (1942).

[28] The applicability of expression (1) in the case of electron capture, with ψ_0 representing the state of the initial atom with one electron missing from the K shell, requires elucidation.

[29] See a relevant discussion in E. P. Cooper, reference 27, Sec. 2 and especially Table I.

Solutions of Sodium in Liquid Ammonia

WILLIAM N. LIPSCOMB
School of Chemistry, University of Minnesota, Minneapolis 14, Minnesota
(Received July 21, 1952)

Modifications of Ogg's treatment of the electron in a spherical cavity in liquid ammonia lead to a radius of about 4.8A or slightly less, in reasonable agreement with the corrected experimental value of 3.2A. Some specific quantum-mechanical interactions appear to be necessary in order to make the electron stable.

OGG[1] has developed Kraus' proposal that solutions of alkali metals in liquid ammonia consist of positive ions and trapped electrons. Ogg's model for trapped unpaired electrons is a spherical cavity of radius 10A (volume, 4200A^3), and of energy -0.4 ev. The large size of these traps has been the subject of both experimental and theoretical controversy,[2] but it appears likely that the volume of a dilute solution is greater than the sum of the volumes of the constituents by about 43 cc per mole of electrons. Assuming a spherical cavity the experimental radius is thus 2.6A (volume, 72A^3). The experimental value[1] of the energy is -0.8 ev. The present note outlines a physical basis for somewhat more reasonable agreement between these values.

The experimental value of 2.6A is too small, because of the neglect of the volume change when sodium atoms are converted to Na^+ and because of electrostriction effects around Na^+. The volume per sodium atom in the metal may be calculated from the density to be 39.4A^3, from which we subtract the volume, 3.6A^3 of Na^+, to get a volume decrease of 36A^3. The electrostriction effect may be estimated roughly from the densities[3] of solutions of NH_4Cl and NaCl in liquid ammonia at -30°C, which indicate volume contractions of 25A^3/ion-pair of NH_4Cl and 45A^3/ion-pair of NaCl. The greater value for NaCl suggests that the smaller, positive ions are chiefly responsible for the contractions, and one might guess that about 10A^3 would be associated with Cl^-, which would leave 35A^3 as the contraction due to Na^+. Thus the volume to be associated with an electron in liquid ammonia is $72+36+35=143$A^3, corresponding to a sphere of radius, $a=3.2$A.

Ogg's theoretical value was derived from the potential energy function $U_1=-(e^2/2a)(1-1/K)$, and neglects surface tension, electrostriction, and the electronic polarization in the dielectric surrounding the spherical cavity. In the following treatment of the variable parts of the electrostriction and electronic polarization as first-order perturbation effects we shall use for the ground-state wave function

$$\psi^0=\frac{1}{\pi}\left(\frac{\alpha}{2}\right)^{\frac{1}{2}}\frac{\sin\alpha r_1}{r_1},$$

which is the solution of the equation

$$\frac{d^2\psi^0}{dr_1{}^2}+\frac{2d\psi^0}{r_1dr_1}+\alpha^2\psi^0=0,$$

where $\alpha^2=8\pi^2m(E^0-U)/h^2$, r_1 defines the distance of the electron of mass m from the center of a spherical cavity of radius a, and U, the potential energy, is a constant. The total energy E^0 is determined by the first zero of ψ^0 so that $\alpha a=\pi$. Thus we assume that ψ^0 is normalized with respect to integration over the sphere, and therefore that the electron does not penetrate into the dielectric. Modification of this assumption would permit a slightly smaller cavity.

The potential problem must now be solved. We shall assume that the polarization associated with orientation of permanent dipoles cannot follow the electronic motion, and hence gives rise to a constant surface charge density $\sigma_1=e_1/4\pi a^2$. In order to satisfy the potential distribution we require that $e_1=e(1-\nu^2/K)$, where the dielectric has low frequency dielectric constant K and refractive index ν. Now the potentials inside ($V_i=-e/|\mathbf{r}-\mathbf{r}_1|+\varphi$) and outside ($V_0$) of the cavity may be expanded in Legendre polynomials,

$$V_i=-\frac{e}{r}\sum_{n=0}^{\infty}\left(\frac{r_1}{r}\right)^n P_n(\mu)+\sum_{n=0}^{\infty}B_nr^nP_n(\mu),\quad r_1\leqslant r\leqslant a \quad (1)$$

$$V_0=\sum_{n=0}^{\infty}\frac{C_n}{r^{n+1}}P_n(\mu),\qquad r\geqslant a \quad (2)$$

where $\mu=\cos\theta$, and the B_n and C_n are determined by the boundary conditions at $r=a$, $V_i=V_0$, and $(\partial V_i/\partial r)=\nu^2(\partial V_0/\partial r)+4\pi\sigma_1$. Solution of these equations[4] for φ, the second term of (1), yields for the mutual potential energy of the charge distribution,

$$U_2=-\frac{e}{2}(\varphi)_{\substack{r=r_1\\ \theta=0}}=-\frac{e^2}{2a}\left(1-\frac{1}{\nu^2}+\frac{e_1}{e\nu^2}\right)+U_3, \quad (3)$$

[1] R. A. Ogg, Jr., J. Am. Chem. Soc. **68**, 155 (1946); Phys. Rev. **69**, 668 (1946).
[2] A. J. Stosick and E. B. Hunt, J. Am. Chem. Soc. **70**, 2826 (1948); Johnson, Meyer, and Masters, J. Am. Chem. Soc. **72**, 1842 (1950).
[3] S. Kikuti, J. Soc. Chem. Ind. Japan **42**, Suppl. Binding, 15 (1939).
[4] See T. L. Hill, J. Chem. Phys. **16**, 394 (1948); J. G. Kirkwood, J. Chem. Phys. **2**, 351 (1934).

where, defining $x=r_1/a$,

$$U_3=-\frac{e^2}{2a}\left(1-\frac{1}{\nu^2}\right)\sum_{n=1}^{\infty}\frac{x^{2n}}{\left[1+\dfrac{n}{\nu^2(n+1)}\right]}. \quad (4)$$

The correction for electrostriction arises from the fact that the dielectric constant varies with density. For the hydrostatic pressure due to electrostriction we write[5]

$$p=\frac{E_0^2}{8\pi}\rho\frac{\partial K}{\partial\rho}, \quad (5)$$

where ρ is the density of the medium. Now for the term involving permanent polarization of the dielectric of constant K, we assume that $E_0=-e/Kr^2$, as if the electron were at the center of the sphere. Evaluation of $\partial K/\partial\rho$ depends on the model of the liquid, but we shall estimate $\partial \ln K/\partial \ln\rho=1.3$, based on experimental data discussed for a number of other polar liquids.[6] This value is in agreement with that expected from Kirkwood's model, but quite different from that given by the Clausius-Mossotti equation. The potential energy is then

$$U_4=-\int_a^{\infty}p4\pi r^2dr=\frac{-1.3}{2K}\frac{e^2}{a}. \quad (6)$$

Now we must introduce a potential energy U_5 due to electronic polarization of the dielectric. We modify Eq. (5) by replacing K by ν^2, and calculate the mean value of $E_0^2=(\partial V_0/\partial r)^2+r^{-2}(\partial V_0/\partial\theta)^2$ by averaging over all angles,

$$\langle E_0^2\rangle_{Av}=\tfrac{1}{2}\int_0^{\pi}E_0^2\sin\theta d\theta=\sum_{n=0}^{\infty}\frac{C_n^2(n+1)}{r^{2n+4}}.$$

The derivative $\partial\nu^2/\partial\rho$ was evaluated from the Clausius-Mossotti equation, and an integration similar to that of Eq. (6) was carried out to give, for the part of the potential energy not included in (6),

$$U_5=-\frac{e^2}{6a}\frac{(\nu^2+2)(\nu^2-1)}{\nu^4}\times\sum_{n=1}^{\infty}x^{2n}\frac{2n+1}{(n+1)\left[1+\dfrac{n}{\nu^2(n+1)}\right]^2}. \quad (7)$$

For the energy associated with surface tension we take $U_6=4\pi a^2\gamma$, where there is considerable question about the value of γ. However, it seems reasonable[7] to choose a value greater than that ($\gamma=32$ ergs/cm² at -33°C) for the plane surface, and calculations are given for both this value and a value 50 percent greater. A maximum value for γ could be estimated by considering the removal of molecules from within the liquid, and then allowing the weak "bonds" thus broken to reform in the surface layer of the resulting cavity. From the heat of vaporization this excess surface energy can be estimated as roughly 100 ergs/cm² for very small holes.

We now calculate the total energy of the system. The unperturbed value E^0 is

$$E^0=U+\frac{h^2}{8ma^2},$$

where, assuming $K=22$ and $\nu^2=1.9$,

$$U=(U_2-U_3)+U_4+U_6$$
$$=-0.48\frac{e^2}{a}-0.03\frac{e^2}{a}+4\pi a^2\gamma.$$

The integrals arising from the perturbation potentials U_3 and U_5 were evaluated by graphical integration to give,

$$E_3=-0.10\frac{e^2}{a} \quad \text{and} \quad E_5=-0.08\frac{e^2}{a}.$$

Thus, the total energy is

$$E=-0.69\frac{e^2}{a}+4\pi a^2\gamma+\frac{h^2}{8ma^2}. \quad (8)$$

The equilibrium value of a for the ground state may be found from $dE/da=0$, and may then be substituted into (9) to calculate the minimum energy E_m.

Numerical values are, for $\gamma=32$ ergs/cm², $a=4.8$A and $E_m=+0.13$ ev. For $\gamma=48$ ergs/cm², $a=4.5$A and $E_m=+0.40$ ev. The values of the radius are only somewhat larger than the corrected experimental value, and are relatively insensitive to the coefficients. On the other hand, the values of E_m represent the differences between large terms; for the first example the three terms in Eq. (8) are -2.06, 0.58, and 1.61 ev, respectively. Only a small increase in the numerical value of the coefficient 0.69 would be required to make E_m negative. In fact if this coefficient is regarded as a parameter, a choice of 1.00, an increase of 45 percent, would give the values $a=4.2$A and $E_m=-0.87$ ev if $\gamma=32$ ergs/cm², or $a=3.9$A and $E_m=-0.66$ ev if $\gamma=48$ ergs/cm². Thus, this choice of a single parameter[8] would give reasonable agreement for both the radius and energy.

Within the limitations of the assumption of a continuous dielectric medium the agreement between theory and experiment is not unreasonable. Although the attractive potential $-0.69\ e^2/a$ represents about two-thirds that necessary to give good agreement, it seems

[5] W. R. Smythe, *Static and Dynamic Electricity* (McGraw-Hill Book Company, Inc., New York, 1939), p. 33; also pp. 134–135.
[6] I. S. Jacobs and A. W. Lawson, J. Chem. Phys. **20**, 1161 (1952).
[7] R. C. Tolman, J. Chem. Phys. **17**, 333 (1949); J. G. Kirkwood and F. P. Buff, J. Chem. Phys. **17**, 338 (1949).
[8] The agreement with experiment of this parametric treatment of the radius is even better if the experimental energy of -1.7 ev (W. L. Jolly, Chem. Revs. **50**, 351 (1952)) is assumed.

difficult to avoid the conclusion that some additional attractive potential is necessary, and is probably to be associated with interactions of the electrons with the protons oriented toward the center of the cavity. Assuming that the N—H bond is about 20 percent ionic, such additional, quantum-mechanical interactions can probably be treated by perturbation or variation methods. In order to provide a polarization charge of magnitude e_1, and to give a potential energy proportional to a^{-1}, the number of protons interacting quantum mechanically with the electron probably must be assumed to be independent of a.

It is interesting to compare the experimental value of the volume with that associated with one NH_3 molecule. The density of 0.68 g/cm³ of NH_3 at −30°C leads to a volume of 41A³ per molecule, which is equivalent to a sphere of radius, $a=2.1$A. Assuming cubic close packing of spherical molecules of radius a, the total volume remaining inside a sphere of radius $2a$ is about 100A³ (radius of equivalent sphere, 2.9A) with which the theoretical values (250 to 460A³) should be compared. Thus, the type of cavity in which the free electron is trapped is only somewhat greater than the ordinary imperfection caused by complete displacement of one molecule, and hence resembles the expected type of electron traps in molecular crystals.

It is difficult to see how the very large electron traps proposed by Ogg can give high electronic conductivity in very dilute solutions, because the wave function of the electron probably extends less than a diameter away, and because the activation necessary for the process of creation of a new hole and disappearance of the old one will not be available. On the other hand, if the traps are comparable with ordinary imperfections the high electronic conductivity could easily persist even in very dilute solutions.

THE JOURNAL OF CHEMICAL PHYSICS VOLUME 21, NUMBER 1 JANUARY, 1953

On the Temperature Dependence of the Optical Absorption of β−Ag_2S

KURT LEHOVEC*
Signal Corps Engineering Laboratory, Fort Monmouth, New Jersey
(Received July 14, 1952)

The shift with temperature of the absorption edge for β-Ag_2S was measured on a Ag_2S ingot and a Ag_2S sheet prepared by tarnishing of Ag in sulfur vapor. The measurements indicate a shift in energy of about −1.2 to -1.9×10^{-3} ev/degree. This value is used to explain the abnormally high value of the numerical factor in front of the exponential term in the expression of conductivity *vs* temperature. If the change in absorption with temperature is due to the decrease in lattice extension, one should expect a decrease in conductivity with increasing pressure of $(1/\sigma\cdot d\sigma/dp)\sim-0.42/T$ (T in degrees Kelvin, p in atmospheres). In the course of this study the linear expansion coefficients of β-Ag_2S (15.2×10^{-6} per degree) and of α-Ag_2S (37.5×10^{-6} per degree) have been measured.

INTRODUCTION

THE stable modification of silver sulfide below 179°C is β-Ag_2S. If β-Ag_2S is in equilibrium with excess sulfur, the conductivity is comparatively low and can be described by the equation

$$\sigma^s=8\times10^8\exp(-0.92/kT). \quad (1)$$

If β-Ag_2S is in equilibrium with excess silver, the conductivity is comparatively high and can be described by the equation

$$\sigma^{Ag}=6\times10^6\exp(-0.58/kT) \quad (2)$$

(σ in ohm^{-1} cm^{-1}, kT in ev).[1] The equations above given for the conductivity refer to total conductivity (electronic plus ionic conductivity). Transference measurements by Tubandt[2] have shown that β-Ag_2S conducts in part by electrons and in part by silver ions. In sulfur-rich, poorly conducting material the ionic transference number is 0.8 at 170°C and increases slowly with decreasing temperature.[2] Because of the similar order of magnitude of electronic and ionic part of conductivity and because of the slow dependence of ionic transference number on temperature,[2] the equations given for σ^s should describe approximately the electronic part of the conductivity. The increased conductivity of silver-rich material arises presumably from an increase in the electronic conduction.

In the equations for conductivity the large value of the coefficient is worth noticing. In a semiconductor with exponential temperature dependence of the electronic conductivity, we have

$$\sigma=(NZ)^{\frac{1}{2}}eb\exp(-W/kT), \quad (3)$$

where b is the electron mobility; $e=1.6\times10^{-19}$ amp sec (electronic charge); k the Boltzman constant, T the absolute temperature. N and Z are the densities of energy states, from which the electrons are released and to which the electrons are excited, respectively. W is half of the energy needed to transfer an electron from a lower energy state (density N) to an upper energy

* Now at Sprague Electric Company, North Adams, Massachusetts.

[1] H. Reinhold and H. Möhring, Z. physik. Chem. **B28**, 178 (1935).

[2] C. Tubandt, Z. Elektrochemie **26**, 358 (1920).

state (density Z). In case of electronic conduction Z is the equivalent density of energy states in the conduction band: $Z\sim 2.57\times 10^{19}(m^*/m)^{\frac{3}{2}}(T/300)^{\frac{3}{2}}$ (in degrees Kelvin; m^*/m is the effective mass ratio of electrons in the conduction band). The lower energy states may be either impurities (impurity conduction) or the energy states of the "filled band" (intrinsic conduction).[3] In either case we expect $N<10^{22}$ cm^{-3}.

In an attempt to interpret Eqs. (1) and (2) by Eq. (3) one may set $W=0.92$ or 0.58 ev, respectively, and $(NZ)^{\frac{1}{2}}eb=8\times 10^8$ ohm^{-1} cm^{-1}, or 6×10^6 ohm^{-1} cm^{-1}, respectively. From the latter equation one obtains $N=1/Z(6\times 10^6/eb)^2$. The order of magnitude of Z should be 10^{20} cm^{-3}, and that of $b\approx 10^2$ cm^2/volt sec (or smaller). Using these values and $e=1.6\times 10^{-19}$ amp sec, we obtain $N\gtrsim 10^{27}$ cm^{-3}. This value is, of course, impossibly large. Using the numerical value 8×10^8 ohm^{-1} cm^{-1}, even larger values are obtained. The difficulties can be resolved, however, if one assumes that the activation energy W is temperature dependent:

$$W=W_0-(dW/dT)\cdot T;\quad (dW/dT)>0; \qquad (4)$$

then a factor $\exp(dW/kdT)$ enters in front of the temperature dependent exponential term $\exp(-W_0/kT)$ in the expression of conductivity.

ABSORPTION EDGE OF Ag_2S AS FUNCTION OF TEMPERATURE

There is some independent optical evidence of a strong decrease with temperature of an energy gap in β-Ag_2S. Coblentz[4] measured photoelectric response of natural silver sulfide crystals and found a large shift of the sensitivity curve with decreasing temperature. Gudden[5] noticed the unusually large value of the shift of photoelectric response (several tenths of a micron by a change of temperature by 180°C) but considered it as arising from a secondary effect (use of a different electric field strength at room temperature and at liquid air temperature, respectively, in Coblentz' experiments).

We have measured the change in the position of the lattice absorption edge with temperature between room temperature and 179°C. The silver sulfide was prepared by two methods: (a) A silver foil (4 mil thick) was transformed into Ag_2S by exposure to sulfur vapors at 200°C; (b) a Ag_2S ingot with a small excess of Ag was made by slow withdrawal of a melt in a closed evacuated quartz tube from a furnace. A slice of Ag_2S of 0.1 cm thickness was cut from the Ag_2S. The surfaces of the slice were polished.

Figure 1 shows transmission curves as a function of temperature. The width of the absorption edge may

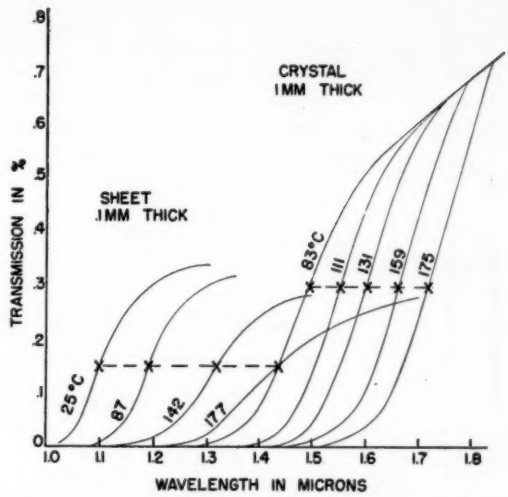

FIG. 1. Spectral transmission of (1) sulfurized silver sheet (sulfur-rich), and (2) β-Ag_2S-crystal grown from a melt (silver-rich) as function of temperature. The temperature in °C is indicated in the figure. The dotted line connects the points from which the dependence of the "absorption edge" on the temperature was calculated.

have been increased due to the comparatively large slit width (of 350–600 microns) used in taking the absorption measurements. The points connected by a dotted line have been used to calculate the dependence of the absorption edge on temperature. The temperature dependence of the photon-energy, corresponding to the absorption edge, can be described by (E in ev, and T in degrees Kelvin)

$E=1.7-1.9\times 10^{-3}T$ (for the tarnished sheet of Ag_2S, sulfur-rich), (5)

and

$E=1.26-1.2\times 10^{-3}T$ (for Ag_2S ingot, silver-rich). (6)

More emphasis should be laid on the temperature coefficient than on the value at $T=0$, since no correction for the shift in the absorption edge with the thickness of the samples was made.

DISCUSSION

Let us attempt to correlate the large shift with temperature of the optical absorption edge with the large value of the coefficient of electric conductivity. Then we have to identify $E/2$ in Eq. (5) and (6), respectively, with W of Eq. (4). We then obtain $W=0.85$ (Eq. 5) and 0.63 (Eq. 6), respectively. These values agree closely with the activation energies derived from the temperature dependence of conductivity measurements on sulfur-rich and sulfur-poor materials (0.58 and 0.92 ev). Since the value for the absorption edge at zero absolute temperature is somewhat uncertain, owing to the differences in the thickness of the sample, the agreement may be fortuitous. From the temperature dependence of the absorption edge follows a factor $\exp(dE/2kdT)=6\times 10^4$ (Eq. 5) and 1.1×10^3 (Eq. 6). Dividing the values of the coefficient in the measured

[3] In this case there should be also a contribution of holes to the conduction; this should not affect, however, the order of magnitude of conductivity, with which we shall be concerned only.

[4] W. W. Coblentz, "Spectrophotoelectrical sensitivity of argentite," Scient. Pap. Bur. of Standards, No. 446 (1922).

[5] B. Gudden, *Lichtelektrische Erscheinungen* (Julius Springer, Berlin, 1929), p. 178.

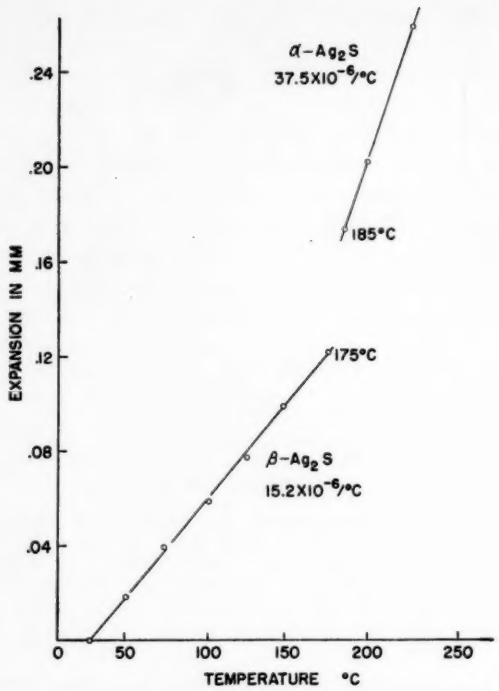

FIG. 2. Expansion of a polycrystalline silver sulfide rod (5 cm long) as function of temperature. Values of expansion coefficient are given in the figure.

expression for conductivity (Eqs. 1 and 2) by these factors, we obtain 1.2×10^4 ohm^{-1} cm^{-1}, and 6×10^3 ohm^{-1} cm^{-1}. These values are still somewhat large, but already of an order of magnitude, which could be explained by the factor $(NZ)^{\frac{1}{3}}eb$.

In spite of the apparent relation between the shift of the absorption edge and the high value of the coefficient in the expression of the conductivity, there remain some points to be cleared up. It is not clear how the increase in conductivity with silver content can be correlated with a shift in the optical absorption edge. One may speculate, perhaps, that the lattice disorder introduced by excess of silver causes a local expansion of the lattice, which is equivalent to an increase in temperature.

PRESSURE DEPENDENCE OF CONDUCTIVITY

The unusually high value of the shift in optical absorption edge with temperature invites some further speculation.

If the shift in absorption with temperature is due to the lattice expansion, one would expect a pressure dependence

$$dE/dp=(dE/dT)\cdot(dT/da)\cdot(da/dp)$$
$$=(dE/dT)\cdot(dT/da)\cdot(a/3V)\cdot(dV/dp).$$

The linear expansion of a polycrystalline β-Ag_2S rod (prepared by tarnishing of silver wire) was measured, and found $da/adT=+15.2\times10^{-6}$ per degree (Fig. 2). The value

$$(1/V)\cdot(dV/dp)=-2.7\times10^{-6} \text{ per atmos}$$

is listed in the International Critical Tables. Using the value $dE/dT=-1.2\times10^{-3}$ ev/degree for our ingot, we have

$$(dE/dp)=(1.2\times10^{-3}\times2.7\times10^{-6})/(15.2\times10^{-6}\times3)$$
$$=+7.1\times10^{-5} \text{ ev/atmos.}$$

Since the conductivity is proportional to $\exp(-E/2kT)$, we have

$$(1/\sigma)\cdot(d\sigma/dp)=-(2kT)^{-1}\cdot(dE/dp)$$
$$=-0.42/T \text{ (per atmos).}$$

This value compares favorably with that of the pressure-conductivity dependence exhibited by tellurium. From the analysis of Bridgman's data[6] by Bardeen,[7] we obtain (at ~15,000 atmos) $dE/dp\approx1.2\times10^{-5}$ ev/atmos. Thus, $(1/\sigma)\cdot(d\sigma/dp)\approx0.07/T$ in the intrinsic range of tellurium.

The pressure dependence of resistivity of Ag_2S is reported to our knowledge only once in the literature,[8] and that paper concerns a polycrystalline sample. The resistance is found to decrease with pressure. The calculations above indicate an increase of resistance with pressure. It is conceivable that the resistance of polycrystalline Ag_2S is determined by grain boundaries. Measurements of the pressure dependence of the resistance of Ag_2S single crystals are highly desirable to clarify the situation.

Alternatively, the shift in the absorption edge with temperature may be due to the increase in lattice disorder. Then one may expect a pressure effect on conductivity also. However, this effect can not be related theoretically in a simple manner to the temperature effect.

In the case of an effect due to expansion, the pressure effect should be rather instantaneous; in the case of an effect due to disorder, the pressure effect should be comparatively slow.

CONCLUSIONS

The numerically high value of the coefficient in front of the exponential term of the conductivity *vs* temperature equation of β-Ag_2S is attributed to a strong decrease of ionization energy of carriers of electric conduction with increasing temperature. The decrease of ionization energy of carriers of conduction with increasing temperature is linked to a strong shift of the absorption edge to a longer wavelength with increasing temperature, and is of the order of -1.2 to -1.9×10^{-3} ev/degree.

The strong temperature dependence of the absorption edge may be related to (a) lattice expansion or (b) disorder. In the first case a strong decrease in conductivity with increasing pressure $((1/\sigma)\cdot(d\sigma/dp)\sim-(0.42/T)$

[6] P. S. Bridgman, Proc. Am. Acad. Sci. **72**, 159 (1938).
[7] J. Bardeen, Phys. Rev. **75**, 1888 (1949).
[8] F. Monten, Ark. Astr. Fys. **4**, No. 31 (1908).

atmos^{-1}) may be expected. In order to clarify the situation, measurements of the effect of pressure on conductivity and on optical absorption of single crystals of β-Ag_2S are desirable.

I wish to express my appreciation to several coworkers, who helped in the preparation of the data: Mr. J. Broder for the preparation of the Ag_2S, Mr. J. Stanley for the growth of the Ag_2S single crystal from a melt, Mr. A. Spell and Mr. M. Polk for the optical transmissency measurements, Mr. L. Tolman for the thermal expansion measurements, and also Mr. J. Rosen for discussion of the manuscript.

THE JOURNAL OF CHEMICAL PHYSICS VOLUME 21, NUMBER 1 JANUARY, 1953

Millimeter Wavelength Dispersion of Water Vapor

GEORGE BIRNBAUM
National Bureau of Standards, Washington, D. C.
(Received June 27, 1952)

Dispersion due to water vapor in the wavelength region ∞ to 0.6 mm is computed by means of quantum-mechanical formulas. The dispersion is attributed to: (1) The contributions of the 11 rotational lines in the region considered; these are obtained with a dispersion equation characteristic of collision theory specialized to sharp lines. (2) The combined contribution of all rotational lines of shorter resonance wavelength. This is obtained with the aid of the well-known shape factor $(\nu_n^2-\nu^2)^{-1}$, which is shown to be valid for sharp lines independent of any special model.

The strongest line, 3_1–4_{-3}, occurs at 0.794 mm, and it gives rise to a maximum change in susceptibility $\epsilon'-1$ of 8.2×10^{-6} for 1 atmos of air containing 1 percent water molecules. The increase in $\epsilon'-1$ from ∞ to 0.6 mm is about twice this value. If the very small effect of the 1.35-cm line is neglected, a simple equation for $\epsilon'-1$ holds from ∞ to 2 mm.

I. INTRODUCTION

THE value of the electric susceptibility of water vapor is required for several different branches of experimental work in the radio and microwave regions of the electromagnetic spectrum; consequently, many measurements of this quantity have been made. Recent measurements at centimeter wavelengths[1] have shown the value to be in close agreement with the one at long wavelengths, but such a result is not likely to be true of the millimeter region where the absorption due to the rotational resonances become quite strong. No measurements have been made as yet in the millimeter region. To obtain values for the susceptibility there as well as to provide a guide for future experiments, we have calculated the dispersion in the wavelength region ∞ to 0.6 mm. Since no similar microwave dispersion problem has been treated thus far, the present calculations are given in some detail. A parallel calculation for the absorption has been reported by Van Vleck.[2]

This paper deals with water vapor under atmospheric conditions for which the rotational lines, except the very weak one at 1.35 cm, may be considered as narrow. The widths of these lines arise almost entirely from molecular collisions; for this reason the effect of a particular resonance is calculated from an equation based on impact theory.

To obtain the effect of the line tails associated with resonances shorter than 0.6 mm, the dispersion form $(\nu_n^2-\nu^2)^{-1}$, is used. This is given by impact theory to be sure. However, it is shown by means of the integral transformation between susceptibility and absorption that this form is generally valid for narrow lines independent of any special model.

II. THEORY OF DISPERSION AND DIELECTRIC CONSTANT

A general quantum-mechanical equation for dispersion has been described by Van Vleck and Weisskopf.[3] This equation, basic to the calculations here, may be written in the form

$$(\epsilon_\nu'-1)(RT/3p)=(4\pi N_0/9hG)\sum_j\sum_i|\mu_{ij}|^2 \times[F(\nu_{ij},\nu)/\nu_{ij}]g_j\exp(-E_j/kT). \quad (1)$$

Here, ϵ_ν' is the dipole contribution to the dielectric constant relative to free space at frequency ν; R is the gas constant; p is the pressure; N_0 is Avogadro's number; ν_{ij} is the characteristic frequency associated with a transition between the states i and j and is defined by $\nu_{ij}=(E_i-E_j)/h$; μ_{ij} is the corresponding electric moment matrix element, $g_j\exp(-E_j/kT)$ is the probability of the state j; and G is the rotational partition function and is defined by $G=\sum_j g_j\exp(-E_j/kT)$. The shape factor $F(\nu_{ij},\nu)$, appropriate for spectral lines in the microwave region when broadening is due to collisions, is defined by

$$F(\nu_{ij},\nu)=\frac{\Delta\nu^2+\nu_{ij}(\nu+\nu_{ij})}{\Delta\nu^2+(\nu+\nu_{ij})^2}+\frac{\Delta\nu^2-\nu_{ij}(\nu-\nu_{ij})}{\Delta\nu^2+(\nu-\nu_{ij})^2}, \quad (2)$$

[1] G. Birnbaum and S. K. Chatterjee, J. Appl. Phys. **23**, 220 (1952).

[2] J. H. Van Vleck, Phys. Rev. **71**, 425 (1947). The following typographical errors were noticed on p. 427: (1) the constant c should be omitted from Eq. (2); and (2) the factor in the last line of note 10 should read $hG\mu_0^2/2kT\bar{\nu}^2$.

[3] J. H. Van Vleck and V. F. Weisskopf, Revs. Modern Phys. **17**, 227 (1945).

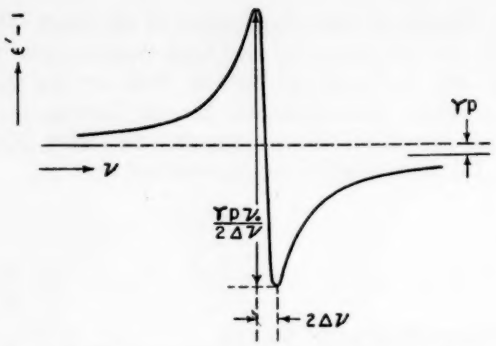

FIG. 1. Dispersion associated with a spectral line [according to Eqs. (9) and (2)].

according to the theory of Van Vleck and Weisskopf.[4] The symbol $\Delta\nu$ represents a line-width parameter; ν_{ij}, ν, and $\Delta\nu$ are in cps. If the line width is small compared with the resonance frequency, Eq. (2) in the immediate vicinity of resonance becomes

$$F(\nu_{ij},\nu)=\nu_{ij}(\nu_{ij}-\nu)/[\Delta\nu^2+(\nu-\nu_{ij})^2]. \quad (3)$$

In addition, if the frequency is sufficiently removed from resonance, i.e., $|\nu-\nu_{ij}|\gg\Delta\nu$, Eq. (2) reduces to

$$F(\nu_{ij},\nu)=2\nu_{ij}^2/(\nu_{ij}^2-\nu^2). \quad (4)$$

To the same degree of approximation, Eqs. (3) and (4) are also obtained from the collision theory of Lorentz. Equation (4) yields a dispersion curve of the familiar Sellmeier form characteristic of classical theory.

Let us consider now Eq. (1) at zero frequency, where $F(\nu_{ij},0)$ takes the value 2. Starting with an equation in this form Van Vleck[5] has derived the well-known equation of Debye, which gives the dipole contribution to the static dielectric constant. We will briefly sketch this derivation not only because of its interest here, but also to exhibit some relations which will be of use later.

If the spacing of the energy levels $h\nu_{ij}$ is small as compared with kT, then[6]

$$\frac{e^{-E_j/kT}}{\nu_{ji}}+\frac{e^{-E_i/kT}}{\nu_{ij}}\simeq\frac{h}{2kT}(e^{-E_j/kT}+e^{-E_i/kT}), \quad (5)$$

where $\nu_{ij}=-\nu_{ji}$. The negative frequency allows for the induced emission of radiation by the molecule. On account of Eq. (5) and the condition $\nu=0$, Eq. (1) becomes

$$(\epsilon_0'-1)\frac{RT}{3p}=\frac{4\pi N_0}{9kT}\frac{\sum_j\sum_i|\mu_{ij}|^2g_j\exp(-E_j/kT)}{\sum_j g_j\exp(-E_j/kT)}. \quad (6)$$

With the additional assumption that the molecule has a permanent moment μ equal for all stationary states, *viz.*,

$$\sum_i|\mu_{ij}|^2=\mu_{jj}^2=\mu^2,$$

Eq. (6) simplifies to

$$(\epsilon_0'-1)(RT/3p)=4\pi N_0\mu^2/9kT, \quad (7)$$

which was first derived by Debye from purely classical considerations.

III. EFFECT OF A SINGLE LINE

Before proceeding further the notation will be specialized to apply directly to the water molecule. This molecule is an asymmetrical top with rotational energy levels specified by the quantum numbers J and τ; thus, j and i are to be replaced by $J\tau$ and $J'\tau'$, respectively. The quantity $g_\tau=2-(-1)^{|\tau|}$ is the statistical weight which is caused by nuclear spin, and $|\mu_{J\tau,J'\tau'}|^2$ is equal to $\mu^2A_{J\tau,J'\tau'}$. Here $\mu=1.84\times10^{-18}$ esu, and $A_{J\tau,J'\tau'}$, which includes the statistical weight $2J+1$, is the so-called line strength. This is the same as $\sum|\Phi|^2$ in the notation of King, Hainer, and Cross,[7] who accurately calculated its value for all possible transitions between energy levels through $J=6$. Line frequencies can be calculated from the rotational energy levels of the ground vibrational state.[8]

The dielectric constant associated with a single spectral line is obtained from Eq. (1) as

$$\frac{\epsilon'_{J\tau,J'\tau'}-1}{p}=\frac{4\pi N_0\mu^2g_\tau A_{J\tau,J'\tau'}F(\nu_{J\tau,J'\tau'},\nu)}{3hGRT\nu_{J\tau,J'\tau'}}\times(e^{-EJ\tau/kT}-e^{-EJ'\tau'/kT}). \quad (8)$$

This may be written in the compact form

$$(\epsilon'_{J\tau,J'\tau'}-1)/p=\gamma_{J\tau,J'\tau'}F(\nu_{J\tau,J'\tau'},\nu)/2, \quad (9)$$

TABLE I. Lines in the pure rotational spectrum of water vapor from 0 to 19 cm^{-1}. The first and second columns list the quantum numbers of the lower and upper states, respectively, and the third column lists the resonance wave numbers. The quantities listed in the fourth and fifth columns are defined in Fig. 1. $p=7.6$ mm Hg, $\Delta\nu=0.1$ cm^{-1}.

$J\tau$	$J'\tau'$	$\nu_{J\tau,J'\tau'}/c$	$\gamma_{J\tau,J'\tau'}p\times10^3$	$(\gamma_{J\tau,J'\tau'}p\nu_{J\tau,J'\tau'}/2\Delta\nu)10^3$
5_{-1}	6_{-5}	0.742[a]	1.994	0.074
2_2	3_{-2}	6.15	5.292	1.63
9_{-3}	10_{-7}	10.78	0.04823	0.0260
4_0	5_{-4}	10.80	1.902	1.03
3_1	4_{-3}	12.59	12.98	8.2
11_{-8}	10_{-4}	13.00	0.003919	0.00255
5_5	6_1	14.60	0.7725	0.56
3_3	4_{-1}	14.87	9.682	7.2
5_4	6_2	15.54	0.2577	0.200
4_4	5_0	15.71	1.054	0.83
7_{-6}	6_{-2}	16.25	0.1879	0.153
1_{-1}	1_1	18.60	395.2	3.77×10^2

[a] This is the experimentally determined value. All the others are calculated from the energy levels.

[4] This shape factor has also been derived by H. Fröhlich, Nature **157**, 478 (1946).

[5] J. H. Van Vleck, *The Theory of Electric and Magnetic Susceptibilities* (Oxford University Press, London, 1932), Chap. 7.

[6] It may be sufficiently accurate to equate the sum of the exponentials to $2\exp(-E_j/kT)$, a form which is convenient for estimating the effect of temperature.

[7] King, Hainer, and Cross, Phys. Rev. **71**, 433 (1947).

[8] Randall, Dennison, Ginsburg, and Weber, Phys. Rev. **52**, 160 (1937); D. M. Dennison, Revs. Modern Phys. **12**, 175 (1940).

where $p\gamma_{J\tau, J'\tau'}$ is the contribution of a line to the static dielectric constant. Figure 1 shows the shape of a sharp line. A noteworthy feature of this curve is that the maximum and minimum excursions may be very much greater than the line contribution at zero frequency.

The lines in the wave number interval 0–19 cm^{-1} are listed in Table I; the quantities associated with these lines are computed at a temperature of 293°K, where G is approximately 170,[9] and at a pressure of 7.6 mm Hg. These parameter values were chosen in order to have a basis for comparing the present results with the absorption calculations of Van Vleck. However, it is easy to adapt the results to other temperatures and pressures.[10]

For water vapor which is in air at atmospheric pressure Van Vleck[2] used the round value $\Delta\nu\sim 0.1$ cm^{-1}, since it reflected rather closely the combined results of the experiments of Becker and Autler on the microwave line at 0.74 cm^{-1} and Adel[11] on several lines in the infrared region 540–620 cm^{-1}. Recently Cloud[12] indirectly derived the preliminary value $\Delta\nu\sim 0.04$ cm^{-1} as an average for several other lines from measurements in the region 500–580 cm^{-1}. He found a variation of width for different lines, but the spread in values of about 0.02 cm^{-1} was equal to the estimated experimental error.

Except for the 0.74 cm^{-1} line, the widths of the other lines in the interval 0–19 cm^{-1} have as yet not been determined. In the light of present knowledge it is thought that the value 0.1 cm^{-1} is reasonable for these lines, although it would not be surprising if the widths were found to vary somewhat.

IV. EFFECT OF ALL THE LINES

Equation (1) will be modified here so that it exhibits essentially the effect of each line in the region from 0 through 19 cm^{-1} and lumps together the effect of all other lines whose resonance frequencies are higher. The latter effect will be considered first.

If the frequency of the incident radiation is much lower than the resonance frequency, Eq. (4) may be approximated by

$$F(\nu_{ij}, \nu)\simeq 2[1+(\nu/\nu_{ij})^2]. \quad (10)$$

Substituting Eq. (10) in (1), we find that

$$(\epsilon_\nu'-1)(RT/3p)=(8\pi N_0/9hG)\sum_j'\sum_i'|\mu_{ij}|^2 \times(g_j/\nu_{ij})\exp(-E_j/kT)+\nu^2(8\pi N_0/9hG) \times\sum_j'\sum_i'|\mu_{ij}|^2(g_j/\nu_{ij}^3)\exp(-E_j/kT), \quad (11)$$

where for simplicity in writing the ij notation is used. The primed summation signs mean that all the lines from 0 through 19 cm^{-1} are to be excluded. The second term on the right side of Eq. (11) can be put in a more convenient form by making use of a centroid frequency defined by

$$1/\bar{\nu}^2=(2kT/hG\mu^2)\sum_j'\sum_i'|\mu_{ij}|^2 \times(g_j/\nu_{ij}^3)\exp(-E_j/kT). \quad (12)$$

With the aid of the results of King, Hainer, and Cross we find that $\bar{\nu}/c=70.3$ cm^{-1}. The error involved in omitting the levels higher than $J=6$ is estimated to be less than one percent.

With regard to the first term in Eq. (11), it has already been shown that it reduces to Eq. (7) provided the summations extend over all the lines of the rotational spectrum. As a consequence of this and the use of the centroid frequency, it follows that Eq. (11) can be simplified to

$$(\epsilon_\nu'-1)/p=[4\pi N_0\mu^2/3kRT^2] \times[1+(\nu/70.3c)^2]-\sum\gamma_{J\tau, J'\tau'}, \quad (13)$$

where the sum is taken only over all the lines in Table I.[13] We now take account of the individual resonances to obtain as the final result

$$(\epsilon_\nu'-1)/p=(4\pi N_0\mu^2/3kRT^2)[1+(\nu/70.3c)^2] +\tfrac{1}{2}\sum\gamma_{J\tau, J'\tau'}[F(\nu_{J\tau, J'\tau'}, \nu)-2]. \quad (14)$$

Equation (14) gives only the dipole contribution to the dielectric constant of water vapor. To obtain the total value one must add to the dipole part the sum of the contributions arising from the nuclear and electronic vibrations of the molecule. This is known[1] and is certainly constant throughout the region under consideration.

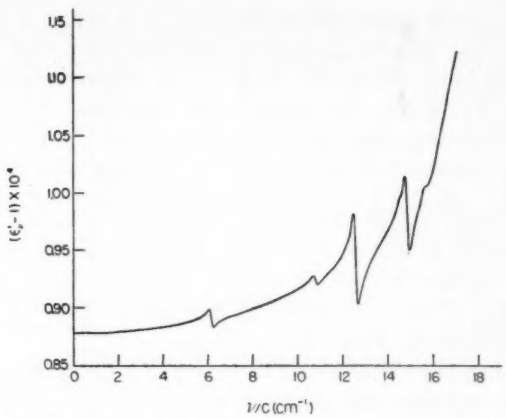

FIG. 2. Variation of the dipole contribution to the dielectric constant of water vapor in the region 0 to 17 cm^{-1}, at the temperature 293°K and pressure 7.6 mm Hg, and for $\Delta\nu=0.1$ cm^{-1}. At $\nu=0$, $\epsilon_0'-1=0.879\times10^{-4}$ ($\mu=1.84\times10^{-18}$ esu). These results are easily adapted to other pressures since $\epsilon_\nu'-1$ is directly proportional to pressure (neglecting the small effect of H_2O-H_2O collisions on $\Delta\nu$).

[9] W. M. Elsasser, Astrophys. J. **87**, 497 (1938), evaluated G at 20-degree intervals in the range 200–320°K. His values can be represented within one percent by the equation $G=0.819T-69.1$.

[10] See note 10 of reference 2, and references 6 and 9 of the present paper.

[11] A. Adel, Phys. Rev. **71**, 806 (1947).

[12] W. H. Cloud, Ph.D. dissertation, The Johns Hopkins University (1952).

[13] The lines at 13.00 and 16.25 cm^{-1} were omitted from Table I when the calculations in this paper were performed. However, these lines are far too weak to influence appreciably the results. The author is indebted to Dr. W. S. Benedict for bringing this omission to his attention.

The curve generated by Eq. (14) is shown in Fig. 2, where the general increase of susceptibility with frequency[14] arises from the wings of the higher frequency lines. To obtain the shape of a particular line, the approximation Eqs. (3) and (4) are used.[15] The distorted appearance of the line in the neighborhood of 15 cm^{-1} is due to the superposition of several lines. In the vicinity of 17 cm^{-1} the accelerated rise of susceptibility is due for the most part to the tail of the very intense line at 18.6 cm^{-1}. This line alone contributes about 2 percent to the dipole part of the static dielectric constant.

It should be noted that the vertical scale of Fig. 2 is rather expanded and that the increase in $\epsilon_\nu'-1$ between 0 and 17 cm^{-1} is only about 28 percent of the zero wave-number value. On the contrary, the situation is entirely different when dealing with the absorption. This is substantially zero at long wavelengths and increases to such an extent at millimeter wavelengths that the atmosphere is virtually closed for transmission except over very short distances.

Aside from the question of line width the principal inaccuracy in these calculations is most likely due to the use of Eq. (10), which requires that $\nu \ll \nu_{ij}$. As 17 cm^{-1} is approached this assumption becomes less warranted because of the proximity of numerous strong resonances.[16] The 18.6 cm^{-1} line was treated separately rather than lumped together with the higher frequency lines in an effort to improve the accuracy of the results. The error which remains is estimated to be no greater than several percent, and it rapidly decreases with decreasing wave number. A discussion dealing with the correctness of the line shape is given in Sec. VI.

V. DISPERSION FROM 0 TO 10 CM^{-1}

It appears from Fig. 2 that the dispersion in the region 0–5 cm^{-1} may be expressed in a simple analytical form. To do this the contribution of the line at 0.742 cm^{-1} is neglected. This causes negligible error, however, since the contribution $\gamma_{5_1 6_5 p}=2.0\times10^{-8}$ (see Table I) is insignificant in comparison with the total dipole contribution of 0.879×10^{-4}. Even the difference between the maximum and minimum points of this line is only 0.7×10^{-7}. It follows then from this discussion and the one leading to Eq. (13) that the dispersion equation in question is

$$(\epsilon_\nu'-1)(RT/3p)=(4\pi N_0\mu^2/9kT)[1+(\nu/52.3c)^2]. \quad (15)$$

This equation may be written in the form

$$(\epsilon_\nu'-\epsilon_0')/(\epsilon_0'-1)=(\nu/52.3c)^2, \quad (16)$$

which is independent of temperature and pressure. Here 52.3 cm^{-1} is clearly the centroid frequency calculated from Eq. (12) by summing over all lines except the one at 0.742 cm^{-1}.[17] Equations (15) and (16) apply for wave numbers up to about 5 cm^{-1}. Beyond this limit the effect of the 6.15 cm^{-1} line would have to be considered. It is simple to find now that at 5 cm^{-1}, for example, the fractional variation in susceptibility is only 1.1 percent.

If the effect of the 6.15 cm^{-1} line is neglected, Eqs (15) and (16) hold up to about 10 cm^{-1}. Because 10 cm^{-1} is not sufficiently small as compared with the resonance wave numbers, these equations are in error there by less than 10 percent. At 5 cm^{-1} the error falls to about 1 percent.

VI. LINE SHAPE

Van Vleck[2] found that the theoretical value of water vapor absorption due to all lines other than the one at 0.742 cm^{-1}, the residual absorption, was smaller than the experimental value by a factor of about 4. In speculating as to the reason for this serious discrepancy, he considered the possibilities that different widths were associated with different lines and that the collision broadening theory of Van Vleck and Weisskopf might be incorrect in the wings of the lines.

On the other hand, the situation with regard to what may be called by analogy the residual dielectric constant, i.e., Eqs. (13) and (15), is considerably more satisfactory. The shape factor used in these equations, an approximate form of $(\nu_n^2-\nu^2)^{-1}$, does not contain the parameter $\Delta\nu$, and furthermore, it is identical with the dispersion form that has found considerable success in applications to optical and infrared spectra. If this shape factor (more exactly, Eq. (4) is substituted in (1)), the Kramers dispersion formula[18] is obtained. This equation has been derived from quantum mechanics on the conditions that the mean lifetime of a single molecule in any state is large compared with its period of vibration, and that the period of the incident radiation is sufficiently removed from this period. One might suspect that this equation applies whenever the conditions $\nu_n \gg \Delta\nu$ and $|\nu-\nu_n| \gg \Delta\nu$ are satisfied regardless of the assumptions involved in the derivation of the line shape. As an example of interest the line shapes predicted by the pressure broadening theories of Lorentz,

[14] M. A. Greenfield and F. W. Brown, J. Opt. Soc. Am. **40**, 643 (1950), represent this dispersion in water vapor by a formula that applies to polar molecules in the liquid state. This formula gives a dielectric constant that always decreases with increasing frequency.

[15] These approximations begin to fail for the 0.742 cm^{-1} line.

[16] For example, there is a line at 25 cm^{-1} whose intensity is 3/4 that of the 18.6 cm^{-1} line. There are about 20 lines of comparable intensity from 25 to 200 cm^{-1}.

[17] Van Vleck has previously evaluated this sum in calculating the microwave absorption of water vapor (see reference 2). Our values for this sum and also the numerical coefficients in the basic absorption formula in reference 2 [p. 428, Eq. (6)] are in good agreement. There is, however, an arithmetical error in reference 2 (p. 427, note 10) in the centroid wave number, which is derived from the rather complicated sum. As verified by correspondence with Professor Van Vleck, the value of the centroid wave number given there, namely, 47 cm^{-1}, should be changed to 52 cm^{-1}.

[18] This equation is briefly described in reference 5, pp. 361–362. P. Debye, *Polar Molecules* (The Chemical Catalog Company, Inc., New York, 1929), Chap. 10, derived an equation in this form, specialized, however, for diatomic molecules. See also C. Manneback, in *Zeeman Verhandelingen* ('s-Gravenhage, Martinius Nijhoff, 1935), pp. 293–301.

and Van Vleck and Weisskopf may be compared. Although these give absorptions that disagree in the line wings, both show that for the conditions under consideration $(\epsilon_\nu'-1)\propto(\nu_n^2-\nu^2)^{-1}$. A proof of the general validity of this relation is given in the Appendix.

In concluding this paper, the author wishes to thank Professor Van Vleck for reading the manuscript and for his comments. It is also a pleasure to thank Dr. W. S. Benedict and Dr. D. M. Kerns for illuminating discussions concerning this work, and Dr. H. Lyons for his encouragement and interest.

APPENDIX

To demonstrate the generality of the dispersion factor $(\nu_n^2-\nu^2)^{-1}$, we make use of a very general relation between the real and imaginary parts of the complex constant, $\epsilon'-i\epsilon''$. The relation in question is[19]

$$\epsilon_\nu'-\epsilon_\infty'=\frac{2}{\pi}\int_0^\infty\frac{\nu'\epsilon_{\nu'}''d\nu'}{\nu'^2-\nu^2}. \tag{18}$$

For the case $\nu=0$, Eq. (18) gives the connection between the static dielectric constant and the integrated absorption, *viz.*,

$$\epsilon_0'-\epsilon_\infty'=(2/\pi)\int_0^\infty(\nu')^{-1}\epsilon_{\nu'}''d\nu'. \tag{19}$$

We suppose that the absorption line is sharp, i.e., ϵ'' is effectively zero except in a sufficiently small interval about the resonance frequency ν_n. Within this interval ν' is very nearly constant and may be set equal to ν_n; and if ν is restricted to values removed from the immediate vicinity of resonance, $\nu'^2/(\nu'^2-\nu^2)$ will be sensibly constant. Then,

$$\epsilon_\nu'-\epsilon_\infty'=[(2\nu_n^2)/\pi(\nu_n^2-\nu^2)]\int_0^\infty(\nu')^{-1}\epsilon_{\nu'}''d\nu', \tag{20}$$

and after substituting Eq. (19) in (20), we obtain the well-known dispersion equation,

$$\epsilon_\nu'-\epsilon_\infty'=(\epsilon_0'-\epsilon_\infty')\nu_n^2/(\nu_n^2-\nu^2).$$

[19] This equation and an inverse transform between ϵ' and ϵ'' were first noted by H. A. Kramers, Atti del Congresso Internazionale dei Fisici, Como **2**, 545 (1927). A brief description of these equations and further references are given by J. H. Van Vleck in *Propagation of Short Radio Waves*, edited by D. E. Kerr (McGraw-Hill Book Company, Inc., New York, 1951), Sec. 8.1.

THE JOURNAL OF CHEMICAL PHYSICS VOLUME 21, NUMBER 1 JANUARY, 1953

Intramolecular Carbon Isotope Effects in the Decarboxylation of Malonic Acid and Bromomalonic Acid

PETER E. YANKWICH AND EDWARD C. STIVERS
Department of Chemistry, University of Illinois, Urbana, Illinois

(Received June 9, 1952)

The intramolecular isotope effects in the decarboxylation of C^{13} and C^{14} carboxyl-labeled malonic and bromomalonic acids have been determined. The observed C^{13} effects are in agreement with the results of other investigators; the C^{14} effects are in partial agreement with earlier published results of one of the authors. The ratio of C^{14} to C^{13} effects is found to be near 3.6.

ISOTOPE effects in the thermal decarboxylation of C^{14} labeled malonic acids were reported first by Yankwich and Calvin,[1] who found 1.12 for the intramolecular frequency of rupture ratio $(C^{12}-C^{12}/C^{12}-C^{14})$ in the case of unsubstituted malonic acid and about 1.4 in the case of bromomalonic acid. These decarboxylation reactions were treated theoretically in terms of two different models, one of which[2] led to the prediction of effects considerably smaller than those observed, while the other,[3] said subsequently[4] to be in error, appeared to account satisfactorily for the results of malonic acid decarboxylation. In the case of either model, rather drastic explanation would have been required to account for the results reported for bromomalonic acid decarboxylation.

Considerable experimentation has followed this early work. The isotope effect for C^{13} labeling has been determined for the unsubstituted acid in several laboratories[5–7] and is in essential agreement with Bigeleisen's theory. The isotope effect for C^{14} labeling has been the object of further work on both substituted and unsubstituted malonic acids;[8,9] the results are not in agreement with the theoretical predictions. The experimental findings and the theoretical predictions are collected in Table I.

The purpose of this research was to achieve careful redetermination of the isotope effects in the decar-

[1] Peter E. Yankwich and M. Calvin, J. Chem. Phys. **17**, 109 (1949).
[2] Jacob Bigeleisen, J. Chem. Phys. **17**, 425 (1949).
[3] Kenneth S. Pitzer, J. Chem. Phys. **17**, 1341 (1949).
[4] A. Bothner-By and J. Bigeleisen, J. Chem. Phys. **19**, 755 (1951).
[5] J. Bigeleisen and L. Friedman, J. Chem. Phys. **17**, 998 (1949).
[6] Lindsay, Bourns, and Thode, Can. J. Chem. **29**, 192 (1951).
[7] Bernstein, J. Phys. Chem. **56**, 893 (1952).
[8] A. Roe and M. Hellman, J. Chem. Phys. **19**, 660 (1951).
[9] Fry and Calvin, J. Phys. Chem. **56**, 901 (1952).

TABLE I. Summary of intramolecular isotope effect results; malonic acids: COOH·CHR·C*OOH.

R	x	State	T, °C	$100[(k_4/k_3)-1]$[a]	Reference
H	14	liquid	145	12±3	1
H	14		153	6±2	8
Br	14		122	41±13	1
α-Naphthyl	14		163	7.6±0.5	9
Phenyl	14		163	8.8±1.6	9
α-Naphthyl	14	dioxane-aq. HCl soln	73	9.8±1.2	9
α-Naphthyl	14		88	9.5±0.8	9
Phenyl	14		73	13.2±1.7	9
Theory Any	14		27–227	3.8	2
H	13	liquid	138	1.9±0.1[b]	5
H	13		138	2.6±0.4[b]	6
H	13		138–199	2.1±0.1[c]	6
H	13		160	3.3	7
Theory Any	13		27–227	2.0	5

[a] Appended errors are average deviations calculated by the present authors.
[b] See reference 10.
[c] See reference 11.

boxylations of malonic acid and bromomalonic acid so that the relation between the C^{13} and C^{14} intramolecular isotope effects might be indicated with certainty. Since there was some agreement as to the magnitude of the C^{13} intramolecular effect,[5,6] this quantity could be used as a check on determinations of the corresponding quantity for C^{14} labeling. Accordingly, malonic acid and bromomalic acid carboxyl-labeled with C^{14} were prepared and decarboxylated; the effluent carbon dioxide and that obtained from oxidation of the product monoacid were subjected to analysis for both C^{13} and C^{14}.[12]

EXPERIMENTAL

Preparation[13] of Malonic Acid-1-C^{14}

Ten grams of chloroacetic acid were dissolved in 15-ml water; the *p*H of the solution was adjusted to 8.0 with saturated sodium carbonate solution. Eight milligrams of C^{14} labeled sodium cyanide were added to 4.9 grams of the unlabeled salt and the mixture dissolved in a minimal quantity of water. The cyanide and acetate solutions were mixed, care being taken to maintain the temperature of the mixture below 90°C; after the cessation of exothermic reaction, the mixture was heated on a steam bath for 1.5 hours, then evaporated to dryness in vacuum. The resultant mixture of chloride and cyanoacetate salts was treated with sufficient concentrated hydrochloric acid to produce a mixture whose *p*H was 1; the mixture was evaporated to dryness in vacuum. One milliliter of concentrated hydrochloric acid was stirred with the solid reaction product and the mixture again evaporated to dryness in vacuum.

The product of the final evaporation was suspended in 60 ml of concentrated HCl; the suspension was transferred to a bomb tube fitted with a high pressure stopcock;[14] the bomb tube and its contents were heated for 3 hours in a boiling water bath. The contents of the bomb were then transferred to a flask; the product mixture was evaporated to dryness in vacuum; final drying was accomplished by continuation of evacuation for 24 hours, the product being maintained at a temperature of 70°C during this period. The dried white solid was extracted with eight 50-ml portions of absolute ether; the combined ether solutions were evaporated to dryness and the crude malonic acid product twice recrystallized from a 1:1 mixture of acetone and benzene.

Yield: 70 percent based on cyanide.
Melting point: 134–135°C; reported figure: 130–137.5°C.[5,15]
Analysis: Calculated for $C_3H_4O_4$: C, 34.62 percent; H, 3.87 percent.
Found: C, 34.60 percent; H, 4.00 percent.

Preparation of Bromomalonic Acid-1-C^{14}

Ten grams of pure labeled malonic acid were stirred into 75 ml of *moist* ether contained in a 200-cc round-bottom three-neck flask; the flask was fitted with a dropping funnel, reflux condenser, and stirrer. One milligram of benzoyl peroxide was added to the contents of the flask and 6 ml (18.7 g) of bromine run in through the dropping funnel; stirring was continuous throughout the bromine addition. The resultant greenish amber solution was transferred to a 200-cc boiling flask and evaporated to dryness in vacuum; evacuation was continued for 72 hours. (In this and all subsequent operations care was exercised to prevent contact between the product and moisture from any source.) The crude bromomalonic acid was dissolved in 6 ml of pure anhydrous trifluoroacetic acid (heating to 85°C was required); the solution was filtered through sintered glass, transferred to a tube-like evaporator of 20-cc volume and evaporated to dryness in vacuum. The product was

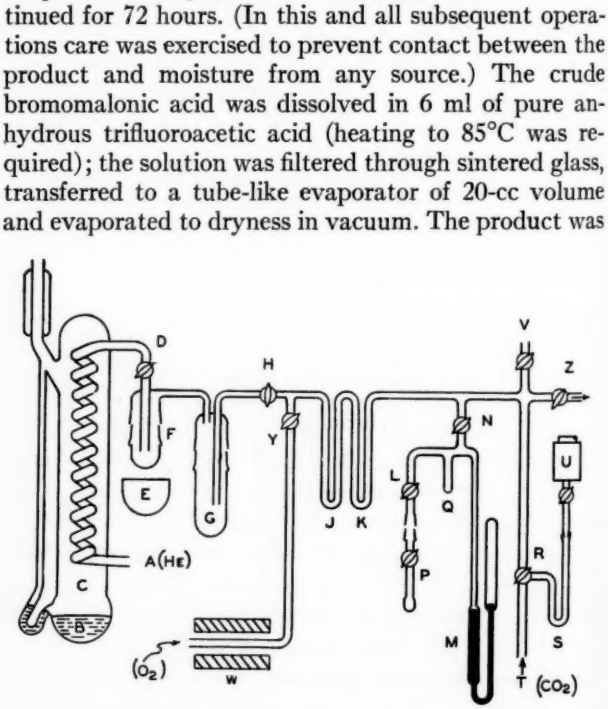

FIG. 1. Decarboxylations and sample preparation apparatus (schematic).

[10] Eastman Kodak Company malonic acid.
[11] British Drug Houses malonic acid. See discussion at end of paper in reference 9.
[12] Preliminary results were presented at the December, 1951 meeting of the American Physical Society at Berkeley, California, and have been reported previously: Yankwich, Stivers, and Nystrom, J. Chem. Phys. **20**, 344 (1952); Phys. Rev. **85**, 753 (1952).
[13] After N. Weiner in *Organic Syntheses* (John Wiley and Sons, Inc., New York, 1943), Coll. Vol. II, p. 376.
[14] Gal and Shulgin, J. Am. Chem. Soc. **73**, 2938 (1951).
[15] Hinshelwood, J. Chem. Soc. **117**, 156 (1920); Biltz and Balz, A. Anorg. Chem. **170**, 339 (1928); Vogel, J. Chem. Soc. **1929**, 1478.

dissolved again in 6 ml of trifluoroacetic acid and filtered through sintered glass; the filtrate was frozen in a dry ice-alcohol bath. The solid filtrate was allowed to warm to room temperature, fractionation of the product being achieved due to the slowness with which pure bromomalonic acid dissolves in trifluoroacetic acid at room temperature or below. The acid was recrystallized three times; after the last recrystallization, the bromo acid was freed of solvent by evacuation at room temperature for 72 hours.

Yield: 47 percent based on malonic acid.
Melting point: 112–113°C; reported figure: 112–113°C.[16,17]
Analysis: calculated for $C_3H_3O_4Br$:
C, 19.69 percent; H, 1.65 percent; Br, 43.70.
Found: C, 19.68 percent; H, 1.93 percent; Br, 43.45.

Apparatus and Procedure

The apparatus, shown in Fig. 1, consisted of sweep-gas and sample heaters A through E, reaction vessel and gas purification train F through K, and sample collection and measurement devices L through U.

The following occurred in a typical experiment: The boiling rate of the preheater working fluid B, o-xylene, was so adjusted that the temperature of pure dry helium passing from A through heating coil C and entering the decarboxylation vessel through D was the same as that of the oil bath E, whose temperature was regulated to ±1°C. The helium flow was 20–30 cc per minute. When thermal balance was achieved, trap G was cooled in a dry ice-alcohol bath, trap J was cooled in liquid nitrogen, and a small cup containing a weighed quantity of solid acid put in place at F; bath E was raised, and decarboxylation started. During the decarboxylation, for which 3–5 hours were allowed, effluent carbon dioxide was freed at G of entrained acetic acid and trapped at J; L and Z were kept closed, and the helium vented at V.

At the end of the decarboxylation H and V were closed, the system evacuated between H and Z, and the carbon dioxide purified by successive sublimations between traps J and K and sample tube P; the sublimations were carried out between dry ice and liquid nitrogen temperatures. The gas in P was reserved for C^{13} analysis.

Bath E was removed and vessel F and trap G cooled in liquid nitrogen; H was opened and the system evacuated between D and Z. F was warmed and all acetic acid sublimed into G. A portion of the acetic acid was removed mechanically from G and burned in W over copper oxide wire; the resultant carbon dioxide was trapped at J, purified by sublimation, as above, and collected at P for mass spectrometer analysis.

In the malonic acid runs bath E was heated to 137°C. Essentially quantitative transfer of acetic acid between F and G was noted in all cases; no appreciable sublimation of malonic acid occurred while the runs were in progress.

It was necessary to remove the last traces of trifluoroacetic acid and other volatile impurities from the solid bromomalonic acid by 3 hours heating at 90°C in vacuum; inappreciable weight loss was noted as a consequence of this treatment, but the melting point of the bromoacid rose to 116–117°C. During the bromoacid decarboxylations bath E was heated to 117°C; little bromoacetic acid distilled into G during the runs. The samples for combustion were obtained after vacuum sublimation as described above.

Sample tubes containing carbon dioxide which had been subjected to mass spectrometer analysis were reconnected to the vacuum system at L and their entire contents transferred to trap Q; with L and N closed, Q was warmed. The quantity of gas was measured by the deflection of the calibrated manometer M. Following the quantity determination, the carbon dioxide was transferred to trap S; R was closed to S and opened to tank carbon dioxide whose pressure was regulated accurately to 76.0 cm. S was warmed, and this permitted the sample to fill the volume RSU; U is an ionization chamber of 250-cc volume. The transfer of the sample to U was made complete and standard carbon dioxide pressure achieved by admission of tank carbon dioxide from T through R.

Isotope Analyses

The ($C^{13}O_2/C^{12}O_2$) ratios R of the various samples were determined with a Consolidated-Nier Isotope-Ratio Mass Spectrometer. The ratio of ion currents (mass 45/mass 44) was corrected for incomplete resolution and for the contribution to the mass 45 current of the species $C^{12}O^{16}O^{17}$. The corrected ratios are collected in Table II.

The ionization currents due to the radioactive decay of C^{14} in the several samples were measured with an

TABLE II. C^{13} intramolecular isotope effect in malonic acids. From total combustion: corrected ratio ($C^{13}O_2/C^{12}O_2$), $R_D = 0.010929$.

Run	mM diacid	Corrected Ratio ($C^{13}O_2/C^{12}O_2$) CO_2, R_C	Acid, R_A	100 [(k_4/k_3) − 1] from R_C	from R_A
MA-1	1.21	0.010750	···	3.3	···
MA-2	2.15	0.010789	0.010996	2.6	2.5
MA-3	0.49	0.010784	···	2.7	···
BrMA-1	2.05	0.010838	0.010999	1.7	2.6
BrMA-2	1.20	0.010768	0.010989	3.0	2.2

TABLE III. C^{14} intramolecular isotope effect in malonic acids. From total combustion: specific activity diacid $S_D = 1.716$ μc/mM.

Run	mM diacid	Specific Activity μc/mM CO_2, S_C	acid, S_A	100 [(k_4/k_3) − 1] from S_C	from S_A
MA-2	2.15	0.816	0.901	10.3±0.8	10.6±0.8
MA-3	0.49	0.817	0.894	10.0±1.0	8.8±1.1
BrMA-1	2.05	0.809	0.908	12.1±0.8	12.3±0.8
BrMA-2	1.20	0.813	0.899	11.1±0.8	10.0±0.8
BrMA-3	2.49	0.807	···	12.6±1.1	···
BrMA-4	2.53	0.811	···	11.6±1.2	···

[16] Lutz, Ber. deut. chem. Ges. **35**, 2552 (1902).
[17] Conrad and Reinbach, Ber. deut. chem. Ges. **35**, 1816 (1902).

Applied Physics Corporation Vibrating-Reed Electrometer, whose output was recorded continuously. The background correction was determined from such a measurement with the ionization chamber filled with inactive carbon dioxide. The net specific activities are collected in Table III.

The malonic acid and bromomalonic acid experiments were performed several months apart; during this period the response of each analytical instrument varied somewhat. A correction for these effects was made by conversion of the corrected ratios and specific activities observed to values based on the average isotope ratio and specific activity of a standard sample. The largest corrections made were about 0.2 percent to a corrected ratio, and about 0.35 percent to a specific activity.

It will be noted that the spread in C^{13} results is much greater than that of the corresponding C^{14} results obtained with the same samples. This situation is the reverse of that expected and was traced to inadequate electronic stabilization of our mass spectrometer. The error appended to the calculated values in the last two columns of Table III is the estimated sum of sample pressure determination and radioactivity measurement errors, the latter being by far the smaller. The sum of S_A and S_C averages 1.714 ± 0.003; this is quite good agreement with the value 1.716 for S_D.

CALCULATIONS

The decarboxylation of liquid malonic acid has been shown to be first order with respect to the acid;[18–20] substituted malonic acids would be expected to behave similarly. Rate constants for the several rupture processes are defined[5] as follows:

$$A_1A_2C^n(C^nOOH)_2 \xrightarrow{k_1} C^nO_2+C^nA_1A_2HC^nOOH, \quad (1)$$

$$A_1A_2C^x(C^nOOH)_2 \xrightarrow{k_2} C^nO_2+C^xA_1A_2HC^nOOH, \quad (2)$$

$$A_1A_2C^n(C^xOOH)(C^nOOH) \xrightarrow{k_3} C^xO_2+C^nA_1A_2HC^nOOH, \quad (3)$$

$$A_1A_2C^n(C^nOOH)(C^xOOH) \xrightarrow{k_4} C^nO_2+C^nA_1A_2HC^xOOH. \quad (4)$$

where A_1 and A_2 are substituents which do not contain carbon, and n and x denote different isotopes or distributions of isotopes of carbon. Analysis of carbon dioxide in the mass spectrometer yields a value for the ratio of the heavy and light isotopes in the sample; in such experiments $n=12$ and $x=13$, and the obtained datum is $R=(C^{13}O_2)/C^{12}O_2)$. Radiometric analysis of carbon dioxide yields a value for its specific activity S, which is proportional to the quantity $(C^{14}O_2)/(C^{14}O_2+C^nO_2)$; here n represents the (presumably unaltered) normal mixture of stable isotopes.[21]

It is possible to evaluate the rate constant ratio k_4/k_3 from continuous measurements of the quantities R and S. In practice, however, these measurements are commonly made on the carbon dioxide which results from total decarboxylation. Determinations of the C^{13} isotope effects have been carried out with malonic acid of normal isotopic constitution and distribution. In these experiments the isotope ratio of the effluent carbon dioxide $-R_C-$ is compared with that $-R_D-$ of carbon dioxide obtained from a total combustion of the diacid. In terms of these corrected ratios,

$$(k_4/k_3)=2(R_D/R_C)-1. \quad (5)$$

Evaluations of the C^{14} isotope effects[1,8,9] have been carried out under conditions such that the mole fraction of C^{14} in the label position was extremely small. In these experiments the specific activity of the effluent carbon dioxide $-S_C-$ is compared with that $-S_D-$ of the parent diacid. In terms of these specific activities,

$$(k_4/k_3)=(S_D/S_C)-1. \quad (6)$$

Additional data may be obtained from analysis of the monoacid which is the other product of decarboxylation. Determinations of corrected ratios and specific activities are made ordinarily on the effluent product obtained from complete decarboxylation. In C^{13} isotope effect experiments, the isotope ratio $-R_A-$ of carbon dioxide obtained from combustion of the monoacid effluent is compared with R_D. In terms of these corrected ratios,[6]

$$(k_4/k_3)=(2R_A-R_D+R_AR_D)/(3R_D-2R_A+R_AR_D). \quad (7)$$

In C^{14} isotope effect experiments, the specific activity of the effluent monoacid $-S_A-$ is compared usually with S_D. In terms of these specific activities,

$$(k_4/k_3)=S_A/(S_D-S_A). \quad (8)$$

Equations (5)–(8) were employed in the calculation of results shown in Tables II and III. The correct application of these equations is based upon two assumptions. (1) In the case of C^{13} label, i.e., the acids of normal isotopic constitution, the assumption is made in the calculation that the C^{13}/C^{12} ratio is the same at each carbon atom. Lindsay, Bourns, and Thode[6] found this actually to be the case for Eastman Kodak Company malonic acid. A similar analysis of the type of synthetic product employed in this research demonstrated iden-

[18] Hinshelwood, J. Chem. Soc. **117**, 156 (1920).
[19] Laskin, Trans. Siberian Acad. Agr. Forestry **6**, 7 (1926).
[20] Hall, J. Am. Chem. Soc. **71**, 2691 (1949).

[21] The effects measured are comparisons of the behavior of C^{14} with the average behavior of the stable carbon isotopes. Because of the relatively low natural abundance of C^{13}, these comparisons are not much different from those which would be observed for labeled molecules in which that nuclide were entirely absent.

tity of the ratios to within 0.1 percent. (2) It is assumed that none of the C^{14} label has found its way into the central carbon atom. A simple calculation shows that about 3–4 percent of the radioactive label would have to have wandered into the 2 position in order that this phenomenon be the source of the discrepancy between the C^{14} results recorded in Table III, the presently or previously reported results for C^{13}, and the prediction of Bigeleisen's theory. The possibility of this very improbable migration has been investigated previously. Ropp[22] prepared malonic acid-2-C^{14} from bromoacetic acid-2-C^{14} by the same procedure as employed in this research. By conversion of the product to 3-(2-Furanyl)-propenoic acid-2-C^{14} it was demonstrated, within about 1 percent experimental error, that no carbon from the 2 position of the bromoacetic acid appeared in the 1 position of the product malonic acid. We conclude, therefore, that the migration suggested above, does not occur to an extent sufficient to influence strongly the results reported here.

RESULTS

In Tables II and III are collected experimentally determined values for the C^{13} and C^{14} isotope effects in the decarboxylation of malonic acid and bromomalonic acid; unity has been subtracted from (k_4/k_3) and the result multiplied by 100 to simplify the tabulation.

The averages of the C^{13} effects are 2.8 ± 0.2 (standard error appended) for malonic acid and 2.4 ± 0.3 for bromomalonic acid; while the latter results leave much to be desired, those for both compounds are in accord with the findings of previous investigators.

The averages of the C^{14} effects are as follows: malonic acid-dioxide basis, 10.2 ± 0.9, -monoacid basis, 9.7 ± 0.9, all determinations, 9.9 ± 0.5; bromomalonic acid-dioxide basis, 11.9 ± 0.6, -monoacid basis, 11.2 ± 0.8, -all determinations, 11.6 ± 0.4. The results for malonic acid indicate a somewhat smaller effect than that reported by Yankwich and Calvin,[1] are in moderate conflict with these reported by Roe and Hellman,[8] and do not conform at all to the theoretical estimates of Bigeleisen.[2] The results for bromomalonic acid are in line with expectation based on the values found for the isotope effect in the case of the unsubstituted acid. There seems to be no explanation for the extremely high result reported for bromomalonic acid by Yankwich and Calvin other than that of impurity of sample as mentioned by them.

The results reported by Yankwich and Calvin were obtained from radioactivity measurements on solid barium carbonate samples. Though that technique is not so sensitive as others employed later, counting procedure error alone could not account for their results with bromomalonic acid. The result for malonic acid reported here is within the limits stated by them, even though the present ionization chamber technique for radioactivity determination has yielded data more precise by an order of magnitude.

More difficult to explain is the discrepancy between the results reported here for malonic acid and those which were published by Roe and Hellman. In the absence of more complete experimental data, speculation concerning their results can be entertained on one point only, the use of the rate-of-drift method for the radioactivity determinations. Experiments in this laboratory have demonstrated that the precision of specific activity determinations on samples so weak as to require use of the rate-of-drift rather than the amplified-developed voltage method is of the order of 1.5 percent, or more than three times the error found when the latter technique is employed. An error of 1.5 percent in determination of the specific activity of carbon dioxide, acetic acid, or malonic acid would result in $100[(k_4/k_3)-1]=10.0\pm3.0$ at the ten percent isotope effect level, and 6.0 ± 3.1 at the six percent isotope effect level. In the present research amplified-developed voltages of 400–1000 millivolts were encountered; the error in their measurement is about one-fourth as large as that in gas quantity determination, which is a feature common to both the present work and that of Roe and Hellman.

CONCLUSIONS

The simplified statistical methanical treatment predicts a value of 2 for the ratio of the C^{14} and C^{13} intramolecular isotope effects that observed here is 3.6 ± 0.5 for malonic acid (maximum possible range, 2.7–4.4) and 4.8 ± 0.9 for bromomalonic acid (maximum possible range, 3.3–8.0). Stevens, Pepper, and Lounsbury[23] have found that the corresponding ratio for the mesitoic acid decarboxylation is about 2.7. The findings in this research are not strictly comparable to their results because of the large differences in temperature of decarboxylation and in nature of reactants.[24,25]

We believe that, within the limits of error stated, the results reported here indicate a C^{14} isotope effect much

[22] Ropp, J. Am. Chem. Soc. **72**, 4459 (1950).

[23] Stevens, Pepper, and Lounsbury, J. Chem. Phys. **20**, 192 (1952).

[24] Fry and Calvin (see reference 9) have reported C^{14} and C^{13} isotope effects in the decomposition of oxalic acid in 99.4 percent sulfuric acid at 80.1 and 103°C. At these temperatures they obtain 2.06 ± 0.14 and 2.04 ± 0.20, respectively, for the ratio of C^{14} and C^{13} isotope effects. Although these results are in agreement with Bigeleisen's theory, they are not strictly comparable to those reported for malonic or mesitoic acid decarboxylations since a carbon-oxygen rupture, rather than a carbon-carbon, is evidently involved in the rate determining step.

[25] In the course of our work two runs were made with bromomalonic acid in an effort to determine the intermolecular isotope effect $k_1/2k_3$. The acid samples were small (0.8 mM), and rather extensive decomposition was required to yield a measurable quantity of CO_2. The extents of decarboxylation and calculated values of $k_1/2k_3$ were $P1$, 5.9 percent, $1.12_1\pm0.04$; $P2$, 13.4 percent, $1.11_8\pm0.02$. When the average of these is combined with $k_4/k_3=1.116\pm0.004$, there results $k_1/2k_4=1.00\pm0.03$. For the C^{13} intermolecular effect with normal malonic acid, $k_1/2k_4$ has been found to be about 1.016; comparison of the result just calculated with this figure is not possible because of the large experimental error associated with the former.

larger than that predicted by theory. Combination of these data with any presently or previously reported data for the C^{13} isotope effect in the decarboxylation of normal unsubstituted malonic acid in no case results in a ratio of isotope effects smaller than 3.

ACKNOWLEDGMENT

This research was supported by the Atomic Energy Commission. We are indebted to Professor Robert F. Nystrom for generous assistance in many phases of the work.

THE JOURNAL OF CHEMICAL PHYSICS VOLUME 21, NUMBER 1 JANUARY, 1953

Regularities in the Spectra of Molecular Complexes*

H. McConnell,† J. S. Ham,‡ and J. R. Platt
Department of Physics, University of Chicago, Chicago, Illinois

(Received June 30, 1952)

The intense so-called "intermolecular charge-transfer spectra" shown by a large number of molecular complexes in solution are found to exhibit certain regularities in regard to wavelength and intensity. The wavelengths of these transitions show an excellent correlation with the ionization potentials of the electron donor partners of the complexes. The intensities of the charge-transfer transitions are markedly dependent on the electron acceptor partner of the complex. These results are examined in terms of possible theoretical interpretations of the charge-transfer transitions.

INTRODUCTION

MOLECULAR complexes between electron donors (D's) and electron acceptors (A's) often show intense electronic absorption transitions not found in either the D or A molecules alone. For example, the frequently discussed molecular complex between benzene (a D) and iodine (an A) shows a transition with peak at 297 mμ with molar extinction coefficient, $\epsilon = 18{,}000$.[1] Benzene or iodine alone are comparatively transparent at this wavelength. Within this last three years about thirty-five similar molecular complexes have been studied spectroscopically,[2] all of which show intense absorption bands not found in either of the partners alone. In this paper we shall adopt the terminology of Mulliken and refer to these new bands of the complexes as intermolecular charge-transfer transitions.[3]

The purpose of this paper is to present some regularities which are useful for predicting empirically the wavelengths and intensities of these charge-transfer transitions.[4] In addition, the theoretical implications of these regularities are discussed insofar as this is possible without elaborate numerical calculations. For simplicity, only electrically neutral D's and A's with closed shell electronic structures will be considered. The discussion is also limited to those molecular complexes whose heats of formation in the ground electronic states are of the order of a few kcal/mole.

EFFECT OF ACCEPTOR ON CHARGE-TRANSFER WAVELENGTH AND INTENSITY

Figure 1 gives the absorption maxima (molar extinctions, ϵ_{max}, and wavelengths, λ_{max}, for the charge-transfer transitions in complexes of the donor benzene with the acceptors, iodine, bromine, chlorine, iodine chloride, sulfur dioxide, oxalyl chloride, and s-trinitrobenzene.[2] Even for apparently quite different A molecules, the charge-transfer wavelengths are the same to within 20 mμ. In fact, the points are nearly on a straight line which extrapolates to 272 mμ at zero intensity. Deviations from this line cannot be separated from experimental error since the absorption maxima are broad and a change of solvent composition can change λ_{max} by as much as 8 mμ.[5] Changes in solvent composition can also affect ϵ_{max} by 20 percent.[1,5]

Unfortunately, insufficient data are available at present to give plots similar to that in Fig. 1 for other D molecules. Such plots would be exceedingly important theoretically. As discussed later, one theoretical description (charge-transfer) of the excited states of these complexes indicates that the regularities in Fig. 1 are to a considerable degree accidental; another theory predicts that similar regularities should hold for every D molecule and that the extrapolation to zero intensity will give the wavelength of a singlet-triplet transition of the D molecule.

There is apparently no correlation between the positions of the charge-transfer transitions in Fig. 1 and

* Supported in part by the ONR under Task Order IX of Contract N6ori with the University of Chicago.

† National Research Council Postdoctoral Fellow, 1950–1952. Present address: Shell Development Company, Emeryville, California.

‡ AEC Predoctoral Fellow, 1951–1952.

[1] H. A. Benesi and J. H. Hildebrand, J. Am. Chem. Soc. **71**, 2703 (1949).

[2] See references to figures.

[3] R. S. Mulliken, (a) J. Am. Chem. Soc. **72**, 600 (1950); (b) J. Chem. Phys. **19**, 514 (1951); (c) J. Am. Chem. Soc. **74**, 811 (1952); and forthcoming papers.

[4] Hastings, Franklin, Schiller, and Matsen have recently found regularities in iodine solutions similar to those described below and have extended the work to several other D molecules. See abstracts to the Symposium on Molecular Structure and Spectroscopy at Ohio State University, June 1952.

[5] E. Cohn and H. McConnell, unpublished.

the positions of singlet transitions of the A molecules alone. The available experimental evidence (which is scanty) shows that the energies and intensities of the singlet transitions of the A molecules are not greatly affected by complex formation with D molecules.[6] As will be seen later, these facts rule out a number of previous theoretical interpretations of charge-transfer spectra.

EFFECT OF DONOR ON CHARGE-TRANSFER WAVELENGTH AND INTENSITY

Figure 2 shows a plot of the lowest observed ionization potentials of the D molecules *vs* the charge-transfer absorption frequencies of $D \cdot A$ complexes in which the A molecule is always iodine.[2] In spite of the markedly different electronic structures of these D molecules, it is seen that there is an excellent correlation between the charge-transfer transition energies and the (vapor) ionization potentials of the D molecules. All the points in Fig. 2 are within 4000 cm^{-1} in ionization potential (or 2000 cm^{-1} in charge transfer energy) of the straight line drawn in this figure.

In Fig. 2 spectroscopic values of ionization potentials have been used whenever the data were available; otherwise, electron impact or estimated ionization potentials are used. The regularity in Fig. 2 appears to be sufficiently definite that it may be used to predict the wavelengths of new charge-transfer spectra with I_2 as the A molecule whenever the ionization potentials of the D molecules are known. Conversely, ionization potentials might be estimated from charge-transfer wavelengths. By employing the straight line approximation in Fig. 2, we have assembled in Table I a set of predicted charge-transfer absorption frequencies for iodine complexes with a variety of D molecules. For

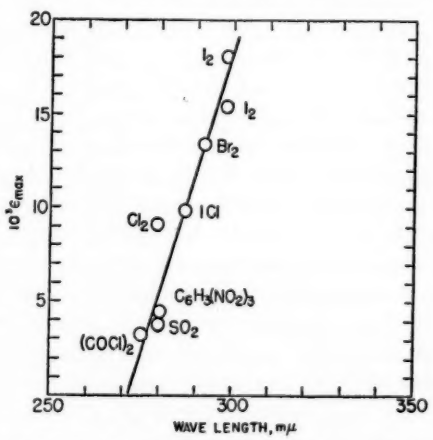

FIG. 1. Intensity (ϵ_{max}) of the charge transfer transition *versus* wavelength for a series of A molecules with benzene.

Iodine—reference 1. Bromine—R. M. Keefer and L. J. Andrews, J. Am. Chem. Soc. **72**, 4677 (1950). Chlorine—L. J. Andrews and R. M. Keefer, J. Am. Chem. Soc. **73**, 462 (1951). Iodinemonochloride—R. M. Keefer and L. J. Andrews, **72**, 5170 (1950). *s*-trinitrobenzene—reference 6. Sulfur dioxide—reference 8. Oxalyl chloride—B. D. Saksena and R. E. Kagarise, J. Chem. Phys. **19**, 994 (1951).

[6] D. Lawrey and H. McConnell, J. Am. Chem. Soc. (to be published).

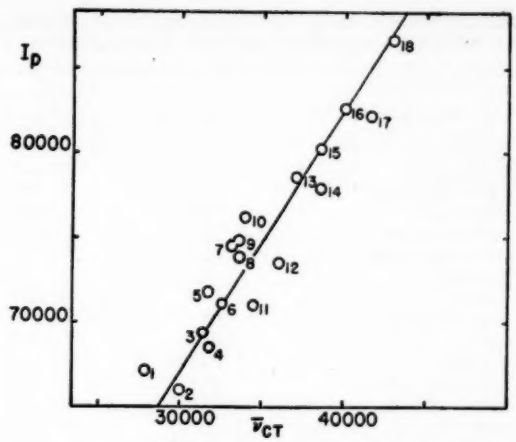

FIG. 2. Ionization potential of the B molecules *versus* the frequency of the charge-transfer transition maximum of its complex with iodine, 1. naphthalene, 2. mesitylene, 3. *o*-xylene, 4. *p*-xylene, 5. 2-methylbutadiene, 6. toluene, 7. cyclohexene, 8. *trans*butene-2, 9. benzene, 10. *cis*butene-2, 11. chlorobenzene, 12. butadiene, 13. propene, 14. *cis*dichloroethylene, 15. *trans*dichloroethylene, 16. diethyl ether, 17. cyclopropane, 18. *t*-butyl alcohol.

Abbreviations:

WCP—W. C. Price, Chem. Revs. **41**, 257 (1947).
API—American Petroleum Institute Catalog of Ultraviolet Spectrograms.
FS—S. Freed and K. M. Sancier, J. Am. Chem. Soc. **74**, 2703 (1949).

The first reference given for each compound is for ionization potential; the second is for the charge transfer frequency; and the third for the frequency of the strongest singlet-singlet absorption. (Values obtained in vapor phase are reduced by 2000 cm^{-1} for comparison with solution values.)

1. Naphthalene—WCP; reference 9; API.
2. Mesitylene—WCP; reference 1; API.
3. *O*-xylene—Price, Hammond, Teegan, and Walsh, Faraday Soc. Disc. **9**, 53 (1950); reference 1; API.
4. *P*-xylene—same as compound 3.
5. 2-methylbutadiene—WCP; FS; API.
6. Toluene—W. C. Price and A. D. Walsh, Proc. Roy. Soc. (London) **A191**, 22 (1947); reference 1; API.
7. Cyclohexene—W. C. Price and W. T. Tutte, Proc. Roy. Soc. (London) **A174**, 207 (1949); L. J. Andrews and R. M. Keefer, J. Am. Chem. Soc. **74**, 458 (1952); W. J. Potts, Jr. (unpublished data).
8. *Trans*butene-2—V. H. Dibeler, J. Research Natl. Bur. Standards **38**, 329 (1947); FS; E. P. Carr and H. Stucklen, J. Chem. Phys. **4**, 760 (1936).
9. Benzene—WCP; reference 1; API.
10. *Cis*butene-2—same as compound 8.
11. Chlorobenzene—WCP; (estimated from data on the bromine complex), R. M. Keefer and L. J. Andrews, J. Am. Chem. Soc. **72**, 4677 (1950); W. C. Price and A. D. Walsh, Proc. Roy. Soc. (London) **A191**, 22 (1947).
12. Butadiene—WCP; FS; API.
13. Propene—WCP; FS.
14. *Cis*dichloroethylene—WCP; L. J. Andrews and R. M. Keefer, J. Am. Chem. Soc. **74**, 458 (1952); A. D. Walsh, Trans. Faraday Soc. **41**, 35 (1945).
15. *Trans*dichloroethylene—same as compound 14.
16. Diethyl ether—WCP; J. S. Ham, J. Chem. Phys. **20**, 1170 (1952); G. Scheibe and H. Grieneisen, Z. physik Chem. **B25**, 52 (1934).
17. Cyclopropane—F. H. Field and E. A. Hinkle, J. Chem. Phys. **18**, 1122 (1950); FS.
18. *t*-butyl alcohol—estimated; J. S. Ham, J. Chem. Phys. **20**, 1170 (1952).

theoretical reasons, these predictions are limited to closed shell A and D molecules and to weak complexes having heats of formation of the order of a few kcal/mole. In practice, chemical reactions, low absorption intensities, or interfering absorptions by solvent molecules may prevent verifications of some predictions. Inaccurate or inappropriate ionization potentials can lead to false predictions. The almost constant wavelengths in Fig. 1 for the charge-transfer complexes of benzene with a number of A molecules suggest that the predictions of Table I may also be approximately correct for complexes containing A molecules other than iodine.

We have noted that the *intensities* of the charge-

TABLE I. Predicted charge-transfer absorption frequencies for iodine complexes with a variety of donor molecules.

Compound	Lowest I_p[a]	Predicted frequency
tetramethylethylene	8.30	30,000
chloroprene	8.83	33,000
diethylthioether	9.30	35,000
ethyl iodide	9.34	35,000
trimethylamine	9.4	36,000
ethylmercaptan	9.70	37,000
pyridine	9.8	38,000
acetone	10.1	39,000
t-butyl chloride	10.2	40,000
carbon disulfide	10.3	40,000
n-butane	10.34	41,000
hydrogen sulfide	10.47	41,000
ethyl bromide	10.92	44,000
acetylene	11.41	46,000
water	12.61	52,000

[a] The ionization potentials are in ev and are taken from W. C. Price [Chem. Revs. **41**, 257 (1947)] with the exception of the values for carbon disulfide [W. C. Price and T. M. Sugden, Trans. Faraday Soc. **44**, 108 (1948)] and pyridine [Hastrulid, Kusch, and Tate, Phys. Rev. **54**, 1037 (1938)].

transfer transitions of the complexes in Fig. 2 show no strong correlation with the ionization potentials of the D molecules, the equilibrium constants of the complexes or with the wavelengths of the transitions.

As strong singlet transitions in molecules are often approximately correlated with their ionization potentials, it is of interest to see whether or not such singlet transition energies can be closely correlated with the charge-transfer energies. As discussed later in this paper, such a correlation is also predicted by one of the possible theoretical interpretations of charge-transfer spectra.

Figure 3 shows a plot of the strongest (allowed) singlet-singlet transition energies of D molecules *vs* the charge-transfer absorption energies of the $D \cdot A$ complexes where A is always iodine.[2] There is evidently some correlation, but several points fall wide of any smooth curve drawn in Fig. 3. The correlation in this figure is evidently not as good as that in Fig. 2. Therefore, for empirical purposes, it would appear better to predict charge-transfer energies from ionization potentials rather than singlet-singlet transition energies.

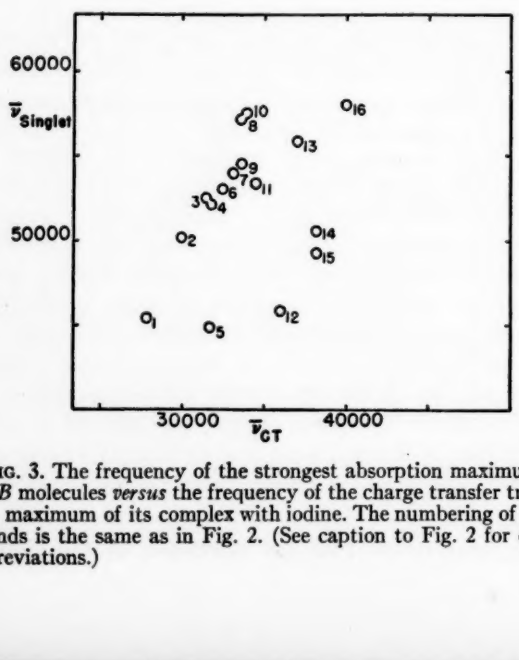

FIG. 3. The frequency of the strongest absorption maximum of the B molecules *versus* the frequency of the charge transfer transition maximum of its complex with iodine. The numbering of compounds is the same as in Fig. 2. (See caption to Fig. 2 for other abbreviations.)

INTERPRETATION OF THE SPECTRA OF MOLECULAR COMPLEXES

Some of the spectroscopic transitions referred to in the present paper as charge-transfer transitions have been given widely divergent theoretical interpretations. Bayliss regarded the charge-transfer transition in the benzene-iodine complex as solvent-induced modification of the intense iodine absorption near 188 mμ.[7] Andrews and Keefer suggested that the charge-transfer transition in the sulfur dioxide–benzene complex might represent an intensification of a transition of the sulfur dioxide molecule.[8] Blake, Winston, and Patterson treated the charge-transfer transitions of the benzene and naphthalene-halogen complexes as perturbed transitions of the aromatic molecules.[9] Mulliken originally regarded the charge-transfer transition of the benzene-iodine complex as an intensified transition of the benzene molecule,[3a] but later changed this interpretation to one from which the term "intermolecular charge-transfer" is derived.[3b,c]

In view of the great diversity of molecular complexes which show intermolecular charge-transfer transitions, it is a reasonable hope that all of these transitions are essentially similar from a theoretical point of view and that their interpretations must employ quantities common to all A and D molecules which have been found to form colored molecular complexes. When this view is adopted, it is easily seen from the data assembled in Figs. 1–3 that the above-mentioned theories of Bayliss, Blake, Winston, and Patterson, Andrews and Keefer and the *original* theory of Mulliken cannot be accepted in general, although such theories might conceivably prove to be the correct interpretations in particular cases. In the following, only those theories which appear to be sufficiently general to provide theoretically similar interpretations of the spectra of a great variety of molecular complexes are considered.

According to the theory finally adopted by Mulliken,[3c] the charge-transfer excited states of molecular complexes can be approximately described by regarding the electron donor as a positive ion and the electron acceptor as a negative ion. These charge-transfer excited states would be correlated at infinite separations with these ions in doublet electronic states. Accordingly we may express the charge-transfer energy by the equation,

$$h\nu = I_p - E - W \quad \text{(in ev)}, \tag{1}$$

where h is Planck's constant, ν is the transition frequency, I_p is the vertical ionization potential of the B molecule, E is the vertical electron affinity of the A

[7] N. S. Bayliss, J. Chem. Phys. **18**, 292 (1950).

[8] L. J. Andrews and R. M. Keefer, J. Am. Chem. Soc. **73**, 4169 (1951).

[9] Blake, Winston, and Patterson, J. Am. Chem. Soc. **73**, 4437 (1951).

molecule, and W is the dissociation energy of the charge-transfer excited state. The ground-state dissociation energy is omitted from (1) as it is negligible ($\sim$0.1 ev). By adopting the straight line approximation for the data in Fig. 2, the quantity $h\nu$ may be expressed empirically by the equation,

$$h\nu = 0.67I_p - 1.9 \quad \text{(in ev)}. \tag{2}$$

The first coefficient of Eq. (2) may have any value from 0.4 to 1.0 with little loss in accuracy. In particular, the data can be fitted by the following especially simple equations:

$$h\nu = 0.47I_p \tag{2'}$$

(strict proportionality: the line passes through the origin), and

$$h\nu = I_p - 4.96. \tag{2''}$$

(The quantity $E+W$ in Eq. (1) is constant. Studies on complexes whose donors have much lower I_p's are greatly needed, to show whether the points continue to lie on a straight line, and if so, determine the slope more accurately.)

By combining the theoretical Eq. (1) with the empirical Eq. (2), we obtain for the dissociation energy of the charge-transfer excited state the equation,

$$W = 0.33I_p + 1.9 - E. \tag{3}$$

The vertical electron affinity of the iodine molecule (in a molecular complex) has been estimated[3c] as *ca* 1.8 ev. Therefore, according to (3), for D molecules with ionization potentials in the 8–10 ev range, the dissociation energies of the charge-transfer states are 3.3–3.8 ev. These dissociation energies are generally about 1.5 ev greater than the Coulombic energy of plus and minus electronic charges separated by the van der Waals intermolecular distances (3–4A) for the complexes of Fig. 2. Only detailed calculations can tell whether or not this rather large energy ($\sim$1.5 ev) can be accounted for in terms of intermolecular covalent binding and polarization energies of the charge-transfer excited states, or in terms of solvent effects. (The classical solvation energy of a dipole of the dimensions of the complex can easily be shown to be negligible.)

In addition to this problem of the absolute magnitudes of the various terms in (3) there is also the question of why the dissociation energies of the charge-transfer excited states should increase with increasing ionization potential of the base molecules. Since the effective van der Waals radii of the donor molecules may decrease with increasing ionization potential, and the Coulombic energy of the excited state increases with decreasing intermolecular distances, the increase in W with I_p may simply be due to the variation in the effective van der Waals radii of the base molecules with I_p.

It is instructive to show that this explanation for the variation of W with I_p is correct as to order of magnitude. From (3) we have the approximate experimental relationship: $dW/dI_p \approx 0.33$. To estimate dW/dI_p theoretically we first write $dW/dI_p = (dW/dr)(dr/dI_p)$. The first factor dW/dr measures the slope of the excited state potential curve; assuming this potential is essentially Coulombic and that the average intermolecular separation is 3.5A, we obtain $dW/dr \approx 0.6$ ev/A. The second term dr/dI_p gives the rate of change of the van der Waals radii of the base molecules with I_p. There is no simple way for getting this quantity for the molecules in Fig. 2; however, from data on the van der Waals radii of F, Cl, Br, and I, and from atomic ionization potentials, we can obtain for these atoms, $dr/dI = 0.14 \pm 0.03$ A/ev. Assuming dr/dI_p to be of this magnitude for the donor molecules, we obtain $dW/dI_p = 0.6 \times 0.14 \approx 0.1$, which is of the same order of magnitude as that obtained from (3).

The charge transfer theory does predict the correct order of magnitude for charge-transfer transition intensities.[3c] On the basis of this theory, there is no reason to believe that the regularities in Fig. 1 will be general for all donor molecules. This is especially true for cases where steric factors could act to keep the D and A molecules well separated. On the other hand, such regularities are expected for a series of A molecules with similar electron affinities *or* similar van der Waals radii. In this connection, it may be of interest to point out the possibility that there might be intramolecular charge-transfer spectra having an ϵ_{max} *vs* λ_{max} behavior similar to that in Fig. 1. For example, the 250 mμ band of nitrobenzene ($\epsilon \approx 8000$) moves slightly to shorter wavelengths (by 5 mμ) but decreases in intensity by a factor of five when the nitro group is gradually twisted by increasing the size of ortho-substituents.[10] In this case, the nitro group can be regarded as the electron acceptor portion of the molecule and the benzene nucleus can be regarded as the electron donor.

From the preceding discussion, it may be seen that there is a strong possibility that the theoretical charge-transfer theory, if sufficiently refined in its quantitative aspects, will be able to account for the spectroscopic regularities presented in this paper. Until a satisfactory refinement is achieved, however, we believe it important to consider other possibilities regarding interpretations of charge-transfer spectra.

An interesting alternative interpretation of the charge-transfer spectra of molecular complexes is suggested by the recent data of Kasha[11] and Reid.[12] Kasha showed that the lowest energy singlet-triplet absorption transition in alpha-chloronaphthalene is strongly enhanced in ethyl iodide solvent. If this enhancement were attributed to weak molecular complex formation, the corresponding singlet-triplet transition of the complex might be 10–1000 times stronger than the corresponding transition in alpha-chloronaphthalene alone, depending on the percentage of complex present.

Reid showed that the phosphorescence intensities of a variety of catacondensed hydrocarbons were strongly

[10] W. G. Brown and H. Reagan, J. Am. Chem. Soc. **69**, 1032 (1947).

[11] M. Kasha, J. Chem. Phys. **20**, 71 (1952).

[12] C. Reid, J. Chem. Phys., **20**, 1212 (1952). We are indebted to Dr. Reid for showing us his manuscript in advance of publication.

enhanced in the presence of *s*-trinitrobenzene (an *A* molecule). The trinitrobenzene seemed to shorten the lifetimes for these phosphorescences to about 10^{-4} seconds, which represents a *ca.* 10^4 increase in the transition probability for these compounds.

However, the lowest triplets, or phosphorescent triplets studied by these authors, do not give very strong transitions to the ground state (in the absence of possible complexing agents) and, in fact, are expected to give the weakest triplet-singlet transitions in these molecules because the transition is "orbitally forbidden."[13] Singlet-triplet transitions which are "orbitally allowed" are 10–100 times stronger than the orbitally forbidden transitions and have molar extinction coefficients of the order of one. If by complex formation these strong singlet-triplet transitions were enhanced to the same degree as the apparent enhancement of the weak singlet-triplets, then the estimated singlet-triplet absorption intensities in the complexes would be of the same order of magnitude as the intensities observed for the charge-transfer transitions.

The above discussion implies that the dissociation products of the charge-transfer excited states of molecular complexes are *D* molecules in triplet states and *A* molecules in singlet states. At present, there is apparently no completely satisfactory theory which accounts for the enhancement of these singlet-triplet transition probabilities in complexes containing only light atoms. The data in Fig. 3 indicate the extent to which available data shed light on this second theory. One would expect a correlation between the energies of charge-transfer transitions and the strongest singlet-singlet transitions of a series of *D* molecules if the separations of the excited singlet and excited triplet states of the *D* molecules were approximately constant. The correlation between these singlets and charge transfer energies is not very good, as shown in Fig. 3, but, of course, the assumption regarding the constancy of the excited singlet-triplet separations is not certain since the energies of the triplet states of many of the *B* molecules are not known. It may be noted also that the extrapolation in Fig. 1 to zero intensity gives a wavelength which is close to that estimated[14] for the strong singlet-triplet transition in benzene.

Of the various theoretical interpretations which could be proposed for the charge-transfer spectra the two discussed above are the most promising; of these two, the theory of Mulliken appears to be the more successful at present.

[13] J. R. Platt, J. Chem. Phys. **17**, 484 (1949).

[14] C. C. J. Roothaan and R. S. Mulliken, J. Chem. Phys. **16**, 118 (1948).

THE JOURNAL OF CHEMICAL PHYSICS VOLUME 21, NUMBER 1 JANUARY, 1953

Equilibrium in the Exchange of Deuterium between Ammonia and Hydrogen*

MORRIS PERLMAN, JACOB BIGELEISEN, AND NORMAN ELLIOTT
Department of Chemistry, Brookhaven National Laboratory, Upton, Long Island, New York

(Received June 9, 1952)

Equilibrium in the reaction $NH_{3(g)}+HD_{(g)}=NH_2D_{(g)}+H_{2(g)}$ was measured in the temperature range 210°K to 295°K. The results may be expressed by the relation $K=0.972\ \exp.\ 509/T$. The zero-point energy difference between NH_3 and NH_2D is calculated to be 635 ± 3 cm^{-1}.

INTRODUCTION

THE equilibrium in the exchange reaction

$$NH_{3(g)}+HD_{(g)}=NH_2D_{(g)}+H_{2(g)} \qquad (1)$$

was studied above room temperature by Farkas,[1] Wirtz,[2] and Herrick and Sabi.[3,4] The recent experiments of Claeys, Dayton, and Wilmarth[5] show that this reaction in the liquid is fairly rapid when catalyzed by KNH_2. The work reported here was undertaken to obtain equilibrium data at and below room temperature.

EXPERIMENTAL METHOD

Equilibration

The apparatus in which the equilibration of ammonia and hydrogen was allowed to take place is shown in Fig. 1. Measurements were made at temperatures below the normal boiling point of ammonia with liquid ammonia and at room temperature with ammonia gas. In all experiments the gas equilibrium was measured.

For the low temperature experiments 18.5 ml of liquid ammonia containing approximately five atom percent deuterium was condensed onto approximately one gram of KNH_2 in vessel *A*. The preparations of these matrials are described below. Constant temperature was maintained in the system by a bath of melting solid held in the Dewar *B*; the temperature was measured with a calibrated copper-constantan thermocouple and was constant to better than 0.1°C. Tank H_2-HD mixture (approximately 5 atom percent D),

* Research carried out at the Brookhaven National Laboratory, under the auspices of the AEC.

[1] A. Farkas, Trans. Faraday Soc. **32**, 416 (1936).

[2] K. Wirtz, Z. Physik. Chem. **B30**, 289 (1935).

[3] C. E. Herrick, Jr., and N. Sabi, Columbia University Secret Report A-765, July 30, 1943.

[4] I. Kirshenbaum, *Physical Properties and Analysis of Heavy Water* (McGraw-Hill Book Company, Inc., New York, 1951), pp. 55–65.

[5] Claeys, Dayton, and Wilmarth, J. Chem. Phys. **18**, 759 (1950).

released from UH_3-UH_2D, was metered into the calibrated bulb *C* to a pressure of 25 cm; and it was then transferred into vessel *A* by application of gas pressure to the mercury reservoir. The rotating inverted cone, driven by a shaft passing through a Wilson seal, served to lift the solution continuously and to throw it out as a spray. The liquid pumping rate was approximately 10 ml per second. The gas phase was circulated by the motion of the fan blades. At intervals small gas samples for isotopic analysis were withdrawn into the side arm volumes at *D* and *E*. It was demonstrated that the time for complete gas mixing in vessel *A* was less than 15 seconds. The reaction was allowed to continue until the isotopic composition of the components of the gas samples became constant. In a separate experiment it was found that the half-time for exchange of deuterium between the amide catalyst and liquid ammonia was short compared with the equilibration times.

For the room temperature measurements gaseous ammonia and hydrogen were metered into vessel *A*, which contained a small quantity of a commercial solid catalyst, either platinized charcoal or a mixture of supported nickel and ruthenium. In all other respects the procedure was the same as that used for the low temperature measurements.

The gas samples for analysis were pumped through a trap cooled by liquid nitrogen to separate the hydrogen from the ammonia.

Analysis

For deuterium analyses all samples were in the form of hydrogen gas. Conversion of the ammonia was effected by reaction with cleaned uranium metal turnings at a temperature of about 475°C.[6]

The isotopic analyses were performed with a General Electric Company mass spectrometer by comparison with standards.[7] A glass pinhole leak was installed in the instrument. Corrections, amounting to about 0.15 percent of the H_2^+ peak height, were made for the H_3^+ ion.

PREPARATION OF MATERIALS

Ammonia containing about 5 atom percent deuterium was prepared by the addition of NaOH and NH_4NO_3 to an excess of 5 percent D_2O–95 percent H_2O mixture. The ammonia was dried by means of cold traps and sodium metal; it was stored as liquid in a nickel cylinder.

Potassium amide was prepared in a nickel apparatus by the passage of ammonia through liquid potassium at 350°C. The reaction was judged complete when no more hydrogen was present in the exit gas. The amide was stored in closed containers and showed little deterioration on standing. This material was easily handled in air, in contrast to the inflammable material prepared by catalyzed reaction in liquid ammonia.

[6] Bigeleisen, Perlman, and Prosser, Anal. Chem. **24**, 1356 (1952).
[7] R. E. Weston, Jr., and J. Bigeleisen, J. Chem. Phys. **20**, 1400 (1952).

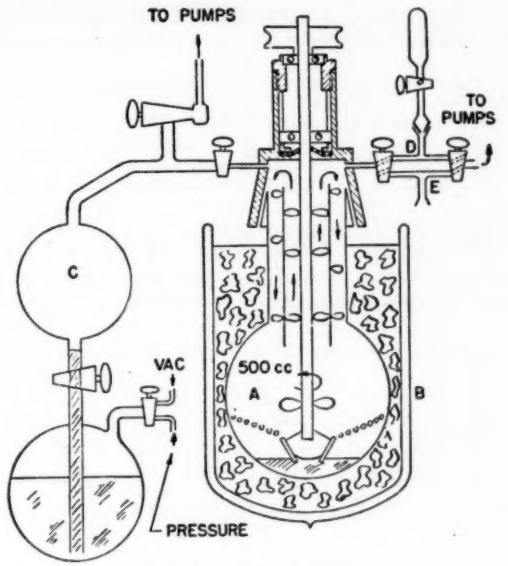

FIG. 1. Equilibration apparatus.

Results

From the analytical data the HD/H_2 and NH_2D/NH_3 ratios for the gaseous equilibrium were calculated in the following manner.

For the hydrogen gas

$$D_H=\frac{HD+2D_2}{2(H_2+HD+D_2)}, \tag{2}$$

where D_H is the atom fraction of deuterium and the other symbols are numbers or concentrations of the particular species. Adequate correction for the small amounts of D_2 present in these experiments may be made with the assumption that for the reaction

$$H_2+D_2=2HD, \tag{3}$$

the equilibrium constant is equal to four. It follows that

$$(HD)/(H_2)=2D_H/(1-D_H). \tag{4}$$

For ammonia gas

$$D_N=\frac{NH_2D+2NHD_2+3ND_3}{3(NH_3+NH_2D+NHD_2+ND_3)}, \tag{5}$$

where D_N is the atom fraction of deuterium in the hydrogen obtained from the ammonia. Because the atom fraction of deuterium did not exceed 0.05, the ND_3 concentration may be neglected. It is assumed that for the reaction

$$NHD_2+NH_3=2NH_2D, \tag{6}$$

the distribution of deuterium is random, $K_6=3$. This assumption is supported by the calculations of Kimball and Stockmayer.[8]

It follows that

$$NH_2D/NH_3=3D_N(1-D_N)/(1-2D_N). \tag{7}$$

Results are summarized in Table I.

In experiments 1, 2, and 3 the isotopic composition

[8] See reference 4, p. 59.

TABLE I. Equilibrium in the reaction $NH_{3(g)}+HD_{(g)}=NH_2D_{(g)}+H_{2(g)}$.

Exp. No.	T°K	Catalyst	Approach	$D_H \pm$av. dev.	$D_N \pm$av. dev.	$(HD/H_2)_g$	$(NH_2D/NH_3)_g$	K_1
5	295	Ni+Ru	5 atom % NH_3-D; H_2	0.0108±0.0002	0.0367±0.0004	0.0218	0.115	5.26±0.1
8	295	Pt	6 atom % H_2-D; NH_3	0.0091±0.0000	0.0318±0.0003	0.0184	0.0988	5.37±0.1
6	295	Ni+Ru	5 atom % NH_3-D; H_2	0.0122±0.0001	0.0384±0.0002	0.0247	0.121	4.92±0.1
1	231	KNH_2	5 atom % NH_3-D; 5 atom % H_2-D	0.0091±0.0001		0.0184		
					0.0509±0.0007		0.163[a]	8.86±0.2
3	231	KNH_2	5 atom % NH_3-D; 0.7 atom % H_2-D	0.0091		0.0184		
2	210	KNH_2	5 atom % NH_3-D; 1 atom % H_2-D	0.0072±0.0002	0.0513±0.0012	0.0145	0.161[a]	11.1 ±0.2

[a] These values were obtained by use of a smoothing procedure discussed in the text.

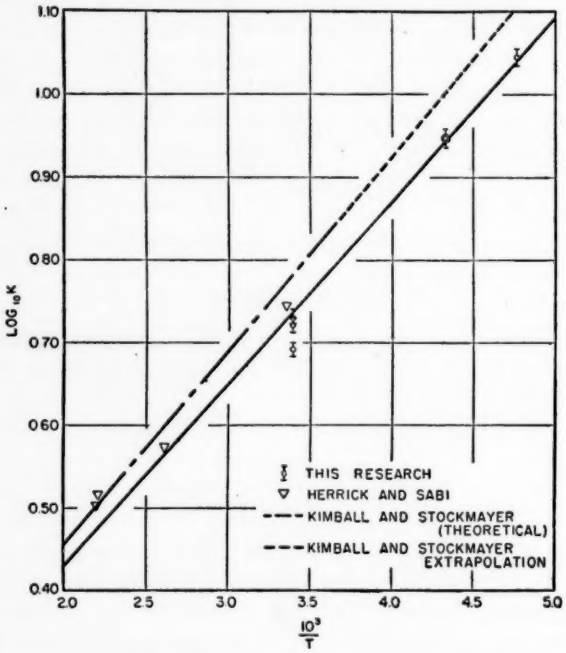

FIG. 2. Equilibrium constant for the reaction $HD_{(g)}+NH_{3(g)}=NH_2D_{(g)}+H_{2(g)}$ as a function of temperature.

of the liquid was constant. The logarithms of the $(NH_2D/NH_3)_g$ ratios derived from the deuterium analyses of the ammonia vapor over the liquid at the temperatures of the experiments and at room temperature were plotted *versus* $1/T$. Through the three points a line was drawn whose slope corresponded to the proper change of vapor pressure ratio with temperature.[9] The desired $(NH_2D/NH_3)_g$ values were read from this line.

In experiments 5 and 6 a calculation of the material balance showed that an over-all dilution of the deuterium by protium had occurred. That this dilution arose from an adsorbed layer, probably water, on the catalyst, is demonstrated by the fact that no dilution was observed in experiment 8, in which the quantity of catalyst was reduced about 100-fold.

Figure 2 shows the values of log K plotted against $1/T$. The results of Herrick and Sabi[3] as corrected by Kirshenbaum[4] and the theoretical line of Kimball and Stockmayer[8] are included. In the temperature range 200° to 500°K the data may be represented by an equation of the form

$$\ln K_1 = A + B/T, \tag{8}$$

in accord with theoretical expectations; at higher temperatures, however, K_1 must approach 3/2 asymptotically. A value for A was calculated theoretically by the method of Bigeleisen and Mayer[10] from the ratio of the classical frequencies of H_2 and HD,[11] from the masses and moments of inertia of NH_3 and NH_2D, and from the symmetry numbers. The products of the moments of inertia were calculated[12] from the internuclear distances.[13] The line in Fig. 2 was drawn through the calculated point at $1/T=0$ ($\ln K=A$) and the experimental points of this work. In Eq. (8) $A=-0.029$; the value of B, derived from the slope of line, is 509°K.

Zero-Point Energy Calculation

The vibrational spectrum of ammonia has not been sufficiently well analyzed to permit the calculation of its zero-point energy.[14] For this reason the theoretical line of Kimball and Stockmayer deviates from the experimental data. From the value of B in Eq. (8), from the difference in the zero-point energies of H_2 and HD, and from the rotational constants of H_2 and HD, the difference in the zero-point energies of NH_3 and NH_2D may be calculated.[10] The relation is

$$(E^0_{0(NH_3)}-E^0_{0(NH_2D)})/k = B+(E^0_{0(H_2)}-E^0_{0(HD)})/k + (\sigma_{(HD)}-\sigma_{(H_2)})T/3, \tag{9}$$

where k is the Boltzmann constant. The zero-point energies and values of σ for H_2 and HD were calculated from the data in Herzberg.[15] The value obtained for $(E^0_{0(NH_3)}-E^0_{0(NH_2D)})/k$ is 914±5°, which is equivalent to $(E^0_{0(NH_3)}-E^0_{0(NH_2D)})/hc=635\pm3$ cm^{-1}

We thank Mr. A. P. Irsa for carrying out the analyses with the mass spectrometer and Mr. H. C. Prosser for his help in the preparation of standards and materials.

[9] I. Kirshenbaum and H. C. Urey, J. Chem. Phys. **10**, 706 (1942).

[10] J. Bigeleisen and M. G. Mayer, J. Chem. Phys. **15**, 261 (1947).

[11] G. Herzberg, *Molecular Spectra and Molecular Structure I* (Prentice-Hall, Inc., New York, 1939), p. 141.

[12] J. O. Hirshfelder, J. Chem. Phys. **8**, 431 (1940).

[13] M. V. Migeotte and E. F. Barker, Phys. Rev. **50**, 418 (1936).

[14] G. Herzberg, *Infrared and Raman Spectra of Polyatomic Molecules* (D. Van Nostrand Company, Inc., New York, 1945), p. 294.

[15] G. Herzberg, *Molecular Spectra and Molecular Structure I* (Prentice-Hall, Inc., New York, 1939), p. 487.

Molecular Images with the Projection Microscope. The Ionization Potential of Zinc Phthalocyanine

ROBERT GOMER AND DONALD A. SPEER
Institute for the Study of Metals, University of Chicago, Chicago, Illinois
(Received June 10, 1952)

The current emerging from single molecules of zinc phthalocyanine in field emission has been measured as a function of voltage. The data permit estimation of the ionization potential at *ca* 7 volts. Comparison of the experiments with a simple theory based on the emission of electrons from the molecule itself supports this view of image formation. It is shown that the images found are not diffraction patterns, but the result of electron optical effects. Emission measurements on molecules adsorbed on clean tungsten substrates show that irregularities of 5–10A exist on the best and cleanest of these surfaces.

I. INTRODUCTION

AMONG the more spectacular discoveries made with the field emission microscope is the observation due to Müller[1] that small quantities of such substances as phthalocyanine, hemin or anthracene on the emitter give rise to patterns that can best be explained as "images" of single molecules. The size of these patterns implies $\sim 10^7$-fold enlargement at resolutions of 3 to 5A. A recent investigation[2] of the transverse velocity distribution of electrons in field emission has shown that resolutions of *ca* 30A can be attained with the projection microscope; if the emerging electrons had no statistical momentum transverse to the direction of emission, a resolution of roughly 10A would be expected from diffraction considerations. These facts seem to contradict the molecular "images."

The difficulty can be resolved if it is assumed that the electrons responsible for molecular images originate in the molecules themselves and thus do not belong to the Fermi sea of the substrate. There must also be a considerable distortion of the field in the vicinity of a molecule. This results not only in increased emission where the field is highest, but also in electron optical effects. The latter are responsible for the very high magnification obtained and together with the selective field enhancement result in the apparent structure of these images. It was decided to test this hypothesis by attempting to measure the current coming from a single molecule as a function of applied voltage, and incidentally to see whether the projection microscope is suitable for the determination of ionization potentials of substances of very low vapor pressure.

II. EXPERIMENTAL

The microscope tube was constructed from a 100-cc round-bottom Pyrex vessel. The lower half of this bulb was coated with a suspension of willemite in a nitrocellulose solution to which a few drops of butyl phthalate had been added as plasticizer. The nitrocellulose was burned off after evaporation of the diluent (amyl acetate) leaving a deposit of willemite on the bulb. A layer of aluminum, thick enough to show metallic reflection and no transparency in ordinary light, was evaporated over the fluorescent screen. This served as a convenient anode, physical binder for the screen and as a reflector to increase light intensity on the outside of the bulb. A tungsten through Nonex seal was connected electrically to the aluminum coating with Hanovia liquid platinum paint and served as anode contact. A two-lead pressed seal (tungsten through Nonex to Pyrex) served as the support for the cathode. In order to avoid difficulties in outgassing these leads, they were coated with Nonex glass to within 3 mm of their ends. Two 10-milt ungsten wires whose ends had been preformed into spirals of a size small enough to insure a tight fit and good contact were slipped over the "open" ends of the lead-in wires. The end of one of the 10-mil wires was bent into a sharp hairpin so that the other wire could rest in the bend and project 2 to 3 mm beyond it. The projecting end was etched to a point electrolytically at *ca* 2 to 10 volts ac in a concentrated sodium hydroxide solution until the point could no longer be resolved in a light microscope at 500-fold magnification. After careful rinsing in distilled water the cathode assembly was then sealed into the microscope tube.

The microscope bulb was supplied with three sidearms, one of which contained some zinc phthalocyanine, which had previously been purified by repeated vacuum sublimation. The other sidearm ended in a tubular expansion shaped somewhat like a small light bulb; this bulb contained a filament of 12-mil tantalum wire which could be heated electrically, and served as getter. The filament was so located that evaporating tantalum could not hit the tungsten tip. The third sidearm, of *ca* 10-mm inside diameter, was constructed of very thick Pyrex, and connected the microscope assembly to the vacuum system. Figure 1 shows a photograph of the microscope.

The vacuum system consisted of a D.P.I. three-stage fractionating oil diffusion pump and two liquid air traps in series. Between the microscope and the nearest trap an RCA 1949 ion gauge was located. It has been amply demonstrated that ion gauges other than thin wire collector types read erroneously at low pressures because of soft x-ray bombardment of all inner surfaces. In the present case the microscope tubes were always sealed off

[1] E. W. Müller, Z. f. Naturforschung **59**, 473 (1950).
[2] R. Gomer, J. Chem. Phys. (to be published).

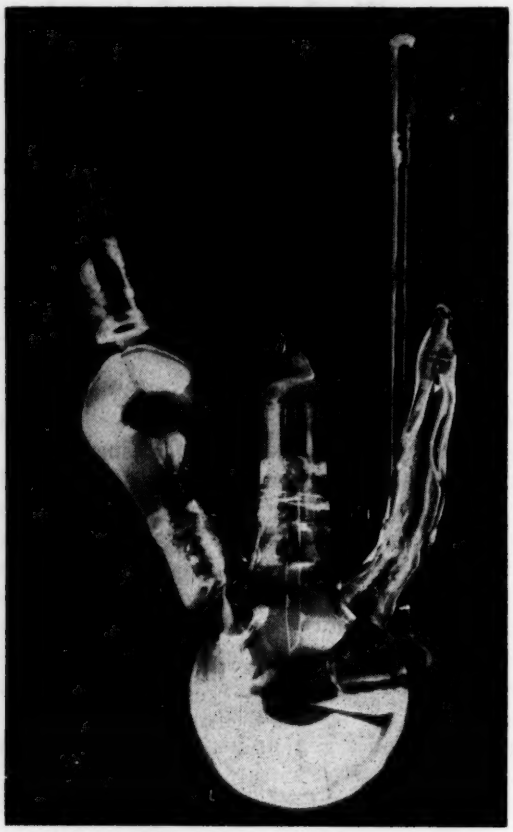

FIG. 1. Photograph of microscope assembly.

before significant experiments were attempted, so that high readings on the ion gauge were unimportant. The microscope assembly, ion gauge, and first liquid air trap were outgassed at 350–400C for several hours. During this and subsequent operations liquid nitrogen was kept in the second trap. After this preliminary outgassing, all parts of the assembly except the sidearm containing phthalocyanine were again outgassed by careful flaming with a hand-torch just below softening temperature. The tungsten tip and the tantalum filament were then heated to *ca* 2500C until ion gauge readings indicated pressures of not over 10^{-7} mm of Hg with all metal parts hot. These processes were repeated as often as necessary. Care was also taken to sublime the phthalocyanine several times within its sidearm without distilling too much away. The thickened seal-off tube connecting the microscope to the vacuum system was heated several times to partial collapse and finally sealed off at as low a temperature as possible. During seal-off, the ion gauge reading did not rise above $2 \cdot 10^{-7}$ mm of Hg. With very thorough outgassing it was sometimes possible to achieve cutoff of the ion gauge before seal-off, but this was not found essential. After sealoff, the pressure inside the tube was estimated to be of the order of 10^{-7} to 10^{-8} mm, from the speed with which the clean tip surface became contaminated, and also from the frequency of fluctuations of the adsorbed phthalocyanine molecules.[2]

FIG. 2. Thick layer of phthalocyanine evaporated onto a tungsten tip from the side. Tip constant $k=3.5 \cdot 10^9$ cm^{-1}. Photograph at 12 000 volts.

FIG. 3. Clean tungsten tip, showing two molecules of phthalocyanine. Tip constant $k=6.53 \cdot 10^9$ cm^{-1}. Photograph at 8000 volts.

The tube was now gettered by prolonged heating of the tantalum filament at a rate sufficient to deposit a visible layer in an hour. It was noticed that best results were achieved if the phthalocyanine sidearm was immersed in liquid nitrogen during this operation. After the tantalum filament had been allowed to cool, the phthalocyanine could be warmed up without rise in pressure. This suggests that a moderately volatile impurity was present in the phthalocyanine and kept decomposing on the hot tantalum filament. No such difficulties were encountered in the absence of phthalocyanine. With proper care it was possible to obtain pressures at which tips remained uncontaminated for periods of days.

A voltage doubler, using two surplus VT 255 tubes capable of delivering 10 milliamperes of filtered dc current at 20 000 volts was used. A sensitive microammeter was used above 10^{-6} ampere and a 4.7-megohm load and vacuum tube voltmeter for currents

below this value. The tip could be heated electrically through the two lead-in wires; the heating current could also be utilized in a sensitive Wheatstone bridge, one arm of which consisted of the tip and its leads.

Photometric measurements consisted of determining the light output of the screen per unit current as a function of voltage. It was found that light output varied linearly with accelerating voltage and current for currents below 10^{-6} ampere. At high currents, saturation of the screen occurred, especially at low voltages. Measurements were carried out by mounting an RCA 931A photomultiplier at the focal plane of a viewing camera equipped with an Ektar, f 4,5 127-mm focal length lens. The camera was focused by means of a removable ground glass viewing screen, so that the total microscope image appeared as a region small enough to be accomodated by the sensitive area of the phototube. The object distance was 83 cm, so that cosine corrections were small. This camera was also used for all photographic work. After calibration of the screen, all but one molecular pattern was covered up and the light

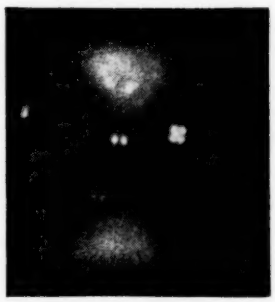

FIG. 4. Clean tungsten tip of Fig. 3 with more molecules of phthalocyanine. Photograph at 8000 volts. Positives printed to emphasize molecules.

output from a single image was then determined as a function of applied voltage. The photomultiplier was equipped with neutral density filters cut from sections of fine-grained film negatives. These were calibrated in a Beckman spectrophotometer and found constant to ½ percent over the entire visible spectrum. The data of Table III were obtained by using the phototube with a small Lucite probe, held directly against the microscope screen.

In order to gain an idea of the field enhancement near adsorbed molecules, scale models of phthalocyanine were constructed of clay and painted with glyptal lacquer and silver paint. The field distribution around the models was then measured in a three-dimensional electrolytic trough, containing two large plane electrodes. The models were fastened flat at the center of one of these so that fields could be measured relative to the undisturbed surface field at the plane. The dimensions of the tank were *ca* 70×70×70 cm and those of the models 5 to 10 cm. Measurements were carried out with an accurate potentiometer, using a tuned amplifier and oscilloscope as null detector and a 400-cycle

FIG. 5. Tip of Fig. 3 with more phthalocyanine. Photograph at 8000 volts. Positives printed to emphasize molecules.

oscillator as source. A small hemispherical boss on the plane electrode was used as control and showed that theoretical values[3] could be approached to within 10 percent or so.

III. RESULTS

In the process of subliming phthalocyanine onto the tip, the latter was generally contaminated with oxygen and other gases desorbed in the sublimation process. For most purposes this was desirable, as emission from the tip itself could thereby be reduced to a negligible amount. Figure 2 shows a thick layer of phthalocyanine sublimed onto the tip from the side. It will be seen that the emitting layer resembles a waning moon. This shows nicely that the tip is spheroidal. It was found possible, however, to sublime phthalocyanine onto a perfectly clean tip by successive flaming of the side arm. After a few sublimations, only phthalocyanine would come off and, if the tip was clean at this point, the desired result could be achieved. Figures 3–5 show a clean tip with a few molecules on it. It will be noted in Figs. 3 to 5 that some of these are apparently flat on the substrate and show the well-known four-leaf structure, while others seem to be resting on end and show only two nodes.

Table I shows current voltage relations for several single molecules and Table II for total emission from tips covered completely with phthalocyanine. In the latter instances, it is possible to derive average values for one molecule by knowing the number of molecules responsible for emission. Figure 6 shows the state of the tip responsible for *I* and *II*; the number of participating molecules in *III* was estimated as 30. Figure 7 shows a Fowler-Nordheim plot for a typical clean tungsten tip. From the slope of this plot, based on the fact[4] that

$$I = \text{const. } V^2 \exp\left(-\frac{6.84\cdot 10^7 \chi^{\frac{3}{2}}}{kV}\right), \qquad (1)$$

the constant k is evaluated to be $6.53\cdot 10^8$ cm^{-1}. The tip radius is calculated to be $3.0\cdot 10^{-5}$ cm from k, using the

[3] J. Jeans, *Mathematical Theory of Electricity and Magnetism* (Cambridge University Press, 1946), p. 197.

[4] See for instance J. A. Becker, Bell System Tech. J. **30**, 907 (1951).

TABLE I. Field emission from single molecules. Tip constant $k=6.53\cdot10^3$ cm^{-1}.

Molecule	Voltage (volts)	Current (amperes)
1	5200	$0.12\cdot10^{-9}$
	5600	0.27
	6000	1.42
2	5200	0.34
	5600	1.30
	6000	4.39
3	5200	0.31
	5600	0.87
	6000	3.76
4	5200	0.076
	5600	0.35
	6000	1.80
	6400	5.63
5	5200	0.04
	5600	0.094
	6000	0.40
	6400	0.75
6	5600	0.25
	6000	0.88
	6400	3.07
7	5600	0.19
	6000	0.54
	6400	1.3
8	5200	0.11
	5600	0.30
	6000	0.84
	6400	2.73
	6600	3.59
9	5200	0.11
	5600	0.30
	6000	0.73
	6400	1.81
	6800	4.76
10	5600	0.28
	6000	0.44
	6400	1.47
	6800	4.03

relation[5]

$$k=F/V=1/0.4r\ \ln x/r, \qquad (2)$$

x being the screen to tip distance, 3.5 cm. The geometric magnification resulting from this curvature, corrected for field compression[2] is $0.76\cdot10^5$. The compression factor β, as determined from the apparent angular separation of the 211 planes, was 1.54. The actual size of the molecular images on the screen was *ca* 0.25 cm, so that they appeared at a magnification of $3.1\cdot10^6$, or magnified over the tip by a factor of 40.

Figure 8 shows a photograph of the actual model used in the electrolytic trough determinations and a schematic diagram summarizing the results obtained. It will be noted that the field enhancement is greatest at the corners of the molecule and least in the center. It was found that the exact curvature at the rim of the model was not critical. For a model of twice the thickness of the one used, enhancements increased by a factor of 1.15.

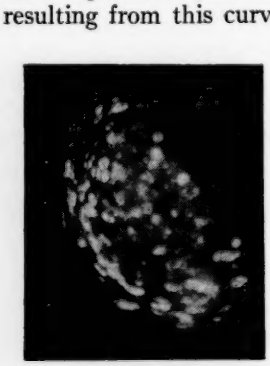

FIG. 6. Tungsten tip covered with phthalocyanine, corresponding to tip conditions of runs *I* and *II*. Tip constant $k=7.03\cdot10^3$ cm^{-1}. Photograph taken at 7000 volts.

[5] Private communication from W. W. Dolan, Linfield College, McMinnville, Oregon. See also reference 4, p. 912.

IV. DISCUSSION

Before attempting to evaluate any quantitative information it may be well to point out several pieces of qualitative evidence which strongly suggest that the observed patterns are images of single molecules:

(1) It will be seen from Figs. 4–6 that individual patterns of fourfold and twofold symmetry occur frequently. It can be seen by eye, although not readily recorded, that these frequently change from one to the other. This suggests strongly that the molecule responsible for the pattern has changed its position from flat adhesion to an "upright" one.

(2) It is frequently observed that four- or two-leaf patterns rotate and librate as a unit, but never that only one component of such pattern breaks away from the rest. When phthalocyanine is first sublimed onto the tip, no structure having less than two leaves is ever seen. These facts suggest that the two- or four-leaf forms (which interchange) are the smallest units ever to occur on a molecular scale.

(3) It will be seen from Figs. 3–6 and Table III that patterns of somewhat varying brightness and size occur on the same tip. It can be verified by visual observation that occasionally a bright pattern will change to a

TABLE II. Field emission from phthalocyanine covered tungsten tips. Tip constant $k=7.03\cdot10^3$.

	Voltage (volts)	Current (amperes)
I	6000	$0.34\cdot10^{-6}$
	6400	$0.78\cdot10^{-6}$
	6800	$1.80\cdot10^{-6}$
	7200	$2.40\cdot10^{-6}$
II	6400	$0.25\cdot10^{-6}$
	6800	$0.80\cdot10^{-6}$
	7200	$1.30\cdot10^{-6}$
	7600	$3.60\cdot10^{-6}$
III	5200	$1.14\cdot10^{-9}$
	5600	$5.78\cdot10^{-9}$
	6000	$14.7\cdot10^{-9}$
	6400	$23.5\cdot10^{-9}$
	6800	$57.8\cdot10^{-9}$

dimmer one and vice versa. Occasionally, patterns will seem to lose their structure and appear as one large bright spot; the latter will revert after some time to a two- or four-leaf structure. These facts suggest strongly that the size and brightness of the patterns depend on the field enhancement near individual molecules. This would be expected to vary with the position of the molecules on the surface. In this connection it should be mentioned that molecular patterns invariably seem to get brighter and larger when the tip is heated slightly below the volatilization temperature (*ca* 400C), although it is difficult to photograph the effect.

(4) There is a very definite correlation between the frequency of movement of the patterns and the pressure in the tube. In a previous communication[6] it was stated that this fact could be used for determining the pressure absolutely. It has since been found, however, that the rate of fluctuation is also proportional to the total current. This suggests that the ions responsible for the bombardment and hence the fluctuations of the patterns are secondary in origin and proportional to the total electron current. It is still possible, of course, to use the tube as a pressure gauge by proper calibration, although the previous claim of absolute measurement is erroneous.

TABLE III. Relative emission from single molecules and tungsten. Tip constant $k=6.53\cdot10^3$. $V=8000$ v.

Relative brightness
(1) Molecules: 10, 43, 16, 4, 15, 5, 8, 8, 14, 4
(111) direction: 9
(310) direction: 23

Nevertheless, the order of magnitude of the fluctuations suggests that one is dealing with areas of the order of 100A.[2]

These considerations make it highly plausible that the patterns are caused by individual molecules. The current voltage relations obtained will now be interpreted on this basis. For simplicity we assume that the molecule may be represented by a three-dimensional potential well in which the π-electrons are considered non-localized. It is assumed that only the highest filled levels in the ground state contribute to emission. The current is then given by

$$I=n\cdot z\cdot D, \tag{3}$$

n being the number of participating electrons, z the rate of impact of the electrons on the sides of the box, and D the chance that an electron will tunnel through the barrier. The impact frequency is given by

$$z=v/a\lambda=h/ma\lambda^2, \tag{4}$$

where v is the velocity of the electrons in the box and λ their wavelength, which can be taken as the box length divided by a, a being a small integer. We use for D the

[6] R. Gomer, J. Chem. Phys. 19, 1072 (1951).

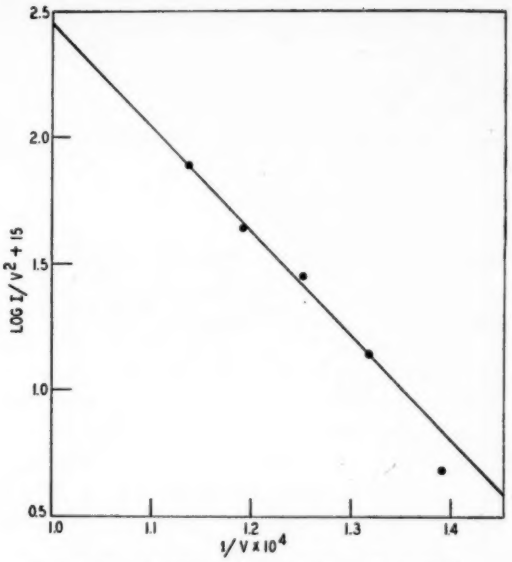

FIG. 7. Fowler-Nordheim plot for a clean W tip.

transmission coefficient worked out by Nordheim[7] for a one-dimensional barrier.

$$D=\frac{4[E(\chi+\mu-E)]^{\frac{1}{2}}}{\chi+E}\cdot\exp\left(-\frac{6.84\cdot10^7(\chi+\mu-E)^{\frac{3}{2}}}{F}\right). \tag{5}$$

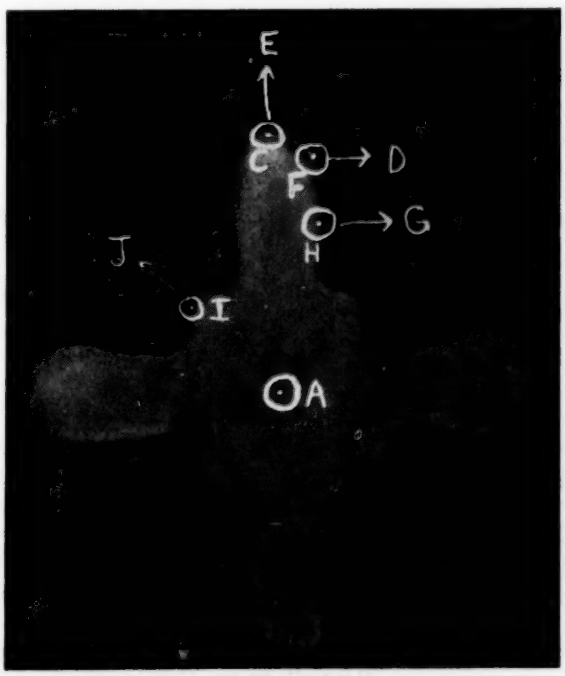

FIG. 8. Photograph of phthalocyanine model, used in electrolytic trough determinations. The model is based on C—C bond distances of 1.44A and is 1.4A thick. ⊙ corresponds to potential gradients normal to the plane of the paper at the point indicated. → corresponds to gradients measured parallel to the plane of the paper at points indicated. The following values were found for F/F_0, the ratio of gradient to gradient at the unperturbed plane substrate: $A=1.67$, $C=2.0$, $D=2.67$, $E=2.14$, $F=2.5$, $G=1.03$, $H=2.47$, $I=1.6$, $J=1.32$.

[7] R. H. Fowler and L. W. Nordheim, Proc. Roy. Soc. (London) A119, 173 (1928).

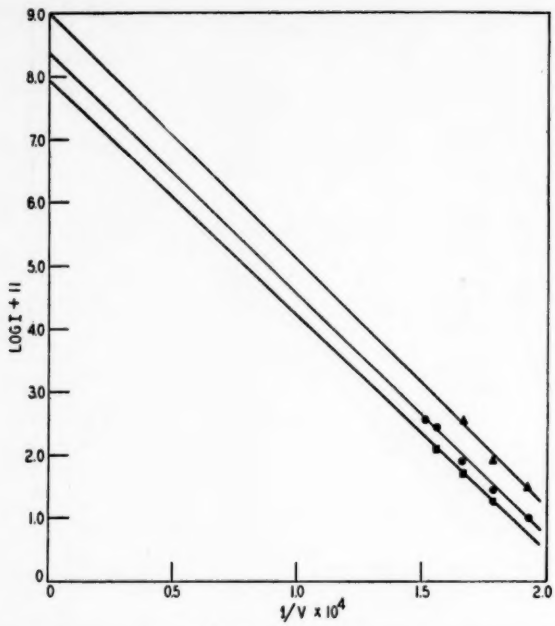

FIG. 9. Plots of log$I$ *vs* $1/V$ for several single molecules of zinc phthalocyanine. Numbers refer to those listed in Tables I or IV: ▲=3, ●=8, ■=7.

Here χ is the work function, μ the height of the Fermi sea, E the energy of the tunneling electrons, and F the surface field. In the present case we assume that χ becomes the ionization potential and that $E=\mu=h^2/2\lambda^2m$, i.e., that only electrons in the highest filled levels contribute. The emitted current should then be

$$I=2\sqrt{2}n\frac{h^2}{a\lambda^3m^{\frac{1}{2}}}\cdot\frac{\chi^{\frac{1}{2}}}{\chi+(h^2/2m\lambda^2)}\cdot\exp\left(-\frac{6.84\cdot10^7\chi^{\frac{3}{2}}}{k\epsilon V}\right), \quad (6)$$

where ϵ is the field enhancement factor, that is, the factor by which the field kV at the surface of the clean tip must be multiplied to give the effective field at a molecule.

The following assumptions are implicit in the derivation of Eq. (6). It is assumed that the forces active in holding the molecule to the surface are sufficiently weak to perturb the orbitals of the former only to a minor extent. Since the molecules seem to retain their identity and are not decomposed (as would be the case in strong chemisorption), this is probably reasonable. Thus ionization potential and work function are thought of as identical. The error should at most amount to the heat of adsorption, i.e., 0.5 volt or so. It is assumed that electrons from the substrate metal can enter the molecule with sufficient ease to replenish all electrons lost by emission. This assumption hinges on two factors: (1) The number of electrons arriving at unit surface in unit time is sufficiently large; (2) the barrier between metal surface and molecule is sufficiently low to permit ready tunneling. It can readily be shown that the total number of electrons arriving at unit surface in unit time is given by

$$\int_0^\mu N(E)\cdot v\cdot dE=\frac{2\pi m}{h^3}\mu^2 1.6\cdot10^{-19}\ \text{ampere/cm}^2, \quad (7)$$

where μ is the height of the Fermi sea of the metal, v the velocity, and $E=\frac{1}{2}mv^2$. Using a value of 5 volts for μ in tungsten, it is seen that this number is $2\cdot10^{11}$ amperes/cm^2. Assuming an area of $6.4\cdot10^{-15}$ cm^2 for phthalocyanine, the current arriving at one molecule is seen to be $1.3\cdot10^{-3}$ ampere. Since the actual currents drawn in the experiments testing Eq. (6) were of the order of 10^{-9} ampere/molecule, it is seen that the transmission coefficient from metal to molecule due to contact potential could be as low as 10^{-6} before a steady state seriously different from the equilibrium assumptions of Eq. (6) would result. Since there seems to be a work function difference of only 1 to 2 volts between the metal and the molecule, this is improbable. It might be mentioned in passing that the electron affinity of phthalocyanine, which is what matters here, is probably not different from its ionization potential by more than 1 volt, since the large molecule with its π-electrons can be thought of as a relatively good electron sink as well as source, or a small piece of metal.

Equation (6) predicts that plots of log$I$ *vs* $1/V$ should result in straight lines. A knowledge of k and ϵ permits evaluation of the ionization potential from the slopes; the pre-exponential term in Eq. (6) can be determined directly from the intercepts. Figures 9 and 10 show such plots for representative single molecules and total coverages. It is seen that reasonably good straight lines result. It should be pointed out that it is difficult to obtain higher accuracy, especially in the case of individual molecules, since molecules frequently change

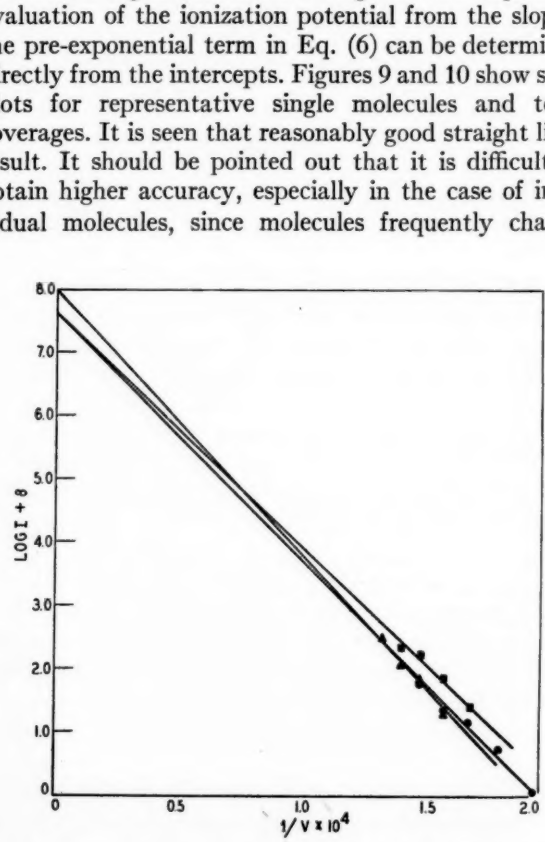

FIG. 10. Plots of log$I$ *vs* $1/V$ for polymolecular coverings. Numbers refer to data of Tables II or V. ■=I, ▲=2, ●=III.

TABLE IV. Summary of results for single molecules.

Molecule	Slope	Intercept	$\chi/\epsilon^{\frac{1}{2}}$ volts
1	4.0	−2.0	4.26
2	4.43	−1.0	4.56
3	3.48	−2.0	3.90
4	5.00	−0.6	4.95
5	4.00	−2.7	4.26
6	4.70	−1.0	4.70
7	3.90	−3.0	4.20
8	3.85	−2.6	4.15
9	3.60	−3.0	3.97
10	4.10	−2.4	4.32
Average		−2.0	

their position during measurements, especially at higher currents, possibly because of local heating or increased chance of ion bombardment. Small errors in current values will not affect the slopes and hence the calculated ionization potential markedly, but will cause very substantial errors in the intercepts since these are obtained by extrapolation, essentially to infinite voltage. This explains why in a few cases very high or very low intercepts were found.

Tables IV and V summarize the results. It will be seen that an ionization potential of 4.7 volts results if no field enhancement is assumed. If an average enhancement of 2.5 (as determined from the electrolytic trough) is used for the lowest values, the ionization potential becomes of the order of 7 ± 0.5 volts. This is a reasonable value. It should be pointed out that the transmission coefficient used in all present calculations is that of Eq. (5) and has not been corrected for image potential.[8] However, the value of k used here was computed from a plot of the clean tungsten tip also uncorrected for image forces, so that any errors are due only to the *difference* in image potential experienced by an electron outside the clean metal and outside the molecule. Since the total correction is small, this error should be much less than the experimental one.

The average intercept for the single molecule curves leads to a pre-exponential term of antilog (−2.0) amperes. If the logarithm of the number of emitting electrons is subtracted from the intercepts of the multimolecular emission curves, a value of antilog (−2.07) amperes results. This agreement is fortuitously good. Evaluation of the pre-exponential term in Eq. (6) gives the value $0.571[n\chi^{\frac{1}{2}}/a\lambda^3(\chi+E)]$ amperes. If χ is chosen as 7 volts and $\lambda\sim4$A so that $a=2$, this becomes $1.2\cdot10^{-3}n$ ampere. The number of electrons contributing significantly to emission is roughly 6 if we consider the highest levels of the three Cartesian coordinates only, and probably nearer to 12, but in no case over 40, the total number of π-electrons. It is seen that a pre-exponential term of $\sim$ antilog (−2.2) amperes results. The agreement with experiment is therefore somewhat better than experimental error on the one hand and the crudity of the theory on the other would lead one to expect.

It remains to show that the patterns are "images" in the sense here used and not simply diffraction patterns. It can be shown[2] that the resolution obtainable is given by

$$\delta'=r\beta\lambda/2\pi\delta, \tag{8}$$

where δ' is the separation of the emitting regions of width δ, and λ the average de Broglie wavelength of the electrons, which is practically equal to their final wavelength $12.5/V^{\frac{1}{2}}$ A. In Eq. (8) r is the effective radius of curvature of the tip. In view of the additional enlargement of the molecules, caused by local field distortion, it is simplest to put $x/r\beta$ equal to the total magnification obtained, in this case $3\cdot10^6$. If the four "corners" of the molecule, each *ca* 3A in extent, are considered as the emitting regions, it is seen from Eq. (7) that $\delta'=6.4\lambda$. For a voltage $V=6000$ volts, $\lambda=0.16$A, so that the minimum distance which two emitting regions of 3A width may be separated without leading to interference is 1A. Since the emitting regions in phthalocyanine are separated by nearly 3A, it is seen that no interference is to be expected. It is seen from Eq. (7) that the size of the patterns should vary with λ, that is, with $V^{-\frac{1}{2}}$, if the patterns were diffraction patterns. To test this, patterns were photographed at voltages from 6000 to 12000 volts. No reduction in size was found on measurement or observed visually. The only factor governing the size of the images that could be discovered is the tip radius. This is in accord with the assumption that the lines of force originating on neighboring elements of the tip tend to "compress" the lines originating in the molecule itself. The higher the curvature of the tip, the less compression is to be expected.

The argument just presented is based on the assumption of no lateral momentum of the electrons. Actually, the kinetic energies of the electrons inside the molecule amount to *ca* 4 volts; however, the proposed mechanism assumes preferential emission from the regions of highest field so that these energies will always be utilized in tunneling through the barrier in a direction outward from the center of the molecule. This is in agreement with the observation that applied voltage has no effect on the image size, since all field components are equally enhanced. It will be seen from careful observation of the photographs that occasionally very bright molecules seem to have a minimum of structure. This

TABLE V. Summary of results for total tip coverages.

Run	Number of emitting molecules	Intercept $-\log N$	$\chi/\epsilon^{\frac{1}{2}}$ volts
I	100	−2.04	4.20
II	100	−2.0	4.58
III	30	−2.07	4.31

[8] L. W. Nordheim, Proc. Roy. Soc. **A121**, 628 (1928).

observation indicates that at very high fields a larger fraction of the molecule becomes emitting, so that in the limiting case a structureless spot should be seen.

The observations listed in Table III permit some interesting conclusions about the nature of a clean heat-polished single crystal surface. It will be seen that the largest variation in brightness is given by a factor of 10. This means that variations in field enhancement from 2.0 to 2.5 are involved if the work function of phthalocyanine is taken as 7 volts and the average enhancement as 2.5. This corresponds to a variation by a factor of 1.3. Electrolytic trough experiments showed that such a variation could be caused by increasing or reducing the effective thickness of the molecules by a factor of 2 or so. Hence it can be concluded that irregularities of 1 to 3A depth and 5 to 10A width exist on the tungsten surface. Irregularities covering smaller regions (even if deep) would not be noticed by a phthalocyanine molecule. These findings support the essentially heterogeneous nature of surfaces.

It is a pleasure to thank Dr. J. R. Platt for most helpful discussions on the electronic structure of conjugated systems.

This work was supported in part by Contract AF 33(038)-6534 with the United States Air Force.

It is a pleasure to acknowledge the gift of phosphors and binders from Dr. Samuel Isenberg and the Sampson Chemical and Pigment Corporation.

THE JOURNAL OF CHEMICAL PHYSICS VOLUME 21, NUMBER 1 JANUARY, 1953

The Optical Absorption of Sulfur*

A. M. Bass†
Laboratory for Insulation Research, Massachusetts Institute of Technology, Cambridge, Massachusetts
(Received September 5, 1952)

The optical absorption of sulfur has been studied in the vapor and liquid state and in solution. These measurements indicate the presence of S_8 ring molecules which disappear at high temperature. The absorption edge in the liquid shifts at the rate of 6.20A/°C toward longer wavelengths with increasing temperature. It is believed that this displacement is related to the thermal excitation of the vibration levels of the sulfur molecules.

As part of an extended research program on the interrelation between structure and dielectric properties of the elements of the VI_b group of the periodic system,[1] Gilleo[2] has described studies on the optical absorption and photoconductivity in hexagonal and amorphous selenium, and Lizell[3] has measured the electrical conductivity of liquid selenium and selenium-tellurium mixtures. The present paper continues the optical studies by an investigation of sulfur in the liquid and gaseous state and in ethyl alcohol solution.

The optical absorption of plastic sulfur was studied by Fukuda[4] over the temperature range 0° to 300°C. For a film 0.3 mm thick he found that the edge of the absorption region shifted about 2A/°C toward the red with increasing temperature. Mondain-Monval[5] and co-workers, using films of sulfur about 40 mm thick, found that the shift in the absorption edge is 2.94A/°C up to about 160°C, and 7.4A/°C at higher temperatures. The marked change in absorption which occurs at about 160°C is associated with the abrupt variation in the viscosity characteristic of sulfur studied carefully by Bacon and Fanelli.[6] This behavior has been explained in terms of a change in molecular structure. The S_8 ring molecules, established for the solid rhombic modification by Warren and Burwell,[7] are assumed to break open and to polymerize into long chain molecules.[1,8]

EXPERIMENTAL PROCEDURE

The absorption spectrum of liquid sulfur was studied for sample thicknesses ranging from 19μ to 317μ and temperatures from 110° to 400°C. The liquid samples were prepared by depositing a layer of sulfur by vacuum evaporation on a pair of 1-in. diam quartz or glass disks. One face of these disks was flat; a uniform circular depression of $\frac{5}{8}$-in. diam was ground in the other, ranging in depth from 0.75 to 3 mils for the various plates. The depression and the surrounding ring-shaped surface were polished optically flat.

To form a liquid sulfur film of a given thickness, high

* Sponsored by the ONR, the Army Signal Corps, and the Air Force under ONR Contracts N5ori-07801 and N5ori-07858.

† Present address: National Bureau of Standards, Washington, D. C.

[1] A. von Hippel, J. Chem. Phys. **16**, 372 (1948).
[2] M. A. Gilleo, J. Chem. Phys. **19**, 1291 (1951).
[3] B. Lizell, J. Chem. Phys. **20**, 672 (1952).
[4] M. Fukuda, Mem. Coll. Sci. Kyoto Imp. Univ. **4**, 351 (1921).
[5] Mondain-Monval, Job, and Galet, Bull. soc. chim. [4] **47**, 545 (1930).
[6] R. F. Bacon and R. Fanelli, J. Am. Chem. Soc. **65**, 639 (1943).
[7] B. E. Warren and J. T. Burwell, J. Chem. Phys. **3**, 6 (1935).
[8] R. E. Powell and H. Eyring, J. Am. Chem. Soc. **65**, 648 (1943); N. S. Gingrich, J. Chem. Phys. **8**, 29 (1940); K. H. Meyer, Trans. Faraday Soc. **32**, 148 (1936); J. A. Prins and N. J. Poulis, Physica **15**, 696 (1949); H. Gerding and R. Westrik, Rec. trav. chim. **62**, 68 (1943).

purity sulfur‡ was evaporated into the depression and on the plane face of the opposing disk. The two disks were then placed in an electrically heated monel block with the two sulfur surfaces in contact. The sample holder was heated and, when the film was observed to melt, the disks were forced together. The close fit of the polished surfaces prevented the molten sulfur from escaping from the cavity.

The temperature of the film was measured by a thermocouple at the bottom of a hole drilled in the sample holder nearly to the edge of the quartz disks.

The spectra were obtained by means of a Cary recording spectrophotometer§ with a useful absorbance range from 0 to 3.2 and a wavelength range from 2100 to 7000A.

The thinnest films of liquid sulfur obtained by this technique were still too thick to permit measurements below *ca* 3800A. The absorption spectrum of the vapor was therefore examined over the same temperature range.

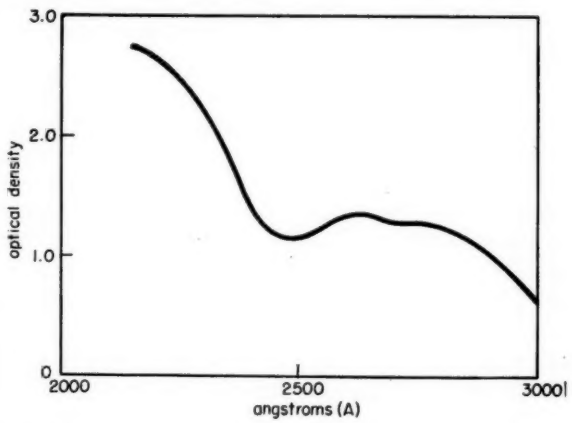

FIG. 1. Absorption spectrum of sulfur in ethyl alcohol.

RESULTS

A. Sulfur in Solution

The absorption spectrum of sulfur in ethyl alcohol was measured for a 1-cm path length of a saturated solution at about 22°C. This spectrum (Fig. 1) is in agreement with that reported earlier by Baer and Carmack[9] with regard to the location of the double maximum in the region 2600 to 2800A. However, we could not observe any indication of the short wavelength maximum which they reported near 2250A. If we assume that in the solution the sulfur molecules have the form of S_8 rings as in rhombic sulfur, the stronger absorption maximum at 2625A has a molar absorptivity ϵ‖ given by $\log\epsilon = 3.60$. Baer and Carmack found for this peak $\log\epsilon = 3.8$.

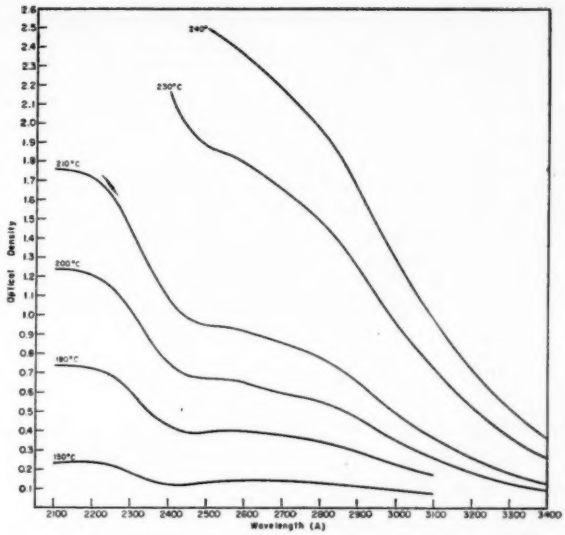

FIG. 2. Absorption spectrum of saturated sulfur vapor.

B. Sulfur Vapor

The spectrum of sulfur vapor is well known at high temperatures where the absorption is almost entirely due to S_2 molecules.[10,11] However, very little information is available as to the sulfur-vapor spectrum at temperatures below 300°C. Henri[10] described the spectrum at lower temperatures as showing only a continuous absorption. We found that below 250°C the absorption spectrum for a 6-cm path length shows broad unresolved maxima at 2100, 2550, and 2850A. (Fig. 2), similar to the absorption in ethyl alcohol. Assuming that this spectrum is produced by S_8 ring molecules and that the value $\log\epsilon = 3.60$ for the molar absorptivity of S_8 at 2550A applies, we can determine the fraction (ρ) of sulfur ring molecules over the range of temperatures indicated. Typical values computed from Fig. 2 are listed in Table I and compared with data

TABLE I. Dissociation of sulfur vapor.

T	ρ (fraction of vapor appearing as S_8)	ρ (reference 19)
140°C	1.0	0.76
160	0.70	0.74
180	0.45	0.75
200	0.39	0.74
220	0.38	0.73

‡ Kindly furnished by R. Fanelli, Texas Gulf Sulfur Company, New York.

§ Model 12M, Applied Physics Corporation, Pasadena, California.

[9] J. E. Baer and M. Carmack, J. Am. Chem. Soc. **71**, 1215 (1949).

‖ ϵ is defined by $I = I_0 \times 10^{-A}$, where $A = \epsilon cd/M$. A is absorbance or optical density; c, concentration in g/liter; d, optical path in cm; and M, molecular weight.

[10] V. Henri, *Structure des Molécules* (Lib. Scient. J. Hermann, Paris, 1925), p. 92 ff.

[11] J. I. Graham, Proc. Roy. Soc. (London) **A84**, 311 (1910); A. Christy and S. M. Naudé, Phys. Rev. **37**, 903 (1931); E. Olsson, Z. Physik **108**, 40 (1938); B. Rosen and L. Neven, J. chim. phys. **35**, 58 (1938); G. Herzberg and L. G. Mundie, J. Chem. Phys. **8**, 263 (1940).

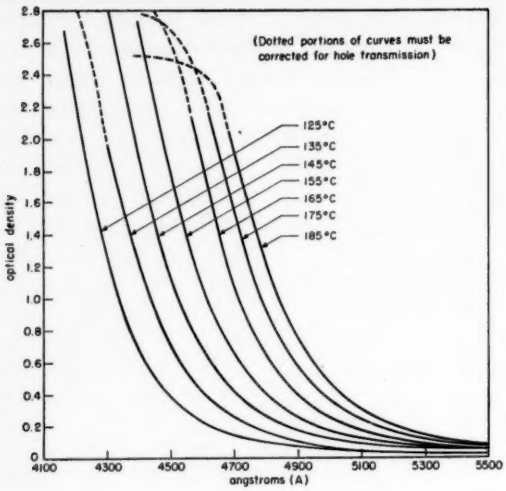

FIG. 3. Absorption spectrum of liquid sulfur (123μ thickness).

obtained from the vapor pressure of sulfur.[12] In contrast to the results of Braune *et al.*, we find a rapid decrease in the relative number of ring molecules, as one would expect from the breaking open of rings observed in the liquid phase. Rings are broken as the temperature increases; this follows also from our observation that above 250°C the concentration of S_2 becomes great enough to be observed spectroscopically and that it masks at higher temperature the diffuse bands described above.

C. Liquid Sulfur

The absorption spectrum of liquid sulfur is continuous, showing a monotonically increasing absorption toward shorter wavelengths; a typical set of data is given in Fig. 3. It may be seen that with increasing temperature the position of the absorption edge (arbitrarily defined as the wavelength at which the film has unit optical density) shifts to longer wavelengths, as found by earlier observers.[4,5] For the particular film of Fig. 3 the total shift of the absorption edge from 120° to 185°C amounts to about 545A. At higher temperatures small holes tend to appear in some of the films; in such cases the optical densities were corrected for the radiation transmitted by the holes. For all the samples observed the average displacement of the absorption edge with rising temperature is 6.20A/°C. This value is higher than those reported previously[4,5] and is, in addition, somewhat dependent upon the rate of heating of the sample. No clear difference could be observed in the shift rate of the absorption edge for temperatures below and above the transition region near 160°C.

Following the suggestion of Gilleo,[2] it is instructive to plot the log of optical density (or absorption coefficient) *vs* reciprocal temperature at constant wavelength. The resulting curves (e.g., Fig. 4) show a regular increase in slope as the temperature is raised, interrupted only by an abrupt change in the temperature range 155° to 175°C, the temperature at which the S_8 ring molecules break open the polymerize to longer chain segments. For temperature variations lying either wholly below or wholly above 160°C the resulting curves are the same whether the sulfur is heated or cooled. However, when the sulfur is first heated above and then cooled below the transition temperature, the original curve is not reproduced; instead, the slope of the high temperature portion is retained. This behavior is to be expected, since the ring structure reforms only slowly.[4]

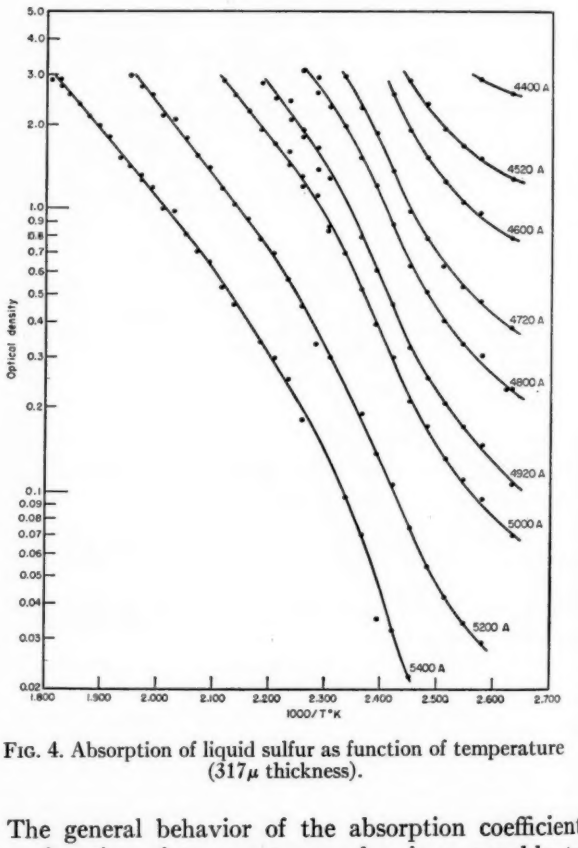

FIG. 4. Absorption of liquid sulfur as function of temperature (317μ thickness).

The general behavior of the absorption coefficient as a function of temperature makes it reasonable to believe that the mechanism for the displacement of the absorption edge is similar to that described for the case of selenium.[2] The long wavelength tail of the absorption band seems to be connected primarily with the excited vibrational energy states and thus is very sensitive to changes in temperature.

It is a pleasure to thank Professor A. von Hippel and Dr. M. A. Gilleo for many helpful discussions in the course of this investigation.

[12] Braune, Peter, and Neveling, Z. Naturforsch. **6a**, 32 (1951).

Interactions in Vibrating Molecules*

P. TORKINGTON
British Rayon Research Association, Manchester, England
(Received December 3, 1951)

Theories of the origin of interactions in the vibrational potential function are briefly discussed. It is concluded that the present accepted theory, based on the assumption of orbital hybridization changes, and van der Waals forces between nonbonded atoms, is in need of some modification. Consistent results are obtained if the orbital amplitude, directly relatable to the valence angle, is employed as the parameter deciding signs of interactions, the determining factor then being the energy increment in the system of oscillating bonds, relative to the increment without change of amplitude. This puts the orbital valence theory of dynamic interactions on a more fundamental basis.

I. INTRODUCTION

UNTIL a few years ago, the origin of interaction terms in molecular potential functions had not received any serious consideration, though there was sufficient evidence to show that their occurrence was common, if not universal. The best-known early examples were the interaction between CH_2 deformation and C=C stretching in ethylene, and later the analogous interaction in the methyl halides. The existence of interaction between the stretchings of adjacent bonds had also been accepted as proved in carbon dioxide. The reason for neglecting their study would seem to be the complete acceptance of the valence force field as a basic potential function for molecules. The Dennison-Urey-Bradley field, which included terms for van der Waals forces between nonbonded atoms, has only fairly recently been revived; it can be regarded as a combination of central- and valence-force fields, and, if transformed to the latter only, immediately accounts for the existence of interaction terms.[1] Recently it has been shown that changes in hybridization of bonding orbitals during molecular vibrations would lead to interactions, and the signs of various interaction constants arising from this effect can be predicted.[2] It would seem that most interactions can be accounted for by one or both of these effects. A particular case which is exceptional is π-electron interactions in conjugated systems.

II. DEFECTS IN THE PRESENT THEORY OF INTERACTIONS

The principal defect is the presence of ambiguity in the predicted sign of an interaction constant arising from hybridization changes. This is discussed later in some detail. The position with respect to the van der Waals components is more definite; the approximate potential function can sometimes be carried over from the corresponding rare gas,[3] and otherwise it is generally safe to assume repulsion between near neighbors, leading to the empirical rule that nonbonding interactions give rise to a positive length-length interaction for adjacent bonds. Duchesne[4] has shown how length-length interaction constants of either sign may arise from interatomic repulsion, but the potential function he deduces for van der Waals forces would seem in need of confirmation, as the usual attractive and repulsive terms are interchanged. There is one detail it would seem worth correcting. If the van der Waals function for pairs of nonbonded atoms be written

$$V=\sum_{i,j} A_{ij}\cdot\Delta R_{ij}+\sum_{i,j} B_{ij}(\Delta R_{ij})^2,$$

where ΔR_{ij} is the change in interatomic distance between atoms i and j, then the constants A_{ij} and the balancing constants A_k' going with linear terms in the valence force potential function should not appear in the frequency formulas. The matter has been considered in a recent publication[1] on the transformation between Urey-Bradley and valence-force fields. The constants A_{ij} and A_k' are small, and the error should not alter any conclusions drawn up till now, but it may be important when dealing with the systematics of small increments.

Passing to the hybridization changes, we first note that these cannot yet be put on any quantitative theoretical basis, though the calculations of Linnett and others on the overlap during nonplanar ethylenic bending[5] and, working the other way, of the orbital-following constants in the methanes,[2] show that this might well be possible. A method for approximations has been indicated by Coulson,[6] *viz.*, by relating to the change in the $s-p$ hybridization ratio for a given angle change. The general problem is complex; a given increment in a hybridization ratio determines related increments to the lengths and strengths of the bonds involved, but the system cannot adjust itself naturally since its center of gravity must remain fixed with respect to its constituent atoms. It would seem impossible to disentangle interaction effects from anharmonicity;

* This paper was delivered at the meeting of spectroscopists at the University, Basle, Switzerland, in June 1951.

[1] P. Torkington, Trans. Faraday Soc. **47**, 105 (1951), where further references are given.

[2] J. W. Linnett and P. J. Wheatley, Trans. Faraday Soc. **45**, 33, 39 (1949).

[3] J. W. Linnett and D. F. Heath, Trans. Faraday Soc. **44**, 561, 873 (1948).

[4] J. Duchesne and A. Monfils, J. Chem. Phys. **17**, 586 (1949).

[5] P. J. Wheatley and J. W. Linnett, Trans. Faraday Soc. **45**, 897 (1949).

[6] C. A. Coulson, V. Henri Mem. Vol. (Desoer, Liege, 1948), p. 15.

Linnett's treatment of the water molecule[7] has shown that the cubic and quartic terms are those for each individual O—H bond, but he does not point out that hybridization changes must lead to a change of force constant during displacement, and that there is therefore no essential difference between interactions due to hybridization changes, and anharmonicity. To make the point quite clear, consider the valence force function

$$2V=\sum_i d_{ii}\Delta_i^2$$

containing only square terms. Conventional anharmonicity correction is equivalent to replacing d_{ii} by d_{ii}', defined as below:

$$d_{ii}'=d_{ii}(1+\sum_j a_j\Delta_j+\sum_{j,k} b_{jk}\Delta_j\Delta_k+\cdots),$$

where the a_j, b_{jk} and further coefficients are constants. The introduction of a cross term $d_{ij}\Delta_i\Delta_j$ into the original square term expression means that $(d_{ii}\Delta_i^2+d_{jj}\Delta_j^2)$ has been replaced by

$$d_{ii}(1+a_i\Delta_j/\Delta_i)\Delta_i^2+d_{jj}(1+a_j\Delta_i/\Delta_j)\Delta_j^2,$$

where

$$(a_id_{ii}+a_jd_{jj})=2d_{ij}.$$

Thus the cross term can be considered as due to a variation of principal force constant with the relative displacements of the two coordinates involved. This picture may be the simplest one for *a priori* calculations of interactions. However, it is only put forward here as a suggestion, and no conclusions are derived from it.

As an example of ambiguity in deductions from the orbital valency theory of interactions, consider the symmetrical triatomic system AB_1B_2. The argument of Coulson, Duchesne, and Manneback[8] runs as follows: Increase in length of bond AB_1 weakens it, resulting in an increase in p character. Therefore in bond AB_2 the p character is decreased, since there is only a certain amount of both s and p orbitals. This decrease in p character must be associated with increase in strength and contraction. Therefore the natural signs of Δr_{AB_1} and Δr_{AB_2} are opposed and their product is negative. Consequently the corresponding interaction constant must be positive for the whole term to have negative sign. Actually the constant is negative in H_2O; and repulsions between the hydrogen atoms would give rise to a positive constant. So if the orbital valency theory is correct it must account for a negative constant here. Linnett and Heath's argument[7] runs that increase in length of either bond results in an increase in p character of both bonds, so that the natural sign of the product of the displacements is positive, and hence that of the interaction constant negative. Both sets of workers agree as to the predicted sign of the constant for interaction between bending and stretching; it is positive, because decrease in bond-length is associated with increase in s character, which would accompany opening of the angle between the bonds. It must be decided whether the assumption of Coulson, Duchesne, and Manneback concerning availability of orbitals is incorrect, or whether there is some additional factor to be considered. It would seem that it was definitely incorrect in a symmetrical triatomic system, for it can be shown that there is no allowed set of orbitals derivable from the system sp_3 of symmetry c_s.[9] Therefore if it is assumed that the two lone pairs, present in all single-bonded triatomic systems, remain equivalent, then so must the two valence orbitals.

III. FURTHER DEVELOPMENT OF THE ORBITAL-VALENCY BASIS OF MOLECULAR VIBRATIONS

Consider the possible effect of equilibrium bond angle, a parameter not so far included. In the more classical valency theory of Pauling,[10] the strength of a bond AB is proportional to the product P_AP_B† of the overlapping bonding orbitals from A and B. Let us see how the general arguments are affected by including changes of amplitudes. As before, we assume that shortening is associated with an increase in s character. But now for a bonding angle $\theta<\theta_t$, where θ_t is the tetrahedral angle, the increase in s character produces an increase of P from the central atom, while for $\theta>\theta_t$ it would produce a decrease. If we assume that an increase in P produces a more stable system, relative to the same displacement without increase in P, then symmetrical stretching will be less or more difficult than antisymmetrical stretching, in the symmetrical triatomic system, according as θ is less than or greater than θ_t. This agrees with the sign of the length-length interaction in water. Further, there is fairly good evidence for a dependence of sign of this interaction on equilibrium bonding angle in the series of triatomic molecules, the rule appearing to be essentially independent of bond order.[11] The change of sign in passing from ammonia to arsine[12] is also accounted for. It remains to include the angle parameter in the treatment of bond/angle interactions. The above change of sign in ammonia and arsine also occurs in the constant for interaction between stretching of a bond and deformation of an opposite angle, (positive in ammonia and negative in arsine). Arguing without considering the amplitudes, it would appear that availability of orbital was a function of bond-angle (cf. Coulson, Duchesne, and Manneback, Sec. II). In arsine, with an angle of about 90°, increase of s character in a pair of opening bonds must be associated with decrease in s character in the third bond.

[7] D. F. Heath and J. W. Linnett, Trans. Faraday Soc. **44**, 556 (1948).

[8] Coulson, Duchesne, and Manneback, Nature **160**, 793 (1947); V. Henri Mem. Vol. (Liege, 1948), p. 33.

[9] P. Torkington, J. Chem. Phys. **19**, 528 (1951).

[10] L. Pauling, *Nature of the Chemical Bond* (Cornell University Press, Ithaca, New York, 1945).

† P is the amplitude as defined by Pauling.

[11] P. Torkington, J. Chem. Phys. **17**, 357 (1949).

[12] J. Duchesne and I. Ottelet, J. Chem. Phys. **17**, 1354 (1949); J. Phys. Rad. **11**, 119 (1950).

In ammonia, symmetry C_{3v} must be favored, all bonds taking up more s orbital simultaneously as the angle increases. Now, as previously mentioned, C_{1s} orbitals are forbidden, so the argument is not valid for arsine. Now introducing the amplitudes as variables, in arsine more s orbital in all the bonds satisfies the requirements of the sign of the coordinate product, since the amplitudes are increased with its introduction. In ammonia, the amplitudes are almost certainly decreased by its introduction, the angle being only slightly less than tetrahedral, and the natural sign of the coordinate product for orbital following will thus be opposite to that of arsine. This lends support to the suggested refinement of orbital valency theory.

IV. APPLICATION TO ETHYLENE-TYPE MOLECULES

The case of ethylene type molecules is of interest in introducing a new principle, *viz.*, orbital-following with no change in the sum total of the valence angles in a plane. Planar trigonal molecules have been studied using an orbital valency field[3]; if orbital-following is accepted as a proved phenomenon from the results obtained with the methanes, the very good fit with the

TABLE I. Hybridization ratios for perpendicular-type displacements in trigonal systems. ($\alpha=120°$).

β	γ	λ_a	λ_b	λ_c
90°	150°	∞ (pure p)	0 (pure s)	∞ (pure p)
100°	140°	1.939	0.673	2.970
109°28′	130°32′	1.519	1.013	1.975
120°	120°	1.414	1.414	1.414
130°32′	109°28′	1.519	1.975	1.013
140°	100°	1.939	2.970	0.673
150°	90°	∞ (pure p)	∞ (pure p)	0 (pure s)

vibration frequencies in the above work must be partly fortuitous, since no allowance was made for change in hybridization, only for rotation of the undistorted set of orbitals. Since the fit with a simple valency field, without interaction, is quite good with the methanes, it is not possible to find definitely the relative effects of orbital-following and orbital-rotation. On general grounds, it would be thought that the former was of more importance in systems having symmetry elements, the latter possibly occurring in unsymmetrical systems only, where the lack of symmetry of the displacements would forbid orbital-following. The deutero-methanes probably occupy the second group. With heavier atoms, van der Waals forces undoubtedly become of comparable magnitude, so that it does not seem that a definite answer can be obtained except by accurate determinations of potential functions from isotopic molecules and explicit transformations of the constants. We shall assume here that orbital following is the determining factor.

For the parallel vibrations of ethylene-type molecules the relative signs of the displacements with orbital following are $\{+\Delta\theta_{CH_2}, -\Delta r_{CH}, +\Delta r_{C=C}\}$, and for the perpendicular vibrations $\{\pm\Delta\theta_{CCH}, \mp\Delta r_{CH}, +\Delta r_{C=C}\}$,

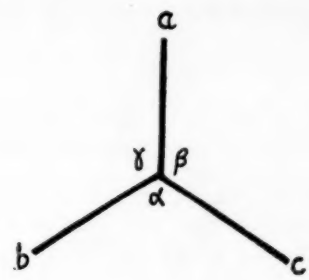

FIG. 1. Diagram of angles.

where the r_{CH} is adjacent to the θ_{CCH}. First it must be stated that all except the A_g vibrations are best treated as of two coupled triatomic CH_2 groups, presumably because of the rigidity of the C=C bond in these modes. The general results are given here for completeness. The hypothetical displacements can be worked out from the formulas given by Coulson[6] for the variation of hybridization ratios with angle in trigonal systems. He gives curves for the case corresponding to parallel vibrations, and it can be seen that $\Delta\theta_{CH_2}\cdot\Delta r_{CC}$ coupling is more important than $\Delta\theta_{CH_2}\cdot\Delta r_{CH}$ coupling. For perpendicular-type displacements, referring to Fig. 1, for constant α (i.e., $\Delta\beta+\Delta\gamma=0$), the hybridization ratios are given by

$$\lambda_a=(\tfrac{1}{2}\sec\beta\sec\gamma)^{\frac{1}{2}},$$
$$\lambda_b=(2\cos\beta\sec\gamma)^{\frac{1}{2}},$$
$$\lambda_c=(2\sec\beta\cos\gamma)^{\frac{1}{2}}.$$

Typical sets of values are shown in Table I. It is seen that $(\partial\lambda_a/\partial\beta)$ is quite small and negative, and $(\partial\lambda_b/\partial\beta)$ and $(\partial\lambda_c/\partial\beta)$ relatively large and respectively positive and negative. Thus if bond a is the σ component of C=C, then planar wagging of the CH_2 group in ethylene is naturally accompanied by a small decrease in s character of the C=C bond, and larger increments to the CH bonds, that adjacent to the decreasing angle undergoing a decrease in s character, and the other an increase. Then the displacements going with orbital-following are as given above, and coupling with $\Delta r_{C=C}$ is relatively slight and can probably be neglected.

Considering now the experimental results, it seems definite[13] that the order of the CH stretching constants is $k_{A_g}\gtrsim k_{B_{1g}}>k_{B_{2u}}>k_{B_{3u}}$, and of the bending constants $f_{A_g}>f_{B_{3u}}$; $f_{B_{2u}}>f_{B_{1g}}$. The constants for interaction[14] between C—H stretching and bending are both small and positive in the perpendicular modes, and small and negative in the B_{3u} factor; the value in the A_g factor cannot be proved. There appears to be a fairly large positive constant for $\Delta r_{CH}\cdot\Delta r_{CC}$ interaction, and a smaller negative one for $\Delta r_{CC}\cdot\Delta\theta_{CH_2}$. The effect of van der Waals forces of all three types on the ethylene potential function has been worked out.[1] It is found that H···C repulsion makes the same contribution to all four-valence constants k_{CH}, and that the additional

[13] P. Torkington, Proc. Phys. Soc. (London), 64, 32 (1951).
[14] For the coordinates going with the signs see reference 13.

increments due to H···H repulsions are

$$\Delta k_{A_g}=(B_\sigma+3B_\pi)/8,$$
$$\Delta k_{B_{1g}}=0,$$
$$\Delta k_{B_{2u}}=B_\sigma/8,$$
$$\Delta k_{B_{3u}}=3B_\pi/8,$$

where B_π, B_σ are the H···H repulsion constants for perpendicular and parallel displacements. Hence with van der Waals forces operating the order would be $k_{A_g}>k_{B_{3u}}>k_{B_{2u}}>k_{B_{1g}}$, and some other factor must determine the other order found. This suggests that the small difference $(f_{A_g}-f_{B_{3u}})$ might be due to the same effect, though a small constant B_σ would suffice here. It may be significant that the relative signs of the displacements Δr_{CC}, $\Delta\theta_{CH_2}$ in the mode δ_{CH_2} are such that orbital-following is opposed.[15] This would account for an increment to f_{CH_2}; but in ν_{CC} the displacements allow of orbital-following, and this frequency has a considerable influence on the calculated value of f_{CH_2}. The difference $(f_{B_{2u}}-f_{B_{1g}})$ requires a relatively large value of B_σ to satisfy it; the order of the interaction constants in the B_{1g} and B_{2u} factors suggests that B_σ is negligible. If the new assignment for ethylene[16] is correct, then the order of $f_{B_{1g}}$ and $f_{B_{2u}}$ is reversed; it would seem more likely that they would be nearly equal in magnitude.[17] But even disregarding the two perpendicular factors the differences $(k_{A_g}-k_{B_{3u}})$ and $(f_{A_g}-f_{B_{3u}})$ cannot be correlated on the basis of an H···H van der Waals repulsion. Now if the displacements in the normal modes are worked out, ν_{CH} in the A_g factor is found to involve opposition to orbital-following in both the subsidiary coordinates Δr_{CC}, $\Delta\theta_{CH_2}$, while in the B_{3u} C−H stretching mode the displacements allow of orbital following (except, of course, that Δr_{CC} here is of zero order).

Hence there is some evidence for there being orbital-following components in the valence constants, these being dependent on the directions of the displacements in the normal modes. The differences between constants in different symmetry factors leads to the "difference constants" mentioned previously; in the case of ethylene there is apparently interaction between the two ends of the molecule which can almost definitely be proved not to be due to H···H repulsions, and since orbital-valency theory can supply the above explanation one hesitates to postulate any conjugation effects. These latter can then be minimized in tetra-chloro-ethylene, leading to a more consistent picture; if they were present in ethylene then they would presumably be of a high order in the chloro-ethylene. Regarding the interaction constants, in the A_g mode one can predict a negative constant for $\Delta r_{CC}\cdot\Delta\theta_{CH_2}$ interaction, and a much less important positive interaction constant for the product $\Delta r_{CH}\Delta\theta_{CH_2}$; also a positive constant for $\Delta r_{CC}\cdot\Delta r_{CH}$ interaction. The B_{3u} interaction constant should also be small and positive (the same sign is obtained by treating it as a triatomic system; a negative sign could be obtained if CCH, HCH, were regarded as two opposed triatomic systems). The real sign is almost certainly negative, but there is a fairly obvious reason for this discrepancy, *viz.*, the opposition to orbital-following associated with rigidity of the C=C bond. Whether or no this constant remains negative in the A_g factor cannot be proved. The variation of all the remaining A_g force constants with this interaction constant, d, has been studied,[13] and it is found that the constant for $\Delta r_{CC}\cdot\Delta r_{CH}$ interaction becomes zero at about $d=+0.030\times10^5$ dynes/cm. So this interaction may possibly be really zero; it is in any case difficult to account for it being larger than the constant for $\Delta r_{CC}\Delta\theta_{CH_2}$ interaction.

On comparing C_2Cl_4 with C_2H_4, the point of most interest is the existence of solutions for the A_g factor with negative constants for the products $\Delta r_{CC}\cdot\Delta\theta_{CCl_2}$ and $\Delta r_{CC}\cdot\Delta r_{CCl}$.[18] The latter is only small for normal values of k_{CC} and may possibly be near zero, though not small and positive. So the two molecules may be quite similar in their electronic properties, in spite of the electro-negativity of chlorine and possible resonance effects. Former analyses of the vibrations of C_2Cl_4 had led to the acceptance of a large positive constant for $\Delta r_{CC}\cdot\Delta r_{CCl}$ interaction.[19] The other interaction constants are larger than in ethylene, and the signs appear to be all positive, in agreement with them being orbital-following constants; van der Waals repulsions would probably lead to negative A_g and B_{3u} $\Delta r_{CCl}\Delta\theta_{CCl_2}$ interaction constants (see reference 1).

A clear picture of the process of orbital-following is obtained from the non-planar rocking modes of ethylenic molecules. Here there is a negative component in the bending constant arising from the decrease in energy with increased overlap of the π-bond p-orbitals; the effect is stronger in the B_{1g} than in the B_{2u} mode, so the former has the lower total constant. In the expanded valence-force potential function, the difference $(f_{B_{1u}}-f_{B_{2g}})$ appears as a positive constant for interaction between the bendings of the two CH_2 groups. There is a similar positive constant for interaction between CH_2 and CH bendings in the vinyl group.[20] It appears probable that in trans-1:2 dichloroethylene there is a fairly large positive constant for interaction between the bendings of the two C−H bonds, while in the cis-compound this is replaced by a smaller negative constant; and the vinyl constant is approximately the algebraic sum of the *cis*- and *trans*-constants. As would follow from simple reasoning, the overlap of πp-orbitals is greater in *trans*-1:2 ethylenic C−H nonplanar

[15] It is well to remember that systems often never carry out the motions from which hypothetical potential functions are deduced; the actual potential function and the displacements occurring in the normal modes would appear to be subtly related.

[16] Rank, Shull, and Axford, J. Chem. Phys. **18**, 116 (1950); R. L. Arnett and B. L. Crawford, J. Chem. Phys. **18**, 118 (1950).

[17] P. Torkington, J. Chem. Phys. **18**, 758 (1950).

[18] P. Torkington, Proc. Phys. Soc. (London) **63**, 804 (1950); J. Chem. Phys. **18**, 773 (1950).

[19] J. Duchesne, V. Henri Mem. Vol. (Liege, 1948), p. 47.

[20] P. Torkington, Proc. Roy. Soc. (London) **A206**, 17 (1951).

bending than in ethylenic CH_2 bending, while in the *cis*-1:2 compound it is less. It is of interest that in benzene if interactions are assumed between adjacent C—H groups only then the corresponding interaction constant in nonplanar bending is large and negative, while if mutual interactions between all CH groups are assumed then the constant becomes small and negative and identical in value with the *cis*-1:2 dichloro-ethylene interaction constant. This latter field gives a better fit with C_6D_6 and is probably a better approximation to the true field with its three constants for interaction between *ortho*, *meta*, and *para* groups. (Equal interaction between all CH groups is the limiting case for perfectly mobile π-electrons.) Finally in acetylene there is found to be a large positive difference constant corresponding to interaction between the bendings of the two C—H bonds; the larger value, relative to ethylene, is probably to be ascribed to the shorter C—C distance rather than to the double π-bond, for in diacetylene, where the distance between the two C—H groups is large, there is only a very small, though still definite and positive, constant.

V. CONCLUSION

The fact that orbital-amplitude appears to be the parameter deciding interactions (see Sec. III) suggests that the ultimate determining factor is the energy-increment in the system of bonds, relative to the increment without change of amplitude. This seems quite a satisfactory correlation. The simpler argument based on the relation between *s* character and bond-length gives the same answer as that based on the amplitudes for all systems in which the hybridization is such that the amplitudes have a maximum value, e.g. for tetrahedral and planar trigonal structures with ideal bonding angles. The difference is apparent when inert pairs are present, as in symmetrical and unsymmetrical triatomic molecules, and in ammonia and arsine.

THE JOURNAL OF CHEMICAL PHYSICS VOLUME 21, NUMBER 1 JANUARY, 1953

An Analytical Method of Calculating Variable Diffusion Coefficients*

LEWIS D. HALL
School of Mineral Sciences, Stanford University, Stanford, California
(Received September 5, 1952)

The Matano-Boltzmann method of graphical calculation of diffusion coefficients in solutions is replaced by an analytical method in certain systems. This procedure enables accurate calculation of diffusion coefficients near the concentration extremes. An equation is derived for the diffusion coefficient D as a function of concentration c. The equation predicts a variation of D with c which is not exponential in metallic systems, contrary to the proposal of Wagner. Comparison of D values with those obtained graphically, for the system copper-nickel, indicates that the graphical values may be appreciably in error at that extreme where the diffusion coefficient is greatest.

INTRODUCTION

A METHOD of calculating diffusion coefficients for uni-directional atomic diffusion in systems of solutions with constant end concentrations was suggested by Boltzmann[1] and first used by Matano.[2] The end concentrations are hereafter designated as 0 and c_0. In the fundamental equation for diffusion,

$$\frac{\partial c}{\partial t}=\frac{\partial}{\partial x}\left(D\frac{\partial c}{\partial x}\right), \tag{1}$$

Boltzmann assumed that (a) the concentration c is a function of a single variable $\lambda=x/t^{\frac{1}{2}}$, and (b) the diffusion coefficient D is a function of concentration only. With these simplifying assumptions, the following expression for D is obtained:

$$D(c)=-\frac{1}{2}\frac{d\lambda}{dc}\int_0^c \lambda dc. \tag{2}$$

Experimenters, for example, da Silva and Mehl,[3] have used this expression to calculate diffusion coefficients by evaluating the quantities in Eq. (2) graphically from the concentration profile of the system (Fig. 2). da Silva and Mehl[3] plot their data on probability paper to eliminate dubious points (Fig. 1), then re-plot the curve to a linear scale to obtain the concentration profile (Fig. 2). The shape of the curves of D *vs* c which they obtain in this way (Fig. 3) has led Wagner[4] to propose that in such systems the dependence of D on c is exponential.

The graphical method has certain serious disadvantages, as is well known. It entails the measurement of slopes and areas of a curve whose ordinates and slopes tend to infinity at the ends of the concentration range (Fig. 2). Diffusion coefficients calculated in this way for concentrations near the limiting values are therefore subject to considerable uncertainty. Since the diffusion coefficients of low concentrations are of great importance in the discussion of diffusion mechanisms for

* This work was supported by the Office of Ordnance Research, U. S. Army, under Contract DA-04-200 ORD 178.
[1] L. Boltzmann, Ann. Physik **53**, 959 (1894).
[2] C. Matano, Japan J. Phys. **8**, 109 (1933).
[3] L. C. C. da Silva and R. F. Mehl, J. Metals **3**, 155 (1951).
[4] C. Wagner, J. Metals **4**, 91 (1952).

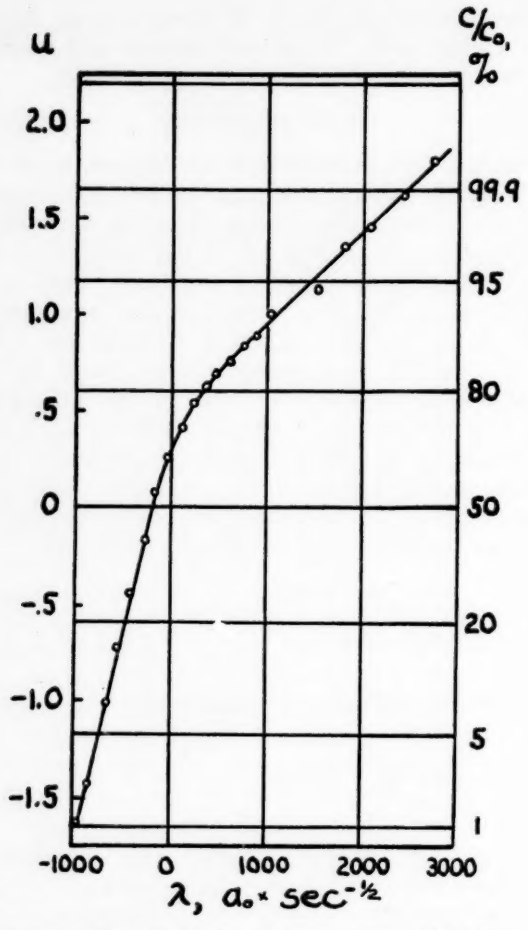

FIG. 1. Probability plot of c/c_0 *vs* λ for Cu−Ni at 1054°C. $c_0=100$ percent; $c=c_{Cu}$. $t=1.12\times10^6$ sec. Data of da Silva and Mehl.

solutions, it is obviously desirable to be able to calculate them accurately. It is interesting to note that as pointed out by Zener[5] and by Nowick,[6] the data reported in the literature for so-called chemical diffusion in metals seldom agree with theory. They discuss probable physical reasons for the deviations; it may be also that where the values of D have been calculated graphically, the method of calculation itself has introduced an inherent error.

ANALYTICAL METHOD

An examination of the probability plot (Fig. 1) suggests an analytical method which will yield accurate results at low concentrations and avoid graphical calculation. Since for a given experiment t is constant, the curve of concentration ratio *vs* λ or x has the shape shown in Fig. 1. It is convenient to use λ as the independent variable. Now a straight line on a plot of this kind is the graph of an equation of type

$$c/c_0=erfc(h\lambda+k), \tag{3}$$

$$=erfcu, \tag{3a}$$

where *erfcu* can be defined by the relation

$$erfcu\equiv\frac{1}{\pi^{\frac{1}{2}}}\int_{-\infty}^{u}\exp(-z^2)dz. \tag{4}$$

Other forms of the probability integral might have been used; these differ from each other essentially by additive or multiplicative constants, and all yield straight lines on probability paper. For purposes of calculation, the following expression is convenient:

$$erfcu\equiv\tfrac{1}{2}(1+erfu),$$

where

$$erfu\equiv\frac{2}{\pi^{\frac{1}{2}}}\int_{0}^{u}\exp(-z^2)dz,$$

values of which are tabulated by Peirce,[7] and more extensively in the W.P.A. tables.[8]

The parameters h and k are, respectively, the slope and intercept of the linear portion of the concentration ratio curve. From (3), (3a), and (4),

$$\frac{d(c/c_0)}{d\lambda}=\frac{h}{\pi^{\frac{1}{2}}}\exp(-u^2), \tag{5}$$

$$\frac{d\lambda}{dc}=\frac{\pi^{\frac{1}{2}}}{hc_0}\exp(u^2), \tag{6}$$

$$\int_0^c\lambda dc=\frac{hc_0}{\pi^{\frac{1}{2}}}\int_{-\infty}^{\lambda}\lambda\exp[-(h\lambda+k)^2]d\lambda, \tag{7}$$

$$=\frac{hc_0}{\pi^{\frac{1}{2}}}\left(-\frac{1}{2h^2}\int_{-\infty}^{\lambda}d\{\exp[-(h\lambda+k)^2]\}\right.$$

$$\left.-\frac{k}{h^2}\int_{-\infty}^{h\lambda+k}\exp(-z^2)dz, \right. \tag{8}$$

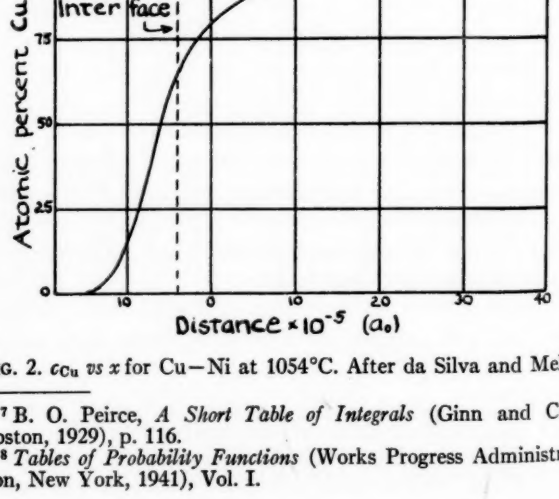

FIG. 2. c_{Cu} *vs* x for Cu−Ni at 1054°C. After da Silva and Mehl.

[5] C. Zener, J. Appl. Phys. **22**, 372 (1951).
[6] A. S. Nowick, J. Appl. Phys. **22**, 1182 (1951).
[7] B. O. Peirce, *A Short Table of Integrals* (Ginn and Co., Boston, 1929), p. 116.
[8] *Tables of Probability Functions* (Works Progress Administration, New York, 1941), Vol. I.

$$= -\frac{c_0}{2h\pi^{\frac{1}{2}}} \exp[-(h\lambda+k)^2] - \frac{c_0 k}{h} erfc(h\lambda+k), \quad (9)$$

$$= -\frac{c_0}{2h\pi^{\frac{1}{2}}} \exp(-u^2) - \frac{kc}{h}. \quad (10)$$

Substituting in (2),

$$D(c) = \frac{\pi^{\frac{1}{2}}}{2c_0 h^2} \exp(u^2)\left(\frac{c_0}{2h\pi^{\frac{1}{2}}} \exp(-u^2) + kc\right), \quad (11)$$

$$= \frac{1}{4h^2} + \frac{k\pi^{\frac{1}{2}}}{2h^2} \exp(u^2)\frac{c}{c_0}, \quad (12)$$

$$= \frac{1}{4h^2} + \frac{k\pi^{\frac{1}{2}}}{2h^2} \exp(u^2) erfcu. \quad (12a)$$

In using (12) to calculate D, one works from c/c_0 near zero upward to the end of the linear range. Thus in the copper-nickel system, in the low copper region, $c = c_{Cu}$, while the high copper region, $c = c_{Ni}$. The parameters h and k are evaluated accordingly. In the low copper region, k is positive, while in the high copper region, reversing the paper, k is negative. In the intermediate curved portion (Fig. 1), slopes and increments of area must be measured graphically from Fig. 2.

DISCUSSION

From (12a) it is evident that the exponential variation of D with concentration assumed by Wagner[4] and taken as the basis for calculations by his method does not hold true. The variation, as long as h and k are constant, is that of the function $\exp(u^2)erfcu$.

From Fig. 3 it is seen that the graphical and analytical curves of D *vs* c are very similar in the region of low D, but diverge sharply as D begins to increase appreciably. It is interesting to note that both the upper and lower linear portions of the curve of Fig. 1 are reflected in decreased slope of the analytical curve of D *vs* c. However, in the case of the graphical curve, while the lower linear portion is reflected in the shape of the corresponding part of the $D-c$ curve, the upper linear portion is not. This lends support to the belief that the shape of the graphical curve in the high D region is a function of the method by which it was calculated. In addition, since the curve of c *vs* λ for a system in which D is constant would plot on probability paper as a straight line through the origin, one might expect intuitively that linear portions of probability plots in general should correspond to regions in which D does not vary rapidly. This expectation is born out by the

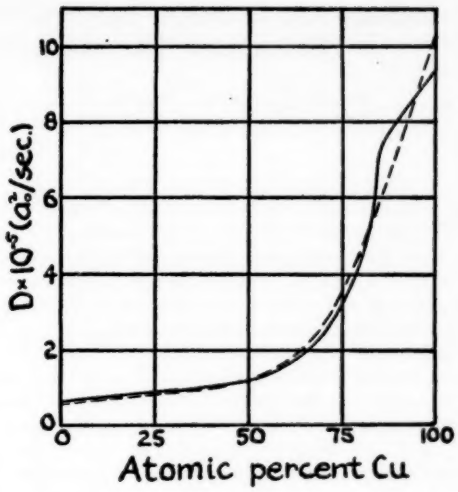

FIG. 3. D *vs* c_{Cu} for Cu–Ni at 1054°C. Dotted curve: da Silva and Mehl (graphical). Solid curve: calculated by Hall (analytical) from data of da Silva and Mehl.

shape of the analytical curve of D *vs* c. In most of the systems studied by da Silva and Mehl,[3] their plotted values of D *vs* c show at least a slight, and sometimes marked tendency to decrease slope in part of the region where D is large, but the authors have usually continued the curves upward with increasing slope. It was this behavior of their curves of D *vs* c which led Wagner[4] to assume an exponential variation of D with c.

In any event, the analytical method should give results equal or superior to the graphical procedure, particularly at and near the limits of the concentration range, and has the advantages of greater ease, simplicity, and directness. It should, of course, be remembered that diffusion coefficients calculated from the Matano-Boltzmann equation will, regardless of the method of calculation, be valid only in so far as the assumptions stated earlier are valid. It is difficult to find in the literature any rigorous experimental investigations of their validity. The tests of assumption (a) which have been made, such as those of Beckmann and Rosenberg[9] on high polymers and of Rhines and Mehl[10] on the system copper-alpha-brass cover too small a range of times to be conclusive. Experiments designed to verify or disprove assumption (b) are almost totally lacking in the literature. It is therefore apparent that such experimental studies would fill an important gap, and investigations of this kind are being initiated at this laboratory, using liquid metals as the diffusion media.

[9] C. O. Beckmann and J. L. Rosenberg, Ann. N. Y. Acad. Sci. **46**, 329 (1945).
[10] F. N. Rhines and R. F. Mehl, Trans. Am. Inst. Mining Met. Engrs. **128**, 185 (1938).

Raman and Infrared Spectral Data, Assignments, Potential Constants, and Calculated Thermodynamic Properties for Oxalyl Chloride*

JOSEPH S. ZIOMEK,† ARNOLD G. MEISTER, FORREST F. CLEVELAND, AND CHARLOTTE E. DECKER
Spectroscopy Laboratory, Department of Physics, Illinois Institute of Technology, Chicago 16, Illinois
(Received August 25, 1952)

Raman displacements, semiquantitative relative intensities, quantitative depolarization factors (single-exposure method), and infrared wave numbers have been obtained for liquid oxalyl chloride (ClOC—COCl) at room temperature. A critical examination of the present and previous data has been made and probable values have been determined. Normal coordinate treatments have been made for both the *cis*- and *trans*-forms. A satisfactory assignment of the present and previous Raman and infrared bands has been made, assuming the sample to be in the *trans*-form. Only binary combinations and 1st overtones were used, except for the 2 highest bands at 3740 and 5140 cm^{-1}. Fermi resonance occurs in 4 cases. Not more than 10 percent of the *cis*-form can be present, and the presence of even this much rests solely upon Saksena and Kagarise's reported temperature variation in the intensity of the 533-cm^{-1} Raman band, though the normal coordinate treatment does indicate that the strongest *trans*-Raman line at 620-cm^{-1} could occur near 533 for the *cis*-structure. The moderately polarized resonance triplet 450, 471, 488 can hardly be accounted for by the presence of a polarized fundamental in this region, for either the *cis*- or the *trans*-form. The heat content, free energy, entropy, and heat capacity were calculated (rigid rotator, harmonic oscillator approximation) for 11 temperatures from 100° to 1000°K for the ideal gaseous state at 1 atmos pressure.

RAMAN[1–6] or infrared[5,6] spectral data for oxalyl chloride have been obtained in previous investigations, and Saksena and Kagarise[6] (SK) have discussed the possibility of the coexistence of *cis*- and *trans*-isomers. In this paper, the available Raman and infrared data are critically compared and probable values are selected. Normal coordinate treatments for both the *cis*- and *trans*-forms were made and a satisfactory assignment on the basis of a *trans*-form was possible. Using the *trans*-fundamentals, thermodynamic properties were calculated.

EXPERIMENTAL

The sample of ClOC—COCl was purchased from Eimer and Amend and was purified by fractionation, retaining the middle portion which boiled at 62–63°C. The Raman displacements were obtained with a 2-prism spectrograph which has a dispersion of 162 cm^{-1}/mm (33A/mm) at 4500A. The spectrograms were taken on Eastman 103-J plates with Hg 4358A as the exciting line, using previously described[7] experimental arrangements and methods.

The depolarization factors were obtained with a Hilger E-518 spectrograph, which has a dispersion of 307 cm^{-1}/mm (63A/mm) at 4500A, by a single-exposure method.[8]

The infrared spectral data were obtained with a Beckman IR-2 spectrophotometer (KBr optics). The region scanned was from 400 to 10 000 cm^{-1}, but bands were observed only between 480 and 5200 cm^{-1}.

RAMAN AND INFRARED SPECTRAL DATA

The Raman spectral data are summarized in Table I. The values reported by Kohlrausch and Wittek[4] (KW) were obtained with high dispersion and, consequently, their values were given the greatest weight in determining the probable values of the Raman displacements. The earlier values of Kohlrausch and Pongratz,[1] Thatte and Joglekar,[2] and Saksena[3] were not given as much weight, since they were unable to resolve several bands and did not agree too well with later values for the ones which were resolved. However, it may be noted that the relative intensities of KW do not agree very well with the present values or with those of SK.

SK reported a doublet 175, 201 cm^{-1} although all others measured only a single line near 189 cm^{-1}. Since lines 10 cm^{-1} apart can be resolved in this laboratory, and since KW had even greater dispersion, SK's resolution of this doublet seems questionable, especially since they were unable to resolve the doublets at 260, 277 and 346, 367 and the triplet at 450, 471, 488. Also, SK reported 2 lines (1230 and 1530 cm^{-1}) which no one else observed. However, since reasonable assignments could be made for these, they were included in the probable value column of Table I.

There also is some question about the polarization state of several lines. The 346, 367 doublet was taken as depolarized, though the reported values of (P), D, and (0.96) in the 3 investigations do not establish this with certainty. Also, the 1780 line has been taken as polarized despite the rather high value (0.66 or 0.79) of its depolarization factor. SK, for their observed doublet 175(12), 201(8) designated the low component as *P*, the high one as *D*. If this were true, it would seem quite improbable that the depolarization factor of the un-

* Reported in part at the Symposia on Spectroscopy and Molecular Structure, Ohio State University, June, 1950, and June, 1952.

† Based in part on a thesis presented in partial fulfillment of the requirements for the Ph.D. degree. Present address: Chemistry Department, De Paul University, Chicago 14, Illinois.

[1] K. W. F. Kohlrausch and A. Pongratz, Ber. deut. chem. Ges. **67**, 976 (1934).
[2] V. N. Thatte and M. S. Joglekar, Phil. Mag. **23**, 1067 (1937).
[3] B. D. Saksena, Proc. Indian Acad. Sci. **12A**, 416 (1940).
[4] K. W. F. Kohlrausch and H. Wittek, Z. physik. Chem. **B48**, 177 (1941).
[5] Ziomek, Cleveland, and Meister, J. Chem. Phys. **17**, 669 (1949).
[6] B. D. Saksena and R. E. Kagarise, J. Chem. Phys. **19**, 987 (1951).
[7] F. F. Cleveland, J. Chem. Phys. **11**, 1, 227 (1943).
[8] F. F. Cleveland, J. Chem. Phys. **13**, 101 (1945).

TABLE I. Raman spectral data for liquid oxalyl chloride (ClOC−COCl).[a]

KP		TJ		S		KW			SK			ZCM			Probable values		
RD	I	RD	I	RD	I	RD	I	DF	RD	I	PS	RD	I	DF	RD	I	PS
188	7	187	1	184	3	189	5	0.84	175 201	12 8	P D	193	5	0.88	189	5	D
260 274	6 7b	271	2	272	6	260 277	4 4vb	0.41	276	39b	P	261 279	33	0.37	260 277	33	P
351	1	345	1	352	0	346 367	1 1	(P)	350	6	D	354	3	(0.96)	346 367	3	(D)
...	...	...	...	...	...	396	2	...	400	0	P	...	...	...	398	vw	(P)
453	6b	458	4b	450–500	5	450 471 488	4vb 4 4	0.44	465	50vb	P	443 465 483	21 28 30	0.51 0.48 0.50	450 471 488	21 28 30	P P P
502	5	...	...	...	...	512	6	P	519	8	P	522	7	P	518	7	P
528	3	526	2	534	2	533	3b	P	533	20	P	533	12	P	533	12	P
616	12b	617	6	619	12b	620	12b	0.14	619	92	P	620	100	0.17	620	100	P
...	...	...	...	...	...	672	0	...	...	...	...	...	...	...	672	vw	...
699	0	...	...	696	0	704	½	...	707	2	P	709	1	...	707	1	(P)
811	00	...	...	...	...	818	0b	...	809	1vb	D	802	vw	...	810	vw	(D)
1077	4b	1076	1d	1078	3	1079	4b	0.40	1078	14	P	1081	5	0.32	1079	5	P
...	...	...	...	...	...	...	...	...	1230	0	...	...	...	...	(1230)	vw	...
1412	0	...	...	...	...	1411	00	...	1417	1	P	1416	vw	...	1414	vw	(P)
...	...	...	...	...	...	...	...	...	1530	0	...	...	...	...	(1530)	vw	...
1772	8b	1776	2	1777	8	1780	10	0.66	1778	67	P	1781	57	0.79	1780	57	P

[a] KP = Kohlrausch and Pongratz, reference 1; TJ = Thatte and Joglekar, reference 2; S = Saksena, reference 3; KW = Kohlrausch and Wittek, reference 4; SK = Saksena and Kagarise, reference 6; ZCM = Ziomek, Cleveland, and Meister, reference 5; RD = Raman displacement in cm^{-1}; I = relative intensity; DF = depolarization factor; PS = polarization state (*P* = polarized, D = depolarized); b = broad, d = diffuse, w = weak, v = very; and parentheses enclose data about which there is some uncertainty. S also obtained qualitative polarization information.

resolved doublet could be as great as 0.86. Yet this is the mean of the values obtained by KW and in the present work for the 189-cm^{-1} line. This casts additional doubt upon SK's resolution of the 189-cm^{-1} line. Unless their filters were efficient and carefully used their 201-cm^{-1} line (which falls at 22 737 cm^{-1}) could instead be assigned as the 1780 line excited by Hg 24 516 cm^{-1} (4078A); the difference is 1779 cm^{-1}. It could also be assigned as the 260 line excited by Hg 22 995 cm^{-1} (4348A); the difference in this case is 258 cm^{-1}. The 2 lines would have displacements from Hg 22 938 cm^{-1} (4358A) of 202 and 203 cm^{-1}, respectively, as compared with their observed value of 201. The 2 lines would thus be superimposed and each would contribute to the intensity of the observed line. It thus seems quite probable that the 201-cm^{-1} line does not belong in the Raman spectrum, and that the low value of 175 obtained by SK represents experimental error caused by the proximity of the 189 line to their (probably) incorrectly assigned 201 line.

The infrared data obtained by SK are in essential agreement with the present results (Table II and Fig. 1), although at least 2 of the intense bands for the liquid (752 and 1058 cm^{-1}) were too broad for comparison. The wave numbers reported by SK for oxalyl chloride in benzene solution are in general agreement with the probable values for the liquid, except for the 1752-cm^{-1} band which appeared at 1777 in the solution. The bands at 1262, 2060, 2100, and 2060 cm^{-1} reported by SK for the gaseous state have never been observed for the liquid. This is difficult to understand since the bands for the liquid are usually stronger than for the gaseous state. Also, their liquid band at 986 cm^{-1} is weaker than the corresponding gas bands, which is just the reverse of what one would expect.

STRUCTURE AND ASSIGNMENTS

Nonspectroscopic Evidence

Previous nonspectroscopic investigations indicated a planar symmetrical structure for oxalyl chloride. The electron diffraction data of Wierl[9] and Morino[10] indicated that the most stable structure was *trans*, with oscillations about this position. Fröschl, Maier, and Heuberger[11] from chemical reaction evidence considered an unsymmetrical structure to be more probable, but Martin and Partington[12] concluded that the calculated value of the refractivity for the symmetrical *trans*-form agreed better with the observed value than did the one for the unsymmetrical structure.

The static *trans*-structure should have zero dipole moment, but Martin and Partington[12] obtained a value of 0.92 D in benzene solution, and this value was confirmed in the laboratory of Morino.[13] If, as the electron diffraction evidence indicates, there is oscillation about C−C axis, the dipole moment would not be zero and

[9] R. Wierl, Physik. Z. **31**, 366 (1930).
[10] Y. Morino, private communications, December 5 and 30, 1949.
[11] Fröschl, Maier, and Heuberger, Monatsh. Chem. **59**, 256 (1932).
[12] G. T. O. Martin and J. R. Partington, J. Chem. Soc. 1175 (1936).
[13] Y. Morino, private communication, May 24, 1952.

TABLE II. Infrared spectral data for oxalyl chloride (ClOC—COCl).[a]

Liquid						Benzene solution	Gas			
Saksena Kagarise		Ziomek Cleveland Meister		Probable values		Saksena Kagarise	25°C Saksena Kagarise		150°C Saksena Kagarise	
WN	I	WN	I	WN	I	WN	WN	I	WN	I
...	...	488	s	488	s	...	...	...	...	...
...	...	532	s	532	s	...	...	...	...	...
...	...	594	s	594	s	...	...	...	...	...
...	...	...	...	...	...	...	724	w	...	...
									774	...
						757	777	vvs	781	...
...[b]	vvs	752	vvs	752	vvs	771	795	vvs	795	...
932	w	942	s	937	m	...	...	...	...	...
986	w	...	...	986	w	980	980	ms	980	...
							988	ms	988	...
							1060	s	1060	...
...[b]	vvs	1058	vvs	1058	vvs	1060	1077	ms	1077	...
...	...	...	...	...	...	...	...	...	1262[c]	w
(1286)	vw	1310	vs	1298	m	...	...	...	...	...
...	...	1388	s	1388	s	...	...	...	...	...
1750	vs	1754	vvs	1752	vs	1777	1790	vs	1794	...
1824	s	1826	vvs	1825	s		1852	s	...	...
1964	ms	...	...	1964	ms		1970[c]	ms	...	...
...	...	...	...	...	...	...	2060[c]	ms	...	...
...	...	...	...	...	...	...	2100[c]	ms	...	...
...	...	...	...	...	...	...	2160[c]	ms	...	...
2480	m	2510	s	2495	ms	...	2530	m	...	...
2828	m	2830	vs	2829	s	...	2855	m	...	...
...	...	3740	vs	3740	s	...	...	...	...	...
...	...	5140	w	5140	w	...	...	...	...	...

[a] WN = wave number in cm^{-1} corresponding to maximum absorption in the infrared band; I = relative intensity (s = strong, m = medium, w = weak v = very); and parentheses enclose data about which there is some uncertainty.
[b] Very intense absorption, wave number not reported.
[c] Recorded strongly at 150°C with high vapor pressure.

this may account for the observed moment. However, it is known that for many compounds the moments obtained with benzene solutions are too large.[14] Hence the observed value may be larger than would be the actual value for the gaseous state.

According to the electron diffraction data,[15] the C—C bond distance is 1.50A, which is less than the normal value of 1.54A. Although the difference is not much greater than the possible experimental error, and may be partly due to a shortening of the single-bond radii, this is nevertheless in the direction one would expect if the C—C bond has some double-bond character. If the bond does have some double-bond character, the molecule must be planar. Besides this, a consideration of dipole-dipole interactions and steric hindrance indicates that the structure should be not only planar, but also *trans*. Figure 2, for example, shows the van der Waals radii drawn about the chlorine and oxygen atoms for the *cis*-form; the considerable overlapping suggests that this structure would be unstable. Figure 3 shows the van der Waals radii for the *trans*-structure: while there is still some overlapping, it is less than for the *cis*, and therefore suggests that the *trans*-form would be more stable. For any nonplanar structure, the resonance forms which contribute to the double-bond character could not exist; hence such a structure would be expected to be less stable than either the *cis* or the *trans*.

Everything considered, then, the *trans*-form seems to be more probable than any other structure.

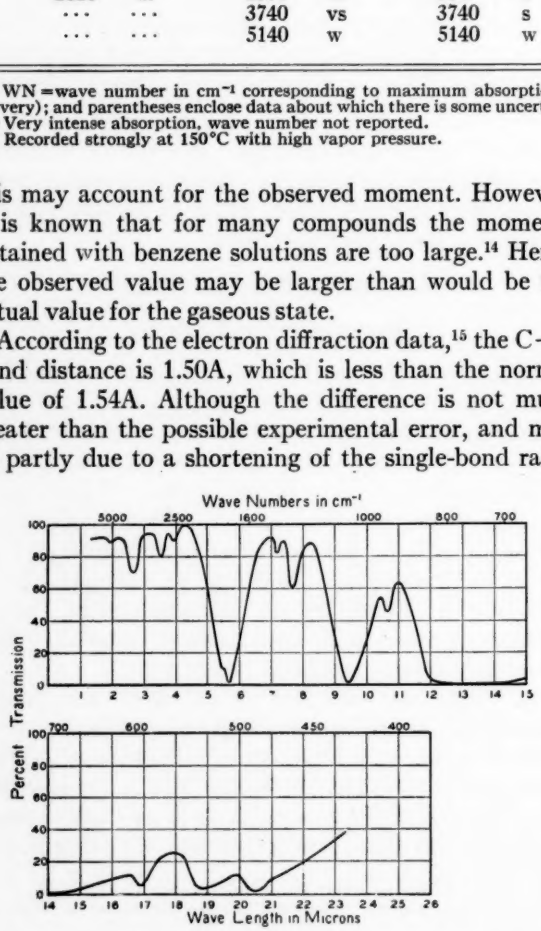

FIG. 1. Infrared bands for oxalyl chloride (ClOC—COCl).

The *Trans*-Structure

In view of these considerations, it seems best to attempt first an interpretation of the spectral data on the basis of the *trans*-model. For this structure (C_{2h}), there should be 5 A_g fundamentals (polarized in the Raman, forbidden in the infrared); 1 B_g (depolarized in the Raman, forbidden in the infrared); 2 A_u (forbidden in the Raman, parallel bands in the infrared); and 4 B_u

[14] R. J. W. Le Fevre, *Dipole Moments* (Methuen and Company, Ltd., London, 1948), second edition, p. 100.
[15] P. W. Allen and L. E. Sutton, Acta Cryst. 3, 49 (1950).

TABLE III. Probable Raman spectral data, calculated wave numbers, and assignments for liquid oxalyl chloride (ClOC—COCl), assuming a *trans*-structure.[a]

RD	I	PS	ν_c	Assignment	Type
189	5	D	*187*	$\nu_{10}'-\nu_5''=173$; $\nu_{10}'-\nu_5'=190$ $\nu_{10}''-\nu_5''=194$; $\nu_8-\nu_{12}=188$	B_g; B_g B_g; B_g
260 277	33	P	**258**	$\left.\begin{matrix}\nu_5'\\ \nu_5''\end{matrix}\right\}2\nu_{12}=268$ $(\nu_3-\nu_4''=253;\ \nu_3-\nu_4'=274)$	$\left.\begin{matrix}A_g\\ A_g\end{matrix}\right\}A_g$ A_g; A_g
346 367	3	(D)	**355**	$\left.\begin{matrix}\nu_4'\\ \nu_4''\end{matrix}\right\}2\nu_9=346$ $(\nu_3-\nu_5''=343;\ \nu_3-\nu_5'=360)$	$\left.\begin{matrix}A_g\\ A_g\end{matrix}\right\}A_g$ A_g; A_g
398	vw	(P)	*414*	$\nu_{11}+\nu_{12}$	A_g
450 471 488	21 28 30	P P P	**483**	$\left.\begin{matrix}\nu_{10}'\\ \nu_{10}''\\ \nu_{10}'''\end{matrix}\right\}\begin{matrix}\nu_9+\nu_{11}=453\\ \nu_8+\nu_{12}=456\end{matrix}$ $(\nu_2-\nu_8=459;\ \nu_7'-\nu_{11}=477)$	$\left.\begin{matrix}B_g\\ B_g\\ B_g\end{matrix}\right\}B_g$ A_g; B_g
518	7	P	*520*	$2\nu_5'=520$	A_g
533	12	P	*545*	$\nu_5'+\nu_5''=537$; $2\nu_5''=554$	A_g; A_g
620	100	P	**624**	ν_3	A_g
672	vw	···	*692*	$2\nu_4'=692$	A_g
707	1	(P)	*716*	$\nu_5'+\nu_{10}'=710$; $\nu_2-\nu_4''=712$ $\nu_4'+\nu_4''=713$; $\nu_5''+\nu_{10}'=727$	B_g; A_g A_g; B_g
810	vw	(D)	*814*	$\nu_2-\nu_5''=802$; $\nu_4'+\nu_{10}''=817$ $\nu_4''+\nu_{10}'=817$; $\nu_2-\nu_5'=819$	A_g; B_g B_g; A_g
1079	5	P	**1087**	ν_2	A_g
(1230)	vw	···	*1240*	$2\nu_3$	A_g
1414	vw	(P)	*1419*	$\nu_1-\nu_4''=1413$; $\nu_2+\nu_4'=1425$	A_g; A_g
(1530)	vw	···	*1537*	$\nu_7'+\nu_7''=1528$; $\nu_2+\nu_{10}'=1529$ $\nu_2+\nu_{10}''=1550$; $2\nu_7''=1542$	A_g; B_g B_g; A_g
1780	57	P	**1779**	ν_1	A_g

[a] ν_c = calculated wave number; other symbols have same meaning as in the previous tables.

(forbidden in the Raman, perpendicular bands in the infrared). There should thus be 6 Raman fundamentals (5 polarized, 1 depolarized) and 6 infrared fundamentals, with no coincidences.

Probable values of the Raman and infrared spectral data, calculated wave numbers, and assignments—made on the assumption that all of the molecules are in the *trans*-form—are given in Tables III and IV. In general, the assignment is quite satisfactory. All observed Raman and infrared bands are reasonably accounted for as fundamentals, allowed resonance multiplets, or as allowed binary combinations and first overtones—except for the 2 highest infrared bands for which a ternary combination and a second overtone had to be used. Fermi resonance doublets occur in 3 cases (260, 277; 346, 367; 777, 795 for the gas or 757, 771 cm^{-1} for the benzene solution); and the 3 lines at 450, 471, 488 are interpreted as a Fermi resonance triplet arising from interaction between ν_{10} and 2 allowed binary combinations. This accounts satisfactorily for the exceptional broadness of the infrared band at 752 cm^{-1} and of several of the Raman lines below 500 cm^{-1}. In a number of cases—especially for the 189-cm^{-1} Raman line and the 488-cm^{-1} infrared band—several allowed combina-

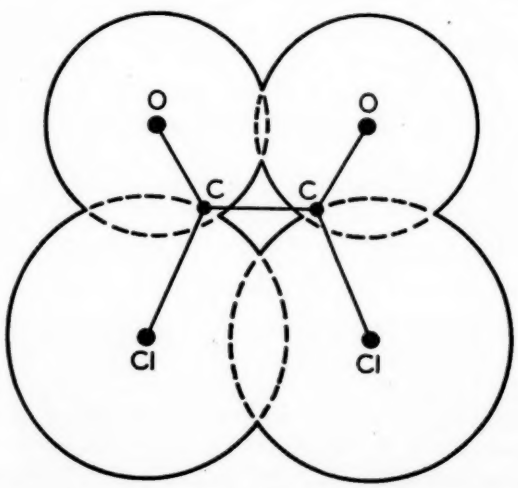

FIG. 2. Overlapping of the van der Waals radii for the *cis*-form.

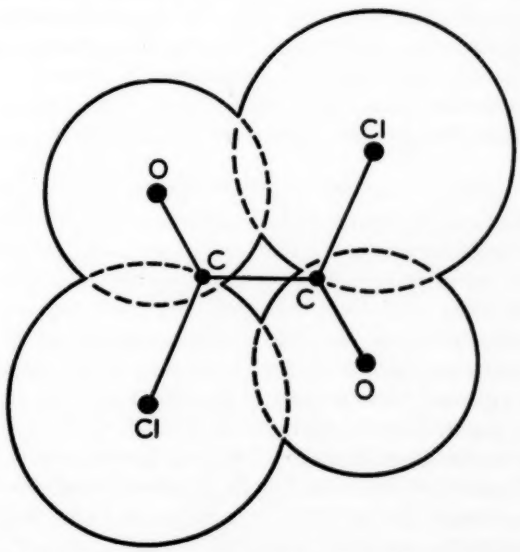

FIG. 3. Overlapping of the van der Waals radii for the *trans*-form.

TABLE IV. Probable infrared spectral data, calculated wave numbers, and assignments for oxalyl chloride (ClOC−COCl), assuming a *trans*-structure.

Liquid		Gas 25°	Gas 150°	ν_c	Assignment	Type
...[a]	...	...	...	**134**	ν_{12}	A_u
...	...	...	...	**173**	ν_9	B_u
...	...	...	...	**280**	ν_{11}	A_u
...	...	...	...	**322**	ν_8	B_u
488	s	...	...	*492*	$\nu_7'-\nu_5''=480;\ \nu_3-\nu_{12}=486$ $\nu_7''-\nu_5''=494;\ \nu_7'-\nu_5'=497$ $\nu_4''+\nu_{12}=501$	$B_u; A_u$ $B_u; B_u$ A_u
532	s	...	...	*540*	$\nu_5'+\nu_{11}=540;\ \nu_4''+\nu_9=540$	$A_u; B_u$
594	s	...	...	*602*	$\nu_{10}''+\nu_{12}=605;\ \nu_5''+\nu_8=599$	$B_u; B_u$
...	...	724	...	*730*	$\nu_{10}'+\nu_{11}$	B_u
752	vvs	777 795	774 781 795	**748**	$\nu_7'\{\nu_{10}'''+\nu_{11}=768;\ \nu_{10}''+\nu_{11}=751;\ \nu_3+\nu_9=739$[b] ν_7''	$B_u\{B_u, B_u, B_u$ B_u
937	m	...	...	*943*	$\nu_2-\nu_{12}=945;\ \nu_3+\nu_8=942$	$A_u; B_u$
986	w	980 988	980 988	*1017*	$\nu_5'+\nu_7'$	B_u
1058	vvs	1060 1077	1060 1077	*1041*	$\nu_5''+\nu_7'=1034;\ \nu_5''+\nu_7''=1048$	$B_u; B_u$
...	...	...	1262	*1258*	$\nu_2+\nu_9=1252;\ \nu_6-\nu_{10}'''=1264$	$B_u; A_u$
1298	m	...	...	*1302*	$\nu_6-\nu_{10}'$	A_u
1388	s	...	...	*1388*	$\nu_6-\nu_4''=1385;\ \nu_3+\nu_7''=1391$	$B_u; B_u$
1752	vs	1790	1794	**1758**	ν_6	B_u
1825	s	1852	...	*1843*	$\nu_2+\nu_7'=1836;\ \nu_2+\nu_7''=1850$	$B_u; B_u$
1964	ms	1970	...[c]	*1953*	$\nu_1+\nu_9$	B_u
...	...	2060	...[c]	*2060*	$\nu_1+\nu_{11}$	A_u
...	...	2100	...[c]	*2111*	$\nu_1+\nu_8=2102;\ \nu_4''+\nu_6=2119$	$B_u; B_u$
...	...	2160	...[c]	*2202*	$\nu_6+\nu_{10}'$	A_u
2495	ms	2530	...	*2537*	$\nu_1+\nu_7'$	B_u
2829	s	2855	...	*2831*	$\nu_2+\nu_6$	B_u
3740	w	...	...	*3733*	$2\nu_1+\nu_9$	B_u
5140	w	...	...	*5256*	$3\nu_6$	B_u

[a] Not investigated below 400 cm^{-1}.
[b] Also $\nu_2-\nu_8=747$, B_u; $\nu_3+\nu_{12}=754$, A_u; and $\nu_3+\nu_{10}'=782$, A_u.
[c] Were recorded strongly at 150°C with high vapor pressure.

tions or overtones fall together and thus increase the intensity of the observed band, while for the Raman lines at 518 and 533 cm^{-1}, and the infrared band at 1825 cm^{-1}, the intensities are enhanced by proximity to intense fundamentals of the same symmetry type. The 2 coincidences, out of 40 possibilities, in Raman and infrared wave numbers are considered to be accidental. Many combinations of the intense infrared fundamental ν_7 with other fundamentals were observed in the infrared, usually as intense bands; but only a few such combinations were observed in the Raman, and even for these, other allowed assignments were possible.

The A_g fundamentals

The totally symmetrical stretching frequencies involving largely the C=O, C−C, and C−Cl bonds can with considerable certainty be expected to fall in the 1700–1800, 800–1100, and 600–800 cm^{-1} regions, respectively. These would be A_g fundamentals and should be polarized in the Raman spectrum and missing in the infrared. On the basis of the depolarization factors and intensities, the Raman lines 1780, 1079, and 620 cm^{-1} were selected as 3 of the 5 A_g fundamentals. The 620 and 1079 lines are highly polarized; and the 1780 line, though its depolarization factor is rather large, is nevertheless definitely polarized.

On the basis of intensity and depolarization factor, 1 of the 3 lines in the 450–488 cm^{-1} region would seem to have been the logical choice for the next A_g fundamental. However, the normal coordinate treatment showed that the calculated wave number could not be this high without using potential constants which distorted the calculated values of the 620, 1079, and 1780 cm^{-1} wave numbers. (The 620 cm^{-1} value increased 20 percent, while the 1079 value decreased 8 percent.) Consequently, the doublets 260, 277, and 346, 367 were considered to correspond to the 2 remaining A_g fundamentals. The first of these doublets is definitely polarized. The second is not so certain: it was reported as (P), D, and (0.96) by KW, SK, and ZCM, respectively. Nevertheless, the normal coordinate treatment indicates that it should be chosen as an A_g fundamental. So the A_g fundamentals were taken as 258, 355, 620, 1079, and 1780 cm^{-1}. These were the values used to establish the potential constants in the A_g equations.

The B_u fundamentals

Fortunately, some of the F matrix elements which appeared in the B_u equations were nearly equal to corresponding F matrix elements in the A_g equations. Making reasonable estimates for these, and the others, values of the B_u fundamentals were calculated. The results were 1813, 760, 308, and 167 cm^{-1}. Strong observed infrared bands at 1752 and 752 were considered

to correspond to the 2 highest calculated values. For the 2 lowest calculated values (ν_8 and ν_9), unfortunately, no direct comparison with experiment was possible, since the infrared spectrum has not been investigated in the region below 400 cm^{-1}. However, ν_8 occurs 5 times and ν_9 7 times in a combination or overtone frequency, and $2\nu_9$ accounts for the resonance doublet at 346, 367 cm^{-1}; this may be considered as evidence in support of the calculated values. After some modification of the F matrix elements, to obtain better agreement with the 2 observed values, the calculated wave numbers 1758, 748, 322, and 173 cm^{-1} were obtained. The fact that this set of F matrix elements reproduced satisfactorily the observed values of 7 of the 12 fundamentals seemed to be a good indication that a satisfactory interpretation on the basis of the *trans*-structure might be possible.

The B_g fundamental

The B_g fundamental was considered to fall in the region 450–488 cm^{-1}, despite the fact that the depolarization factors for the lines in this region are 0.50 rather than the expected 0.86 for a depolarized line. The reasons for doing this follow: (1) the 3 lines in this region are quite intense and it therefore seemed probable that at least one of them must correspond to a fundamental, rather than to a combination or overtone frequency. (2) The normal coordinate treatment indicated that a line in this region could not be a polarized A_g fundamental. (3) Only 1 Raman fundamental remained to be assigned and it seemed that it must correspond to the most intense of the remaining observed Raman lines. (4) The analogous molecule phosgene has a fundamental at 444 cm^{-1} which is regarded,[16] like the present B_g fundamental, as an out-of-plane motion.

The A_u fundamentals

The A_u fundamentals, like the B_g, correspond to out-of-plane motions and should therefore appear in the low wave number region of the infrared spectrum, which unfortunately has not been observed. To find the regions in which they should occur, the value 483 cm^{-1} for the B_g fundamental was used to determine 1 of the potential constants necessary for the calculation of the A_u wave numbers. This, with reasonable values of the other necessary constants, yielded calculated values of the A_u fundamentals in the regions 273–332 and 104–176 cm^{-1}. If these fundamentals are taken as $\nu_{11}=280$ and $\nu_{12}=134$ cm^{-1}, simple and reasonable assignments of all the remaining Raman and infrared bands can be made. In particular, the existence of 3 strong lines, rather than 1, in the 450–488 cm^{-1} region becomes explicable as a Fermi resonance interaction between $\nu_9+\nu_{11}$, $\nu_8+\nu_{12}$, and the B_g fundamental at 483 cm^{-1}. Resonance interaction involving $2\nu_{12}$ and the A_g fundamental at 258 cm^{-1} also accounts for the Raman doublet at 260, 277 cm^{-1}; and ν_{11} in 2 binary combinations, interacting with the B_u fundamental at 748 cm^{-1}, accounts for the infrared bands observed near 752 cm^{-1}. Besides this, the Raman line at 398 cm^{-1} can be explained only as $\nu_{11}+\nu_{12}$; and ν_{11} in combination with another fundamental provides the only interpretation for the infrared bands at 724 and 2060 cm^{-1}. Altogether, ν_{11} and ν_{12} each appear in 8 combination or overtone frequencies. This cumulative evidence seems to establish fairly well the values for the 2 A_u fundamentals.

It appears, therefore, that a reasonable and satisfactory interpretation of the Raman and infrared spectral data can be made upon the basis of the *trans*-structure. Possible objections and appropriate comments follow: (1) The 450, 471, 488 triplet has the intermediate depolarization factor 0.50, rather than 0.86 which it should have if it is a B_g fundamental. Part of this may arise from the 459 difference band which is of type A_g, but this would hardly be intense enough to account entirely for this effect. Hence, if the structure is *trans* for all the molecules, it seems that this effect can be accounted for only by some unknown effect connected with the resonance interaction between the B_g fundamental and the 2 combination frequencies. (2) The doublet 346, 367 seems depolarized, rather than polarized. The experimental evidence, though, is not unambiguous on this point. (3) The depolarization factor of the 1780 cm^{-1} line is rather large for a polarized line. However, the line is definitely polarized, and pending further theoretical investigation one cannot be sure that the depolarization factor should be smaller than the observed value. (4) The infrared band at 1058 cm^{-1} is rather strong for just 2 coincident binary combinations, and the calculated values are lower than the observed value, rather than higher as is usual. It may be noted, however, that both of these combinations involve the very intense infrared fundamental at 752 cm^{-1}, and that other combinations involving this fundamental are also usually quite intense. Furthermore, since the 752 band is very broad and has 2 or more resonance components, the calculated values for the 1058 band may not be very exact. For other molecules, too, combination and overtone bands in the infrared are often quite strong.

Everything considered, the evidence against the *trans*-structure seems much weaker than the evidence in its favor.

Mixture of *Cis* and *Trans*

Since it seemed possible that some of the effects given above might arise from the presence of some of the *cis*-form, a normal coordinate treatment was carried out to establish the approximate location of the fundamentals for this structure. First of all, an assignment was attempted on the assumption that all the molecules were in the *cis*-form, but no satisfactory assignment could be found.

If any appreciable amount of the *cis*-form is present,

[16] H. W. Thompson, Trans. Faraday Soc. 37, 251 (1947).

there should have been 3 Raman lines in the 1700–1800 cm^{-1} region (the *trans* A_g, and the *cis* A_1 and B_1 lines), but only 1 line of normal width was observed. Hence, unless one or more of the lines was so weak as to escape observation (which from experience with other molecules does not seem probable), it is necessary to assume nearly exact coincidence of these 3 lines. Consistent with this assumption is the fact that the observed depolarization factor of the 1780 line is rather large (0.66 or 0.79), which could be due to the coincidence of polarized and depolarized lines, though it could equally well result from a single line which is only slightly polarized. Also, the normal coordinate treatment indicates that one can make the frequencies coincident, without disturbing the stretching frequency patterns too greatly, if modifications of the stretching constants are made. However, in some cases, these changes would be as large as 20 percent of the values used in the *trans*-calculations. Hence, since it seems difficult to justify such large changes in going from the *trans*- to the *cis*-model, the assumption of coincidence of frequencies becomes improbable. Besides this, experience with other molecules does not make it seem plausible that such a coincidence of frequencies would occur.

The normal coordinate treatment also shows that a polarized *cis*-fundamental can hardly fall in the 450–488 cm^{-1} region, and that the 1058-cm^{-1} band can hardly be a *cis*-fundamental. Thus, these two possible objections to the *trans*-structure cannot be removed by postulating the presence of some *cis* in the sample.

Another reason for doubting the presence of any appreciable portion of the *cis*-form is the absence in the observed spectrum of the requisite number of depolarized Raman lines.

If an observable amount of the *cis*-form is present, one would certainly expect that the *cis*-counterpart of the strongest Raman line (620 cm^{-1} for the *trans*) should appear in the Raman spectrum, and—according to the selection rules—also in the infrared. From the normal coordinate treatment, one would expect this *cis*-line to appear at a smaller displacement than 620, for the calculated values were 552 and 564. The closest observed Raman line is at 533 and it is polarized, as it should be; moreover, an infrared band was observed at 532. SK reported an increase in intensity of this Raman band with temperature. (Whether the infrared band also increased in intensity with temperature, as it should if the Raman and infrared bands have the same origin, was not investigated by them, since this was outside the range of their spectrometer.) All this is consistent with the supposition that the 533 band is the *cis*-counterpart of the 620 cm^{-1} Raman line.

One cannot be certain of this, however. For the 533 Raman line can be explained on the basis of the *trans*-structure as a coincident overtone and combination band, both of which are of the proper symmetry type to gain intensity from the highly intense 620 line by resonance interaction. In favor of this is the fact that the nearby 518 Raman line, of the same type, is also rather strong, as if by resonance. That it is not quite as strong can be ascribed to the fact that it is a little farther away from the 620 line and therefore does not gain quite as much in intensity. Also, the infrared band at 532 can be explained as 2 coincident binary combinations, both different from the one used to explain the Raman line at 533. Only the increase with temperature reported by SK for the 533 Raman line remains inexplicable, therefore, on the basis of the *trans*-structure. It seems, then, that before one concludes that the 533 band is the result of the *cis*-structure it would be desirable to investigate very carefully whether the intensity of the 532 infrared band also increases with temperature, and perhaps also to check this result for the Raman line.

Moreover, if an observable amount of the *cis*-form is present, one would expect the *cis*-counterpart of the strongest infrared band (752 for the *trans*) to appear in the infrared, and—according to the selection rules—also in the Raman spectrum. The normal coordinate treatment indicates that the *cis*-frequency should occur in the 692–788 cm^{-1} region. A weak infrared band was reported by SK at 724 for the gas at 25°C, but not for the gas at 150°C, nor for the benzene solution, nor for the liquid. The 724 band can be given a reasonable assignment on the basis of the *trans*-structure. However, the *cis*-band could easily be covered up by the strong *trans*-band in the infrared, and a better place to look for it would be in the Raman spectrum. Here one has only the very weak line at 672, the weak line at 707, and the very weak line at 810. The polarization state of the first is not known, that of the second is polarized (but not certainly so) where it should be depolarized, and that of the third is depolarized (but not certainly so) as it should be. All 3 have satisfactory *trans*-assignments, and are weaker than one would expect for a fundamental if the intensities of the 533 Raman and infrared bands were from the *cis*-form. Hence one cannot be certain of the presence of the *cis*-form from bands in this region.

Everything considered, the evidence in favor of the existence of even a small amount of the *cis*-form in the sample seems quite unconvincing, either at room or at higher temperatures. The only thing for which an explanation on the basis of the *trans*-form is lacking is the increase in intensity reported by SK for the 533 cm^{-1} Raman band. One may conclude, therefore, that the present evidence is greatly in favor of the *trans*-structure for oxalyl chloride.

NORMAL COORDINATE TREATMENT

From the previous discussion, the *trans*- or C_{2h} structure seems to be preferred. In order to establish the fundamental frequencies for this structure and to find what frequency differences could be expected for the *cis* and *trans*, normal coordinate treatments were made

TABLE V. Potential constants for ClOC−COCl.[a]

	Δm	Δc_1	Δc_2	Δo_1	Δo_2	Δo_1c_1	Δo_2c_2	Δmo_1	Δmc_1	Δmo_2	Δmc_2
Δm	f_m	$f_m{}^c$	$f_m{}^c$	$f_m{}^o$	$f_m{}^o$	$f_m{}^{oc}$	$f_m{}^{oc}$	$f_m{}^{mo}$	$f_m{}^{mc}$	$f_m{}^{mo}$	$f_m{}^{mc}$
Δc_1		f_c	$\bar{f}_c{}^c$	$f_c{}^o$	$\bar{f}_c{}^o$	$f_c{}^{oc}$	$\bar{f}_c{}^{oc}$	$f_c{}^{mo}$	$f_c{}^{mc}$	$\bar{f}_c{}^{mo}$	$\bar{f}_c{}^{mc}$
Δc_2			f_c	$\bar{f}_c{}^o$	$f_c{}^o$	$\bar{f}_c{}^{oc}$	$f_c{}^{oc}$	$\bar{f}_c{}^{mo}$	$f_c{}^{mc}$	$f_c{}^{mo}$	$f_c{}^{mc}$
Δo_1				f_o	$\bar{f}_o{}^o$	$f_o{}^{oc}$	$\bar{f}_o{}^{oc}$	$f_o{}^{mo}$	$\bar{f}_o{}^{mc}$	$f_o{}^{mo}$	$\bar{f}_o{}^{mc}$
Δo_2					f_o	$\bar{f}_o{}^{oc}$	$f_o{}^{oc}$	$\bar{f}_o{}^{mo}$	$f_o{}^{mc}$	$\bar{f}_o{}^{mo}$	$f_o{}^{mc}$
Δo_1c_1						f_{oc}	$\bar{f}_{oc}{}^{oc}$	$f_{oc}{}^{mo}$	$f_{oc}{}^{mc}$	$\bar{f}_{oc}{}^{mo}$	$\bar{f}_{oc}{}^{mc}$
Δo_2c_2							f_{oc}	$\bar{f}_{oc}{}^{mo}$	$\bar{f}_{oc}{}^{mc}$	$f_{oc}{}^{mo}$	$f_{oc}{}^{mc}$
Δmo_1								f_{mo}	$f_{mo}{}^{mc}$	$\bar{f}_{mo}{}^{mo}$	$\bar{f}_{mo}{}^{mc}$
Δmc_1									f_{mc}	$\bar{f}_{mc}{}^{mo}$	$\bar{f}_{mc}{}^{mc}$
Δmo_2										f_{mo}	$f_{mo}{}^{mc}$
Δmc_2											f_{mc}

[a] Since $f_{ij}=f_{ji}$, the elements below the diagonal are not given.

for both forms, using the Wilson FG matrix method.[17]

The symbols used for the equilibrium values of the bond distances and interbond angles are[18]

$o_1=C_1=O_1$, $o_2=C_2=O_2$, $c_1=C_1-Cl_1$,
$c_2=C_2-Cl_2$, $m=C-C$, $mo_1=C-C-O_1$,
$mo_2=C-C-O_2$, $mc_1=C-C-Cl_1$, $mc_2=C-C-Cl_2$,
$o_1c_1=O_1-C_1-Cl_1$, $o_2c_2=O_2-C_2-Cl_2$,
m, o_1c_1 = angle between C−C bond and $O_1-C_1-Cl_1$ plane,
m, o_2c_2 = angle between C−C bond and $O_2-C_2-Cl_2$ plane, and
oc, oc = torsional angle between the O−C−Cl planes.

Whenever it is unnecessary to distinguish between identical atoms, the subscripts will be dropped. The equilibrium values of these are[15] $o=1.20$A (assumed): $c=172$A; $m=1.50$A; $mo=123°$; $mc=114°$; $oc=123°$; $m, oc=180°$; and $oc, oc=0°$. It was found that the 5 A_g symmetry coordinates transformed as A_1 under the operations of the C_{2v} group, and hence the same symmetry coordinates could be used for the A_g coordinates of the *trans*, and the A_1 coordinates of the *cis*-form. Thus, since $F=UfU^{-1}$, the F matrices for the *cis*- and *trans*-forms are formally identical. The G matrices, however, are not the same since the different orientation for the *cis* and *trans* affects the g's in the expression $G=UgU^{-1}$.

The symmetry coordinates are, for the A_g and A_1 vibrations,

$R_1=\Delta m$,
$R_2=2^{-\frac{1}{2}}(\Delta c_1+\Delta c_2)$,
$R_3=2^{-\frac{1}{2}}(\Delta o_1+\Delta o_2)$,
$R_4=3^{-\frac{1}{2}}(\Delta mo_1+\Delta mc_1+\Delta mo_2+\Delta mc_2-2\Delta o_1c_1-2\Delta o_2c_2)/2$,
$R_5=\frac{1}{2}(\Delta mo_1+\Delta mo_2-\Delta mc_1-\Delta mc_2)$, and
$R_6=6^{-\frac{1}{2}}(\Delta o_1c_1+\Delta o_2c_2+\Delta mo_1+\Delta mo_2+\Delta mc_1+\Delta mc_2)\equiv 0$ redundant);

and for the B_u and B_1 vibration types

$R_7=2^{-\frac{1}{2}}(\Delta c_1-\Delta c_2)$,
$R_8=2^{-\frac{1}{2}}(\Delta o_1-\Delta o_2)$,
$R_9=3^{-\frac{1}{2}}(\Delta mo_1+\Delta mc_1-\Delta mo_2-\Delta mc_2-2\Delta o_1c_1+2\Delta o_2c_2)/2$,
$R_{10}=\frac{1}{2}(\Delta mo_1-\Delta mc_1-\Delta mo_2+\Delta mc_2)$, and
$R_{11}=6^{-\frac{1}{2}}(\Delta o_1c_1-\Delta o_2c_2+\Delta mo_1-\Delta mo_2+\Delta mc_1-\Delta mc_2)\equiv 0$ (redundant).

These symmetry coordinates are normalized and orthogonal. The potential function used has the coefficients given in Table V. From the potential energy matrix and the matrix formed from the coefficients contained in the symmetry coordinates, one gets the following F matrix elements: for the A_g and A_1 type,

$F_{11}=f_m$,
$F_{12}=2^{\frac{1}{2}}f_m{}^c$,
$F_{13}=2^{\frac{1}{2}}f_m{}^o$,
$F_{14}=3^{-\frac{1}{2}}(f_m{}^{mo}+f_m{}^{mc}-2f_m{}^{oc})$,
$F_{15}=f_m{}^{mo}-f_m{}^{mc}$,
$F_{22}=f_c+\bar{f}_c{}^c$,
$F_{23}=f_c{}^o+\bar{f}_c{}^o$,
$F_{24}=6^{-\frac{1}{2}}(f_c{}^{mo}+f^c{}_{cm}+\bar{f}_c{}^{cm}+\bar{f}_c{}^{mc}-2f_c{}^{oc}-2\bar{f}_c{}^{oc})$,
$F_{25}=2^{-\frac{1}{2}}(f_c{}^{mo}+\bar{f}_c{}^{mo}-f_c{}^{mc}-\bar{f}_c{}^{mc})$,
$F_{33}=f_o+\bar{f}_o{}^o$,
$F_{34}=6^{-\frac{1}{2}}(f_o{}^{mo}+f_o{}^{mc}+\bar{f}_o{}^{mo}+\bar{f}_o{}^{mc}-2f_o{}^{oc}-2\bar{f}_o{}^{oc})$,
$F_{35}=2^{-\frac{1}{2}}(f_o{}^{mo}+\bar{f}_o{}^{mo}-f_o{}^{mc}-\bar{f}_o{}^{mc})$,
$F_{44}=(4f_{oc}+4\bar{f}_{oc}{}^{oc}+f_{mo}+f_{mc}-4f_{oc}{}^{mo}-4f_{oc}{}^{mc}-4\bar{f}_{oc}{}^{mo}-4\bar{f}_{oc}{}^{mc}+\bar{f}_{mo}{}^{mo}+\bar{f}_{mc}{}^{mc}+2f_{mo}{}^{mc}+2\bar{f}_{mo}{}^{mc})/6$,
$F_{45}=3^{-\frac{1}{2}}(f_{mo}-f_{mc}-\bar{f}_{mo}{}^{mc}+\bar{f}_{mo}{}^{mo}+2f_{oc}{}^{mc}+2\bar{f}_{oc}{}^{mc}-2f_{oc}{}^{mo}-2\bar{f}_{oc}{}^{mo})/2$, and
$F_{55}=\frac{1}{2}(f_{mo}+f_{mc}+\bar{f}_{mo}{}^{mo}+\bar{f}_{mc}{}^{mc}-2f_{mo}{}^{mc}-2\bar{f}_{mo}{}^{mc})$;

and for the B_u and B_1 type,

$F_{11}=f_c-\bar{f}_c{}^c$,
$F_{12}=f_c{}^o-\bar{f}_c{}^o$,
$F_{13}=6^{-\frac{1}{2}}(2\bar{f}_c{}^{oc}-2f_c{}^{oc}+f_c{}^{mo}-\bar{f}_c{}^{mo}+f_c{}^{mc}-\bar{f}_c{}^{mc})$,
$F_{14}=2^{-\frac{1}{2}}(f_c{}^{mo}-\bar{f}_c{}^{mo}-f_c{}^{mc}+\bar{f}_c{}^{mc})$,
$F_{22}=f_o-\bar{f}_o{}^o$,
$F_{23}=6^{-\frac{1}{2}}(2\bar{f}_o{}^{oc}-2f_o{}^{oc}+f_o{}^{mo}-\bar{f}_o{}^{mo}+f_o{}^{mc}-\bar{f}_o{}^{mc})$,
$F_{24}=2^{-\frac{1}{2}}(f_o{}^{mo}-\bar{f}_o{}^{mo}-f_o{}^{mc}+\bar{f}_o{}^{mc})$,

[17] E. B. Wilson, Jr., J. Chem. Phys. **7**, 1047 (1939); **9**, 76 (1941).
[18] See descriptive notation for methanes and ethanes: Davis, Cleveland, and Meister, J. Chem. Phys. **20**, 454 (1952).

$$F_{33}=(4f_{oc}-4\bar{f}_{oc}{}^{oc}-4f_{oc}{}^{mo}-4f_{oc}{}^{mc}+4\bar{f}_{oc}{}^{mo}+4\bar{f}_{oc}{}^{mc}+f_{mo}-\bar{f}_{mo}{}^{mo}+f_{mc}-\bar{f}_{mc}{}^{mc}+2f_{mo}{}^{mc}-2\bar{f}_{mo}{}^{mc})/6,$$
$$F_{34}=3^{-\frac{1}{2}}(2\bar{f}_{oc}{}^{mo}-2f_{c}{}^{mo}+2f_{oc}{}^{mc}-2\bar{f}_{oc}{}^{mc}+f_{mo}-\bar{f}_{mo}{}^{mo}-f_{mc}+\bar{f}_{mc}{}^{mc})/2,$$
$$F_{44}=\tfrac{1}{2}(f_{mo}-\bar{f}_{mo}{}^{mo}+f_{mc}-\bar{f}_{mc}{}^{mc}-2f_{mo}{}^{mc}+2\bar{f}_{mo}{}^{mc}).$$

The elements of the G matrix were obtained from relations given by Wilson[17] and also from the expressions for the g's derived by Decius[19] and Lohman.[20] The results for the *trans*-configuration are, for the A_g type,

$$G_{11}=2\mu_C,$$
$$G_{12}=2^{\frac{1}{2}}\mu_C\cos mc,$$
$$G_{13}=2^{\frac{1}{2}}\mu_C\cos mo,$$
$$G_{14}=-3^{\frac{1}{2}}\mu_C(c^{-1}\sin mc+o^{-1}\sin mo),$$
$$G_{15}=-\mu_C(o^{-1}\sin mo-c^{-1}\sin mc),$$
$$G_{22}=\mu_C+\mu_{Cl},$$
$$G_{23}=\mu_C\cos oc,$$
$$G_{24}=\tfrac{1}{2}\mu_C o^{-1}6^{\frac{1}{2}}\sin oc,$$
$$G_{25}=2^{\frac{1}{2}}\mu_C(2m^{-1}\sin mc+\tfrac{1}{2}o^{-1}\sin oc),$$
$$G_{33}=\mu_C+\mu_O,$$
$$G_{34}=\tfrac{1}{2}c^{-1}\mu_C 6^{\frac{1}{2}}\sin oc,$$
$$G_{35}=-2^{\frac{1}{2}}\mu_C(2m^{-1}\sin mo+\tfrac{1}{2}c^{-1}\sin oc),$$
$$G_{44}=3[c^{-2}\mu_{Cl}+o^{-2}\mu_O+\mu_C(c^{-2}+o^{-2}-2c^{-1}o^{-1}\cos oc)]/2,$$
$$G_{45}=3^{\frac{1}{2}}[o^{-2}\mu_O-c^{-2}\mu_{Cl}+\mu_C(o^{-2}-c^{-2}+4c^{-1}m^{-1}\cos mc-4o^{-1}m^{-1}\cos mo)]/2,$$
$$G_{55}=\tfrac{1}{2}o^{-2}\mu_O+\tfrac{1}{2}c^{-2}\mu_{Cl}+\mu_C(8m^{-2}+\tfrac{1}{2}c^{-2}+\tfrac{1}{2}o^{-2}+c^{-1}o^{-1}\cos oc-4o^{-1}m^{-1}\cos mo-4c^{-1}m^{-1}\cos mc);$$

TABLE VI. F matrix elements for *trans*- and *cis*-oxalyl chloride.[a]

Type	Element	*Trans*	Type	*Cis* Set I	*Cis* Set II	*Cis* Set III
	F_{11}	4.8360[b]		4.8360	4.8360	
	F_{12}	0.75		0.75	0.75	
	F_{13}	0.80		0.80	0.80	
	F_{14}	0.15226		0.15226	0.15226	
	F_{15}	0.0000		0.0000	0.0000	
	F_{22}	3.2744		3.2744	3.2744	
	F_{23}	0.75		0.75	0.75	
A_g	F_{24}	0.000	A_1	0.000	0.000	
	F_{25}	−0.40		−0.30	−0.30	
	F_{33}	12.318		12.318	12.318	
	F_{34}	0.000		0.000	0.000	
	F_{35}	0.400		0.200	0.200	
	F_{44}	0.66125		0.88	0.99188	
	F_{45}	−0.150		−0.150	−0.15	
	F_{55}	0.721		0.73	0.60	
	F_{11}	2.65		2.65	2.65	2.65
	F_{12}	0.75		0.75	0.75	0.75
	F_{13}	0.20		0.20	0.20	0.20
	F_{14}	−0.30		−0.40	−0.18	−0.40
B_u	F_{22}	12.50	B_1	12.50	12.50	12.50
	F_{23}	0.30		0.30	0.30	0.30
	F_{24}	0.20		0.40	0.12	0.40
	F_{33}	0.50		0.50	0.50	0.50
	F_{34}	−0.15		−0.15	−0.09	−0.15
	F_{44}	0.75		0.721	0.45	0.50
	F_{11}	0.19366		0.18970	0.17590	0.19366
A_u	F_{12}	0.049020	A_2	0.044737	0.04390	0.04902
	F_{22}	0.21524		0.21762	0.30000	0.21524
B_g	F_{11}	0.19366	B_2	0.18970	0.17590	0.19366

[a] The F matrix elements are given rather than the potential constants, since there are more potential constants than matrix elements and many of the potential constants are extremely sensitive to values which may be assumed for some of the constants in order to make the determination of the other constants possible.

[b] F matrix elements containing only bond-stretching constants are in md/A, only bond-angle interaction constants in md/rad and only angle-angle constants in md A/rad².

[19] J. C. Decius, J. Chem. Phys. **16**, 1025 (1948).

[20] J. Lohman, ONR Technical Report 17, February, 1951.

and for the B_u type,

$$G_{11}=\mu_{Cl}+\mu_C,$$
$$G_{12}=\mu_C\cos oc,$$
$$G_{13}=\tfrac{1}{2}o^{-1}6^{-\frac{1}{2}}\mu_C\sin oc,$$
$$G_{14}=2^{-\frac{1}{2}}o^{-1}\mu_C\sin oc,$$
$$G_{22}=\mu_O+\mu_C,$$
$$G_{23}=\tfrac{1}{2}c^{-1}6^{\frac{1}{2}}\mu_C\sin oc,$$
$$G_{24}=-2^{-\frac{1}{2}}c^{-1}\mu_C\sin oc,$$
$$G_{33}=3[c^{-2}\mu_{Cl}+o^{-2}\mu_O+\mu_C(c^{-2}+o^{-2}-2c^{-1}o^{-1}\cos oc)]/2,$$
$$G_{34}=3^{\frac{1}{2}}[o^{-2}\mu_O-c^{-2}\mu_{Cl}+\mu_C(o^{-2}-c^{-2})]/2, \text{ and}$$
$$G_{44}=\tfrac{1}{2}[c^{-2}\mu_{Cl}+o^{-2}\mu_O+\mu_C(c^{-2}+o^{-2}+2c^{-1}o^{-1}\cos oc)].$$

The elements of the G matrix for the *cis*-form are, for the A_1 and B_1 vibrations,

$G_{ik}{}^{A_1}=G_{ik}{}^{A_g}$ and $G_{ik}{}^{B_1}=G_{ik}{}^{B_u}$, except for $G_{25}{}^{A_1}=G_{14}{}^{B_u}$, $G_{35}{}^{A_1}=G_{24}{}^{B_u}$, $G_{45}{}^{A_1}=G_{34}{}^{B_u}$, $G_{55}{}^{A_1}=G_{44}{}^{B_u}$, $G_{14}{}^{B_1}=G_{25}{}^{A_g}$, $G_{24}{}^{B_1}=G_{35}{}^{A_g}$, $G_{34}{}^{B_1}=G_{45}{}^{A_g}$, and $G_{44}{}^{B_1}=G_{55}{}^{A_g}$.

For the nonplanar vibrations (A_u and B_g, or A_2 and B_2), the method of Eliashevich[21] as given by Bernstein and Ramsay[22] was used. The potential energy expression was

$$2V=f_{m,\,oc}(\Delta m,\,oc)^2+2f_{m,\,oc}{}^{oc,\,oc}(\Delta m,\,oc)(\Delta oc,\,oc)+f_{oc,\,oc}(\Delta oc,\,oc)^2,$$

in which the interaction term $\bar{f}_{m,\,oc}{}^{m,\,oc}(\Delta m,\,o_1c_1)\times(\Delta m,\,o_2c_2)$ has been considered as negligible. The equations for the A_2 frequencies are

$$4\pi^2c^2(\nu_1{}^2+\nu_2{}^2)=a_1f_{m,\,oc}+a_2f_{oc,\,oc}-2a_3f_{m,\,oc}{}^{oc,\,oc}, \text{ and}$$
$$16\pi^4c^4\nu_1{}^2\nu_2{}^2=f_{m,\,oc}f_{oc,\,oc}-(f_{m,\,oc}{}^{oc,\,oc})^2(a_1a_3-a_2{}^2),$$

where c is the velocity of light, ν is the wave number in cm^{-1},

$$a_1=h'^2\mu_{Cl}+f'^2\mu_C+k'^2\mu_O,$$
$$a_2=h'c^{-1}\mu_{Cl}(\sin mc)^{-1}+gf\mu_C+k'o^{-1}\mu_O(\sin mo)^{-1},$$
$$a_3=c^{-2}\mu_{Cl}(\sin mc)^{-2}+g^2\mu_C+o^{-2}\mu_O(\sin mo)^{-2},$$
$$h'=h/[p(h+k)],$$
$$k'=k/[p(h+k)],$$
$$f'=p^{-1}+2m^{-1},$$
$$g=(o\sin mo)^{-1}-(c\sin mc)^{-1},$$

p = distance from the nearest C atom to the line joining the O and Cl atoms, measured along the C−C axis extended, h = distance from the O atom to the C−C axis extended, measured along the line connecting the O and Cl atoms, and k = the corresponding distance from the Cl atom to the C−C axis extended measured along the same line as h.

The B_2 frequencies may be obtained from these by setting $m=\infty$, $f_{oc,\,oc}=0$, and $f_{m,\,oc}{}^{oc,\,oc}=0$. Also the A_u frequencies may be obtained by setting $m=\infty$, and the B_g frequencies by setting $f_{oc,\,oc}=0$ and $f_{m,\,oc}{}^{oc,\,oc}=0$. The condition that $m=\infty$ eliminates the contribu-

[21] M. A. Eliashevich, Compt. rend. acad. sci. U.R.S.S. **28**, 604 (1940).

[22] H. J. Bernstein and D. A. Ramsay, J. Chem. Phys. **17**, 556 (1949).

TABLE VII. Comparison of calculated and probable values of the wave numbers corresponding to the fundamental vibrational frequencies of oxalyl chloride.

Probable values (used for thermodynamic properties)	Calculated *Trans* Type	*Trans* Wave number	*Cis* Type	*Cis* Wave number Set I	Set II	Set III
1780		1779		1787	1790	
1079		1087		1129	1140	
620	A_g	624	A_1	552	564	
357[a]		355		311	337	
269[a]		258		200	133	
1792[b]		1757		1735	1760	1844
786[b]	B_u	748	B_1	750	788	692
332[c]		332		491	425	416
173[c]		173		294	288	261
280[c]	A_u	280	A_2	471	457	474
134[c]		134		149	175	148
470[a]	B_g	488	B_2	281	271	284

[a] Mean of resonance values; units are cm^{-1}.
[b] Gas value.
[c] Calculated values.

tion to the potential energy from the relative motion of the C atoms.

The Trans-Calculations

The F_{ij}'s for the A_g matrix were estimated, using some values transferred from phosgene and ethane. After several modifications, it was found that the set corresponding to the F values given in Table VI gave 1779 as ν(C=O), 1087 as ν(C−C), and 624 cm^{-1} as ν(C−Cl), and gave 355 and 258 cm^{-1} for the in-plane deformation wave numbers. Since the observed Raman lines in the 460-cm^{-1} region were intense and polarized, as would be expected for an A_g frequency, an attempt was made to raise the calculated value of ν_4 (355 cm^{-1}) up to this region. This, however, upset the frequency pattern too greatly. It appears, therefore, that the upper limit for ν_4 is approximately 365 cm^{-1}. To check the reasonableness of the A_g set of F_{ij} values, the corresponding F's were used to form a set of F_{ij}'s for the B_u secular equation. This calculation gave ν_6 as 1813 cm^{-1} instead of 1752 as observed, and the C−Cl wave number at 760 as compared with the observed value at 752 cm^{-1}. Later the F_{ij} values corresponding to the 2 deformation frequencies were varied, and it was found that to prevent the other B_u frequencies from changing too much, F_{33} had to have a value of $4.55–6.00 \cdot 10^{-12}$ and F_{44} a value of $6.00–7.5 \cdot 10^{-12}$ ergs/rad.^{2} Finally, a satisfactory set of values was found which gave ν_6(C=O) at 1757, ν_7(C−Cl) at 748, ν_8 (deformation) at 332, and ν_9 (deformation) at 173 cm^{-1}. The F values corresponding to these also are given in Table VII. The ν_8 and ν_9 frequencies are allowed only in the infrared spectrum, which unfortunately has not been investigated below 400 cm^{-1}.

A value of $0.19366 \cdot 10^{-11}$ ergs/rad for $f_{m,\,oc}$ gives a value of 488 cm^{-1} for the B_g fundamental. The values 134 cm^{-1} for the torsional mode and 280 for the flapping mode were chosen from values in the calculated ranges 104–176 and 332–273 cm^{-1}, respectively. They receive additional support by their appearance in combination frequencies. The associated constants for these are $f_{oc,\,oc}=0.21524$, $f_{m,\,oc}{}^{oc,\,oc}=0.049020$, and $f_{m,\,oc}=0.19366$ md A/rad^2.

The *Cis*-Calculations

For the *cis*-calculations, it was assumed that the bond-stretching F matrix elements were the same as those found for the *trans*-model, and these values were used with various sets of bending F matrix elements. The main purpose of the calculation was to give a picture of the direction and approximate magnitude of the differences between corresponding *cis*- and *trans*-frequencies. A few of these sets are given in Table VI and the resulting frequencies are given in Table VII.

TABLE VIII. Heat content, free energy, entropy, and heat capacity of *trans* oxalyl chloride (ClOC−COCl) for the ideal gaseous state at 1 atmos pressure.

T (°K)	$(H^0-E_0{}^0)/T$	$-(F^0-E_0{}^0)/T$	S^0	$C_p{}^0$
other:	8.86[a]	50.66	59.52	11.23
100 torsional:	0.65[b]	0.31	0.96	1.47
total:	9.51	50.97	60.48	12.70
	11.50	57.61	69.11	16.62
200	1.18	0.95	2.13	1.84
	12.68	58.56	71.24	18.46
	13.22	61.45	74.67	19.10
273.16	1.37	1.35	2.72	1.91
	14.59	62.80	77.39	21.01
	13.75	62.63	76.38	19.77
298.16	1.41	1.48	2.89	1.92
	15.16	64.11	79.27	21.69
	15.57	66.94	82.51	21.92
400	1.55	1.91	3.46	1.95
	17.12	68.85	85.97	23.87
	17.00	70.57	87.57	23.46
500	1.63	2.26	3.89	1.96
	18.63	72.83	91.46	25.42
	18.18	73.78	91.96	24.64
600	1.68	2.57	4.25	1.97
	19.86	76.35	96.21	26.61
	19.17	76.66	95.83	25.55
700	1.73	2.83	4.56	1.97
	20.90	79.49	100.39	27.52
	20.01	79.27	99.28	26.27
800	1.76	3.06	4.82	1.98
	21.77	82.33	104.10	28.25
	20.74	81.67	102.41	26.84
900	1.78	3.27	5.05	1.98
	22.52	84.94	107.46	28.82
	21.38	83.89	105.27	27.29
1000	1.80	3.46	5.26	1.98
	23.18	87.35	110.53	29.27

[a] The units are cal deg^{-1} $mole^{-1}$.
[b] The contribution of the torsional vibration (134 cm^{-1}) is listed separately to facilitate revision of the table if and when a better way is found to calculate the contribution for this frequency.

THERMODYNAMIC PROPERTIES

The probable values of the wave numbers given in Table VII were used to calculate values of the heat content, free energy, entropy, and heat capacity for the ideal gaseous state at 1 atmos pressure (rigid rotator, harmonic oscillator approximation). The previously given bond distances and interbond angles were used to calculate the product of the principal moments of inertia, using the Hirschfelder[23] formula. The value obtained was $I_A I_B I_C = 1.7617 \cdot 10^6$ (awu A^2)^3. The symmetry number was 2, and the molecular weight used was 126.94. Nuclear spins and isotopic mixing were neglected. The contributions of the torsional frequency were calculated on the assumption of small displacements, as in the ethylenes. These contributions are listed separately in Table VIII, which gives the calculated values, to facilitate revisions of these values if it becomes possible at a later time to calculate the torsional contributions more exactly.

[23] J. O. Hirschfelder, J. Chem. Phys. 8, 431 (1940).

ACKNOWLEDGMENTS

This work was a part of a research program which is supported in part by the Office of Ordnance Research (Contract No. DA-11-022-ORD-464), and which was further aided by research grants from the American Academy of Arts and Sciences, and from the Society of the Sigma Xi. Correspondence with Professor G. W. Wheland, University of Chicago, about the nonspectroscopic evidence, was also of great help. The authors greatly appreciate this assistance.

THE JOURNAL OF CHEMICAL PHYSICS VOLUME 21, NUMBER 1 JANUARY, 1953

Investigation of Crystal Growth by Thermal Etching and Oriented Overgrowth

ALEXANDER SMAKULA* AND MYRON W. KLEIN
Engineer Research and Development Laboratories, Fort Belvoir, Virginia
(Received July 17, 1952)

Thermal etching of perfect thallium halide single crystals in vacuum takes place preferably at points where the crystal is distorted. The etching proceeds in regular steps forming pits bounded always by (110) planes. High temperature produces a disordered etching and marked surface striation. The formation of oriented hillocks indicates a surface migration of molecules. Crystal overgrowth from the vapor takes place on single points of the surface with preferably the same orientation as the substrate. The population distribution of microcrystals depends on the crystal orientation. The crystals, although grown at very low speed, show surface striations.

I. INTRODUCTION

THE process of crystal growth is generally divided into two steps; the formation of primary three-dimensional nuclei, and the subsequent growth of crystalline faces.

The first step is a submicroscopic phenomenon and unaccessible to a direct observation. The primary nucleation requires supercooling of the phase from which the nuclei are formed. From thermodynamical considerations the size and the rate of nuclei formation can be computed.[1–3] So far as primary nucleation is concerned, the theoretical results are in agreement with experiments.

The subsequent growth of nuclei to form crystalline faces is more complicated. At present there are three theories of crystal growth:

(1) The surface nucleation theory, developed by Kossel[4] and Stranski[5] for ideal crystals assumes an already existent, flat, crystalline surface. The formation of a new monomolecular surface layer takes place rapidly by repeatable steps which add one atom or molecule after another along kinks and steps until the surface is completed. To start a new layer a two-dimensional nucleus must be formed. This depends strongly on supercooling, but its rate, calculated from the supersaturation is several orders of 10 too low. Thus, the surface nucleation theory developed for ideal crystals requires very high supersaturation in which case, experimentally, only poor crystals can be obtained.

(2) To eliminate this difficulty Burton, Cabrera, and Frank[6] introduced the screw dislocation theory. This assumes that crystals are not perfect and always contain dislocations which make possible a continuous growth even at low supersaturation, without any direct surface nucleation. Thus we have a theory for real crystals with defects, but applicable to conditions (low supersaturation) where experimentally perfect crystals are grown.

(3) The lamellar theory has been proposed recently by Graf[7] to explain the lamellar steps (of the order of

* Present address: Laboratory for Insulation Research, Massachusetts Institute of Technology, Cambridge, Massachusetts.

[1] Disc. Faraday Soc., No. 5 (1949).
[2] M. Volmer, *Kinetik der Phasenbildung* (Steinkopf, Dresden, 1939).
[3] R. Becker and W. Doering, Ann. Physik 24, 719 (1935).
[4] W. Kossel, Nachr. Ges. Wiss., Göttingen, p. 135 (1927).
[5] I. N. Stranski, Z. physik Chem. 136, 259 (1928).
[6] Burton, Cabrera, and Frank, Nature 163, 398 (1949).
[7] L. Graf, Z. Metallkunde 42, 336 and 401 (1951).

microns) which are formed during very fast crystal growth. According to Graf, the primary nucleus has a spherical form as long as the surface tension is greater than the shear strength of the crystal; then it assumes a polyhedric form at a low growth rate, or lamellar, at a high growth rate. The thickness of the lamellae is determined by the ratio of the surface tension to mechanical strength of the crystal.

The decisive factors in the crystal growing process are the primary and secondary nucleation. Experimental study has been done mostly on primary nucleation.[8] We bring here some interesting data on secondary nucleation in single crystals, obtained in connection with our study of the annealing process.

II. METHOD

The secondary nucleation process can be studied either on the dissolution of a single crystal or on its formation. Since the simplest conditions are in the transition from solid to vapor phase or vice versa, (a) the thermal etching and (b) the oriented overgrowth from the vapor were used. These were applied to single crystals of thallium bromo-iodide, a substance with a comparatively high vapor pressure and sufficient hardness for the preparation of optical surfaces.[9] The crystals (ca. 1.5×1.5×0.5 cm) were cut along cubic (100) dodecahedron (110) or octahedron (111) planes. To avoid any surface-structure difference, caused by grinding or polishing, crystals with three different cuts were ground and polished together on an optical disk. For dissolution the polished crystals were heated in vacuum (10^{-5} mm) in a sealed Pyrex tube in a furnace with a small temperature gradient (*ca.* 2° C/cm). The crystals at the middle of the tube had the highest temperature (300°C) and the top of the tube 10 cm distant, the lowest (280°C).

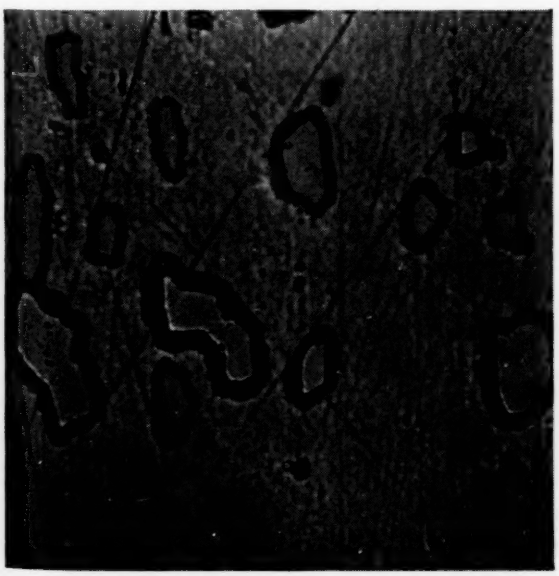

FIG. 1. Irregular pits formed on an unannealed crystal surface (110) after 30 hr at 300°C. Magnification 1000 ×.

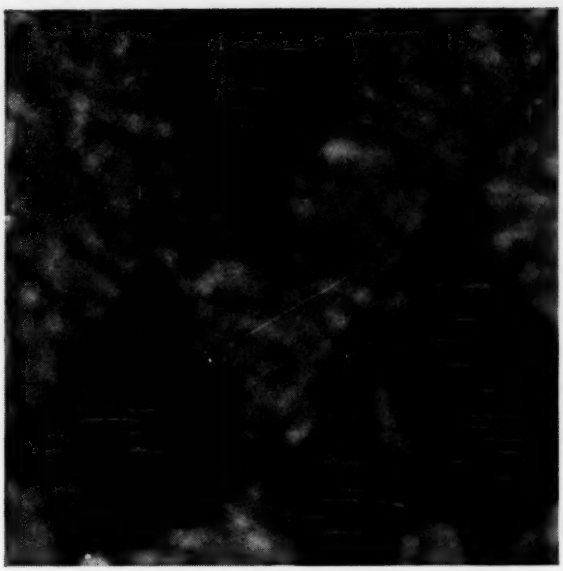

FIG. 2. Irregular pits with striation formed on an annealed surface (110) after 20 hr at 320°C. Magnification 1000 ×.

For study of crystal formation the bottom of the evacuated tube had the highest temperature (300°C) and the crystal at the middle the lowest (280°C). A small piece of material on the bottom of the tube delivered the vapor which deposited on crystals 10 cm above. The substrate and the vapor were of the same material. After treatment, the crystal surfaces were examined by a microscope with 250 to 1000× magnification.

III. RESULTS

A. Thermal Etching

It is known, particularly from metals, that sufficiently high temperature produces on surfaces of single crystals, regular pits distributed at random over the surface.[10] To obtain well-formed pits on thallium bromo-iodide crystals the temperature has to be quite low and the crystal surface not destroyed. For our experiments the temperature was 300°C, while the melting point is 414°C. When a crystal with a polished but not annealed surface was quickly heated to 300°C, so that the recrystallization of the surface destroyed by grinding could not take place, the evaporation produced very irregular pits, but clean background, as is shown in Fig. 1. On the other hand, if the temperature was too high (320°C) the formed pits are very irregular also, and the background of the pits shows striation (Fig. 2). In Fig. 3 is shown the result obtained on (100), (110)

[8] G. Tammann, *Kristallisieren und Schmelzen* (Leipzig, 1903).
[9] A. Smakula and M. W. Klein, J. Opt. Soc. Am. **40**, 748 (1950).
[10] E. N. DaC. Andrade, Proc. Phys. Soc. (London) **B63**, 198 (1950).

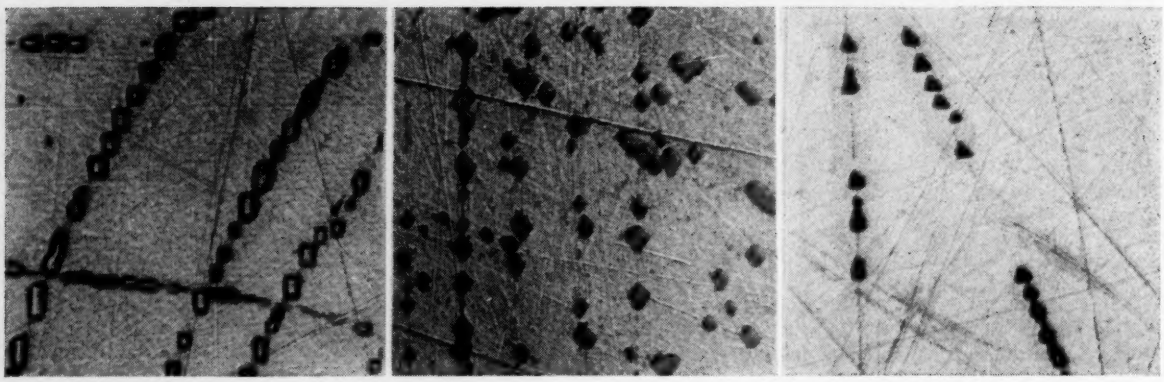

(a) (b) (c)

FIG. 3. Distribution of pits formed after 24 hr at 300°C. Magnification 250 ×.
(a) (100) surface, (b) (110) surface, (c) (111) surface.

and (111) surfaces at 300°C after 24 hr. The shape of the pits is rectangular on the (100), rhombic on the 110), and triangular on the (111) surface. By a goniometric determination of the angles between the pit surfaces, it has been found that pits are always limited by (110) planes which are the most stable planes in body-centered cubic crystals.[11] The distribution of the pits is preferably along scratches caused by grinding and polishing, but there are some scratches which do not contain any pits. Thus it is quite evident that mechanical distortion of the crystal lattice favors the nucleation for thermal dissolution. The surface density of the pits is practically the same on the (100) and (110) surface, but much less on the (111) surface. Since the pits on all three surfaces do not differ much in size, one may conclude that the evaporation from (111) surfaces is the lowest.

If the polished crystal surfaces were well annealed, the visible scratches have no influence on the formation of evaporation nuclei as can be seen in Fig. 4. The biggest and most perfect pits were formed on (110) surfaces.

The evaporation from single spots of the crystal surface may take place in a direct or indirect way. The molecules can evaporate directly into the vacuum or migrate onto the free surface, forming hillocks as shown in Figs. 5, 6, and 7. The arrangement of hillocks formed on the (100) surface is shaped like double wings with an angle of about 120° and a preferred orientation of one wing parallel to one of the pit sides. The arrangement of hillocks on the (110) surface shows a twofold symmetry with preferred orientation perpendicular to one side of the pits and of those on (111) planes has a threefold symmetry with a not well-pronounced orientation.

B. Oriented Overgrowth (Autoepitaxis)[12]

Deposition from vapor of thallium bromo-iodide at a very low rate in vacuo on a heated single-crystal surface does not form a uniform layer but single crystals far apart from each other. The crystals formed from

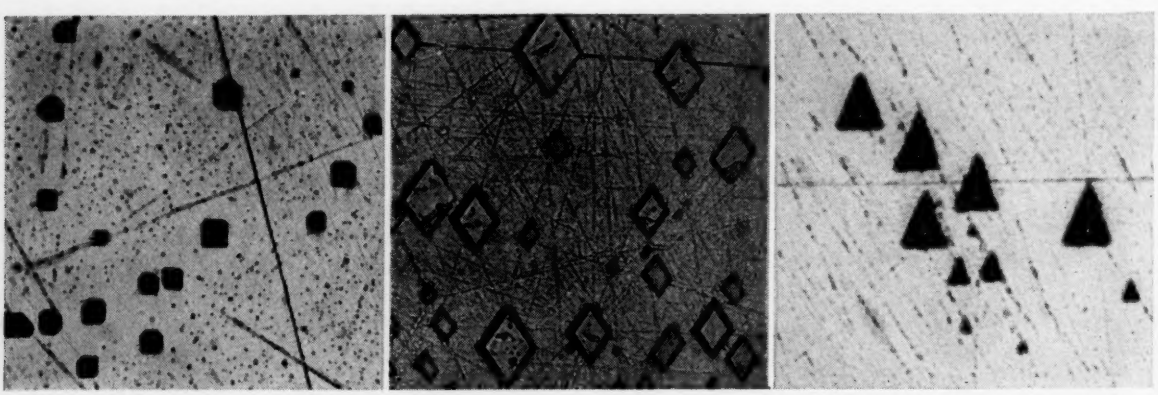

(a) (b) (c)

FIG. 4. Evaporation pits on well-annealed surfaces after 16 hr at 300°C. Magnification 1000 ×.
(a) (100) surface, (b) (110) surface, (c) (111) surface.

[11] W. Kleber, Zentr. Mineral. Geol. **A353** (1938).
[12] L. Royer, Bull. Soc. Franç. Minéral **51**, 7 (1928) introduced the term "epitaxie" for oriented overgrowth.

the vapor are very similar in shape to pits as can be seen from Fig. 8. The microcrystals have a square shape on the (100) face, while they are hexagonal on the (110) and (111) face. On all three substrate surfaces the crystals are bounded by (110) planes. The square shape on the (100) surface is actually a composition of four (110) planes projected in the [100] direction. Correspondingly, the hexagonal shapes on (110) and (111) surfaces are projections of dodecahedron in [110] and [111] directions. The distribution of crystals is approximately equal on (100) and (110) planes but very rare on the (111) plane. The scratch lines do not influence the nuclei formation. Generally, the orientation of the crystals formed from the vapor corresponds to the orientation of the substrate. However, some mismatches may be seen.

Although the growing speed was very low, about 1 micron per hour, the planes of crystals are not perfect, as can be seen in Fig. 9. The (110) planes show rough linear structure in the [110] direction.

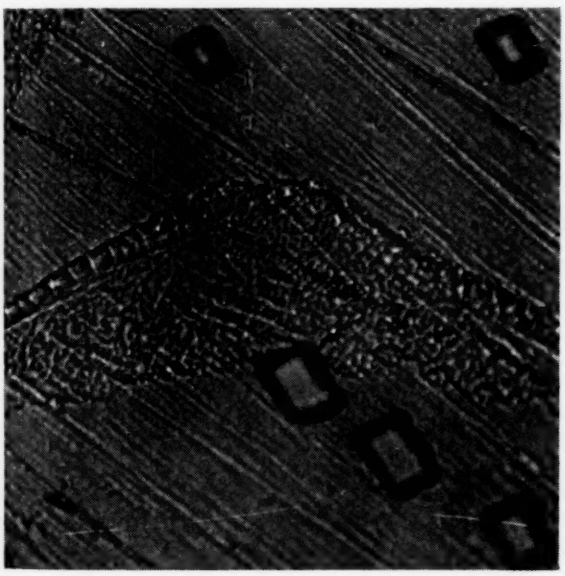

FIG. 5. Evaporation pits and hillocks on well-annealed (100) surface after 26 hr at 300°C. Magnification 1000 ×.

IV. DISCUSSION

The experimental results obtained on cubic body-centered thallium bromo-iodide crystals show that the evaporation of single crystals starts on definite points of the surface. Mechanical deformation of the crystal surface favors the start of evaporation. At low temperature, the evaporation proceeds in regular steps forming very regular pits bounded always by (110) planes. At higher temperature, the evaporation mechanism is more complicated, the formed pits are irregular and striation appears. The density of pits varies considerably over the surfaces, but the average density is highest on the (110), somewhat lower on the (100), and lowest on the (111) plane. This result indicates that the nucleation of evaporation pits increases with the reticular density of the crystal plane. Since the potential energy of a molecule in a crystal lattice increases with the reticular density, we must conclude that the starting of the evaporation does not take place in a direct process. According to Rideal and Wiggins,[13] the initial evaporation of single crystals starts at kinks from which the single molecules can escape more easily. When a

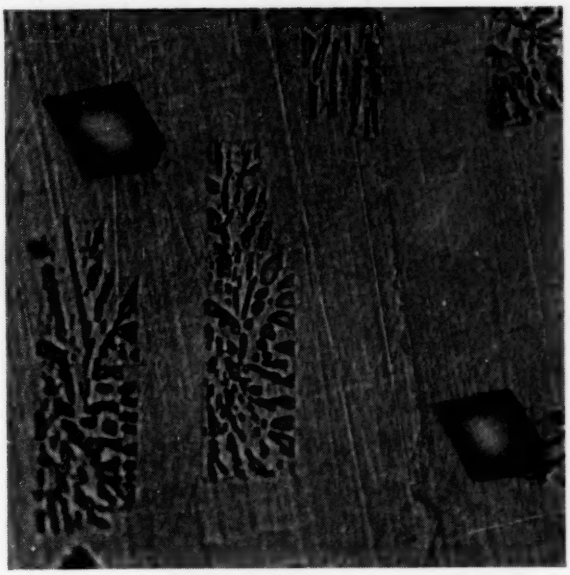

FIG. 6. Evaporation pits and hillocks on well-annealed (110) surface after 26 hr at 300°C. Magnification 1000 ×.

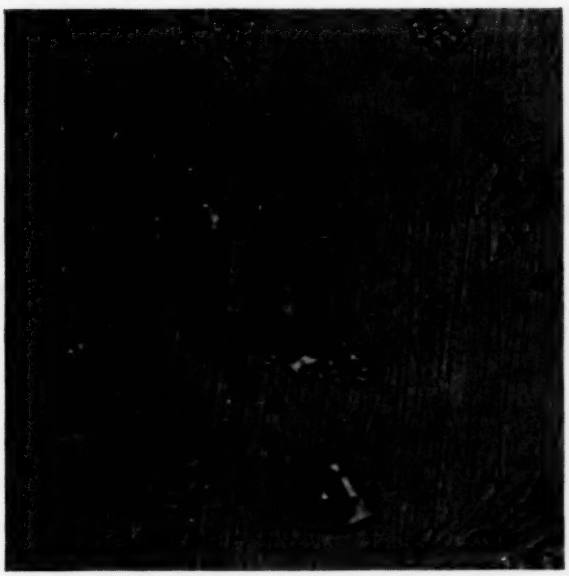

FIG. 7. Evaporation pits and hillocks on well-annealed (111) surface after 26 hr at 300°C. Magnification 1000 ×.

[13] E. Rideal and P. M. Wiggins, Proc. Roy. Soc. (London) **A210**, 291 (1952).

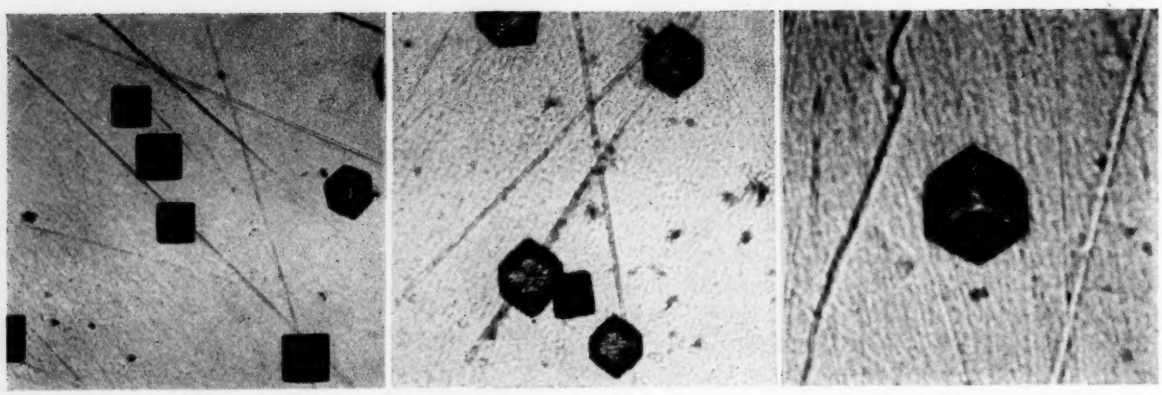

(a) (b) (c)

FIG. 8. Overgrowth crystals on well-annealed surfaces after 24 hr at 300°C. Magnification 250 ×.
(a) (100) surface, (b) (110) surface, (c) (111) surface.

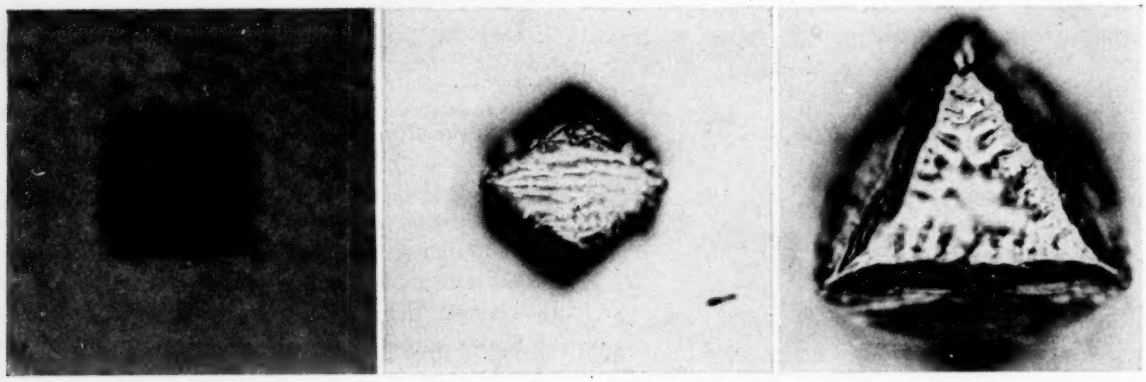

(a) (b) (c)

FIG. 9. Surface structure of overgrowth crystals on well-annealed surfaces after 24 hr at 300°C. Magnification 1000 ×.
(a) (100) surface, (b) (110) surface, (c) (111) surface.

molecule leaves its original place, it can migrate along the crystal surface.[14] The hillocks shown in Figs. 5–7 may be formed by such a migration. The outside shape of the hillocks may be connected with the migration directions, the inner structure with a layer coagulation.[15]

The formation of nuclei from the vapor phase is very similar to evaporation and can be considered as a reversed process. At low vapor pressure single nuclei are formed on the crystal surface, bounded always by (110) planes. The orientation is determined by the surface on which the vapor is deposited. A small number of nuclei do not match with the orientation of the main crystal. The population density of nuclei is again highest on (110) and lowest on (111) planes. The uniform three-dimensional growth of nuclei indicates a high degree of surface migration. Although the crystals have a very uniform shape, the surfaces disclose a rough structure quite similar to the surface structure obtained by evaporation.

[14] See, e.g., Knacke, Stranski, and Wolff, Z. physik Chem. **198**, 157 (1951).
[15] E. N. DaC. Andrade, Trans. Faraday Soc. **31**, 1157 (1935).

Molecular Constants of Cesium Chloride by the Molecular Beam Electric Resonance Method*†

R. G. LUCE‡ AND J. W. TRISCHKA
Syracuse University, Syracuse, New York

(Received July 10, 1952)

The electric resonance method of molecular beam spectroscopy was used to observe the CsCl spectra arising from transitions of the type $J,m_J \rightarrow J,m_J'$, where J is the rotational quantum number and m_J the electric quantum number. The following transitions were identified and studied: 2,0→2,1; 3,0→3,1; 4,0→4,1; 4,1→4,2; and 5,1→5,2. An analysis of the spectra for several values of the electric field intensity gave the following molecular constants for the ground vibrational state of $Cs^{133}Cl^{35}$: $\mu_0=10.46\pm0.14$ debye; $A_0=(385\pm9)\times10^{-40}$ g cm²; $B_0=(72.7\pm1.7)\times10^{-3}$ cm⁻¹; $r_0=(2.88\pm0.03)\times10^{-8}$ cm. μ_0 is the electric dipole moment, A_0 is the moment of inertia, B_0 is the rotational constant, and r_0 is the internuclear distance. If μ is assumed to be proportional to the internuclear distance, and if the potential function is assumed to be a cubic, then the vibration-rotation constant α_e is calculated to be $(0.53\pm0.08)\times10^{-3}$ cm⁻¹. From measurements of line widths it was possible to set upper limits on the quadrupole interaction constants of Cs and Cl; *viz*, $|eqQ/h|_{Cs} \lesssim 4$ mc/sec and $|eqQ/h|_{Cl} \lesssim 3$ mc/sec.

I. INTRODUCTION

THE radiofrequency spectra of CsCl were studied by the molecular beam electric resonance method.[1–3] This method makes possible the measurement of the energy level differences between two adjacent m_J states of a diatomic molecule in a uniform electric field, the rotational quantum number, J, remaining constant. m_J is the electric quantum number.

CsCl differs in two important respects from molecules previously studied by this method: (1) both nuclei have an electric quadrupole moment, (2) the moment of inertia, A, and the electric dipole moment, μ, are considerably larger. The first difference resulted in more complex spectra than were found for molecules in which only one nucleus had a quadrupole moment. The second difference enabled larger J states to be refocused in the apparatus; i.e., CsCl states of $J \lesssim 5$ were refocused, whereas states of $J \lesssim 2$ were refocused heretofore.

II. EXPERIMENTAL

A. Apparatus

The general apparatus design, as seen in Fig. 1, was similar to that described in reference 1. However, several new features of the apparatus are worthy of description.

When observations were made at small C field voltages in the previous apparatus, difficulties were experienced with nonadiabatic transitions in the regions between the uniform field and the inhomogeneous fields. To reduce the number of these transitions separate, uniform fields called "buffer fields" were placed on either side of the C field, and their field strengths were adjusted to minimize the number of nonadiabatic transitions.

The collimator was made of two microscope cover glasses mounted on a mycalex frame to create a slit of the desired width. When the collimator was located between the A field and the adjacent buffer field, the refocused beam showed erratic fluctuations, indicating fluctuations in the number of nonadiabatic transitions in the interfield regions. It was hypothesized that these variations were caused by changes in the accumulation of electric charge on the glass surfaces of the collimator. Therefore, the collimator was placed between this buffer field and the C field, where the electric fields were weaker. The erratic behavior of the refocused beam was then absent as long as the glass surfaces were clean.

A knife-edge, also made of a microscope cover glass, was used in place of the usual stop wire in the B field, reducing by half the scattered beam reaching the detector. The position of the knife-edge was controlled from outside the vacuum system through a sylphon bellows used as a vacuum seal. A dial gauge was used to determine the position of the knife-edge. Settings were repeatable to 1.3×10^{-3} cm.

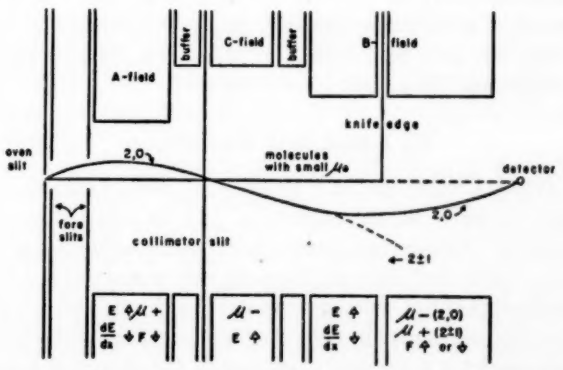

FIG. 1. Diagram of electric resonance apparatus. Dimensions along undeflected beam path are to scale. The distance from oven slit to detector wire is 64.5 cm.

* Supported in part by the ONR.
† Submitted by Robert G. Luce in partial fulfillment of the requirements for the degree of Doctor of Philosophy at Syracuse University.
‡ Now at Knolls Atomic Power Laboratory, General Electric Company, Schenectady, New York.
[1] H. K. Hughes, Phys. Rev. 72, 614 (1947).
[2] J. W. Trischka, Phys. Rev. 74, 718 (1948).
[3] A preliminary report of this work has been made in Phys. Rev. 83, 851 (1951). The results in the present paper differ slightly from those previously reported.

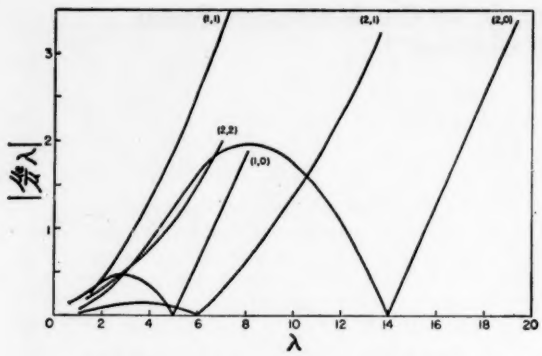

FIG. 2. $|(\mu_e/\mu)\lambda|$ *vs* λ for $J=1$ and $J=2$.

The *C* field, similar in construction to that in reference 2, but twice as long, was 10 cm long in the beam direction and 6.25 cm high. The radiofrequency voltage was applied over a length of 8 cm in the middle of the *C* field. The plates were chromium plated to reduce and to stabilize the contact potential. Two different sets of three glass spacers were used—0.65253±0.00015 cm and 0.31356±0.00025 cm. The spacers were compared with a Sheffield visual gauge and measured absolutely with a micrometer. Absolute measurements were also made with the visual gauge and Hoke precision gauge blocks made by Pratt and Whitney.

B. Resolution

Experience has shown[2] that a conservative estimate of the line width—i.e., the full width at one-half maximum—can be made by adding to the homogeneous field width[4] the frequency spread produced in a perfectly homogeneous field, when the field values are varied over the range of values present in the actual, inhomogeneous field. For a CsCl beam issuing from an oven at a temperature of 900°K, as in these experiments, the line width for a perfectly homogeneous field 8 cm long is 4.4 kc/sec. A conservative estimate of the inhomogeneity in the field results from the addition of the uncertainty in the spacer value given above and the deviations from planeness of the field boundary plates. Each plate differs from a plane by ±0.00062 cm. The estimated effect of inhomogeneity on a line at a frequency of 1 mc/sec is a broadening of 4 kc/sec for the larger spacing and 10 kc/sec for the smaller.

C. Refocusing Conditions

When a molecule in a given J, m_J state traverses a sigmoid path, as shown in Fig. 1, it is said to be "refocused." In these experiments the inhomogeneous fields were such that the effective dipole moment, μ_e, was positive in the *A* field and negative in the *B* field. Consequently, molecules in only one or two J, m_J states were refocused for a particular setting of the A and B fields. Transitions to the state J, m_J' were observed as a drop in beam flux caused by the "defocusing" of the beam, since, in general, a significant change in moment occurred as a consequence of a transition.

With the *A* and *B* fields arranged as described above, for a given apparatus and a given substance, only molecules with J values in a definite range can be refocused and only a fraction of the allowed transitions can be observed. In order to determine which J, m_J' states can be refocused it is necessary to know the force acting on the molecule in the inhomogeneous fields. Figures 2 and 3 are plots of a quantity, $|\mu_e\lambda/\mu|$, proportional to this force, *vs* the field parameter λ for the J, m_J states of interest in the present experiments. $\lambda=\mu E/(\hbar^2/2A)$, where E is the electric field intensity. It will be noted that for a number of states the curve has a cusp touching the λ axis for one value of λ. For λ less than this value μ_e is negative, while for λ greater than this value μ_e is positive. These curves were derived from solutions of an equation developed by Lamb.[1,5]

Since μ_e must be negative in the *B* field, of the states shown in Figs. 2 and 3 only the following can be expected to be refocused: 1,0; 2,0; 3,0; 3,1; 4,0; 4,1; 4,2; 5,0; 5,1; 5,2. In the present apparatus the maximum force in the *B* field is not sufficient, however, to permit refocusing of the CsCl molecules in the states 1,0; 2,1; 3,1; 4,2. In general, even when the force in the *B* field is adequate the force in the *A* field may not be sufficient if too large a value of λ is required. This is illustrated in the present apparatus, for which the maximum value of λ is 60, by the 5,0 state of CsCl. Because of insufficient forces in one or the other field, or in both fields, no CsCl molecules with $J>5$ can be refocused in this apparatus.

To obtain all of the observable transitions it is necessary to refocus the CsCl molecules in only the following states: 2,0; 3,0; 4,1; 5,1. Figures 2 and 3 make it clear that to refocus these states in an ideal apparatus four distinct sets of voltages on the *A* and *B* fields are required. However, the inhomogeneous field design and beam height of the present apparatus are such that molecules in the 3,0 and 4,1 states are refocused for the

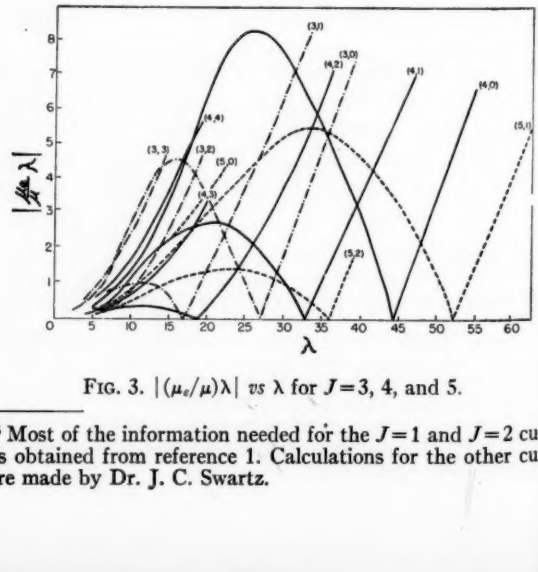

FIG. 3. $|(\mu_e/\mu)\lambda|$ *vs* λ for $J=3$, 4, and 5.

[4] H. C. Torrey, Phys. Rev. **59**, 293 (1941).

[5] Most of the information needed for the $J=1$ and $J=2$ curves was obtained from reference 1. Calculations for the other curves were made by Dr. J. C. Swartz.

same setting of the field voltages. For another setting of these voltages molecules in the 4,0 and 5,1 states are simultaneously refocused. The failure to discriminate between molecules in particular states is also illustrated by an inability to allow the observation of the 5,1→5,0 transition. A portion of the 5,0 curve is drawn in Fig. 3. It will be noted that the force in the B field acting on a 5,0 molecule is quite similar to that acting on a 5,1 molecule, whereas the force on a 5,2 molecule is considerably less. Thus, when a 5,1 molecule, which is initially refocused by the apparatus, undergoes a transition in the C field to a 5,0 state, the force on it in this new state in the B field is virtually the same as before and no drop in beam flux occurs at the detector. However, with a transition to a 5,2 state the force in the B field is sufficiently less for a drop in beam flux to occur

D. Beam Properties

All observations were made with oven and collimator slits 7.6×10^{-3} cm wide and a detector wire 13×10^{-3} cm wide. The beam height was 0.5 cm. A total beam flux of 325 000 cm of galvanometer deflection was measured on the highest sensitivity of the amplifier. This flux produced an ion current of 1.36×10^{-9} amp. The magnitude of the refocused beams varied with different states as follows: for the 2,0 state, 5 cm deflection; for the 3,0 and 4,1 states (refocused together). 10 cm; and for the 5,1 and 4,0 states (refocused together), 12 cm. Most of the observations were made with the knife edge set 18×10^{-3} cm from the beam center line. The beam produced a 50 cm deflection with the knife-edge in position, the A and B fields off and a pressure of 2×10^{-7} mm of Hg in the apparatus. For positions of the knife-edge greater than 14×10^{-3} cm no once-scattered molecules could reach the detector; hence, double scattering accounted for the observed beam.

E. Measuring Equipment

Two General Radio oscillators were used. One was the standard signal generator type 805-C with a range from 50 kc/sec to 50 mc/sec, the other a type 857-A with a range from 95 to 515 mc/sec. A General Radio 620-A heterodyne frequency meter was used to determine the oscillator frequency to 1 part in 10 000. The meter was checked to 1 part in 10 000 against the Bureau of Standards' station WWV. A Leeds and Northrup volt box accurate to 2 parts in 10 000 was used in conjunction with a Rubicon potentiometer, which had an accuracy of 1 part in 10 000, and an Eppley standard cell, standardized before and after the experiment by the Bureau of Standards to 1 part in 10 000. The random error for a given setting of the potentiometer was 4 parts in 100 000.

F. Spectra

Measurements were made in three different regions of electric field intensity of the C field. In the first

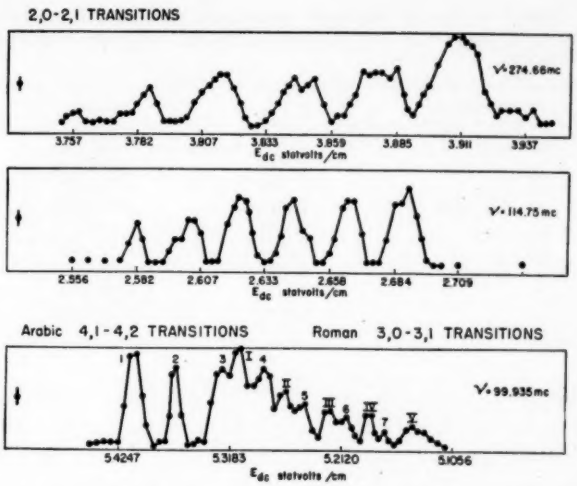

FIG. 4. Spectra resulting from 2,0→2,1; 3,0→3,1 and 4,1→4,2 transitions. Vertical lines at left indicate observational error.

region the transition frequencies were 100 mc/sec and greater. Data in this region were necessary in order to determine μ and A. In the second region the transition frequencies were of the order of 5 mc/sec, frequencies large in comparison with the fine structure resulting from the quadrupole interactions. This was a suitable region in which to expect the appearance of quadrupole fine structure. The third region was a region of very weak fields in which the Stark effect was small compared with the effects produced by the quadrupole interactions. As the resolution was a maximum here, this region was also suitable for the discovery of quadrupole effects.

Figure 4 shows examples of data taken at frequencies of 100 mc/sec and greater. The large C field spacers were used for the 2,0→2,1 observations, the small spacers for the 3,0→3,1 and 4,1→4,2 observations. The distinct lines in Fig. 4 were produced by molecules in different vibrational states. No fine structure resulting from the quadrupole interactions is resolved. The width of each line for a given vibrational state is greater than that predicted from the field inhomogeneity. To insure that no line broadening was caused by excessive rf voltage, this voltage was adjusted until a region was found for which the width did not depend on the voltage. Thus, it is concluded that the quadrupole interactions are responsible for the broadening of the peaks.

Since the abundance ratio of $Cs^{133}Cl^{35}$ and $Cs^{133}Cl^{37}$ is 3:1, it is clear that the spectra in Fig. 4 were produced by $Cs^{133}Cl^{35}$. Calculations for the 2,0→2,1 transitions of the positions of the $v=0$ and $v=1$ lines for $Cs^{133}Cl^{37}$ showed that they should appear at slightly lower fields than do the $v=3$ and $v=4$ lines of the $Cs^{133}Cl^{35}$ spectrum. v is the vibrational quantum number. An examination of Fig. 3 shows an asymmetry in the $v=3$ line and a "bump" on the side of the $v=4$ line of the 2,0→2,1 spectrum. The "bump" occurs at the position of the

TABLE I. Energy difference parameter, $\Delta\epsilon$, as a function of the field parameter λ, calculated from the solutions of Lamb's equation.

Transition	λ	$\Delta\epsilon$
2,0→2,1	2.000	0.055740
	2.400	0.084868
	2.700	0.111989
3,0→3,1	3.864	0.046340
	4.700	0.072674
	5.577	0.110190
4,1→4,2	3.939	0.046378
	5.000	0.075755
	5.850	0.105060

predicted $v=1$ line for $Cs^{133}Cl^{37}$. However, since the various asymmetries, peaks and valleys in the other lines of the observed spectrum in each case are not real, the identification of the $Cs^{133}Cl^{37}$ lines is dubious.

Investigations in the region of 5 mc/sec failed to reveal either resolved vibrational effects or quadrupole fine structure in the lines produced by any of the five observable transitions.

At very weak fields a few relative maxima and minima were found, but no distinct lines.

III. RESULTS

A. μ and A

The values of μ and A were calculated from data taken at two different electric field intensities by the method now to be described. The equation due to Lamb[1] for the energy levels of a rigid rotator in an electric field was solved for three different values of the parameter λ in the λ range covered by the experimental data. Table I gives values of $\Delta\epsilon$ *vs* λ for the transitions of interest in our experiments. $\Delta\epsilon=h\nu/(\hbar^2/2A)$. The quantity $\Delta\epsilon/\lambda^2$ was then calculated and a parabola, $\Delta\epsilon/\lambda^2=f(\lambda^2)$, fitted to the three points for each transition. This gave,

for the 2,0→2,1 transition,

$$\Delta\epsilon/\lambda^2=(118.1426+5.831\lambda^2-0.1323\lambda^4)\times10^{-4}; \quad (1)$$

for the 3,0→3,1 transition,

$$\Delta\epsilon/\lambda^2=(27.588+0.21187\lambda^2+0.00130\lambda^4)\times10^{-4}; \quad (2)$$

and for the 4,1→4,2 transition,

$$\Delta\epsilon/\lambda^2=(29.222+0.04290\lambda^2+0.0000013\lambda^4)\times10^{-4}. \quad (3)$$

From each of these equations an equation of the following form was derived:

$$1/\mu^2A=g[E, \nu, (\mu A)^2]. \quad (4)$$

If the experimental fields used are designated by E_1 and E_2 and the corresponding frequencies by ν_1 and ν_2, then the following relation is true:

$$g[E_1, \nu_1, (\mu A)^2]=g[E_2, \nu_2, (\mu A)^2]. \quad (5)$$

This equation, a quadratic in $(\mu A)^2$, was solved for $(\mu A)^2$. Substitution of this value of $(\mu A)^2$ in (4) then gave μ^2A. Finally, μ and A were calculated from $\mu=\mu^2A/\mu A$ and $A=(\mu A)^2/\mu^2A$. Table II shows the data and results for the 2,0→2,1 and 3,0→3,1 transitions for the ground vibrational state, $v=0$. Although values of μ and A in close agreement with the values presented in Table II were obtained from the data for the 4,1→4,2 transition, the large errors made these results useless. These errors were a result of the small size of the second term in (3) in comparison with the first.

Each field value in Table II was calculated from the average of the voltages at half-maximum of the observed lines, corrected for the contact potential difference, −0.17 v, between the plates of the C field. The errors in the field values are composed almost entirely of the random errors in the determination of the line positions. Systematic errors in the measurement of electric field intensity, such as the error in the C field spacer values, do not contribute to the error in A and contribute a negligible amount to the error in μ.

Since no details of the quadrupole interactions were discovered in these experiments, it was not possible to calculate the location of the hypothetical, unperturbed Stark line within the extent of the broad, featureless, observed lines. A general consideration of the theory indicates that the Stark line should be near the center of the observed line. However, more conclusive evidence is needed to demonstrate the adequacy of the method, given in the preceding paragraph, for selecting the position of the Stark line. Therefore, calculations were made in which the position of this line was assumed to be at the voltage corresponding to the half-maximum value of the observed line. The resulting values of μ and A differed from those given in Table II by less than 1 percent.

In Table III values of μ_0, A_0, and $(\mu^2A)_0$ are given which are grand means of the values in Table II. The subscript 0 indicates that these values are for the

TABLE II. Data and molecular constants calculated for the ground vibrational state from the observed transitions.

Transition	Frequency mc/sec	Field statvolts/cm	λ	$(\mu^2A)_0$ 10^{-73} cgs units	μ_0 10^{-18} esu	A_0 10^{-40} g cm^2
2,0→2,1	274.66±0.05	3.9104±0.0010	2.84	42.23±0.20	10.46±0.20	385.8±12.6
	114.89±0.02	2.6894±0.00077	1.95			
3,0→3,1	237.12±0.05	7.6593±0.0027	5.55	42.26±0.23	10.46±0.20	384.7±12.3
	99.935±0.020	5.3086±0.0053	3.84			

ground vibrational state. In addition, calculated values of the rotational constant B_0 and the internuclear distance r_0 are presented.

B. Vibrational Effects

An equation for the variation of μ^2A with vibration may be derived from each of the equations (1), (2), and (3). To a first approximation it is found that twice the fractional change in the voltage difference between adjacent vibrational lines is equal to the fractional change in μ^2A between the two vibrational states. A more refined calculation requires a knowledge of the individual variations of μ^2 and A. Because the least refinement is needed if the 4,1→4,2 data are used, only these data were used in the calculations. In this case, twice the fractional change in voltage per vibrational state is (1.52±0.08) percent. Since the experiments gave no information about the individual variations of μ^2 and A, a more refined calculation required some reasonable assumption about these variations. Table III gives the value of $[(\mu^2A)_1-(\mu^2A)_0]/(\mu^2A)_0$ resulting from a calculation in which it was assumed that both μ^2 and A increase with vibration and increase by equal fractions. Within experimental error μ^2A changes an equal amount between adjacent vibrational states.

The vibration rotation constant, α_e, was calculated from the variation of μ^2A with vibration by a method previously outlined.[6] This method makes the assumptions that μ is proportional to the internuclear distance and that the potential function is a cubic. The value of ω_e, 229 cm^{-1}, used in the calculation is the theoretical one computed by Rittner[7] by a semiclassical method. Where his values can be compared with experiment agreement is within about 10 percent. The value of α_e is given in Table III. The error given assumes a 10 percent error in ω_e; an error which causes only a 1 percent change in α_e.

C. Quadrupole Interactions

A width of about 500 kc/sec was attributed to each vibrational state after the line widths in the 5 mc/sec region were corrected for the vibrational effects determined from the higher frequency data. When this figure is divided by the expected width of a fine structure line, 25 kc/sec, it is clear that less than 20 such lines could have been resolved by the apparatus. Although the theory for the 2,0→2,1 line predicts a total of 92 fine structure transitions, some structure would have been resolved were either quadrupole interaction very small compared with the other. The absence of resolved lines indicates that the ratio of the two interactions is probably less than 10.

As it was not possible to determine the magnitudes of the quadrupole interactions, upper limits were found. Two calculations were made, one on the assumption that the Cs interaction, and the other that the Cl interaction was solely responsible for the observed line width. The conservative values obtained in this way are given in Table III.

TABLE III. Results.

Quantity	Value
μ_0, 10^{-18} esu	10.46±0.14
A_0, 10^{-40} g cm^2	385 ±9
$(\mu^2A)_0$, 10^{-78} esu^2 g cm^4	42.24±0.16
B_0, 10^{-3} cm^{-1}	72.7 ±1.7
r_0, 10^{-8} cm	2.88±0.03
μ/er_0	0.76
$[(\mu^2A)_1-(\mu^2A)_0]/(\mu^2A)_0$, percent	+1.65±0.09
α_e, 10^{-3} cm^{-1}	0.53±0.08
$\lvert eqQ/h\rvert_{Cs}$, mc/sec	≤4
$\lvert eqQ/h\rvert_{Cl}$, mc/sec	≤3

IV. DISCUSSION

It is of interest to compare the above value of the internuclear distance with that obtained by electron diffraction.[8] It is noteworthy that the electron diffraction result represents an average over the vibrational and rotational states present. The center of the electron diffraction population for the stated 1200°C source is about $v=3$. Centrifugal stretching effects, even for the large values of J in the electron diffraction work, can be neglected within the present limits of error. When the values of r_0 and α_e in Table III are used, $r_3=(2.92\pm0.03)\times10^{-8}$ cm. This is to be compared with the electron diffraction result of $(3.06\pm0.03)\times10^{-8}$ cm. The discrepancies are 5 percent between the two values and 3 percent outside the margins of experimental error.

The authors wish to thank Dr. J. C. Swartz for his assistance in the laboratory and Mr. D. T. F. Marple for his aid in the calculation of results. We also wish to thank Mr. C. Johnson of the Physics Department Machine Shop for his invaluable aid in the construction of the apparatus used in these experiments.

[6] J. W. Trischka, Phys. Rev. **76**, 1365 (1949).
[7] E. S. Rittner, J. Chem. Phys. **19**, 1030 (1951).
[8] Maxwell, Hendricks, and Mosley, Phys. Rev. **52**, 968 (1937).

The Infrared and Raman Spectra of Dicyanoacetylene*

FOIL A. MILLER
Department of Research in Chemical Physics, Mellon Institute

AND

ROY B. HANNAN, JR.†
Department of Chemistry, University of Pittsburgh and Mellon Institute, Pittsburgh 13, Pennsylvania

(Received July 14, 1952)

The preparation of dicyanoacetylene, N≡C−C≡C−C≡N, is outlined and its infrared and Raman spectra are presented. An assignment is given for 8 of the 9 fundamental frequencies which explains the observed combination tones very satisfactorily. All features of the spectra are compatible with $D_{\infty h}$ symmetry, including particularly the infrared band contours, the lack of coincidences between infrared and Raman frequencies, and the operation of selection rules for the combination tones. Results of a normal coordinate treatment are included.

INTRODUCTION

DICYANOACETYLENE, N≡C−C≡C−C≡N, was first reported by Moureu and Bongrand in 1909.[1] They published several papers on the physical and chemical properties of the substance, and summarized their findings in a review in 1920.[2] Only one later paper mentioning this compound has been found,[3] and it is concerned chiefly with by-products of the synthesis.‡

Dicyanoacetylene is unique in combining both a linear chain of six atoms and a system of three conjugated triple bonds. Only one other six-atom linear molecule is known (diacetylene, H−C≡C−C≡C−H), and no molecule having a system of three conjugated triple bonds has been subjected to a vibrational analysis. This paper summarizes the results obtained from the vibrational spectra. An x-ray determination of the crystal structure[4] has shown that the molecule is linear and symmetrical, with the nitrogen atoms at the ends. The interatomic distances are: C≡N, 1.14A; C−C, 1.37A; C≡C, 1.19A.

EXPERIMENTAL

The dicyanoacetylene used in this work was prepared by a method very similar to the one originally described by Moureu and Bongrand.[2] The reactions employed were

$$\mathrm{HOOC-C\equiv C-COOH} \xrightarrow{\mathrm{CH_3OH}} \mathrm{CH_3OOC-C\equiv C-COOCH_3} \xrightarrow{\mathrm{NH_4OH}} \mathrm{NH_2OC-C\equiv C-CONH_2} \xrightarrow{\mathrm{P_2O_5}} \mathrm{N\equiv C-C\equiv C-C\equiv N}.$$

The final product was a colorless liquid which solidified at 20°C and boiled at 76°C. A mass spectrographic analysis indicated a purity of about 98.2 percent by weight.[5]

A Perkin-Elmer Model 12B spectrometer was used to obtain the infrared spectra from 420 to 3400 cm^{-1}. Prisms of KBr, NaCl, and CaF_2 were employed. During the recording of the spectra the housings of the instrument were continuously flushed with a stream of dry nitrogen gas in order to reduce the absorption due to atmospheric water vapor and carbon dioxide.

For the liquid state spectra, ordinary vapor-tight cells were used in thicknesses of 0.4 and 0.02 mm. A Perkin-Elmer one-meter cell was used in obtaining the spectrum for the vapor. The gas-handling system used for filling the latter was designed to permit a crude fractionation of the sample. An examination of the spectra of three fractions resulted in the identification of ten impurity bands.

The uncertainty in the measured frequencies was estimated to be less than ±1 cm^{-1} in the 400-1200 cm^{-1} interval, ±3 cm^{-1} in the 1200–2600 cm^{-1} interval, ±5 cm^{-1} in the 2600–3000 cm^{-1} interval, and ±10 cm^{-1} in the 3000–3400 cm^{-1} interval.

The Raman spectrograph and illuminator have been described elsewhere.[6] For this work, samples were

* From a thesis submitted by R. B. Hannan in partial fulfillment of the requirements for the degree of Doctor of Philosophy at the University of Pittsburgh, June, 1952.

† Present address: Standard Oil Company of Indiana, Whiting, Indiana.

[1] C. Moureu and J. C. Bongrand, Bull. Soc. Chim. **V**, 846 (1909).

[2] C. Moureu and J. C. Bongrand, Ann. Chem. **14**, 5 (1920).

[3] H. Mommaerts, Bull. classe sci., Acad. roy. Belg. **28**, 363 (1942); *Chem. Abstracts* **40**, 4670–8.

‡ *Note added in proof.*—The synthesis has also been repeated by A. T. Blomquist and E. C. Winslow, J. Org. Chem. **10**, 149 (1945) (especially p. 156).

[4] R. B. Hannan and R. L. Collin, Acta Cryst. (to be published).

[5] The mass spectrographic analysis was obtained through the courtesy of Dr. R. A. Friedel of the Synthetic Fuels Research Laboratories of the Bureau of Mines, Bruceton, Pennsylvania.

[6] F. A. Miller and R. G. Inskeep, J. Chem. Phys. **18**, 1519 (1950).

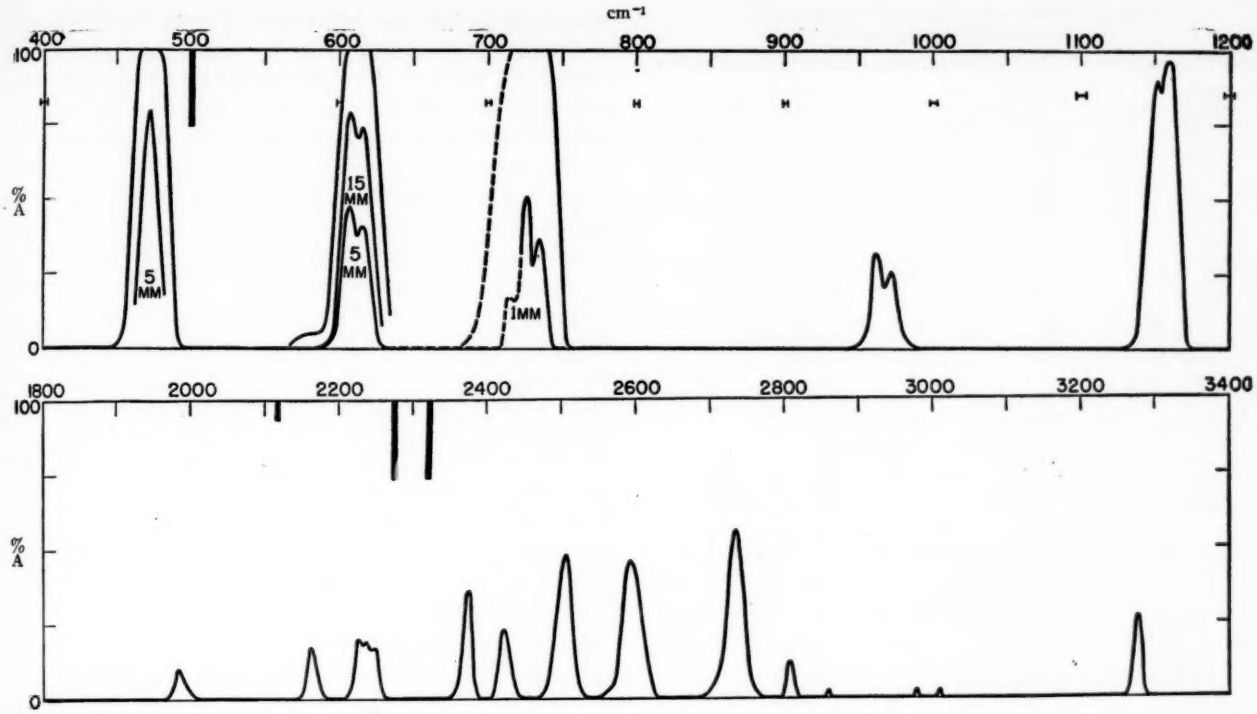

FIG. 1. Infrared and Raman spectra of dicyanoacetylene. The infrared absorption is for a sample in a one-meter cell at 90 mm pressure unless otherwise indicated. Raman frequencies are indicated by bars. The dotted portion of the 730 cm^{-1} band is due to an impurity.

vacuum distilled and sealed into 10 cm long Raman tubes having a volume of about two ml.

The infrared spectrum of the vapor and the four observed Raman lines are given in Fig. 1 and Table I.

ASSIGNMENT OF FREQUENCIES

On the basis of valence theory, the only reasonable structure for dicyanoacetylene is the linear symmetrical configuration belonging to point group $D_{\infty h}$. This structure accounts so well for all the features of the observed spectra that it will be the only one considered here.

Of the thirteen normal vibrations for this structure, four are doubly degenerate. Table II summarizes the notation, selection rules, and expected frequency ranges for the fundamentals. The notation follows Herzberg.[7] Schematic pictures of the nine modes are shown in Fig. 2.

Infrared Band Contours

P and *R* branches were resolved only for the parallel bands. For the perpendicular ones, the *Q* branch is so intense that the appearance is that of a single absorption maximum. Using the interatomic distances from the x-ray study, the spacing between the *P* and *R* maxima was calculated to be 8.7 cm^{-1}.[8] The five observed doublet separations were between 8.9 and 10.0 cm^{-1}, which is quite satisfactory.

[7] G. Herzberg, *Infrared and Raman Spectra of Polyatomic Molecules* (D. Van Nostrand Company, New York, 1945), p. 119.
[8] Reference 7, p. 391.

Assignment of Observed Fundamental Frequencies

Of the three totally symmetrical stretching vibrations belonging to the Raman active species Σ_g^+, ν_1 and ν_2 were readily identified with the strong Raman lines at 2333 and 2267 cm^{-1}. However, no Raman line was found which could be assigned as ν_3. The analogous symmetrical C—C stretching mode is also extremely weak in the Raman spectrum of cyanogen and diacetylene.

The line at 504 cm^{-1} can be assigned to one of the Raman active bending fundamentals of species Π_g. The other member of this species was not observed.

The two infrared active fundamentals belonging to species Σ_u^+ are parallel vibrations. The double maxima of ν_4 could have been taken as 2226 and 2236 cm^{-1} or as 2236 and 2246 cm^{-1}. The latter set was chosen because it provided a more nearly complete assignment of the observed summation and difference frequencies. This choice of $\nu_4 = 2241$ cm^{-1} is further substantiated by the fact that a very strong band appears in the liquid spectrum at the same frequency. For ν_5 either 967 or 1155 cm^{-1} are possibilities. The 1155 cm^{-1} band was adopted because of its greater intensity and because it could not be readily interpreted as a combination tone. On the other hand, 967 can be explained as $\nu_6 + \nu_8$.

The two remaining fundamental vibrations are perpendicular bands of the infrared active species Π_u. The intense band at 472 cm^{-1} is reasonable for one of these vibrations, but the other was again not observed.

All the assignments are collected in Table I.

TABLE I. Observed vibrational frequencies of dicyanoacetylene (in cm^{-1}).

Raman (Liq.)	I	IR (vapor)	I	Assignment
		3276	w	$\nu_4+\nu_5-\nu_9=3288$
		3007	vw	$\nu_4+\nu_6+\nu_7=3005$
		2978	vw	...
		2858	vw	...
		2808	w	$\nu_1+\nu_8=2805$
		2735	w	$\nu_2+\nu_8=2739$
		2591	w	$\nu_4+\nu_8-\nu_9=2606$
		2505	w	$\nu_4+\nu_7=2501$
		2442	w	$\nu_1+\nu_9=2440$
		2375	w	$\nu_2+\nu_9=2374$
2333	s			ν_1
2267	s			ν_2
		2246 (max)		
		2241 (min)	w	ν_4
		2236 (max)		
		2226	w	$\nu_1-\nu_9=2226$
		2162	w	$\nu_2-\nu_9=2160$
2119	vw			$\nu_1-2\nu_9=2119$
		1982	w	$\nu_4-\nu_7=1981$
		1159.3 (max)		
		1154.4 (min)	m	ν_5
		1150.1 (max)		
		971.4 (max)		
		967.5 (min)	w	$\nu_6+\nu_8=976$
		961.8 (max)		
		734.4 (max)		
		729.9 (min)	vs	$\nu_7+\nu_8=732$
		725.4 (max)		
		616.0 (max)		
		611.6 (min)	s	$\nu_6+\nu_9=611$
		607.1 (max)		
504	m			ν_6
		472	vs	ν_8
[260]				ν_7
		[107]		ν_9

vs = very strong w = weak
s = strong vw = very weak
m = medium
[ ] Estimated from combination tones

Assignment of Unobserved Fundamental Frequencies

There are three fundamental frequencies which were not directly observed (ν_3, ν_7, and ν_9). In such cases the values can sometimes be determined from a consideration of the remaining frequencies, which must be interpreted as summation or difference tones subject to the selection rules of $D_{\infty h}$.

The infrared bands observed at 612, 730, and 967 cm^{-1} are all parallel bands. Because of the intensity of 612 and 730, one would like to assign them as fundamentals, but no parallel fundamentals can be this low. A consideration of the direct products shows that they must represent combinations of Σ_g^+ and Σ_u^+ or Π_g and Π_u vibrations.[9] The binary sum of a Σ_g^+ and Σ_u^+ fundamental would be much higher than these observed values (see Table II). Likewise a difference tone involving Σ_g^+ and Σ_u^+ fundamentals is out of the question, for it requires that the transition originate from a level at least 800 cm^{-1} above the ground state. At room temperature, the population of such a level would be insufficient to account for the observed intensities. Finally, all three of these observed frequencies are too high to be the difference between a Π_g and a Π_u fundamental. Therefore, it is concluded that they represent various sums of Π_g and Π_u frequencies, i.e., sums of Raman active bending with infrared active bending fundamentals. For instance, the sum of the two observed bending frequencies is $504+472=976$ cm^{-1}, which is in reasonable agreement with the observed value of 967 cm^{-1}. The bands at 612 and 730 cm^{-1} are then presumed to be due to combinations involving the two unobserved bending frequencies (ν_7 and ν_9). This leads to six pairs of possible values for ν_7 and ν_9. The particular set $\nu_7=260$ cm^{-1}, $\nu_9=107$ cm^{-1} was the only one which led to a satisfactory interpretation of the remaining observed frequencies. There can be little doubt as to the reality of these frequencies, for ν_7 was used four times and ν_9 eight times in explaining various combination bands. Furthermore, the numerical values must be correct to within ± 3 cm^{-1}, for both were observed as difference tones.

It was not possible to locate ν_3 from the combination bands.

Explanation of Remaining Frequencies

All but six of the remaining vapor phase bands have been satisfactorily explained as binary combinations, and four of these six can be accounted for as ternary combinations (Table I). This leaves only the very weak bands at 2978 and 2858 cm^{-1}. Since these are in the C—H stretching region at the positions for methylene or methyl groups, they may be due to an impurity.

The only remaining Raman line, at 2119 cm^{-1}, can be nicely explained as $\nu_1-2\nu_9=2119$. It is quite unusual to observe a ternary combination in the Raman effect.

Liquid State Infrared Spectrum

It was hoped that ν_3 could be observed in the spectrum of a thick liquid sample owing to the breakdown of selection rules. The breakdown is demonstrated by the appearance of bands at 2337, 2267, and 504 cm^{-1} in the liquid which correspond to the Raman active

TABLE II. Predicted properties of the fundamental vibrations for $D_{\infty h}$ symmetry.

Species	Notation	Activity	Band type	Description	Expected frequency in cm^{-1}
Σ_g^+	ν_1	Raman		C≡N stretch	2050–2400
	ν_2			C≡C stretch	2050–2300
	ν_3			C—C stretch	800–1150
Σ_u^+	ν_4	Infrared	Parallel	C≡N stretch	2050–2400
	ν_5			C—C stretch	800–1150
Π_g	ν_6	Raman		Bend	Less than 600
	ν_7			Bend	
Π_u	ν_8	Infrared	Perpendicular	Bend	Less than 600
	ν_9			Bend	

[9] Reference 7, pp. 123–131, 380.

fundamentals ν_1, ν_2, and ν_6. An additional twenty-five new bands, most of them very weak, were found in the liquid which had no counterpart in either the vapor infrared nor in the Raman spectra. It is probable that most of them are caused by impurities. In the region where ν_3 is expected (800–1150 cm^{-1}), bands were observed at 814, 890, 917, 950, 1074, and 1145 cm^{-1}. Because no further evidence for or against any of these values was found, ν_3 is left unassigned.

Conclusions

Eight of the nine fundamental frequencies have now been assigned, and are shown to account for the considerable number of combination bands quite satisfactorily. The missing frequency is that for the symmetrical C—C stretching mode.

There can be little doubt that the symmetry of the molecule is $D_{\infty h}$. The parallel and perpendicular band envelopes, the separations of the P and R maxima, the lack of coincidences between infrared and Raman spectra, and the obvious operation of selection rules in the fundamentals and combination bands constitute strong evidence for this structure. Thus the chemical, x-ray, and spectroscopic evidence each independently and convincingly lead to the same conclusion.

CALCULATION OF FORCE CONSTANTS

The most general quadratic function for the vibrational potential energy of the $D_{\infty h}$ model of dicyanoacetylene would contain fifteen force constants. There are, however, only nine fundamental frequencies. Consequently a valence force field has been assumed in which the interactions between nonadjacent bonds and angles are assumed to be zero. This leaves nine force constants in the potential function:

$$2V=2f_1(\Delta d_1)^2+2f_2(\Delta d_2)^2+f_3(\Delta d_3)^2+4f_{12}(\Delta d_1)(\Delta d_2)+4f_{23}(\Delta d_2)(\Delta d_3)+2f_\alpha(\Delta\alpha)^2+2f_\beta(\Delta\beta)^2+4f_{\alpha\beta}(\Delta\alpha)(\Delta\beta)+2f_{\beta\beta'}(\Delta\beta)(\Delta\beta'),$$

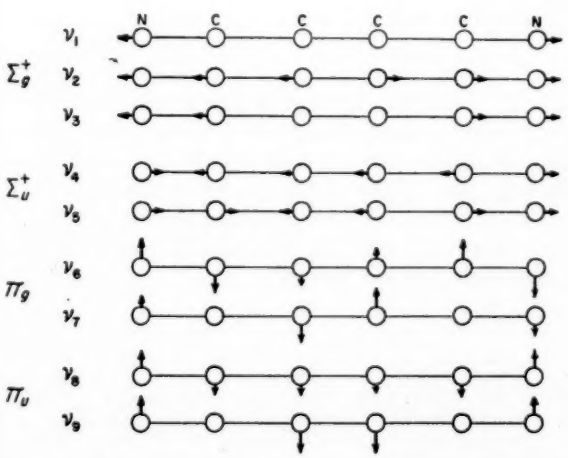

FIG. 2. Normal vibrations of dicyanoacetylene (schematic).

TABLE III. Force constants for Σ_u^+ vibrations (in units of 10^5 dynes/cm).

f_{12} (assumed)	f_1	f_2
0	15.7	7.9
0.2	16.1	7.7
0.4	16.6	7.5
0.6	16.9	7.3
0.8	17.3	7.2
1.0	17.6	7.1

where the internal coordinates are defined as the changes in the following bond lengths and angles:

$$N\overset{d_1}{\text{—}}C(\alpha)\overset{d_2}{\text{—}}C(\beta)\overset{d_3}{\text{—}}C(\beta')\overset{d_2'}{\text{—}}C(\alpha')\overset{d_1'}{\text{—}}N.$$

Wilson's F and G matrix method was used.[10] The matrices are given explicitly in the Appendix. The G matrices have been verified by an independent derivation using the generalized approach developed by Decius[11] and applied to linear molecules by Ferigle and Meister.[12]

Stretching Force Constants

Since ν_3 has not been observed, it is impossible to solve the equations for the Σ_g^+ and Σ_u^+ species to obtain specific values for the five force constants involved in the stretching vibrations. However, by treating f_{12} as a variable parameter, frequencies for ν_4 and ν_5 can be used in the Σ_u^+ equations to solve for corresponding values of f_1 and f_2. These results are shown in Table III. f_1 is the nitrile stretching force constant and would be expected to have a value between 16.5×10^5 and 17.5×10^5 dynes/cm. f_2 is the C—C stretching force constant for a single bond in a highly conjugated system, and its value is anticipated to be between 6.0×10^5 and 7.5×10^5 dynes/cm. The interaction constant is normally found to be less than 1×10^5 dynes/cm. Table III shows that a reasonable range of values for these three constants is obtainable from the assigned frequencies even though it is impossible to solve for a unique set of values.

It was also hoped that a reasonable value for ν_3 could be derived from the equations for the stretching frequencies. By subtracting the linear equation of the Σ_u^+ species from that of the Σ_g^+ species the following is obtained:

$$\lambda_3=\lambda_4+\lambda_5-\lambda_1-\lambda_2+2\mu_C(f_3-2f_{23}),$$

where μ_C = the reciprocal of the mass of carbon, and $\lambda_i=4\pi^2c^2\nu_i^2$.

[10] E. B. Wilson, Jr., J. Chem. Phys. **7**, 1047 (1939); **9**, 76 (1941).
[11] J. C. Decius, J. Chem. Phys. **16**, 1025 (1948); **20**, 511 (1952).
[12] S. M. Ferigle and A. G. Meister, J. Chem. Phys. **19**, 982 (1951).

TABLE IV. Force constants for the bending vibrations [in units of 10^{-11} (dyne cm/radian^2)].

	Set I	Set II
f_α	0.36	0.70
f_β	0.24	0.37
$f_{\alpha\beta}$	0.012	0.42
$f_{\beta\beta'}$	0.081	0.042

The unknown quantities in this equation are ν_3, f_3, and f_{23}. f_3, the C≡C stretching constant, should have a value between 14.5×10^5 and 15.5×10^5 dynes/cm. The interaction constant is anticipated to be between zero and 1.0×10^5 dynes/cm. Therefore, the quantity (f_3-2f_{23}) would be expected to have a value between 12.5×10^5 and 15.5×10^5 dynes/cm. It was found, however, that this quantity had to have a value of about 17×10^5 to 19×10^5 in order that the calculated value of ν_3 fall within the expected range of 800 to 1150 cm^{-1}. This discrepancy may be due to the neglect of interactions between nonadjacent bonds or angles, or to incorrect estimates for the ranges of ν_3, f_3, or f_{23}. It seems that there is little that can be done with the stretching force constants until ν_3 is determined experimentally.

Bending Force Constants

Expressions for all four bending frequencies were combined to give a quartic equation in f_α, two of the roots of which were imaginary. The remaining roots gave the sets of values listed in Table IV. Set II was rejected because it contains an interaction constant which is larger than a principal force constant.

APPENDIX

The factored F and G matrices are given below, with the symbols having the following meanings:

$S_1, S_2, \cdots$ = valence force symmetry coordinates for fundamental vibrations ν_1, ν_2, $\cdots$ (see Table II),
μ_N = the reciprocal of the mass of nitrogen,
μ_C = the reciprocal of the mass of carbon,
d_1 = C≡N bond length,
d_2 = C−C bond length,
d_3 = C≡C bond length,
ν_i = frequency,
$\lambda_i = 4\pi^2c^2\nu_i^2$ = a root of the secular equation.

Species Σ_g^+

F matrix

	S_1	S_2	S_3
S_1	f_1	0	f_{12}
S_2		f_3	$2^{\frac{1}{2}}f_{23}$
S_3			f_2

G matrix

	S_1	S_2	S_3
S_1	$\mu_N+\mu_C$	0	$-\mu_C$
S_2		$2\mu_C$	$-2^{\frac{1}{2}}\mu_C$
S_3			$2\mu_C$

Species Σ_u^+

F matrix

	S_4	S_5
S_4	f_1	f_{12}
S_5		f_2

G matrix

	S_4	S_5
S_4	$\mu_N+\mu_C$	$-\mu_C$
S_5		$2\mu_C$

Species Π_g

F matrix

	S_6	S_7
S_6	f_α	$f_{\alpha\beta}$
S_7		$f_\beta-f_{\beta\beta'}$

G matrix

	S_6	S_7
S_6	$\mu_C[1/d_1^2+2/d_2^2+2/d_1d_2]+\mu_N/d_1^2$	$-[1/d_1+2/d_2+2/d_3]\mu_C/d_2$
S_7		$2\mu_C[1/d_2^2+2/d_3^2+2/d_2d_3]$

Species Π_u

F matrix

	S_8	S_9
S_8	f_α	f_β
S_9		$f_\beta+f_{\beta\beta'}$

G matrix

	S_8	S_9
S_8	$\mu_C[1/d_1^2+2/d_2^2+2/d_1d_2]+\mu_N/d_1^2$	$-[1/d_1+2/d_2]\mu_C/d_2$
S_9		$2\mu_C/d_2^2$

Explicit equations for the frequencies are not given here. Wu[13] has given them for diacetylene, and these apply also to dicyanoacetylene if the appropriate masses and bond lengths are used. Our equations for Σ_g^+, Σ_u^+, and Π_u agree with Wu's. His equations for Π_g, however, bear no apparent resemblance to those from this work. No attempt was made to see whether algebraic manipulation would bring agreement, for it was known from other sources that the F and G matrices are correct (*viz.*, from the independent derivation of the matrices by Decius' method).

[13] T. Y. Wu, *Vibrational Spectra and Structure of Polyatomic Molecules* (J. W. Edwards, Ann Arbor, Michigan, 1946), second edition, p. 256.

The Mechanism of Acetone Vapor Fluorescence*

HAROLD J. GROH, JR.,† G. W. LUCKEY, AND W. ALBERT NOYES, JR.
Department of Chemistry, University of Rochester, Rochester, New York

(Received July 29, 1952)

The decay rates for the fluorescence of acetone vapor have been determined at several temperatures and pressures, and in the presence and absence of foreign gases, particularly oxygen. The quenching of the fluorescence has also been studied over a similar range of conditions. Since both the presence of oxygen and an increase in temperature tend to eliminate the fluorescence from one of the upper states, it has proved possible to obtain rate constants for the state not so eliminated. Approximate constants for the other state may be obtained by use of the data on total fluorescence in conjunction with data on the temperature and oxygen insensitive state. The data indicate that these two states are formed by independent or nearly independent paths so that molecules in one state are not transformed into molecules in the other under the conditions of these experiments. A consideration of this and previous work permits a further elucidation of the fluorescence phenomena.

IT has been recognized for some time that the fluorescence of acetone vapor is complex and that its quantitative description must be based on at least two and possibly more upper emitting states.[1] One of these states, i.e., the one present at room temperature in the absence of oxygen but which is eliminated either by increase in temperature or by oxygen, gives a fluorescence spectrum with a demonstrable structure.[2] No structure can be found in the spectrum emitted by the other state, although this is probably due to its complexity rather than to the total absence of structure.

In the present work, advantage is taken of the possibility of eliminating or reducing the emission of one of the upper states in order to obtain quenching and decay constants for the other. With this information at hand it is possible to discuss the entire mechanism of fluorescence in somewhat greater detail than heretofore.

EXPERIMENTAL

The preparation of materials has already been described.[1] The fluorescence decay rates were studied with an apparatus described by Kaskan and Duncan.[3] Light from a single condenser discharge through an argon filled tube was collimated and passed through 5 mm of Corning 9863 glass and 2 cm of 1.78-m nickel chloride solution before entering the T-shaped cell. The filter combination transmitted from approximately 2950 to 3500A. The fluorescent light passed through a Corning 7380 filter to eliminate scattered incident light before impinging on the photomultiplier tube. Quartz fluorescence was minimized by confining the incident beam to the center of the cell and by painting the outside cell walls black. The only modification of the electrical system was to increase the cathode-ray post-deflection accelerating potential from 1400 to 2500 volts. This brightened the transient screen images so that traces as brief as 10^{-6} second could be photographed. Fresh samples of acetone were used for each determination. Mixtures of acetone and oxygen were stirred for at least thirty minutes with an all glass, magnetically driven stirrer. Low oxygen pressures were measured with a McLeod gauge.

The blank due to scattered incident radiation and a small magnetic disturbance was always subtracted from the intensity of the "fast" fluorescence. This blank amounted to one-fourth to one-fifth of the fluorescent intensity. The subtraction probably over corrects for scattered radiation since acetone will absorb some of the scattered radiation. Further evidence that fluorescence from the 7380 filter was not responsible for the "fast" fluorescence ascribed to acetone was obtained by use of a Corning 3060 filter. The same effects were observed as for 7380 and yet the lifetime of the fluorescence of 3060 is about 10^{-4} second. Thus, the two types of fluorescence to be described later are believed to be real and not caused by spurious effects.

The apparatus for the steady state quenching determinations has already been described.[1] For these experiments no stirrer was used, but mixtures were allowed to stand for at least eight hours before an experiment was started.

RESULTS

Preliminary experiments showed that acetone vapor at 50° did not show a fluorescence which decayed as a simple exponential function of time. After a flash excitation there was a very fast decay followed by a slow, exponential decay. The mean life of the short-lived component is less than $8 \cdot 10^{-6}$ sec, the mean duration of the source flash. The long-lived component has a mean life of $2 \cdot 10^{-4}$ sec at 25°.[3] These experiments also showed that the long-lived component was quenched

* This work was supported in part by a contract with the ONR.

† Eastman Kodak Company Fellow in Physical Chemistry at the University of Rochester during 1951–2.

[1] See G. W. Luckey and W. A. Noyes, Jr., J. Chem. Phys. **19**, 227 (1951). Many references to earlier work have been given by R. E. Hunt and W. A. Noyes, Jr., J. Am. Chem. Soc. **70**, 467 (1948). The present paper deals entirely with the so-called "blue" fluorescence since it has been shown that the "green" fluorescence is almost certainly due to the presence of biacetyl. See M. S. Matheson and J. W. Zabor, J. Chem. Phys. **7**, 536 (1939).

[2] Luckey, Duncan, and Noyes, J. Chem. Phys. **16**, 407 (1948).

[3] W. E. Kaskan and A. B. F. Duncan, J. Chem. Phys. **16**, 223 (1948). See also W. E. Kaskan, Ph.D. thesis, University of Rochester, 1949. The authors wish to express their appreciation to Professor Duncan for the loan of this apparatus.

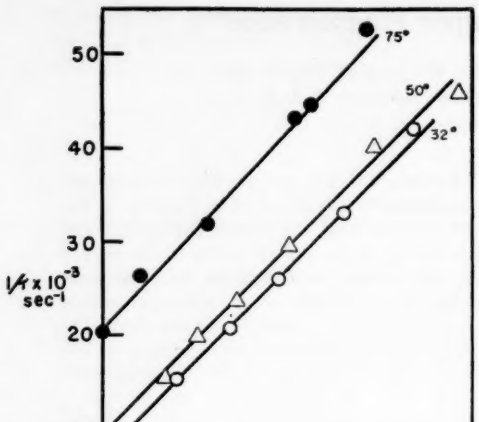

FIG. 1. Inverse mean life *vs* oxygen concentration for the long-lived component of acetone fluorescence. The acetone concentration was $6.34 \cdot 10^{18}$ molecules/cc.

strongly by oxygen, whereas the fast decay seemed unaffected by even 5 mm pressure of oxygen. These results were always reproducible.

It proved possible, therefore, to study the quenching of the long-lived state by measuring the inverse lifetime as a function of oxygen concentration at constant acetone concentration. Figure 1 shows the results at 32, 50, and 75°. The graphs are all straight lines which are parallel within experimental error. The slopes are $8.25 \cdot 10^{12}$ sec^{-1} mole^{-1} cc. From the intercepts it can be shown that in the absence of oxygen an increase in temperature of 25° reduces the mean life by one-half.

The steady-state measurement of fluorescent intensity includes radiation emitted by all states, whereas the flash method may, under certain restricted conditions, differentiate one emitting species from another. The inverse of relative fluorescence efficiency $1/Q$ rises sharply as oxygen is added and finally becomes nearly constant.[1] Oxygen pressures of 10 to 15 mm at 50° in 200 mm of acetone produce the limiting value of $1/Q$. This corroborates the flash method which shows that the short-lived state is unaffected by oxygen while the long-lived state can be completely quenched by this gas. Hence removal of the long-lived state permits a study to be made of the oxygen-insensitive portion. The behavior of the long-lived state may then be deduced from a study of total fluorescence. If the phenomenon were simple, one could subtract the fluorescence efficiency for one state from the total fluorescence efficiency to obtain the fluorescence efficiency due to the other state.

It was evident, however, that the total fluorescent yield increased with the intensity of the incident light at constant pressure. This effect disappears at 150° and could be eliminated by interposition of a blue filter in the path of the fluorescent radiation. The photochemically-formed biacetyl is, therefore, almost certainly responsible for this phenomenon. The number of quanta absorbed per cubic centimeter per second must be kept constant as the pressure is varied in order to ascertain the true nature of quenching by acetone. This can be done by varying the incident intensity as the pressure is varied. Figure 2 shows two curves, one at constant incident intensity and one at constant number of quanta absorbed per cubic centimeter per second.

The procedure was as follows: (1) The data for a plot of $1/Q$ *vs* acetone pressure at 50° were determined. This plot agrees with previous work.[1] (2) By interposition of neutral density filters, $1/Q$ was determined as a function of acetone pressure at constant number of quanta absorbed per cubic centimeter per second. (3) Oxygen was introduced at each acetone pressure and the residual yield subtracted from the yield at constant I_a to give $1/Q^{**}$, the inverse of the relative fluorescent efficiency for the oxygen-sensitive portion of the fluorescence. (4) The residual fluorescent intensities were only 10 to 15 percent of the total so that calculation of $1/Q^{*}$ for the oxygen-insensitive portion involves large errors. Figure 3 shows the results.

The results may be summarized briefly as follows: (1) The oxygen-sensitive portion of the fluorescence follows a Stern-Volmer relationship as regards quenching by oxygen (flash technique) and quenching by acetone (steady-state technique). (2) The oxygen-insensitive portion of the fluorescence probably obeys the Stern-Volmer relationship as regards quenching by acetone, although for reasons given the calculations of this quenching are subject to considerable error.

Any mechanism advanced must account not only for the above facts but be consistent with other data on

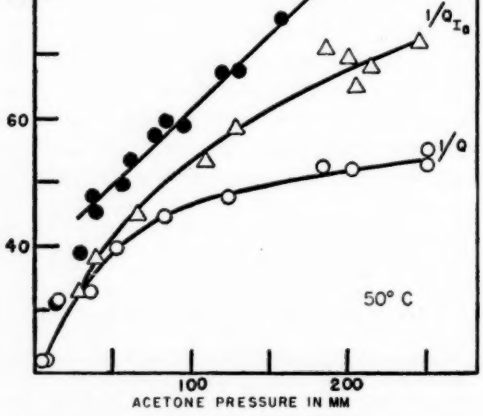

FIG. 2. Two lower curves: Inverse of relative fluorescent efficiency at constant incident intensity and at constant number of quanta absorbed per cubic centimeter per second (I_a). Upper curve: Inverse of fluorescent efficiency for the long-lived state alone.

(1) quenching; (2) spectroscopy; (3) photochemistry, both with and without added foreign gas.

DISCUSSION

One of the striking facts which emerge from the present work is that the intensity of the short-lived fluorescence is independent of the extent to which the long-lived fluorescence is removed either by oxygen or by increase in temperature. This indicates strongly that the short-lived state does not form the long-lived state reversibly. It cannot be decided whether or not the long-lived state is formed irreversibly from the same short-lived state from which fluorescence is observed.

The spectra of both fluorescences are at considerably longer wavelengths (roughly 3800 to 4700A) than the absorption band of acetone vapor (roughly 3300 to 2300A). No resonance fluorescence has been observed for this molecule. Thus the upper state responsible for the short-lived fluorescence differs at least in vibrational (and possibly also in electronic) energy from the state initially formed by the act of absorption. The state responsible for the long-lived fluorescence almost certainly is a different electronic state from the other one (or two) states.

In view of the foregoing facts it seems necessary to conclude that both fluorescing states are formed by independent paths from the initially formed state (or states). This might result from two different simultaneous absorptions leading to different upper electronic states which would merely lose vibrational energy by collision. It is possible to account for the facts also by the formation of a single upper state by absorption with transfer to the two fluorescing states by collision. The ratio of the amounts formed would be constant in the absence of foreign gas at constant temperature. Since the long-lived state is quenched strongly by oxygen and also has a much shorter mean life at high temperatures than at low, it is impossible to prove that the ratio of the amounts of the two states formed is independent of all conditions.

Certain steps previously given[1] are either redundant or wrong, and one or two new steps must be added. We may write the following initial steps:

$$A+h\nu=A', \tag{1}$$

$$A'=D, \tag{2}$$

$$A'+A=A^*+A, \tag{3}$$

$$A'+A=A^{**}+A, \tag{4}$$

where D represents dissociation products (free radicals), and A* and A** are the short- and long-lived fluorescing states, respectively. A fifth step $A'+O_2=?$ might be included, but is not necessary to explain the facts since (3) and (4) must be fast reactions and the mole fraction of the oxygen was always low.

The necessity for reaction (2) must be discussed.

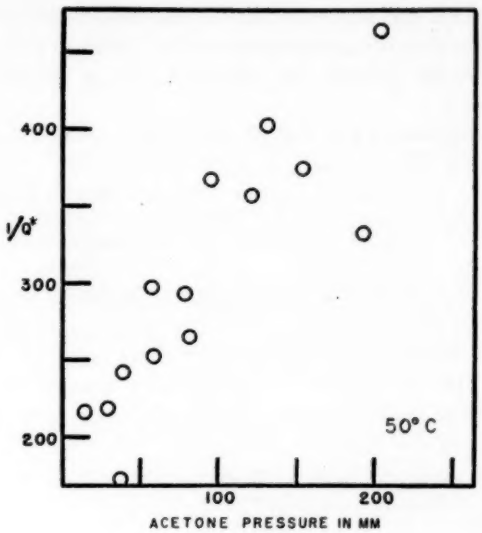

FIG. 3. Inverse of relative fluorescent efficiency for the oxygen-insensitive portion of acetone fluorescence.

Pitts and Blacet[4] find some primary dissociation of acetone in the presence of about 4 mm pressure of iodine. Iodine has a large effect in reducing the quantum yield of acetone decomposition and may be presumed, therefore, to deactivate the excited states of acetone. It would be advantageous to know whether or not there would be dissociation of acetone at even higher iodine pressures, but such data would be impossible to obtain at temperatures of importance in this work. Possibly acetone decomposition would be negligible at sufficiently high iodine pressures.[5] If this is true, (2) can be neglected, and in any case it is not essential to the explanation of the present data. If (2) is not included, dissociation must follow from either A* or A** or both and must be nearly but not quite 100 percent at temperatures over 150°.

The following steps must be included to account for the facts:

Reactions of A*:

$$A^*=A+h\nu^*, \tag{5}$$

$$A^*+A=2A, \tag{6}$$

$$A^*(+A)=D(+A). \tag{7}$$

(*Note:* Oxygen does not quench A*).

Reactions of A**:

$$A^{**}=A+h\nu^{**}, \tag{8}$$

$$A^{**}+A=2A \tag{9}$$

$$A^{**}+O_2=A+O_2. \tag{10}$$

[4] J. N. Pitts, Jr., and F. E. Blacet, J. Am. Chem. Soc. **74**, 455 (1952).

[5] Private communication from G. R. Martin and H. C. Sutton, University of Durhan. This work has been submitted for publication in the Transactions of the Faraday Society. These authors present data to show that acetone decomposition is still decreasing slowly with iodine pressure at the highest iodine pressure studied.

(*Note:* It is not necessary to include dissociation of A** since the amount of this state will be small in any case. Dissociation cannot be excluded as a possibility, however.)

Assumption of the steady state leads to the following expressions:

$$1/Q^* = I_a/I_f^* = [k_5+k_7+k_6(\mathrm{A})]/\alpha k_5, \quad (11)$$

$$1/Q^{**} = I_a/I_f^{**} = [k_8+k_9(\mathrm{A})+k_{10}(\mathrm{O_2})]/(1-\alpha)k_8, \quad (12)$$

and

$$1/Q = I_a/I_f = \frac{(k_3+k_4)[k_5+k_6(\mathrm{A})+k_7(\mathrm{A})][k_8+k_9(\mathrm{A})+k_{10}(\mathrm{O_2})]}{k_3k_5[k_8+k_9(\mathrm{A})+k_{10}(\mathrm{O_2})]+k_4k_8[k_5+k_6(\mathrm{A})+k_7(\mathrm{A})]}, \quad (13)$$

where $\alpha = k_3/(k_3+k_4)$ = fraction transferred to A*. Reaction (2) is assumed to be of minor importance (see above). These equations have the right forms to fit the facts. The evaluation of some of the constants may be made from the data, and rough estimates may be made of some of the others.

After flash excitation, in which the mean life of the source is as long as 8×10^{-6} sec,

$$1/\tau^* = k_5+k_7+k_6(\mathrm{A}), \quad (14)$$

$$1/\tau^{**} = k_8+k_9(\mathrm{A})+k_{10}(\mathrm{O_2}), \quad (15)$$

if one assumes that (7) is first order and not second. Data on this point are not very conclusive but tend to indicate that the primary quantum yield is pressure independent.[6] Equation (15) does not agree with the nonlinear plot of $1/\tau$ *vs* (A) as given by Kaskan and Duncan.[7] These authors show, however, that the inverse lifetime increases with increasing absorbed intensity. This effect has been verified in the present work. Consequently, a plot of inverse lifetime *versus* acetone pressure at constant incident intensity will represent the change in mean life due to acetone pressure plus the change due to increasing absorbed intensity as pressure increases. It is thought that this effect is large enough to account for the nonlinearity.

The plot of Eq. (15) [at constant (A)] permits k_{10} to be obtained from the slope (Fig. 1). One finds $k_{10} = 8.2\times10^{12}$ cc/mole sec. Since the slopes at various temperatures are identical, $E_{10} = 0$. The "collision efficiency" for deactivation of the long-lived state by oxygen is high.

At 50°,

$$1/Q^* = 1.8\times10^3+2.5\times10^8(\mathrm{A}), \quad (16)$$

where (A) is expressed in moles/cc. Ordinates in Figs. 2 and 3 must be multiplied by a factor of about 12[1] to obtain absolute inverse fluorescence efficiencies. These constants may be compared with 3×10^3 and 1.5×10^8 obtained at 300° in previous work.[1] Since the agreement is within experimental error, one finds $k_6/\alpha k_5 = k_6/k_5 = 2\times10^8$ cc/mole since $\alpha\cong1$; also $k_7/k_5 = 2\times10^3$. k_6/k_5 thus seems to be nearly independent of temperature, but k_7 has an activation energy roughly estimated at 5000 cal/mole.[8]

An estimate, based on absorption coefficients, of the lifetime of the excited state of acetone, has been made.[3] If it is proper to use this lifetime for A*, k_5 may be estimated to have a maximum value of 3.4×10^5 sec^{-1}, and hence $k_6 = 5\times10^{13}$ cc/mole sec and $k_7 = 6\times10^8$ sec^{-1} (both also maximum values). These figures are self-consistent but should not be considered to have absolute significance.

A very rough estimate can be made of the activation energy for (9) from the inverse lifetimes of A** at 50 and at 75°. Thus $E_9\cong10\,000$ cal/mole. The value of k_8 can be estimated as 5×10^3 sec^{-1} from the data of Kaskan and Duncan.[3]

The minimum mean life of A* at 100 mm pressure is about 10^{-9} sec. This is probably long enough to permit iodine to reduce the primary quantum yield appreciably[4] if the collision efficiency for this process is high. Finally, the primary quantum yield for dissociation may be estimated to be 0.7 at 50° and 0.99 at 300°.

Thus the techniques employed permit determination of ratios of rate constants for the two fluorescing states of acetone. The absolute values are based on an assumption which cannot be proved to be valid. Indeed, it is impossible as of the present moment to think of an experimental procedure which would permit the determination of the absolute constants without ambiguity.

[6] D. S. Herr and W. A. Noyes, Jr., J. Am. Chem. Soc. **62**, 2052 (1940). See, however, J. J. Howland, Jr., and W. A. Noyes, Jr., J. Am. Chem. Soc. **66**, 974 (1944), who show that the over-all quantum yield of acetone decomposition tends to decrease with increasing pressure. This might suggest some deactivation by collision.

[7] W. E. Kaskan and A. B. F. Duncan, J. Chem. Phys. **18**, 427 (1950).

[8] W. A. Noyes, Jr., and L. M. Dorfman, J. Chem. Phys. **16**, 788 (1948).

The Formation of Negative Ions of Sulfur Hexafluoride

A. J. AHEARN AND N. B. HANNAY
Bell Telephone Laboratories, Murray Hill, New Jersey
(Received July 28, 1952)

Negative ion production in SF_6 has been studied in a mass spectrometer; SF_6^-, SF_5^-, F_2^-, and F^- were identified. The SF_6^- and SF_5^- are produced in very large quantities by a resonance capture process at an electron energy of about 2 ev, and are formed in approximately equal amounts.

At higher electron energies, the same capture occurs by a secondary process, in which low energy electrons released by other excitation and ionization processes suffer the resonance capture.

Partial dissociation after electron capture accounts for the appearance of F^- and F_2^- ions below 16 ev. Above this energy, other processes will also produce these ions.

Possible explanations of the primary resonance capture mechanism are discussed.

1. INTRODUCTION

SULFUR hexafluoride is one of several compounds of polyatomic molecules that have a high dc breakdown voltage relative to nitrogen. With some of these polyatomic molecules, stable systems are possible in which an electron has been added to the molecule or to one of its dissociation products to form a negative ion. If the probability of negative ion formation for low speed electrons is high enough, an electron released by one or another mechanism would become attached to a heavy carrier before it attained sufficient energy in the field to initiate an avalanche and breakdown. These considerations have suggested that negative ion formation in SF_6 may be an important factor contributing to its high electrical breakdown strength.

No studies of the negative ions in SF_6 appear to have been made. The formation of positive ions of SF_6 under electron impact has been studied by Dibeler and Mohler.[1] They report appearance potentials and relative abundance of various dissociation products, and they suggest one mechanism whereby one dissociation product (a fluorine atom) may form a negative ion.

Some experiments of McAfee[2] indicated that negative ions in SF_6 were formed at low electron speeds and that the probability of negative ion formation increased rapidly with decreasing electron speed.

Since sulfur hexafluoride is of considerable importance as a dielectric, an understanding of negative ion formation and its bearing on the breakdown strength of this gas is desirable. Consequently, an investigation was made in which several negative ions differing in m/e were observed and studied. The measurements reported herein indicate that low speed electrons are readily captured by SF_6 molecules to form negative ions, including resonance captures occurring at approximately 2 electron volts with a relatively high capture cross section.

2. METHOD AND APPARATUS

The measurements were made with a Consolidated mass spectrometer[3] Model 21–103. This instrument, although designed for positive ion analysis, is readily adapted to the study and measurement of negative ions by reversing the magnetic field and the two electric fields which serve to accelerate the ions after they are formed. In most of the studies, -5 volt was applied to the pusher electrode in the ion chamber. A separate negative voltage power supply adequately filtered was used to accelerate the ions just prior to the magnetic deflection since the voltage supply of the commercial instrument could not be readily reversed.

In this instrument, the gas under analysis is admitted through a molecular flow leak. The pressure on the inlet side of this leak is determined from a simple U-tube mercury manometer measurement followed by an expansion with known volumes. SF_6 pressures from about 200 microns to a fraction of a micron were used on the high pressure side of the leak. The corresponding pressure in the ionization chamber ranged from 2×10^{-4} mm Hg to $<10^{-6}$ mm Hg.

Electron beam currents from 6 to 100 μa are available in the commercial instrument from 40 to 100 volts. A slight modification readily extended this range to nearly zero volts, although inhomogeneity in the energies of the electrons at low beam voltages is undoubtedly important.

The electron beam energy scale was calibrated by measurements of the O^- negative ion of oxygen, the appearance potential of which is well established.[4] Using this scale, the position of the O^- peak from carbon monoxide was in good agreement with Hagstrum's value.

3. RESULTS

3.1 Negative Ions Identified

The following four negative ions of SF_6 and its dissociation products were observed: SF_6^-, SF_5^-, F^-, and F_2^-.

An ion with an apparent m/e that was 16.4 mass units lighter than SF_5 was also observed. This corresponds to the metastable transition $(SF_6^-)^* \rightarrow SF_5^- + F$ occurring after the ion has passed through the accelerating

[1] V. H. Dibeler and F. L. Mohler, J. Research Natl. Bur. Standards **40**, 25 (1948).
[2] K. B. McAfee (to be published).
[3] Consolidated Engineering Company, Pasadena, California.
[4] H. D. Hagstrum, Revs. Modern Phys. **23**, 185 (1951).

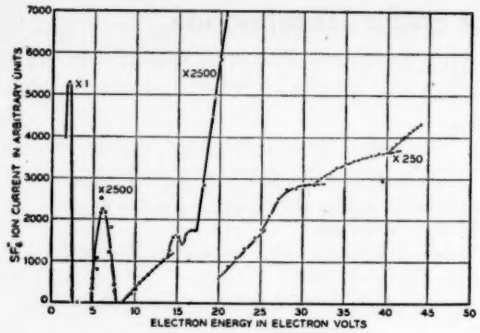

FIG. 1. SF_6^- ion current as a function of electron energy.

electric field but before it has suffered appreciable magnetic deflection.[5]

3.2 Variation of Ion Current with Electron Energy

The dependence of the SF_6^- negative ion yield on the electron beam energy from nearly zero to 45 volts is shown in Fig. 1. In Figs. 1–3 the measurements were either made at, or adjusted to, 20 μa electron beam current and 100μ pressure on the high pressure side of the molecular flow leak to the ion chamber. The ion current is expressed in arbitrary units,[6] and the electron beam energy scale has been calibrated in the manner already indicated.

The SF_6^- negative ion current rises rapidly to a large maximum value at about 2 ev and then plunges rapidly to zero. This large peak of current is followed at higher voltages by a much weaker SF_6^- current. Note the amplification factors needed to plot these currents on the ordinate scale. As shown in Fig. 1, when these data are plotted on an appropriate scale, considerable detail appears in the form of critical changes in slope of the curve. The significance of this detail and other features of the data will be discussed in a later section.

Figure 2 shows corresponding data for the SF_5^- negative ion current as a function of electron energy. A striking similarity between these data and those for

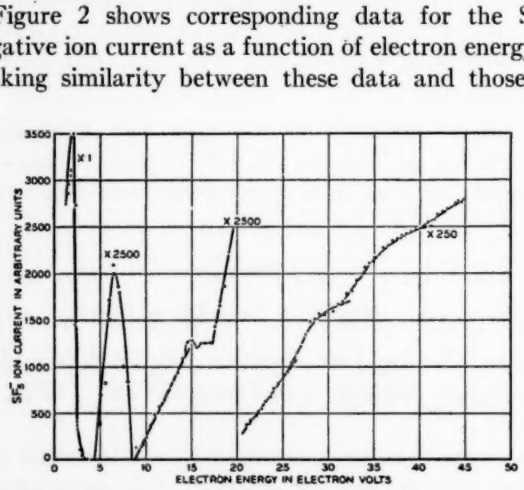

FIG. 2. SF_5^- ion current as a function of electron energy.

[5] J. A. Hipple and E. U. Condon, Phys. Rev. 68, 54 (1945).
[6] Microamperes in the output of the dc amplifier measuring collector current.

SF_6^- in Fig. 1 is immediately apparent. The SF_5^- current rises to a large maximum value at about 2 ev, falls rapidly to zero, and at higher voltages the small ion current indicated appears. Just as in Fig. 1, detail in the form of critical changes in slope are revealed when the data are presented in detail.

Figure 3 contains data for the variation of the F^- negative ion current with electron energy. At the lowest voltage indicated (2 ev) this current appears to be rising rapidly with decreasing voltage. The current falls to a minimum value at 4 ev and is followed by a series of three well-defined current onsets leading to maxima, and two further critical slope changes. At no point does the ion current fall to zero, as contrasted with the SF_6^- and SF_5^- curves.

No data on the variation of the F_2^- negative ion current with electron energy are presented, because the currents obtained were too small to measure very accurately. The current varies only gradually with voltage and in that general sense the F_2^- ion current resembles the F^- ion current. Two maxima were located, as shown in Fig. 5, although the voltage scale was not as well established as for the other data presented.

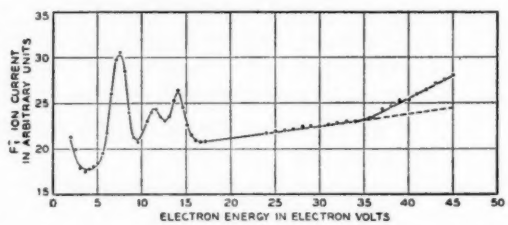

FIG. 3. F^- ion current as a function of electron energy. Note that ordinates do not start at zero.

3.3 Variation of Negative Ion Currents with Pressure

Figure 4 displays the relative abundance of the various negative ions of SF_6 as well as their dependence on the pressure. These data may be summarized as follows:

(1) The peak ion currents for SF_6^- and SF_5^- at 2 ev vary linearly with the pressure, but the much feebler currents at, for example, 15 ev and 35 ev are proportional to the square of the pressure.

(2) At 2 ev the SF_5^- and the SF_6^- negative ions are formed with approximately equal abundance.

(3) The F^- negative ion current at 35 ev varies linearly with the pressure. A rough measurement indicated that this linearity also applies at the first maximum in the F^- curve of Fig. 3. Presumably, the F^- ion current throughout the voltage range of Fig. 3 is linearly proportional to the pressure.

(4) The data on the F_2^- negative ion are too scanty to determine the pressure dependence.

(5) The SF_5^- and SF_6^- ion currents at 2 ev are 100 times greater than the F^- ion current at 35 ev. Similarly,

the F^- current is about 100 times greater than the F_2^- ion current, at 35 ev.

Some of the experimental results are summarized in Fig. 5. Here the positions of the critical changes in ion current for the various observed negative ions of SF_6 are indicated on the electron beam energy scale. These values are of course taken from Figs. 1–3.

In addition, the appearance potentials for the various positive ions of SF_6, as reported by Dibeler and Mohler, are also indicated, the width of the shaded area giving the assigned probable error. The numbers just above the shaded areas give the relative abundance of the various ions at 50 ev. The electron affinity (E.A.$=3.6$ ev) of fluorine,[7] the ionization potential [I.P. $(F^+)=18.6$ ev] of fluorine, the energy of dissociation [D $(SF_6)=22.4$ ev] for the process $SF_6 \rightarrow S+6F$, and the energy of dissociation of molecular fluorine,[8] [D $(F_2)=1.7$ ev] are the energy data of interest which are known.

4. DISCUSSION AND INTERPRETATION OF RESULTS

The various processes that can occur when an electron impinges upon a molecule XY are shown in Table I.

TABLE I.

(*A*) Resonance capture	$e+XY \rightarrow (XY^-)^* \rightarrow X+Y^-$
(*B*) Excitation and dissociation	$e+XY \rightarrow (XY)^* + e \rightarrow X+Y+e$
(*C*) Formation of a positive ion	$e+XY \rightarrow (XY^+)^* + 2e \rightarrow X^+ + Y + 2e$
(*D*) Formation of a positive and a negative ion	$e+XY \rightarrow (XY)^* + e \rightarrow X^+ + Y^- + e$

In the following discussion, asterisks are used to denote excited states, which may or may not be the same state for different processes under discussion.

In the resonance capture process (*A*), the attachment can occur only when the electron energy is essentially equal to the energy difference between the ground state and the excited state $(XY^-)^*$. In the case of the remaining three processes, however, the electron energy may exceed that just necessary for the onset of the process, as there are free electrons to carry off the excess energy.

For a polyatomic molecule such as SF_6, X and Y may be atoms or radicals. Furthermore, three or more fragments may result from the dissociation in this case. The dissociations shown in the table need not occur, of course, and the end product will then be the intermediate shown in the table.

4.1 Primary Capture Processes in SF_6

The very large, narrow peaks at 2 ev for SF_6^- and SF_5^- ions represent resonance capture processes of type

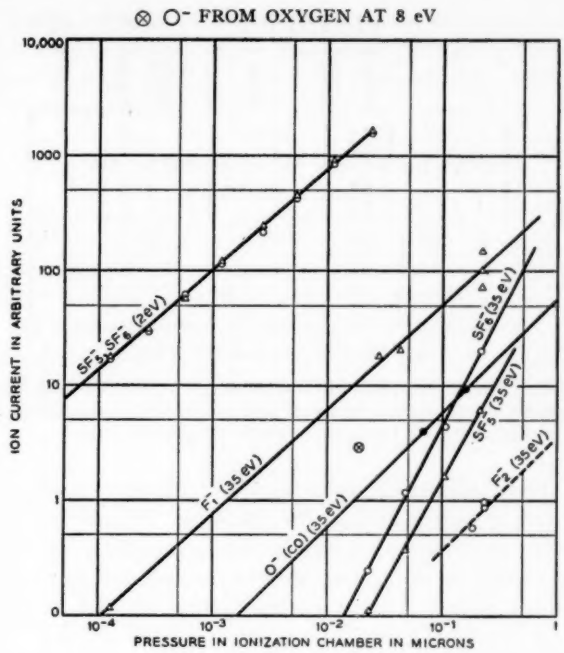

FIG. 4. Pressure dependence and relative magnitudes of negative ion currents in SF_6.

(*A*). They may be represented by

$$e+SF_6 \rightarrow (SF_6^-)^* \begin{cases} \rightarrow SF_6^- & (1) \\ \rightarrow SF_5^- + F. & (2) \end{cases}$$

It appears that some of the excited ions $(SF_6^-)^*$ dissociate as indicated by reaction (2), whereas others do not [reaction (1)]. The approximate equality of the peak sizes indicates that (1) and (2) are about equally likely. The very large magnitude of these peaks, as compared with typical negative ion peaks such as O^- from CO, can be seen from Fig. 4.

One might expect to find similar processes leading to a more extensive dissociation, producing ions SF_4^-, SF_3^-, etc., as, for example,

$$e+SF_6 \rightarrow (SF_6^-)^* \rightarrow SF_4^- + 2F, \text{ etc.} \quad (3)$$

That no such reactions do in fact occur is indicated by the nonappearance of the ions SF_4^-, SF_3^-, etc.

The dissociation may also produce a negative fluorine ion, by processes such as

$$e+SF_6 \rightarrow (SF_6^-)^* \rightarrow SF_5 + F^-, \quad (4)$$

$$e+SF_6 \rightarrow (SF_6^-)^* \rightarrow SF_4 + F + F^-, \text{ etc.} \quad (5)$$

The dissociation energy (22.4 ev) for $SF_6 \rightarrow S+6F$ indicates that on the average about 4 ev are required to strip off successive fluorine atoms. To a rough approximation, the excited states in (4), (5), etc., might then represent energy transitions successively increasing by this 4-ev increment. The situation will be complicated

[7] R. B. Bernstein and M. Metlay, J. Chem. Phys. **19**, 1612 (1951).
[8] R. N. Doescher, J. Chem. Phys. **19**, 1070 (1951).

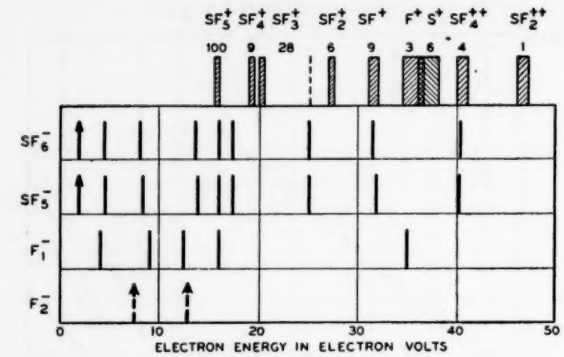

FIG. 5. Onset potentials for ions produced in SF_6. Vertical lines represent onsets, arrows represent maxima. Width of shaded areas for positive ion data represents assigned probable errors.[1]

by the possibility of processes producing an F_2 molecule as well as two F atoms. Processes (4), (5), etc., would predict recurrent increases in the F^- negative ion current as the electron energy passed through the resonance capture energy values corresponding to the excited states in (4), (5), etc. The experimental data for F^- in Fig. 3 show three well-defined onsets below 15 ev, the spacing of which is not inconsistent with the expectation that the energy difference for the removal of successive fluorine atoms is approximately 4 ev. Thus, the low voltage details of the F^- ion current can be accounted for in terms of a resonance capture by the parent molecule followed by dissociation in which one of the fluorine atoms is expelled as a negative ion. On this basis the F^- ion current should be linearly proportional to the gas pressure. The data of Fig. 4 show that at 35 ev the F^- ion current varies linearly with the pressure, and data not included on the graph indicate that this dependence persists at lower voltages.

In a similar manner, dissociation may lead to the appearance of F_2^- ions:

$$e+SF_6 \rightarrow (SF_6^-)^* \rightarrow SF_4+F_2^-, \quad (6)$$

$$e+SF_6 \rightarrow (SF_6^-)^* \rightarrow SF_3+F+F_2^-, \text{ etc.} \quad (7)$$

Considerations like those discussed for F^- would suggest similar onsets in the F_2^- negative ion current. As shown in Fig. 5, two maxima were observed in the F_2^- ion current, one falling at about 7.7 ev and the other at 12.7 ev. In this picture, the F_2^- ion current should vary linearly with the pressure. Unfortunately, the data of Fig. 4 are too scanty to reveal the pressure dependence.

4.2 Secondary Capture Processes

Processes (*B*), (*C*), and (*D*) of Table I, all yield free electrons as an end product, and the energy of these is determined by the excess energy of the impinging electron. For SF_6, there are a large number of possible processes corresponding to each of the three types:

Type *B*: $e+SF_6 \rightarrow (SF_6)^*+e \rightarrow SF_5+F+e$, etc. (8)

Type *C*: $e+SF_6 \rightarrow (SF_6^+)^*+2e \rightarrow SF_5^++F+2e$, etc. (9)

Type *D*: $e+SF_6 \rightarrow (SF_6)^*+e \rightarrow SF_5^++F^-+e$, etc. (10)

Among the electrons released in these processes, those of the critical speed (up to 2.5 ev) may experience resonance capture to form SF_6^- as in reactions (1). This would predict that SF_6^- negative ions would reappear a bit beyond the initial, large resonance capture peak and that, with increasing electron energy, there would be recurrent critical changes of slope in the ion current *vs* electron energy curve as fresh supplies of low voltage electrons were made available for resonance capture. A similar behavior for SF_5^- is expected. The data for SF_6^- and SF_5^- in Figs. 1, 2, and 5 show considerable detail which is not inconsistent with this thesis. To illustrate this secondary process, which is a phenomenon that has not been reported in the literature, the onset at 17.3 ev will be first discussed. The large increase at 17.3 ev can be explained in terms of a resonance capture of a low voltage electron released by a process of type (9) or (10), which produces a SF_5^+ ion. In the positive ion spectrum of SF_6, the SF_5^+ ion is the most abundant, and has the lowest appearance potential: 15.9 ev.[1] Measurements were made of the shape of the SF_5^+ ion current near the onset, and it was found that the tail of the curve extended from 15.9 to about 17.5 or 18 ev, and that the large increase in current began at the latter energy. An electron of 17.3 ev energy can produce the ion SF_5^+ and release an electron with as much as 1.4 ev energy. This electron is in the proper energy range to undergo capture by an SF_6 molecule. The electron energy at the onset of the secondary capture process (e.g., 17.3 ev) exceeds that corresponding to the onset of the ionization process producing the low speed electron (e.g., 15.9 ev). The amount of the excess energy is not subject to exact interpretation and will vary from one process to another. Factors that contribute to this uncertainty are the variation in probability for the excitation and ionization processes producing the low voltage electrons, the considerable uncertainty in the shape of the onset region of the primary low voltage capture peak, the distribution in energy of the released electrons, and the relatively small size of the secondary capture currents.

The other increases in the SF_6^- and SF_5^- ion currents can be accounted for in the same general way. The SF_6^- and SF_5^- ion currents in the region between 2 and 16 volts can be accounted for in terms of a dissociation of the parent molecule into neutral fragments, [Process (8)], with the release of a low speed electron which in turn experiences resonance capture to form the SF_6^- and SF_5^- negative ions that are observed. Above 15.9 ev, processes of types (9) and (10) will enter. Each successive appearance potential would initiate the introduction of a fresh supply of low speed electrons, which in turn could suffer resonance capture by an SF_6 molecule. In this picture, critical changes in the SF_6^- and SF_5^- ion current above 15.9 ev should correspond to appearance potentials for positive ions, all of which are produced by processes of the types represented by (9) and (10). The data of Fig. 5 show four critical increases

in negative ion current in the region where positive ions appear, the first of which has already been discussed. The large number of appearance potentials for positive ions together with the probable errors and uncertainties like those revealed in Fig. 6 preclude a complete correlation with the negative ion increases. Nevertheless, there are ample processes whereby low speed electrons are introduced to account for the remaining critical increases in SF_6^- and SF_5^- negative ions shown in Fig. 5. At first glance, it appears that the second most abundant positive ion SF_3^+ which appears at 20.1 ev has no corresponding increase in SF_6^- and SF_5^- ion current. However, a measurement of the shape of the appearance potential curve for SF_3^+ ions, revealed that there are two processes producing SF_3^+ ions, one setting in at 20.1 ev as reported by Dibeler and Mohler, and the second at about 25 ev. These processes may be identified with reactions of type (10) and (9), respectively. Since the type (9) process produces ions in much greater abundance, it is this appearance potential which may properly be correlated with the next break in the SF_6^- and SF_5^- curves, in view of the much larger number of secondary electrons being released beginning with 25 ev primary electron energy.

The number of low speed electrons available for these secondary resonance captures is linearly proportional to the gas pressure. Since the probability of capture depends on the product of the electron density and the gas density, the ion current beyond 2 ev should vary linearly with the square of the gas pressure. The data of Fig. 4 show substantially this dependence for both SF_6^- and SF_5^-. The low voltage peak in both cases varies linearly with pressure, as expected.

4.3 Processes Producing a Negative and a Positive Ion

The critical slope increases at about 15.7 and 34.3 ev in the F^- ion current remain to be explained. The proximity of the former to the appearance potential (15.9 ev) for SF_5^+ ions suggests that processes (10), etc., set in at 15.9 ev. The F^- negative ion current expected from these reactions would vary linearly with the pressure, in agreement with the experimental indications.

The critical slope increase at 34.3 ev in the F^- ion current is in fairly good agreement with the appearance potential for F^+. Dibeler and Mohler[1] suggest that since F^+ appears at a higher voltage than any of the polyatomic singly charged ions it only results from complete dissociation of SF_6. The reaction

$$e+SF_6 \rightarrow (SF_6^+)^* \rightarrow S+5F+F^+ \qquad (11)$$

requires $22.4+18.6=41$ ev, whereas the reaction

$$e+SF_6 \rightarrow (SF_6)^* \rightarrow S+4F+F^-+F^+ \qquad (12)$$

only requires $22.4+18.6-3.6=37.4$ ev.

Since reaction (12) is in reasonable agreement with the value of 35.8 ev for the onset of F^+, Dibeler and Mohler infer that the onset of F^+ would be accompanied by the production of F^- ions. That this is in fact the case is suggested by the critical slope change in the F^- ion current in Fig. 3 at 34.3 ev.

4.4 Mechanism of the Low Voltage Capture Process

The data of Fig. 4 shows that at 2 ev the SF_6^- and the SF_5^- ion currents are substantially equal. This suggests that reactions (1) and (2) are equally probable.

For the diatomic molecule the potential energy diagram is a simple two-dimensional case in which the potential energy *vs* internuclear separation is plotted. SF_6 would require a 15-dimensional surface to represent the potential energy as a function of the configurational coordinate representing internuclear distances. However, to consider the removal of only one fluorine atom from the SF_6 molecule this complex diagram reduces to the simple two-dimensional diagram of the diatomic molecule consisting of an SF_5 radical and a fluorine atom. This is sketched in Fig. 6a. Here the potential energy is plotted *vs* the configurational coordinate representing the separation of the above fluorine atom from the SF_5. The dashed vertical lines bound the Franck-Condon region. The asymptote to the curve is indicated by the dashed horizontal line, and its height

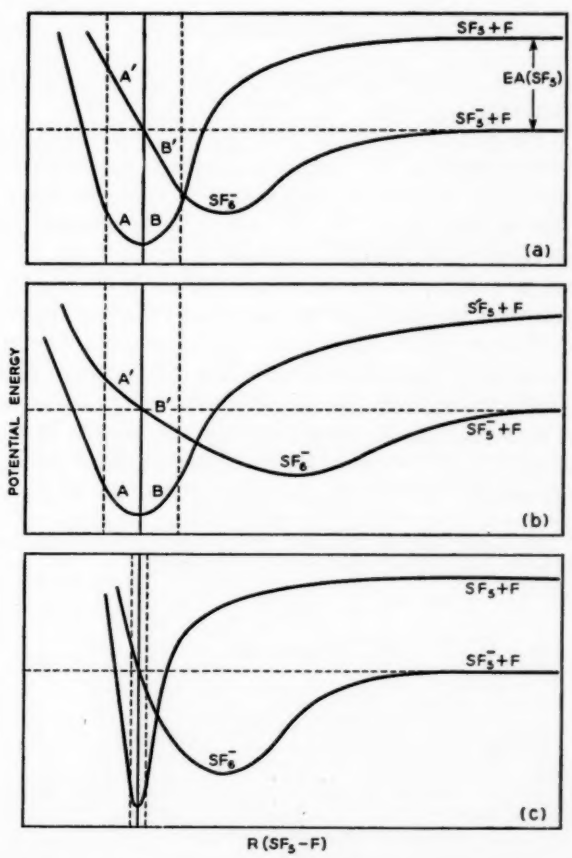

FIG. 6. Possible potential energy diagrams for capture process (see text).

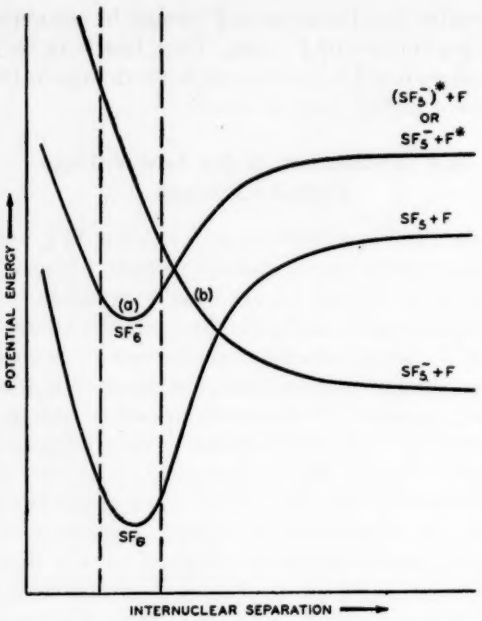

FIG. 7. Alternative potential energy diagram for capture process (see text).

above the minimum of the curve designates the minimum[9] energy required to achieve the dissociation indicated. The second curve represents reaction (2),

$$e+SF_6 \rightarrow (SF_6^-)^* \rightarrow SF_5^-+F, \qquad (2)$$

where the indicated separation of the asymptotes of the curves equals the electron affinity (E.A.) of SF_5.

If the resonance capture of a 2-ev electron results in a transition from A to A' reaction (2) would occur yielding an SF_5^- ion. If the transition is from B to B', the energy of the excited state $(SF_6^-)^*$ would be insufficient for dissociation and the SF_6^- ion would be observed. Now since transitions to A' and B' are equally probable, this furnishes a plausible interpretation of the experimental fact that the SF_6^- and the SF_5^- ion currents at 2 ev are substantially equal, by virtue of the *ad hoc* assumption that the asymptote cuts the potential energy curve for the excited state in approximately the middle of the Franck-Condon region. However, the potential energy diagram sketched in Fig. 6a predicts that the SF_5^- ion would appear at larger electron energies than the SF_6^- ion. This disagrees with the experimental data of Figs. 1 and 2 which show that the low voltage maximum for each of the two ions appears at 2 ev.

Alternative diagrams that avoid this difficulty are sketched in Figs. 6b and 6c. In sketch (B) the excited level is relatively flat in the Franck-Condon region. Consequently, the energy difference $B'-B$ is nearly equal to $A'-A$. In sketch (C) a narrow steep potential valley is assumed. Here the region B' is only slightly lower in energy than A' since the Franck-Condon region is quite narrow.

Another method of explaining the features of the SF_6^- and SF_5^- capture processes is by the predissociation process illustrated in Fig. 7. A transition to curve (a) might occur, with the possibility that the SF_6^- ion thus produced might undergo dissociation by thermal excitation over the potential hump to curve (b). The experimental observation noted earlier that SF_6^- ions do go over to SF_5^- after a lapse of time (e.g., after acceleration by the electric field), thus indicating a metastable state, is consistent with this suggested picture.

There are, in addition, other possibilities that may explain the mechanism of the low voltage resonance capture process, but it does not appear possible at the present time to choose between the suggested processes.

From the data of Fig. 4 some interesting comparisons can be made. In the resonance capture, to form SF_5^- and SF_6^-, the ion current is 1000 times greater than that of O^- ions formed in carbon monoxide at 35 ev, and it is about 400 times greater than that of O^- ions formed in oxygen at 8 ev. The measurements of Lozier[10] (giving relative intensities of O^- and CO^+ in CO) indicate that in this resonance capture the SF_6^- and SF_5^- ion currents each are about equal to that of the CO^+ ion in CO at 35 ev. These data of Lozier,[11] together with quantitative data by Tate and Smith,[11] indicate that for this resonance capture of an electron the SF_6 molecule capture cross section is about 10^{-16} cm^2.

The authors would like to express their appreciation to E. E. Francois for aid in adapting the instrument for the experiments, to H. D. Hagstrum for several valuable discussions, and to H. D. Hagstrum, G. H. Wannier, and E. J. Murphy for a critical reading of the manuscript.

[9] This tacitly assumes that the dissociation can be achieved in which the end products have zero kinetic energy.

[10] W. W. Lozier, Phys. Rev. **46**, 268 (1934).

[11] J. T. Tate and P. T. Smith, Phys. Rev. **39**, 270 (1932).

Electron Traps in the Thallium-Activated Potassium Chloride Phosphor

PETER D. JOHNSON AND FERD E. WILLIAMS
General Electric Research Laboratory, Schenectady, New York
(Received July 14, 1952)

The effects of activator concentration, added impurities, infrared stimulation, and temperature of excitation on the thermoluminescence of KCl:Tl permit the identification of the two principal trapping levels as the $^3P_0^0$ and $^3P_2^0$ states of isolated Tl^+. The energy of activation necessary to fill these metastable states, following excitation to the $^3P_1^0$ and $^1P_1^0$ states, is provided by the polarization energy. The concentration of traps simultaneously filled is limited primarily by re-excitation of metastable Tl^+. *F* and *V* centers are created by multiple excitation of Tl^+. These interpretations are quantitatively correlated by a configuration coordinate model and are shown to be in accord with the band theory.

INTRODUCTION

THERMOLUMINESCENCE or "glow" measurements have been of considerable use in elucidating the mechanism of phosphorescent decay.[1-3] Much emphasis has been placed on the kinetics governing untrapping. However, except for color centers,[4] the precise identifications of traps have been uncertain.

In the present work, thermoluminescence in conjunction with related experiments is used to identify the electronic states as well as the sites responsible for trapping. Thallium-activated potassium chloride was selected because its luminescent properties are understood fundamentally better than any other phosphor.[5-8] The identification of the principal traps should substantially complete the detailed delineation of the mechanism of luminescence of KCl:Tl.

With proper conditions of excitation, KCl:Tl exhibits at least eight individual glow peaks which can be separated using slow heating rates. Attention will be confined mainly to two peaks which are generally much more intense than the others.

APPARATUS AND PHOSPHOR PREPARATION

The thermoluminescence apparatus is shown in Fig. 1. A fused quartz disk and retaining ring hold the phosphor in place. The coolant and heating unit are placed in the well at the top of the copper block. Measurements show that the thermocouple is within one C° of the temperature of the surface of the phosphor. Ultraviolet excitation and the emission pass through a 1.5-mm thick fused quartz window. The sample chamber is evacuated to one micron pressure with a mechanical pump and liquid nitrogen trap. Three shutters are provided in the outer housing: one for excitation, another between the sample and the 5819 photomultiplier sensitized with Cenco pump oil, and a third for stimulation with visible or infrared radiation. Slots for color filters are provided for selection of excitation, emission, or stimulation wavelength. The output of the photomultiplier is amplified[9] and goes to a G-E photoelectric recorder. The temperature is controlled to within one C° by a Brown Air-O-Line controller which pneumatically adjusts the variac which supplies the current to the heating coil. A cam, shaped to give the desired heating schedule and driven by a synchronous motor, actuates the control mechanism. Temperature checks during the glow period are made with a separate potentiometer.

The source of ultraviolet excitation was either the 4-watt G-E germicidal lamp giving predominately 2537A or a low voltage hydrogen discharge lamp[10] giving a continuous spectrum from 1800 to 3600A. Most of the thermoluminescent measurements here reported were made at a linear heating rate of 0.083 C°/sec. No significant differences were obtained at 0.033 C°/sec. The apparatus is capable of a controlled heating schedule from 20 to 750°K; however, in KCl:Tl

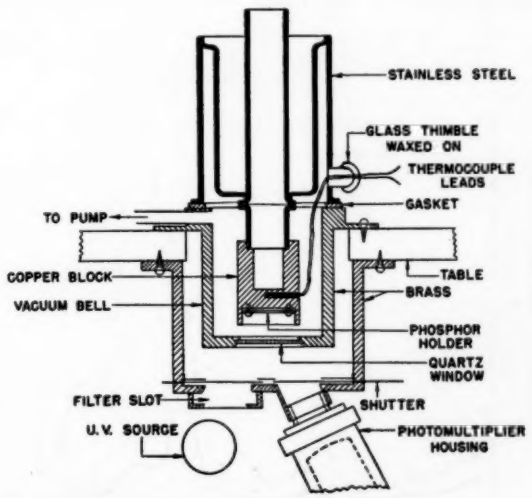

FIG. 1. Thermoluminescence apparatus.

[1] J. T. Randall and M. A. F. Wilkins, Proc. Roy. Soc. (London) A184, 366 (1945).
[2] F. E. Williams and H. Eyring, J. Chem. Phys. **15**, 289 (1947).
[3] M. E. Wise, Physica **17**, 1011 (1951).
[4] F. Seitz, Revs. Modern Phys. **18**, 384 (1946).
[5] F. Seitz, J. Chem. Phys. **6**, 150 (1938).
[6] F. E. Williams, J. Chem. Phys. **19**, 457 (1951); Phys. Rev. **82**, 281 (1951).
[7] F. E. Williams and M. H. Hebb, Phys. Rev. **84**, 1181 (1951).
[8] P. D. Johnson and F. E. Williams, J. Chem. Phys. **18**, 1477 (1950); **20**, 124 (1952).
[9] S. Roberts, Rev. Sci. Instr. **10**, 181 (1939).
[10] P. D. Johnson, J. Opt. Soc. Am. **42**, 278 (1952).

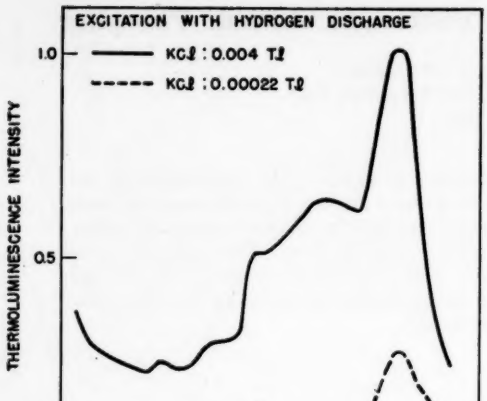

FIG. 2. Effect of activator concentration on thermoluminescence.

all important reproducible glow peaks occur between 80 and 400°K; consequently, most of the measurements were confined to this temperature range. The glow peak heights are reproducible to 3 percent.

Stimulation measurements were made by noting the initial deflection of the recorder when the stimulating radiation is turned on, following a standard excitation and decay procedure. To eliminate the inertia of the recorder, the bursts of stimulated emission were checked by connecting the photomultiplier output to an oscilloscope with a long persistence P-7 screen. A 150-watt tungsten projection lamp operated at $\frac{2}{3}$ of rated voltage, in conjunction with Corning filters 2600, 2408, 5970, and 2540 for the infrared and interference filters for the visible, provided the radiation for stimulation.

Measurements on single crystals of KCl:Tl gave essentially the same glow curves as measurements on samples prepared by rapid fusion and cooling in a platinum crucible. Because a fresh, completely unexcited sample was used for each experiment and since approximately 100 thermoluminescent experiments were required to establish the results reported here, fused and powdered samples were used primarily. The concentrations of impurities reported are those added since it was established that the rapid preparative procedure resulted in negligible loss of volatile constituents. Tl^+, Cd^{++}, Ca^{++}, Sr^{++}, and Ba^{++} were added as chlorides, and $O^=$ was introduced as KNO_3 which decomposes to oxide under the conditions of preparation. The amounts of impurity added were generally close to or below their solubility limit in KCl.

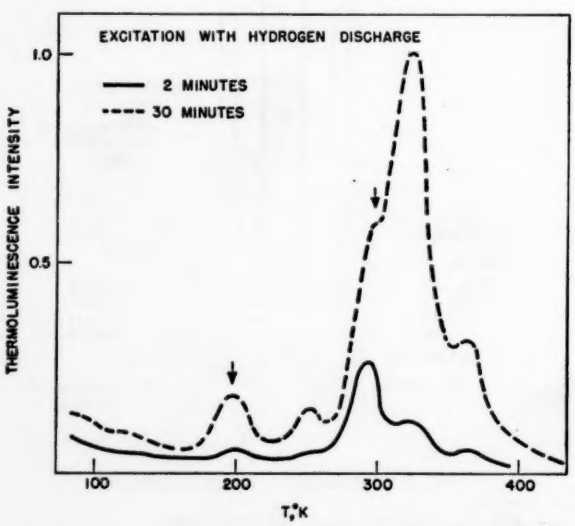

FIG. 3. Thermoluminescence of KCl: 0.00027Tl single crystals.

RESULTS AND DISCUSSION

Representative thermoluminescent curves are shown in Figs. 2–6. In addition to the two principal thermoluminescent peaks at 205 and 300°K, there are peaks, after excitation with the germicidal lamp, at 110, 140, 170, 188, 325, and 375°K. These traps have concentrations of 10^{10} to 10^{11}/cm³ as estimated from the photomultiplier sensitivity and geometry of the apparatus. These peaks are observable because of the inefficiency of filling the 205 and 300°K traps with 2537A excitation. With excitation by the hydrogen discharge lamp, the 205 and 300°K peaks increase in intensity by a factor of 10^3 indicating an occupied trap concentration of the order of 10^{14}/cm³, and the other peaks are almost completely obscured. The 110°K peak is prominent only in freshly prepared samples. A broad glow peak at 250°K shown in Fig. 2 is most pronounced with high Tl^+ concentration. Its intensity follows the activator concentration dependence of luminescent emission from interacting activator ions[8] shown in Fig. 7. This trap probably dominates the room temperature phosphorescence of KCl:Tl in accord with the conclusions of Seitz,[5] which follow from the concentration dependence of afterglow intensity. The 325°K peak develops with long time excitation. The thermoluminescent peaks of single crystals, shown in Fig. 3, are about 3 C° narrower than the powdered samples.

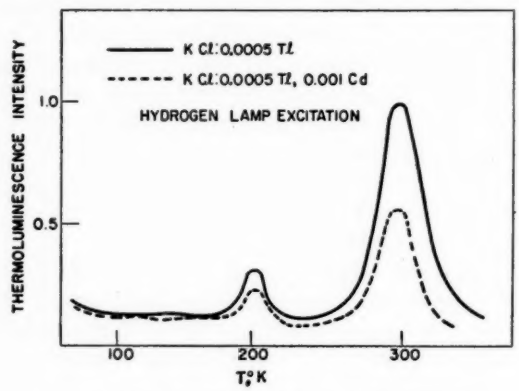

FIG. 4. Effect of Cd^{++} on thermoluminescence.

The heights of both the 205 and 300°K thermoluminescence peaks have the same dependence on gross activator concentration as the efficiency of luminescent emission characteristic of isolated activator ions.[8] Isolated activator ions are understood to be sufficiently removed from other activator ions so that no interaction affecting luminescent properties occurs. In Fig. 7 the correlation of the height of the 300°K peak and of luminescent efficiency *versus* Tl^+ concentration is shown.

The addition of Ca^{++}, Sr^{++}, and Ba^{++} to KCl:Tl in concentrations as great as 0.1 mole percent to introduce cation vacancies or of oxide for anion vacancies fails to affect the glow curve, indicating that none of the traps being studied are lattice vacancies. If, however, Cd^{++} is introduced, the two principal thermoluminescent peaks are suppressed as shown in Fig. 4. It has been previously reported[8] that the addition of Cd^{++} to KCl:Tl

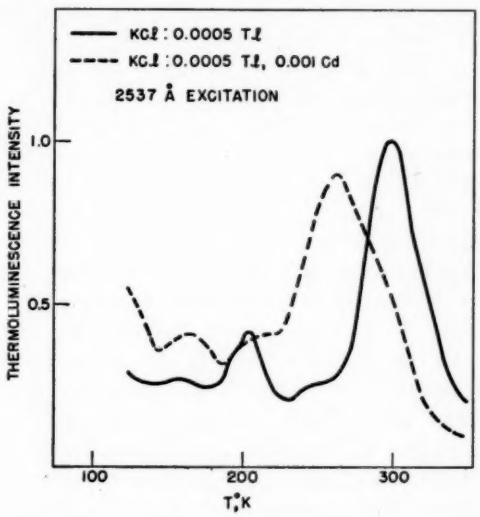

FIG. 5. Effect of Cd^{++} on thermoluminescence.

yields additional luminescent emission bands which were attributed to the $^3P_2{}^0 \rightarrow {}^1S$ and $^3P_0{}^0 \rightarrow {}^1S$ transitions of Tl^+. The presence of a nearby Cd^{++} or Tl^+, which have a strong tendency for homopolar binding, breaks down the optical selection rules for these transitions. The 205 and 300°K traps, therefore, behave as the metastable $^3P_2{}^0$ and $^3P_0{}^0$ states of isolated Tl^+, and become emitting states on interacting with nearby Cd^{++} or Tl^+. Concurrent with the decrease in concentrations of the principal traps by the addition of Cd^{++}, the 250°K thermoluminescent peak is enhanced and shifted to 270°, as shown in Fig. 5. This is in accord with the identification of this trap with a metastable state of Tl^+ interacting with a nearby homopolar cation, either Tl^+ or Cd^{++}.

The use of filters permits the measurement of thermoluminescence of the individual emission bands of KCl:Tl. There is no significant difference in glow curves obtained by observing the 3050 and 4750A emission

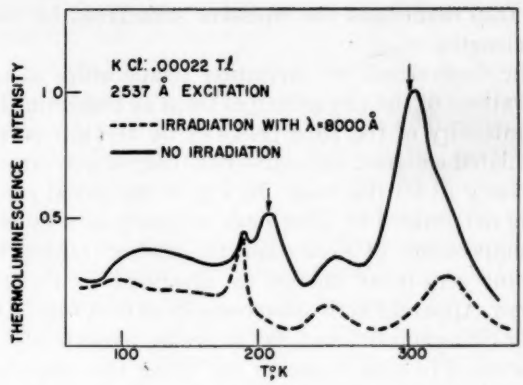

FIG. 6. Effect of infrared stimulation on thermoluminescence.

separately, except for a slightly higher intensity at higher temperature when observing the shorter wavelength emission. The previously reported[8] thermal equilibrium between the $^3P_1{}^0$ and $^1P_1{}^0$ emitting states of the isolated Tl^+ adequately explains the difference.

Irradiation with infrared should excite metastable Tl^+. As shown in Fig. 6 stimulation by 7500–8500A radiation, subsequent to ultraviolet excitation but prior to warming, selectively, empties the 205 and 300°K thermoluminescent peaks. It will be shown quantitatively in the next section that the 1.5-ev stimulating radiation has insufficient energy for excitation to the conduction band of KCl, and therefore, the two principal traps are localized states of Tl^+. The spectrum for the stimulation of phosphorescence of KCl:Tl reported by Bunger and Flechsig[11] is in accord with this conclusion. The dependence of emission intensity stimulated by red or infrared radiation on temperature of excitation is the same as that of the intensity of the 300°K glow peak. This shows that optical emptying of

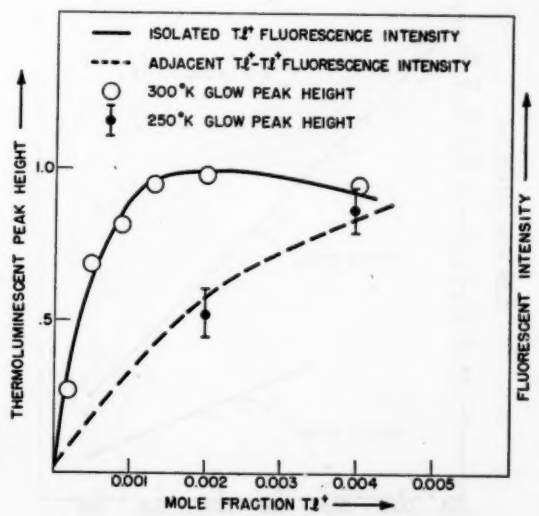

FIG. 7. Correlation of trap concentration with fluorescent efficiency.

[11] W. Bunger and W. Flechsig, Z. Physik 69, 637 (1932).

this trap dominates the emission stimulated by these wavelengths.

The dependence on excitation temperature of concentrations of the two principal traps as determined by the intensity of the glow peaks or by the intensity of stimulated emission indicates that thermal activation is necessary to fill the traps. In Fig. 8 the initial rate of filling determined by glow peak intensity as a function of temperature of excitation are plotted taking into account zero-point energy as described in the next section. Apparent activation energies of 0.019 and 0.047 ev for filling the 205 and 300°K peaks, respectively, are deduced. The time constant for filling the traps with the hydrogen source is of the order of minutes but is days for the 2537A source. The limiting concentration under optimum conditions is approximately 10^{15} cm^{-3}.

From the thermoluminescent curves, trap depths of 0.35 and 0.72 ev are calculated for the 205 and 300°K peaks, respectively, assuming first-order kinetics with no retrapping. The frequency factors for untrapping are found to be approximately 10^8 sec^{-1}, the same order of magnitude as the frequency factors for transfer between the emitting $^3P_1{}^0$ and $^1P_1{}^0$ states.

THEORY

The dependence of number of traps filled on Tl^+ concentration, the specific effect of Cd^{++}, and selective emptying by infrared radiation indicate that the two principal traps are metastable states of isolated Tl^+. Energy and selection rule considerations strongly suggest the $^3P_0{}^0$ and $^3P_2{}^0$ states. The energies of these states with respect to the conduction band of KCl should reveal the degree of binding and will directly give the ionization energies of $^3P_0{}^0$ and $^3P_2{}^0$ Tl^+ in KCl. The energy of the ground state $^1S_0$ of Tl^+ in the band

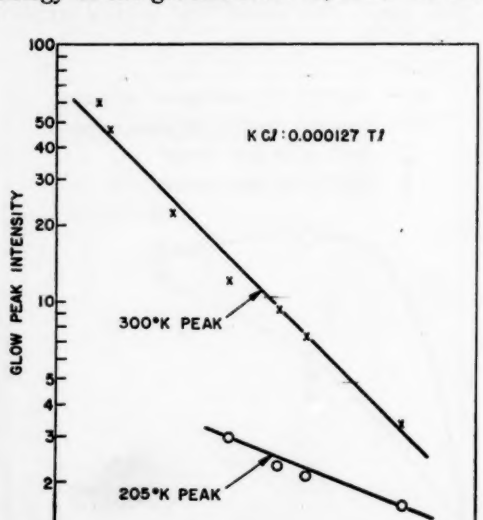

FIG. 8. Dependence of filled trap concentration on excitation temperature.

structure of KCl can be computed by considering the following cycle:

$$\begin{array}{ccc} Tl^+(g)+KCl(s) & \xrightarrow{I_2} & Tl^{++}(g)+KCl(s)+e \\ \downarrow \Delta E & & \downarrow \Delta E'-F \\ KCl:Tl^+(s)+K^+(g) & \xrightarrow{I_2^*} & KCl:Tl^{++}(s)+K^+(g)+e(s), \end{array}$$

where I_2 is the second ionization energy of Tl and equals +20.3 ev;[12] F is the electron affinity of KCl in the lowest conduction state and equals +0.07 ev;[13] ΔE and $\Delta E'$ are the changes in lattice energy arising from substituting Tl^+ and Tl^{++}, respectively, for K^+ in KCl, and $I_2{}^*$ is the ionization energy of Tl^+ in KCl and is, therefore, the energy from the $^1S_0$ Tl^+ state to the conduction band. ΔE is the +0.16 ev.[6] The repulsion and van der Waals energy components of $\Delta E'$ are computed by the same methods used for ΔE and are found to equal −0.40 and −0.27 ev, respectively. The Madelung energy arising from the extra positive charge is simply $-Ae^2/a$ or −8.01 ev. The polarization energy is the same as the polarization energy arising from a positive ion vacancy since each dipole induced on a particular ion is the same magnitude in the two cases but opposite in direction. The polarization energy equals −1.96 ev.[14] Summing components, $\Delta E'$ is −10.6 ev. Therefore, $I_2{}^*$ is 9.5 ev; and since the band gap of KCl is 9.4 ev,[13] the $^1S_0$ state of Tl^+ is approximately a tenth of an electron volt below the top of the filled band. The energy of the $^3P_1{}^0$ state of Tl^+ in KCl has already been determined with respect to the $^1S_0$ state,[6] and is also shown in Fig. 9 for its equilibrium configuration. The $^3P_0{}^0$ and $^3P_2{}^0$ states are also shown, having been located with respect to the $^3P_1{}^0$ state by the differences in atomic energies since the lattice interactions are the same. It is concluded that approximately 4.5 ev is necessary to ionize the metastable states of Tl^+ in KCl; therefore, the tight-binding approximation is appropriate for treating the trapping states as well as the emitting and ground states. The conclusion that 4.5 ev is required to ionize the metastable activator is confirmed by the observation made during this investigation that F centers can be formed in KCl:Tl by 1850A radiation from a quartz low pressure hydrogen lamp or by a quartz window hydrogen discharge lamp, but cannot be formed in this way in pure KCl. Presumably, there is excitation first to the $^3P_0{}^0$ or $^3P_2{}^0$ states and then further excitation to the conduction band with subsequent trapping at anion vacancies to form F centers. With the ionization of the Tl^+ ion, it is also possible for an electron to pass from the filled band into the ground state of the Tl^+. The hole thus formed may be trapped at a cation vacancy resulting in formation of a V center.

[12] R. F. Bacher and S. Goudsmit, *Atomic Energy States* (McGraw-Hill Book Company, Inc., New York, 1932).
[13] N. F. Mott and R. W. Gurney, *Electronic Processes in Ionic Crystals* (Oxford University Press, London, 1948), p. 97.
[14] duPré, Hutner, and Rittner, J. Chem. Phys. 18, 379 (1950).

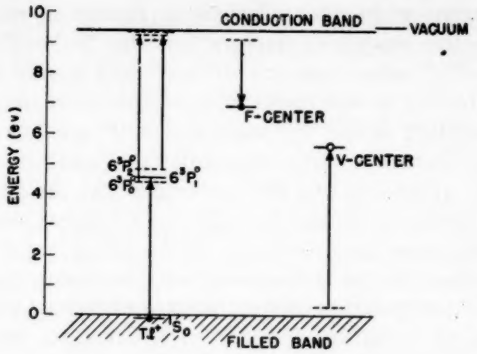

FIG. 9. Band theory model of KCl:Tl.

Experimental confirmation of the formation of V centers in KCl:Tl by near uv excitation at liquid helium temperature has been observed previously.[15] Since there is a 4.5-ev gap between the metastable states and the conduction band, the stimulation spectrum observed by Bunger and Flechsig[11] must correspond to transitions to higher states of Tl^+. It is probable that the two weak stimulation peaks at 11 500A and 15 500A coincide with direct transitions from the $^3P_0^0$ to the $^3P_1^0$ and $^1P_1^0$ emitting states.

Insight into the atomic rearrangements and activation energies accompanying trapping and untrapping can be obtained from the configuration coordinate model which is particularly appropriate for localized systems. In Fig. 10 the energies of the states of Tl^+ are shown as a function of the distance between the Tl^+ and its nearest Cl^- neighbors with the condition that the remainder of the lattice rearranges to minimize the potential energy. The $^1S_0$ and $^3P_1^0$ states were computed fundamentally.[6] The $^1P_1^0$ state was determined from absorption and emission spectra and from the equilibrium between the $^1P_1^0$ and $^3P_1^0$ states.[8] Since the radial charge density of $^1P^0$ states is more extensive than $^3P^0$ states, as shown by Hartree-Fock calculations,[16] the minimum for the $^1P_1^0$ state is at a smaller interatomic distance. The $^3P_0^0$ and $^3P_2^0$ states are approximately parallel to the $^3P_1^0$ state and differ by free ion energies but are very slightly modified to yield the observed activation energies for emptying the traps thermally.

Incidentally, the identification of $^3P_2^0$ Tl^+ as a trap removes the possibility of the $^1S \rightarrow {}^3P_2^0$ transition[8] being responsible for the absorption band at 2060A in KCl:Tl with low activator concentration. This band probably arises from an electron transfer process as suggested by Pringsheim.[17] Modifying the calculations of von Hippel[18] on the electron transfer absorption in KCl at 1625A by the difference in ionization energies of Tl and K yields for KCl:Tl an absorption band at 2108A in striking agreement with experiment.

Since each isolated Tl^+ is independent, is capable of existing in metastable states, and in the metastable states has a lifetime of days, the question arises as to why only approximately the fraction 10^{-4} can be excited with long-time excitation. Two explanations are theoretically sound and can be distinguished experimentally by the dependence of concentration of filled traps at saturation on activator concentration. It must first be recognized that direct optical excitation to the trapping states cannot occur since these transitions are forbidden by selection rules, as are obviously the reverse transitions. Excitation occurs by excitation first to one or the other of the emitting states and then transition with low probability γ to the trapping states. This mechanism will be discussed quantitatively later in this section.

The first possible reason for the low saturated concentrations of traps is that excitation of the metastable Tl^+ to higher states by the incident radiation empties the traps. With excitation intensity J, the rates of formation and annihilation of metastable activator ions are, respectively,

$$+dX/dt = J\sigma(X_m - X)\gamma, \tag{1}$$

$$-dX/dt = J\sigma' X, \tag{2}$$

where σ and σ' are the cross sections for excitation from the ground to the emitting state and from the metastable to higher states, and γ is the probability of trapping following initial excitation. Obviously, σ, σ', and γ are dependent on wavelength of excitation. Under steady state conditions the ratio of concentration of activator ions in the metastable state X to the concentration of activator ions capable of excitation to the

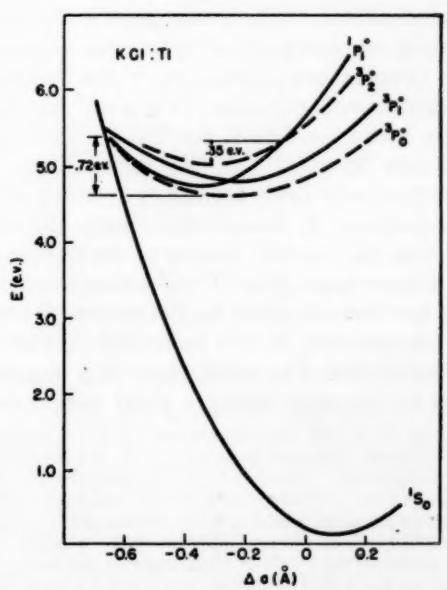

FIG. 10. Configuration coordinate model of KCl:Tl.

[15] P. D. Johnson and F. J. Studer, Phys. Rev. **82**, 976 (1951).
[16] D. R. Hartree and W. Hartree, Proc. Roy. Soc. (London) **150**, 9 (1935).
[17] P. Pringsheim, Revs. Modern Phys. **14**, 132 (1942).
[18] A. von Hippel, Z. Physik **101**, 680 (1936).

emitting or metastable states X_m is

$$X/X_m=\gamma/(\sigma'/\sigma+\gamma). \quad (3)$$

Incidentally,

$$X_m=C(1-C)^z, \quad (4)$$

where C is the gross activator concentration, and Z is the number of sites surrounding an excited activator which if occupied by a second unexcited activator results in radiationless de-excitation.[8]

The second possibility is that concentration de-excitation of the metastable activators occurs by interaction with activators in the emitting or metastable states. The rate of formation of metastable activator ions is again given by (1), but the rate of annihilation is

$$-dX/dt=J\sigma Z'XC, \quad (5)$$

where Z' is the number of sites surrounding a metastable activator which if occupied by a second excited activator results in untrapping. Under steady state conditions,

$$X/X_m=\gamma/(Z'C+\gamma). \quad (6)$$

The first mechanism predominates since Eq. (3) predicts that the correlation between filled trap concentration and luminescent efficiency shown on Fig. 7 should be independent of the degree of saturation as observed. Contrary to experiment, Eq. (6) predicts a lower trap concentration with higher gross activator concentration. It should be pointed out that the conclusions as to the identity of the trapping sites were established from concentration dependence of traps at short excitation times where only Eq. (1) is operative. There is some evidence for the second mechanism operating at low activator concentration for the 205°K peak. An average $\bar{\gamma}$ weighted according to wavelength can be evaluated from Eq. (3), since $X\simeq 10^{-4}\,X_m$ and $\sigma'/\sigma\simeq 1$: $\bar{\gamma}\simeq 10^{-4}$ for excitation with the hydrogen lamp.

The mechanism of filling the traps is elucidated by the limiting concentration of metastable activator ions and the temperature dependence of the concentration of metastable activator ions. It is clear that trapping occurs by excitation first to the $^3P_1^0$ (or $^1P_1^0$) state and then transfer to the $^3P_0^0$ or $^3P_2^0$ states. From Fig. 10 it is seen that only those activators in which excitation is to a condition of polarization energy sufficient for passage over the thermal barrier to the trapping states can participate in trapping. The observed low activation energies are those required for the system to attain the proper configuration in the unexcited ^1S state at the time of excitation. The small value of $\bar{\gamma}$ suggests that trapping occurs only during a short period following excitation while the polarization energy is retained. Since the frequency factors for the $^3P_0^0\rightarrow{}^3P_1^0$ and $^3P_2^0\rightarrow{}^3P_1^0$, transitions are 10^8 sec^{-1} and should be the same for the reverse transitions; and since the frequency of vibration of the $^3P_1^0$ state is 2×10^{12} sec^{-1} as determined from the force constant,[6] the maximum γ is clearly approximately 10^{-4} assuming that the polarization energy is retained for only one vibration. At lower temperatures than the optimum for filling traps, γ will be reduced by the Boltzmann factor for the probability of the configuration of the $^1S_0$ state necessary to yield, following excitation, the critical polarization energy ϵ' for trapping; therefore,

$$\gamma=10^{-4}\exp(-\epsilon/kT_{\text{eff}}), \quad (7)$$

where $T_{\text{eff}}=\theta\coth\theta/T$ and corrects for the zero-point energy $k\theta$.[7] Utilizing the values of ϵ obtained from Fig. 8, ϵ' of 0.54 and 0.62 ev for trapping into the $^3P_2^0$ and $^3P_0^0$ states are obtained and appear plausible from Fig. 10. Following excitation, the probability of radiationless de-excitation may be comparable or even large compared to the probability of trapping; however, emission is the dominant process competing with trapping. The magnitude of $\bar{\gamma}$ for hydrogen discharge excitation was further verified using Eq. (1), from the rate of build-up of the trap concentration, 10^{13} sec^{-1}, the experimental σ of 10^{-18} cm^2, X_m of 10^{18} cm^{-3}, and J of 10^{17} photons sec^{-1} cm^{-2}.

CONCLUSIONS

The two principal traps of KCl:Tl are identified as the $^3P_0^0$ and $^3P_2^0$ states of isolated Tl^+. The $^1S_0$ state of Tl^+ is just below the top of the filled band of KCl and the $^3P^0$ states are approximately 4.5 ev below the conduction band. Multiple excitation of activator ions is feasible in KCl:Tl and is responsible for the limited concentration of traps simultaneously occupied as well as for infrared stimulation and for the formation of F and V centers. The polarization energy following excitation is retained for approximately one oscillation, thereby facilitating trapping. The $^3P_0^0$ and $^3P_2^0$ Tl^+ are capable of representation in the configuration coordinate model formulated for $^3P_1^0$ and $^1S_0$ Tl^+ and also used for $^1P_1^0$ Tl^+.

ACKNOWLEDGMENTS

The authors are indebted to Mr. D. Sullenger, Mr. G. Schlotzer, and Mr. M. Zucker for assistance in obtaining many of the glow curves, to Dr. S. Roberts for many features of the design of the apparatus, and to Dr. M. Hebb for helpful discussions.

Anomalous Adjustment of Indicator Concentration in Moving Boundary Measurements of Transference Numbers

A. R. GORDON AND R. L. KAY
Chemistry Department, University of Toronto, Toronto, Canada
(Received June 30, 1952)

If in a measurement with a rising boundary, the initial concentration of the indicator solution is greater than the critical Kohlrausch concentration, it has long been known that the concentration of the column of solution formed behind the boundary will have the Kohlrausch value, i.e., there is downward adjustment of indicator concentration. It is here shown that if the initial indicator concentration be less than the Kohlrausch concentration, there can be upward adjustment of concentration. Similarly, with a falling boundary, there can be downward adjustment if the initial indicator concentration be greater than the Kohlrausch value. A mechanism for the adjustment process is proposed, and it is shown that the reason such anomolous adjustment is effective, is the extreme slowness of mixing under a density gradient in narrow channels. The significance of these results for moving boundary measurements is discussed, and a simple method is described for determining the adjusted indicator concentration with reasonable precision.

MANY years ago, Kohlrausch[1] pointed out that for a steady state with a two-salt boundary *MA–MB*, the condition must hold

$$C_i/C = t_i/t = r, \qquad (1)$$

where C_i and C are the concentrations of the indicator ion B and of the leading ion A, t_i and t the corresponding transference numbers, and r is the so-called Kohlrausch ratio. Thus, with a rising boundary, if C_i^0, the concentration of the indicator when the junction is formed, be greater (for the given C) than the critical Kohlrausch value C_i^*, defined by Eq. 1, a diffusion boundary results at the initial position of the junction, and the column of indicator solution formed behind the boundary will have the concentration C_i^*, i.e., there is downward adjustment of indicator concentration. This case has been discussed in detail, notably by MacInnes,[2] Longsworth,[3] and Dole.[4]

Recent measurements in this laboratory[5] have shown for several two salt systems, both in aqueous and methanolic solution, that there could be *upward* adjustment of indicator concentration behind a rising boundary if C_i^0 were *less* than C_i^*. This rather unexpected result suggested that if the effects of stirring under a density gradient could be minimized by cell design, upward adjustment to the Kohlrausch value could be complete, and this was in fact found to be the case. Here, we report the results of similar measurements with falling boundaries, and additional data for rising boundaries as well. It must be admitted at once that the results reported here suggest that the phenomenon of indicator concentration adjustment is more complex than was at first suspected,[5] and that our earlier discussion did not take into account all the factors involved.

Experimental: The preparation of the chemicals and of the solutions and the general experimental technique have been previously described.[6,7] Cadmium and silver-silver chloride electrodes on the closed side of the cells served for cation and anion boundaries, respectively; in all cells the tube in which the boundary moved was 2.5-mm internal diameter, and in all cases the observed transference numbers have been corrected for solvent conductance and volume change at the electrode.[2]

The shearing mechanisms for the various cells for use with falling boundaries are shown in Fig. 1, the position of the stopcock in each case being that for filling. For cell VI, the junction is formed by rotating the cock 90° counter-clockwise, and the same is true for VII if it is desired to form the boundary in the conventional position at the top of the graduated tube—"top shearing"; if, however, the boundary is to be formed in the vertical plane at *b*, the cock is rotated 90° clockwise—"side shearing." For cell VIII, the leading solution is run into the cell from below until it is just above the cock, the cock is closed, and the tube above it is then repeatedly flushed from the bottom through a fine capillary with indicator solution; the junction is then formed by restoring the cock to its original position. Cells III, IV, and V are the analogs for rising boundaries of cells VI, VII, and VIII, re-

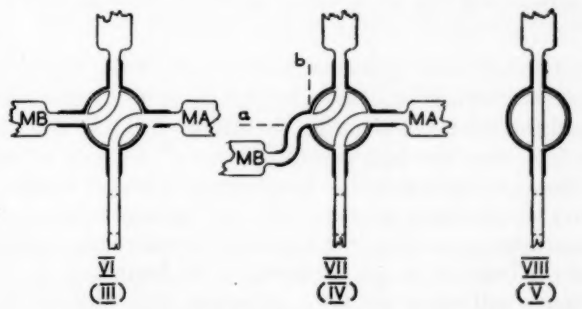

FIG. 1. Shearing mechanism of falling boundary cells.

[1] F. Kohlrausch, Ann. Phys. Chem. **62**, 209 (1897).
[2] D. J. MacInnes and L. G. Longsworth, Chem. Revs. **11**, 171 (1932).
[3] L. G. Longsworth, J. Am. Chem. Soc. **67**, 1109 (1945).
[4] V. P. Dole, J. Am. Chem. Soc. **67**, 1119 (1945).
[5] A preliminary account of this work was presented at the Symposium on Electrochemical Constants, September 19, 1951, at the National Bureau of Standards, Washington, D. C.
[6] Allgood, LeRoy, and Gordon, J. Chem. Phys. **8**, 418 (1940).
[7] The lithium chloride was supplied by Mr. R. E. Jervis of this department; it had been prepared from the carefully purified carbonate and redistilled constant-boiling hydrochloric acid; it was fused in platinum in an atmosphere of dry hydrogen chloride, and cooled in dry carbon dioxide-free nitrogen preparatory to weighing. Barium chloride was three times crystallized as the dihydrate, and the concentration of the resulting stock solutions was determined by differential titration with silver nitrate which had been standardized with potassium chloride.

spectively; in fact Fig. 1, observed upside down, would serve for the shearing mechanisms of these cells.

To determine the concentration of the indicator solution behind the boundary with reasonable precision[8] and under conditions comparable with those obtaining during an actual moving boundary measurement, the cells shown in Fig. 2 were constructed after several trials—*A* for falling boundaries and *B* for rising. When the boundary, formed at stop-cock *a*, has passed cock *c*, *b*, and *c* are closed, the upper part of the cell is lifted from the upper standard taper, and a small platinum electrode, mounted on a similar male taper, is inserted and carefully aligned by means of etched marks on the male and female parts of the joint. The cell is then inverted, and the second electrode inserted. After coming to equilibrium in a constant temperature bath, the apparent resistance of the column of solution thus isolated is determined by an alternating current bridge with Wagner ground. For each indicator, the cell was calibrated by measuring the apparent resistance of a series of solutions of the indicator in question whose concentrations covered that being investigated; in this way, since all measurements were effected at the same frequency and the same input, systematic errors in the interpretation of concentration as a function of apparent resistance are minimized. While the precision of such measurements is better than a part in a thousand, their accuracy is less than this owing to the possibility of small amounts of leading solution being trapped in dead spaces around the joints and subsequently diffusing into the column of indicator solution after the boundary had passed.

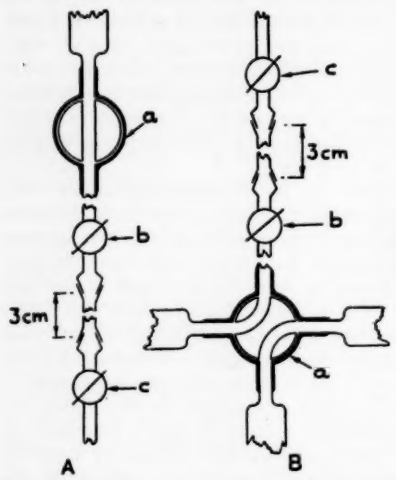

FIG. 2. Cells for determination of adjusted indicator concentration.

A theoretical treatment was first given at Washington[5] for the case of a rising boundary when the indicator concentration C_i, actually obtaining at the boundary, is less than the Kohlrausch value C_i^*. Let V_f be the volume swept out by the boundary in liters per faraday, and C the concentration of the leading solution in equivalents per liter; the apparent transference number of the leading A ion, computed from boundary movement, will then be CV_f. Consider the flux of the common M ion in a volume between fixed reference planes enclosing the boundary; it follows from conservation[9] that

$$(1-t)-(1-t_i)=V_f(C_i-C). \qquad (2)$$

In (2) replace C_i by C_i^*-x, and (noting Eq. 1) rearrange; there results

$$CV_f=t(1-r)/(1-r+rx/C_i^*), \qquad (3a)$$

$$y=t-CV_f=(t_ix/C_i^*)/(1-r+rx/C_i^*). \qquad (3b)$$

Equation (3b) at once suggests a mechanism for the observed upward adjustment process of indicator concentration under these conditions. From a material balance for the A ion in the volume of leading solution lying between the boundary and the upper reference plane, it is obvious that this volume will contain y equivalents per Faraday less of A than if its bulk concentration had been maintained. Moreover, since from Eq. 2

$$C_iV_f=t_i-y, \qquad (4)$$

there will be an equal excess of the B ion in the volume of indicator solution lying between the lower reference plane and the boundary. Thus, for electrical neutrality, there will be an excess of y equivalents of the common M ion in the leading solution and an equal deficit in the indicator. Neutrality can then be preserved if y equivalents of the common ion per faraday cross the boundary in addition to the one equivalent normally carrying the current. The net result is that the leading solution, lying between the boundary and the upper reference plane, will contain y equivalents less of MA than if its bulk concentration had been preserved, while the indicator solution lying between the lower reference plane and the boundary will contain y equivalents more of MB. Density stirring will then tend to reduce the concentration of the leading solution as a whole and to increase that of the indicator, thus causing adjustment.

For a falling boundary when the indicator concentration is less than C_i^*, one would expect on the basis of this mechanism that a thin layer of indicator solution of concentration C_i^* would be formed above the leading solution with the first passage of the current, and that subsequent boundary movement would be normal, i.e., $CV_f=t$, since the indicator solution as a whole is here density stable.[10] It should be noted in passing that this process in reverse accounts for the familiar downward adjustment of indicator concentration with a rising boundary when $C_i^0>C_i^*$.

For a falling boundary when $C_i^0=C_i^*+x$ (x a positive quantity), an argument similar to that leading to Eq. 3 gives

$$CV_f-t=y=(t_ix/C_i^*)/(1-r-rx/C_i^*), \qquad (5)$$

and a mechanism analogous to that discussed for rising boundaries would predict downward adjustment of indicator concentration and upward adjustment in the leading solution through passage of the common ion from the indicator to the leading solution.

[8] The method employed in the preliminary measurements, *viz.*, determination of the resistance of the indicator solution between fine platinum wires sealed opposite one another in the walls of the cell channel, could at best yield results precise to a percent or so.

[9] This implies that the assumption be made, valid for steady state boundaries, that the physical boundary may be treated as a mathematical plane. See, in particular, references 3 and 4.

[10] This assumes that the density of the indicator solution is an increasing function of concentration. If, as with a few salts, the density is a decreasing function, stable falling boundaries will result if the initial indicator concentration is above the Kohlrausch value.

To test this, the system chosen was 0.04 N KCl–LiCl in aqueous solution at 25°C. A series of measurements in cell A gave $C_i^* = 0.0265_5$ N for a range of initial indicator concentrations less than this value.[11] It should be noted that the adjusted indicator ion concentration was the same within experimental error regardless of the length of time the electrolysis proceeded after the boundary had passed stop-cock c. For $C_i^0 > C_i^*$, there was downward adjustment of indicator concentration; for example, with $C_i^0 = 0.045$ N, the concentration of the isolated sample of solution was 0.0278 N, so that the solution in the channel of the cell had a density approximately 0.5 mg/cc less than that for the solution in the reservoir above it. Moreover, this is an average value for a column of solution 3 cm in length, and the actual concentration of the indicator in contact with the boundary should be less than this. In support, is the fact that in a duplicate measurement in which cocks b and c were closed before the boundary had reached b, the concentration of the leading potassium chloride solution was found to be indistinguishable from its initial value, i.e., there had been no upward adjustment of concentration in the leading solution, and a transference measurement in cell VIII (see below) with $C_i^0 = 0.046$ N gave the correct value of the transference number.

As a further test, a concentration boundary was formed in cell A between 0.045 N LiCl in the reservoir and 0.0266 N in the channel. After 105 minutes—the normal time for a run—with no current passing, analysis showed that the sample isolated had only risen in concentration to 0.0269 N. In a similar measurement but with a current of 2 milamp passing, normal for these measurements, the concentration had risen only to 0.0279 N, a result which may be compared with that obtained above. One may therefore conclude that in the absence of Joule heating, convective stirring under a density gradient in narrow channels is an exceedingly slow process, analogous to diffusion, and that even when reinforced by thermal convection the process is still relatively slow under the conditions obtaining here.

In the light of these data, the results of the transference measurements, shown in Fig. 3, are perhaps not surprising. Here the measured CV_f is plotted as a function of initial indicator concentration; the solid line in the figure corresponds to the known[6,12] value of t_+ for 0.04 N KCl, *viz.*, 0.4900, and the arrow indicates the Kohlrausch concentration. It should be noted that in none of the measurements with $C_i^0 < 0.046$ N was there any change within experimental precision in the measured CV_f as the boundary moved down the tube, that a 50 percent change in current had no effect on the measured transference number, and that below the Kohlrausch concentration $CV_f = t_+$ as predicted. This last is in agreement with modern experience[13] with falling boundaries, since the present practice is to use an initial indicator concentration slightly below the Kohlrausch value. Figure 3 shows that within reason, any initial indicator concentration less than C_i^* will result in a stable falling boundary.

The results with C_i^0 between 0.027 N and 0.046 N are not inconsistent with the measurement of adjusted indicator concentration discussed above, and suggest that as long as the boundary is moving with sufficient speed to ensure even a thin layer of indicator with concentration C_i^* in contact with it, any convective process occurring above this level will not disturb boundary movement. Above 0.046 N, the apparent transference number tends to be low, and there are two possible explanations for this. (1) Under a sufficiently high density gradient, the indicator concentration at the boundary may rise above the Kohlrausch value. The adjustment process will then maintain the concentration of the leading solution above its initial value so

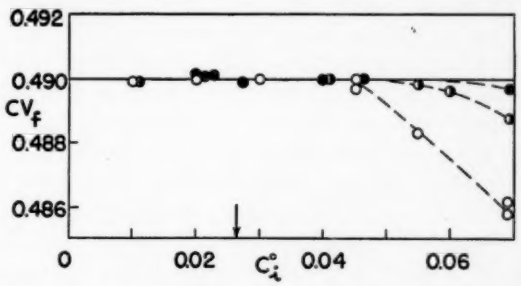

FIG. 3. Apparent transference numbers for the system 0.04 N KCl–LiCl as a function of initial indicator concentration. Normal current, 2 milamp.; current range, 1.6–2.9 milamp. ○ cell VI; ◑ cell VII, side shearing; ● cell VIII.

that boundary movement is actually at a concentration greater than that obtaining initially, and this will of course result in an apparent decrease in boundary velocity; see appendix. (2) In any moving boundary measurement, there is always some thermal convection due to Joule heating in both solutions;[2,12] reinforced by density stirring, actual "blurring" of the boundary may occur so that what is being observed is not a true two-salt boundary, but rather a KCl+LiCl concentration boundary. Longsworth[3] and Dole[4] have shown in their discussion of polysalt boundaries that this will also result in decreased boundary velocity. Unfortunately, it does not seem possible to decide experimentally between these two possibilities, since in either case the effect would be noticeable only in a small volume immediately adjacent to the boundary.

The results obtained with cells VI and VII are consistent with either explanation since with VII, when side shearing is employed, the only reservoir of indicator solution significant as far as density stabilization is concerned is that between the planes a and b in the

[11] From the known value of the transference number for potassium ion (see below) Eq. 1 would predict t for $Li_+ = 0.325_3$; interpolation of Longsworth's data (J. Am. Chem. Soc. 54, 2741 (1932)) gives t_+ for 0.02655 N LiCl = 0.3247.

[12] L. G. Longsworth, J. Am. Chem. Soc. 54, 2741 (1932).

[13] L. G. Longsworth, J. Am. Chem. Soc. 66, 449 (1944).

side arm; see Fig. 1. The results obtained with cell VIII as compared with those for cell VI are more difficult to understand. The explanation we believe lies in the fact that VI has a 90° channel in the stop-cock. If density mixing is in fact analogous to diffusion there will in VI be horizontal density gradients at every level in the channel in the cock, thus favoring convective stirring in the channel; in contrast, in VIII the process of mixing under a density gradient will be more nearly unidirectional.

In view of the results with falling boundaries, further measurements were carried out with the system 0.01 N KCl–KIO_3 at 25°C in aqueous solution. A series of measurements in cell B gave $C_i^* = 0.00691$ N when the initial indicator concentration was greater than this value;[14] and a measurement with $C_i^0 = 0.00501$ N gave an adjusted indicator concentration of 0.00679 N, i.e., adjustment was nearly complete even with this type of shearing mechanism. The transference numbers (including some of the earlier data) are shown in Fig. 4, the line in the figure corresponding[6,12] to $t_- = 0.5098$. If the effects of density differences are minimized as in cell IV with side shearing, correct values of t_- are obtained down to $C_i^0 = 0.003$ N. With cells III and V, one would expect on the basis of downward adjustment of concentration of the leading solution, that the apparent transference number for $C_i^0 < C_i^*$ would be high, while in fact it is low. Here, however, in contrast to a falling boundary, blurring of the boundary by convective mixing will oppose the effect of downward adjustment of leading ion concentration, and the results suggest that the former effect predominates.

The results differ in another respect from those with falling boundaries, since with cells III and V the correct transference number is no longer obtained when C_i^0 is even slightly below C_i^*. There is, however, one important difference in the two cases. With a falling boundary,

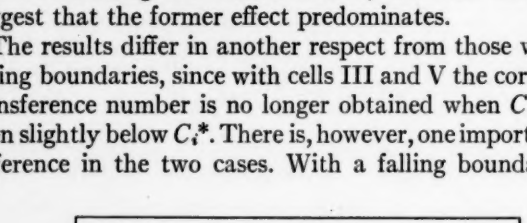

FIG. 4. Apparent transference numbers for the system 0.01 N KCl–KIO_3 as a function of initial indicator concentration. Normal current, 0.5 milamp; current range, 0.4–0.65 milamp. ○ cell III; ◒ cell IV, top shearing; ◑ cell IV; side shearing; ● cell V.

[14] From the transference data for KCl solutions (references 6 and 12) and the equivalent conductance (Shedlovsky, Brown, and MacInnes, Trans. Electrochem. Soc. 66, 165 (1934); Benson and Gordon, J. Chem. Phys. 13, 473 (1945)), the conductance for potassium ion in 0.00691 N KCl solution is 69.91. The equivalent conductance for 0.00691 N KIO_3 is 107.13 (Krieger and Kilpatrick, J. Am. Chem. Soc. 64, 7 (1942)). If one assumes independent ionic mobilities, one obtains for the transference number of iodate 0.3474, which may be compared with that computed by Eq. 1—0.3522. The poor agreement here is probably due to the assumption of independent ionic mobilities at this concentration for an electrolyte such as KIO_3.

not only is the warmer solution above the colder, but there will actually be a smaller differential between the bulk temperatures of the two solutions if $C_i^0 > C_i^*$ than if the Kohlrausch concentration had obtained; this of itself will tend to reduce thermal convection at the boundary. With a rising boundary, the hotter solution is below, and the temperature differential between leading and indicator solutions will increase with decrease in indicator concentration below the Kohlrausch value. This may be the explanation of the fact that the apparent transference number with a rising boundary is so sensitive to a deficit in indicator concentration unless, as in cell IV, the effects of any density stabilization are minimized. That cell V does not show this effect as markedly as cell III is what would be expected from the results with falling boundaries.

A further series of measurements for the system 0.03 N KCl–$BaCl_2$ in aqueous solution at 25°C were carried out to obtain data for rising cation boundaries when the indicator is an unambiguous strong electrolyte. The adjusted Kohlrausch concentration,[15] determined in cell B, is here 0.0268_2 N, and the transference measurements are shown in Fig. 5, the line in the figure corresponding to $t_+ = 0.4901$.[6,12] It is at once evident that the results are similar to those for the potassium chloride-potassium iodate case, and to the earlier data[5] for aqueous potassium chloride—cadmium chloride and methanolic potassium chloride—potassium di-iodobenzoate boundaries.

While there are still some doubtful points, we believe certain conclusions are justified:

(1) In any system, whether the boundary is rising or falling, there is adjustment of concentration toward a stable boundary. The mechanism proposed—transfer of the common ion across the boundary during adjustment to preserve electrical neutrality—seems generally consistent with the facts.

(2) Equalization of concentration under a density gradient in a narrow channel is a slow process, and with proper cell design can be largely eliminated as a disturbing factor.

(3) If the adjustment process results in density instability in the solutions, the consequent convection plus that due to Joule heating may cause mixing at the boundary unless the cell design ensures that such disturbances do not reach the boundary.

(4) Falling boundaries, contrary to general opinion, are no more difficult to employ than are rising boundaries. This may be of some importance in future work in nonaqueous solvents, since many of the obvious

[15] The equivalent conductances of 0.02682 N calcium and barium chlorides are 113.45 and 116.76; Shedlovsky and Brown, J. Am. Chem. Soc. 56, 1066 (1934). The transference number of calcium ion at this concentration is 0.4211; Keenan, McLeod, and Gordon, J. Chem. Phys. 13, 466 (1945); thus the chloride ion conductance in the calcium chloride solution is 65.68. If one assumes independent ionic mobilities for salts of the same valence type, the transference number of the barium ion is 0.4375; this is in reasonable agreement with the value 0.4381, obtained from Eq. 1.

indicators suitable for such solvents can only be used with falling boundaries.

(5) In any work with a new indicator, new salt or new solvent, considerable effort will be saved if an approximate value of the Kohlrausch ratio for the given experimental conditions is determined by some simple device such as that described in this paper.

(6) The fact that even with the present technique, one can obtain moderately accurate values of the Kohlrausch ratio, suggests an interesting possibility. If the ratio be determined for a range of concentration of the leading salt MA, and if an unambiguous extrapolation of the ratio to zero concentration be possible, multiplication of the resulting limiting value by the ratio of the limiting equivalent conductance of MB to that of MA will obviously give the ratio of the limiting conductance of the B ion to that of the A. Since the difference of the limiting ionic conductances is known, this should fix both ion conductances, i.e., one could obtain limiting ionic conductances without carrying out any transference measurements in the ordinary sense of the term. This possibility is now being investigated in this laboratory.

In conclusion, we wish to express our thanks to the National Research Council of Canada for a grant in aid of this research, and for the award to one of us (R.L.K.) of a Studentship and a Fellowship.

APPENDIX

In the limiting case of assumed uniformity of concentration at all times in both solutions as a result of density stabilization, the rate of adjustment can be calculated approximately. Assume, following Dole,[4] that the transference numbers are independent of concentration and that diffusion may be ignored. With a falling boundary when $C_i^0 > C_i^*$, let the initial volume of indicator solution be V_i^0; in cell VII with side shearing, this would be the volume in the side arm enclosed between the planes a and b—approximately 0.03 cc in the actual cell. Let the initial volume of the leading solution be V^0, in cell VII, this would be the channel in the stop-cock, the graduated tube and the reservoir at its base—approximately 5 cc in all. Let the initial concentration of the leading solution be C^0, and at some later instant of the electrolysis let the concentrations be C_i and C, the volumes V_i and V; note that $V_i+V = V_i^0+V^0=A$. During a short interval in which df faradays pass, it follows from Eqs. 2 and 5 that

$$(t_i+y)\cdot df = C_iV_f\cdot df = C_i\cdot dV_i. \tag{6}$$

During this interval, the indicator solution will lose $y\cdot df$ equivalents of the indicator salt with a resultant change in concentration given by

$$y\cdot df = -V_i\cdot dC_i. \tag{7}$$

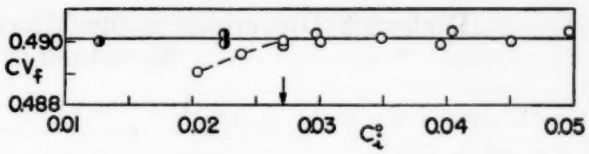

FIG. 5. Apparent transference numbers for the system 0.03 N KCl–$BaCl_2$ as a function of initial indicator concentration. Normal current, 1.7 milamp.; current range, 1.6–2.1 milamp. ○ cell III; ◑ cell IV, side shearing.

Subtract (7) from (6), and there results

$$t_i\cdot df = d(C_iV_i), \tag{8a}$$

$$t_if = C_iV_i - C_i^0V_i^0. \tag{8b}$$

Similarly,

$$tf = C^0V^0 - CV. \tag{9}$$

From (8b) and (9), one obtains $C=(B-C_iV_i)/rV$ where $B=rC^0V^0+C_i^0V_i^0$. The Kohlrausch concentration of the indicator at any instant is obviously rC, so that the excess indicator concentration x (see Eq. 5) is given by

$$x = C_i - rC = (AC_i - B)/(A - V_i). \tag{10}$$

From Eqs. 6 and 7, one obtains by elimination of df:

$$C_i\cdot dV_i/V_i\cdot dC_i = -(t_i+y)/y. \tag{11}$$

In (5) replace C_i^* by C_i-x, and the expression on the right of (11) becomes $-C_i(1-r)/x$. After substituting for x by means of (10), Eq. 11 becomes after rearranging

$$dV_i/(AV_i - V_i^2) = -(1-r)\cdot dC_i/(AC_i - B), \tag{12a}$$

$$\ln(V_iV^0/V_i^0V) = (1-r)\cdot\ln(AC_i^0 - B)/(AC_i - B). \tag{12b}$$

On the assumption of complete density stabilization, Eq. 12b thus predicts the bulk concentration of the indicator solution (and consequently of the leading solution) as a function of boundary movement. In the case of a rising boundary with $C_i^0 < C_i^*$, one obtains a similar relation except that all signs in the argument of the logarithm on the right must be changed. If the volume of the indicator solution is at all times negligible in comparison with that of the leading solution, Eq. 12b reduces to the relation previously reported.[5]

The significance of Eq. 12b, if density stabilization were operative, can be best illustrated by a numerical example. Consider an experiment with a KCl–LiCl boundary in which $C^0=C_i^0=0.04$ N, with cell VII and side-shearing (see above). The Kohlrausch ratio is here 0.664. With $V_i^0=0.03$ cc, $V^0=5$ cc, Eq. (12b) predicts that when the boundary reaches the first line in the graduated tube ($V_i=0.37$ cc) C_i will be 0.02665 N and C will be 0.04012 N, i.e., adjustment will be complete within a part in three thousand, and a stable boundary will henceforth move down the tube. A calculation of t_+ from subsequent observed boundary movement with $C=0.04000$ N instead of $C=0.04012$ N, would, however, lead to the erroneous value 0.4885.

Dielectric Dispersion in the Microwave Region of Six Tetrasubstituted Methanes in the Solid State*

J. G. Powles,† D. E. Williams, and C. P. Smyth
Frick Chemical Laboratory, Princeton University, Princeton, New Jersey
(Received July 31, 1952)

A method is described for the measurement of dielectric constant and loss at microwave frequencies and low temperatures. The dielectric constant and loss at 3.22 cm wavelength (9.32×10^9 cycles/sec) have been measured over a range of temperature in the solid state and in the liquid near the melting point for *t*-butyl chloride, *t*-butyl bromide, 2,2-dichloropropane, methyl chloroform, 2-chloro-2-nitropropane, and 2,2-dinitropropane. 1,1-Dichloro-1-nitropropane also has been measured as a supercooled liquid. The six tetrasubstituted methanes, previously found to show molecular orientational freedom in the solid state for some distance below the melting point, give evidence of very short dielectric relaxation times in this region. The relaxation times increase from a very low value for *t*-butyl chloride to values such that large dielectric loss is observed near 3 cm for 2-chloro-2-nitropropane and 2,2-dinitropropane. The relaxation times in the solid rotator phases and in the liquid are compared, and the results are discussed in terms of intermolecular forces which give rise to potential energy barriers restricting rotation.

INTRODUCTION

MANY substances whose molecular shapes are symmetrical about one or more axes have been found to show polymorphism, the molecules in the solid state apparently possessing a more or less restricted rotational freedom for some distance below the melting point.[1,2] Such solid phases are sometimes called rotator phases,[3] and the transitions at which the degree of orientational freedom changes may be called rotational transitions, although they may be regarded as a type of order-disorder transition. Tetrasubstituted methanes may have molecular shapes sufficiently close to spherical to permit rotational orientation in the solid state. Dielectric constants high enough to indicate rotational freedom have been observed for the dipolar molecules of *t*-butyl chloride,[4,5] *t*-butyl bromide,[4,5] *t*-butyl iodide,[4] 2,2-dichloropropane,[6] methyl chloroform,[6,7] 2-methyl-2-nitropropane,[7] 2-chloro-2-nitropropane,[7] 2-bromo-2-nitropropane,[7] 2,2-dinitropropane,[7] and dinitroneopentane.[7] Transitions which are presumably rotational have also been observed for other molecules of similar shape but zero dipole moment, e.g., methane,[8] deuteromethane,[9] neopentane,[10] and carbon tetrachloride.[11] When the symmetry of the molecule is reduced too far, orientational freedom in the solid state does not occur, as in the case of 1,1,2-trichloroethane,[7] $CHCl_2\cdot CH_2Cl$, in contrast to methyl chloroform, $Cl_3C\cdot CH_3$, which is nearly spherical in molecular shape and has a rotator phase. With the exception of *t*-butyl iodide, these substances show no dielectric loss at frequencies from 0.5 to 50 kc other than that attributable to the presence of traces of ionic impurities in the less stable substances. As judged by the static dielectric constant, the orientational freedom of the molecules in the rotator phases is comparable to that in the liquid state. In order to investigate the hindrance to this rotational orientation, measurements of dielectric constant and loss have been made at 3.22 cm wavelength over a range of temperature and are reported in this paper.

EXPERIMENTAL METHOD

The method employed to measure the dielectric constant ϵ' and loss ϵ'' was necessitated by certain special conditions. Because all of the materials, except 2,2-dinitropropane, were liquids at room temperature, it was not convenient to employ methods normally used for the measurement of solids,[12] which involve manipulation of the sample or measurement under various conditions. The following method[12] has, therefore, been chosen, although its accuracy is probably lower than that usually attained in microwave measurements of dielectric properties. The dielectric specimen is formed in a rectangular wave guide, one end having a plane transverse air-dielectric interface and the other having a long taper with the resultant space in the wave guide

* This research has been supported in part by the ONR. Reproduction, translation, publication, use or disposal in whole or in part by or for the United States Government is permitted.

† Visiting Research Fellow supported by a grant from E. I. du Pont deNemours and Company to the Department of Chemistry of Princeton University.

[1] C. P. Smyth, Chem. Revs. **19**, 329 (1936); see also L. Deffet, *Répertoire des composés organiques polymorphes* (Desoer, Liège, 1942).

[2] R. W. Crowe, Ph.D. thesis, Princeton University, Princeton, New Jersey, 1951.

[3] J. D. Hoffman and C. P. Smyth, J. Am. Chem. Soc. **72**, 171 (1950).

[4] W. O. Baker and C. P. Smyth, J. Am. Chem. Soc. **61**, 2798 (1939); Ann. N. Y. Acad. Sci. **40**, 447 (1940).

[5] Kushner, Crowe, and Smyth, J. Am. Chem. Soc. **72**, 1091 (1950).

[6] A. Turkevich and C. P. Smyth, J. Am. Chem. Soc. **62**, 2468 (1940).

[7] R. W. Crowe and C. P. Smyth, J. Am. Chem. Soc. **72**, 4009 (1950).

[8] K. Clusius, Z. physik. Chem. **B3**, 63 (1929); K. Clusius and A. Perlick, Z. physik Chem. **B24**, 313 (1934).

[9] K. Clusius and L. Popp, Z. physik. Chem. **B46**, 63 (1940).

[10] J. G. Aston and G. H. Messerly, J. Am. Chem. Soc. **58**, 2354 (1936).

[11] W. P. Conner and C. P. Smyth, J. Am. Chem. Soc. **63**, 3424 (1941).

[12] R. M. Redheffer, Radiation Laboratory Series (McGraw-Hill Book Company Inc., New York, 1947), Vol. 11, p. 561, gives a summary to 1947.

filled with a wedge of lossy material. A slotted line carrying a probe served to measure the standing wave pattern in the wave guide in front of the interface. The experimental arrangement is shown schematically in Fig. 1. If the wedge is a perfectly nonreflecting termination, the real and imaginary parts of the dielectric constant are given by

$$\epsilon' = \frac{1+\lambda_c^2(B^2-A^2)}{1+(\lambda_c/\lambda_g)^2}, \tag{1}$$

$$\epsilon'' = \frac{2\lambda_c^2 AB}{1+(\lambda_c/\lambda_g)^2}, \tag{2}$$

where

$$A = \frac{\tan 2\pi x_0/\lambda_g(\rho^2-1)}{\lambda_g(1+\rho^2\tan^2 2\pi x_0/\lambda_g)}, \tag{3}$$

$$B = \frac{\rho}{\lambda_g}\cdot\frac{1+\tan^2 2\pi x_0/\lambda_g}{1+\rho^2\tan^2 2\pi x_0/\lambda_g}, \tag{4}$$

λ_c is the cut-off wavelength in the air-filled guide, λ_g is the wavelength in the air-filled guide, ρ^2 is the power standing wave ratio, and x_0 is the distance of the first minimum in the standing wave from the front face of the dielectric. If $\alpha+i\beta$ is the propagation constant in the dielectric filled guide, then $\alpha=2\pi A$ and $\beta=2\pi B$. If the dielectric loss is low, (3) and (4) reduce to

$$A = (2\pi x_0/\lambda_g^2)(\rho^2-1) \tag{5}$$

and

$$B = \rho/\lambda_g, \tag{6}$$

so that the dielectric constant is determined primarily by ρ^2 and the loss by x_0.

In the apparatus the wave guide was supported vertically and the air-dielectric interface was horizontal. A window was formed in the guide by a thin mica sheet, 0.001 inch thick or less, held between the flanges of two sections of wave guide and made liquid tight by a little silicone grease at its edges. When, in one case, the mica was removed after the specimen was formed, the absence of detectable difference in the readings showed that the window had exerted no adverse effect. There was no detectable reflection from the sheet, which was strong enough to support the dielectric without appreciable distortion. The cell was surrounded by a jacket, in which circulated, according to the temperature range required, either acetone, water, or glycerine, which was heated or cooled in an adjacent apparatus. The temperature range $-80°$ to $120°$ could be covered. The lower end of the jacket extended to the end of the dielectric, but the wave guide was well insulated for some distance below the interface. The slotted line section was maintained close to room temperature, being protected by a length of about 10 cm of guide and a thermal choke. As a result of the unavoidable influx of heat at the lower end of the cell, there was a temperature difference over a 7 cm length of dielectric of about 5° at $-75°$ and 1.5° at $-20°$. This temperature gradient was not serious unless the dielectric properties varied rapidly with temperature as in the regions of the transitions. Even then it was not important when the dielectric loss was high, since then only a short section of dielectric near the front face was effective. In the earlier experiments another mica sheet was placed just above the slotted line to prevent condensation of moisture inside the cold guide, but this precaution was found to be unnecessary.

The wedge termination alone had a power standing wave ratio of 1.08, which was unimportant in most of the measurements where the loss in the dielectric was high. This source of error would normally be avoided by taking another specimen differing in length by one quarter wavelength. When the loss was low, the results were checked by using a short circuit plunger termination, but these measurements were considered generally less reliable. The measurements with the short-circuit plunger, which followed essentially the method of Roberts and von Hippel,[13,14] were valuable in giving an independent check on the other measurements. The poor reproducibility was ascribed to the difficulty in forming a sufficiently good upper end to the specimen, which was particularly important when the material had a high dielectric constant. The essential ambiguity in the results was a serious disadvantage since the measurement of a different length required reforming the specimen and very slight macroscopic differences might render the results difficult to interpret. The short-circuit method was somewhat superior to ours for the measurement of the low dielectric constants (about 3) of the lowest temperature phases. For methyl chloroform and *t*-butyl bromide, for which the dielectric constants of the lowest temperature phase was not measured in this way, the agreement with the lower frequency measurements was not so good.

The dielectric specimen was formed by cooling slowly through the freezing point, a good interface being observed visually and the results being satisfactorily

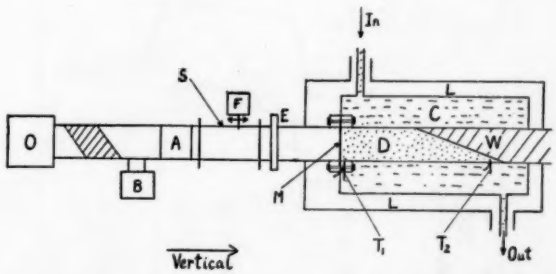

FIG. 1. Schematic experimental arrangement: *A*, variable attenuator 15–30 db; *B*, wavemeter; *C*, circulating fluid; *D*, dielectric specimen; *E*, thermal choke; *F*, detector; *L*, lagging; *M*, mica sheet; *O*, microwave oscillator modulated at 1 kc; *S*, slotted section with traveling probe; *T*, thermocouples; *W*, wedge termination.

[13] S. Roberts and A. von Hippel, J. Appl. Phys. **17**, 610 (1946).
[14] W. B. Westphal, M.I.T. Laboratory for Insulation Research Report No. 36, p. 113 (1950).

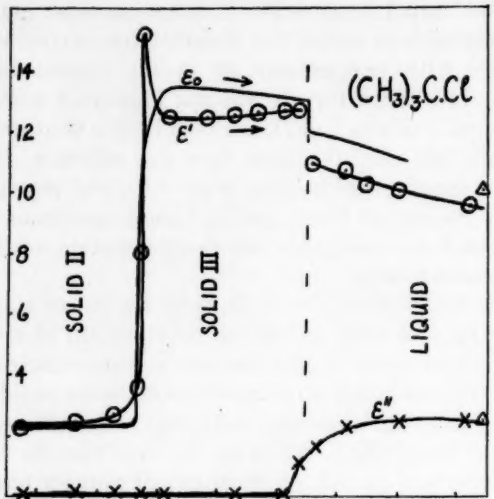

FIG. 2. Static dielectric constant, ϵ_0, (see reference 5) and dielectric constant, ϵ', and loss, ϵ'', at 3.22 cm wavelength *versus* temperature (°C) for *t*-butyl chloride.

reproducible. The power standing wave ratios did not exceed 60 and were obtained by direct measurement of the maximum and minimum of the standing wave by means of a calibrated attenuator in the audio stage of the detector and a microammeter. x_0 was obtained by comparing the position of the minimum of the standing wave in front of the specimen with that measured in a preliminary experiment in which the specimen was replaced by a short-circuit plate. $(\lambda_g/2)-x_0$, which was of the order of a millimeter, was measured with an accuracy of about 0.01 mm. Nevertheless, the accuracy of x_0 was the limiting factor in the determination of ϵ''.

PURIFICATION OF MATERIALS

All the materials were measured either immediately or, at the most, one day after purification.

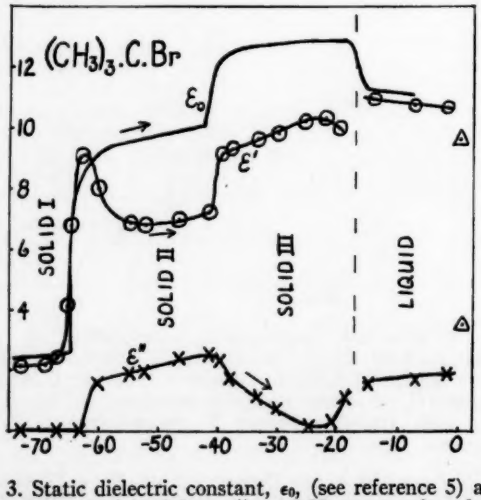

FIG. 3. Static dielectric constant, ϵ_0, (see reference 5) and dielectric constant, ϵ', and loss, ϵ'', at 3.22 cm wavelength *versus* temperature (°C) for *t*-butyl bromide.

t-Butyl chloride, supplied by The Matheson Company, Inc., was washed with sodium carbonate and distilled water, dried over calcium chloride, and fractionally distilled. bp 50.8°; literature bp 50.6°,[4] 51.0°;[15] n_D^{20} 1.3856; literature n_D^{20} 1.3847,[4] 1.3853,[16] 1.3839.[17]

t-Butyl bromide was purified in the same way as *t*-butyl chloride. bp 72.9°; literature bp 73.2°,[4] 73.25°;[16] n_D^{20} 1.4275; literature n_D^{20} 1.4276,[4] 1.4275–7.[18]

2,2-Dichloropropane, supplied by Halogen Chemicals, was purified in the same way as *t*-butyl chloride. bp 69.5°; literature bp 69.3°,[6] 70.5°.[15]

Methyl chloroform, supplied by The Matheson Company, Inc., was purified in the same way as *t*-butyl chloride. bp 74.0°; literature bp 74.0°;[6] mp −33.0°, literature mp −32.7°;[6] n_D^{20} 1.4378; literature n_D^{20} 1.4379.[6]

2-Chloro-2-nitropropane, given by Commercial Solvents Corporation, was purified in the same way as

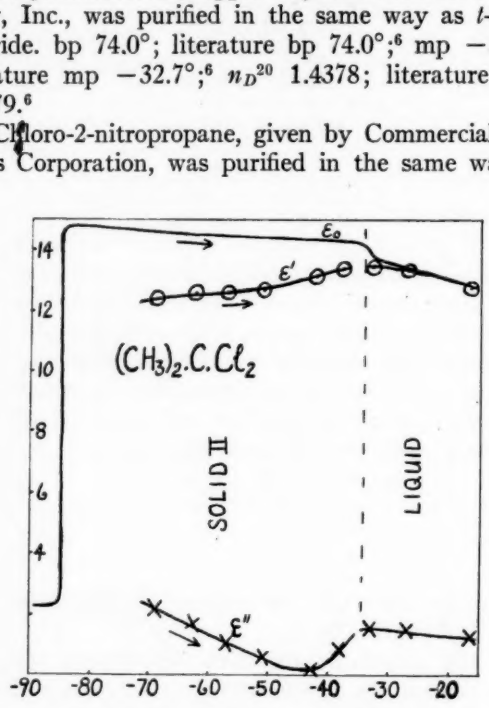

FIG. 4. Static dielectric constant, ϵ_0, (see reference 6) and dielectric constant, ϵ', and loss, ϵ'', at 3.22 cm wavelength *versus* temperature (°C) for 2,2-dichloropropane.

t-butyl chloride, except that it was distilled at reduced pressure, bp 65.0° (80 mm).

2,2-Dinitropropane, given by Commercial Solvents Corporation, was crystallized three times from alcohol, fragmented, and dried under vacuum for three days, mp 53.2°.

1,1-Dichloro-1-nitropropane, given by Commercial Solvents Corporation, was measured as received.

EXPERIMENTAL RESULTS

The measurements of dielectric constant and loss at 3.22 cm wavelength (9.32×10^9 cycles/sec) are plotted

[15] J. Timmermans and Y. Delcourt, J. chim. phys. **31**, 85 (1934).
[16] C. P. Smyth and R. W. Dornte, J. Am. Chem. Soc. **53**, 545 (1931).
[17] G. B. Kistiakowsky and C. H. Stauffer, J. Am. Chem. Soc. **59**, 165 (1937).
[18] M. S. Kharasch and W. M. Potts, J. Am. Chem. Soc. **58**, 57 (1936).

against temperature for six tetrasubstituted methanes in Figs. 2–7, together with values for three of the liquids as previously measured[19–21] in this laboratory at the same wavelength. Also shown are the so-called static dielectric constants[4–7] measured at frequencies between 0.5 and 50 kc, at which the loss is zero except for the effect of dc conductance resulting from ionic impurities in some of the less stable substances. The agreement between the 3.22 cm values for the liquids in the present work and the results of previous measurements is satisfactory for *t*-butyl chloride and methyl chloroform. For liquid *t*-butyl bromide, which is very subject to the effect of impurities because of its instability, the loss is considerably lower and the dielectric constant higher than that previously reported.[19] When the loss is small, the agreement of the dielectric constant with the static values is sufficient to warrant confidence in the reasonable accuracy of the measurements. Because of the large thermal inertia of the cooling system, supercooling had a pronounced effect, since the evolution of heat by a

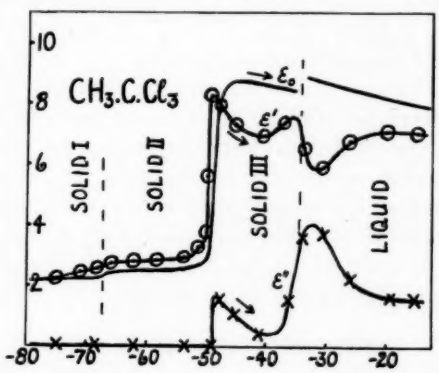

FIG. 5. Static dielectric constant, ϵ_0, (see reference 7) and dielectric constant, ϵ', and loss, ϵ'', at 3.22 cm wavelength *versus* temperature (°C) for methyl chloroform.

highly supercooled specimen in transforming might not be sufficient to bring the temperature back up to the correct value for the transition point. For this reason results are given for rising temperature only, except in the case of 2,2-dinitropropane.

Some of these materials show a small peak in the dielectric constant at the transition with rising temperature, which was not found in the static dielectric constant. This peak value does not exceed the static value except in *t*-butyl chloride. Where the transition is to a phase having high dielectric loss, the loss rises only slowly to its normal value with rising temperature when the peak in ϵ' is present. It seems that the material when close to the transition has low loss and, therefore, high ϵ', which is brought down at slightly higher temperatures by the onset of the loss. It may be that this effect is in part caused by the temperature gradient in

[19] H. L. Laquer and C. P. Smyth, J. Am. Chem. Soc. **70**, 4097 (1948).
[20] Curtis, McGeer, Rathmann, and Smyth, J. Am. Chem. Soc. **74**, 644 (1952).
[21] A. A. Anderson (unpublished measurements).

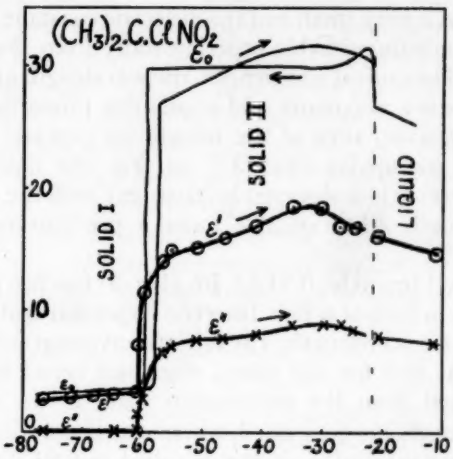

FIG. 6. Static dielectric constant, ϵ_0, (see reference 7) and dielectric constant, ϵ', and loss, ϵ'', at 3.22 cm wavelength *versus* temperature (°C) for 2-chloro-2-nitropropane.

the specimen, and the apparent measured values are incorrect. However, no peak was observed in 2-chloro-2-nitropropane, where the loss rose sharply at the transition, and in 2,2-dinitropropane the transition occurred at a temperature such that the temperature gradient was much smaller than in the other cases. It is possible, however, that the effect may result from lack of attainment of equilibrium in the specimen, giving rise to an inhomogeneous dielectric near the transition, which would give anomalous results. The transition proceeded appreciably more slowly in the nitro compounds than in the others, possibly because of the larger barrier to rotation in the nitro compounds, which is discussed later.

For *t*-butyl chloride, $(CH_3)_3CCl$, (Fig. 2) the loss of

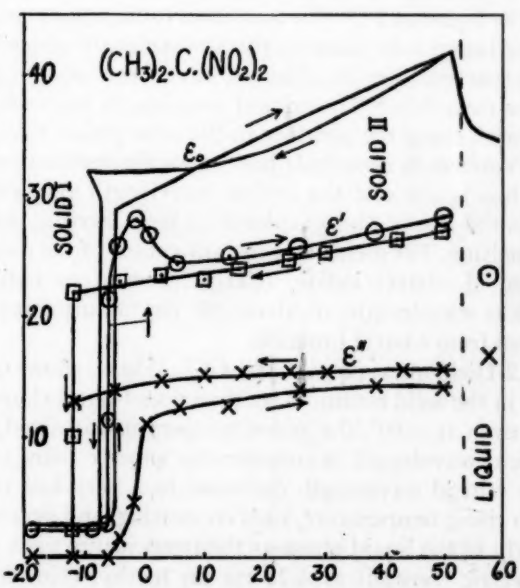

FIG. 7. Static dielectric constant, ϵ_0 (see reference 7), and dielectric constant, ϵ', and loss, ϵ'', at 3.22 cm wavelength *versus* temperature (°C) for 2,2-dinitropropane.

the solid is very small and the dielectric constant at 3.22 cm is indistinguishable experimentally from the static value. The critical wavelength, the wavelength at which the loss is a maximum and a quantity proportional to the relaxation time of the orientation process, is evidently far smaller than 3.2 cm. For the liquid, the considerable loss observed is consistent with the critical wavelength of 1.06 cm at 4° found in previous measurements.[22]

t-Butyl bromide, $(CH_3)_3CBr$, (Fig. 3) has two rotator phases, in both of which dielectric dispersion is observed at 3.22 cm wavelength. The critical wavelengths for this material and for the others discussed below may be estimated from the relationship that, at the critical wavelength, $\epsilon' = (\epsilon_0 + \epsilon_\infty)/2$, where ϵ_0 is the static dielectric constant and ϵ_∞ is the so-called optical dielectric constant. Similarly the dielectric loss, ϵ'', at the same point, will have a value which is less than or equal to $(\epsilon_0 - \epsilon_\infty)/2$. The extent to which the loss is less than $(\epsilon_0 - \epsilon_\infty)/2$ at the critical wavelength is an indication of the extent of the distribution of relaxation times. If, therefore, the dielectric constant is $>$ (or $<$) $(\epsilon_0 + \epsilon_\infty)/2$ and $\epsilon'' \ll (\epsilon_0 - \epsilon_\infty)/2$, it is reasonable to deduce that the critical wavelength is shorter (or longer) than the wavelength of measurement. In the lower temperature rotator phase of *t*-butyl bromide, the critical wavelength is estimated in this manner to be rather shorter than 3 cm and is possibly comparable with the value 1.6 cm found for the liquid at 1°.[22] The transition to the upper rotator phase brings a decrease in critical wavelength which is to be expected. Similar changes have been observed in other materials.[23] The critical wavelength continues to fall with rising temperature in the same phase, which is also commonly observed. Just below the melting point, the loss is low and the critical wavelength very short. As in the case of *t*-butyl chloride, a large increase occurs on melting. The dielectric constant values[4] of the rotator phase of *t*-butyl iodide, $(CH_3)_3CI$, seem to indicate critical wavelengths of about 10^7 cm, a surprising increase from *t*-butyl bromide.

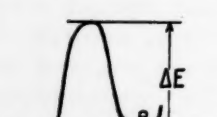

FIG. 8. Rotational potential energy curve for a molecule in the crystal.

2,2-Dichloropropane, $(CH_3)_2CCl_2$, (Fig. 4) shows more loss in the solid rotator state than does *t*-butyl chloride, but even at −69°, the lowest temperature attained, the critical wavelength is considerably shorter than 3 cm. The critical wavelength decreases to a very low value with rising temperature, rises on melting, and decreases slowly in the liquid phase as the temperature rises. The dielectric constant at 3.22 cm for methyl chloroform, CH_3CCl_3, (Fig. 5) shows some indication of the lower transition established by heat capacity and dielectric constant measurements.[7] The critical wavelength of the rotator phase below the melting point is evidently much shorter than 3 cm, while, for the liquid just above the melting point, it is close to 3 cm. In fact, it may be estimated from the measurements quoted[21] that, for liquid methyl chloroform at the freezing point, the critical wavelength is approximately 2.4 cm, while for *t*-butyl chloride[20] the corresponding value is estimated as only 1.3 cm.

For 2-chloro-2-nitropropane, $(CH_3)_2C(NO_2)Cl$, (Fig. 6) the dielectric constant in the rotator phase has a value close to $(\epsilon_0 + \epsilon_\infty)/2$ so that the critical wavelength cannot be very different from 3 cm throughout the temperature range of this phase. However, the loss is only about half of $(\epsilon_0 - \epsilon_\infty)/2$, possibly indicating a distribution of relaxation times. In contrast to the other tetrasubstituted methanes just considered, the critical wavelength of the liquid just above the melting point is close to that of the solid rotator phase. The more polar 2,2-dinitropropane, $(CH_3)_2C(NO)_2$, (Fig. 7) is rather similar to 2-chloro-2-nitropropane in behavior. The rotator phase seems to have a critical wavelength close to 3 cm at 0°, which decreases slightly with rising temperature. On melting, the critical wavelength rises slightly. The effect of molecular asymmetry is shown by 1,1-dichloro-1-nitropropane, $C_2H_5C(NO_2)Cl_2$, which was found not to freeze above −80° but to become very viscous.[24] The liquid was lossy at 3.2 cm, showing a falling dielectric constant and rising loss as the temperature decreased.

INTERPRETATION OF RESULTS

The interactions of a molecule with its neighbors in the crystal result in a variation of its potential energy with angular position having the general form shown in Fig. 8. *A* is the more populated equilibrium position and *B*, a second equilibrium position higher than *A* by an amount *Q*, is separated from it by an energy barrier ΔE. It may be shown that *Q* is very approximately proportional to the transition temperature, while ΔE determines the order of magnitude of the dielectric relaxation time or critical wavelength by the following approximate relation:

$$\tau \propto \lambda_m \propto e^{\Delta E/kT}.$$

The actual potential energy curve is much more complicated, and it is possible that the representation of the molecular interaction by an average potential energy curve for a single molecule is not valid, especially when the motion of the molecules in a rotator phase is highly cooperative. Nevertheless, this representation enables us to form some picture of the dielectric relaxation process in these materials. It is not likely that *Q* and ΔE are simply related. At a transition, *Q* is very much reduced and ΔE is probably reduced at the same time, if only

[22] Hennelly, Heston, and Smyth, J. Am. Chem. Soc. **70**, 4102 (1948).

[23] See J. G. Powles, J. phys. **13**, 121 (1952).

[24] Compare reference 9.

because of the lattice expansion which occurs. This is in accord with the observation of a fall in critical wavelength at the transition from the lower to the upper rotator phase in *t*-butyl bromide. We are unable to predict, in general, the relation of Q and ΔE in the present state of our knowledge. However, if the molecule is very symmetrical and the intermolecular forces are small, both ΔE and Q will be small, which is exemplified by the very low transition temperature of methane,[8] 20.4°K.

In the case of polar and less spherical molecules the values of Q and ΔE depend on both the magnitude and the asymmetry of all the intermolecular forces involved. The van der Waals radii of the methyl group, 2.0A, and chlorine, 1.80A,[25] are sufficiently close to give molecular symmetry permitting rotational orientation of the molecules of the methyl chloromethanes in the solid state, but the rotational transition temperatures do not show a consistent variation with molecular structure.[6] This absence of consistent variation of transition temperature and of Q can be accounted for by the presumable differences in molecular packing in the anisotropic lattices existing below the transitions.[6]

Again in the series of the *t*-butyl halides the rotational transition temperature of *t*-butyl bromide is 11° lower than that of the chloride, but Figs. 2 and 3 show the critical wavelength to be longer. The transition temperature of *t*-butyl iodide is 15° lower than that of the bromide and the critical wavelength of the rotator phase is greater by a factor of about 10^7, as previously indicated. Evidently, in the *t*-butyl halides, increase in the height of the potential barrier hindering rotation does not substantially raise the transition temperature or the value of Q. Increase in radius from 1.80A for chlorine to 1.95A for bromine should increase the molecular symmetry and thus tend to lower the hindering potential barrier in *t*-butyl bromide, but the greater polarizability of the bromine atom increases the intermolecular attraction, thus tending to raise the barrier. The increase in radius from that of bromine to that of iodine, 2.15A, increases both the molecular asymmetry and the intermolecular attraction, thus raising the hindering potential barrier. The great increase in the critical wavelength is less surprising when it is recalled that the change of a methyl group in *t*-butyl chloride to an ethyl to give *t*-amyl chloride appears to prevent rotation entirely.[26] The results for *t*-butyl chloride, 2,2-dichloropropane, and methyl chloroform show that the potential barrier to rotation increases with successive replacement of the methyl groups by chlorine atoms and consequent increase in the number of strong local dipoles. This increase in the hindering potential barriers parallels an apparent effect of dipole-dipole forces observed in the liquid state.[20]

The replacement of a chlorine atom in 2,2-dichloropropane by a nitro group increases the dipole moment considerably and the volume slightly, and decreases the molecular symmetry slightly, all of which factors should contribute to the large increase observed in the hindering potential barrier. The replacement of the remaining chlorine atom by a second nitro group further increases the dipole moment without greatly altering the spatial symmetry of the molecule or the consequent potential barrier. In view of the prevention of molecular rotation by the insertion of a CH_2 group in the *t*-butyl chloride molecule, it is at first surprising to find[7] a rotator state in dinitroneopentane, $(CH_3)_2C(CH_2NO_2)_2$, but examination of a model of the molecule shows that it can take up a shape which does not differ greatly from a sphere.

It is, perhaps, remarkable to find that the critical wavelength in the crystal is shorter than that in the liquid in some cases. In terms of our simple picture, this means that the energy barrier is lower in the crystal than in the liquid. Another example of the short critical wavelength in the solid state is found in *n*-docosyl bromide.[27] The similarity in some respects between the solid rotator phase and the liquid gives added interest to the fact that these materials are soft or waxy in the rotator phase.

The authors wish to thank Dr. J. K. Dale and the Commercial Solvents Corporation for the gift of three of the substances investigated.

[25] L. Pauling, *Nature of the Chemical Bond* (Cornell University Press, Ithaca, New York, 1940), p. 189.

[26] A. Turkevich and C. P. Smyth, J. Am. Chem. Soc. **64**, 737 (1942).

[27] Private communication from Dr. J. D. Hoffman; also J. D. Hoffman, J. Chem. Phys. **20**, 541 (1952).

The Infrared Spectra and the Molecular Structure of Pyramidal Molecules*

HARALD H. NIELSEN
Department of Physics and Astronomy, The Ohio State University, Columbus, Ohio.

(Received July 21, 1952)

It is necessary to have explicit expressions for the rotational term values for the vibration states ν_2 and ν_4 in order to make use of the analysis of the data on the low frequency bands in the spectra of pyramidal XH_3 molecules. These frequencies are coupled by a Coriolis interaction which gives rise to a submatrix, for each value of J, in the complete energy matrix which has $3(2J+1)$ rows and columns. These submatrices further break up into smaller ones which have at most three rows and columns. Explicit relations for the term values ν_2 and ν_4 require that these be diagonalized independently.

It has been possible to expand the determinants of these submatrices in special cases where, for example, the quantum number $K=J$ and where $K=0$ so that explicit relations for these states may readily be had. Using the frequency positions of lines involving transitions to these states permits the evaluation of the Coriolis factor $\zeta_4^{(z)}$. The structure of the molecules may also be fixed if then $B^{(xx)}$and $\zeta_3^{(z)}$ can be determined, use being made of the zeta-sum for XH_3 molecules, i.e., $\zeta_3^{(z)}+\zeta_4^{(z)}=-1+B^{(xx)}/2B^{(zz)}$.

I. INTRODUCTION

THE pyramidal XY_3 molecule is one which lends itself admirably to investigation by infrared spectroscopy. The model has been studied theoretically by Shaffer[1] and is known to have four distinct and different modes of vibration, two of which induce electrical moments parallel to the axis of symmetry and two others which induce electrical moments normal to the axis of symmetry. The latter two represent oscillations of the atomic nuclei in force fields which are two dimensionally isotropic and are, therefore, two-fold degenerate. The four modes of oscillation of this type of molecule are illustrated in Fig. 1, where they are identified using the notation of Herzberg. ν_1 and ν_2 are the parallel vibrations, ν_1 being the higher frequency; ν_3 and ν_4 are the perpendicular vibrations where ν_3 is the higher frequency.

Accompanying a parallel vibrational transition are transitions among the rotation levels governed by the selection rules $\Delta J=0, \pm1$; $\Delta K=0$; J and K being, respectively, the quantum numbers of total angular momentum and of the angular momentum directed along the axis of symmetry. These produce a series of sub-bands, a sub-band for each value of K (see, for example, G. Herzberg, *Infrared and Raman Spectra*, D. Van Nostrand Company Inc., New York, 1945, p. 418). The transitions $\Delta J=-1$, 0 and $+1$ give rise, respectively, to lines in the P, Q and R branches. The frequency interval between P lines and R lines permit the determination of $B^{(xx)}$, $B^{(xx)}$ being equal to $h/8\pi^2 I_{xx}c$, where I_{xx} is one of the two equal moments of inertia.

A perpendicular vibrational transition is accompanied by the rotational transitions $\Delta J=0, \pm1$; $\Delta K=\pm1$. These give rise, also here, to a series of overlapping, although not coincident, sub-bands; a sub-band for each value of K. The frequency interval between the Q branches (i.e., $\Delta J=0$) in one of the perpendicular bands ν_t permits the determination of $[(1-\zeta_t)B^{(zz)}-B^{(xx)}]$ where $B^{(zz)}=h/8\pi^2 I_{zz}c$, I_{zz} being the third moment of inertia and ζ_t being the Coriolis factor coupling the angular momentum associated with the frequency ν_t to the angular momentum of rotation of the molecule about its axis of symmetry. While the constant ζ_t depends in an involved manner upon the normal coordinates it may be shown[1,2] that $\zeta_3+\zeta_4=[(I_{zz}/2I_{xx})-1]$. This enables one to evaluate I_{xx} and I_{zz}, which, in turn, fixes the size and shape of the molecule.

An analysis of these bands in XH_3 molecule is not made without difficulty, however. This is so, particularly because ν_1 and ν_3 are almost completely superimposed and because ν_2 and ν_4 overlap and badly perturb each other. An alternative method which suggests itself is to analyze a parallel band, say ν_1, in the spectrum of XH_3 and a parallel band in the deuterium equivalent. The moments of inertia I_{xx} and I_{xx}^* may be evaluated from such an analysis, the asterisk referring to the isotopic molecule. One may then show that

$$(I_{xx}/I_{xx}^*)=(m/m^*)\left\{\frac{\frac{1}{2}\tan^2\beta+[M/(3m+M)]}{\frac{1}{2}\tan^2\beta+[M/(3m^*+M)]}\right\}, \quad (1)$$

where β is the angle between the altitude of the pyramid and an XH bond, m is the mass of H, m^* is the mass of D and M is the mass of X. Once β is determined, the altitude h may be evaluated from a knowledge of I_{zz}. This simple method is subject to the objection that β is extremely sensitive to the ratio (I_{xx}/I_{xx}^*). Thus, for example, in the case of the stibine molecule, if the angle β is to be real (i.e., lie between 0 and $\pi/2$) the ratio (I_{xx}/I_{xx}^*) must lie between the values 0.50037 and 0.51247. It will be seen that extremely accurate determination of the B values is required to yield a dependable value for β. It, therefore, becomes desirable to re-examine the method, referred to earlier, of an-

* This work was assisted by the Office of Naval Research under Contract No. N6onr-22526, NRO19-123 with Ohio State University.

[1] W. H. Shaffer, J. Chem. Phys. 9, 607 (1941).

[2] D. M. Dennison and M. Johnston, Phys. Rev. 47, 93, 868 (1935).

alyzing the four fundamental bands in the spectrum of the molecule.

II. THE TERM VALUES OF THE XH_3 MOLECULE

The term values evaluated by Shaffer[1] are valid as long as no resonances exist between vibration frequencies. Unfortunately, in virtually all pyramidal molecules of the XH_3 variety such resonances do exist and it becomes necessary to investigate what these are and how they will affect or modify the term values given in reference 1.

The only resonance interactions which can seriously affect the term values of the first excited states of the four fundamental modes of oscillation are the Coriolis interaction terms. The vibrations ω_1 and ω_2 are linked to the frequencies ω_3 and ω_4 by such interaction terms. These are introduced in the first-order Hamiltonian through the operator $\frac{1}{2}(p_x \pm ip_y)(P_x \pm iP_y)/I_{xx}$, where p_x and p_y are the x and y components of the incipient internal angular momentum resulting from oscillation and P_x and P_y are the x and y components of the angular momentum of the molecule. The operators $(p_x \pm ip_y)$ are of the form

$$(p_x \pm ip_y) = \sum_{s=1}^{2} \sum_{t=3}^{4} \zeta_{s,t}^{(x)} e^{\pm i\chi_t} \times \{(\omega_s/\omega_t)^{\frac{1}{2}} q_s [p_{rt} \pm (i/r_t) p_{\chi t}] - (\omega_t/\omega_s)^{\frac{1}{2}} r_t p_s\}, \quad (2)$$

where ω_s is a parallel normal frequency and ω_t is a perpendicular normal frequency. q_s and p_s in Eq. (2) are the normal coordinate and conjugate momentum associated with the normal frequency ω_s. r_t and χ_t in Eq. (2) are the polar equivalents of the normal coordinates associated with the doubly degenerate normal frequencies ω_t; p_{rt} and $p_{\chi t}$ are the corresponding momentum operators.

The interacting frequencies $\omega_1 : \omega_4$ and $\omega_2 : \omega_3$ are far separated from each other and their effect upon each other may satisfactorily be taken into account by the usual methods of the perturbation theory. The interacting frequencies ω_1 and ω_3 are, however, nearly coincident. One may, nevertheless, convince oneself that for XH_3 molecules, where the motions of the nuclei are essentially along the valence bonds, the factor $\zeta_{1,3}^{(x)}$ is very nearly equal to zero. Here also the effect may be taken into account by the usual methods of the perturbation theory. One may conclude from this that the term values stated by Shaffer are entirely valid for the first excited states of vibrations ω_1 and ω_3 and that the two bands ν_1 and ν_3 may be expected to show no anomalies in rotational structure. These may, therefore, be analyzed according to standard methods if the lines can be identified.

The interacting frequencies ω_2 and ω_4 are also near to each other in molecules of this kind. Moreover, the coefficient $\zeta_{2,4}^{(z)}$ is not nearly equal to zero so that the Coriolis resonance operator (2) becomes of first-order importance and must be treated by special methods.[3] The operator (2) will have elements in the energy matrix which are nondiagonal in the vibration quantum numbers V_2 and V_4, l_4 and in the rotation quantum number K. The nondiagonal elements of (2) which are of interest have been given by Nielsen[3] and are the following:

$$(V_s-1, V_t, l_t, K | H^{(1)}/hc | V_s, V_t-1, l_t \pm 1, K \pm 1) = -(V_s, V_t-1, l_t \pm 1, K \pm 1 | H^{(1)}/hc | V_s-1, V_t, l_t, K)$$
$$= \pm[(\omega_s+\omega_t)/\omega_s^{\frac{1}{2}}\omega_t^{\frac{1}{2}}][\zeta_{s,t}^{(z)} B_e^{(zz)}/2][V_s(V_t \mp l_t)]^{\frac{1}{2}}[(J \mp K)(J \pm K+1)]^{\frac{1}{2}}, \quad (3)$$

where l_t is the quantum number of angular momentum of vibration associated with the twofold degenerate vibration ω_4 and $|l_t|$ takes the values V_t, V_t-2, ...1 or 0.

The energy matrix will, therefore, to second order of approximation have elements only along the principal diagonal except where the quantum numbers V_2, V_4, l_4 and K are concerned. These elements may be grouped in such a manner that for any value of J all the elements involving these quantum numbers will lie about the principal diagonal, forming a submatrix which may be diagonalized by itself. This is accomplished by setting the determinant of the matrix equal to zero and solving for the roots.

The secular determinant for the energies of the two perturbing states $V_2=1$, $V_4=l_4=0$ and $V_2=0$, $V_4=1$, $l_4=\pm 1$ will have $3(2J+1)$ rows and columns, but breaks up into subdeterminants. The general subdeterminant will be of the following form:

	$V_t=1, l_t=1, V_s=0$ $K=K+1$	$V_t=l_t=0, V_s=1$ $K=K$	$V_t=1, l_t=-1, V_s=0$ $K=K-1$
$V_t=1, l_t=1, V_s=0$ $K=K+1$	$-K-1-\epsilon$	$[\frac{1}{2}(J-K)(J+K+1)]^{\frac{1}{2}}\alpha$	0
$V_t=l_t=0, V_s=1$ $K=K$	$[\frac{1}{2}(J-K)(J+K+1)]^{\frac{1}{2}}\alpha$	$\Delta-\epsilon$	$-[\frac{1}{2}(J+K)(J-K+1)]^{\frac{1}{2}}\alpha$,
$V_t=1, l_t=-1, V_s=0$ $K=K-1$	0	$-[\frac{1}{2}(J+K)(J-K+1)]^{\frac{1}{2}}\alpha$	$K-1-\epsilon$

(4)

[3] H. H. Nielsen, Revs. Modern Phys. 23, 132 (1951).

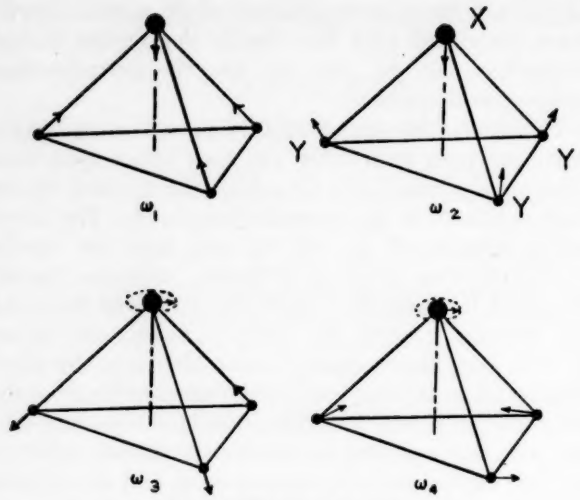

FIG. 1. The normal modes of oscillation for pyramidal XY_3 molecules.

where

$$\Delta=(-\delta/2\pi c)+(B_e^{(zz)}-B_e^{(xx)}),$$

$$\alpha=\{[(\omega_s+\omega_t)/(\omega_s\omega_t)^{\frac{1}{2}}]\zeta_{st}^{(x)}(B_e^{(xx)}/2)\}/[(1-\zeta_t^{(z)})B_e^{(zz)}-B_e^{(xx)}],$$

and

$$\epsilon=-\{T(V)+J(J+1)B_e^{(xx)}+(K^2-1)(B_e^{(zz)}-B_e^{(xx)})\}/2[(1-\zeta_t^{(z)})B_e^{(zz)}-B_e^{(xx)}],$$

with $\delta=(\omega_t-\omega_s)$ and $T(V)$ equal to the vibration term value. The value of $K-1$ may not exceed J; neither may $K+1$ be less than $-J$. Evidently, then there will be two identical single roots obtained by setting $K+1=-J$ and $K-1=J$ in Eq. (4); two identical subdeterminants of two rows and columns obtained by setting $K+1=-J+1$ and $K-1=J-1$ in Eq. (4) and $(2J-1)$ other subdeterminants of three rows and columns each. $J-1$ of the latter are repeated twice, and one (i.e., where $K+1=1$) is unique. This last instance of the above subdeterminant is of particular interest because it removes the degeneracy of the levels $K=l=\pm 1$.

Diagonalization of these submatrices is simple in principle, but rather difficult in practice. In general, the term values can be calculated only by the solution of a cubic equation and for this reason methods using combination relations are not particularly helpful. One may observe, however, that if the value of K in (4) is set equal to $J-1$ (i.e., $K+1=J$) two of the off diagonal elements reach their minimum value $\sqrt{J}$. This corresponds to the classical case where the molecule is rotating entirely about the axis of symmetry. Classically when $P_z=P$ and $P_x=P_y=0$. Correspondingly, $p_xP_x+p_yP_y$ should be zero and the perturbation would vanish. Quantum mechanically this is not quite so, but the perturbation is so small that the determinant of the submatrix may be expanded by a suitable method, for example, through continued fractions. Carrying this through the first term only, one obtains for the term value of the state where $K+1=J$:

$$E/hc\cong T(V)+J(J+1)B_e^{(xx)}+J^2(B_e^{(zz)}-B_e^{(xx)})-2\zeta_4B_e^{(zz)}[1-2(\zeta_{2,4}^{(x)})B_e^{(xx)2}/\zeta_4\delta B_e^{(zz)}], \quad (5)$$

where $\delta=\omega_4-\omega_2$. Expanding (4) in the same manner for $K=J-2$ (i.e., $K+1=J-1$) one obtains the slightly less rigorous expression for E/hc:

$$E/hc\cong T(V)+J(J+1)B_e^{(zz)}+(J-1)^2(B_e^{(zz)}-B_e^{(xx)})-2(J-1)\zeta_4B_e^{(xx)}[1-4(\zeta_{2,4}^{(x)})^2B_e^{(xx)2}/\zeta_4\delta B_e^{(xx)}]. \quad (5a)$$

The result of the perturbation may, evidently, be summarized by saying that the usual degenerate Coriolis coupling factor ζ_4 must be replaced by an effective factor which varies with K. The ${}^RR$ frequencies where the above term values are involved are readily shown to be

$$\nu=\nu_0+2JB_e^{(xx)}+2J[(1-\zeta_4)B_e^{(zz)}-B_e^{(xx)}]+4J(\zeta_{2,4}^{(x)})^2B_e^{(xx)2}/\delta \quad (6)$$

and

$$\nu=\nu_0+2JB_e^{(xx)}+2(J-1)[(1-\zeta_4)B_e^{(zz)}-B_e^{(xx)}]+4(2J-1)(\zeta_{2,4}^{(x)})^2B_e^{(xx)2}/\delta.$$

The interval between two lines $\nu(J+1,\ K+1=J+1)$ and $\nu(J,\ K=J)$ will then be equal to $2[(1-\zeta_4)B_e^{(zz)}+2(\zeta_{2,4}^{(x)})^2B_e^{(xx)2}/\delta]$ and between two lines $\nu(J+1,\ K+1=J)$ and $\nu(J,\ K=J-1)$ the spacing will be $2[(1-\zeta_4)B_e^{(zz)}+4(\zeta_{2,4}^{(x)})^2B_e^{(xx)2}/\delta]$. If, therefore, the lines indicated above can be identified the values the constants ζ_3, $\zeta_4B_e^{(xx)}$ and $(\zeta_{2,4}^{(x)})^2$ can all be determined. Recalling that the zeta-sum for this type of molecule is $\zeta_3+\zeta_4=[(B_e^{(xx)}/2B_e^{(zz)})-1]$ the value of $B_e^{(zz)}$ is also calculable. This determines the shape and size of the molecule.

The perturbation produces anomalies also in the structure of the parallel band ν_2. The anomaly manifests itself in the respect that it causes the sub-bands comprising the parallel band to be resolvable. In this instance, i.e., the first excited state of ν_2, it is the states where $K=0$ which are most readily studied. When K is set equal to zero the submatrix (4) factors into a single root and a double root. One of the double roots applies to the state ν_2 and, if one neglects the inversion doubling, leads to the term value

$$E/hc\approx T'(V)+(3\omega_4+\omega_2)/2+J(J+1)B_e^{(xx)}+[(\delta/2)^2+4(\zeta_{2,4}^{(x)})^2B_e^{(xx)2}J(J+1)]^{\frac{1}{2}}. \quad (7)$$

An expression for the frequency positions of the lines in the P branch of the sub-bands where $K=0$ may be derived from (7), remembering that $\Delta J=-1$ and $\Delta K=0$. It is the following:

$$\nu\cong(\omega_4+\omega_2/2)-2JB_e^{(xx)}-[(\delta/2)^2+4J(J+1)(\zeta_{2,4}^{(x)})^2B_e^{(xx)2}]^{\frac{1}{2}}. \quad (8)$$

Since $B_e^{(xx)}$ is already known these lines enable an independent check to be made on the value $\zeta_{2,4}^{(x)}$.

THE JOURNAL OF CHEMICAL PHYSICS VOLUME 21, NUMBER 1 JANUARY, 1953

Crystal Structure and Lattice Energy of Orthorhombic Hexachloroethane

YOSHIO SASADA AND MASAO ATOJI*
Faculty of Science, Osaka University, Nakanoshima, Osaka, Japan
(Received August 5, 1952)

As a part of an investigation of the crystal structures of hexachloroethane, the orthorhombic phase of hexachloroethane has been investigated by x-ray methods. The unit cell, of dimensions

$$a=11.56\text{A},\quad b=10.18\text{A},\quad \text{and}\quad c=6.42\text{A},$$

contains four molecules. The space group is $D_{2h}^{16}-Pnma$. The two- and three-dimensional Fourier series were calculated and atomic coordinates determined. Detailed discussions have been given for the lattice energy and molecular interaction of this crystal.

PART 1. CRYSTAL STRUCTURE OF ORTHORHOMBIC HEXACHLOROETHANE

Introduction

HEXACHLOROETHANE has three modifications as follows:

$$\text{orthorhombic} \underset{45.0^\circ\text{C}}{\rightleftarrows} \text{triclinic} \underset{71.4^\circ\text{C}}{\rightleftarrows} \text{cubic}.$$

In order to explain much of the thermal data for these transitions,[1,2] the authors have studied the crystal structure of each phase.[3] As a part of these investigations, the determination of the accurate atomic parameters of orthorhombic hexachloroethane has been carried out by x-ray methods.

In the electron diffraction study of gaseous hexachloroethane[4] it was pointed out that the valency angles $\angle$Cl−C−Cl in this molecule are somewhat smaller than the regular tetrahedral angle because of repulsion between chlorine atoms attached to different carbon atoms. It might be an interesting problem to compare these valency angles in the crystalline state with those in the gaseous state.

Early in 1927, K. Yardley (Lonsdale)[5] gave valuable suggestions on the crystal structures of a series of halogen derivatives of ethane including orthorhombic hexachloroethane, but the atomic parameters could not be obtained accurately. The crystal structure of orthorhombic hexabromoethane was reported by Snaauw and Wiebenga.[6] The result of our investigation shows that orthorhombic hexachloroethane is isostructural with the former, though the parameters of corresponding atoms have considerably different values.

Experimental

Hexachloroethane (Kahlbaum, A. G.), recrystallized from a mixture of alcohol and ether, has a melting point of 185°C. The crystal exhibits the planes {100}, {210}, {010}, and {111}, and, when viewed along the [010] direction, it presents a pseudohexagonal appearance.[5] Neither twinning, cleavage, nor etch-figures could be observed. These features may be understood from the arrangement of molecules in the crystal, described later. A crystal was sealed in a thin-walled capillary tube to prevent vaporization. Laue and oscillation photographs around the three principal axes were obtained using Cu−Kα radiation (at about 15°C). There is no noticeable diffuse scattering in Laue pictures. Oscillation photographs give

$$a=11.56\text{A},\quad b=10.18\text{A},\quad c=6.42\text{A}$$

and $a:b:c=1.136:1:0.6306$, in good agreement with Yardley's[5] and Groth's[7] results. Assuming four molecules per unit cell, the calculated density is 2.081 gcm^{-3}, which agrees well with the observed value of 2.091 gcm^{-3}. The possible space group is $D_{2h}^{16}-Pnma$ or $C_{2v}^{9}-Pna$. The relative intensities of reflections were visually estimated with the aid of calibrated scales and corrected for Lorentz, polarization, and absorption factors.

Atomic Arrangement

From the consideration of the molecular symmetry of hexachloroethane, which is undoubtedly $D_{3d}-\bar{3}m$,[8] and the molecular packing in this crystal together with Yardley's, and Snaauw and Wiebenga's investigations, an approximate structure was obtained. The refinement of atomic parameters was made by successive Fourier series methods. The final projections of electron density on [100] and [001] are given in Fig. 1 and Fig. 2, respectively. In order to obtain more accurate parameters, the three-dimensional Fourier syntheses in the planes of $(x, \frac{1}{4}, z)$ and $(x, \frac{1}{8}, z)$ were calculated by the following formulas (see Fig. 3).

---

* Present address: School of Chemistry, University of Minnesota, Minneapolis 14, Minnesota.

[1] K. J. Ivin and F. S. Dainton, Trans. Faraday Soc. **43**, 32 (1947).

[2] S. Seki and M. Momotani, Bull. Chem. Soc. Japan **23**, 30 (1950).

[3] A detailed discussion of the disordered structure of cubic hexachloroethane has been offered (T. Oda, M. Atoji, and T. Watanabé, The Second Congress of the International Union of Crystallography, 1951). The single crystal investigation of triclinic hexachloroethane is now in progress.

[4] Y. Morino and M. Kimura, J. Chem. Soc. Japan **68**, 78 (1947).

[5] K. Yardley, Proc. Roy. Soc. (London) **A118**, 449 (1928).

[6] G. J. Snaauw and E. H. Wiebenga, Rec. trav. Chim. **61**, 253 (1942).

[7] P. Groth, Chem. Krystallographie III, 38 (1908).

[8] For example: Y. Morino and M. Yuwasaki, J. Chem. Phys. **17**, 591 (1949).

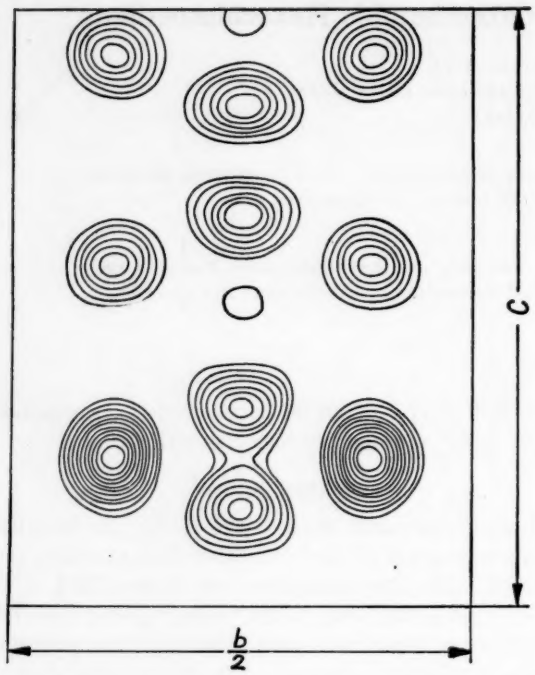

FIG. 1. Fourier projection on (100). Contours are drawn at equal intervals on an arbitrary scale.

$$\rho(x,\tfrac{1}{4},z)=1/V\sum_h\sum_k\sum_l F(hkl)[\cos 2\pi(hx+lz)\cos\tfrac{1}{2}\pi k - \sin 2\pi(hx+lz)\cos\tfrac{1}{2}\pi k],$$

$$\rho(x,\tfrac{1}{8},z)=1/V\sum_h\sum_k\sum_l F(hkl)[\cos 2\pi(hx+lz)\cos\tfrac{1}{4}\pi k - \sin 2\pi(hx+lz)\cos\tfrac{1}{4}\pi k].$$

The former plane includes the centers of two carbon atoms and two chlorine atoms, and the latter passes close to the centers of the other two chlorine atoms. The most probable values of the atomic parameters are listed in Table I.[9] The calculated structure factors using these parameters (which show $D_{2h}^{16}-Pnma$ symmetry) and the observed ones are given in Table II. In the calculated structure factors the effect of thermal motion is taken into account by applying a temperature factor, $\exp[-B(\sin\theta/\lambda)^2]$, where B is 3.7. The intramolecular distances and valency angles which show $D_{3d}-\bar{3}m$ symmetry within experimental errors are listed in Table III. The carbon to chlorine distances are in good agreement with those in gaseous hexachloroethane. The valency angles of the carbon atom are somewhat larger than those in the gaseous state. These values might be understood as the averaged effect of intermolecular forces in the crystalline field. The packing of the molecules and the intermolecular distances are shown in Figs. 4–6. From those figures, it will be seen that there are no remarkable cleavage planes in this crystal. The intermolecular Cl—Cl distances are 3.7–4.1A, which are larger than the ordinary van der Waals distance of 3.60A. The detailed discussion of intermolecular forces in orthorhombic hexachloroethane is given in the next part.

[9] Internationale Tabellen zur Bestimmung von Kristallstrukturen (Borntraeger, Berlin, 1935).

PART 2. LATTICE ENERGY OF ORTHORHOMBIC HEXACHLOROETHANE

Introduction

The transition phenomena occuring in crystalline hexachloroethane should be understood on the basis of the crystal structures and molecular interactions for each phase. In this part, the van der Waals attraction energy of orthorhombic hexachloroethane, the atomic structure of which has been accurately determined by the authors (Part 1), is estimated using the well-known expressions derived by Slater and Kirkwood,[10] Kirkwood,[11] London,[12] and Margenau.[13] The influence of repulsive forces calculated by the Lennard-Jones expression[14] and the electrostatic field resulting from the dipole moments are also considered. Discussions are given for the anisotropic interaction in the lattice from which we have attempted to explain the anisotropic volatility of this crystal pointed out by Yardley.[5]

Calculations of Attraction Energy

(a) *The Slater and Kirkwood Method*

In the first stage, we have used the approximate van der Waals force formula derived by Slater and Kirkwood,[10] and Kirkwood.[11]

$$E=-k\frac{Neh}{\sqrt{m}}\left\{(n_1\alpha_1^3)^{\frac{1}{4}}\sum\frac{1}{R_1^6}+\frac{2\alpha_1\alpha_2}{\left(\frac{\alpha_1}{n_1}\right)^{\frac{1}{2}}+\left(\frac{\alpha_2}{n_2}\right)^{\frac{1}{2}}}\times\sum\frac{1}{R_{12}^6}+(n_2\alpha_2^3)^{\frac{1}{4}}\sum\frac{1}{R_2^6}\right\},$$

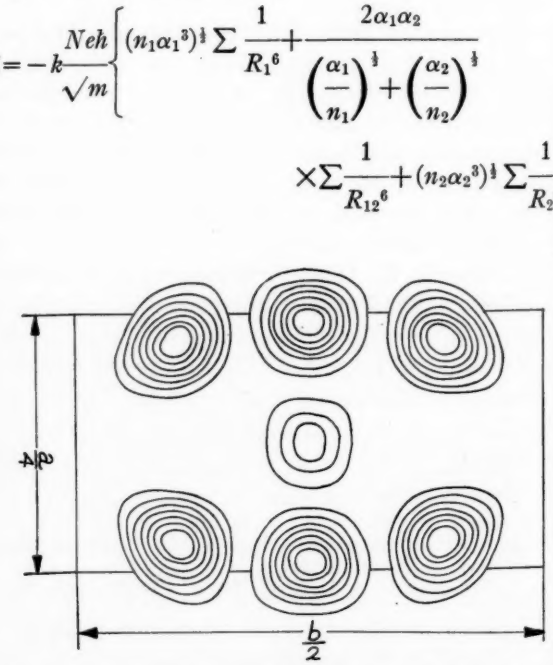

FIG. 2. Fourier projection on (001). Contours are drawn at equal intervals on an arbitrary scale.

[10] J. Slater and J. G. Kirkwood, Phys. Rev. **37**, 682 (1931).
[11] J. G. Kirkwood, Physik Z. **33**, 57 (1932).
[12] F. London, Z. physik Chem. **B11**, 222 (1930).
[13] H. Margenau, Phys. Rev. **38**, 747 (1931).
[14] J. E. Lennard-Jones, Proc. Roy. Soc. (London) **A106**, 463 (1924).

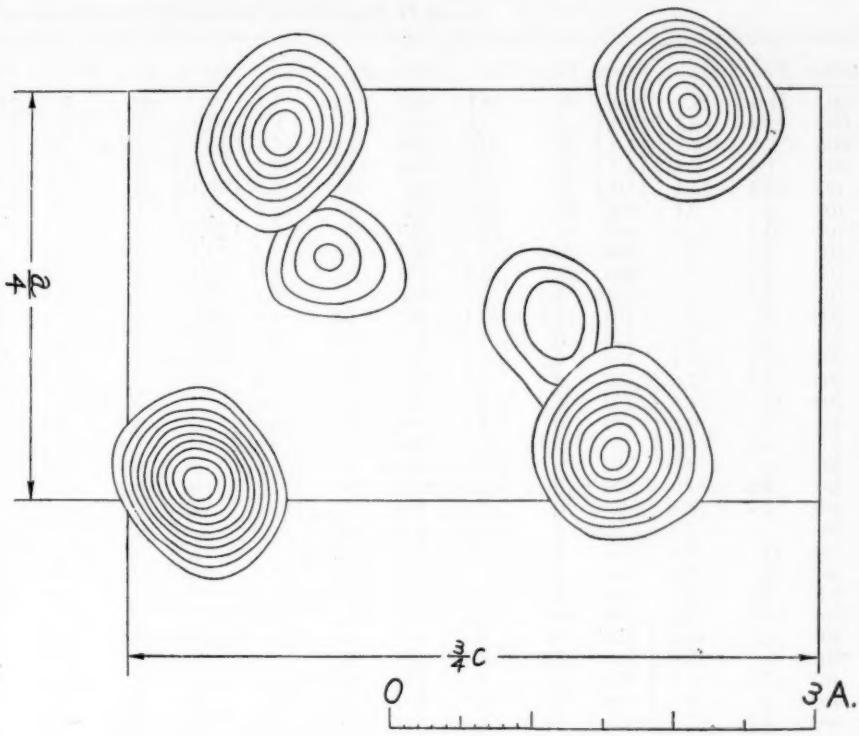

FIG. 3. Composite three-dimensional Fourier sections, $\rho(x, \frac{1}{4}, z)$ and $\rho(x, \frac{3}{4}, z)$. Contours are drawn at equal intervals on an arbitrary scale.

where k is 0.68 and 0.75 for Slater and Kirkwood's, and Kirkwood's expressions, respectively; N is Avogadro's or Loschmidt's number; $\hbar = h/2\pi$; m is the mass of an electron; n the number of electrons in the outermost electronic shell of the atom under consideration; α is the polarizability of the atom or atomic group; R's are the distances from one center of force to all the others in the lattice, and suffixes 1 and 2 denote the two kinds of centers.

The summation is taken over a sphere with its center on a molecule and a radius of about 10A (about 2000 terms). For the contribution of the outer part, the summation is replaced by integration. Since the latter contribution is only 0.4 percent of the total, it will be seen that the number of terms taken for summation is sufficient. In the present case, use is made of the two modes of division to get the center of forces as discussed by Müller,[15] and Nitta and Seki.[16] The two modes are

(1) The centers of force are placed on the nuclei of the chlorine and carbon atoms.
(2) Each C−C and Cl−Cl bond is taken as a whole and the centers of force are placed on the scattering centers (electronic center of gravity considering the polarizability of each atom), that is, at the middle point of the C−C bond and at a point 0.17A from the chlorine of the C−Cl bond for which the weighting factor of $\frac{1}{4}$ is taken for the carbon.

Next, we shall proceed with the estimation of the polarizability. For orthorhombic hexachloroethane, the anisotropy and the dispersion of the refractive index is not reported. However, for the purpose of calculating lattice energies of molecular crystals, the polarizability may be estimated from the refractive index of the liquid.[17] Making use of the refractive indices of liquid halogenated ethanes for $H\alpha$, $H\beta$, $H\gamma$, and $Na-D$ lines and Cauchy's dispersion formula, the refractive indices corresponding to infinite wavelength are obtained by extrapolation. From these results and the Lorenz and Lorentz equation we have obtained the molecular refraction of each compound (see Table IV). On the other hand, the atomic or bond refractivity of carbon, hydrogen, C−C and C−H bond in the saturated aliphatic compounds are 2.3808 cc,[18] 1.0696 cc,[18] 1.185 cc[19] and 1.663 cc,[19] respectively. Assuming atomic and bond refractivities to be additive, we can find the atomic refractivity of a chlorine attached to an aliphatic carbon

TABLE I.[a] Atomic coordinates.

	x	y	z
$4C_1(c)$	0.111	0.250	−0.212
$4C_2(c)$	0.139	0.250	0.023
$4Cl_1(c)$	0.246	0.250	−0.360
$4Cl_2(c)$	0.008	0.250	0.168
$8Cl_3(d)$	0.030	0.393	−0.278
$8Cl_4(d)$	0.221	0.108	0.086

[a] See reference 9.

[15] A. Müller, Proc. Roy. Soc. (London) **A154**, 624 (1936).
[16] I. Nitta and S. Seki, J. Chem. Soc. Japan **64**, 475 (1943).
[17] S. Seki and H. Chihara, Sci. Papers Osaka Imp. Univ. No. 1 (1949).
[18] F. Eisenlohr, Z. physik Chem. **75**, 585 (1910); **79**, 129 (1912).
[19] K. Fajans and C. A. Knorr, Ber. deut. chem. Ges. **59**, 256 (1926).

TABLE II. Observed and calculated structure factors.

Indices	F_{obs}	F_{calc}	Indices	F_{obs}	F_{calc}	Indices	F_{obs}	F_{calc}	Indices	F_{obs}	F_{calc}	Indices	F_{obs}	F_{calc}	Indices	F_{obs}	F_{calc}
002	11.9	−18.7	12,0,0	0	−2.7	037	0	3.2	915	0	0.5	11,2,2	0.7	−1.9	144	7.7	7.2
004	2.9	−4.3	12,0,1	2.1	3.8	042	0	1.1	10,1,1	5.6	−6.2	11,2,3	0	3.5	145	11.7	9.3
006	3.1	−4.1	12,0,2	0	0.2	044	7.8	−7.1	10,1,2	2.4	2.9	11,2,4	0	0.2	146	4.2	2.5
101	7.0	9.8	12,0,3	0	−0.2	046	14.1	11.3	10,1,3	0	−1.2	12,2,1	0	2.9	241	0	−0.7
102	22.4	−32.1	13,0,1	0	2.7	051	0	−0.5	10,1,4	0	0.8	12,2,2	0	1.5	242	13.0	14.6
103	0	0.4	020	18.2	−24.6	053	4.1	6.1	11,1,1	1.1	−3.0	12,2,3	0	0.8	243	6.4	6.2
104	10.2	−7.4	040	11.2	−10.5	055	0	0.8	11,1,2	2.0	3.2	13,2,1	0	0.7	244	9.6	−8.6
105	3.6	−4.5	060	28.0	−32.2	062	5.6	7.3	11,1,3	3.2	2.0	131	12.1	−19.5	245	0	0.9
106	2.1	2.3	080	23.3	22.4	064	0	3.0	11,1,4	2.2	2.2	132	0	−0.2	246	0	−1.1
107	4.2	3.9	0,10,0	4.0	3.2	066	0	0.3	12,1,1	0	−1.5	133	4.0	5.7	341	9.7	11.5
200	0	0	210	18.1	−24.4	071	6.8	−5.4	12,1,2	4.7	4.1	134	0	1.1	342	0	−1.0
201	6.9	8.2	220	0	0.2	073	15.4	14.1	12,1,3	0	2.3	135	11.2	10.0	343	12.2	−11.9
202	21.9	−32.1	230	6.3	−5.7	075	0	−0.6	13,1,1	0	2.3	136	4.2	−4.5	344	12.3	10.8
203	13.6	−12.6	240	0	0.3	082	5.6	4.8	121	5.3	−8.5	137	0	0.1	345	0	1.8
204	18.5	17.3	250	6.8	−2.9	084	0	−2.4	122	5.7	6.1	231	15.3	41.7	346	0	0.7
205	0	0.3	260	0	−0.3	091	0	−0.6	123	8.1	8.8	232	1.5	2.3	441	13.3	−15.1
206	4.4	4.3	270	15.3	11.1	093	0	2.7	124	3.1	−2.8	233	4.5	4.7	442	0	−0.7
207	0	−0.2	280	0	−0.3	0,10,2	0	−0.5	125	5.6	−5.2	234	0	0	443	0	1.6
301	9.0	−10.0	290	0	−1.4	0,11,1	0	1.5	126	2.1	−2.7	235	0	−0.2	444	11.4	−8.1
302	17.3	19.4	2,10,0	0	0.1	111	5.9	−9.7	127	0	0.1	236	3.1	3.5	445	0	2.6
303	3.3	−2.7	2,11,0	0	1.4	112	10.2	−16.3	221	0	−1.9	237	0	−1.6	446	10.2	7.7
304	11.4	9.3	410	0	0.3	113	7.7	−7.8	222	1.5	−1.6	331	13.4	21.9	541	5.0	−5.8
305	0	−0.6	420	9.2	−7.7	114	9.2	7.7	223	0	−0.5	332	8.9	7.5	542	2.4	2.1
306	5.5	−5.7	430	0	−0.8	115	1.8	3.1	224	0	0.5	333	9.5	−10.3	543	4.6	−5.3
307	5.0	6.2	440	12.4	8.8	116	2.3	−3.1	225	0	0.6	334	0	3.8	544	3.8	2.9
400	52.1	46.7	450	0	0.1	117	6.2	3.8	226	1.6	−0.4	335	0	−2.2	545	6.5	7.3
401	16.3	18.0	460	18.0	−18.2	211	0	2.1	227	0	0.6	336	2.4	−3.4	546	4.8	4.3
402	12.7	−11.6	470	0	0	212	2.6	2.8	321	5.7	−6.2	337	0	−2.2	641	6.8	−5.1
403	0	0	480	12.6	13.1	213	2.3	−2.3	322	6.8	−5.8	431	7.5	7.5	642	8.6	5.2
404	8.9	−7.3	490	0	0.4	214	0	−1.5	323	9.5	10.1	432	9.7	10.8	643	12.9	15.0
405	7.6	7.6	4,10,0	0	2.7	215	15.3	13.3	324	4.9	4.9	433	15.7	−18.8	644	0	−2.1
406	2.2	−2.3	4,11,0	0	−0.1	216	0	1.2	325	0	−1.2	434	7.2	−6.9	645	0	1.1
407	2.9	−2.5	610	21.1	−18.2	217	3.4	−3.7	326	2.6	1.4	435	0	1.1	646	0	0.2
501	12.1	10.9	620	0	−0.3	311	0.1	1.6	327	0	−0.2	436	0	−1.4	741	11.8	12.5
502	19.5	−20.3	630	21.5	−19.2	312	4.6	−4.2	421	7.3	6.5	531	10.4	−10.1	742	3.2	2.8
503	1.9	−0.7	640	0	0.5	313	6.7	4.7	422	5.7	4.3	532	0	−2.5	743	5.2	−5.5
504	3.8	3.7	650	1.5	2.9	314	13.2	12.3	423	0	1.0	533	0.6	−1.3	744	4.6	−4.3
505	5.2	−7.2	660	0	0	315	2.4	−2.1	424	11.2	8.6	534	7.4	−5.9	745	0	−1.5
506	0	−1.0	670	14.5	14.6	316	3.7	−3.4	425	0	−0.7	535	7.1	7.4	841	14.6	−15.4
600	0	−0.4	680	0	−0.2	317	4.2	−4.7	426	6.7	−5.0	536	0	−1.9	842	2.7	−2.4
601	5.9	5.2	690	1.8	1.2	411	1.4	1.0	427	0	−0.4	631	15.5	17.9	843	0	−1.4
602	10.2	−8.5	6,10,0	0	−0.1	412	11.4	11.8	521	1.4	0.8	632	3.8	3.1	844	4.7	−2.9
603	13.9	−15.7	810	0	0.6	413	7.1	−6.5	522	7.5	5.2	633	0	2.6	845	0	−2.6
604	6.9	6.9	820	13.6	−10.5	414	8.1	−6.3	523	4.7	4.2	634	5.5	−4.3	941	4.0	−5.2
605	1.9	1.2	830	0	−1.1	415	0	0.6	524	4.1	−3.3	635	0	−2.2	942	2.5	−2.6
606	1.6	2.4	840	6.7	8.0	416	0	−1.1	525	2.6	−2.9	636	4.5	5.8	943	3.4	−1.1
701	4.2	−4.7	850	0	0.2	417	0	−1.1	526	2.0	−2.9	731	8.2	7.7	944	0	−1.6
702	2.1	1.9	860	5.8	−8.1	511	2.2	2.1	621	3.7	2.3	732	9.2	8.9	10,4,1	2.5	−1.9
703	3.6	−3.6	870	0	−0.3	512	13.4	−16.9	622	0.6	−1.1	733	6.5	−8.1	10,4,2	1.0	−3.7
704	7.7	7.3	880	9.4	5.7	513	6.5	−5.4	623	8.5	−5.8	734	0	4.1	10,4,3	7.9	8.0
705	2.9	5.5	890	0	0.4	514	3.2	4.0	624	0	−0.8	735	0	1.4	10,4,4	0	1.9
706	4.6	−5.6	10,1,0	13.1	14.0	515	2.9	4.5	625	0	0.4	736	0	0	11,4,1	4.4	4.6
800	15.3	13.4	10,2,0	0	−0.4	516	0.6	−1.2	626	0	−1.0	831	0	−0.9	11,4,2	2.6	3.7
801	11.9	11.0	10,3,0	4.9	7.1	611	6.7	−6.2	721	8.7	−7.8	832	11.0	11.4	11,4,3	0	−2.5
802	3.1	−3.0	10,4,0	0	0.6	612	5.6	4.9	722	3.8	−2.8	833	0	−2.0	12,4,1	4.4	−5.8
803	0	0.4	10,5,0	0	−1.3	613	0	−1.4	723	3.7	5.3	834	4.2	−6.1	12,4,2	0	−2.1
804	1.7	−3.4	10,6,0	0	0	614	0	2.2	724	0	0.7	835	0	0.2	151	6.2	7.0
805	4.8	6.8	10,7,0	10.4	10.7	615	8.6	7.0	725	2.4	−0.8	931	0	1.3	152	0	−4.3
806	0	2.2	10,8,0	0	0	616	0	2.9	726	2.9	1.2	932	0.8	−1.2	153	4.0	−4.8
901	8.3	8.5	12,1,0	0	0	711	0	−0.8	821	8.4	7.7	933	0	−1.2	154	0	2.0
902	7.9	−7.5	12,2,0	4.3	4.4	712	2.4	2.8	822	3.2	2.8	934	3.9	−6.1	155	4.8	−3.7
903	2.9	−2.8	12,3,0	0	−0.1	713	0	1.9	823	0	0.8	935	3.1	3.7	156	0	1.0
904	3.8	5.6	12,4,0	5.2	7.2	714	4.0	6.4	824	2.6	3.1	10,3,1	0	1.3	251	15.0	−16.0
905	1.3	−1.6	12,5,0	0	0.1	715	0	2.7	825	0	−0.4	10,3,2	0.7	1.4	252	0	−0.1
10,0,0	0	−0.2	011	5.0	10.7	716	0	−1.9	921	0	0.9	10,3,3	0	1.2	253	2.6	−3.1
10,0,1	4.1	3.8	013	13.4	−17.3	811	0	1.1	922	5.9	4.5	10,3,4	0	1.9	254	0	−0.6
10,0,2	0	0.5	015	0	0.4	812	8.7	7.4	923	0	1.7	11,3,1	1.0	1.1	255	7.5	4.4
10,0,3	8.5	−10.0	017	2.1	−1.8	813	0	0.1	924	0	−0.7	11,3,2	2.6	4.3	256	0	−1.2
10,0,4	0	−1.0	022	4.9	4.7	814	5.8	−6.3	925	0	−2.5	11,3,3	2.7	−4.5	351	10.4	−8.5
10,0,5	0	0.3	024	9.4	6.9	815	0	−0.3	10,2,1	0	0.2	12,3,1	0	−0.8	352	2.7	−4.6
11,0,1	0	−2.3	026	9.5	7.1	911	0	1.7	10,2,2	0	2.6	12,3,2	0	2.9	353	6.6	6.0
11,0,2	1.6	−2.5	031	5.6	7.9	912	8.4	−9.0	10,2,3	2.0	−2.5	141	6.1	6.3	354	2.8	2.2
11,0,3	4.6	−4.9	033	15.7	−25.1	913	5.5	−4.0	10,2,4	0	−1.0	142	5.9	5.3	355	0	0.5
11,0,4	0	0.9	035	0	2.3	914	0	−0.9	11,2,1	1.0	−2.6	143	11.9	−11.3	356	0	0.4

TABLE II.—*Continued.*

Indices	F_{obs}	F_{calc}	Indices	F_{obs}	F_{calc}	Indices	F_{obs}	F_{calc}	Indices	F_{obs}	F_{calc}	Indices	F_{obs}	F_{calc}	Indices	F_{obs}	F_{calc}
451	3.1	−2.5	165	0	0.9	961	2.7	−3.5	575	2.6	−4.2	484	4.4	−3.6	592	0.7	−2.2
452	2.3	−1.3	166	0	−1.6	962	6.2	4.3	671	0	1.4	581	0	3.1	593	2.1	−0.6
453	6.9	6.5	261	2.6	−2.7	10,6,1	0	−1.7	672	4.7	−3.7	582	7.8	−6.8	691	2.3	−4.8
454	0	1.1	262	12.3	11.1	10,6,2	0	0.3	771	0	−0.6	583	0	−0.8	692	0	0
455	0	−0.2	263	4.4	4.8	11,6,1	0	0.4	772	3.8	−3.2	584	0	1.6	791	0	−1.8
456	0	0.4	264	6.8	−7.4	171	8.3	6.4	871	0	−0.6	681	0	1.1	792	0	−1.4
551	6.1	4.9	265	0	0	172	9.5	8.9	872	8.3	−6.8	682	3.4	−2.5	891	0	0.4
552	5.1	−3.9	266	0	−2.0	173	3.6	4.0	971	0	−1.3	781	0	−0.5	1,10,1	0	−1.9
553	0	−1.2	361	2.2	2.0	174	6.2	−5.4	972	5.0	6.4	782	0	1.0	1,10,2	0	−1.6
554	0	4.7	362	8.3	−8.2	175	2.7	−3.6	10,7,1	4.0	4.0	881	3.6	2.4	1,10,3	3.1	4.0
555	3.2	−2.0	363	3.4	3.1	271	9.0	−6.1	10,7,2	0	−2.2	882	0	−1.3	2,10,1	0	0.4
556	0	0.4	364	2.3	−3.0	272	0	−1.9	181	0	2.7	981	0	2.6	2,10,2	7.1	−4.8
651	13.1	−9.9	365	0	0.1	273	0	0.8	182	10.8	−8.7	191	0	2.4	2,10,3	0	−2.1
652	0	0.4	461	7.5	−5.3	274	0	1.0	183	0	−1.1	192	0	−2.1	3,10,1	2.7	−4.2
751	5.8	−3.7	462	4.9	5.5	275	12.8	−9.1	184	0	−2.0	193	4.0	−2.3	3,10,2	1.0	0.2
752	0	−3.3	463	0	0.4	371	4.5	−3.8	185	0	−0.6	194	0	0.9	3,10,3	4.5	4.2
851	0	0.8	464	3.4	4.9	372	0	1.4	281	0	1.7	291	5.2	−7.4	4,10,1	5.5	5.0
852	0	−2.8	465	4.4	−3.5	373	0	−1.6	282	9.8	−7.9	292	0	−0.1	4,10,2	0	0.2
951	0	0	561	5.3	−4.1	374	10.5	−9.0	283	0	−3.5	293	0	−1.1	4,10,3	0	0.5
952	2.0	−2.3	562	8.1	9.4	375	0	1.8	284	7.1	5.3	294	2.5	−0.2	5,10,1	0.7	1.9
10,5,1	3.1	−2.6	563	1.8	1.1	471	2.3	−1.7	285	0	0	391	3.0	−3.8	5,10,2	0	−0.7
10,5,2	0	0.4	564	0	−2.4	472	10.4	−8.7	381	0	−1.6	392	3.1	−2.0	6,10,1	0	1.9
11,5,1	0	−1.4	565	0	2.5	473	7.0	7.1	382	6.6	6.0	393	0	3.0	1,11,1	2.9	−4.1
11,5,2	0	−1.0	661	0	−1.9	474	7.0	5.4	383	0	−2.2	394	0	1.2	1,11,2	0	−0.1
12,5,1	0	−0.2	662	2.8	3.4	475	0	−0.6	384	2.3	2.3	491	0	−1.5	2,11,1	8.5	8.6
161	5.9	−3.9	761	0	0.3	571	0	0.2	385	0	0	492	0	−0.5	2,11,2	0	0.5
162	10.8	12.0	762	2.9	−1.4	572	10.8	11.3	481	2.9	3.8	493	0	3.0	3,11,1	4.6	4.7
163	0	1.5	861	2.9	−3.3	573	4.4	3.8	482	3.8	−3.7	494	0	0.5			
164	0	2.5	862	0	1.9	574	2.4	−1.7	483	0	0	591	0.6	2.3			

and a C—Cl bond refractivity for each compound. It will be seen that the assumption of additivity of the refractivities is reasonable. This is shown in Table IV. From the averaged value of each refractivity, the polarizabilities could be obtained using the Lorenz and Lorentz equation (Table V).

The final results for the attraction energy together with the estimations of summation terms are shown in Table VI. The observed sublimation energy is 14.1 kcal mole^{-1}.[20] However, the calculated values are in the range 18.61–22.05 kcal mole^{-1}. This agreement is not so good, if the dipole-quadrupole interactions, the repulsion, and the electrostatic energy described later are taken into consideration. As already pointed out,[12,15] it is very difficult to estimate how reliable this method is, especially with regard to n (the number of electrons in the outermost electronic shell of the atom). No previous estimation of the lattice energies of molecular crystals containing chlorine atoms has been reported, but we may say for the chlorine in hexachloroethane that "n" in the Slater and Kirkwood expression is probably too large. Deitz[21] has concluded empirically that for halogens $n=4$ might give a good value in the case of the lattice energies of alkali halides. In the present case, the lattice energy corresponding to $n=4$ is 15.43 kcal mole^{-1} for Slater and Kirkwood's method, 17.02 kcal mole^{-1} for Kirkwood's method, which applies to the first mode of division. This value is closer to the observed value of 14.1 kcal mole^{-1}.

[20] I. Nitta and S. Seki, J. Chem. Soc. Japan **62**, 581 (1941).
[21] V. Deitz, J. Franklin Inst. **219**, 459 (1935).

(b) *London's Method*

London[12] has given an approximate expression for the van der Waals energy considering only dipole-dipole interaction.

$$E=-\tfrac{3}{4}Nh\left[\frac{\alpha_1^2\nu_1}{2}\sum\frac{1}{R_1^6}+\frac{\nu_1\nu_2}{\nu_1+\nu_2}\alpha_1\alpha_2\sum\frac{1}{R_{12}^6}+\frac{\alpha_2^2\nu_2}{2}\sum\frac{1}{R_2^6}\right],$$

where $h\nu$ is a characteristic amount of energy corresponding to the principal specific frequency, ν, which is taken from the dispersion equation of the particle in question, or is approximately equal to the ionization energy.

In our evaluation of London's method the first ionization energy of chlorine and carbon has been used

TABLE III. The molecular dimensions of hexachloroethane in the crystalline state compared with those in the gaseous state.

	Crystal	Gas
C_1-C_2	1.54A	1.54A (assumed)
C_1-Cl_1	1.76A	1.77A
C_1-Cl_3	1.76A	
C_2-Cl_2	1.77A	
C_2-Cl_4	1.77A	
$\angle Cl_1C_1Cl_3$	109.5°	109°
$\angle Cl_2C_1Cl_3$	111.5°	
$\angle Cl_2C_2Cl_4$	109.5°	
$\angle Cl_4C_2Cl_4$	109.0°	

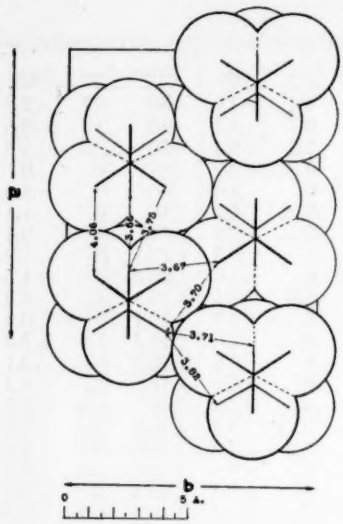

FIG. 4. Molecular arrangement projected on (001) and intermolecular distances (in A).

instead of the principal specific frequency. The final values are listed in Table VII. The agreement between the calculated and observed lattice energies shows that London's first approximation method using the first ionization potential of each atom in the molecule is useful to get the order of magnitude of the lattice energy of the molecular crystal. These suggestions are confirmed by the calculation shown in Table VIII which includes the theoretical and observed lattice energies of AX_4-type molecular crystals.[16,22]

In both London's, and the Slater and Kirkwood methods, a similar assumption is made, that is, each molecule in the crystal is separated into spherical atoms. Generally speaking, it will be seen that the observed value lies in the range between the results of the two methods and that the Slater and Kirkwood method gives higher values than London's method.

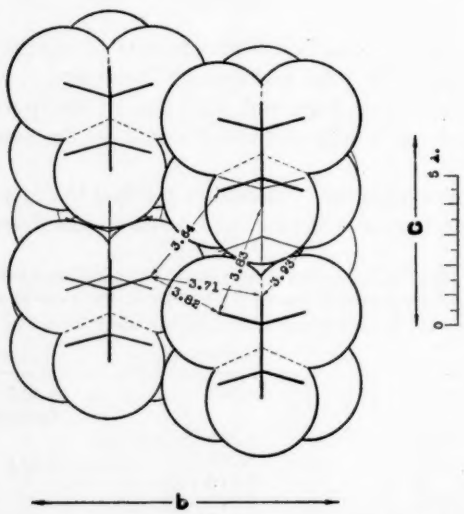

FIG. 5. Molecular arrangement projected on (100) and interatomic distances (in A).

[22] S. Seki, J. Chem. Soc. Japan 62, 789 (1941).

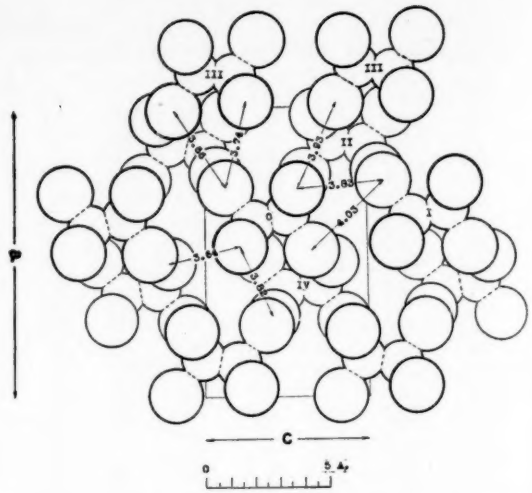

FIG. 6. View of molecular arrangement projected on (010) showing pseudohexagonal appearance. The intermolecular distances are also shown in A. Numbers expressed by Roman numerals are given for the discussion of anisotropy of molecular interaction.

(c) *Margenau's Term*

For the second approximation to the van der Waals force, Margenau[13] has given a formula of the dipole-quadrupole interaction as follows:

$$E=-15/8N\alpha^3(h\nu/\epsilon)^2\sum 1/R^8.$$

The estimation of this term has been limited to the chlorine chlorine interactions, because the magnitude of the other contributions was less than about 3 percent of the former contribution. The result of the summation, which is taken over a sphere with a radius of 10A, is

$$\sum 1/R^8=12.35\times10^{-4}\text{A}^{-8} \text{ for Cl}-\text{Cl},$$

which includes the integration part of $0.05\times10^{-4}\text{A}^{-8}$. When the first ionization potential of chlorine (12.90 ev) is used, we can get 7.44 kcal mole^{-1} as an energy of dipole-quadrupole interactions. When the first ionization energy of C_2H_5Cl is used, Margenau's term becomes 5.26 kcal mole^{-1} which may be taken as a lower limit, approximately, because the ionization potential of the similar compounds $CHCl_3$, CH_3Cl, and C_2H_5Cl are 11.5 ev,[23] 11.17 ev,[23] and 10.79 ev,[24] respectively.

TABLE IV.

Substance	Molecular refractivity	Difference	Atomic ref. of chlorine bonded to carbon	C—Cl bond refractivity
C_2HCl_5	34.84_3		5.802	6.39_9
		4.765		
$C_2H_2Cl_4$	30.07_8		5.794	6.39_2
		4.705		
$C_2H_3Cl_3$	25.37_3		5.801	6.39_9
		4.734		
$C_2H_4Cl_2$	20.63_9		5.800	6.40_1
		Average: 4.735	5.799	6.39_8

[23] W. C. Price, J. Chem. Phys. 4, 539 (1936).
[24] W. C. Price, J. Chem. Phys. 3, 365 (1935).

TABLE V. The atomic and bond polarizabilities.

Carbon;	0.9437×10^{-24} cc
Chlorine;	2.299×10^{-24} cc
C−Cl bond;	2.536×10^{-24} cc
C−C bond;	0.4697×10^{-24} cc

Energy of Repulsion

Born and Mayer[25] have expressed the repulsive force, which results from the quantum mechanical kinetics of elementary charges, as an exponential function. However, their equation involves the compressibility as well as the thermal expansion coefficient, neither of which has been reported for the present case. Therefore, we have used Morino and Miyagawa's[26] experimental formula for the Cl−Cl interaction, which is of the Lennard-Jones type[14] as follows:

$$E=-N/2\sum \chi/R^{12} \quad \text{with} \quad \chi=1.620\times10^{-7}\ \text{erg A}^{12}.$$

The summation was done over a sphere with a radius of 8A and gave 5.278×10^{-6} A^{-12}. The repulsive energy becomes 6.15 kcal mole^{-1}. As already pointed out,[17] the repulsive energy (6.15 kcal mole^{-1}) is almost equal to the Margenau energy (7.44–5.26 kcal mole^{-1}).

Electrostatic Energy

Hexachloroethane has C−Cl dipoles compensating each other. Their moment has been reported by Smyth[27] as $\mu=1.56$ Debye units. Sponer and Willstätter[28] have pointed out that the charge distribution is much better described assuming a model consisting of point charges rather than dipoles. We have represented it in a very simplified way by means of an expression like

$$N/2\sum\sum e_i^*e_j^*/R_{ij},$$

where e^*'s are the formal charge of the dipoles: $-\mu/d=e^*$, where the bond distance $d=1.76$A. We have taken the chlorine atoms as the centers of the negative charges and the carbon atoms as the centers of the positive charges. These assumptions are not strictly true, but the order of magnitude of the electrostatic energy may be evaluated in this manner. The summation over the electrostatic terms gives a repulsive energy of only 0.3 kcal mole^{-1}. In the case of crystalline carbon dioxide,[28] the electrostatic energy was estimated to be 0.1–0.5 kcal mole^{-1}. These results show that in molecular crystal electrostatic forces should not produce large energy, when compared to the other terms which constitute the total energy.

TABLE VI. The results of the summations[a] are classified by the modes of subdivision. The R's are measured in A. The second row in each section shows the magnitude of the contribution to the total energy. The third row shows the lattice energy using Slater and Kirkwood's expression. The values estimated by Kirkwood's expression are put in parentheses.

(1) First mode of division. Centers are nuclei of chlorines and carbons.

$\Sigma 1/R_1^6$: Cl−Cl	$\Sigma 1/R_{12}^6$: Cl−C	$\Sigma 1/R_2^6$: C−C
22376.6×10^{-6}	8677.5×10^{-6}	933.0×10^{-6}
$E_{1a}=-16.94$ (−18.68)	$E_{1b}=-2.919$ (−3.219)	$E_{1c}=-0.141$ (−0.155)

$E_1=E_{1a}+E_{1b}+E_{1c}=-20.00$ kcal mole^{-1} (−22.05 kcal mole^{-1}).

(2) Second mode of division. Centers are placed on the center of scattering of C−Cl and C−C bonds.

$\Sigma 1/R_1^6$: CCl−CCl	$\Sigma 1/R_{12}^6$: CCl−CC	$\Sigma 1/R_2^6$: CC−CC
19086.9×10^{-6}	3734.7×10^{-6}	203.5×10^{-6}
$E_{2a}=-17.90$ (−19.74)	$E_{2b}=-0.697$ (−0.769)	$E_{2c}=-0.007$ (−0.008)

$E_2=E_{2a}+E_{2b}+E_{2c}=-18.61$ kcal mole^{-1} (−20.52 kcal mole^{-1}).

[a] The small contribution evaluated by integration is included.

TABLE VII. London's method.

First ionization potential[a] of chlorine atom	12.90 ev
First ionization potential of carbon atom	11.27 ev
Energy contribution of Cl−Cl interactions	−13.10 kcal mole^{-1}
Energy contribution of Cl−C interactions	−1.94 kcal mole^{-1}
Energy contribution of C−C interactions	−0.08 kcal mole^{-1}
Total energy	−15.12 kcal mole^{-1}
Observed value	−14.1 kcal mole^{-1}

[a] Landolt-Börnstein, *Zahlenwerte und Funktionen*, "Atom und Molekular Physik," 1 Band, Tabellen, 6 Auflage, 1 Teil, p. 211 (Springer-Verlag, Berlin, 1950).

Anisotropic Volatility

By measuring the variation in the intensities of the x-rays diffracted from particular crystal planes, Yardley[5] has reported the anisotropic volatility of orthorhombic

TABLE VIII. Comparison of Slater and Kirkwood's, and London's methods.

Crystal	Observed value (kcal mole^{-1})	Slater and Kirkwood (kcal mole^{-1})	London (kcal mole^{-1})	First ionization potential (ev)
$TiBr_4$	14.9	16.41	14.27[a]	Ti 6.84 Br 11.76
$PSBr_3$	14.6	15.01	12.92[a]	P 10.9 S 10.36 Br 11.76
CHI_3	16.7	18.37	15.27[a]	C 11.27 H 13.59 I 10.44
I_2	14.6	15.5	14.1	I 9.76[b]
C_2Cl_6	14.1	18.61*–20.00*	15.12[a]	C 11.27 Cl 12.90

[a] The numbers marked by the asterisk were calculated by the authors using Nitta and Seki's results for the summation terms. All the other terms except the ionization potentials (see Table VII, reference a) have been reported by Nitta and Seki (see references 17, 21, and 23).
[b] This value was cited by Nitta and Seki (see reference 17).

[25] M. Born and J. E. Mayer, Z. Physik **75**, 1 (1932).
[26] Y. Morino and I. Miyagawa, J. Chem. Soc. Japan **68**, 62 (1947).
[27] C. P. Smyth, J. Phys. Chem. **41**, 209 (1937).
[28] H. Sponer and M. B. Willstätter, J. Chem. Phys. **5**, 745 (1937).

TABLE IX. The anisotropy of molecular interaction.

Molecule	Attraction energy (erg. molecule^{-1})
I	2.49
II	1.75
III	1.02
III'	2.49
IV	2.57

hexachloroethane as described below. When the crystal is left in air, it shortens in the direction of the [100] axis and, even after the other crystal planes have disappeared, the (100) plane remains clearly defined. These observations might be explained qualitatively from the molecular interaction. The van der Waals attraction between molecule 0 and its first neighbors *I*, *II*, *III*, *III'*, and *IV* (see Fig. 6) were calculated by Slater and Kirkwood's method to get the relative value of the anisotropy of molecular interaction in this crystal (Table IX). The interaction between molecule 0 and *I* or *IV*, for which the directions of force are parallel to the (100) plane or almost parallel to that plane, is stronger than the others. These estimations not only give good agreement with the anisotropic volatility but also will yield some information about the mechanism of the transitions.

Appendix: Estimation using Axilrod and Teller's Expression

In the calculations mentioned above, the van der Waals attraction is assumed to be a sum of the interactions between pairs of atoms. According to Axilrod and Teller,[29] however, if the perturbation of the third order is applied, the interaction between triplets of atoms is given by the following equation:

$$E=C(3\cos\gamma_1\cos\gamma_2\cos\gamma_3+1)/r_{12}^3r_{23}^3r_{31}^3,$$

where γ_1, γ_2, and γ_3 are the angles of the triangle formed by atoms 1, 2, and 3; r_{12}, r_{23}, and r_{31} are the interatomic distances in this triangle; C is a positive quantity of the order of $I\alpha^3$, where I is the first ionization potential and α is the atomic polarizability.

We have attempted a derivation of the van der Waals forces considering second-order perturbation. Since the straightforward summation is very tedious, we have made the following assumptions.

(1) The six chlorine atoms in orthorhombic hexachloroethane have approximately similar surroundings, therefore we have calculated the interaction between only one chlorine in molecule 0 (see Fig. 6) and two chlorines in the other molecules. The total energy estimated by this expression is assumed to be equal to six times this interaction. The chlorines under consideration form triangles which might be classified into three types, that is, equilateral, right, and obtuse triangles.

(2) Only the interactions between chlorine atoms have been calculated, because other contributions do not amount to more than 10 percent of the total.

(3) Summation is taken over the range of a sphere with a radius of 6A from the center of gravity of molecule 0. The contribution of the outer part is negligible.

(4) When the triplet of atoms forms an obtuse triangle, the contribution is very small, so that we may neglect terms of this type.

We have obtained $\sum 1/r_{12}^3r_{23}^3r_{31}^3=43.39\times10^{-15}$ A^{-9} for the equilateral triangles[30] (6 terms) and $\sum 1/r_{12}^3r_{23}^3r_{31}^3=58.99\times10^{-15}$ A^{-9} for the right triangles[31] (40 terms). Using the approximation $C=I\alpha^3$ with $I=12.90$ ev[32] and $\alpha=2.299\times10^{-24}$ cc (Table V), we have obtained

$$E=2.57 \text{ kcal mole}^{-1}.$$

Since these evaluations involve many assumptions, the result is not completely reliable, but it seems likely that the contribution obtained by Axilrod and Teller's expression give rise to considerable repulsive forces.

ACKNOWLEDGMENTS

The authors wish to thank Dr. I. Nitta and Dr. T. Watanabé for their continued encouragement and Dr. S. Seki for his helpful discussions on the calculation of lattice energy. One of authors (M. A.) is indebted to Dr. W. N. Lipscomb, Mr. L. Lavine, and Mr. C. E. Nordman for their kind advice in the preparation of this manuscript. This research was helped by the research grant given by the Ministry of Education.

[29] B. M. Axilrod and E. Teller, J. Chem. Phys. **11**, 299 (1943).

[30] For $r_{12}=r_{23}=r_{31}$, $E=C(11/8/r_{12}^3r_{23}^3r_{31}^3)$.

[31] For $\gamma_1=90°$, $E=C(1/r_{12}^3r_{23}^3r_{31}^3)$.

[32] See Table VII, reference a.

Thermal Diffusion in Isotopic Mixtures in the Critical Region*

F. E. CASKEY AND H. G. DRICKAMER
Department of Chemistry, University of Illinois, Urbana, Illinois
(Received July 25, 1952)

Thermal diffusion ratios have been measured for the system $C^{14}O_2-CO_2$ temperature range −15°C to +50°C and to 160-atmospheres pressure. One isotherm at −15°C has also been measured for the system $CH_4-CH_3H^3$. The results deviate completely from the predictions of the kinetic theory of Enskog and Chapman and correspond closely to the previous results for the xenon-ethane system. The thermodynamics of irreversible processes qualitatively predicts the results obtained.

THERMAL diffusion is a transport phenomenon occuring in mixtures, whereby a temperature gradient results in a concentration gradient. This can be expressed quantitatively by the equation

$$\mathbf{J}_1=-D_{12}\left[\frac{\partial N_{10}}{\partial x}-\alpha N_{10}N_{20}\frac{\partial \ln T}{\partial x}\right]. \quad (1)$$

The direction and degree of the separation is expressed by the sign and magnitude of the thermal diffusion ratio α. In general, the separation depends on the shape as well as the mass of the molecules involved, but for isotopes α is considered positive if the light molecule concentrates at the hot wall. $\mathbf{J}_1$ then refers to the flux of the light component.

THEORY

The first quantitative expression for the thermal diffusion ratio was obtained (for ideal gases) from the kinetic theory of Enskog and Chapman.[1] For gases dilute in one component the result can be written

$$\alpha=(C-1)(S_1/Q_1), \quad (2)$$

where S_1 and Q_1 depend on molecular masses, collision diameters, and suitably averaged effective collision cross sections. C depends only on the collision cross sections.

Thermal diffusion is most sensitive to the type of molecular interaction, and the only model which gives reasonably quantitative results, even at very low pressures, is the Lennard-Jones potential, wherein the interaction energy is expressed as

$$E=-4\epsilon[(r_0/r)^6-(r_0/r)^{12}], \quad (3)$$

where ϵ = attractive energy in the configuration of maximum attractive interaction and r_0 = collision diameter. For this model the effective average collision cross sections ($W^{(i)}_{(j)}$) depend only on kT/ϵ, where k = Boltzmann's constant and T = absolute temperature. These integrals have been evaluated by Hirschfelder, Bird, and Spotz.[2] The ratio S_1/Q_1 is a very slowly varying function of temperature, but, at temperatures near the critical and below, $(C-1)$ varies rapidly with temperature and actually changes sign well below the critical temperature. This behavior is qualitatively confirmed by experiment on dilute gases.

The dense gas theory of Enskog[3] predicts a slight variation of α with pressure at high pressures, but no changes in magnitude or sign. This has proved to be totally inconsistent with experiment.[4–7] The results for the system ethane-xenon indicate that, along an isotherm just above the critical temperature, α decreases and changes sign at a pressure of 5–15 atmospheres, then decreases to a large negative value near the critical point. At higher densities it increases and finally changes sign again at a density 1.5–2 times the critical density.

It was found[8,9] that the behavior described above could be qualitatively predicted from the theory of irreversible phenomena known as the "thermodynamics of irreversible processes." The expression for α from this theory[10] is

$$\alpha=\frac{M_1M_2}{\bar{M}RT}\left[\frac{\bar{H}_1}{M_1}-\frac{\bar{H}_2}{M_2}-Q^*\right], \quad (4)$$

where M_i = molecular mass of component i, $\bar{M}$ = mean molecular mass, R = gas constant, T = absolute temperature, $\bar{H}_i$ = partial molal enthalpy of component i, Q^* = "heat of transport," i.e., the heat transported isothermally with unit mass. The equation cannot be used directly because it is impossible to evaluate Q^* theoretically or to obtain absolute values for the enthalpies.

Equation (4) can be written

$$\alpha=\alpha_0+\frac{M_1M_2}{\bar{M}RT}\left[\frac{\bar{H}_1'}{M_1}-\frac{\bar{H}_2'}{M_2}-Q^{*\prime}\right], \quad (5)$$

* This work was supported in part by the AEC.

[1] S. Chapman and T. G. Cowling, *Mathematical Theory of Non-Uniform Gases* (Cambridge University Press, Cambridge, 1939), pp. 134–167.

[2] Hirschfelder, Bird, and Spotz, J. Chem. Phys. **16**, 968 (1948).

[3] Reference 1, pp. 273–294.

[4] Pierce, Duffield, and Drickamer, J. Chem. Phys. **18**, 950 (1950).

[5] Giller, Duffield, and Drickamer, J. Chem. Phys. **18**, 1027 (1950).

[6] L. H. Tung and H. G. Drickamer, J. Chem. Phys. **18**, 1031 (1950).

[7] E. W. Becker, J. Chem. Phys. **19**, 131 (1951).

[8] W. L. Robb and H. G. Drickamer, J. Chem. Phys. **18**, 1380 (1950).

[9] W. L. Robb and H. G. Drickamer, J. Chem. Phys. **19**, 818 (1951).

[10] S. R. De Groot, *Thermodynamics of Irreversible Processes* (Interscience Publishers, Inc., New York, 1951).

where α_0 = the thermal diffusion ratio for an ideal gas at the temperature T. This can be evaluated from Eq. (1). $\bar{H}_1'$ = the partial molal enthalpy above that of an ideal gas at temperature T. This can be evaluated from p-v-t data. $Q^{*\prime}$ = heat of transport above the value for an ideal gas. This was assumed to be zero in the calculations of Robb and Drickamer.[8,9] For a mixture of iso-

TABLE I. Thermal diffusion ratio for $CO_2-C^{14}O_2$.

T°C	P atmos	ρ g/cc	q[a]	α
−15	62.0	1.024	0.796	+0.0083
	100.4	1.034	0.908	+0.0035
	101.0	1.035	0.841	+0.0063
	142.3	1.048	0.831	+0.0067
	224.0	1.070	0.746	+0.0092
0	48.0	0.932	0.939	+0.0019
	80.2	0.963	0.784	+0.0048
	103.0	0.978	0.696	+0.0090
	154.0[b]	0.998	0.581	+0.0123
	191.5	1.015	0.499	+0.0299
	224.0	1.030	0.751	+0.0137
15°	19.9[c]	0.0425	0.933	+0.0247
	47.6[c]	0.135	0.800	+0.0128
	70.0	0.850	1.090	−0.0082
	135.0	0.915	1.090	−0.0060
20°	44.9	0.118	1.090	−0.0274
	53.8	0.170	1.075	−0.0146
	59.5	0.775	1.060	−0.0075
	61.4	0.781	1.126	−0.0124
	82.5	0.828	1.101	−0.0084
	90.9	0.841	1.094	−0.0079
	109.9	0.865	1.030	−0.0020
	143.3	0.899	0.982	+0.0010
	144.5	0.900	1.066	−0.0046
32.1°	45.0	0.106	1.078	−0.0134
	64.4	0.200	0.940	+0.0083
	72.5	0.300	0.980	+0.0078
	73.4	0.330	1.050	−0.0175
	73.9	0.356	1.023	−0.0234
	74.0	0.380	1.06	−0.0532
	74.3	0.400	1.266	−0.1450
	74.3	0.400	1.114	−0.0625
	74.4	0.425	1.202	−0.1225
	74.7	0.490	1.188	−0.113
	75.3	0.575	1.200	−0.0864
	80.0	0.663	1.202	−0.0520
	90.5	0.725	1.266	−0.0282
	137.5	0.820	1.233	−0.0116
	151.0	0.838	1.000	0.000
	224.0	0.901	0.969	+0.0022
40.1°	47.0	0.105	1.057	−0.0158
	69.2	0.200	0.911	+0.0131
	80.8	0.300	0.964	+0.0067
	82.7	0.330	1.050	−0.0175
	84.1	0.356	1.088	−0.0234
	85.2	0.380	1.150	−0.0478
	86.0	0.400	1.170	−0.0519
	89.5	0.500	1.352	−0.0662
40.1°	99.5	0.635	1.222	−0.0299
	136.0	0.760	1.245	−0.0150
	136.0	0.760	1.182	−0.0115
	138.4	0.764	1.061	−0.0064
49.7°	83.9	0.251	0.953	+0.0022
	95.6	0.353	1.003	+0.0009
	100.0	0.420	1.119	−0.0338
	106.8	0.490	1.188	−0.0470
	113.8	0.558	1.212	−0.0463
	114.0	0.560	1.059	−0.0143
	137.2	0.675	1.035	−0.0054

[a] $q = \left(\frac{\text{conc } C^{14}O_2}{\text{conc } C^{12}O_2}\right)_{\text{btm}} \left(\frac{\text{conc } C^{12}O_2}{\text{conc } C^{14}O_2}\right)_{\text{top}} = \frac{(\text{conc } C^{14}O_2)\ \text{btm}}{(\text{conc } C^{14}O_2)\ \text{top}}$.
[b] Amplifier tube failure.
[c] Dc voltage fluctuated due to weak batteries.

TABLE II. Thermal diffusion ratio for $CH_4-CH_3H^3$.

T°C	P atmos	ρ g/cc	q[a]	α
−15°C	55.8	0.053	0.846	+0.0372
	58.0	0.056	0.679	+0.0925
	108.0	0.122	0.810	+0.0234
	138.0	0.162	0.941	+0.0044
	172.0	0.200	0.969	+0.0028
	222.0	0.237	0.875	+0.0098
	224.0	0.238	0.844	+0.0106

[a] $q = \left(\frac{\text{conc } C^{14}O_2}{\text{conc } C^{12}O_2}\right)_{\text{btm}} \left(\frac{\text{conc } C^{12}O_2}{\text{conc } C^{14}O_2}\right)_{\text{top}} = \frac{(\text{conc } C^{14}O_2)\ \text{btm}}{(\text{conc } C^{14}O_2)\ \text{top}}$.

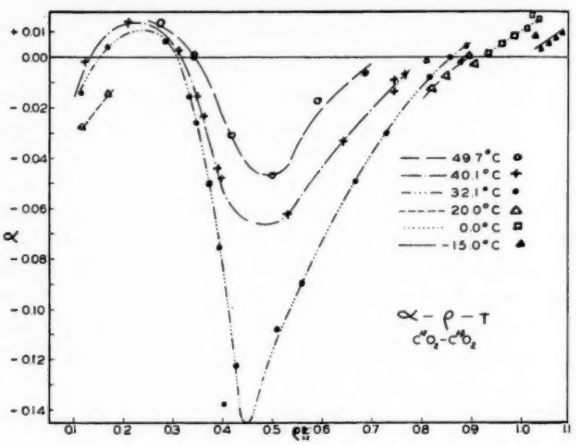

FIG. 1. Thermal diffusion ratio α as a function of density and temperature for the system $CO_2-C^{14}O_2$.

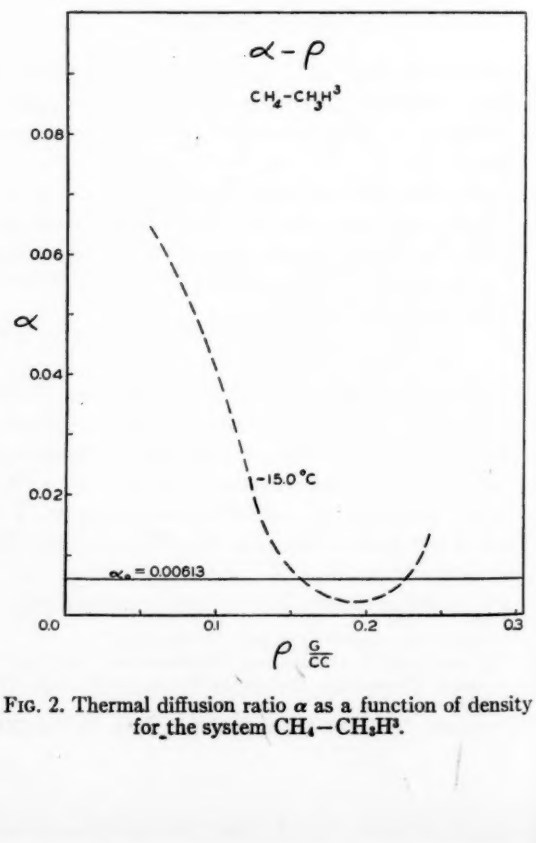

FIG. 2. Thermal diffusion ratio α as a function of density for the system $CH_4-CH_3H^3$.

topes Eq. (5) becomes

$$\alpha=\alpha_0+\frac{1}{\bar{M}RT}[\bar{H}'(M_2-M_1)-Q^{*\prime}]. \qquad (6)$$

Equation (6) predicts that the behavior obtained for the ethane-xenon mixture would also occur in isotopic mixtures. As will be seen below, this is confirmed by experiment.

EXPERIMENTAL PROCEDURE

Thermal diffusion ratios were measured in the system $C^{14}O_2-CO_2$ in the temperature range from $-15°C-50°C$ and the pressure range 15 atmos–160

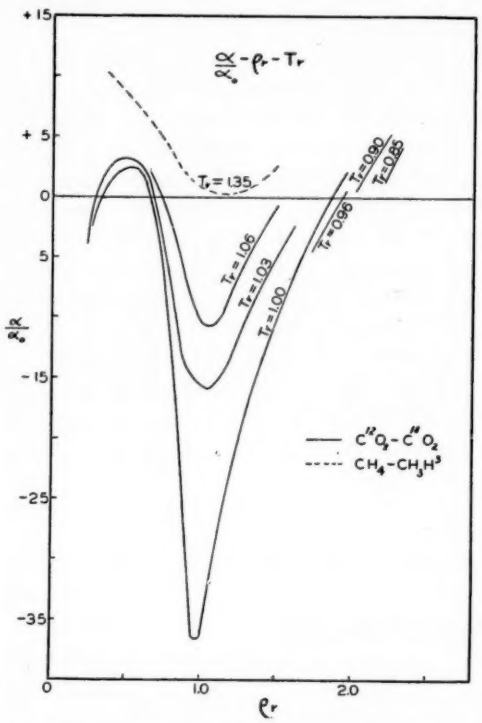

FIG. 3. Reduced plot for the thermal diffusion ratio.

atmos. (The critical point is $t_c=31.6°C$ $p_c=73.6$ atmos.) One isotherm (at $-15°C$) was also measured for the system $CH_3H^3-CH_4$. The radioactive $C^{14}O_2$ was generated from $BaC^{14}O_3$ obtained from the Oak Ridge National Laboratory of the Atomic Energy Commission. The tritium tagged CH_3H^3 was purchased from Tracerlab.

The CO_2 was 99.9 percent pure, while the CH_4 was Research Grade, obtained from Phillips Petroleum Company.

The measurements were made in a thermal diffusion column essentially identical with that described by Giller *et al.*[5] except that a gap width of 0.0318 cm was used.

The values of α were predicted from the column

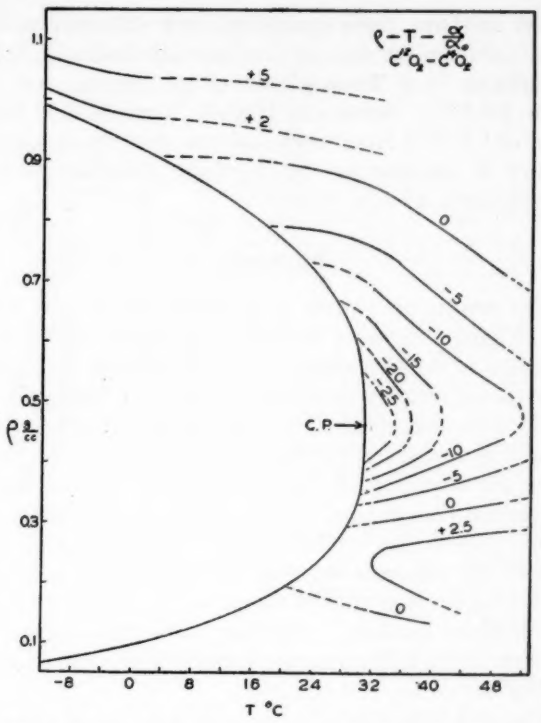

FIG. 4. Lines of constant α on a temperature-density plot.

theory of Furry, Jones, and Onsager[11] as modified by Drickamer, Mellow, and Tung.[12] The physical properties necessary for this calculation are (a) $(\partial\rho/\partial T)_p$, (b) the viscosity μ, and (c) the diffusion coefficient D_{12}. For CO_2 (a) was obtained from the data of Michels and Michels,[13] (b) was calculated from Enskog's dense gas theory, and (c) was obtained from the data of Robb[14] and Timmerhaus.[15]

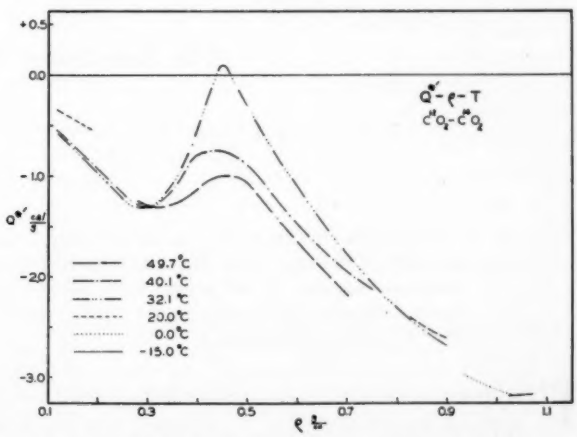

FIG. 5. The heat of transport above that for an ideal gas as a function of temperature and density.

[11] Furry, Jones, and Onsager, Phys. Rev. **55**, 1083 (1939).
[12] Drickamer, Mellow, and Tung, J. Chem. Phys. **18**, 945 (1950).
[13] A. Michels and C. Michels, Proc. Roy. Soc. (London) **A153**, 201 (1936); **A160**, 348 (1937).
[14] W. L. Robb and H. G. Drickamer, J. Chem. Phys. **19**, 1504 (1951).
[15] K. D. Timmerhaus and H. G. Drickamer, J. Chem. Phys. **20**, 981 (1952).

For methane these quantities were obtained as follows: (a) from the data of Kvalnes and Gaddy,[16] (b) by calculation from Enskog's dense gas theory, and (c) from Enskog's dense gas theory. (Unpublished data obtained in this laboratory indicate that the dense gas theory is satisfactory for methane diffusion to 150 atmospheres, at least.)

RESULTS

The results are shown in Tables I and II and Figs. 1–5. Figure 1 shows α for the system $CO_2-C^{14}O_2$ as a function of density along various isotherms. It can be seen that α actually undergoes a triple sign change along some of the isotherms. This corresponds exactly to the results obtained for the ethane-xenon system. Figure 2 gives the isotherm for the $CH_4-CH_3H^3$ system. While α does not change sign, it decreases to a value very near zero at about the critical density ($\rho=0.163$ g/ml). It should be remembered that this isotherm is about 67.5°C above the critical temperature. Because of the low counting efficiency for tritium, these data are not so reliable as the CO_2 data, particularly at the low density end of the curve.

Figure 3 is a plot of α/α_0 as a function of reduced density and temperature. α_0 is the value of α for an ideal gas at the same temperature, calculated from Eq. (2).

[16] H. M. Kvalnes and V. L. Gaddy, J. Am. Chem. Soc. **53**, 394 (1931).

It can be seen that the methane data fit quite well with the carbon dioxide data. Figure 4 is a contour map showing lines of constant α/α_0. The plot corresponds to Fig. 2 of the paper by Giller *et al.*

Figure 5 shows a plot of $Q^{*\prime}$, the heat of transport above that for an ideal gas, as a function of density and temperature. $Q^{*\prime}$ necessarily approaches zero at low density. In view of the difficulty of evaluating molecular properties in the critical region and the complexity of column theory in this region, it is doubtful if the variations in $Q^{*\prime}$ in the critical region are significant. However, at high density $Q^{*\prime}$ definitely tends to larger negative values and appears to be nearly independent of temperature. If $Q^{*\prime}$ continued its decrease at the same rate to very high density, α would be very large and positive in that region. A molecular interpretation of the heat of transport would be most useful.

These deviations for isotopic mixtures from the kinetic theory Chapman and Enskog, particularly in the rather low density region where the other transport coefficients are accurately predicted, are a little surprising. It must be admitted that CO_2 is far from spherically symmetrical, but the CH_4 is reasonably so. It appears doubtful if the deviations can be laid only to lack of spherical symmetry. In any case, it is clear that thermal diffusion offers a fruitful field for investigation of intermolecular forces, particularly in condensed systems.

F. E. Caskey would like to acknowledge financial support from the Standard Oil Company (Indiana) and from Tau Beta Pi.

THE JOURNAL OF CHEMICAL PHYSICS VOLUME 21, NUMBER 1 JANUARY, 1953

The Electronic Structure of Ferrocene

H. H. Jaffé
Venereal Disease Experimental Laboratory, U. S. Public Health Service, School of Public Health, University of North Carolina, Chapel Hill, North Carolina

(Received September 12, 1952)

The electronic structure of ferrocene (*bis*cyclopentadienyl iron) is considered by constructing MO's from the AO's of the iron atom and the MO's of the cyclopentadienyl radicals. The 18 valence electrons of the compound are distributed among these MO's so that 16 occupy bonding, and 2 nonbonding MO's. This electron distribution permits an interpretation of the stability, the magnetic susceptibility and the absorption spectrum of ferrocene.

THE preparation of *bis*cyclopentadienyl iron, a new type of metallo-organic compound, has recently been reported.[1] This compound has been shown to possess some remarkable properties[2] and has been given the name ferrocene to stress its aromatic character. Two structures have been proposed in which the iron atom lies in the center of a pentagonal prism or antiprism which have the cyclopentadienyl radicals for pentagonal faces.[2a] We shall show that either of these structures can give rise to very strong bonding between the metal and the organic radical, and hence to the observed stability of the compound.

The following discussion is based on molecular orbital (MO) theory, and the orbitals for ferrocene will be obtained as linear combinations of the atomic orbitals (AO) of iron and the MO's of the cyclopentadienyl

[1] T. J. Kealy and P. L. Paulson, Nature **168**, 1039 (1951); Miller, Tebboth, and Tremaine, J. Chem. Soc. 632 (1952).

[2] (a) Wilkinson, Rosenblum, Whiting, and Woodward, J. Am. Chem. Soc. **74**, 2125 (1952); (b) Woodward, Rosenblum, and Whiting, J. Am. Chem. Soc. **74**, 3458 (1952).

radicals. The structures proposed for ferrocene belong to the symmetry groups C_{5v} or D_{5h},[3] but intermediates between the proposed structures, of symmetry C_5, can be written.* Both the AO's of the iron and the MO's of cyclopentadienyl can be divided in groups according to their symmetry with respect to the fivefold axis, which is also chosen as the z-axis of iron. Since the MO's of cyclopentadienyl with one or more nodes occur in degenerate pairs, linear combinations of such MO pairs can always be constructed so that common nodal planes exist for corresponding obritals of the two radicals, whatever their relative orientation. Hence, the exact point group to which the compound belongs does not influence the conclusions of this discussion.

The available orbitals with their symmetry classifications are listed in Table I. The orbitals of the separate cyclopentadienyl radicals are replaced by linear combinations of corresponding orbitals from both radicals. From these orbitals the following MO's for ferrocene can be constructed:

$$\psi_1=(s\cos a+d_z\sin a)\cos\alpha_1+2^{-\frac{1}{2}}(\phi_1+\phi_1')\sin\alpha_1,$$
$$\psi_2=p_z\cos\alpha_2+2^{-\frac{1}{2}}(\phi_1-\phi_1')\sin\alpha_2,$$
$$\psi_3=p_x\cos\alpha_3+2^{-\frac{1}{2}}(\phi_2+\phi_2')\sin\alpha_3,$$
$$\psi_4=d_{x+z}\cos\alpha_4+2^{-\frac{1}{2}}(\phi_2-\phi_2')\sin\alpha_4,$$
$$\psi_5=p_y\cos\alpha_5+2^{-\frac{1}{2}}(\phi_3+\phi_3')\sin\alpha_5$$
$$\psi_6=d_{y+z}\cos\alpha_6+2^{-\frac{1}{2}}(\phi_3-\phi_3')\sin\alpha_6,$$
$$\psi_7=d_{x+y}\cos\alpha_7+2^{-\frac{1}{2}}(\phi_4+\phi_4')\sin\alpha_7,$$
$$\psi_8=d_{xy}\cos\alpha_8+2^{-\frac{1}{2}}(\phi_5+\phi_5')\sin\alpha_8,$$
$$\psi_9=s\sin a-d_z\cos a,$$
$$\psi_{10}\doteq 2^{-\frac{1}{2}}(\phi_4-\phi_4'),$$
$$\psi_{11}=2^{-\frac{1}{2}}(\phi_5-\phi_5'),$$
$$\psi_{12}=d_{xy}\sin\alpha_8-2^{-\frac{1}{2}}(\phi_5+\phi_5')\cos\alpha_8.$$

Orbitals ψ_{13} to ψ_{19} follow as negative combinations corresponding to ψ_1 to ψ_7.

ψ_1 to ψ_8 are bonding orbitals, and all are doubly occupied; ψ_9 to ψ_{11} are nonbonding, and ψ_{12} to ψ_{19} are antibonding orbitals. The value of the α_i may be determined by solution of the secular equations and will depend on the energies of the component orbitals and the overlap and resonance intergrals between them. Since ϕ_4 and ϕ_5 are normally unoccupied high energy orbitals of cyclopentadienyl, and s and d_z are normally occupied low energy orbitals of iron, it is reasonable to assume that the two electrons which remain after orbitals ψ_1 to ψ_8 are filled will occupy ψ_9. Consequently these electrons are paired and the compound is diagmagnetic.[2a] According to Hund's rule, ferrocene would be paramagnetic if these two electrons were to occupy the degenerate orbitals ψ_{10} and ψ_{11}.

TABLE I.

Iron	Cyclopentadienyl[a]	Symmetry
s, p_z, d_z	$2^{-\frac{1}{2}}(\phi_1\pm\phi_1')$	a_1
p_x, d_{x+z}	$2^{-\frac{1}{2}}(\phi_2\pm\phi_2')$	b_1
p_y, d_{y+z}	$2^{-\frac{1}{2}}(\phi_3\pm\phi_3')$	b_2
d_{x+y}, d_{xy}	$2^{-\frac{1}{2}}(\phi_4\pm\phi_4')$; $2^{-\frac{1}{2}}(\phi_5\pm\phi_5')$	a_2

[a] The ϕ are the MO of the radical; the primed orbitals belong to one radical, the unprimed to the other. The oribtals are numbered in the order of increasing energy; ϕ_2 and ϕ_3, and ϕ_4 and ϕ_5 are degenerate pairs.

The great stability of ferrocene is thus the result of two factors: (1) the rare gas electron configuration of the iron atom,[2a] and (2) the existence of eight bonding MO's, so that the iron may be said to be bound to each of the organic radicals by four covalent bonds. The present treatment suggests that no barrier exists against free rotation of the radicals around the fivefold axis.

The present discussion also permits an interpretation of the ultraviolet absorption spectrum of ferrocene.[2a] The longest wavelength absorption band ($\lambda=440m\mu$)† can be attributed to a charge transfer transition, $\psi_9\rightarrow\psi_{10,11}$. This transition is forbidden by symmetry and can occur only since the symmetry is distorted by vibrational motion. This assignment is supported by the low intensity of this band ($\epsilon_{max}=87$). The second absorption band ($\lambda=326m\mu$, $\epsilon_{max}=50$) again must be a forbidden transition. It may be of the same nature as the first band, the upper level arising from a splitting of the degenerate orbitals ψ_{10} and ψ_{11}, or it may be a transition to the lowest antibonding orbital ($\psi_9\rightarrow\psi_{12}$). The intense far ultraviolet absorption("end absorption," at $\lambda=225m\mu$, $\epsilon=250$) must arise from excitation of one of the bonding electrons to a nonbonding or antibonding MO ($\psi_8\rightarrow\psi_{10,11}$ or ψ_{12}). Since the orbitals ψ_8 and ψ_{10} to ψ_{12} all belong to class a_2, either transition is allowed. Thus, the observed high intensity is consistent with the proposed structure.

[3] Structures II and III of reference 2a, respectively.

* *Note added in proof:*—Since this paper was submitted for publication the structure of ferrocene has been determined by x-ray diffraction [E. O. Fischer and W. Pfab, Z. Naturforsch. **7b**, 377 (1952); P. F. Eiland and R. Pepkinsky, J. Am. Chem. Soc. **74**, 4971 (1952)]. The compound is found to have symmetry C_{5v}, and no free rotation appears to occur, at least in the crystal.

† *Note added in proof:*—The ultraviolet absorption spectrum of ferrocene has been published in detail since this paper was submitted for publication [Kaplan, Kester, and Katz, J. Am. Chem. Soc. **74**, 5531 (1952)]. The data are essentially in agreement with those cited. The width of the band at 440 mμ suggests that this band may consist of a superposition of two bands where the two upper levels arise from a splitting of the degenerate orbitals ψ_{10} and ψ_{11}.

Substituted Methanes. XI.* Potential Constants for CBr_3Cl†

ARNOLD G. MEISTER AND FRED L. VOELZ
Spectroscopy Laboratory, Department of Physics, Illinois Institute of Technology, Chicago 16, Illinois
(Received September 30, 1952)

A new set of potential constants has been obtained for CBr_3Cl using the Wilson FG matrix method and a potential energy function containing all possible second degree terms. These constants are in better agreement with those determined for CBr_2Cl_2, CBr_2ClH, CBr_2ClD, and CCl_3Br than the set given previously.

NOW that 21 of the 123 possible deuterium and halogen substituted methanes have been investigated in this laboratory, it seems appropriate to compare the results for the potential constants to see if there are any serious inconsistencies. A study of Table I, which compares the original potential constants of CBr_3Cl[1] with those of CBr_2Cl_2,[2] CBr_2ClH,[3] and CCl_3Br,[4] indicates that the original values of f_e, $f_b{}^{b'e}$, f_{be}, and $f_{be}{}^{b'e}$ for CBr_3Cl differ considerably from the values found for the other molecules. Hence, an attempt was made to calculate the fundamental frequencies of CBr_3Cl using only potential constants transferred from CBr_2Cl_2, with the exception of $f_b{}^{b'b}$, $f_{bb}{}^{b'e}$, and $f_{bb}{}^{b'b}$ which do not occur in the most general quadratic potential energy function for CBr_2Cl_2. The values of $f_b{}^{b'b}$ and $f_{bb}{}^{b'b}$ were taken from the other CBr_3X molecules,[1] while $f_{bb}{}^{b'e}$ was assumed to be zero as was done originally. This set was called the test set and it led to the frequencies given in the column labeled test set in Table II. The observed frequency values are also given in this table, and one sees that the transferred constants predict the frequencies very well. One also notices that these constants place the ν_5 type *e* fundamental at 217.8 cm^{-1}, which is much closer to 211.3 cm^{-1} than 268.3 cm^{-1} as chosen by some observers.[5,6]

Next the transferred constants were modified in order to improve the agreement between the calculated and observed values, and this set of constants is given as the final set in Table I. While the agreement is not exact as it was for the original set, the worst difference for the final set is 2 cm^{-1}. However, because the constants given as the final set agree much better with those determined for the other molecules, it is felt that they are a better set even if they do not reproduce the frequencies exactly. It appears that for some molecules, if one tries to get too close a fit between the observed and calculated values of the fundamental frequencies, considerable distortion of some of the potential constants may result.

TABLE I. Potential constants for CBr_3Cl.

Type[a]	Original set	Test set	Final set	CBr_2ClH	CCl_3Br
f_b	2.8976[b]	2.7530	2.7525	2.8704	2.8976
f_e	2.9565	3.3713	3.2659	3.4204	3.4580
$f_b{}^{b}$	0.29910	0.21296	0.15400	0.27187	···
$f_b{}^{e}$	0.20890	0.32465	0.31177	0.32037	0.37782
$f_b{}^{bb}$	0.33734	0.34088	0.33734	0.30000	···
$f_b{}^{b'b}$	−0.20788	−0.20788[c]	−0.20788	···	···
$f_b{}^{be}$	0.31643	0.35007	0.33337	0.36345	0.35007
$f_b{}^{b'e}$	0.18036	−0.17178	−0.16343	−0.18178	···
$f_e{}^{bb}$	···	−0.20547	−0.20547	−0.22500	···
$f_e{}^{be}$	···	0.36022	0.32007	0.30000	0.42630
$f_e{}^{bb}-f_e{}^{bc}$	−0.47402	−0.56569	−0.52554	−0.52500	···
f_{bb}	1.2136	1.2391	1.1475	1.2458	···
f_{be}	0.92910	1.1383	1.0509	1.1798	1.3038
$f_{bb}{}^{b'b}$	0.24314	0.24314[c]	0.17704	···	···
$f_{bb}{}^{be}$	0.079853	0.12944	0.079855	0.23083	···
$f_{bb}{}^{b'e}$	0.0000	0.0000[c]	0.0000	···	···
$f_{be}{}^{b'e}$	−0.070262	0.087897	0.051650	0.15793	···

[a] f_b is C−Br bond stretching constant; $f_b{}^{b}$ is C−Br bond interaction constant; $f_b{}^{bb}$ is C−Br bond, Br−C−Br angle interaction constant with C−Br bond in common; $f_b{}^{b'b}$ is the same as $f_b{}^{bb}$ except C−Br bond is not in common; f_{be} is the Br−C−Cl angle bending constant; $f_{bb}{}^{be}$ is the Br−C−Br and Br−C−Cl angle interaction constant with C−Br bond in common; $f_{bb}{}^{b'e}$ is the same as $f_{bb}{}^{be}$ except the C−Br bond is not in common; the other constants have similar meanings.

[b] Bond stretching constants are in md/A; bond-angle interaction constants are in md/rad; and angle-angle interaction, or angle bending constants, are in mdA/rad².

[c] These constants were transferred from CBr_3H, while all the remaining constants of this set were transferred from CBr_2Cl_2, with the exception of $f_{bb}{}^{b'e}$ which was assumed to be zero.

TABLE II. Calculated and observed values of the fundamental frequencies of CBr_3Cl in cm^{-1}.

Type	Frequency	Original set	Test set	Final set	Observed
a_1	ν_1	744.9	759.2	747.0	745.0
	ν_2	326.7	335.2	326.5	326.7
	ν_3	211.5	219.0	212.7	211.3
e	ν_4	677.0	675.4	677.0	677.0
	ν_5	211.3	217.8	211.3	211.3
	ν_6	140.3	139.5	140.3	140.3

* For previous papers of this series, see J. Chem. Phys. **18**, 346, 1073, 1076, 1081 (1950); **19**, 119, 784, 1561 (1951); **20**, 454, 1979 (1952); **21**, 189 (1953).

† Part of a research program aided by a grant from the American Academy of Arts and Sciences and by a contract (DA-11-022-ORD-464) with the Office of Ordnance Research.

[1] Meister, Rosser, and Cleveland, J. Chem. Phys. **18**, 346 (1950).

[2] Davis, Cleveland, and Meister, J. Chem. Phys. **20**, 454 (1952).

[3] Pontarelli, Meister, Cleveland, Voelz, Bernstein, and Sherman, J. Chem. Phys. **20**, 1949 (1952).

[4] Zietlow, Cleveland, and Meister, J. Chem. Phys. **18**, 1076 (1950).

[5] Lecomte, Volkringer, and Tchakirian, Compt. rend. **204**, 1927 (1937).

[6] M. L. Delwaulle and F. Francois, Compt. rend. **214**, 226 (1942).

Letters to the Editor

THIS section will accept reports of new work, provided these are terse and contain few figures, and especially few half-tone cuts. The Editorial Board will not hold itself responsible for opinions expressed by the correspondents. Contributions to this section should not exceed 600 words in length and must reach the office of the Editor not later than the 15th of the second month preceding that of the issue in which the Letter is to appear. No proof will be sent to the authors. A publication charge of $10.00 per Letter is made which, when honored, will entitle the Institution to 100 free reprints.

Dipole Loss in Polystyrene and Derivatives

EDWARD B. BAKER, ROBERT P. AUTY, AND GROVER J. RITENOUR
Dow Chemical Company, Midland, Michigan
(Received November 13, 1952)

WITH the automatic dielectric bridge previously described[1] recordings of ϵ'' and ϵ' for pure polystyrene, cross-linked polystyrene, and polystyrene plasticized with diphenyl have been made *vs* $1/T$. Correction for expansion is included. The loss is plotted as $\log \epsilon'' T/T_0$, where T_0 is 40°C, to convert to straight lines the exponential tails of the absorption peak and to eliminate the expected $1/T$ dependence of $(\epsilon_0' - \epsilon_\infty')$. In all cases a characteristic dipole loss peak above the second-order transition point is attributed to the residual phenyl group dipole moment of about 0.2 D.U. Such a peak is to be expected from analogy to the Cl tagged phenyl groups of polychlorostyrene previously reported.[2] A preliminary curve for polystyrene was previously published.[1]

Results for polystyrene cross-linked with 6 percent divinylbenzene are shown in Fig. 1A. The dipole peak has straight line

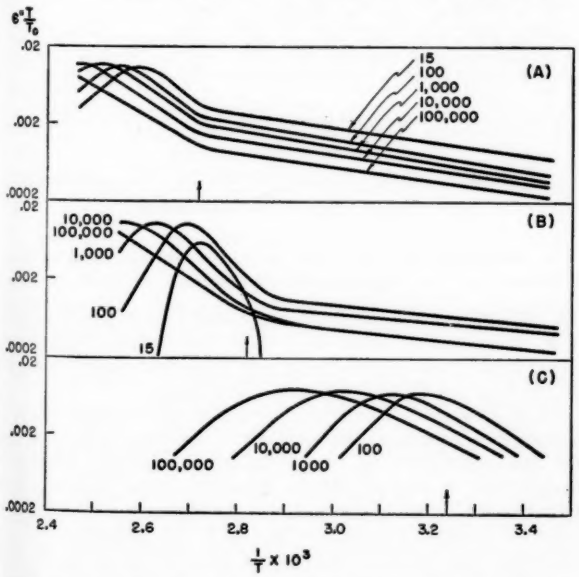

FIG. 1. Curves of $\epsilon'' T/T_0$ *vs* $1/T$ at various frequencies in cps for (A) cross-linked polystyrene, (B) pure polystyrene, and (C) polystyrene plasticized with 20 percent diphenyl. Second-order transition temperatures are indicated with arrows.

sides on the log plot, and just below the second-order transition the low temperature side has a rather sharp decrease in slope (the same temperature for all frequencies), following a new straight line to low temperatures. The region below the second-order transition, we believe, is due to a very much wider distribution of relaxation times, still, however, involving the phenyl dipole, since such a loss is absent in polyethylene.

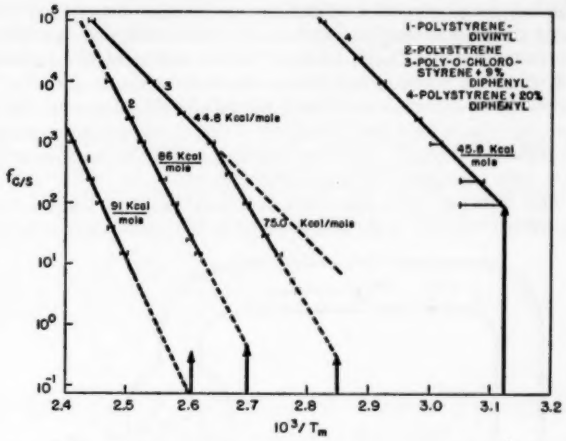

FIG. 2. Plots of log frequency *vs* $1/T_m$ for four polystyrenes, with slopes and second-order transitions indicated.

A similar behavior is exhibited by polystyrene (Fig. 1B) except that the loss below the transition is much less reproducible and often absent at low frequencies. The loss peaks occur at lower temperatures for polystyrene than for the more rigid cross-linked polystyrene, and at still lower temperatures if plasticizer is added (Fig. 1C). With sufficient plasticizer the sudden change at the transition is absent, the sides of the peaks passing through undisturbed. The dipole peak for polystyrene above the transition is quite reproducible.

The loss peaks for all of these materials exhibit an asymmetry (even if replotted against $\log f$ at constant T), and individual curves (above the transition) may be accurately fitted with the asymmetrical distribution of relaxation times τ based on $\epsilon^* = (\epsilon_0' - \epsilon_\infty')1/(1+jw\tau)^\beta$ recently proposed for glycerine by Davidson and Cole,[3] assuming Arrhenius dependence for τ on T. This procedure is questionable if β and the activation energy are functions of T. However, the asymmetry is on the correct side to be accounted for by such a distribution, which has a sharp cut off τ_m in τ such that $\tau < \tau_m$. If applicable in this case, it would indicate an upper limit to the size of an aggregate of dipoles effective in the loss mechanism. Figure 2 shows plots of $\log f$ *vs* $1/T_m$ which are straight lines for all except plasticized polychlorostyrene indicating an Arrhenius dependence of τ (if β and activation energy are independent of T).

The dielectric constant of polystyrene and cross-linked polystyrene shows a decrease of 0.03 from room temperature to the dipole peak (after expansion correction) which has not been explained. The samples were chemically silvered after cleaning with chromic acid and then had the edges turned off to a clean surface. The dielectric constant at room temperature is then 2.55, which is greater than with a bare sample by an amount not accounted for by series air films of known dimensions.

[1] E. B. Baker, Rev. Sci. Instr. **20**, 716 (1949); **22**, 34, 373, 376 (1951); E. B. Baker, Annual Report 1950, NRC Conference on Insulation.
[2] E. B. Baker, Annual Report 1951, NRC Conference on Insulation.
[3] D. W. Davidson and R. H. Cole, J. Chem. Phys. **19**, 1484 (1951).

Diffusion in Porous Catalysts

C. BOKHOVEN AND J. HOOGSCHAGEN
Central Laboratory of Staatsmijnen in Limburg, Geleen, Holland
(Received November 4, 1952)

IN porous catalyst particles the reactants have to move by diffusion to the internal surface in order to react. When the reaction is reasonably fast and the particle size is not too small, the diffusion rate may be insufficient to maintain an equal concentration of reactants inside and outside the particle and consequently the reaction rate will decrease. As pointed out by

Thiele,[1] the degree of retardation by diffusion depends on the value of a dimensionless modulus to which Wagner[2] has given the form $m=R(k/D_{eff})^{\frac{1}{2}}$, where R is the radius of the particle, k is the true (pseudo first-order) reaction constant and D_{eff} is the effective diffusion coefficient in the porous substance. Up to now there have been published only a few direct measurements[3,4] on diffusion through porous substances, and in no case have the data been correlated with catalytic activity.

The diffusion rate has been measured with a simple glass apparatus (Fig. 1). Atmospheric oxygen diffuses through a porous

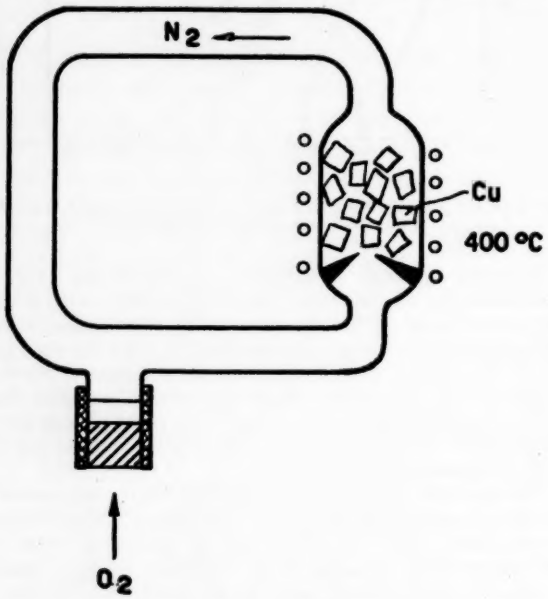

FIG. 1. Simple glass apparatus.

tablet connected to the apparatus by means of a rubber tubing. By heating the widened part of the closed circuit, where active copper absorbs the oxygen completely, a circulation flow is set up. From the weight gain of the apparatus (total weight 15 grams) in about 20 hours, D_{eff} for O_2-N_2 at room temperature and atmospheric pressure can easily be calculated. D_{eff} for the reactants at reaction conditions follows from well-known formulas[5-7] which are different for Knudsen and for normal diffusion.

For a number of catalysts D_{eff} ranged from 4 to 12 percent of free gas diffusion coefficients. A model of catalyst particles, each consisting of loose subparticles, would yield a much higher value for the same porosity. The structure of the porous catalysts investigated thus rather resembles a sponge where interconnections between subparticles retard diffusion.

A plot of the reaction constant (according to the Temkin-Pyzhev theory[8]) at 1 atmos of a commercial ammonia synthesis catalyst (crushed down to particle size 0.5–0.7 mm) against the reciprocal absolute temperature showed a bend near 400°C (Fig. 2). After correction for retardation by diffusion, using the *Knudsen* formula in the calculation of D_{eff} for NH_3 at reaction conditions, a straight line for the true activity between 350 and 450°C was obtained. In this case the value observed for O_2-N_2 was $D_{eff}/D_{gas}=0.040$. From this it may be concluded that at atmospheric pressure the diffusion has a Knudsen character which is in agreement with the mean pore size (400A) calculated from the B.E.T. surface area. As the value of D_{eff} is lowest if Knudsen diffusion is assumed, an additional transport by normal gas diffusion or surface migration cannot be appreciable. Further experiments will be carried out at high pressures.

The activity line at atmospheric pressure for a commercial watergas shift catalyst (tablets of Fe_2O_3-Cr_2O_3, crushed down to 2.8–3.4 mm) showed a bend near 350°C (Fig. 2). Correction with the observed value of $D_{eff}/D_{gas}=0.054$ yields a straight line for

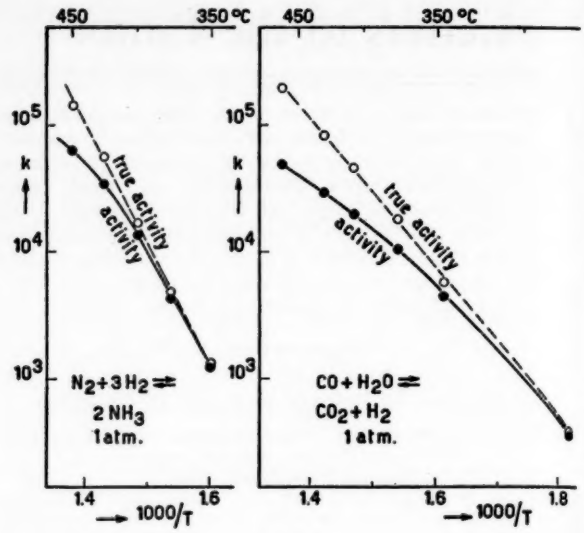

FIG. 2.

the true activity between 275 and 450°C provided *normal gas diffusion* is assumed. The dependency of the activity on the particle size at 350°C could also be accounted for satisfactorily. Although the mean pore size (300A) suggests Knudsen diffusion, the normal gas diffusion character can be naturally explained by the presence of macropores originating from the tableting of the catalyst powder.

A detailed account of the work will be published elsewhere.

[1] E. W. Thiele, Ind. Eng. Chem. **31**, 916 (1939).
[2] C. Wagner, Z. phys. Chem. **A193**, 1 (1943).
[3] E. Wicke and R. Kallenbach, Kolloid Z. **97**, 135 (1941).
[4] H. L. Penman, J. Agr. Sci. **30**, 437, 570 (1940).
[5] H. J. Arnold, Ind. Eng. Chem. **22**, 1091 (1930).
[6] C. R. Wilke, Chem. Eng. Progress **46**, 95 (1950).
[7] M. Knudsen, Ann. phys. **28**, 75 (1909).
[8] Temkin and Pyzhev, Acta Physicochim. U.R.S.S. **12**, 327 (1940).

A Magnesium Oxide Phosphor Activated by Tetravalent Manganese

J. S. PRENER
General Electric Research Laboratory, Schenectady, New York
(Received October 27, 1952)

A LARGE number of inorganic phosphors containing divalent manganese as an activator show fluorescence in a comparatively broad band. A few phosphors have been found, however, which show red fluorescence with a fine structure.[1-4]

These phosphors have been found to contain manganese in an oxidation state greater than two, and it has been concluded that the ion responsible for the emission is probably tetravalent manganese.[1,5,6] The phosphors presently known showing these multibanded emission spectra are of a complex and in some cases unknown crystal structure. The need was therefore felt for obtaining this type of luminescent emission in a simple host crystal of known structure, in order that theoretical calculations as to the nature of the emission process could be carried out.

We found that magnesium oxide, which has the rocksalt structure, could be activated by manganese so as to yield the fluorescence spectrum shown in Fig. 1(a), if magnesium oxide is fired, together with 0.1 mole percent of manganese sulfate and 5 mole percent lithium carbonate, at 1000°C in an oxygen atmosphere. If the above mixture is fired in hydrogen or if the lithium carbonate is omitted and the mixture fired in oxygen, the resulting product in either case is not excited by ultraviolet light. In the former case, magnesium oxide activated by divalent manganese is formed.[7-9] This is excited by cathode rays, and its

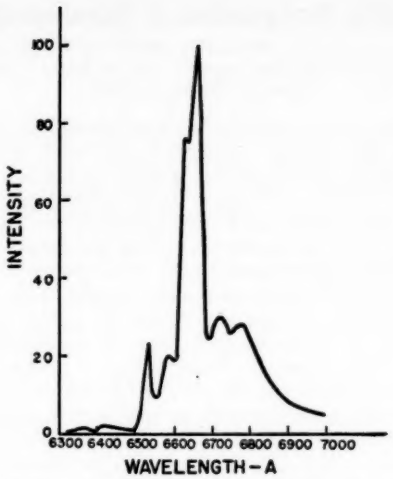

FIG. 1(a). Emission spectrum at 93°K. 100 MgO:0.1 Mn:5 Li_2CO_3 (O_2 at 1000°C). 3650 excitation.

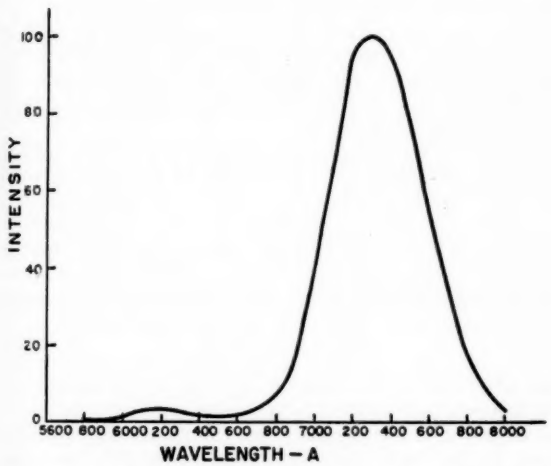

FIG. 1(b). Emission spectrum at room temperature. 100 MgO:0.1 Mn: 5 Li_2CO_3 (H_2 at 1000°C). Cathode-ray excitation.

emission spectrum is shown in Fig. 1(b). In the latter case, although chemical analysis indicates the presence of tetravalent manganese, the average oxidation state being 3.7, presumably no appreciable quantity of the higher valence manganese is incorporated in the lattice.

In the presence of lithium carbonate, one Mn^{++} and two Li^+ ions may replace three Mg^{++} ions in the magnesium oxide lattice. Precision lattice constant determinations of pure MgO, 100 MgO:1 Mn and 100 MgO:1 Mn:5 Li_2CO_3 all fired in oxygen, seem to support this view. The values of a_0 were found to be (1) pure MgO:a_0=4.211±0.002A, (2) 100 MgO:1 Mn:a_0=4.213 ±0.002A, (3) 100 MgO:1 Mn:5 Li_2CO_3:a_0=4.207±0.002A. The unit cell dimensions of samples one and two are the same within the limits of precision of the determination which is consistent with the fact that the oxidized manganese does not enter the MgO lattice. The unit cell dimension of the sample containing Li^+ is smaller by 0.004A, which is what one would calculate considering the fact that the ionic radii of both Li^+ and Mn^{+4} are smaller than those of Mg^{++}. Paramagnetic resonance measurements on two phosphors whose compositions were 100 MgO:0.1 Mn:5 Li_2CO_3, one being fired in hydrogen and the other in oxygen, were carried out by Leifer and Hershberger.[10] The one fired in oxygen gave a microwave absorption spectrum as a result of divalent manganese, with an intensity one-tenth that of the one fired in hydrogen. This would indicate that the manganese in the oxygen-fired sample had an average oxidation state of 3.8, in fair agreement with the chemical analysis of the oxidizing power of the manganese which yielded an average valence of 3.5.

We are now making a fundamental study of the nature of the emission process in this phosphor.

[1] F. A. Kroeger, *Some Aspects of the Luminescence of Solids* (Elsevier Publishing Company, Houston, 1948).
[2] F. E. Williams, J. Opt. Soc. Am. **37**, 302 (1947).
[3] S. H. Patten and F. E. Williams, J. Opt. Soc. Am. **39**, 702 (1949).
[4] Travnicek, Kroeger, Botden, and Zalm, Physica **18**, 33 (1952).
[5] F. A. Kroeger and van den Boomgaard, J. Elec. Soc. **97**, 377 (1950).
[6] L. Thorington, J. Opt. Soc. Am. **40**, 579 (1950).
[7] E. Tiede, Ber. deut. chem. Ges. **72**, 611 (1939).
[8] J. T. Randall, Nature **142**, 113 (1938).
[9] J. T. Randall, Proc. Roy. Soc. (London) **A17**, 272 (1939).
[10] Report 52-14, July, 1952, Department of Engineering, University of California, Los Angeles.

Formation and Excitation of Atomic Sodium in Hydrogen Diffusion Flames*

LORÉ LINDNER, W. E. SCOTT, AND E. R. STEPHENS
The Franklin Institute Laboratories for Research and Development, Philadelphia, Pennsylvania
(Received October 7, 1952)

RECENT studies of candoluminescence[2] reported by British workers have disclosed some interesting phenomena involving the sodium *D* lines which occur in diffusion flames of hydrogen in air. When hydrogen is passed through a porous block coated with a luminescent material (such as calcium oxide containing a small percentage of a bismuth compound as activator) and allowed to burn in air, the coating is observed to luminesce with a color characteristic of the activator. This luminescence was correlated by Smith[2] with the presence of hydrogen atoms in the flame, since he was able to excite the luminescence with hydrogen atoms from a Wood's discharge tube. Further experiments by Arthur[3] showed that both the luminescence and the sodium *D* line emission of the flame itself could be quenched by the addition to the hydrogen stream of a small, seemingly critical percentage of any one of a number of additives. Ethyl benzene, sulfur dioxide, toluene, benzene, and several others were reported by Arthur as being effective quenching agents. The fact that both the sodium emission and the luminescence are quenched by the same concentration of additive was interpreted as evidence that hydrogen atoms were responsible either for the production or excitation of sodium atoms. These possibilities may be represented by

$$\text{production:}\quad (1)\ H+NaX\rightarrow Na+HX$$
$$\text{or}$$
$$\text{excitation:}\quad (2)\ Na+H+H\rightarrow Na^*+H_2$$
$$Na^*\rightarrow Na+h\nu.$$

Reaction (2) is analogous to the mechanism proposed for the excitation of the luminescent surface. A distinction may be made between these two possibilities by observing the spectral absorption of such a flame at the *D* line wavelengths as a function of concentration of a quenching agent. If (1) is the important reaction, then the absorption at these wavelengths would be expected to decrease as the quencher, which presumably removes the hydrogen atoms necessary for (1), is added. If (2) is of primary importance, the absorption should remain substantially constant with increasing concentration of quenching agent. We carried out this experiment (using sulfur dioxide as quenching agent) and found that the absorption at the *D* line wavelengths did become weaker as the concentration of sulfur dioxide was increased.

A special burner consisting of ten ceramic tubes in a row fed by a common manifold was constructed for these studies. The light from a tungsten strip filament was brought to a focus in the flame by a lens. A second lens focused this image on the entrance slit of a small glass constant-deviation spectrograph which was provided with an exit slit and a photomultiplier tube. Suitable circuits were provided to buck out the bulk of the signal from the photomultiplier, so that the output could be read on a sensitive galvanometer.

A set of curves of flame transmission *versus* wavelength are shown in Fig. 1 for a series of percentages of sulfur dioxide added. Although the measured absorption was small due to the low resolving power of the instrument used, it is clear that the absorption at the *D* lines becomes progressively weaker as sulfur dioxide is added. A parallel decrease in the intensity of the *D* lines in emission with increasing sulfur dioxide concentration was also observed. The quenching of the luminescence and *D* lines increased regularly with increasing concentration of sulfur dioxide with no true critical concentration as reported by Arthur. However, at 2.3 percent sulfur dioxide, the "critical" concentration given by Arthur, the quenching of both *D* lines and luminescence was almost complete. Thus, it is quite clear that the sodium atom concentration decreases rapidly as sulfur dioxide is added to the flame. Since the quenching agent presumably reduces the hydrogen atom concentration in the flame, this may be interpreted to mean that hydrogen atoms are involved in the production rather than the excitation of sodium atoms in the flame and a reaction such as (1) is probably involved. Of course, this result could be explained by assuming that the production of atomic sodium is a

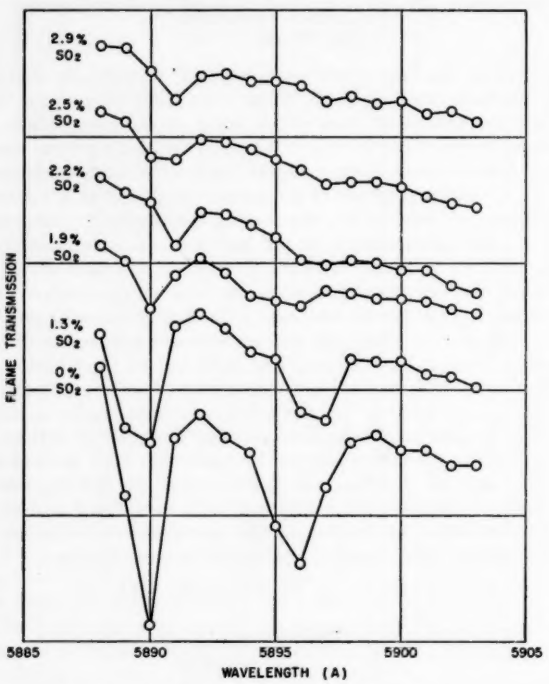

FIG. 1. Transmission of hydrogen diffusion flame.

purely thermal process and that addition of a quenching agent causes a marked decrease in flame temperature, although this latter seems very unlikely. Alternatively, if hydrogen atoms are involved in the excitation of sodium atoms [reaction (2)], it would be expected that the reversal temperature of the *D* lines would be abnormally high but would decrease as the quencher is added. For this reason attempts were made to measure the reversal temperature of the *D* lines as a function of sulfur dioxide concentration. Although no change in temperature was observed, the accuracy of the measurement was very poor because of the smallness of the absorption signal when the lamp and the flame were at nearly the same temperature. Attempts will be made to improve this measurement.

* The work described in this paper was supported by contract with the Office of the Chief of Ordnance, Department of the Army.

[1] A. G. Gaydon, *Spectroscopy and Combustion Theory* (Chapman and Hall, Ltd., London, 1948), p. 34.

[2] E. C. W. Smith, Inst. of Gas Engineers, Publication No. 237 (1940); D. T. A. Townend, Chemistry and Industry **23**, 346 (1945); *Symposium on Energy Transfer in Hot Gases*, Natl. Bur. Standards (September, 1951).

[3] J. R. Arthur, Nature **165**, 557 (1950); Arthur, Bangham, Baulk, and Whittingham, Nature **166**, 358 (1950).

Molecular Configuration of Polyelectrolytes*

PAUL J. FLORY
Department of Chemistry, Cornell University, Ithaca, New York
(Received October 23, 1952)

THE expansion of polyelectrolyte molecules has been treated by several authors[1-3] through consideration of the electrostatic free energy which arises as a result of the net loss to the surrounding solution of some of the counter ions of opposite charge. Kimball, Cutler, and Samelson[1] have shown that disregard of the resulting net excess charge (giving $\nabla^2\psi=0$), in accordance with the Donnan approximation, is to be preferred over series expansion of the Poisson-Boltzmann equation with neglect of higher terms. The Donnan approximation can be shown to be legitimate for a system which is large in comparison with its peripheral double layer, the latter having a thickness approximately equal to the Debye-Hückel characteristic length $1/\kappa$. This condition holds for polyelectrolytes of high molecular weight in media of not too low ionic strength ($>10^{-4}$ molar in water), and it is, therefore, permissible to assume the net charge to be substantially zero throughout the greater portion of the molecular domain. The electric potential is extraneous under these conditions, and its introduction needlessly complicates previous attempts to treat the molecular configuration of polyelectrolyte molecules. It is the purpose of this communication to point out that consideration of the osmotic effects of mobile ions offers a more direct approach to the problem, which may be treated by straightforward extension of the molecular configuration theory for uncharged molecules.[4]

Consider a system comprising a single polyelectrolyte molecule immersed in an infinite bath of solution of a simple electrolyte $M_{\nu_+}{}^{z+}A_{\nu_-}{}^{z-}$ (herein referred to as "salt") at a concentration c_s^*. The polymer molecule is represented as a spherically symmetric distribution of units, with a density which is approximated satisfactorily by a Gaussian function of the distance from the center of the distribution.[4] The free energy of formation of the system may be written

$$\Delta F=\Sigma_j \Delta F_{Mj}+\Delta F_{el}, \tag{1}$$

where ΔF_{Mj} is the free energy of formation of the solution of x_j units, solvent, and mobile ions occurring in the jth shell of the domain, and ΔF_{el} is the elastic free energy associated with expansion of the chain configuration. Assuming that the osmotic forces cause the molecule to expand uniformly so that all linear dimensions are altered by the factor α, at equilibrium

$$\partial\Delta F/\partial\alpha=0=\sum_j(\partial\Delta F_{Mj}/\partial n_{1j})(\partial n_{1j}/\partial \mathcal{V}_j)(\partial \mathcal{V}_j/\partial\alpha)+\partial\Delta F_{el}/\partial\alpha$$
$$=\sum_j[(\mu_{1j}-\mu_1^*)/v_1](\partial \mathcal{V}_j/\partial\alpha)+(\partial\Delta F_{el}/\partial\alpha), \tag{2}$$

where n_{1j} is the number of solvent molecules in shell j of volume $\mathcal{V}_j$, v_1 is the molar volume of the solvent, and $\mu_{1j}-\mu_1^*$ represents the difference in chemical potential of the solvent within the shell and at an infinite distance from the molecule. The chemical potential consists of two terms, one (previously considered[4]) due to the polymer units and the other to the difference in mobile ion concentrations in the jth shell and in the outer solution. Thus,

$$\mu_{1j}-\mu_1^*=-RT\{\psi_1(1-\Theta/T)c_{2j}{}^2v_u{}^2+(\nu c_{sj}+ic_{2j}/z_-)-\nu c_s^*\}, \tag{3}$$

where ψ_1 and Θ are previously defined[4] thermodynamic parameters relating to the polymer units, v_u is the molar volume of a polymer unit, c_{2j} is the concentration of polymer units in the jth shell, i is the number of electronic charges (assumed positive for definiteness) attached to the polymer chain per unit, z_- is the number of charges borne by the mobile counter anion, $\nu=\nu_++\nu_-$, and c_{sj} is the concentration of the salt in shell j. Activity coefficients are omitted. The second term in Eq. (3) may be written $(ic_{2j}/z_-)-\eta_j\nu c_s^*$, where $\eta_j=(c_s^*-c_{sj})/c_s^*$. It is readily shown that the concentration of salt in the jth layer at Donnan equilibrium is specified by the general relationship

$$(1-\eta_j)^{-h}-(1-\eta_j)=Y_j, \tag{4}$$

where h is the valency ratio $z_-/z_+=\nu_+/\nu_-$ for the salt and $Y_j=ic_{2j}/\nu_-z_-c_s^*$. Expanding η_j in powers of Y_j,

$$\eta_j=(h+1)^{-1}Y_j-(1/2)h(h+1)^{-2}Y_j^2+(1/3)h(h-1)(h+1)^{-3}Y_j^3 -(1/8)h(2h-1)(h-2)(h+1)^{-4}Y_j^4+\cdots. \quad (5)$$

When we substitute Eq. (5) in (3), and (3) in (2) and sum by integration over the Gaussian distribution exactly as in the treatment of the uncharged polymer molecule,[4] there is obtained after[4] setting $\partial F_{el}/\partial\alpha$ equal to $3kT(\alpha-1/\alpha)$,

$$(\alpha^5-\alpha^3)=2C_M\psi_1(1-\Theta/T)M^{\frac{1}{2}} +2iM\alpha^3\{C_I(i/M^{\frac{1}{2}}S^*\alpha^3)+C_I'(z_+-z_-)(i/M^{\frac{1}{2}}S^*\alpha^3)^2 +C_I''[z_+^2-(5/2)z_+z_-+z_-^2](i/M^{\frac{1}{2}}S^*\alpha^3)^3+\cdots\}, \quad (6)$$

where S^* is the ionic strength of the external solution in moles per liter, C_M has been previously defined,[4] and

$$C_I=10^3(2^{-5/2}2^{-2})(3\pi^{-1/2})^3[(M/\bar{r}_0^2)^{3/2}/\mathrm{N}M_u]/\nu_1M_u$$
$$C_I'=10^6(3^{-5/2}2^{-3})(3\pi^{-1/2})^6[(M/\bar{r}_0^2)^{3/2}/\mathrm{N}M_u]^2/\nu_1M_u \quad (7)$$
$$C_I''=10^9(4^{-5/2}2^{-4})(3\pi^{-1/2})^9[(M/\bar{r}_0^2)^{3/2}/\mathrm{N}M_u]^3/\nu_1M_u,$$

where $\bar{r}_0^2$ is the mean-square end-to-end distance for the unperturbed chain and M_u is the molecular weight of a unit. The series expansion is unsatisfactory at larger values of $i/M^{1/2}\alpha^3S^*$; more elaborate methods of integrating over the polymer distribution are then required.

The principal ionic term with coefficient C_I in Eq. (6) is identical with that which may be obtained by appropriate use of the electrostatic free energy as calculated by Hermans and Overbeek.[1,5] It corresponds also to the first ionic term derived by Hill[3] from consideration of the electrostatic free energy. Kimball, Cutler, and Samelson[2] predict a much smaller expansion as a consequence of their consideration of each chain unit as a statistically independent entity.

The similar treatment of polyelectrolyte gels will be presented in a forthcoming paper.

* This investigation was carried out at Cornell University in connection with the Government Research Program on Synthetic Rubber under contract with the Office of Synthetic Rubber, Reconstruction Finance Corporation.

[1] J. J. Hermans and J. Th. G. Overbeek, Rec. trav. chim. **67**, 761 (1948).
[2] Kimball, Cutler, and Samelson, J. Phys. Chem. **56**, 57 (1952).
[3] T. L. Hill, J. Chem. Phys. **20**, 1173 (1952).
[4] P. J. Flory and T. G. Fox, Jr., J. Am. Chem. Soc. **73**, 1904 (1951); P. J. Flory, J. Chem. Phys. **17**, 303 (1949).
[5] I. M. Krieger, thesis, Cornell University (1951).

Kinetics of the Gas Phase Reaction between Acetylene and Ozone

RICHARD D. CADLE AND CONRAD SCHADT
Stanford Research Institute, Stanford, California
(Received November 13, 1952)

PREVIOUSLY reported work has demonstrated that rapid gas phase reactions occur between ozone and various olefins.[1] The over-all reactions are quite complicated. By extrapolating rates back to initial conditions, a relatively simple second-order rate law was observed. The present note reports a study of the gas phase reaction between acetylene and ozone.

The course of the reaction was followed in terms of absorption of infrared radiation (1040 cm^{-1} by ozone and 735 cm^{-1} by acetylene). The reaction products were essentially transparent at these wave numbers. The apparatus used was described previously.[1] The acetylene was obtained from a commercial source and was purified by bubbling it through water and through concentrated sulfuric acid. Initial rates only were studied.

The ozone concentration was varied from 0.48 to 2.36 mm and the acetylene concentration from 0.98 to 6.59 mm. Total pressures varied from 286 to 634 mm with oxygen and nitrogen as carrier gas. Rates were measured for 15 runs at 30°C and for 4 runs each at 40°C and 50°C.

Over the range of conditions studied the reaction is over-all second order, and first order with respect to each reactant. The average value for the rate constant at 30°C was 0.0025 mm^{-1} sec^{-1} with a standard deviation of 0.0009 mm^{-1} sec^{-1}. The value of the rate constant was independent of the pressure of the carrier gas. The activation energy was estimated to be 4.8 kcal $mole^{-1}$. The average stoichiometric ratio of acetylene to ozone estimated from five determinations was 1.26 with a standard deviation of 0.09. The reaction products had absorption bands in the infrared region in the vicinity of 2300, 2100, 1750, 1370, 1300, 1100, and 725 cm^{-1}.

The rate constant can be expressed by the equation

$$k=3.0\times10^7e^{-4.8/RT}.$$

The pre-exponential factor is abnormally low. Possible explanations for this were presented previously.[1]

It is significant that while the 1750 cm^{-1} band corresponding to the carbonyl group was present, the 3300 cm^{-1} band of the hydroxyl group was missing. Bands corresponding to both groups were observed in the spectrum for the products of the gas phase reaction of ethylene with ozone.[1] Likewise, both hydroxyl and carbonyl groups are contained in the products of the liquid phase reaction of ethylene with ozone but only carbonyl groups in the products of the liquid phase reaction of acetylene with ozone.[2-4]

This similarity between gas and liquid phase reactions suggests that the reaction mechanisms, such as those proposed by Criegee,[2] may be similar for the reactions occurring in both the gas and the liquid phases.

[1] R. D. Cadle and C. Schadt, J. Am. Chem. Soc. (to be published).
[2] R. Criegee, *The Ozonolysis of Olefins and Acetylenes*. Paper presented before the Division of Organic Chemistry, 120th Meeting of the American Chemical Society (September, 1951).
[3] L. Long, Jr., Chem. Revs. **27**, 437 (1940).
[4] Dallwigk, Paillard, and Briner, Helv. Chim. Acta **35**, 1377 (1952).

Emission Spectrum of Undecomposed *N* Methylpyrrole

GUILIO MILAZZO
Istituto Superiore di Sanità, Rome, Italy
(Received November 5, 1952)

IF N methylpyrrole is subjected to electrical discharge in a Schüler tube[1] at a relatively high pressure (~1 mm Hg), it shows a faint band-emission spectrum between 34 800 and 41 500 cm^{-1} (2878–2400A). To the knowledge of the author this is the first time that an emission spectrum of a five-membered heterocyclic molecule with only one heteroatom has been observed.

Fifty-two bands were measured; the wave numbers of 10 bands on the ultraviolet side are identical, beyond the experimental error, with the wave numbers of 10 absorption bands on the red side of the absorption spectrum of the N methylpyrrole vapor, so that it is probable that this emission spectrum belongs to the undecomposed molecule and arises from the same electronic transition which is responsible for the absorption spectrum.

The vibrational frequencies found for the ground (final) and the excited (initial) state are collected in the following Table (heavy type, the most probable; normal type, the less probable; italics, the doubtful).

Frequencies of the ground state		Frequencies of the excited state cm^{-1}	
354	*1054*	**284**	**1103**
607	**1084**	**460**	*1138*
660	*1283*	**519**	*1255*
688	**1380**	**767**	**1338**
868	**1415**	**902**	
962	**1504**		

On the basis of these new results it seems that the position of the 0·0 band as previously given[2] (42 008 cm^{-1}), without changing the vibrational frequencies of the ground and the excited state already found, should be displaced towards the red. In fact, the 0·0 band should be located in the spectral region common to the emission and absorption spectra, i.e., between 38 800 and 42 000 cm^{-1}. If the electronic transition is allowed, the 0·0 band

should be present in both the emission and absorption spectra and should be of remarkable intensity.

On this electronic transition vibrations of the total-symmetric type should be superimposed as 0→1 transitions in absorption and as 1←0, 2←0, etc., transitions in emission for every superimposed vibration. In absorption some 1→0 transition should be present too. Under these conditions, if any band, common to emission and absorption spectra, would be interpreted as 0·0 band, the *same* vibrational frequencies should appear as 0⇄1 and 1⇄0 transitions in emission and in absorption. None of the bands common to the spectra can be interpreted without any doubt as 0·0.

On the other hand, if the intensities of the strongest absorption bands are recalculated, in order of magnitude, as molecular extinction coefficients, values of about 40 are found, i.e., a figure corresponding to a forbidden transition, so that it seems probable that as pure electronic transition the 0·0 band cannot be observed. Under these conditions, without knowing the real wave number of the 0·0 band and with so great a number of superimposed vibrations of the ground and the excited state, a complete, sure, and detailed assignment of every band of the emission spectrum is nearly impossible.

It is, however, interesting to draw attention to the stability of this molecule in the excited state. The fact that this molecule is capable of giving an emission spectrum demonstrates that in the excited state it is long-lived enough to return to the ground state, under emission of the corresponding radiation, before it decomposes. This greater stability can be ascribed to a stabilization of an electron sextet of benzenoid type, facilitated, in comparison with the unsubstituted pyrrole, by the methyl group. This stabilization is confirmed by the spectral behavior of the methylpyrrole in absorption[2] and in emission at low pressure[3] (emission of the "*T*" spectrum), and by some aspects of its chemical behavior. This new physico-chemical investigation confirms the greater aromaticity of *N* methylpyrrole in comparison with the simple pyrrole.

A difficulty arises from the comparison between *N* methylpyrrole and thiophene. The latter compound is much more stable than *N* methylpyrrole, and its chemical behavior is also much more of a benzenoid type. In emission at low pressure, it gives a stronger "*T*" spectrum than *N* methylpyrrole, while at a higher pressure in the condition under which the methylpyrrole emits the spectrum of the undecomposed molecule, the thiophene gives no spectrum. It is as if the stability ratio between methylpyrrole and thiophene were reversed in the sense that *N* methylpyrrole in the electronic excited state is stabler than thiophene.

Investigation of this point is in progress. This paper will be published in full in the Gazzetta Chimica Italiana.

[1] For description of the tube and of the methods see H. Schüller, Spectrochim. Acta **4**, 85 (1950).
[2] G. Milazzo, Gazz. chim. ital. **74**, 152 (1944).
[3] G. Milazzo, Gazz. chim. ital. **82**, 362 (1952); Experientia **8**, 259 (1952).

The Dependence of the Intrinsic Viscosity Sodium Polyacrylate on Salt Concentration*

P. J. Flory, W. R. Krigbaum, and W. B. Shultz
Department of Chemistry, Cornell University, Ithaca, New York
(Received October 23, 1952)

EVIDENCE accumulated to date on various uncharged polymers leads to the conclusion that the intrinsic viscosity $[\eta]$ is accurately proportional to the cube of a linear dimension of the polymer chain in dilute solution.[1] It is reasonable to suppose that the same should apply to polyelectrolytes under conditions such that the molecules are not too greatly extended. This is indicated to be true, approximately at least, by the work of Oth and Doty[2] comparing the intrinsic viscosities of polymethacrylic acids neutralized by sodium hydroxide to varying degrees with their sizes obtained from light scattering dissymmetries. The cube of the linear expansion factor α required for test of the theoretical relation (6) of the preceding communication accordingly should be proportional to $[\eta]$. Specifically,[3]

$$\alpha^3=[\eta]/[\eta]_\Theta, \tag{8}$$

where $[\eta]_\Theta$ is the intrinsic viscosity under conditions such that the molecules assume their unperturbed configurations for which $\alpha=1$. The "Θ-point" for a polyelectrolyte should be experimentally definable by means of the same criteria which apply to uncharged polymers.[3] That is to say, a solvent composition and temperature, for which the second virial coefficient in the series expansion of the osmotic pressure vanishes, prescribes the condition for a net intermolecular interaction equal to zero. The intramolecular interaction between different portions of the same molecule should likewise be zero under the same conditions; hence, α should equal unity, and this unique condition may be referred to as the "Θ-point." It is easy to show that it must for the same reason coincide with a critical point in the phase diagram in the limit of infinite molecular weight.

We have prepared a series of fractions of polyacrylic acid covering the molecular weight range from 4.4×10^4 to 1.3×10^6 by successive precipitation from dioxane using *n* heptane as precipitant. Molecular weights were determined by light scattering measurements in anhydrous dioxane. Critical precipitation temperatures T_c of the polyacid fractions were measured in the same

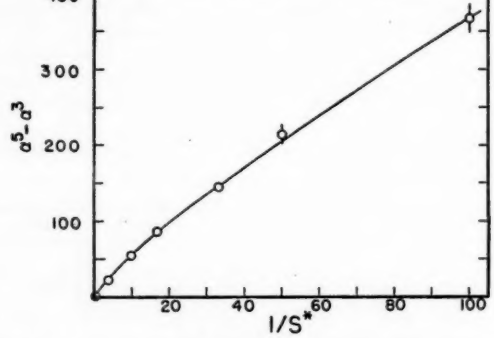

FIG. 1. Plot of $\alpha^5-\alpha^3$ against reciprocal ionic strength of sodium chloride. ○, uncorrected for shear effect; ◌̇, shear corrected.

solvent, in which the solubility *decreases* with rise in temperature. Thus, T_c for the fractions at the extremes of the molecular weight range were 73.4° and 39.7°, respectively. Extrapolation to $M=\infty$ by plotting T_c against $M^{-\frac{1}{2}}$ in the usual way[1] yielded $\Theta=30(\pm1)$°C. The intrinsic viscosity of the fraction of molecular weight 8.4×10^5, on which the preliminary results here reported were obtained, was 0.71 in dioxane at $T=\Theta=30$°C. We assume for the present that the size of the polysodium salt and its intrinsic viscosity would be the same at the Θ-point (if it could be reached in an aqueous medium) as for the polyacid in dioxane. This probably is not exactly true. However, approximate location of the Θ-point for the half-neutralized polyacid by salt precipitation, followed by measurement of the intrinsic viscosity at the Θ-point for this system gave a value within 20 percent of the above.

Solution viscosities of the completely neutralized sodium salt have been measured at 30° in water containing sodium chloride ranging in concentration from 0.01 molar to 4.0 molar. Intrinsic viscosities were obtained by extrapolating η_{sp}/c to infinite dilution in the usual manner. The large shear effect observed at the lower ionic strengths (where $[\eta]$ is large) made correction to zero shear rate necessary. This was accomplished by evaluating the "shear coefficient"[4] using a special viscometer permitting measurements at three pressure heads, the lowest of which provided a shear rate of about 80 sec^{-1}. The factor α^3 was calculated from the corrected intrinsic viscosity using Eq. (8).

Turning to the theoretical Eq. (6) with coefficients given by (7), the second term in the series is zero since $z_+=z_-=1$, and the

third term can be shown to be negligible compared to the first under the conditions of our experiments. Thus, $\alpha^5-\alpha^3$ is predicted to be linear in $1/S^*$. The experimental results are shown in Fig. 1. Although the complete set of data over the entire broad range in $1/S^*$ describe a curve, all points except the two for the greatest ionic strengths could be fitted within experimental error to a single straight line of slope 3.5; the initial slope of the curve as shown in Fig. 1 is about 5. The slope calculated from Eqs. (6) and (7) is 21. The discrepancy may result from retention by the charged carboxyl groups of a large fraction of sodium ions so that their osmotic effect within the domain of the chain is reduced.

We conclude that the extension to polyelectrolytes of the previous interpretation of intrinsic viscosities of non-ionic polymers is at least approximately valid. Further experiments are in progress on the dependence of $[\eta]$ on the molecular weight, the degree of neutralization, and valence type of the added salt.

* This investigation was carried out at Cornell University in connection with the Government Research Program on Synthetic Rubber under contract with the Office of Synthetic Rubber, Reconstruction Finance Corporation.

[1] T. G. Fox, Jr., and P. J. Flory, J. Phys. Colloid Chem. **53**, 197 (1949); J. Am. Chem. Soc. **73**, 1909, 1915 (1951); H. L. Wagner and P. J. Flory, J. Am. Chem. Soc. **74**, 195 (1952); Cragg, Dumitru, and Simkins, J. Am. Chem. Soc. **74**, 1977 (1952); L. Mandelkern and P. J. Flory, J. Am. Chem. Soc. **74**, 2517 (1952); Flory, Mandelkern, Kinsinger, and Shultz, J. Am. Chem. Soc. **74**, 3364 (1952).

[2] A. Oth and P. M. Doty, J. Phys. Chem. **56**, 43 (1952).

[3] P. J. Flory and T. G. Fox, Jr., J. Am. Chem. Soc. **71**, 1904 (1953).

[4] Fox, Fox, and Flory, J. Am. Chem. Soc. **71**, 1901 (1951).

Burning Velocity of Ethylene Oxide Decomposition Flames

RAYMOND FRIEDMAN AND EDWARD BURKE
Westinghouse Research Laboratories, East Pittsburgh, Pennsylvania
(Received November 12, 1952)

BURDEN and Burgoyne[1] have recently shown that a decomposition flame can propagate through pure ethylene oxide, the products of reaction being largely CH_4 and CO. This flame is of particular interest because kinetic studies of the slow decomposition of C_2H_4O in static systems (see Mueller and Walters[2]) indicate a first-order reaction. The only reported value of the burning velocity of an ethylene oxide decomposition flame was very recently given by Gerstein, McDonald, and Schalla,[3] who measured the rate of propagation in a tube at room temperature and atmospheric pressure. They report that their value is in reasonable agreement with burning-velocity theories of Hirschfelder, Corner, and Semenov.

We have been able to obtain a stable ethylene oxide decomposition flame by means of a flat-flame burner, 10 cm in diameter, adapted from a design employed by Powling[4] in studies of very lean hydrocarbon-air flames. The flames which we obtained, while extremely faint, were distinctly visible and gray in color. Burning velocities were obtained from measured flow velocities and flame areas. The slight deviations from flatness were taken into account by measurements of photographs of the flames, taken at $f/1.8$ with 20-second exposures. Corrections for the deviation of the vapor from ideality were applied, using the P-V-T data of Walters and Smith.[5]

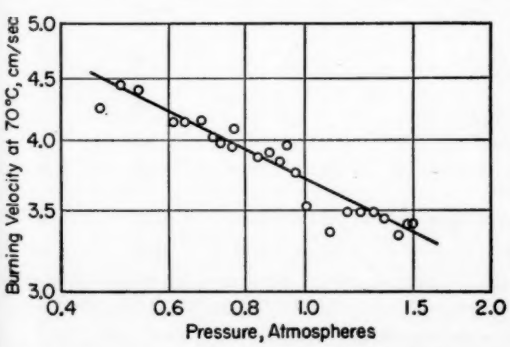

FIG. 1. Variation of burning velocity of ethylene oxide with pressure.

Figure 1 is a log-log plot of burning velocity against pressure, from 0.46 to 1.49 atmospheres. The temperature of the gas just upstream of the flame was 70°C. The linear variation shown in Fig. 1 indicates that the burning velocity varies inversely with the 0.25 power of pressure, whereas for a first-order reaction an inverse 0.50 power would be expected from theory. We are now conducting experiments at lower pressures, employing larger burners, in order to determine this exponent more precisely. Figure 2 shows the variation of burning velocity with temperature

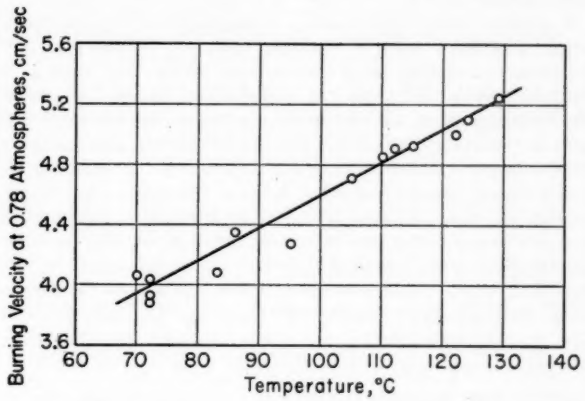

FIG. 2. Variation of burning velocity of ethylene oxide with temperature.

of the gas just upstream of the flame, at a pressure of 0.78 atmosphere and temperatures from 70° to 130°C.

When our data are extrapolated to the conditions of temperature and pressure employed by Gerstein *et al.*, a burning velocity of 2.7 cm/sec is obtained, which may be compared with their value of 12.5 cm/sec. This suggests that the method employed by Gerstein *et al.* may not be well suited to flames of this type.

We are presently engaged in further studies of this flame, including temperature traverses, product-gas analyses, and spectroscopic observations, as well as extension of the burning velocity measurements to lower pressures. A complete account of this work, including the theoretical implications of the results, is in preparation.

[1] F. A. Burden and J. H. Burgoyne, Proc. Roy. Soc. (London) **A199**, 328 (1949).

[2] K. H. Mueller and W. D. Walters, J. Am. Chem. Soc. **73**, 1458 (1951).

[3] Gerstein, McDonald, and Schalla, Fourth Symposium on Combustion, Cambridge, Massachusetts, September, 1952.

[4] J. Powling, Fuel **28**, 25 (1949).

[5] C. J. Walters and J. M. Smith, Chem. Eng. Progress **48**, 337 (1952).

Absorption Spectra of Free Radicals in Continuously Irradiated Photochemical Systems

D. A. RAMSAY
Division of Physics, National Research Council, Ottawa, Canada
(Received November 10, 1952)

EVIDENCE for the existence of free radicals in photochemical systems has been based mainly on the chemical properties of the radicals and on the results of kinetic investigations.[1] Recently, using very high light intensities obtained by photoflash techniques, the absorption spectra of several free radicals have been obtained.[2–4] The method of flash photolysis offers many advantages both for the detection of free radicals by means of their absorption spectra and for the study of free radical reactions. Nevertheless, the method has certain limitations, e.g., (a) it is necessary to use a large excess of inert gas to minimize thermal effects, (b) the system does not reach a stationary state,

(c) the course of the reaction at high light intensities may differ from that at lower light intensities owing to the high radical concentration.

It is of interest, therefore, to be able to detect and measure stationary state concentrations of free radicals in continuously irradiated photochemical systems. The conditions which are favorable for the detection of free radicals under these conditions are (a) long absorbing path and (b) high resolving power. In a previous experiment[4] the absorption spectrum of free NH_2 radicals was obtained by the flash photolysis of ammonia at a few mm Hg pressure using a path length of 1 meter. In an attempt to observe the absorption spectrum of free NH_2 radicals in a continuously irradiated photochemical system the following experiment was carried out.

A glass reaction vessel (Fig. 1) approximately 1 meter in length was fitted with a multiple reflection mirror system.[5,6] A one-meter quartz lamp constructed from thin quartz to transmit 1849A radiation was sealed into the reaction vessel. The lamp was fitted with tantalum electrodes and was filled with neon at ~5 mm pressure and a few droplets of mercury. Radiation from a tungsten filament lamp was focused on the entrance slit of the mirror system and after several traversals was focused on the slit of a 21-ft concave grating spectrograph. Ammonia at a few mm pressure was streamed through the tube with the quartz lamp operating at 320 v and 0.5 amp. An absorption spectrum of the system was taken in the region of 6000A (second order) with 20 traversals through the tube. The exposure time

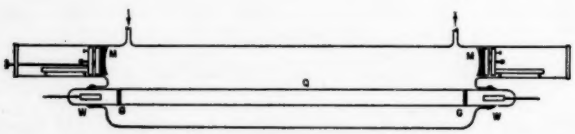

FIG. 1. Apparatus for studying the absorption spectra of free radicals in continuously irradiated systems. *M*—multiple reflection mirror system, *Q*—thin quartz mercury lamp, *G*—graded seals, *W*—wax seals.

using Eastman Kodak 103 aF plates and a slit width of 0.04 mm (resolving power ~100 000) was two minutes. With these conditions the NH_2 bands in the region of 6000A were observed and had an intensity comparable to that obtained in the flash photolysis experiment. It is believed that this is the first time that an absorption spectrum of a free radical has been observed in a continuously irradiated photochemical system.

In a similar experiment cyanogen was irradiated at a few mm pressure, and an absorption spectrum was taken using a path length of 4 meters. Approximately 40 lines of the (0, 0) CN band[7] near 3883A were observed. Attempts to obtain further free radical absorption spectra are in progress.

The main application of the present method from a kinetic point of view lies in the possibility of studying stationary concentrations of free radicals in continuously irradiated systems. For this purpose a calibration scale giving relative radical concentrations may be constructed by measuring the optical density of any absorption line with 4, 8, 12, 16, 20, ··· traversals, other conditions in the experiment being maintained constant. From a spectroscopic point of view, the method is useful for obtaining electronic absorption spectra of free radicals at comparatively low temperatures and as a possible method for obtaining the infrared absorption spectra of free radicals.

I am indebted to Dr. G. Herzberg for helpful discussions and to Mr. G. Ensell for his skilful glassblowing.

[1] E. W. R. Steacie, *Atomic and Free Radical Reactions* (Reinhold Publishing Corporation, New York, 1946), A.C.S. Monograph Series No. 102.
[2] G. Porter, Proc. Roy. Soc. (London) **A200**, 284 (1950); Disc. Faraday Soc. **9**, 60 (1950).
[3] R. G. W. Norrish, Disc. Faraday Soc. (to be published).
[4] G. Herzberg and D. A. Ramsay, J. Chem. Phys. **20**, 347 (1952); Disc. Faraday Soc. (to be published).
[5] J. U. White, J. Opt. Soc. Am. **32**, 285 (1942).
[6] H. J. Bernstein and G. Herzberg, J. Chem. Phys. **16**, 30 (1948).
[7] R. W. B. Pearse and A. G. Gaydon, *The Identification of Molecular Spectra* (John Wiley and Sons, Inc., New York, 1950), second edition.

Strong Hydrogen Bonds in Crystals

R. C. LORD AND R. E. MERRIFIELD
Spectroscopy Laboratory and Department of Chemistry, Massachusetts Institute of Technology, Cambridge, Massachusetts
(Received November 5, 1952)

FOR the past several years, we have been investigating infrared spectra of unusually strong hydrogen bonds. A recent letter by Rundle and Parasol[1] on similar studies prompts a preliminary statement of some of our results and conclusions. As Rundle and Parasol point out, the O—H stretching frequency in crystals containing short hydrogen bonds is often difficult to identify because of the large frequency displacement and breadth of the bands. In addition the bands are characterized by low peak intensity, by relatively flat peaks, and often by the appearance of several maxima of comparable intensity. These factors make the assignment of a single frequency to the band difficult and somewhat arbitrary.

We have investigated the O—H stretching frequencies in a number of crystals for which the O—O distance has been determined by x-ray methods. The results are given in Table I. If the shift in frequency from the "normal" value is plotted against the O—O distance for the crystals in Table I together with several previously reported, the curve shown in Fig. 1 is obtained. A somewhat similar plot has been given by Rundle and Parasol,[1] although we are in disagreement with them as to the frequency of the band center in maleic acid.

The infrared absorption spectra of tertiary amine hydrohalides show features which indicate the presence of strong $N^+—H\cdots X^-$ bonds in these salts. The spectrum of triethylamine hydrochloride in the form of a Nujol mull shows no absorption in the usual $N^+—H$ stretching region, but there is a very strong band centered at 2540 cm^{-1}, which must be the $N^+—H$ frequency. The band is a well-defined doublet with maxima at 2500 cm^{-1} and 2610 cm^{-1}, the latter being the more intense; in addition there are two weaker satellites at 2360 cm^{-1} and 2740 cm^{-1}. The large displacement of the band from its normal spectral location is attributed to a strong $N^+—H\cdots Cl^-$ bond.

These salts are soluble in partially halogenated solvents such as chloroform, and the above-described band persists in the spectra of such solutions. The frequency of the central minimum is the same as in the solid, although there are small changes in the peak frequencies, and the band is broader. The position of the band is the same for the fluoride, chloride, bromide, and iodide, but there are definite differences in the fine structure, principally in the relative intensity of the four components. Aromatic tertiary amine salts (e.g., pyridine hydrochloride) have a broad, structureless band at 2450 cm^{-1}, together with a broad

TABLE I.

Compound	Bond	ν	$\Delta\nu$	Bond length	Notes
1. Maleic acid	O—H—O	2000 cm^{-1}	1700 cm^{-1}	2.47A	a, b
2. Urea oxalate	O—H—O	2100	1600	2.50	b, c, d
	N—H—O	3230	170	2.89	a
3. Oxalic acid dihydrate	O—H—O	1900	1800	2.50	a, c
	O—H—O	3460	240	2.84	
4. Potassium dihydrogen phosphate	O—H—O	2370	1330	2.54	
5. Sodium bicarbonate	O—H—O	2440	1260	2.55	(b?)
6. Succinic acid	O—H—O	2680	1020	2.64	b, d
7. Adipic acid	O—H—O	2775	925	2.68	b, d

[a] Assumed values of nonbonded frequencies: O—H, 3700 cm^{-1}; N—H, 3400 cm^{-1}.
[b] More than one strong component.
[c] Partially overlapped by carbonyl band.
[d] Partially overlapped by C—H band.

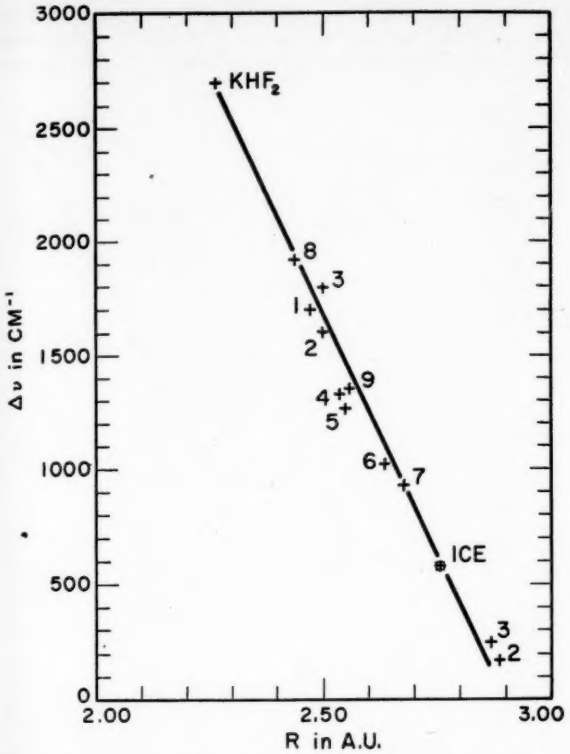

FIG. 1. Shift $\Delta\nu$ in stretching frequency *vs* $X-H\cdots Y$ distance in hydrogen bonding. Numbers refer to compounds in Table I. In addition, 8 = nickel dimethylglyoxime, 9 = acetylglycine, 10 = acetic acid dimer.

doublet with peaks at 1980 cm^{-1} and 2090 cm^{-1}. Such primary and secondary amine hydrohalides as we have investigated in solution show bands at higher frequencies (above 2700 cm^{-1}), but no band at 2540 cm^{-1}.

The effect of deuterium substitution on the hydrogen-bond stretching frequency in a few of the above-mentioned crystals is shown in Table II. The deuterium frequency given for acetylglycine is somewhat uncertain as it is overlapped by the carbonyl and amide frequencies. Rundle and Parasol[1] give curves for deuterated KH_2PO_4 and Ni-dimethylglyoxime, but the curves do not show the deuterium frequencies. The observed isotopic shifts show that the $X-H-Y$ stretching vibration is highly anharmonic, as would be expected[2] from the expansion of short hydrogen bonds on deuterium substitution.[3]

TABLE II.

Compound	Bond	ν(H)	ν(D)	ν(H):ν(D)
Triethylamine hydrochloride	N−H−Cl	2540 cm^{-1}	1965 cm^{-1}	1.29
Pyridine hydrochloride	N−H−Cl	2425	1880	1.29
Potassium dihydrogen phosphate	O−H−O	2370	1750	1.35
N-Acetylglycine	O−H−O	2350	1850	1.27

The striking breadth of these bands in crystals, even at low temperatures,[4] the constancy of the band center in the tertiary amine hydrohalides, the structure of the bands, and the marked anharmonicity are all features that any model must explain. It seems to us that these characteristics are incompatible with a simple electrostatic model of the hydrogen bond and that a quantum-mechanical model is undoubtedly required.[5] As a start in this direction, a complete molecular orbital calculation, including configuration interaction, of the binding in HF and FHF^- is in progress through the cooperation of the Solid State and Molecular Theory Group directed by Professor J. C. Slater.

A detailed report on the above work will be submitted for publication in this Journal at a later date.

[1] R. E. Rundle and M. Parasol, J. Chem. Phys. **20**, 1487 (1952).
[2] C. E. Nordman and W. N. Lipscomb, J. Chem. Phys. **19**, 1422 (1951).
[3] J. M. Robertson and A. R. Ubbelohde, Proc. Roy. Soc. (London) **170A**, 222 (1939); A. R. Ubbelohde, Proc. Roy. Soc. (London) **173A**, 417 (1939).
[4] R. Newman and R. M. Badger, J. Chem. Phys. **19**, 1147, 1207 (1951).
[5] See Kellner, Repts. on Progress in Phys. **15**, 1 (1952).

Crystal Structure of Diethylsilanediol and Its Hydroxyl Groups

MASAO KAKUDO AND TAKEO WATASE
Department of Applied Chemistry, Faculty of Engineering, Osaka University, Osaka, Japan
(Received November 7, 1952)

NO previous x-ray work has been reported on the crystal structure of organosilanols yet; the information regarding hydroxyl groups in organosilanol is significant for the investigation of the mechanism of its condensation to siloxane, and may clear up the characteristic differences between OH groups bound to carbon atoms and those bound to silicon atoms.

The crystal structure analysis of diethylsilanediol, (C_2H_5)-$Si(OH)_2$, has now been completed with these particular purposes in view.

Experimental data were obtained from oscillation photographs and were used to construct Patterson and electron-density projections.

The monoclinic holohedral crystal deposited from ether solution are colorless and flat prismatic in habit. The unit cell dimensions are $a=14.55$, $b=4.96$, $c=10.25$ kx, $\beta=110°\ 10'$.

Space group: $C_{2h}^5-P2_1/a$, $Z=4$, $d=1.134$ (20°C), mp=96°C.

The structure can be described as consisting of molecular chains

$$(\cdots OH-Si(R_2)-OH\cdots OH-Si(R_2)-OH\cdots)$$

parallel to the b axis. These chains are arranged side by side in a plane parallel to (001), and thus form a layer structure, being the repetition of a unit sheet such as

$$\{\cdots OH(R_2)\ OH(R_2)\ OH\cdots\},$$

which is often found in the structure of organic alcohols or fatty acids.

The novel and interesting feature of the structure is the environment of the OH groups arranged nearly in a plane (Fig. 1).

Of the six OH groups surrounding each OH group, two are considerably closer to the central OH, and occurrence of the usual hydrogen bonding is possible only between these two nearest OH neighbors. However, one of them is an intramolecular hydrogen bond with more or less distorted bond angle Si−O−H, which may be an unstable bond. For this reason it may be more reasonable to consider that the location of hydrogen atoms is as in Fig. 1.

The new model explains satisfactorily the considerable shortening of O_1-O_2 distance and other chemical or physical properties[1] of this crystal. The hydrogen atoms now form a kind of bifurcated hydrogen bond, or alternatively these OH−OH linkages may be looked upon as caused by the dipole-dipole interaction between two antiparallel OH-bond dipoles closely confronting each other.

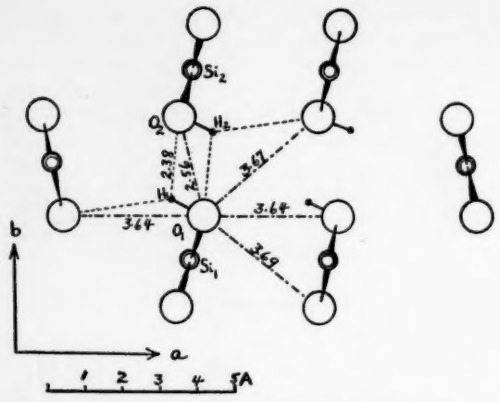

FIG. 1. Schematic representation of hydroxyl groups. (Large circles indicate oxygen atoms, which are nearly on the plane $z=\frac{1}{2}$. Double circles indicate silicon atoms. Ethyl groups are not shown.)

The interatomic distances and bond angles are given below:

$$\text{Si}-\text{OH}=1.63\ \text{kx}, \quad \text{Si}-\text{C}=1.90\ \text{kx},$$
$$\angle\text{OSiO}=110°, \quad \angle\text{CSiC}=111°;$$

(nonbonded)

$$\text{C}\cdots\text{C}=3.94\text{–}4.12\ \text{kx},$$
$$\text{OH}\cdots\text{OH}=2.56\text{–}3.69\ \text{kx}.$$

This new observation of a direct binding of OH groups to silicon may throw light on the bonding of OH groups in organic or inorganic silicon compounds.

The structure analyses of other organosilanols such as

$$(C_6H_5)_2Si(OH)_2, \quad (CH_3)_2(OH)SiCH_2Si(OH)(CH_3)_2,$$

and

$$(CH_3)_2(OH)Si_2(OH)(CH_3)_2$$

have also been carried out. A full account will be given soon.

[1] Digiorgio, Sommers, and Whitmore, J. Am. Chem. Soc. 68, 344 (1946).

T^2 Dependence of the Low Temperature Specific Heat of Gallium

WARREN DE SORBO
General Electric Research Laboratory, Schenectady, New York
(Received November 13, 1952)

TARASOV[1] first demonstrated the applicability of a two-dimensional frequency distribution function to the low temperature specific heat of layer structure graphite. Although the specific heat data on graphite available to Tarasov was rather incomplete, graphical interpolation of the data showed that it obeyed a T^2 law and could not be described by the Debye T^3 law. Recent measurements on the low temperature specific heat of graphite by De Sorbo[2] have verified this T^2 dependence in the region 13–54°K.

More recently Tarasov[3,4] has pointed out an agreement between the experimental specific heat data of the "layer" lattices of the elements gallium, arsenic, antimony, and bismuth with the two-dimensional continuum integrals. For the latter three elements, the comparison was made with data that extended down to liquid nitrogen temperatures only. The author has recently extended the measurements on bismuth and antimony to liquid hydrogen temperatures and has found no T^2 dependence of the specific heat in the lowest temperature region studied. In the case of antimony, however, the deviations can be explained in terms of an anisotropic continuum theory accounting for the interaction between layers and three-dimensional lattice.[5] Reports on this work and that of arsenic, currently being studied, will soon be forthcoming.

In the case of gallium, Tarasov made his comparison with some data of Clusius and Harteck.[6] In this work, large heat transfer corrections caused a wide scattering of the data points. Furthermore, less than a tenth of a gram atom of gallium was available to the authors. Adams[7] has recently published more accurate

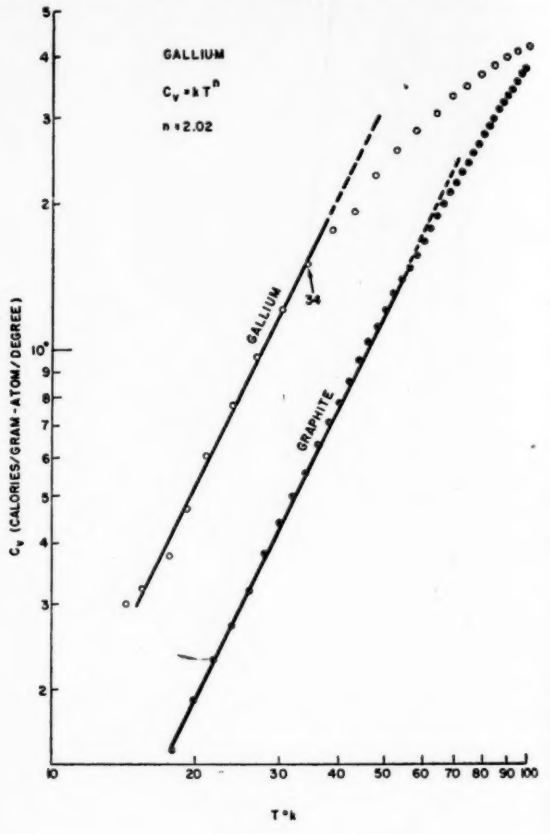

FIG. 1.

specific heat data on gallium. It is the purpose of this note to demonstrate the remarkable T^2 dependence of the specific heat of gallium using Adams' data. This dependence exists in the region 15–34°K. A plot of $\log C_v$ *vs* $\log T$ of Adams' data on gallium and of De Sorbo's data on graphite is shown in Fig. 1. C_v for gallium was calculated using Adams' C_p data and the Nernst and Lindemann formula.[8]

[1] V. V. Tarasov, Compt. rend. acad. sci. U.R.S.S. 1945. Volume XLVI, No. 3.
[2] W. De Sorbo and W. W. Tyler, Phys. Rev. 83, 878 (1951).
[3] V. V. Tarasov, Compt. rend. acad. sci. U.R.S.S. 1946. Volume LIV, No. 9.
[4] V. V. Tarasov, Zhur. Fiz. Khim. XXIV, 1, 111 (1950).
[5] W. De Sorbo, The Eighth Conference on Cryogenics, General Electric Company, Schenectady, New York, October 6–7, 1952.
[6] K. Clusius and P. Harteck, Z. Physik. Chem. 134, 243 (1928).
[7] Adams, Johnston, and Kerr, J. Am. Chem. Soc. 74, 4784 (1952).
[8] W. Nernst and F. Lindemann, Z. Elektrochem. 17, 817 (1911).

Note on Frequency Spectra of Simple Solids from Specific Heat Data

JENN LIN HWANG
Physics Department, Taiwan University, Taipei, Formosa, China
(Received November 13, 1952)

THE difficulties inherent in the problem of finding frequency spectra from specific heat measurements[1–3] have been analyzed exhaustively by Katz.[4] In this note I will show that the Katz' idea which was used in analyzing the specific heat data of low temperature can be extended to the whole temperature range.

The integral equation

$$C(T)=\int_0^{\nu_m}\frac{\left(\frac{h\nu}{kT}\right)^2 e^{h\nu/kT}\rho(\nu)d\nu}{(e^{h\nu/kT}-1)^2} \tag{1}$$

and its restricting condition

$$\int_0^{\nu_m}\rho(\nu)d\nu=1 \tag{1.a}$$

may be converted into convenient forms

$$\frac{C(x)}{x^3}=\int_0^{\mu}\frac{(z/x)^5 e^{z/x}g(z)dz}{z(e^{z/x}-1)^2} \tag{2}$$

and

$$\int_0^{\mu}z^2g(z)dz=1 \tag{2.a}$$

by introducing a parameter ν_0 and new notations

$$\nu/\nu_0=z,\quad kT/h\nu_0=x,$$

$$\nu_m/\nu_0=\mu,\quad\text{and}\quad\rho(\nu)=\frac{1}{\nu_0}\left(\frac{\nu}{\nu_0}\right)^2 g\left(\frac{\nu}{\nu_0}\right). \tag{3}$$

Here for convenience's sake ν_0 must be chosen so as to make $\mu=1$. But unfortunately this requirement cannot be attained in general, because the specific heat data available at present are inadequate for determining the real maximum frequency ν_m beforehand. However, on considering Eqs. (5) and (6) below and applying the method of trial and error to a $C(x)/x^3$ curve, one can choose by a guess a value of ν_0 such that μ becomes substantially less than unity. Therefore, practically the upper limit of each integral may be replaced by 1 instead of μ with the understanding that $g(z)=0$ when $\mu<z\leq 1$.

The first advantage of using the expression (2) is that the specific heat curve of a particular solid would become extremely distinguishable from others; Fig. 1 illustrates that almost all of

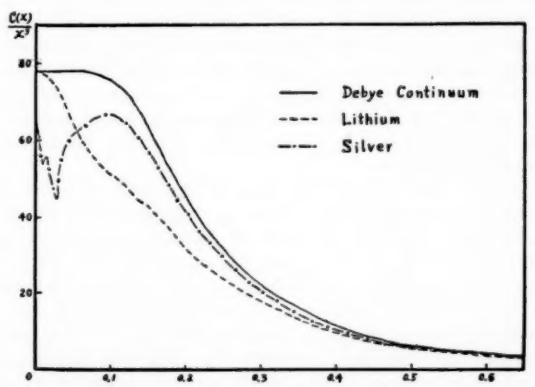

FIG. 1. The character of any specific heat curve may be easily observed from the plotting of $C(x)/x^3$ against $x=T/\theta_0(\theta_0=h\nu_0/k)$. In the Li curve (see reference 5) $\theta_0=314°$ is the value of the effective Debye temperature extrapolated to absolute zero, but for Ag (see reference 6) $\theta_0=200°$ is the one chosen arbitrarily. Either of the values of θ_0 will not fulfill the requirement that $\nu_m/\nu_0\leq 1$.

the special characters of any specific heat curve would appear in the range of lower temperature. The second advantage is more important. According to the definition of integration, we may rewrite Eq. (2) into a summation form

$$\frac{C(x)}{x^3}\simeq\sum_{i=1}^{n}\frac{g(z_i)}{z_i}\frac{(z_i/x)^5 e^{z_i/x}}{(e^{z_i/x}-1)^2}\delta, \tag{4}$$

where $\delta=1/n$ and $z_i=(i-\frac{1}{2})\delta$. Now we can put the following constructions on the Eq. (4) in imitation of Eq. (4) of Katz' paper[4]:

(a) The frequency spectrum is replaced by a substitute spectrum consisting of n designated single frequencies $\nu_0 z_1, \cdots, \nu_0 z_n$ with weights $z_1^2 g(z)\delta, \cdots, z_n^2 g(z_n)\delta$, where

$$\sum_{i=1}^{n} z_i^2 g(z_i)\delta=1. \tag{4.a}$$

(b) Each frequency gives rise to a peak in the $C(x)/x^3$ curve as a function of $x=kT/h\nu_0$. The peaks all have the same basic shape represented in Fig. 1 of Katz' paper or in Fig. 2 of this

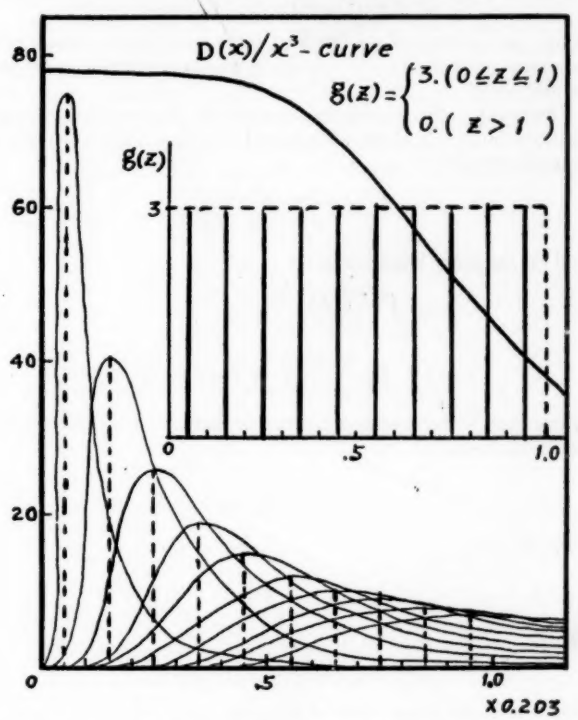

FIG. 2. Analysis of the Debye $C(x)/x^3$ curve in terms of monochromatic frequency peaks. Noting the location and height of each extremum, one can determine $g(z_i)$ from Eqs. (5) and (6) (see reference 7).

paper. The shape is modified by a horizontal scaling factor depending only on z_i and a vertical scaling factor proportional to $g(z_i)\delta/z_i$.

(c) The maximum of each peak lies at

$$x\simeq 0.203 z_i \tag{5}$$

and its height is

$$h_i\simeq 21.3 g(z_i)\delta/z_i. \tag{6}$$

(d) Higher frequencies cause considerably smaller peaks than lower ones with the same $g(z_i)$ values [or spectral weights $z_i^2 g(z_i)\delta$] owing to the factor z_i (or z_i^3).

Since Eqs. (5) and (6) enable us to make a correspondence between the $C(x)/x^3$ curve and its frequency spectrum, not only in the low temperature range but also in the whole range, the above information can be utilized to determine the outline of a frequency spectrum, by analyzing the $C(x)/x^3$ curve in terms of peaks just as was done by Katz.[7] In the higher temperature range, though we cannot expect such a simplicity in interpreting the correspondence as in the lower one, especially when n increases, the present method involves no limitation, such as the one in Katz, in analyzing a $C(x)/x^3$ curve.

A systematic procedure of the analysis, and hence a numerical method for the solution of Eq. (2), is suggested in the following: In order to get a good agreement between the integration and the summation we apply the quadrature formula of Newton-Cotes or Maclaurin to Eqs. (2) and (2.a). Then

$$\frac{C(x)}{x^3}=\sum_{i=1}^{n} W(z_i)\frac{(z_i/x)^5 e^{z_i/x}}{z_i(e^{z_i/x}-1)^2}g(z_i) \tag{7}$$

and

$$\sum_{i=1}^{n} W(z_i) z_i^2 g(z_i) = 1, \tag{7.a}$$

$W(z_i)$ being the weighting factors of the quadrature formula, $\delta = 1/n$, and

$$z_i = \begin{cases} 0, \delta, 2\delta, \cdots, n\delta \text{ for Newton-Cotes' scheme} \\ \delta/2, 3\delta/2, \cdots, (n-\frac{1}{2})\delta \text{ for Maclaurin's scheme.} \end{cases}$$

Thus, for a datum of specific heat corresponding to a value of x, one may get from Eq. (7) a linear equation in which $g(z_i)$ appear as unknowns.

Obviously, $g(0)$ cannot be found with the foregoing scheme, and one must rely upon an alternate method; Eq. (2) may be transformed into

$$\frac{C(x)}{x^3} = \int_0^\infty \frac{\xi^4 e^\xi g(x\xi) d\xi}{(e^\xi - 1)^2},$$

and on the other hand, we know

$$x^n = \lambda_n \int_0^\infty \frac{\xi^4 e^\xi (x\xi)^n d\xi}{(e^\xi - 1)^2},$$

$$\lambda_n = 1 \Big/ \int_0^\infty \frac{\xi^{n+4} e^\xi d\xi}{(e^\xi - 1)^2} = 1/\zeta(n+4)\Gamma(n+5),$$

where $\zeta(\xi)$ is the Riemann's zeta-function and $\Gamma(\xi)$ the gamma-function. Thus, if

$$C(x)/x^3 = \sum_{n=0}^{\infty} a_n x^n,$$

then we have

$$g(z) = \sum_{n=0}^{\infty} a_n \lambda_n z^n.$$

Hence, an exact relation is obtained:

$$g(0) = a_0/\zeta(4)\Gamma(5) = (15/4\pi^4) a_0,$$

where a_0 is the initial value of $C(x)/x^3$.

The exact value of $\mu = \nu_m/\nu_0$ should be determined by extrapolation after the solutions of linear equations have been found.

[1] E. W. Montroll, J. Chem. Phys. **10**, 218 (1942).
[2] H. Grayson-Smith and J. P. Stanley, J. Chem. Phys. **18**, 236 (1950).
[3] W. Kroll, J. Phys. Soc. Japan (to be published).
[4] E. Katz, J. Chem. Phys. **19**, 488 (1951).
[5] F. Simon and R. C. Swain, Z. Phys. Chem. **B28**, 190 (1935).
[6] W. H. Keesom and J. A. Kok, Physica **1**, 770 (1934).
[7] For actual cases, it might be more expedient to deal with the residual portion $[C(x)/x^3] - [D(x)/x^3]$, where $D(x)$ is the Debye function, than the $C(x)/x^3$ curve itself.

Perturbations on Exciton States in Molecular Crystals

HARVEY WINSTON
Research and Development Laboratories, Hughes Aircraft Company, Culver City, California
(Received October 31, 1952)

A METHOD adapted from Slater's[1] treatment of single particles in a perturbed periodic potential can be applied to perturbations on exciton states in molecular crystals. While the method is subject to the same kind of limitations as Slater's, it also shares the major advantage of giving an easily visualizable picture. The results which can be obtained are well known, but the simplicity of the treatment justifies its presentation.

Consider a band of exciton states, each characterized by a crystal momentum $\mathbf{p}_0$, in a crystal containing one perfectly fixed molecule in each unit cell; these states are assumed to be derived from a nondegenerate free molecule state. Let the wave functions of this band be u_{p_0}. From these u_{p_0} functions we form a function $a(\mathbf{Q}_n)$, analogous to Slater's Wannier function:

$$a(\mathbf{Q}_n) = N^{-\frac{1}{2}} \sum_{p_0} \exp(-i\mathbf{p}_0 \cdot \mathbf{Q}_n/\hbar) u_{p_0}. \tag{1}$$

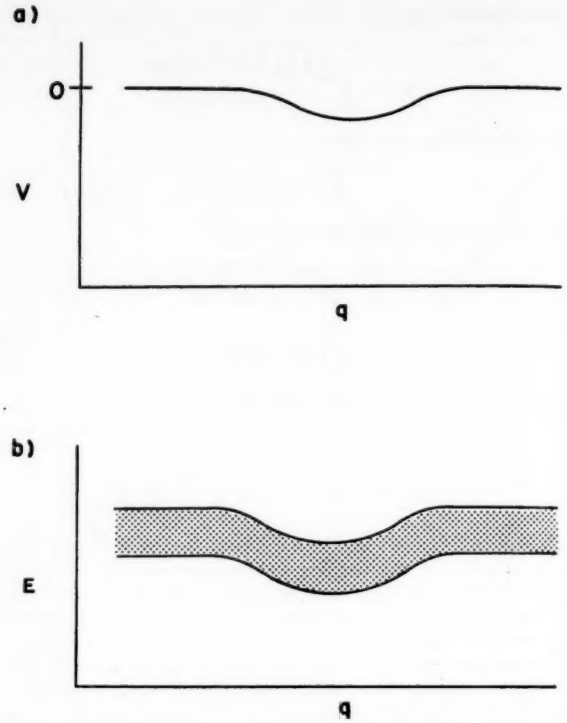

FIG. 1. (a) Effective perturbing potential; (b) perturbing potential superimposed upon the band diagram.

This Wannier-type function $a(\mathbf{Q}_n)$ is, of course, dependent on the coordinates of all the electrons in the crystal; the $\mathbf{Q}_n$ in parenthesis is *not* an argument of the function but instead indicates the cell in which the function localizes the excitation. In fact, $a(\mathbf{Q}_n)$ is not far from being the function constructed from the free molecule functions by placing the molecule at $\mathbf{Q}_n$ in its excited state, placing all others in their ground states, and antisymmetrizing. The localized Wannier-type functions are introduced here only because their special properties make feasible a simple solution for a perturbed problem.

We must now discuss the form of the perturbing potential. To a fairly good approximation, we may think of the perturbation as a function of the cell in which the excitation finds itself, rather than as a function of the actual electron coordinates. This representation is especially well adapted to the method of expressing the wave function as a linear combination of functions $a(\mathbf{Q}_n)$, on account of the way $a(\mathbf{Q}_n)$ localizes the excitation in the nth cell. Perturbations that can be handled in this way include those arising from nuclear displacements and the effect of a foreign molecule with a different excitation energy from the host molecules. This latter disturbance can be idealized as a change in the excitation energy when the excitation finds itself in the foreign molecule's cell.

We now follow Slater in writing the wave function of the perturbed crystal as

$$\psi = \sum_k \Psi(\mathbf{Q}_k) a(\mathbf{Q}_k), \tag{2}$$

and determining $\Psi(\mathbf{Q}_k)$ by solving the following differential equation for $\Psi(\mathbf{q})$, a function of the continuous variable $\mathbf{q}$:

$$[E_0(-i\hbar\nabla) + V(\mathbf{q})]\Psi(\mathbf{q}) = E\Psi(\mathbf{q}). \tag{3}$$

If $E_0(\mathbf{p}_0)$ is the energy of the unperturbed problem as a function of $\mathbf{p}_0$, then $E_0(-i\hbar\nabla)$ is the operator formed by replacing p_{0x} by $(h/2\pi i)(\partial/\partial x)$, etc.; $V(\mathbf{q})$ is the perturbing potential discussed in the preceding paragraph; and $\Psi(\mathbf{q})$ has the physical interpretation that $\Psi^*\Psi$ integrated over a unit cell gives (very nearly) the probability of finding the excitation in that cell.

As an example of the method's application, imagine a displacement of molecular centers over some small region of the crystal. Because of the influence of intermolecular distance on excitation energy, an effective perturbing potential is established, as in Fig. 1(a). As Slater has shown, this perturbing potential can be superimposed upon the band diagram, as in Fig. 1(b), which shows how localized excitation levels can arise in the region of the displacement. The discussion required is similar to the discussions of the similar diagrams in Slater's paper, with the obvious differences between his one-electron functions and our whole-crystal functions. It is not hard to see, given a suitable dependence of E_0 on $\mathbf{p}_0$ and of excitation energy on intermolecular distance, how the excitation can "dig a hole for itself" in the crystal and become localized in a region with distorted intermolecular distances induced by the presence of the excitation. Other well-known results can be discussed qualitatively on the basis of this model. It might also be possible to use Adams'[2] multiband formulation for a more quantitative discussion of the eventual degradation of the whole crystal to its electronic ground state, though this would require a more careful consideration of the effect of vibrations on the scheme.

[1] J. C. Slater, Phys. Rev. **76**, 1592 (1949).
[2] E. N. Adams, II, Phys. Rev. **85**, 41 (1952).

Dielectric Losses of Sodium Chloride Crystals

Y. Haven
Philips Research Laboratories, N. V. Philips' Gloeilampenfabrieken, Eindhoven, Netherlands
(Received November 10, 1952)

As was first pointed out by Breckenridge,[1] lattice defects in alkali halides can give rise to low frequency dielectric losses. The experimental material of Breckenridge, however, is liable to criticism and Henvis, Davisson, and Burstein[2] reported already that Breckenridge's results could not be reproduced. The purpose of this note is to present some further experimental data.

In sodium chloride containing some Ca^{2+} ions, a pair of associated lattice defects, e.g., Schottky defects, or Ca^{2+} ions with Na^+

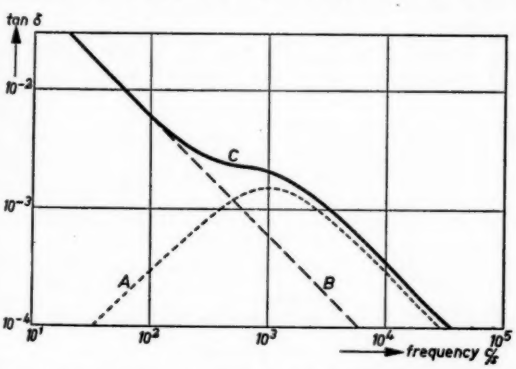

FIG. 1. A = losses resulting from dipoles, B = conductivity losses, C = total losses.

vacancies, can be considered as dipoles which can orient themselves in an electric field and so give rise to Debye-type dielectric losses. The losses resulting from these associated defects can be represented by

$$\tan\delta=\frac{\epsilon_s-\epsilon_\infty}{\epsilon}\cdot\frac{\omega\tau}{1+(\omega\tau)^2}, \tag{1}$$

$$(\epsilon_s-\epsilon_\infty)\epsilon_0=f\cdot n/\mu^2/3kT, \tag{2}$$

whereas free defects (e.g., Na^+ vacancies) give rise to a contribution

$$\tan\delta=\sigma/\epsilon\epsilon_0\omega. \tag{3}$$

Here, ϵ = dielectric constant; $\epsilon_s-\epsilon_\infty$ = contribution of the dipoles to ϵ; ϵ_0 = dielectric constant of free space; $\omega=2\pi\nu$; ν = frequency; τ = relaxation time; f = a factor, near unity, depending on the field that orients the dipoles; μ = electric moment associated with the lattice defects; n = number of dipoles per unit volume; k = Boltzmann's constant; T = temperature in °K; σ = conductivity. The total losses are then the sum of a number of contributions (1) and of (3) (see Fig. 1).

A convenient way of analyzing the dielectric losses is by plotting log tanδ against logν as in Fig. 1. This method of plotting has some advantages over the plotting of tanδ or log tanδ against $1/T$. First, when the dispersion of ϵ is small, (3) is in this plot a straight line, likewise extrapolations of (1) for $\omega\tau\gg1$ or $\ll1$. Secondly, in this way the results are less influenced by other effects, e.g., adsorption of water, which may change with temperature.

In Fig. 2 we present the dielectric losses of sodium chloride

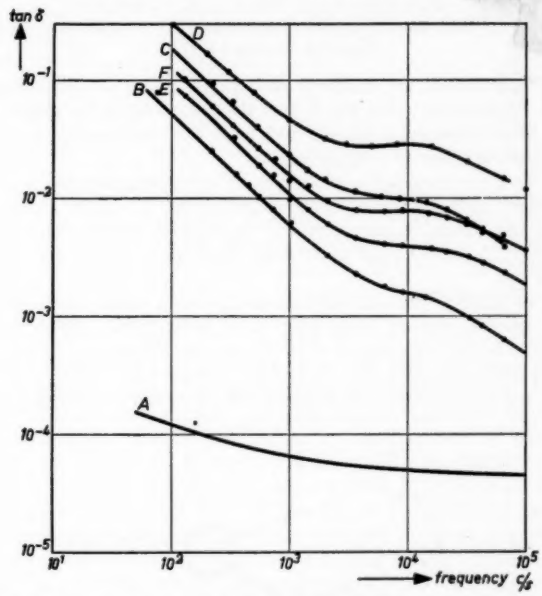

FIG. 2. Dielectric losses of NaCl containing Ca^{2+} or Mn^{2+} at 110°C. A = very pure NaCl, B = NaCl slightly contaminated (0.003 mole percent divalent ions), C = 0.03 mole percent Ca^{2+}, D = 0.14 mole percent Ca^{2+}, E = 0.008 mole percent Mn^{2+}, F = 0.014 mole percent Mn^{2+}.

single crystals containing respectively Ca^{2+} and Mn^{2+} ions. Our specimens were prepared as follows. From the crystals that were prepared from a melt containing the impurities, thin plates were cleaved. These crystals were painted with Ag paste and baked at about 500°C. The samples with Mn^{2+} were sealed in quartz tubes after pumping for about one hour at 150°–200°C and measured in vacuum. The samples with Ca^{2+}, however, were measured in air after having been heated for about 12 hours in air at 140°–150°C. These measures were taken to remove moisture.

By subtracting the conductivity losses, as extrapolated from low frequencies, one obtains Debye curves, which appear to be increased with increasing concentrations of divalent impurities, thus enabling it to be correlated with (Ca^{2+} ion − Na^+ vacancy) pairs. In the frequency range investigated we find one Debye peak for both Mn^{2+} and Ca^{2+} impurities situated at about the same frequency.

In Table I we give the peak frequencies measured on sodium chloride containing Ca^{2+}. The shift of the peak with temperature

TABLE I. Peak frequencies.

Temp.	Frequency
69°C	1000 c/sec
85°C	2600
110°C	12 000
125°C	26 000

corresponds with an activation energy of 0.7 ev. The width of the Debye peaks is about 1.5 times the theoretical width.

Just as Henvis (see reference 2), we too were unable to reproduce the peaks of Breckenridge, and we believe that his results may be incorrect, the more so as the theoretical half-width of the peaks (40°–60°C) is much greater than actually found by Breckenridge in most cases.

More extensive data and the discussion of the results will be published in Philips Research Reports.

[1] R. G. Breckenridge, J. Chem. Phys. **16**, 959 (1948); **18**, 913 (1950).
[2] Henvis, Davisson, and Burstein, Phys. Rev. **82**, 774 (1951).

The Molecular Structure of B_4Cl_4

MASAO ATOJI AND WILLIAM N. LIPSCOMB
School of Chemistry, University of Minnesota, Minneapolis, Minnesota
(Received October 27, 1952)

THROUGH the courtesy of Urry, Wartik, and Schlesinger,[1] who discovered B_4Cl_4 and studied some of its properties, we have obtained a sample and have now completed an x-ray diffraction study of a single crystal.

There are two B_4Cl_4 molecules in a tetragonal unit cell with $a=8.09$ and $c=5.45$A. The space group is $D_{4h}{}^{15}-P(4/n)mc$, and the atomic parameters are $x_{Cl}=0.275$, $y_{Cl}=0$, $z_{Cl}=0.204$, $x_B=0.105$, $y_B=0$, and $z_B=0.385$. Molecular centers are at $00\frac{1}{2}$ and $\frac{1}{2}\frac{1}{2}0$.

The space group and approximate packing require the molecule to have symmetry $D_{2d}-\bar{4}2m$. The interatomic distances are $B_1B_2=B_2B_3=B_3B_4=B_4B_1=1.73$A and $B_1B_3=B_2B_4=1.70$A. All BCl distances are 1.69A. Four ClCl distances are 4.51A and two are 4.45A, all within the molecule. Because of the possibility that

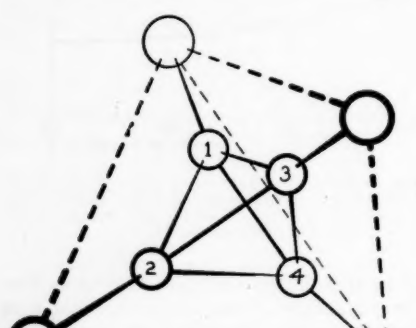

FIG. 1. The molecular geometry of B_4Cl_4.

the slight deviation of the symmetry from tetrahedral might be peculiar to the solid phase, a molecular structure study of the gas phase would be of interest.

Until we know the structures of other electron deficient compounds of boron, there seems little point in remarking on the possible hybridization in B_4Cl_4. However, the bond distances can be treated by the use of Pauling's equation,[2]

$$d=d_1-0.6\log n,$$

for electron deficient molecules. Assuming a single-bond boron radius[3] of 0.80A, and a B–Cl single bond distance[4] of 1.70A, we predict a bond order of 1.04 for the BCl bond, and 0.61 and 0.68 for the two types of BB bonds. The total bond order of 7.96 is quite satisfactory. Thus, the BCl bonds are essentially single bonds, while those between boron atoms are roughly 2/3 bonds.

The boron arrangement in B_4Cl_4 is related to the boron arrangement in B_4H_{10}. The trial structure for B_4H_{10} has now been established by Christer E. Nordman of this laboratory from complete *hkl* data from single crystals. The boron arrangement is at least roughly tetrahedral, and the presence of a disordered phase indicates approximately spherical molecules. While the hydrogen positions have not been determined, it is interesting to guess that the molecule consists essentially of two distorted B_2H_5 groups (one bridge hydrogen missing from each) combined to give a molecule of B_4H_{10} having D_{2d} symmetry.

It is a pleasure to acknowledge the support of this research by the Office of Naval Research.

[1] Urry, Wartik, and Schlesinger, J. Am. Chem. Soc. (to be published).
[2] L. Pauling, J. Am. Chem. Soc. **69**, 542 (1947).
[3] K. Hedberg, J. Am. Chem. Soc. **74**, 3486 (1952).
[4] V. Schomaker and D. P. Stevenson, J. Am. Chem. Soc. **63**, 37 (1941).

The Dissociation of H_2 and N_2 on Tungsten Filaments*

M. FARBER AND A. J. DARNELL
Jet Propulsion Laboratory, California Institute of Technology, Pasadena, California
(Received November 3, 1952)

DURING recent years the dissociation energy of nitrogen has been of a controversial nature with values ranging from 170 to 250 kcal/mole for $D(N_2)$.[1–3] Since the heat of dissociation of N_2 is extremely high for its determination by direct manometric methods, an attempt has been made for the determination of $D(N_2)$ by the hot-wire method.

The hot-wire method was first developed by Langmuir[4] and employed by him for the determination of the dissociation energy of H_2. In the present research the method of Langmuir has been modified in that the gas pressure is low enough (approximately 50 microns) to allow the gas to remain at the temperature of the bulb because of the larger mean free path. A tungsten filament 6 in. long and 0.001 in. in diameter was inserted between two tungsten electrodes 0.10 in. in diameter.

The power necessary to heat the filament in a vacuum and in the presence of the gas to a desired temperature was measured with a Leeds and Northrup type K potentiometer. The temperature was determined from the resistance of the filament[5] and checked with an optical pyrometer. At the temperature employed the power lost to the leads is negligible, and lead corrections can be neglected.

Since the heat of dissociation of H_2 is well known, this gas was used as a check on the method. Figure 1 shows the power vs

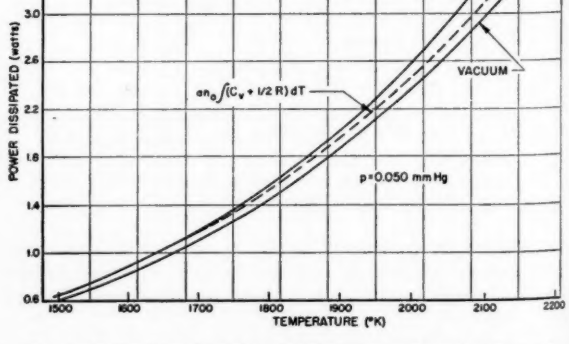

FIG. 1. Thermal conductivity of hydrogen on a tungsten filament.

temperature curve for the filament in the gas and in a vacuum. The accommodation coefficient a in the region of no dissociation is found to be 0.19 and is assumed to remain constant during dissociation. An assumption is also made that the molecules striking the wire either attain the temperature of the wire or are reflected at the incident temperature. The total power difference

is divided between gas conduction and dissociation as

$$\Delta w = an_0\left[\int_{T_i}^{T_w}(C_v+\tfrac{1}{2}R)dT+X\Delta E\right],$$

where $n_0=p/(2\pi MRT_i)^{\frac{1}{2}}$ and X = degree of dissociation.

An analysis of the power data from Fig. 1 leads to a value of ΔH for H_2 of 101±3 kcal/mole and an entropy of 27±1 cal/mole. The entropy from spectroscopic constants in this temperature range is 28 cal/mole.

The experiment was repeated with N_2, and the results are shown in Fig. 2. If the $D(N_2)$ were 170 kcal/mole, the degree of dissociation at a pressure of 50 microns and at a temperature of 3000°K would be nearly 20 percent. This degree of dissociation would indicate a power difference of nearly three times that shown in Fig. 2. Since no evidence of dissociation is found in Fig. 2 at temperatures to 2900°K, it appears that the heat of dissociation of N_2 is greater than 200 kcal/mole. The accommodation coefficient is quite constant over the range studied and is evaluated from the Knudsen equation as 0.55 at 2500 and 2900°K. There was no evidence of a reaction between the N_2 and tungsten since the gas pressure remained constant. Spot determinations were made at 3200 and 3300°K with no apparent trace of dissociation. This fact would tend to support a value for the heat of dissociation of N_2 of at least 225 kcal/mole.

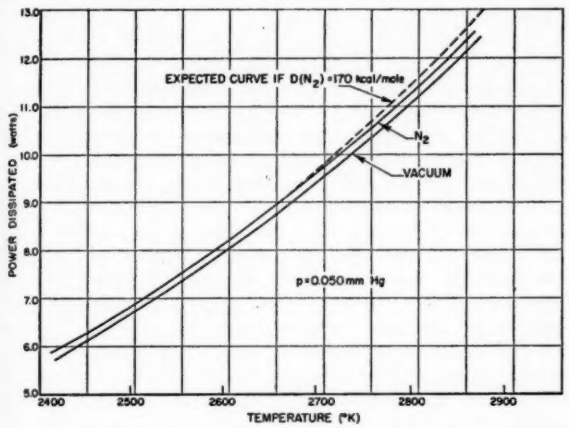

FIG. 2. Thermal conductivity of nitrogen on a tungsten filament.

* This paper presents the results of one phase of research carried out at the Jet Propulsion Laboratory, California Institute of Technology, under Contract No. DA-04-495-Ord 18 sponsored by the Department of the Army, Ordnance Corps.

[1] L. Pauling, *Nature of the Chemical Bond* (Cornell University Press, Ithaca, New York, 1939).
[2] A. G. Gaydon, *Dissociation Energies* (John Wiley and Sons, Inc., New York, 1947).
[3] G. Glockler, J. Chem. Phys. **19**, 124 (1951).
[4] I. Langmuir, Phys. Rev. **34**, 401 (1912); J. Am. Chem. Soc. **34**, 860 (1912); J. Am. Chem. Soc. **37**, 417 (1914).
[5] H. A. Jones and I. Langmuir, Gen. Elec. Rev. **30**, 310, 354, 408 (1927).

Effects of Vibrational State on Rotational Intensity Distributions in OH†

A. M. BASS AND H. P. BROIDA
National Bureau of Standards, Washington, D. C.
(Received November 17, 1952)

As part of a study of the rotational energy distributions in flames, a survey has been made of rotational "temperatures" as determined from the OH ($^2\Sigma^+-{}^2\pi$) emission spectrum. The spectrum was observed in the hot gases above the reaction zone of a flame of a stoichiometric mixture of hydrogen and oxygen. Rotational "temperatures" were measured from the slopes of the usual plots[1] of $\log(I_K/A_K\nu^4)$ *versus* E_K. (I_K is the peak intensity and A_K is the transition probability, including the statistical weight, for a particular transition from the initial energy level E_K which gives rise to emission of radiation of frequency ν.) These measurements have been carried out for the six main branches of the (3,3), (2,2), (1,1), (0,0), (1,0), and (2,1) bands of OH. The spectra were recorded by a Leeds and Northrup grating monochromator.[2,3]

In the hot gases above the reaction zone of the observed flame, previous studies[4] have indicated that there is thermal equilibrium with a calculated adiabatic temperature of 3100°K and a measured sodium line reversal temperature[5] of 2750°K. From the measured values of line intensities and the values of E_K, A_K, and ν as tabulated in the report of Dieke and Crosswhite[6] the "temperatures" determined by the method described above are as shown in Table I. The uncertainty in the "temperature" arises from the difficulty of determining the slope of the line because of the scatter of the measured intensities. In all cases the tabulated limits indicate the extreme temperatures which can be determined from the scatter of the plotted points. To diminish the effects of self-absorption on the measured "temperatures," the emphasis in determining the slopes was placed on the lines of low emissivity (chiefly lines of high K number). The effect of self-absorption would be to give abnormally high "temperatures," and would be more pronounced for lines of high intensity. However, the facts that the 0,0 band gives an intermediate "temperature," and that the 2,1 band gives a "temperature" 17 percent higher than the more intense 1,1 band strongly suggest that self-absorption is not the major cause of the differences in these measurements. The measured "temperature" from the logarithmic plot in the 0,0 band agrees well with that of 2650°K as determined by the use of the iso-intensity method with the R_2 branch.[4]

TABLE I.

Band	T_R°K	$T_{R\max}$°K	$T_{R\min}$°K
3,3	1900	2700	1700
2,2	2450	2600	2300
1,1	2550	2700	2500
0,0	2675	2775	2650
1,0	2950	3100	2950
2,1	3000	3250	2850

In the hot gases above the reaction zone of a methane-oxygen flame, Shuler[7] has observed a similar difference in rotational "temperatures" between the 1,0 and the 0,1 bands of OH.

It is not yet possible to explain fully these measured differences. However, Dieke and Crosswhite[6] state that their calculations of the transition probabilities (A_K) omit the vibration-rotation interaction in the OH molecule. Since different rotational "temperatures" are found in the same initial vibrational state, this would indicate that a possible source of the observed discrepancy may lie in the fact that these terms have been neglected. This effect will be studied further and the measurements extended to other bands in the OH spectrum.

† Supported in part by the Office of Ordnance Research.

[1] G. Herzberg, *Molecular Spectra and Molecular Structure. I. Spectra of Diatomic Molecules* (D. Van Nostrand Company, Inc., New York, 1950), second edition, pp. 126, 205.
[2] W. G. Fastie, J. Opt. Soc. Am. **42**, 641 (1952).
[3] This instrument was constructed by the Research Department of Leeds and Northrup Company and loaned to the Heat and Power Division of the National Bureau of Standards on a field trial arrangement.
[4] H. P. Broida and K. E. Shuler, J. Chem. Phys. **20**, 168 (1952).
[5] H. H. Lurie and G. W. Sherman, Ind. Eng. Chem. **25**, 404 (1933).
[6] G. H. Dieke and H. M. Crosswhite, "The Ultra Violet Bands of OH, Fundamental Data," Bumblebee Series Report No. 87, 1948.
[7] K. E. Shuler, private communication.

On the Statistical Theory of Crystallite Length

MALCOLM DOLE
Department of Chemistry, Northwestern University, Evanston, Illinois
(Received October 30, 1952)

UNDER the above title Simha[1] has discussed the statistical treatment we gave previously[2] for the size distribution of crystallizable sequences between branch points. He points out

that the model adopted by us, namely, of y branches distributed at random on S carbon atoms of the main chain of molecules of uniform length, is erroneous and should be refined to consider the probability that some molecules will have more or less than y branches per molecule. We agree with this but wish to point out that some of the differences between the equations given in Simha's note and our paper are due to the fact that Simha counts the number of zero groups in computing his weight and number fractions and averages while we omitted them. By a "zero group" we mean groups for which ζ, the number of units in a free crystallizable sequence, is equal to zero. A zero group can be formed by two adjacent side chains or by a side chain next to an end group.

By dividing our[2] Eq. (11) by Eq. (13), we obtain the number fraction of groups having ζ free units when the zero groups are also counted or

$$\bar{\nu}_\zeta{}^0=\frac{(S-1-\zeta)\,!(S-y)\,!y}{(S-y-\zeta)\,!S\,!}. \tag{1}$$

The superscript zero on the symbol ν means that the zero groups are included. Following the method of our previous paper, we can now show that

$$\bar{\nu}_\zeta{}^0=\frac{\nu_\zeta{}^0}{\sum_{\zeta=0}^{S-y}\nu_\zeta{}^0}=\frac{\nu_\zeta{}^0}{1+y} \tag{2}$$

in agreement with one of Simha's equations and that

$$\sum_{\zeta=0}^{S-y}\zeta\bar{\nu}_\zeta{}^0=\frac{S-y}{1+y}, \tag{3}$$

which is also obtainable from Simha's equations. For the weight fraction counting each branch point as one unit we now have

$$\bar{W}_\zeta{}^0=\frac{\zeta\cdot y(y+1)}{S}\cdot\frac{(S-1-\zeta)\,!(S-y)\,!}{(S-y-\zeta)\,!S\,!}, \tag{4}$$

and summing over all weight fractions to equal unity

$$1=\sum_{\zeta=1}^{S-y}\bar{W}_\zeta{}^0+\frac{y}{S}. \tag{5}$$

The added term y/S is to allow for the fraction of weight of the branch points. It is through the use of (5) that (3) was obtained. The number average length of a sequence is

$$\langle\zeta\rangle=\frac{\sum_{0}^{S-y}\zeta\nu_\zeta{}^0}{\sum_{0}^{S-y}\nu_\zeta{}^0}=\frac{S-y}{y+1} \tag{6}$$

in agreement with Simha. When the average length is calculated not counting the groups of zero length, the average is $S/y+1$.

The difference between the treatments using the refined model of Simha and ours enters into the value of $\nu_\zeta{}^0$. For the example calculated by us[2] the difference amounts to slightly less than one percent for the number of zero groups, $\nu_0{}^0$, and decreases slowly as ζ increases.

[1] Robert Simha, J. Chem. Phys. **20**, 1654 (1952).
[2] Dole, Hettinger, Larson, and Wethington, J. Chem. Phys. **20**, 781 (1952).

Note on the Generalized Free-Electron Model of Conjugated Polycyclic Hydrocarbons

J. Stanley Griffith*
Department of Theoretical Chemistry, University of Cambridge, Cambridge, England
(Received November 14, 1952)

A GENERALIZATION of the perimetral free-electron model of conjugated polycyclic hydrocarbons has recently been proposed independently by at least three authors: Nakajima and Kon,[1] Perkampus,[2] and Griffith.[3] This generalization involves a new boundary condition at carbon nuclei of atoms linked to three neighbors. It has been shown by Griffith[3] that this condition is necessary in order that the resulting Hamiltonian shall be Hermitian. The new model leads to predictions of long wavelength transitions for porphine, tetrahydroporphine azulene, naphthalene, and benzologs, which are very comparable with those of a simple LCAO theory. For open-chain polyenes and benzene the new model is, of course, the same as the older perimetral one.

The present author has discovered a detailed correspondence between the wave functions of the generalized free-electron model (FE) and a certain algebraic set of secular equations. For polycyclics without side chains, the set of values c_p of an FE wave function at the n nuclei ($p=1, 2, \cdots, n$) are found to satisfy the equations

$$-\tfrac{1}{2}d_p x c_p+\Sigma c_q=0, \tag{1}$$

where the sum extends over all q such that atom p is linked to atom q, and d_p is the number of such q. The simple correspondence holds also for polycyclics with side chains, provided the free-electron path along each side chain is taken to extend one bond-length beyond the last carbon nucleus. When p is the last atom of a side chain the equation involving xc_p is $-xc_p+c_q=0$ (p linked to q) as in the LCAO case. This definition of the position of the end of a chain has also been considered by Hückel[4] and by Jaffé[5] for the particular case of open-chain polyenes. However, while for polycyclics with side chains no other reasonable definition leads to any simple algebraic correspondence; for acyclics, although this is the most natural definition, others can be used provided the c_p are measured at points slightly away from the nuclei. It will be noticed that, if there are no carbon atoms linked to three neighbors, then these equations are identical in form with the LCAO ones.

In the free-electron theory the energy is $\hbar^2\lambda^2/2m$, and the quantity x above is related to λ by the equation $x=2\cos\lambda a$ (a is the CC internuclear distance). When the n vectorial solutions $\mathbf{c}$ of (1) are arranged in order of decreasing x, it is found that they are derived in the manner shown above from the n FE functions of smallest $|\lambda|$, arranged in order of increasing $|\lambda|$ (in cases of degeneracy this situation is modified in a straightforward manner). There is in fact always a 1:1 order—and symmetry—preserving correspondence between the vectors $\mathbf{c}$ and the FE functions of lowest $|\lambda|$.

The π-electron charge density is defined in the FE model as

$$\rho(x)=2\sum_{\text{occ.}}|\psi(x)|^2.$$

From the detailed correspondence outlined above, it can be deduced that, for all alternant hydrocarbons, ρ is unity at every carbon nucleus linked to only one or two neighbors.

* Present address: Christ Church College, Oxford, England.
[1] T. Nakajima and H. Kon, J. Chem. Phys. **20**, 751 (1952).
[2] H.-H. Perkampus, Z. Naturforsch. **7b**, 594 (1952).
[3] J. Stanley Griffith (to be published).
[4] E. Hückel, Z. Elektrochem. **43**, 776 (1937).
[5] H. H. Jaffé, J. Chem. Phys. **20**, 1646 (1952).

A Free-Electron Model for Discussing Reactivity in Unsaturated Hydrocarbons

Kenichi Fukui, Teijiro Yonezawa, and Chikayoshi Nagata
Faculty of Engineering, Kyoto University, Kyoto, Japan
(Received November 4, 1952)

FOR the purpose of accounting for the reactivity of each position in an aromatic hydrocarbon, several methods[1] were proposed since Schmidt's first quantum-mechanical treatment.[2] Most recently in the LCAO MO treatment of aromatic molecules, the possible importance of the electrons in the highest occupied level, concerning the electronic rate process involved in the electrophilic substitution, has been pointed out by Fukui, Yonezawa, and Shingu,[3] who have referred to these as *frontier* electrons. In the present letter a simple approximate prediction

TABLE I. Electron density distributions of every energy level in butadiene, from LCAO MO calculation and from free-electron treatment. λ: $\epsilon=\alpha+\lambda\beta$, α: Coulomb integral, β: exchange integral between two adjacent π-orbitals, ϵ: one-electron energy; $\omega=(2m\epsilon/\hbar)^{\frac{1}{2}}$; $\rho_i=\psi^*\psi/(1/a)$ at carbon atom i; $\rho_i'=\int\psi^*\psi d\tau$; integration is done over the region within the distance $a/2$ from carbon atom i (for a terminal carbon atom integration should be made up to the distance a in the direction of the end); ※ frontier level.

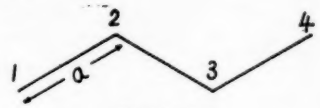

Butadiene

Symmetry property of wave function	LCAO MO treatment[a] λ	Electron density $\lvert C_i\rvert^2$ at 1	2	$\omega a/\pi$	Free-electron treatment Local density ρ_i at 1	2	Integrated density ρ_i' at 1	2
Antis.	−1.6180	0.1382	0.3618	0.8000	0.1382	0.3618	0.2622	0.2378
Sym.	−0.6180	0.3618	0.1382	0.6000	0.3618	0.1382	0.3505	0.1495
※Antis.	+0.6180	0.3618	0.1382	0.4000	0.3618	0.1382	0.3757	0.1243
Sym.	+1.6180	0.1382	0.3618	0.2000	0.1382	0.3618	0.1486	0.3514

[a] See reference 3.

of the reactivity is made, again in the light of the *frontier* electron concept, using a free-electron model.

The free-electron treatment has been reported or suggested by several authors[4–6] related to such problems of the conjugated system as absorption spectra and diamagnetic anisotropy. On the problem of chemical reactivity, however, no free-electron treatment seems to have been reported except Schmidt's method.[2] In Schmidt's model an aromatic system was regarded as a box filled with a Fermi gas of a definite number of π-electrons. In the present model, for the quantum-mechanical treatment of an unsaturated hydrocarbon, free electrons are traveling along a network generally composed of closed circuits and open chains.[5,6]

At a cross link the continuity requirement as to three parts of the wave function must be satisfied. At an end of chain the boundary condition is taken so that the wave function vanishes at the point which is one bond length distant from the terminal carbon atom.

In Tables I and II in the case of butadiene and naphthalene, as an illustration, the electron distributions calculated for every energy level are shown together with the results obtained from the ordinary LCAO MO treatment.[3] A qualitative parallelism is found between the results of two approximations. Especially for the *frontier* level, at sight of the calculated electron density at every carbon atom, it is observed that the density is large at the point which is known from experience as reactive. Besides, in some *alternant* hydrocarbons,[7] such as butadiene, hexatriene, naphthalene, etc., the *frontier* electron density at every carbon atom from the free-electron model coincides exactly with that of the LCAO MO approximation. This fact demonstrates that the free-electron approximation, if adopted together with the *frontier* electron concept, can similarly serve as the LCAO MO treatment to predict the chemical reactivity at any position in a conjugated system. Moreover, as some merits of the free-electron approximation, it can be pointed out that the continuous electron distribution can be obtained automatically in the process of calculation, and especially in a long chain molecule the calculation is simpler than in the LCAO MO treatment. In Fig. 1 the *frontier* electron density at each carbon atom in a straight chain conjugated polyene is shown.

The present method on the basis of the *frontier* electron concept

TABLE II. Electron density distributions of every energy level in naphthalene, from LCAO MO calculation and from free-electron treatment. Symmetry property of wave function: S =sym. and A =antisym. with respect to XX', s =sym. and a =antisym. with respect to YY'. Other notations are the same as in Table I.

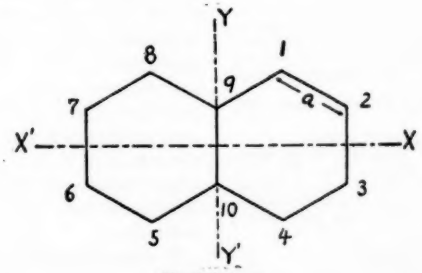

Naphthalene

Symmetry property of wave function	LCAO MO treatment λ	Electron density $\lvert C_i\rvert^2$ at 1	2	9	$\omega a/\pi$	Free-electron treatment Local density ρ_i at 1	2	9	Integrated density ρ_i' at 1	2	9
Sa	−2.3028	0.0903	0.0532	0.2130	1.0000	0.1818	0.1818	0.1818	0.0909	0.0909	0.1364
Aa	−1.6180	0.0691	0.1809	0.0000	0.8000	0.0691	0.1809	0.0000	0.0928	0.1189	0.0766
Ss	−1.3028	0.1597	0.0301	0.1204	0.7010	0.1561	0.0328	0.0813	0.1080	0.0628	0.1584
Sa	−1.0000	0.0000	0.1667	0.1667	0.6392	0.0030	0.1263	0.1611	0.0500	0.1056	0.1887
As	−0.6180	0.1809	0.0691	0.0000	0.6000	0.1809	0.0691	0.0000	0.1408	0.0844	0.0495
※Aa	+0.6180	0.1809	0.0691	0.0000	0.4000	0.1809	0.0691	0.0000	0.1612	0.0766	0.0243
Ss	+1.0000	0.0000	0.1667	0.1667	0.3608	0.0030	0.1263	0.1611	0.0202	0.1187	0.2223
Sa	+1.3028	0.1597	0.0301	0.1204	0.2991	0.1561	0.0328	0.0814	0.1454	0.0395	0.1301
As	+1.6180	0.0691	0.1809	0.0000	0.2000	0.0691	0.1809	0.0000	0.0711	0.1757	0.0065
Ss	+2.3028	0.0903	0.0532	0.2130	0.0000	0.0909	0.0909	0.0909	0.0909	0.0909	0.1364

I. Carbon number $2N$. $C_{2N}H_{2N+2}$

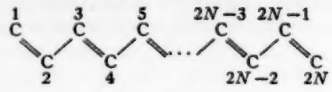

(a) N is even: $\rho_i = \frac{1}{N+\frac{1}{2}} \sin^2\left(\frac{Ni}{2N+1}\pi\right)$ $(i=1, 2, \cdots, N)$

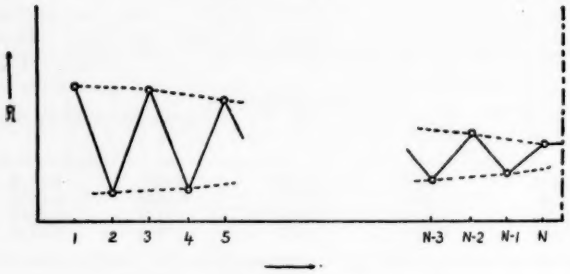

→Number of a carbon atom i in a chain

(b) N is odd: $\rho_i = \frac{1}{N+\frac{1}{2}} \sin^2\left(\frac{Ni}{2N+1}\pi\right)$ $(i=1, 2, \cdots, N)$

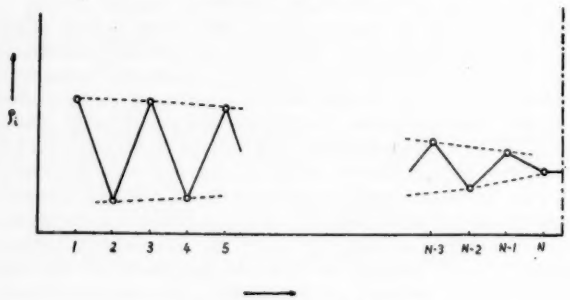

→Number of a carbon atom i in a chain

II. Carbon number $2N+1$: $C_{2N+1}H_{2N+3}$ radical

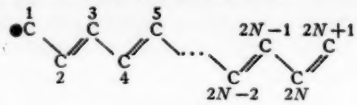

(a) N is even: $\rho_i = \frac{1}{N+1} \sin^2\left(\frac{i\pi}{2}\right)$ $(i=1, 2, \cdots, N, N+1)$

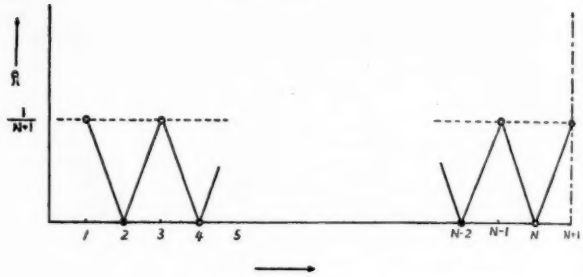

→Number of a carbon atom i in a chain

(b) N is odd: $\rho_i = \frac{1}{N+1} \sin^2\left(\frac{i\pi}{2}\right)$ $(i=1, 2, \cdots, N, N+1)$

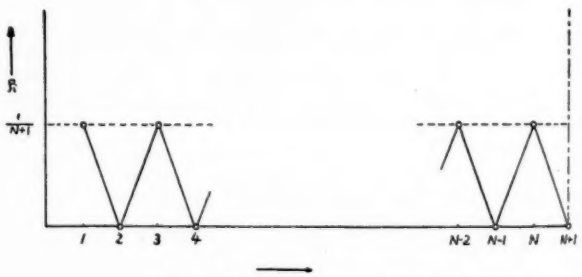

→Number of a carbon atom i in a chain

FIG. 1. Frontier electron density at each carbon atom in a straight chain conjugated polyene.

could easily be extended to the problem of the reactivity in π-electron systems containing heteroatoms or substituents by introducing suitable perturbing potentials.[6]

Financial support for this work has been received from GAFSR (1952-59255), Education Ministry, Japanese Government.

[1] G. W. Wheland, J. Am. Chem. Soc. **64**, 900 (1942); A. Pullman and B. Pullman, Rev. sci. **84**, 145 (1946) and Experientia **2A**, 364 (1946); Buu-Hoi, Daudel, and Vroelant, Bull. soc. chim. France **1949**, 211; C. Vroelant, Compt. rend. **228**, 1029 (1949); Burkitt, Coulson, and Longuet-Higgins, Trans. Faraday Soc. **46**, 553 (1951).
[2] O. Schmidt, Z. physik. Chem. **39**, 59 (1938); **42**, 83 (1939); **44**, 185, 194 (1939); **47B**, 1 (1940).
[3] Fukui, Yonezawa, and Shingu, J. Chem. Phys. **20**, 722 (1952).
[4] L. Pauling, J. Chem. Phys. **4**, 673 (1936); K. Lonsdale, Proc. Roy. Soc. (London) **159**, 149 (1937); W. T. Simpson, J. Chem. Phys. **17**, 1218 (1949); J. R. Platt, J. Chem. Phys. **17**, 484 (1949); H. Kuhn, J. Chem. Phys. **16**, 840 (1948), **17**, 1198 (1949), Helv. Chim. Acta **31**, 1441 (1948), and Chimia **2**, 11 (1948); M. W. Nathans, J. Chem. Phys. **20**, 741 (1952).
[5] H. Kuhn, Helv. Chim. Acta **32**, 2247 (1949).
[6] T. Nakajima and H. Kon, J. Chem. Phys. **20**, 750 (1952).
[7] H. C. Longuet-Higgins, J. Chem. Phys. **18**, 265 (1950).

A Theory of Successive Rotational Transitions in Crystals

THEODORE J. KRIEGER* AND HUBERT M. JAMES
Purdue University, Lafayette, Indiana
(Received October 23, 1952)

THE specific heat curves of certain crystals, such as the hydrogen halides and ammonium salts, show two or three successive λ-point anomalies.[1] These have been associated with changes in the rotational or orientational order of the component molecules or ions. Kirkwood[2] and Chang[3] have considered crystal models consisting of arrays of classical rotators in which the potential energy of the coupling of next neighbors is of the form

$$E(\theta_{ij}) = A\cos\theta_{ij},$$

θ_{ij} being the angle between the axes of symmetry of the molecules. Kirkwood's approximations correspond to those in the Bragg-Williams theory of order-disorder transitions in alloys, Chang's approximations to those in Bethe's more accurate theory. Both calculations indicate the occurrence of a single second-order transition at a temperature determined by A and the number z of next neighbors of any central atom. Tisza[4] has made a qualitative suggestion as to how two (but not three) orientational transitions might occur in the hydrogen halides, but no detailed calculations have previously been made on any model showing more than one transition.

It was supposed by Chang that the qualitative behavior of his model would be little affected by the assumed dependence of the coupling energy on θ_{ij}. This, however, is contrary to the fact (noted by Kirkwood, and easily verified) that a model with $E(\theta_{ij})$ proportional to $\cos^2\theta_{ij}$ gives a transition of the first order, rather than one of the second order. We have investigated the dependence of the transition phenomena on the interaction potential function, assumed to have the form

$$E(\theta_{ij}) = AP_1(\cos\theta_{ij}) + BP_2(\cos\theta_{ij}),$$

where the P's are the Legendre polynomials and A and B are adjustable parameters. For negative A, the first term represents a coupling tending to favor parallel orientations of adjacent molecules over antiparallel orientations; for negative B, the second term favors parallel and antiparallel orientations over per-

pendicular ones. The two terms can be considered as the first terms in the expansion of a general potential for orientational coupling independent of the direction of the line between molecules.

In the Bragg-Williams approximation, the probability per unit solid angle for finding the angle θ between the molecular axis and a preferred direction in space is proportional to

$$\exp[-\alpha P_1(\cos\theta)-\beta P_2(\cos\theta)],$$

where α and β are long-range order parameters that are functions of T, A, B, and z. As T rises, first-order transitions occur when either α or β changes discontinuously, while second-order transitions occur when they vanish without discontinuity. In the Bragg-Williams approximation we find that transitions will occur as follows, as T rises:

$B/A>3.21$	Second-order transition as α vanishes, followed by a first-order transition as β vanishes.
$3.21>B/A>2.89$	Successive first-order transitions as α and β vanish.
$2.89>B/A>0.55$	Single first-order transition as α and β vanish together.
$0.55>B/A>0$	Single second-order transition as α and β vanish together.

As a check, calculations have been made by an extended but much simplified version of Chang's method. The results, as in Chang's theory, are restricted to small deviations from random orientation of the molecules. The qualitative results of the Bragg-Williams calculation have been confirmed, so far as they are accessible to this method, and improved values for some of the numerical constants have been found.

Powles[5] has estimated the magnitudes of the dipolar and van der Waals interactions in hydrogen halides, which would correspond in a general way to the parameters A and B of our model, respectively. He finds a fair correlation of the upper transition temperature T_2 with the van der Waals forces, but a very poor correlation of the lower transition temperature T_1 with the dipole forces. This would be expected from consideration of our model, which indicates that, when two transitions occur, T_2 depends little on the value of A, whereas T_1 depends strongly on both A and B. The successively smaller spacing of T_1 and T_2 in the sequence DI, DBr, DCl is also suggested by our theory, combined with Powles' calculations.

Perhaps the most serious simplification in our model is the neglect of any dependence of orientational coupling on the direction of the line between the two molecules. This, with quantum effects and the need for including more terms in the expansion of $E(\theta_{ij})$, may well contribute to the variety and complexity of observed rotational transitions.

A detailed account of this work is in preparation.

* Now at Battelle Memorial Institute, Columbus, Ohio.
[1] A. Eucken, Z. Elektrochem. **45**, 126 (1939).
[2] J. G. Kirkwood, J. Chem. Phys. **8**, 205 (1940).
[3] T. S. Chang, Proc. Cambridge Phil. Soc. **33**, 524 (1937).
[4] In *Phase Transformations in Solids* (J. Wiley and Sons, Inc., New York, 1951), report on Cornell symposium.
[5] J. G. Powles, Trans. Faraday Soc. **48**, 430 (1952).

Self-Diffusion in the Alkali Metals

D. K. C. MacDonald
Division of Physics, National Research Council, Ottawa, Canada
(Received November 4, 1952)

In a recent paper in this Journal, Gutowsky and McGarvey[1] report that from measurements of the nuclear resonance linewidth in Li and Na, they deduce activation energies for self-diffusion in the solid metals of 9.8±1 kcal/g atom and 9.5±1.5 kcal/g atom, respectively. Measurements of the electrical resistance in Li, Na, and K over a wide range of temperature (see, e.g., Fig. 1) show clearly an "anomalous" rise of resistance starting well below the melting point which permits an independent estimate of an activation energy to be made.

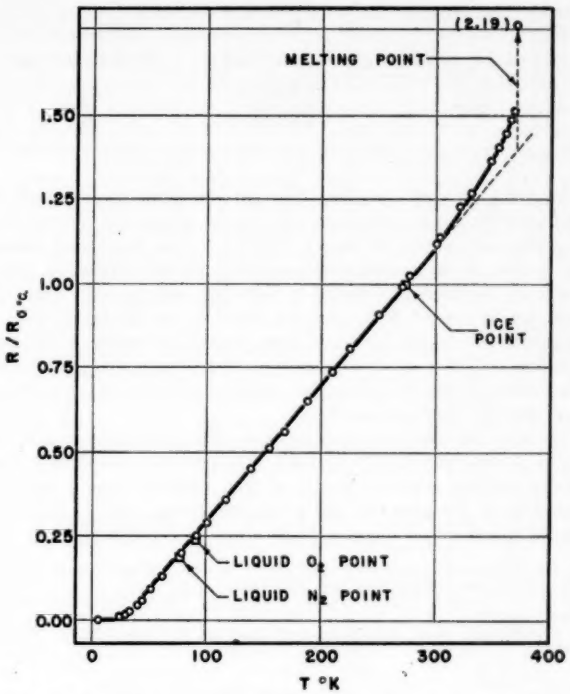

FIG. 1. Electrical resistance of sodium from 0°K to melting point.

Assuming that the equilibrium concentration of "holes" in the lattice at temperature T resulting from self-diffusion is given by

$$(N/N_0)\sim\epsilon^{-U/RT}, \tag{1}$$

where U is the activation energy for self-diffusion. It follows that the relative "excess" resistance ΔR should be given by

$$(\Delta R/R)\propto(1/T)\epsilon^{-U/RT}. \tag{2}$$

Figure 2 then shows $\ln(T\Delta R/R)$ plotted against $1/T$ for the three metals Li, Na, and K. It will be seen that satisfactory straight lines result and the activation energies U deduced are given in Table I.

The excellent agreement for Li and Na with the work of

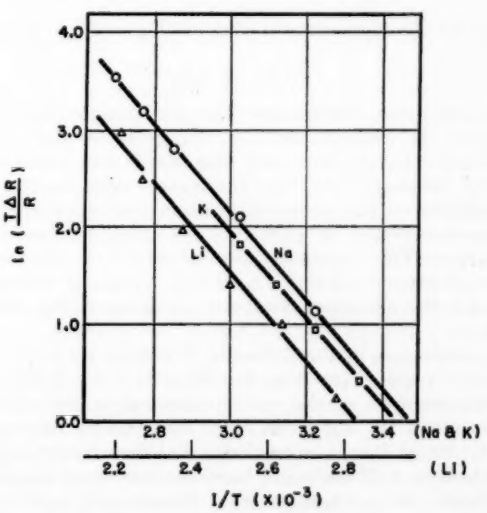

FIG. 2. Determination of activation energy from "excess" electrical resistance.

TABLE I.

	U (kcal/mole)	Lvap (kcal/mole)
Li	9.3±0.35	32.6
Na	9.1±0.1	23
K	9.1±0.1	19.3

Gutowsky is very pleasing, the more so since their results are deduced from a *diffusion-rate* essentially, while ours depend on an equilibrium number of lattice vacancies. The surprising feature, of course, is the remarkable constancy of the activation energy since on the basis of Frenkel or Schottky defects (e.g., Frenkel[2]), one would expect U to depend directly on the latent heat of vaporization which for these three metals is shown in the third column of Table I for comparison. The behavior is perhaps less surprising if one considers the equation $\Delta H=16.5L_{\text{melt}}$ proposed recently by Nachtrieb *et al.*[3]

It may be remarked that no exponential resistance rise of this type is observed in Rb and Cs. This would accord with their lower melting points, since it is then unlikely that a sufficient number of vacancies of an activation energy ~9 kcal/g atom could be generated to produce an observable resistance.

[1] H. S. Gutowsky and B. R. McGarvey, J. Chem. Phys. **20**, 1472 (1952); H. S. Gutowsky, Phys. Rev. **83**, 1073 (1951).
[2] J. F. Frenkel, *Kinetic Theory of Liquids* (Clarendon Press, Oxford, 1946), p. 13.
[3] Nachtrieb, Weil, Catalano, and Lawson, J. Chem. Phys. **20**, 1189 (1952).

The Unimolecular Decompositions of Some Alkyl Bromides

J. H. S. GREEN, G. D. HARDEN, ALLAN MACCOLL, AND P. J. THOMAS
William Ramsay and Ralph Forster Laboratories, University College, Gower Street, London, W.C.1, England
(Received October 28, 1952)

As has been previously reported,[1-3] there is a possible duality of mechanism for the decomposition of alkyl bromides in the gas phase into an olefin and HBr. In the first place, elimination of HBr may proceed in a single step,[3]

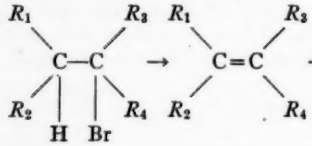

(A)

or secondly the initial process may be the breaking of a C—Br bond,[1,2]

$$R\text{—Br}\rightarrow R+\text{Br}. \qquad \text{(B)}$$

In this latter case, the bromine atom may initiate chains, which will lower the over-all activation energy below the value for breaking the C—Br bond and thus enable mechanism (B) to complete favorably with (A). The present note describes some investigations on the unimolecular elimination mechanism which have been obtained by inhibiting the chain mechanism with cyclohexene. This substance was suggested by the work on cyclohexyl bromide (J.H.S.G.), and its enhanced efficiency as compared with propylene has been demonstrated by one of us (P.J.T.).

The parameters of the Arrhenius equations obtained for the maximally inhibited reactions are shown in Table I. All the decompositions when carried out in seasoned vessels are homogeneous and of the first order. Since the chain mechanisms have been eliminated, it may be concluded that they proceed according to mechanism A. Daniels and his co-workers[4] have examined in some detail, the pyrolysis of ethyl bromide and have come to the conclusion that chains certainly play an appreciable part in the noninhibited reaction. This view is confirmed by our study of

TABLE I.

Molecule	log$A$	E (kcal)
ethyl bromide	13.42	53.9
n-propyl bromide	12.90	50.7
n-butyl bromide	13.18	50.9
iso-butyl bromide	13.05	50.4
sec-propyl bromide[a]	13.62	47.8
sec-butyl bromide[a]	12.63	43.8
cyclo-hexyl bromide[a]	13.38	46.1
tert-butyl bromide[a]	14.00	42.2

[a] For these substances no inhibition was observed.

the unimolecular elimination. That a fine state of balance exists between the chain and the unimolecular mechanisms is shown by a comparison of Daniels' value for the parameter of the over-all reaction ($E=53.0$, log$A=14.06$) with our own. It should be noted, however, that the addition of cyclohexene in the present experiments did reduce the normal rate and also eliminated the induction periods. A further comparison can be made with the work of Kistiakowsky and Stauffer[5] in the case of *tert*-butyl bromide. These authors rightly concluded that the decomposition proceeded by a unimolecular mechanism, although no attempt was made to inhibit the reaction. Our work has shown that in fact the normal rate is uninfluenced by the addition of an inhibitor. Although our parameters for the reaction differ slightly from those of the earlier workers ($E=40.5$ kcal, log$A=13.48$), the disagreement is within the bounds of experimental error. It will also be noted that the limiting rate observed in the case of *n*-propyl bromide is not that of a heterogeneous reaction as suggested previously.[2]

Some tentative conclusions may be drawn from the reported values of the Arrhenius parameters. In the first place, the series further establishes the relationship $A\sim10^{13}$ for unimolecular reactions. Secondly, in the case of the primary bromides, neglecting ethyl bromide, there is no significant difference in the parameter in going from *n*-propyl to *iso*-butyl bromide. This constancy is further being checked by one of us (J.H.S.G.) in the cases of *n*-pentyl and *n*-hexyl bromide. Again, the decompositions clearly divide themselves as regards activation energy into 3 classes dependent upon the nature of the C—Br bond broken. For primary, secondary, and tertiary bromides the activation energies are of the order of 50, 46, and 42 kcals, respectively. There is thus a clear correlation with C—Br bond strength.

The relationship between the nature of the C—Br and C—H bonds broken is brought out by an examination of the rates relative to the rate of decomposition of ethyl bromide at 380°. Reading across Table II, the enormous effect of varying the C—Br

TABLE II.

p-C—Br		*s*-C—Br		*t*-C—Br	
ethyl	1	*sec*-propyl	170[b]	*t*-butyl	32 000[b]
n-propyl	3.6	*sec*-butyl	390[b]		
n-butyl	5.9	*cyclo*-hexyl	370[b]		
n-pentyl	7.7[a]				
iso-butyl	6.5				

[a] Based on observed rate only.
[b] Obtained by extrapolation.

bond from primary to tertiary is seen, the C—H bond remaining primary. In the first column, the effect of changing the C—H bond from primary to tertiary is seen to be small, as is also the case in column two, where the C—H bond changes from primary to secondary. The conclusion that the C—Br bond strength is the major factor in determining the rate is thus amply justified.

Further details respecting this work will be published elsewhere.

[1] Allan Maccoll, J. Chem. Phys. **17**, 1350 (1949).
[2] P. Agius and Allan Maccoll, J. Chem. Phys. **18**, 158 (1950).
[3] Allan Maccoll and P. J. Thomas, J. Chem. Phys. **19**, 977 (1951).
[4] J. Am. Chem. Soc. **72**, 424 (1950) (reference to earlier work will also be found here).
[5] J. Am. Chem. Soc. **59**, 165 (1937).

Asymmetric Internal Rotational Barriers about Single Bonds

N. W. Luft
Cheadle Hulme, Cheshire, England
(Received October 10, 1952)

VALUES for the heights of asymmetric barriers in internal rotation about single bonds may be estimated, with reasonable accuracy, by using simple symmetry considerations together with known data for related molecules. Usually the atoms defining the rotation axis have tetrahedral or planar electron configurations, the sites being occupied by bonds i, k, $\cdots$, and/or lone electron pairs p. Thus, the rotating groups may be denoted by indicial symbols, e.g., (iii) representing a group with trigonal symmetry, (ik) a digonal group, (ipp) a OH group, etc. If in a molecule, at least one of the two rotating groups has a symmetry plane $\sigma_v(z)$ through the rotation axis z, then the Fourier coefficients of its internal rotational barrier are given by

$$c_n = \tfrac{1}{2} \sum_{l,r} c_n{}^{lr} \cos\phi_0{}^{lr} \cdots . \qquad (1)$$

The coefficient $c_n{}^{lr}$ is the nth Fourier coefficient for the interaction between the charge distribution l, on the left of the rotation axis, and another one r to the right; $\phi_0{}^{lr}$ is their initial dihedral angle. A number of coefficients $c_n{}^{lr}$ are known, especially for $n=3$ from threefold barriers.[1] Although in some cases terms up to c_6 have to be considered, usually the first four terms would seem to provide sufficient accuracy. Apart from errors introduced by dropping higher terms, a variation of bond lengths, angles, and moments with environment may reduce the over-all accuracy slightly.

If Eq. (1) is applied to groups of molecules, simple relations between their Fourier coefficients may obtain, as exemplified in Table I for c_3's of three types of compounds. The coefficients c_1, c_2, and c_4 are the same for all three, those for the second type, however, having negative signs.

TABLE I.

Configuration	c_3	Example
$(ikk)(ikk)$	$c_3{}^*$	ClH_2C-CH_2Cl
$(ikk)(kii)$	$c_3{}^*+c_3{}^{ii}+c_3{}^{ik}-2c_3{}^{kk}$	$ClH_2C-CHCl_2$
$(kii)(kii)$	$c_3{}^*+3(c_3{}^{ii}-c_3{}^{kk})$	$Cl_2HC-CHCl_2$

It can be inferred from the signs of the c_n's and the known magnitudes of the coefficients $c_n{}^{lr}$ that $(ikk)^2$ and $(iik)^2$ have stable *trans*-configurations and secondary minima in gauche positions, whereas $(ikk)(kii)$ should attain an energy minimum when the single substituents on each side include a dihedral angle of $\lesssim 60°$ (g-form, rotational angle $\phi \gtrsim 120°$), and another less stable minimum (*cis*- or g'-form, $\phi = 0°$) which may split into two at $\phi \sim \pm 15°$.

Recently[2] the potential barriers of $MeCH_2-CH_2Me$ and $Me_2CH-CHMe_2$ have been calculated by the electrostatic method.[3] By using average values of the Fourier coefficients obtained for the barriers in these two molecules the coefficients c_n for Me_2CH-CH_2Me, and thus the maximum $V_m \sim 8.5$ and $\Delta E(g \to g') \sim 3.8$ kcal/mole can be estimated, which are in reasonable agreement with detailed calculations according to the electrostatic theory.

The position with the corresponding halogen compounds is analogous. In agreement with experiment,[4,5] $ClCH_2-CH_2Cl$ and $Cl_2CH-CHCl_2$ are found to have *trans*-minima and barriers of similar shape; the maximum V_m for the latter compound is calculated to be 3 kcal/mole higher than for the former one. Bernstein's[4] data for $ClCH_2-CH_2Cl$ result in coefficients c_n for Cl_2CH-CH_2Cl, which yield a low minimum in g'-position. This is at variance with dipole moment determinations,[5,6] which would suggest that $\Delta E(g \to g')$ is sufficiently high to have escaped observation, *viz.*, $\gtrsim 3$ kcal/mole, as probably also in the similar, though less symmetrical case of $MeCHCl-CH_2Cl$.[7] Thus one may suppose that Bernstein's figures for $ClCH_2-CH_2Cl$, *viz.*, $V_m \sim 4.5$, $\Delta E = 1.1$ kcal/mole, are somewhat too low, as also indicated by recent[8] electron diffraction results.

Since the configurations of O and N atoms are approximately tetrahedral and the charge distributions in OH and NH bonds very similar, the above considerations can be applied to the three molecules $HO-OH$, $HO-NH_2$, and H_2N-NH_2 by letting $i = OH = NH$, $k-p$, $c_n{}^{ip} = c_n{}^{pp} = 0$ for $n > 2$. Here the coefficients c_3, *viz.*, $c_3{}^{ii}$, $2c_3{}^{ii}$, and $3c_3{}^{ii}$, respectively, are numerically smaller than c_1 and c_2. It follows that $HO-OH$ and H_2N-NH_2 have twofold barriers of similar shape with high *cis*-maxima and lower maxima in *trans*-position, as suggested previously.[3] To the same approximation, H_2N-OH should have a deep minimum in *trans*-position and possibly a shallow minimum superimposed on the *cis*-maximum. The barrier height quoted recently[9] for H_2N-NH_2, *viz.*, $V_0 = 2.8$ kcal/mole, must be regarded as much too low. Because an insufficient knowledge of quadrupole moments of lone electron pairs, it has not been possible, by the electrostatic method, to obtain definite barrier heights for $HO-OH$ and H_2N-NH_2, but only certain rather wide limits (see reference 3), $6 < V_0 < 18$ kcal/mole, say. The pair of torsional frequencies $\delta_t(H_2N-NH_2) \sim 360$,[9] and $\delta_t(HO-OH) \sim 500$ cm^{-1} (see reference 10) is the only known set which satisfies this requirement and at the same time gives similar barrier heights for the two molecules, *viz.*, $V_c \sim 12$, $V_t \sim 4$ kcal/mole.

The writer acknowledges helpful discussions with Dr. G. J. Szasz.

[1] N. W. Luft, Disc. Faraday Soc., **10**, 117 (1951).
[2] N. W. Luft, Trans. Faraday Soc. (to be published).
[3] H. J. Lasettre and L. B. Dean, J. Chem. Phys. **17**, 317 (1949).
[4] H. J. Bernstein, J. Chem. Phys. **17**, 262 (1949).
[5] J. R. Thomas and W. G. Gwinn, J. Am. Chem. Soc. **71**, 2785 (1949).
[6] A. Turkevich and J. Y. Beach, J. Am. Chem. Soc. **61**, 3127 (1939).
[7] Morino, Miyagano, and Haga, J. Chem. Phys. **19**, 791 (1951).
[8] J. Ainsworth and J. Karle, J. Chem. Phys. **20**, 425 (1952).
[9] D. W. Scott *et al.*, J. Am. Chem. Soc. **71**, 2293 (1949).
[10] P. Giguère, Can. J. Research **B28**, 485 (1950).

The System Pyridine-Pyrrole and Hydrogen Bonding

Robert H. Linnell
Department of Chemistry, American University of Beirut, Beirut, Lebanon
(Received October 20, 1952)

MIXTURES of pyridine and pyrrole have been studied by several workers. Deželić[1] and Deželić and Belia[2] studied the viscosity of a series of mixtures of pyridine and pyrrole, and their plot of viscosity *vs* mole fraction pyrrole revealed a small maximum at a mole fraction 0.7 pyrrole. A marked heat of mixing was also observed. These workers interpreted their results as derived from compound formation between one molecule of pyridine and two molecules of pyrrole, although Deželić[1] does mention the possibility of a one-to-one complex that dissociates. Laurent[3] measured the specific inductive capacity of mixtures of pyridine and pyrrole in inert solvents and concluded that a one-to-one mole combination took place. In a study of hydrogen bonding Rodebush and co-workers[4] determined the infrared spectrum of a one-to-one mole ratio mixture of pyridine and pyrrole. Bands were found at 2.95, 3.11, 3.25, and 3.47 microns. The 3.11-micron band is a new band and was attributed to a strong hydrogen bonding between the pyrrole N—H and the pyridine N.

The infrared spectrum of pyrrole has been the subject of several papers. The fundamental N—H vibration of pyrrole is at 2.83 microns (vapor phase, 7 mm pressure, room temperature).[5] The N—H vibration of liquid pyrrole appears at 2.95 microns[6] and when pyrrole is dissolved in CCl_4 two bands apparently resulting from N—H vibration can be separated, one at about 2.86 microns (the so-called "unassociated band") and the other at about 2.92 microns ("associated band").[6] Fuson[6] and his co-workers have interpreted the 2.92-micron band as resulting from hydrogen bonding between pyrrole molecules and call this the "associated

band" (the intensity of this band increases as the concentration of pyrrole increases), while the band at 2.86 microns is regarded as resulting from free pyrrole molecules and is called the "unassociated band" (the intensity of this band increases as the concentration of pyrrole decreases).* In CCl_4 solutions 0.1 molar or less the 2.92-micron band disappears and therefore the pyrrole molecules are probably all unassociated.

We have repeated the viscosity measurements and found the same results as Deželić.[1] The infrared spectra of a large number of CCl_4 solutions of pyridine, pyrrole, and mixtures of pyridine and pyrrole have been run on a Perkin-Elmer model 21 infrared spectrophotometer using NaCl optics and cells. The results are in agreement with those of other workers.[5-7] In mixtures of pyridine and pyrrole the only new band to appear in the region 2–15 microns is the 3.11-micron band. By using dilute CCl_4 solutions of pyrrole (0.1 molar or less) the "associated band" at 2.92 microns was eliminated. The optical density of the 2.84 micron N−H vibration of pyrrole obeys Beer's Law in these dilute solutions and this band can be used to determine the concentration of free pyrrole molecules in the pyridine-pyrrole mixtures. If we assume the equilibrium $C_5H_5N+HNC_4H_4 \rightleftarrows C_5H_5NHNC_4H_4$, where the bond between the pyrrole and pyridine is a strong hydrogen bond, then we can write the equilibrium constant $K=[C_5H_5NHNC_4H_4]/[C_5H_5N][HNC_4H_4]$ and a value for K can be calculated from the optical density of the 2.84 micron band (which gives us the $[HNC_4H_4]$ term and the initial concentrations of pyridine and pyrrole. I have found a value of $K=3.0$ liters$\times$moles^{-1}, this value being independent of the pyrrole:pyridine mole ratio over a range from 0.5 to 2.3. The 2–15 micron spectrum is qualitatively the same regardless of whether the pyridine or pyrrole is in excess. As a further indication of the assumed equilibrium I have plotted the calculated concentration of the $C_5H_5NHNC_4H_4$ complex against the experimentally measured optical density of the 3.11-micron band, and a linear relationship is found. This should be the case if the equilibrium idea is correct. The infrared work, therefore, gives strong support to the suggestion that a 1:1 complex forms between pyridine and pyrrole, a strong hydrogen bond being responsible for this interaction. There is no indication from the infrared of any other complexes than the 1:1 species.

A more complete description of the infrared work on the pyridine-pyrrole mixtures and other experimental work now in progress on this system will be published in this Journal at a later date.

The infrared work described here was done while the author was the guest of the Physics Department of the University of Michigan. The author wishes to express his thanks to the Physics Department staff and especially to Dr. G. B. B. M. Sutherland and Dr. K. Nolan Tanner for their cooperation.

[1] Deželić, Trans. Faraday Soc. **33**, 713 (1937).
[2] Deželić, Belia, Ann. **535**, 291 (1938); Deželić, Belia, Bull. soc. roy Yougoslav. **9**, 151 (1938).
[3] Laurent, Ann. chim. 397 (1938).
[4] Buswell, Downing, and Rodebush, J. Am. Chem. Soc. **61**, 3252 (1939).
[5] N. Fuson and M.-L. Josien, J. Chem. Phys. **20**, 1043 (1952).
[6] Fuson, Josien, Powell, and Utterback, J. Chem. Phys. **20**, 145 (1952).
* The shift in wavelength of the N−H absorption of pyrrole on going from pure liquid pyrrole to CCl_4 solutions could be the result of the changing dielectric constant of the solvent, see P. Tuomikoski, J. Chem. Phys. **20**, 1054 (1952).
[7] Gordy and Stanford, J. Am. Chem. Soc. **62**, 497 (1940).

A Preliminary Magnetic Study of Purple Sulfur*

THOMAS FREUND, STEVEN ADLER, AND CALVIN SPARROW†
Chemistry Department, Northwestern University, Evanston, Illinois
(Received November 6, 1952)

MAGNETIC susceptibility measurements on a new allotropic form of sulfur are consistent with the interpretation that this solid is composed of paramagnetic diatomic sulfur. This purple form of sulfur was first prepared by Rice and Sparrow.[1] The new allotrope is made by freezing out diatomic sulfur vapor on a cold finger at liquid nitrogen temperature. The purple sulfur very rapidly undergoes a transition to the ordinary yellow form when it is allowed to warm above −190°C.

Unfortunately, it was not possible to prepare a pure sample of purple sulfur. The magnetic susceptibility measurements were carried out on a Faraday type magnetic balance[2] using a field intensity of about 7500 oersteds. This balance was calibrated with sucrose which had a known gram susceptibility of -0.566×10^{-6} at 25°C. Precautions were taken to exclude paramagnetic oxygen. The impure sample of purple sulfur had a gram susceptibility of 10×10^{-6} at −196°C. The measured gram susceptibility of this sample of sulfur after it had been allowed to undergo the transition to the ordinary yellow form was -0.43×10^{-6} at 25° and -0.40×10^{-6} at −196°C. The accepted value[3] for diamagnetic solid yellow sulfur is -0.49×10^{-6} and is temperature independent. This would indicate a small impurity in the sulfur used by the present authors. Recently, Scott[4] measured the magnetic susceptibility of diatomic sulfur in the vapor state at elevated temperatures and found the Curie constant to be 0.93. This is in agreement with the calculated value[5] for diatomic sulfur in a $^3\Sigma$ state, with multiplet structures small compared to kT. The molar susceptibility of diatomic sulfur at −196°C calculated from Scott's Curie constant is 120×10^{-4}. Assuming our sample of impure purple sulfur was diatomic sulfur, the molar magnetic susceptibility was 7×10^{-4} at −196°C. While the measured value for the paramagnetic susceptibility of impure purple sulfur was low for diatomic sulfur in the $^3\Sigma$ state, it is felt that some improvement in the technique of preparation of the purple sulfur would increase the value greatly.

The authors wish to thank P. W. Selwood for a discussion of the results, and F. O. Rice for comments concerning the results.

* This work was supported by the ONR.
† Standard Oil of Indiana, Whiting, Indiana.
[1] Dissertation, The Catholic University of America, Washington, D. C., 1952.
[2] P. W. Selwood, *Magnetochemistry* (Interscience Publishers, Inc., New York, 1943).
[3] International Critical Tables.
[4] A. B. Scott, J. Am. Chem. Soc. **71**, 3145 (1949).
[5] J. H. Van Vleck, *Electric and Magnetic Susceptibilities* (Oxford University Press, London, 1932), p. 266.

Ionization and Dissociation of Methyl Siloxanes by Electron Impact

VERNON H. DIBELER, FRED L. MOHLER, AND R. M. REESE
National Bureau of Standards, Washington, D. C.
(Received November 10, 1952)

MASS spectra of hexamethyl disiloxane $(CH_3)_6Si_2O$ and of octamethyl trisiloxane $(CH_3)_8Si_3O_2$ have been obtained with a type 103 Consolidated mass spectrometer. Relative intensities for nominal electron energies of 70 v and corrected appearance potentials of a few ions are given in Table I.

In both spectra the molecule ion is very small, and by far the most abundant ion is that formed by the dissociation of one methyl radical plus an electron. In both compounds the appear-

TABLE I. Abundance and appearance potentials of some ions of methyl siloxanes.

m/e	Ion	Rel. intensity at 70 v	Appearance potential (ev)
	1. $(CH_3)_6Si_2O$		
66	$(CH_3)_4Si_2O^{++}$	12.4	25
73[a]	$(CH_3)_3Si^+$	11.8	15
147	$(CH_3)_5Si_2O^+$	100	9.6
162	$(CH_3)_6Si_2O^+$	0.03	
	2. $(CH_3)_8Si_3O_2$		
63.7	$(CH_3)_6Si_3O_2^{+++}$	0.35	
73[a]	$(CH_3)_3Si^+$	42.9	12
103	$(CH_3)_6Si_3O_2^{++}$	12.8	22, 13.6
221	$(CH_3)_7Si_3O_2^+$	100	9.6
236	$(CH_3)_8Si_3O_2^+$	0.02	

[a] Mass 73 could be Si_2OH^+ or $C_2H_6SiO^+$.

ance potential of this ion is 9.6 ev. The sensitivity for the maximum peak relative to the sensitivity for the mass 43 of *n* butane is 2.6 and 2.9 for the disiloxane and the trisiloxane, respectively.

Exceptionally abundant doubly charged ions are observed in both spectra formed by the dissociation of two methyl radicals plus two electrons from the molecule. In the disiloxane the relative intensity is 12.4 and the appearance potential is about 25 volts. In the trisiloxane the intensity is nearly the same and the appearance potential is about 22 volts. Doubly charged isotopic ions at half-mass units support these interpretations. In the trisiloxane a small singly-charged ion of mass 103 is coincident with the doubly charged ion and produces a second break in the ionization efficiency curve at 13.6 ev.

In the trisiloxane there is a small triply-charged ion resulting from the dissociation of three methyl groups and three electrons from the molecule. The corresponding ion is not observed in the disiloxane. Although a small singly charged ion at mass 29 is observed, a survey of this mass range at about 30 times normal sensitivity gives no evidence of the expected isotopic ions at $m/e=29\frac{1}{3}$ and $29\frac{2}{3}$.

Another large ion in both spectra is at mass 73 with appearance potentials of 15 ev in the disiloxane and 12 ev in the trisiloxane. Isotope ratios calculated from adjacent peaks favor the interpretation as $Si(CH_3)_3^+$, but this is not conclusive, and the difference in appearance potentials in the two compounds is unexpectedly large. Other ions with relative intensities of about 7 percent in both spectra could be CH_3SiH_2 and $(CH_3)_2SiH$. The relative intensities of these ions and other ions in the same mass range are similar to ions found in the spectrum of silicon tetramethyl,[1] and in this compound there is no ambiguity as to the interpretation. In silicon tetramethyl also, the most abundant ion results from the dissociation of one methyl group plus an electron but no doubly charged ions are observed.

It is of interest that in the siloxanes the most probable ionization processes involve removing one methyl radical for single ionization, two radicals for double ionization, and three radicals for triple ionization.[2] The fact that doubly charged ions are not observed in silicon tetramethyl and triply-charged ions are found only in the trisiloxane suggests that in these processes, one electron and one methyl radical are removed from each silicon atom in the molecule.

[1] V. H. Dibeler, J. Research Natl. Bur. Standards (to be published).
[2] Triply-charged ions are very rare in polyatomic spectra. The only other examples that we know of are the molecule ions in the spectra of naphthalene, methyl naphthalenes, and of azulene. See API Catalog of Mass Spectral Data, Carnegie Institute of Technology.

Nonadiabatic Transitions*

HENRY AROESTE†
Cornell University, Ithaca, New York
(Received October 3, 1952)

ZEROTH-ORDER Born-Oppenheimer wave functions and first-order Dirac time-dependent perturbation theory have been used in the consideration of adiabatic transitions. For some nonadiabatic transitions it may only be necessary to extend the theory to the first-order Born-Oppenheimer approximation, as such transitions may occur in the first order of the Dirac theory. It is hoped that the following analysis will be applied to vibrational-electronic energy exchanges, which are presently of interest.[1]

If $k=(m/M)^{\frac{1}{4}}$, where m refers to electron mass and M to nuclear mass, we may expand the total wave function $\psi_n=\psi_n^0+k\psi_n^1+\cdots$, where $\psi_n^0=\chi_n^0\varphi_n^0$ and $\psi_n^1=\chi_n^1\varphi_n^0+\chi_n^0\varphi_n^1$. φ refers to electronic states and χ to nuclear states. Also, the total Hamiltonian $H=H_0+k^4H_1$, where $H_0=T_e+U$. (U is the potential energy, and T_e, the kinetic energy for electrons; $H_1=T_N$ or the kinetic energy for the nuclei.) We may then expand $H=H_0^0+kH_0^1+\cdots$, where terms in H_1 do not enter until the term in k^2. If we now define the perturbation to be $V=H-H^\alpha$, where H^α is the Hamiltonian of the initial configuration, then $V=H_0^0-H_0^{0\alpha}+k(H_0^1-H_0^{1\alpha})+\cdots=\Delta H_0^0+k\Delta H_0^1+\cdots$. We then consider matrix elements $\int\psi_n^*V\psi_i dxd\xi$, where x refers to electronic and ξ to nuclear coordinates. We obtain on expansion the following terms to first order in k:

$$\int\chi_n^{0*}\varphi_n^{0*}\Delta H_0^0\chi_i^0\varphi_i^0dxd\xi, \quad (1)$$
$$k\int\chi_n^{0*}\varphi_n^{0*}\Delta H_0^1\chi_i^0\varphi_i^0dxd\xi, \quad (2)$$
$$k\int\chi_n^{0*}\varphi_n^{0*}\Delta H_0^0\chi_i^1\varphi_i^0dxd\xi, \quad (3)$$
$$k\int\chi_n^{0*}\varphi_n^{0*}\Delta H_0^0\chi_i^0\varphi_i^1dxd\xi, \quad (4)$$
$$k\int\chi_n^{1*}\varphi_n^{0*}\Delta H_0^0\chi_i^0\varphi_i^0dxd\xi, \quad (5)$$
$$k\int\chi_n^{0*}\varphi_n^{1*}\Delta H_0^0\chi_i^0\varphi_i^0dxd\xi, \quad (6)$$

where all $\varphi=\varphi(x,\xi)$ and $\chi=\chi(\xi)$. Expression (1) is the usual adiabatic term. Expressions (3) and (5) are also adiabatic terms as $\int\varphi_n^{0*}\Delta H_0^0\varphi_i^0dx=(V_n^0(\xi)-V_n^{0\alpha}(\xi))\delta_{in}$, where $H_0^0\varphi_n^0=V_n^0\varphi_n^0$. We therefore must consider expressions (2), (4), and (6). Defining $\int\varphi_n^{0*}\Delta H_0^1\varphi_i^0dx=(\Delta H_0^1)_{in}$, it is a result of the work of Born and Oppenheimer that $(H_0^1)_{in}=\mu_{in}(V_i^0-V_n^0)$, where $\varphi_i^1=\Sigma_{n'}\mu_{in'}\varphi_{n'}^0$. Thus, $(\Delta H_0^1)_{in}=\mu_{in}(\Delta V_i-\Delta V_n)$, where $\Delta V_i=V_i^0-V_i^{0\alpha}$, and $\Delta V_n=V_n^0-V_n^{0\alpha}$. Neglecting for the moment integrations over nuclear coordinates, (2) is $k\mu_{in}(\Delta V_i-\Delta V_n)$. Similarly, (4) is $k\mu_{in}\Delta V_n$, and (6) is $k\mu_{ni}\Delta V_n$, so that the nonadiabatic term in first order is $k\int\chi_n^{0*}(\mu_{in}\Delta V_i+\mu_{ni}\Delta V_n)\chi_i^0d\xi$, since, fortunately, (2), (4), and (6) do not contain χ_n^1 and χ_i^1. It is a further result of the work of Born and Oppenheimer that

$$\mu_{in}=\sum_j\zeta_j\int\varphi_n^{0*}\frac{\partial\varphi_i^0}{\partial\xi_j}dx,$$

where ζ_j represents the displacement of the equilibrium nuclear separation ξ_j. Therefore, in theory, at least, one need only know the χ^0 and φ^0 to calculate the nonadiabatic term.

* Nonadiabatic transitions as discussed here refer to those between nondegenerate electronic states.
† Present address: Institute for Nuclear Studies, University of Chicago, Chicago, Illinois.
[1] K. J. Laidler and K. E. Shuler, Chem. Revs. **48**, 153 (1951). In certain cases, it may be necessary to extend the theory to higher orders of the Born-Oppenheimer expansion in order to achieve convergence.

The Raman Spectra of Vinyl- and Dichlorovinyltrichlorosilane

HIROMU MURATA
Osaka Municipal Technical Research Institute, Osaka, Japan
(Received October 20, 1952)

α,β-dichlorovinyltrichlorosilane, prepared by Agre,[1] has been argued to be β,β-dichlorovinyltrichlorosilane by Wagner and Pines.[2] For the purpose of deciding the configuration, I have measured the Raman spectra of vinyl- and dichlorovinyltrichlorosilane. Samples of these compounds were kindly sent to me by Dr. R. Okawara, Osaka University, the vinyltrichlorosilane being prepared by the dehydrochlorination of α-chloroethyltrichlorosilane and the dichlorovinyl-compound by the method of Agre. They were of the properties given in Table I.

TABLE I.

	b.p. (°C)	$n_D^{18.5}$	Active Cl (%)
$CH_2=CHSiCl_3$	91– 92	...	65.41
$CHCl=CClSiCl_3$	159–160	1.4912	45.97

The Raman data obtained for these compounds are given in Table II. When the results obtained for methyltrichlorosilane,[3] ethylene, and dichloroethylene are taken into account, the observed lines are tentatively assigned as shown in Table II. Of course, for the skeletal vibrations of these molecules the vinyl and dichlorovinyl groups should not be considered as one particle. It can, however, be safely said that the skeletal vibrations of these molecules consist of the inner vibrations of vinyl and dichloro-

vinyl groups and the normal vibrations of the tetrahedral molecules assuming vinyl and dichlorovinyl groups as one particle, if one ignores the fact that the interaction of the inner vibrations of vinyl and dichlorovinyl groups with the skeletal vibrations of tetrahedral molecules cause some displacements in their frequencies. From Table II it is clear that the dichlorovinyltrichloro-

TABLE II. Raman spectra of vinyl- and dichlorovinyltrichlorosilane (cm^{-1}).

Modes of vibrations		$CH_2=CHSiCl_3$	$CHCl=CClSiCl_3$
τ[a](Si−C)		77(5*b*)(*e*, *k*)	85(6*b*)(*e*, *k*)
δ(Si−Cl)	*E*	148(8*s*)(*e*±, *k*)	147(5*s*)(*e*±, *k*)
δ(Si−R[b])	A_1	182(3*s*)(*e*±)	188(7*s*)(*e*±)
	E	219(4*s*)(*e*±, *k*)	210(4*s*)(*e*±, *k*)
δ(C−Cl)			289(7*s*)(*e*±, *k*)
δ(C=C)		351(7*s*)(*e*±, *k*)	355(9*s*)(*e*±, *k*)
ν(Si−Cl)	A_1	450(10*s*)(*e*±, *k*)	490(10*s*)(*e*±, *k*)
ν(Si−R)	*E*	593(3*b*)(*e*, *k*)	586(3*b*)(*e*, *k*)
	A_1	...	723(1*b*)(*e*)
ν(C−Cl)			627(5*s*)(*e*, *k*)
			800(2*b*)(*e*, *k*)
δ(C−H)		1262(4*s*)(*e*, *k*)	1216(4*s*)(*e*, *k*)
		1401(7*b*)(*e*, *k*)	
		1492(1*b*)(*e*, *k*)	
ν(C=C)		1601(6*s*)(*e*, *k*)	1560(9*b*)(*e*, *k*)
ν(C−H)		2992(7*s*)(*e*, *k*)	3018(5*s*)(*e*, *k*)
		3075(3*s*)(*e*, *k*)	

[a] τ denotes the internal rotation around the axis of the Si−C bond.
[b] *R* denotes vinyl or dichlorovinyl groups.

silane prepared by the method of Agre is only one type of the isomer, either $\alpha,\beta-$ or $\beta,\beta-$.

The electron diffractions on the vapors of these samples were also investigated. In vinyltrichlorosilane, the CH_2 group has a *cis*-configuration to a Cl atom of the $SiCl_3$ group with regards to the C−Si bond. In dichlorovinyltrichlorosilane, the CHCl group has a staggered configuration to a Cl atom of the $SiCl_3$ group, and the two Cl atoms in dichlorovinyl group were in the *trans*-position to each other. Thus it may be concluded that Agre's compound is *trans*-α,β-dichlorovinyltrichlorosilane. Detailed electron diffraction studies of these molecules will be published at a later date.

[1] C. L. Agre, J. Am. Chem. Soc. **71**, 300 (1949).
[2] G. H. Wagner and A. N. Pines, J. Am. Chem. Soc. **71**, 3567 (1949).
[3] Shimanouchi, Tsuchiya, and Mikawa, J. Chem. Phys. **18**, 1306 (1951).

Production of Fe^{59} by the $Co^{59}(n,p)$ Reaction in the Brookhaven Reactor*

ARTHUR C. WAHL†
Chemistry Department, Brookhaven National Laboratory, Upton, Long Island, New York
(Received November 5, 1952)

TWO one-gram samples of Co_3O_4 (<0.002 percent Fe), one wrapped in 45 mils of cadmium, were each irradiated for one hour in the pneumatic tube in the reactor, where the flux is estimated to 3×10^{12} neutrons/cm^2/sec. The samples were dissolved in warm concentrated hydrochloric acid, and ten milligrams of iron (III) carrier were added. The concentration of hydrochloric acid was adjusted to 8*f*, and the iron (III) chloride was extracted into isopropyl ether saturated with 8*f* hydrochloric acid. The isopropyl ether phase was washed four times with 8*f* hydrochloric acid, ten milligrams of cobalt (II) carrier being added in two of the washes. The iron (III) was then back-extracted into water and aliquots mounted for counting. The bulk of the iron (III) was further purified by an additional isopropyl ether extraction from added cobalt (II) carrier. The activity of the repurified iron was within 10 percent of the activity of the iron before repurification, showing that the original purification was adequate. The activities of aliquots of the repurified iron samples, followed to date for 50 days, have decayed with the expected 47-day period.

The chemical yields were determined to be 85 percent for each sample by comparing the tris-2,2′-dipyridyl iron (II) colors[1] of the repurified iron (III) solutions and the iron (III) carrier solution at 520 mμ on a Beckmann Model DU Spectrophotometer.

Aliquots of the repurified iron (III) solutions and the extracted cobalt (II) solutions were mounted on glass cover slips and counted in a Nucleometer internal proportional counter attached to a scaler. The yields given in Table I were calculated from the

TABLE I. Yields of Fe^{59} and Co^{60} in the Brookhaven reactor (1 g Co_3O_4 for 1 hour at 3×10^{12} n/cm^2/sec).

Sample	Fe^{59}	Co^{60}	
1	0.040 μc	260 μc[a]	(no Cd)
2	0.036 μc	14 μc	(sample wrapped in Cd)

[a] 340 μc from comparison of gamma-activity with Co^{60} standard; 310 μc calculated from flux of 3×10^{12} and 34-barn capture cross section.

counting data, corrections for chemical yield and decay and assumptions of 50 percent geometry and 100 percent counting efficiency for the beta-particles being made.

The fact that the Fe^{59} yields with and without cadmium are the same within experimental error confirms the expectation that no large fraction of the activity was formed by slow neutron capture by the very small iron impurity in the cobalt.

The yield of Fe^{59} per gram of cobalt per day in the 3×10^{12} flux is 1.2 microcuries. Thus, irradiation of 50 g of cobalt for 10 days in the maximum flux of 5×10^{12} would yield nearly a millicurie of Fe^{59} activity at an irradiation cost of 125 dollars.[2] If the irradiation were carried out in cadmium, the millicurie of Fe^{59} would have to be separated from about 400 millicuries of Co^{60}. These figures indicate that the production of carrier-free Fe^{59}, free of Fe^{55}, in the Brookhaven reactor is feasible and is comparable economically to cyclotron production.

* Research carried out under the auspices of the U. S. Atomic Energy Commission, while the author was a summer visitor at Brookhaven National Laboratory, Upton, Long Island, New York.
† Address: Department of Chemistry, Washington University, St. Louis 5, Missouri.
[1] M. L. Moss and M. G. Mellon, Ind. Eng. Chem., Anal. Ed. **14**, 862 (1942).
[2] Isotopes Division, U. S. Atomic Energy Commission, *Isotopes, Catalogue and Price List No. 4* (Oak Ridge, Tennessee, March, 1951), p. 26.

On the Influence of Nonrandomness of Mixing in the Cell Model of Solutions

I. SAROLÉA
Faculté des Sciences de l'Université Libre de Bruxelles, Belgium
(Received November 10, 1952)

IN some recent papers, I. Prigogine and his co-workers, G. Garikian and V. Mathot, have developed a cell model for the statistical thermodynamics of solutions.[1,2] This model takes account of variations of volume and changes of frequencies of the intermolecular vibrations, owing to changes in the intermolecular forces, but it has, till now, been only developed assuming random mixing. The purpose of this short note is to indicate briefly the order of magnitude of the corrections due to the nonrandomness of mixing.

The configurational partition function may be written [see reference 2, Eq. (2.2′)]

$$Q=\sum_{N_{AB}} \Psi_A^{N_A}\Psi_B^{N_B} g(N_A, N_B, N_{AB}) \times\exp\left(-\frac{N_A\omega_A(0)+N_B\omega_B(0)}{2kT}\right), \quad (1)$$

where $g(N_A, N_B, N_{AB})$ is the number of ways to distribute N_A

molecules A and N_B molecules B into N_{AA} neighbors AA, N_{BB} neighbors BB, and N_{AB} neighbors AB. (When nothing is specified, the symbols have the same meaning as in reference 2.) The potential energy of a molecule A at the center of its cell, $\omega_A(0)$, is given by

$$\omega_A(0)=(2,4\alpha-\alpha^2)\left(\frac{2N_{AA}}{N_A}\epsilon_{AA}{}^*+\frac{N_{AB}}{N_A}\epsilon_{AB}{}^*\right). \tag{2}$$

In this equation, the first term contains the contribution of the molecules A surrounding the central A, the second term, that of the neighbors B, for, around N_A molecules A as centers, one may form zN_A pairs, from which $2N_{AA}$ are AA pairs and N_{AB} are AB pairs ($zN_A=2N_{AA}+N_{AB}$). If one uses the smoothed potential model, which fits the liquid state better than the harmonic oscillator model, then $\Psi_A=\Psi_B$, and both are independent of N_{AB}.

For $g(N_A, N_B, N_{AB})$, we shall use the quasi-chemical approximation (see reference 3).

Equation (1) then gives

$$Q=\Psi_A{}^{N_A}\Psi_B{}^{N_B}\frac{N!}{N_A!N_B!}\left(\frac{zN_Ax_B}{2}\right)!^2\left(\frac{zN_Ax_A}{2}\right)!\left(\frac{zN_Bx_B}{2}\right)!$$
$$\times\sum_{N_{AB}}\frac{\exp\left[-\dfrac{(\alpha^2-2,4\alpha)(N_A\Lambda_{AA}+N_B\Lambda_{BB}+N_{AB}w_{AB}}{2kT}\right]}{\left(\dfrac{N_{AB}}{2}\right)!^2\left(\dfrac{zN_A-N_{AB}}{2}\right)!\left(\dfrac{zN_B-N_{AB}}{2}\right)!}, \tag{3}$$

where one has defined

$$w_{AB}=\epsilon_{AA}{}^*+\epsilon_{BB}{}^*-2\epsilon_{AB}{}^*. \tag{4}$$

The corresponding free energy is

$$\frac{F}{NkT}=-\lg Q^{1/N}=-x_A\lg\Psi_A+x_B\lg\Psi_B+x_A\lg x_A+x_B\lg x_B$$
$$-z\left\{x_A\lg\frac{x_A}{[x_A-(N_{AB}{}^*/zN)]^{\frac{1}{2}}}+x_B\lg\frac{x_B}{[x_B-(N_{AB}{}^*/zN)]^{\frac{1}{2}}}\right.$$
$$\left.+\frac{N_{AB}{}^*w_{AB}(\alpha^2-2,4\alpha)}{2zNkT}\right\}$$
$$+\frac{(\alpha^2-2,4\alpha)(x_A\Lambda_{AA}+x_B\Lambda_{AB}+(N_{AB}{}^*/N)w_{AB})}{2kT}. \tag{5}$$

N_{AB} is such that it makes Q a maximum. It is thus given by the condition of maximum:

$$\frac{N_{AB}{}^{*2}}{(zN_A-N_{AB}{}^*)(zN_B-N_{AB}{}^*)}=\exp\left[-\frac{(\alpha^2-2,4\alpha)w_{AB}}{kT}\right]. \tag{6}$$

Deriving (5) with respect to the volume, one gets the equation of state

$$\frac{\Lambda}{kT}=\frac{1}{\alpha[1-(\alpha/2)^{1/6}](2,4-2\alpha)}, \tag{7}$$

where Λ is defined by

$$\Lambda=x_A\Lambda_{AA}+x_B\Lambda_{BB}+N_{AB}{}^*/Nw_{AB}. \tag{8}$$

If one takes into account only the order-disorder effects and not the variations of volume, the excess free energy calculated from Eq. (5) is

$$\frac{F_e}{NkT}=-z\left\{x_A\lg\frac{x_A}{[x_A-(N_{AB}{}^*/zN)]^{\frac{1}{2}}}\right.$$
$$\left.+x_B\lg\frac{x_B}{[x_B-(N_{AB}{}^*/zN)]^{\frac{1}{2}}}\right\}. \tag{9}$$

Expanding (9) with respect to the powers of w_{AB}/kT, and defining

$$\theta=\frac{1}{\Lambda_{AA}}\left(\Lambda_{AB}-\frac{\Lambda_{AA}+\Lambda_{BB}}{2}\right),$$

one finds

$$\frac{F_e}{NkT}=\frac{x_Ax_B(\alpha^2-2,4\alpha)\Lambda_{AA}\theta}{kT}\left(1-\frac{x_Ax_B(\alpha^2-2,4\alpha)\Lambda_{AA}\theta}{zkT}\right). \tag{10}$$

The excess entropy is

$$\frac{S_e}{Nk}=-\frac{\partial F_e/Nk}{\partial T}=-\left(\frac{x_Ax_B(\alpha^2-2,4\alpha)\Lambda_{AA}\theta}{z^{\frac{1}{2}}kT}\right)^2. \tag{11}$$

The excess energy is

$$\frac{E_e}{NkT}=\frac{F_e+TS_e}{NkT}=\frac{x_Ax_B(\alpha^2-2,4\alpha)\Lambda_{AA}\theta}{kT}$$
$$\times\left(1-\frac{2x_Ax_B(\alpha^2-2,4\alpha)\Lambda_{AA}\theta}{zkT}\right). \tag{12}$$

Before discussing the meaning of these equations by comparing them to those obtained when neglecting the order-disorder effects, let us look for a last property, the excess volume. If we compare the equation of state (7) to that obtained when assuming random mixing (4),

$$\frac{\Lambda_0}{kT}=\frac{1}{\alpha_0[1-(\alpha_0/2)^{1/6}](2,4-2\alpha_0)}, \tag{13}$$

where

$$\Lambda_0=x_A\Lambda_{AA}+x_B\Lambda_{BB}+zx_Ax_Bw_{AB}, \tag{14}$$

one sees that the two equations differ only by the meaning of Λ. Using Eqs. (8) and (14), one gets

$$\Lambda=\Lambda_0+w_{AB}\left(\frac{N_{AB}{}^*}{N}-zx_Ax_B\right)=\Lambda_0-\frac{4\theta^2\Lambda_{AA}{}^2x_Ax_B(\alpha^2-2,4\alpha)}{zkT} \tag{15}$$

if one neglects the powers of θ higher than 2. The correction due to the order is thus small (of the second order in θ). To the same approximation

$$\alpha=\left(\frac{v^*}{v}\right)^2=\alpha_0+\frac{2304\theta^2\Lambda_{AA}{}^2x_Ax_B}{\Lambda_0{}^2z}. \tag{16}$$

Using Eq. (16), one finds easily for the excess volume

$$\frac{v_e}{v^*}=\frac{v}{v^*}-x_A\frac{v_A}{v^*}-x_B\frac{v_B}{v^*}=\frac{v_e{}^0}{v^*}-\frac{9033\theta^2\Lambda_{AA}{}^2x_Ax_B}{z\Lambda_0{}^2}, \tag{17}$$

where $v_e{}^0$ is the excess value obtained by the cell model using random mixing.

Let us now compare the excess functions (10)–(12) with those obtained when assuming random mixing, i.e., with Eqs. (6.9), (6.10), (6.11), and (6.12) of reference 2. As a first approximation the corrections due to the nonrandomness of mixing may simply be added to the values of the excess functions obtained in reference 2.

We shall consider three extreme cases (see reference 2).

(1) *Dispersion forces:*

$$\Lambda_{AB}=\Lambda_{AA}\Lambda_{BB}\quad\left(\theta=-\frac{\delta^2}{8}\right)$$

or

$$\Lambda_{AB}=\frac{\Lambda_{AA}+\Lambda_{BB}}{2}\quad(\theta=0). \tag{18}$$

Equations (11) and (17) show in this case that the order-disorder correction, which is of the $4e$ order in δ, is completely negligible compared to the contribution of the variations of volume of $2e$ order in δ. One could expect that result since if Eq. (18) is satisfied, A has no tendency to be surrounded by B or the contrary, and the mixing takes place rigorously at random.

(2) *Addition compound:* $\Lambda_{AA}\approx\Lambda_{BB}\ll\Lambda_{AB}$ ($\delta=0$; $\theta\neq0$) or *association in an inert solvent:* $\Lambda_{AB}\approx\Lambda_{BB}\ll\Lambda_{AA}$ ($\delta\neq0$; $\theta\neq0$).

In those two cases the conclusions are the same: the order-disorder effects give a contribution of the second order in θ and δ. To consider a specific example, we may take the case of an "addition compound" with $x_A=x_B=\frac{1}{2}$, $\Lambda_{AA}/kT=20$, $z=10$. Then Eq. (11) gives

$$\left(\frac{S_e}{Nk}\right)_{\text{order-disorder}}=-3\theta^2.$$

We have to compare with the corresponding value calculated from the cell model [reference 2, Eq. (6.11)],

$$\left(\frac{S_e}{Nk}\right)_{\text{cell method}}=-\tfrac{1}{2}\theta+\tfrac{1}{4}\theta^2.$$

In conclusion, the consideration of nonrandomness of mixing does not alter the conclusions of the paper by Prigogine and Mathot.[2] It introduces effects which are always of a higher order in θ than the effects due to volume changes, and thus may be neglected in many cases.

[1] I. Prigogine and G. Garikian, Physica **16**, 239 (1950).
[2] I. Prigogine and V. Mathot, J. Chem. Phys. **20**, 49 (1952).
[3] Fowler and Guggenheim (Cambridge University Press, Cambridge, 1939), p. 576; for a discussion of the quasi-chemical approximation, see Prigogine, Salorêa, Mathot, and Van Hove, Trans. Faraday Soc. **48**, 485 (1952).
[4] I. Prigogine and V. Mathot, reference 2, Eq. (5.4).

On the Specific Molar Quantities in the Cell Model of Solutions

J. NASIELSKI
Faculté des Sciences de l'Université Libre de Bruxelles, Brussels, Belgium
(Received November 10, 1952)

IT seems interesting to apply the recent theory of binary solutions, based on the cell model applied to molecules of the same size but with different fields of forces, given by Prigogine and Mathot,[1] to the calculation of partial molar quantities. These are derived from their expressions for molar quantities. The smoothed potential has been used. Elementary calculations, based on the definition of partial molar quantities yield the following expression for the activity coefficient (see reference 1, Eq. 5.8):

$$\log f_A = x_B^2\theta(a\alpha^2-b\alpha)\frac{\Lambda_{AA}}{kT}+\frac{\Delta_A}{2}\frac{\Lambda_{AA}}{kT}-\log\frac{\psi}{\psi_A{}^0}, \qquad (1)$$

assuming a zero external pressure. Δ_A stands for $[(a\alpha^2-b\alpha)-(a\alpha_A{}^2-b\alpha_A)]$. The other symbols have the same meaning as in

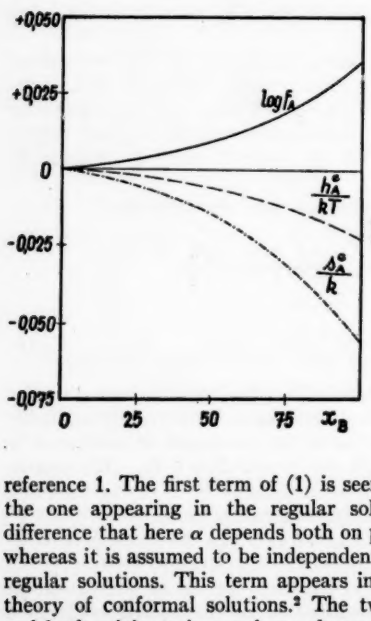

FIG. 1. Specific molar quantities for $\Lambda_{AA}/kT=15$, $\delta=0.2$, $\theta=0$.

reference 1. The first term of (1) is seen to be closely related to the one appearing in the regular solutions theory, with the difference that here α depends both on pressure and composition, whereas it is assumed to be independent of both in the theory of regular solutions. This term appears in the present form in the theory of conformal solutions.[2] The two other terms are new, and both originate in a volume change on mixing. For the heat and entropy of dilution, one finds (see reference 1, Eqs. 5.9 and 5.10)

$$\frac{h_A^e}{kT}=\frac{a\alpha^2-b\alpha}{kT}x_B^2\Theta\Lambda_{AA}+\frac{\Delta_A}{2}\frac{\Lambda_{AA}}{kT}+N\Lambda\frac{2a\alpha-b}{2kT}\frac{\partial\alpha}{\partial N_A}, \qquad (2)$$

$$\frac{s_A^e}{k}=\log\frac{\psi}{\psi_A{}^0}+N\frac{\partial\log\psi}{\partial N_A}. \qquad (3)$$

Introducing the simplified equation of state (reference 2, Eq. 5.6), expanding in powers of θ and δ, and neglecting terms beyond the

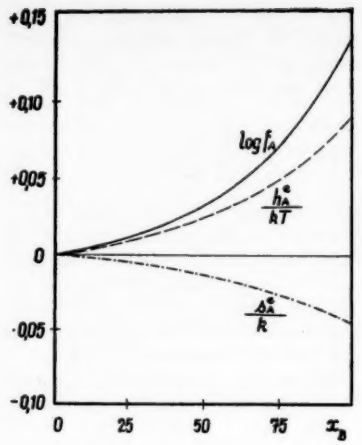

FIG. 2. Specific molar quantities for $\Lambda_{AA}/kT=15$, $\delta=0.2$, $\theta=-(\delta^2/8)$.

second, one finds immediately

$$\log f_A=-1435x_B^2\Theta\frac{\Lambda_{AA}}{kT}-12\,169\frac{kT}{\Lambda_{AA}}x_B^2 \times[-2\theta-\delta^2+4(2x_B-1)\theta\delta+4x_A(3x_B-1)\theta^2], \qquad (4)$$

$$\frac{h_A^e}{kT}=-1435x_B^2\Theta\frac{\Lambda_{AA}}{kT}+8845\frac{kT}{\Lambda_{AA}}x_B^2 \times[-2\theta-\delta^2+4(2x_B-1)\theta\delta+4x_A(3x_B-1)\theta^2], \qquad (5)$$

$$\frac{s_A^e}{k}=21\,015\frac{kT}{\Lambda_{AA}}x_B^2[-2\theta-\delta^2+4(2x_B-1)\theta\delta +4x_A(3x_B-1)\theta^2]=12\,818\frac{1}{v^*}\frac{\partial V_e}{\partial N_A}. \qquad (6)$$

Since it has been assumed that $\Lambda_{AA}\leq\Lambda_{BB}$, a certain asymmetry is introduced in the components. For this reason, the expressions for the second component are slightly different:

$$\log f_B=-1435x_A^2\Theta\frac{\Lambda_{AA}}{kT}-12\,169\frac{kT}{\Lambda_{AA}}x_A^2 \times[-2\theta-\delta^2+8x_B\delta\theta+4x_B(3x_A-1)\theta^2], \qquad (4')$$

$$\frac{h_A^e}{kT}=-1435x_A^2\Theta\frac{\Lambda_{AA}}{kT}+8845\frac{kT}{\Lambda_{AA}}x_A^2 \times[-2\theta-\delta^2+8x_B\delta\theta+4x_B(3x_A-1)\theta^2], \qquad (5')$$

$$\frac{s_A^e}{k}=21\,015\frac{kT}{\Lambda_{AA}}x_A^2[-2\theta-\delta^2+8x_B\delta\theta +4x_B(3x_A-1)\theta^2]=12\,818\frac{1}{v^*}\frac{\partial V_e}{\partial N_B}. \qquad (6')$$

Attention should be drawn to Eqs. (6) and (6'); they are quite analogous to Eq. (5.10) in reference 2.

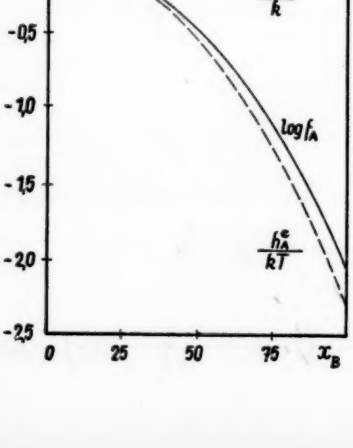

FIG. 3. Specific molar quantities for $\Lambda_{AA}/kT=15$, $\delta=0.2$, $\theta=+(\delta/2)$.

Two important cases have to be considered: (1) θ is very small: $\theta \simeq 0$. This corresponds to what Prigogine and Mathot call "dispersion forces." In this case, the entropy of dilution makes an important contribution to the activity coefficient. This situation is encountered in solutions of nonpolar molecules of the same size, for instance, carbon tetrachloride-neopentane (Figs. 1 and 2). (2) θ is significantly different from zero. This happens generally when one of the components is polar. Here, the entropy of dilution is very small as compared with the heat of dilution, and may be neglected. Figure 3 illustrates the case called "association in an active solvent."

It is interesting to point out that the theory of regular solutions has been verified precisely in those cases where θ is certainly very different from zero, for instance, carbon tetrachloride-iodine.[3] On the contrary, when θ approaches zero, the solutions are no more regular, as is shown by the measurements of Mathot and Desmyter.[4] It is thus seen that the relative importance of entropy and heat of dilution depends strongly on the nature of intermolecular forces.

We are greatly indebted to Professor I. Prigogine for constant advice and interest.

[1] I. Prigogine and V. Mathot, J. Chem. Phys. **20**, 49 (1952).
[2] H. C. Longuet-Higgins, Proc. Roy. Soc. (London) **A205**, 247 (1951).
[3] J. Hildebrand and R. L. Scott, *Solubility of Non-Electrolytes* (Reinhold Publishing Corporation, New York, 1949).
[4] V. Mathot and A. Desmyter (to be published).

The Dependence of Intensity of Sound at Source on Its Absorption Coefficient in Liquids

S. PARTHASARATHY, S. S. CHARI, AND D. SRINIVASAN
National Physical Laboratory of India, New Delhi, India
(Received October 20, 1952)

USING the method of radiation pressure, we have measured the absorption coefficients of ultrasonic waves in a number of liquids which will form the subject of a separate paper to be published. But this note sets forth the results of observation on the relation between the intensity of sound at the source and its absorption coefficient in liquids, obtained in the course of our investigations.

The ratio of absorption coefficient to the square of frequency, i.e., α/ν^2 was determined in a number of liquids by the radiation pressure method. The intensity I_0 of sound at the source in each of the liquids was evaluated from a knowledge of the radiation pressure which was measured, and from the relation given by Langevin regarding the pressure of radiation S as being equal to the energy density $E(=I_0/v)$ at a point or to $2I_0/v$ at a perfectly reflecting wall in a fluid medium, v being the velocity of sound in it. The velocities of sound in the liquid were determined by the light diffraction method at the temperatures indicated or corrected to these wherever necessary.

In all the experiments, the quartz crystal was in contact with the liquid studied. The readings given in the sixth, seventh, and eighth columns have to be multiplied by a constant A, which is the cross section of the ultrasonic beam expressed in square cm. In our experiments, we maintained the crystal at a constant voltage. The frequency of oscillation used was 5 mc/sec. Table I gives the results, $I_0/\rho v$ and $I_0/(\alpha/\nu^2)$ being evaluated from experimentally determined values.

TABLE I.

Liquid	Temp. °C	Velocity v cm/sec $\times 10^{-5}$	ρ density in g/cc	$\alpha/\nu^2 \times 10^{15}$	$I_0 \times 10^{-5}$ ergs/sec	$I_0 \times \rho v \times 10^{-10}$	$I_0/(\alpha/\nu^2) \times 10^{-20}$
Toluene	30	1.320	0.863	1.23	1.69	1.9	1.4
m Xylene	30	1.334	0.861	0.89	1.21	1.4	1.4
Pyridine	25	1.400	0.975	5.20	6.37	8.7	1.2
Nitrobenzene	30	1.490	1.199	0.99	1.61	2.9	1.6
Chlorobenzene	26	1.302	1.120	0.98	1.56	2.3	1.6
Acetone	20	1.203	0.791	0.37	0.48	0.5	1.3
Cyclohexanol	26	1.428	0.946	4.89	6.36	8.6	1.3
Ethyl acetate	20	1.187	0.899	0.90	1.20	1.3	1.3
Butyl alcohol	30	1.315	0.808	0.97	1.43	1.5	1.5
						Mean	1.4

According to the present theoretical concepts,[1,2] the factor $I_0 \times \rho v$, i.e., the product of the sound intensity and the characteristic impedance of the liquid should remain constant for the same voltage, frequency, and the quartz crystal. But this relationship between I_0 and ρv does not appear to hold good experimentally. On the contrary, the ratio $I_0/(\alpha/\nu^2)$ remains constant, departing very little from the mean value of 1.4 for the liquids studied. This is a noteworthy result which leads to the interpretation that at low frequencies and for constant voltage, the initial intensity of sound rises in the same proportion as α/ν^2 whatever the liquid might be.

But in our experiments carried out at 5 mc/sec on anomalously absorbing liquids like benzene and carbon disulfide, the above law of proportionality breaks down, $I_0/(\alpha/\nu^2)$ being 0.475 and 0.160, respectively, for these two liquids. We repeated, further, these experiments at 15 mc/sec for all the above liquids. In none of them does the above law of proportionality between I_0 and α/ν^2 hold good, whether the liquid is normally absorbing or otherwise, the values for $I_0/(\alpha/\nu^2)$ ranging from 3.0 to 16.0; nor does the factor $I_0 \times \rho v$ show any consistent value.

[1] P. Vigoureux, *Ultrasonics* (Chapman & Hall, Ltd., London, 1950), p. 11.
[2] Kinsler and Frey, *Fundamentals of Acoustics* (1950), p. 483.

The Volume Effect in Polymer Chains

T. B. GRIMLEY
Department of Physical Chemistry, University of Liverpool, Liverpool, England
(Received October 28, 1952)

THREE attempts to treat the volume effect on the basis of a generalized Fokker-Planck equation have now been published.[1-3] If the chain elements are numbered 0, 1, 2, $\cdots$, N and element number 0 is fixed at the origin of a coordinate system, one has, in these methods, an equation

$$f_{N+1}(r; m+1) = \int \psi_{N+1}(s, r-s) f_{N+1}(r-s; m) ds \qquad (1)$$

for $f_{N+1}(r; m+1)$, the probability that the mth element is between r and $r+dr$. $\psi_{N+1}(s, r-s)$ is the probability that the link connecting the mth with the $(m+1)$th element is given by s if the mth element is at $(r-s)$. If Eq. (1) is to be of any use, one must assign some form to ψ_{N+1}, and in the three papers referred to above, the only differences lie in the supposed form of this function. It is the main purpose of this note to point out that $\psi_{N+1}(s, r-s)$ can be found from classical statistical mechanics.

According to (1) we determine $f_{N+1}(r; m+1)$ by integrating some function over the coordinates of the mth element, the $(m+1)$th element remaining fixed. The integrand in (1) must, therefore, be the pair distribution function $f_{N+1}(r-s, r; m, m+1)$ and an assumption about ψ_{N+1} is equally an assumption about this pair distribution function. Now classical statistical mechanics may be used to express $f_{N+1}(r-s, r; m, m+1)$ in terms of the distribution functions in a *chain of N elements*. If ternary and higher-order complexes of chain elements may be ignored, one finds

$$f_{N+1}(r-s, r; m, m+1) = c\Big[f_N(r-s, r; m, m+1) + \beta_1 \sum_j \int f_N(r-s, r, r', r'; m, m+1, j, N) dr'\Big] \qquad (2)$$

for $m \neq N$, while for $m = N$ the result is

$$f_{N+1}(r-s, r; N, N+1) = c[f_N(r-s; N) + \beta_1 \sum_j f_N(r-s, r; N, j)]. \qquad (3)$$

c is a normalizing constant to be obtained by integrating (2) or (3) over r and s, the s integration being over all points distant l (the link length in the chain) from r. β_1 is the excluded volume integral for free chain elements. Since no one has hitherto suggested a form for $\psi_{N+1}(s, r-s)$ which makes the integrand in (1) identical with the right-hand sides of (2) and (3), all published treatments of the volume effect which are based on (1) lead to incorrect results.

Equation (3) may be used at once to give information about the volume effect. Integrating over s and converting the result into a differential equation, one finds

$$\partial f_N(r; N)/\partial N-(l^2/6)\nabla^2 f_N(r; N)=\beta_1 \sum_j \Big\{ f_N(r, r; j, N) -[f_N(r; N)+\partial f_N(r; N)/\partial N]\int f_N(r', r'; j, N)dr' \Big\}. \quad (4)$$

The term on the right in (4) is responsible for the volume effect. If this term is small we can apply a perturbation method based on the use of the (known) random flight functions on the right; if not we cannot proceed without some assumption about the form of $f_N(r', r'; j, N)$.

Assuming that the perturbation method is valid, we get $\langle r_N^2\rangle$, the average square end to end distance, by multiplying (4) by r^2, integrating over r, and finally integrating with respect to N. The result is

$$\langle r_N^2\rangle = Nl^2[1-(4/3)(3/2\pi)^{\frac{1}{2}}(\beta_1/l^3)N^{\frac{1}{2}}]. \quad (5)$$

Terms of $0(N^{-\frac{1}{2}})$ are omitted from the square bracket in (5) since they are not obtained accurately in passing from (3) to (4).

Results similar to (5) are obtained for other average dimensions, e.g., the second moment of the radial distribution function which appears in the theory of light-scattering. The result (5) shows, however, that for long chains, the average dimensions can never be calculated on the assumption that the volume effect is a small perturbation.

[1] J. J. Hermans, Rec. trav. chim. **69**, 220 (1950).
[2] H. Hadwinger, Makromol. Chem. **5**, 148 (1951).
[3] Hermans, Klamkin, and Ullman, J. Chem. Phys. **20**, 1360 (1952).

A Contribution to the Theory of Light Absorption of Symmetrical Polymethine Dyes

KENICHI FUKUI, CHIKAYOSHI NAGATA, AND TEIJIRO YONEZAWA
Faculty of Engineering, Kyoto University, Kyoto, Japan
(Received November 4, 1952)

IN recent years some valuable results have been obtained as to the light absorption of polymethine dyes and related compounds by adopting a free-electron gas model for these molecules.[1-3] Kuhn[1] in particular gave a successful explanation of the colors of symmetrical and unsymmetrical polymethines, porphyrines, and polyenes. But the agreements of calculated positions of the absorption maxima with experimental results have not been so entirely satisfactory. This may be mainly owing to the extreme simplicity of the adopted model in addition to the influence of the end groups, as Kuhn has already pointed out.

In the present letter the Kuhn free-electron model for the symmetrical polymethine is subjected to some modification in such a manner that small perturbing potential barriers V and U, considered between two carbon atoms and between carbon and nitrogen atoms, respectively, are added to the uniform field along the polymethine chain as shown in Fig. 1. For the purpose of simplifying the calculation, each small potential barrier is transformed so that it tends to be infinitely high and infinitely thin in such a way that its area remains constant[4] after the exact solution has been obtained for the original model. This leads to the following equation, which gives the one-electron energy spectrum:

$$\frac{1+\cot\gamma_1\chi}{(4\pi^2k'/\chi)+\cot\gamma_1\chi+\cot\gamma_2\chi}-\cot\gamma_1\chi = \left(\frac{2\pi^2k}{\chi}\right)+y^{(N)}(\cos\chi+2\pi^2k\cdot\sin\chi/\chi)/\sin\chi, \quad (1)$$

where

$$\chi=(a/\hbar)(2m\epsilon)^{\frac{1}{2}}, \quad \gamma_1=C_1/a, \quad \gamma_2=C_2/a,$$

$$k=\lim_{\substack{V\to\infty\\ b\to 0}} (2ma/h^2)Vb.$$

$$k'=\lim_{\substack{U\to\infty\\ d\to 0}} (2ma/h^2)Ud, \quad \epsilon=\text{one-electron energy},$$

and $Y^{(N)}(Z)$ is a rational function of $Z\equiv\cosh\varphi$ and is given by the following relations:

$$Y_S^{(N)}=\tanh(N-\tfrac{1}{2})\varphi\cdot\sinh\varphi,$$
$$Y_A^{(N)}=\coth(N-\tfrac{1}{2})\varphi\cdot\sinh\varphi,$$

where subscript S and A designate that the corresponding equation gives the energy levels whose wave functions are symmetric and antisymmetric, respectively.

It is easily seen that, when in Eq. (1) both k and k' are put equal to zero, the roots χ_0's of Eq. (1) become

$$\chi_{0S}=\frac{(n+\frac{1}{2})\pi}{N-\frac{1}{2}+\gamma_1+\gamma_2} \quad (n=0, 1, 2, \cdots), \quad (2a)$$

and

$$\chi_{0A}=\frac{n\pi}{N-\frac{1}{2}+\gamma_1+\gamma_2} \quad (n=1, 2, \cdots), \quad (2b)$$

giving the Kuhn equation

$$\Delta E_{0N}=\frac{h^2(2N+5)}{8mL^2},$$

where $L=(2N-1+2\gamma_1+2\gamma_2)a$, and ΔE is the energy difference between the lowest empty level and the highest occupied level.

Provided that k and k' are small, the roots of Eq. (1) may be expanded in powers of k and k', namely,

$$\chi=\chi_0+\xi_1 k+\xi_1' k'+\cdots, \quad (4)$$

where ξ_1 and ξ_1' are given by

$$\xi_1(\chi_0)=\frac{2\pi^2\cdot\sin^2(\gamma_1+\gamma_2)\chi_0[2N\sin\chi_0+\sin\{2(\gamma_1+\gamma_2)-1\}\chi_0]}{\chi_0(N-\frac{1}{2}+\gamma_1+\gamma_2)\{1-\cos 2(\gamma_1+\gamma_2)\chi_0\}\sin\chi_0},$$

and

$$\xi_1'(\chi_0)=\frac{4\pi^2\cdot\sin^2\gamma_2\chi_0}{\chi_0(N-\frac{1}{2}+\gamma_1+\gamma_2)}.$$

When Eq. (4) is used, ΔE can be calculated from

$$\Delta E_N=\frac{\hbar^2}{2ma^2}\{(\chi_A)^2_{n=[(N+1)/2]+1}-(\chi_S)^2_{n=(N+1)/2}\} \quad \text{for odd } N, \quad (5a)$$

and

$$\Delta E_N=\frac{\hbar^2}{2ma^2}\{(\chi_S)^2_{n=(N/2)+1}-(\chi_A)^2_{n=(N/2)+1}\} \quad \text{for even } N. \quad (5b)$$

By neglecting the terms higher than k and k' in the right-hand side of Eq. (4), the wavelengths of first approximation can easily be calculated.

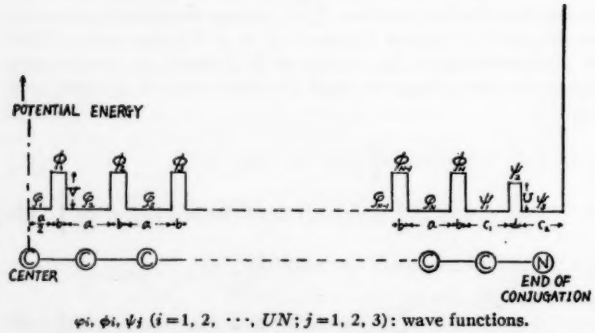

φ_i, ϕ_i, ψ_j $(i=1, 2, \cdots, UN; j=1, 2, 3)$: wave functions.

FIG. 1. Modified potential model for symmetrical polymethines.

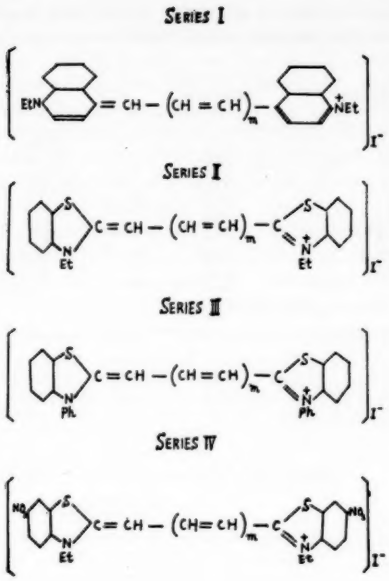

FIG. 2. Several series of symmetrical polymethines.

Related to several series of symmetrical polymethines shown in Fig. 2 the wavelengths of the maximum of the first absorption band are calculated from Eq. (5) and, for the sake of comparison, from Eq. (3). These are tabulated in Table I. The value γ_1 is taken always as constant 1 while the value γ_2 may be adjusted by considering the influence of the end group. The parameters k and k', which are considered to represent the magnitude of the small potential barriers and, accordingly, to be nearly constant for the compounds belonging to a series, are chosen appropriately for each series. The agreement of the calculated results with the observed values is within experimental error for every compound in a series and for every series.

As is seen in Table I, the calculated results on the basis of the Kuhn free-electron model show deviations which are difficult to remove with every effort of adjusting the length of chain L. The present model seems to be useful in approaching nearer to experimental results. As to the relation of the values of parameters k, k', and the chemical constitution of dyes, discussions could be made by the help of far more experimental data.

TABLE I. Comparison of calculated wavelengths with experiment.

Dye			λ_{obs}[a]	λ_{Kuhn}[b]		λ'_{Kuhn}[c]		λ[d]	
Series	m	N	(A)	(A)	Δ	(A)	Δ	(A)	Δ
I	0	3	5910	5790	− 120	5790	−120	5890	−20
	1	4	7050	7055	+ 5	7055	+ 5	7010	−40
	2	5	8130	8325	+ 195	8325	+195	8190	+60
II	0	1	4230	3275	− 955	4060	−170	4235	+ 5
	1	2	5575	4530	−1045	5335	−240	5525	−50
	2	3	6500	5790	− 710	6605	+105	6555	+55
III	0	1	4290	3275	−1015	4245	− 45	4305	+15
	1	2	5645	4530	−1115	5520	−125	5610	−35
	2	3	6625	5790	− 835	6790	+165	6645	+20
IV	0	1	4495	3275	−1220	4440	− 55	4475	−20
	1	2	5835	4530	−1305	5715	−120	5820	−15
	2	3	6820	5790	−1030	6990	+170	6855	+35

[a] Brooker, Keyes, and Williams, J. Am. Chem. Soc. **64**, 199 (1942).

[b] λ_{Kuhn}: Calculated from Eq. (3) in which $\gamma_1=1$, $\gamma_2=1.5$ (the Kuhn nonmodified equation).

[c] λ'_{Kuhn}: Calculated from Eq. (3) in which $\gamma_1+\gamma_2$ is taken by the method of least square in such a way that the agreement of calculated results for a series is the best; namely, $\gamma_1+\gamma_2=2.5$ for Series I, $\gamma_1+\gamma_2=2.8406$ for Series II, $\gamma_1+\gamma_2=2.9151$ for Series III, and $\gamma_1+\gamma_2=2.9936$ for Series IV.

[d] λ: Calculated from Eq. (5) in which $\gamma_1=1$, and γ_2, k, k' are taken as follows:

Series	γ_2	k	k'
I	1.5	0.25	0.1573
II	1.6	0.25	0.1632
III	1.6	0.25	0.1656
IV	1.6	0.25	0.1709

The authors are grateful to the Education Ministry of the Japanese Government for a grant-in-aid.

[1] H. Kuhn, J. Chem. Phys. **16**, 840 (1948); **17**, 1198 (1949); Helv. Chim. Acta **31**, 1441 (1948).
[2] N. S. Bayliss, J. Chem. Phys. **16**, 287 (1948); W. T. Simpson, J. Chem. Phys. **16**, 1124 (1948); H. Kuhn, Chimia **2**, 11 (1948).
[3] H. Kuhn, Helv. Chim. Acta **32**, 2247 (1949); T. Nakajima and H. Kon, J. Chem. Phys. **20**, 750 (1952).
[4] R. de L. Kronig and W. G. Penny, Proc. Roy. Soc. (London) **130**, 499 (1931).

Dilute Solution Hydrodynamic Behavior of Flexible Chain Molecules: Polymethyl Methacrylate*

THOMAS G. FOX, *Rohm and Haas Company, Philadelphia, Pennsylvania*
AND
LEO MANDELKERN, *National Bureau of Standards, Washington, D. C.*
(Received November 17, 1952)

THE dilute solution hydrodynamic behavior of flexible chain molecules of molecular weight M at temperature T has been described by the equations,[1,2]

$$[\eta]=KM^{\frac{1}{2}}\alpha^3, \tag{1}$$
$$K=\Phi(\langle r_0^2\rangle/M)^{\frac{3}{2}}, \tag{2}$$
$$f_0/\eta_0=K_fM^{\frac{1}{2}}\alpha, \tag{1-1}$$
$$K_f=P(\langle r_0^2\rangle/M)^{\frac{1}{2}}, \tag{2-1}$$
$$\alpha^5-\alpha^3=2\psi_1C_M(1-\theta/T)M^{\frac{1}{2}}, \tag{3}$$

where $[\eta]$ is the intrinsic viscosity, f_0 the frictional coefficient at infinite dilution in the solvent of viscosity η_0, and α represents the ratio of $\langle r^2\rangle^{\frac{1}{2}}$, the actual root mean square distance between the ends of the polymer chain in the given solvent to $\langle r_0^2\rangle^{\frac{1}{2}}$, the corresponding distance in an "ideal" solvent wherein the second and higher osmotic virial coefficients are zero. The entropy factor ψ_1, the critical miscibility temperature θ, and the constant C_M are specific for the polymer-solvent pair. K and K_f are constants characteristic of the polymer which depend (slightly) on T, while Φ and P are universal constants for all flexible polymers irrespective of M, T, or solvent. These are determinable by the relations

$$\Phi=[\eta]M/\langle r^2\rangle^{\frac{3}{2}}, \tag{4}$$
$$P=(f_0/\eta_0)/\langle r^2\rangle^{\frac{1}{2}}. \tag{4-1}$$

At infinite dilution the sedimentation constant $S_0=(M/N)\times(1-\bar{v}\rho)/f_0$ and the diffusion constant $D_0=kT/f_0$ where ρ is the solution density, $\bar{v}$ is the partial specific volume of the polymer, and N and k are Avogadro's and Boltzmann's constants. It follows from Eqs. (1), (2), (1-1), and (2-1) that

$$\Phi^{\frac{1}{3}}P^{-1}=[N\eta_0/(1-\bar{v}\rho)][S_0[\eta]^{\frac{1}{2}}/M^{\frac{1}{6}}], \tag{4-2}$$
$$\Phi^{\frac{1}{3}}P^{-1}=(\eta_0/kT)D_0([\eta]M)^{\frac{1}{3}}, \tag{4-3}$$
$$\Phi^{\frac{1}{3}}P^{-1}=(\eta_0/kT)[NkT(1-\bar{v}\rho)]^{\frac{1}{3}}[[\eta]S_0D_0^2]^{\frac{1}{3}}. \tag{4-4}$$

These equations have been successfully applied to extensive data obtained on $[\eta]-T-M$ relationships for a variety of polymers[3] and to the few polymers for which reliable $S_0-[\eta]-M$ data are available.[2,4] It is our purpose to subject them to a further test employing the recently published data of Meyerhoff and Schulz[5] on sedimentation, diffusion, and viscosity studies for polymethyl methacrylate fractions in acetone, together with light scattering and viscosity data obtained by one of us[6] for similar methacrylate fractions.

Values of $\Phi^{\frac{1}{3}}P^{-1}$ calculated by Eq. (4-4) from the $S_0-D_0-[\eta]$ data of Meyerhoff and Schulz (Table I) are independent of M as required by theory. The average value 2.6×10^6 *is the same as that obtained for other polymers,*[2,4] bearing out the universal constancy of Φ and P.

TABLE I. Calculation of the universal hydrodynamic constants from data on polymethyl methacrylate in acetone.

Polymer designation	Meyerhoff-Schulz data[a] $M\times10^{-4}$	$S_0\times10^{13}$	$D_0\times10^{7}$	$[\eta]$ in acetone at 20°C	$\Phi^{\frac{1}{3}}P^{-1}\times10^{-6}$ calc. by Eq. (4-4)[b]	$\langle r^2\rangle^{\frac{1}{2}}\times10^{8}$ [c]	P calc. by Eq. (4-6)
A	744	107	0.95	6.01	2.79	2600	4.90
B	459	82	1.18	4.42	2.67	2100	4.89
C	321	69	1.42	3.19	2.55	1620	5.26
D	202	595	1.95	2.51	2.76	1325	4.70
E	142	48.5	2.25	1.82	2.55	1140	4.70
F	61.1	36.5	3.95	0.902	2.68	605	5.07
G	30.6	25.2	5.45	0.618	2.59	455	4.87
H	14.8	18.8	8.30	0.349	2.56	290	5.02
J	7.72	14.1	12.05	0.188	2.43	182	5.50
					Average 2.62		4.90

[a] See reference 5.

[b] Values of $(1-\theta\rho)=0.369$ given by Meyerhoff and Schulz (see reference 5), and $\eta_0=3.31\times10^{-3}$ poises for acetone at 20°C were used in this calculation.

[c] Calculated from the relationship $\langle r^2\rangle^{\frac{1}{2}}\times10^{8}$ acetone at 30°C $=382\,[\eta]^{0.725}$ $CHCl_3$ at 20°C established for the range 400 to 1300A (see reference 6). It is estimated from $[\eta]-T$ data the $\langle r^2\rangle^{\frac{1}{2}}$ at 30°C is not more than 2 or 3 percent greater than $\langle r^2\rangle^{\frac{1}{2}}$ at 20°C.

Alternately, it can be shown from Eqs. (2) and (2-1) that

$$\Phi^{\frac{1}{3}}P^{-1}=K^{\frac{1}{3}}/K_f. \tag{4-5}$$

From Eqs. (1-1) and (3) and the relation between D_0 and f_0

$$\frac{1}{D_0^2M}=[2C_TK_f^5/(kT/\eta_0)^5]D_0^3M^2+K_f^2/(kT/\eta_0)^2, \tag{5}$$

where $C_T=\psi_1C_M(1-\theta/T)$. Although the experimental data when plotted as $1/D_0^2M$ *vs* $D_0^3M^2$ show some scatter, they may in conformity with Eq. (5) be represented by a straight line. Values of K_f and $2C_T$ determined from the intercept and slope of the least squares line are 2.98×10^{-8} and 2.74×10^{-3}, respectively. K was calculated by Eq. (1) to be 5×10^{-4} from intrinsic viscosity data in di-*n*-propyl ketone at $T=\theta=35$°C, where $\alpha^3=1$.[6] These data according to Eq. (4-5) correspond to $\Phi^{\frac{1}{3}}P^{-1}=2.66\times10^{6}$, in agreement with the value obtained above. It is noteworthy that this determination was based on data obtained in two different laboratories.

P may be evaluated from diffusion and light scattering dissymmetry data since from Eq. (4-1) and the D_0-f_0 relationship,

$$P=(kT/\eta_0)/D_0(\langle r^2\rangle)^{\frac{1}{2}}. \tag{4-6}$$

Values of $\langle r^2\rangle^{\frac{1}{2}}$ calculated from Meyerhoff and Schultz's measurements at 20°C of the intrinsic viscosities in chloroform[5] using an empirical relationship established by one of us[6] are given in Table I. The magnitude of P thus calculated (Table I) is virtually independent of M and agrees closely with the theoretically predicted value of 5.13.[4,7]

From $\Phi^{\frac{1}{3}}P^{-1}=2.6\times10^{6}$ and $P=4.9$ one obtains $\Phi=2.1\times10^{21}$, which is in good agreement with values determined from light scattering and viscosity investigations for a variety of polymers.[6,8]

We can predict from Eqs. (4-2) and (4-3) and the relationship $[\eta]$ acetone 20°C$=5.89\times10^{-5}M^{0.72}$ obtained by one of us[6] that $D_0=8.06\times10^{-4}M^{0.67}$ and $S_0=1.22\times10^{-14}M^{0.43}$. These may be compared with $D_0=6.46\times10^{-4}M^{0.56}$ and $S_0=1.0\times10^{-14}M^{0.44}$ obtained from log-log plots of the data of Table I. Deviations between predicted and observed values are no greater than the uncertainties in the absolute molecular weight determinations.

The successes met here in correlating sedimentation, diffusion, viscosity, and light scattering data on polymethyl methacrylate solutions furnish additional evidence of the validity of the theoretical equations summarized above.

* The work reported here was supported in part by the U. S. Office of Naval Research and the Office of the Quartermaster General as part of Project ONR(QMC)NR-033-314.

[1] P. J. Flory, J. Chem. Phys. **17**, 303 (1949); P. J. Flory and T. G. Fox, J. Am. Chem. Soc. **73**, 1904 (1951).

[2] L. Mandelkern and P. J. Flory, J. Chem. Phys. **20**, 212 (1952).

[3] Bibliography given in reference 4. See also Cragg, Dumitru, and Simpkins, J. Am. Chem. Soc. **74**, 1977 (1952).

[4] Mandelkern, Krigbaum, Scheraga, and Flory, J. Chem. Phys. **20**, 1392 (1952).

[5] G. Meyerhoff and G. V. Schulz, Die Makromolekulare Chemie **7**, 294 (1952).

[6] Work carried out in the Rohm and Haas Laboratories (to be published).

[7] J. G. Kirkwood and J. Riseman, J. Chem. Phys. **16**, 565 (1948).

[8] T. G. Fox and P. J. Flory, J. Am. Chem. Soc. **73**, 1909, 1915 (1951); A. Oth and P. Doty, J. Phys. Chem. **56**, 43 (1952).

Natural Hypsochromic Shifts on Phenyl Substitution

B. PULLMAN, G. BERTHIER, AND J. BAUDET
Institut du Radium, 11 rue Pierre Curie, Paris, France
(Received November 5, 1952)

AS a general rule the substitution of a phenyl group on a conjugated hydrocarbon produces, in the absence of steric interference with coplanarity, a bathochromic displacement of the longest wavelength of absorption (λ_{max}).[1] Recently, however, two cases have been found in which such a substitution brings about a hypsochromic displacement of λ_{max} though no steric effects seem to be present: (a) 2-phenylazulene absorbs at 687 mμ while azulene (I) absorbs at 697 mμ,[2] (b) phenyldibenzoheptafulvene (II, R=Ph) absorbs at 284 mμ while dibenzoheptafulvene (II, R=H) absorbs at 296 mμ.[3] These are evidently *natural* hypsochromic shifts in the sense of the definition that we have proposed previously,[4] similar to such shifts observed in some *methylated* azulenes[5] and fulvenes.[6] Two related compounds are known which show the usual bathochromic shift: (a) 1-phenylazulene absorbs at 735 mμ,[2] (b) phenyldibenzofulvene (III, R=Ph) absorbs at 326 mμ while dibenzofulvene (III, R=H) absorbs at 312 mμ.[7]

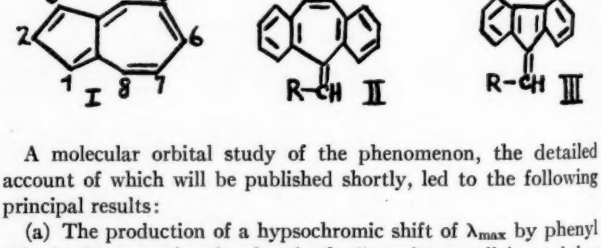

A molecular orbital study of the phenomenon, the detailed account of which will be published shortly, led to the following principal results:

(a) The production of a hypsochromic shift of λ_{max} by phenyl substitution can only take place in the "nonalternant" (containing an odd numbered ring) hydrocarbons.[8]

(b) The phenomenon is related to special features which characterize the conjugation of phenyls in this group of molecules. Thus the substitution of a phenyl on an "alternant" hydrocarbon yields a hydrocarbon which is still alternant and consequently does not produce any modification in the charge distribution; in a compound such as, say, 2-phenylnaphthalene, the charges resulting from the π-electrons are uniformly equal to unity on all the carbon atoms, both of the naphthalene and the benzene nuclei. Things are quite different in "nonalternant" hydrocarbons; the substitution of a phenyl produces there a charge displacement both in the original hydrocarbon and in the substituent. Moreover, the direction of the charge displacement in the phenyl ring depends upon the nature of the compound and even of the *C*

atom to which the phenyl is attached. Thus, in a general way, the charge shift in the phenyl ring follows the general trend present in the parent hydrocarbon[8]; in (II, R=Ph) the phenyl as a whole gains charges, in (III, R=Ph) it gives up charges to the ring. In the same way the phenyl gains charges when placed at the position 2 of azulene and looses them when placed at position 6. It is thus a kind of a substituent which may be called *neutral*, as it may exhibit both $+M$ and $-M$ effects or no effect at all, depending upon the place of substitution.[9]

(c) The possibility of the existence of a natural hypsochromic shift on phenylation is strictly related to the existence of these charge displacements (this is the reason why no such effects can appear in the alternant hydrocarbons), though it is independent of the direction of the displacement. When proper account is being taken (by a perturbation method) of the modifications in the Coulomb integrals of the conjugated system, following the charge shift brought about by phenylation, the numerical results given in Table I are obtained (overlap included) for the previously quoted compounds[10]:

TABLE I.

Compound	$m=\frac{E-E^0}{\gamma}$ Highest filled orbital	Lowest empty orbital	$N\rightarrow V_1$ (in γ-units)
Azulene	0.1717	0.1527	0.3244
2-phenylazulene	0.1785	0.1538	0.3323
1-phenylazulene	0.1686	0.1497	0.3183
6-phenylazulene	0.1627	0.1799	0.3426
Dibenzoheptafulvene	0.2597	0.5425	0.8022
Phenyldibenzoheptafulvene	0.2212	0.6001	0.8213
Dibenzofulvene	0.6372	0.3397	0.9769
Phenyldibenzofulvene	0.4837	0.2819	0.7656

It is seen that in all cases the theory is in agreement with experiment. A prediction is made that a hypsochromic shift should occur on phenyl substitution at the position 6 of azulene.

[1] For a general discussion and numerous examples see B. Pullman and A. Pullman, *Les Théories Electroniques de la Chimie Organique* (Masson Editeur, Paris, 1952).
[2] Plattner, Sandrin, and Wyss, Helv. Chim. Acta **29**, 1604 (1946).
[3] Bergmann, Fischer, Ginsburg, Hirshberg, Lavie, Mayot, Pullman, and Pullman, Bull. soc. chim. **18**, 684 (1951).
[4] A. Pullman and B. Pullman, Disc. Faraday Soc. **9**, 46 (1950).
[5] Pl. A. Plattner and E. Heilbronner, Helv. Chim. Acta **30**, 910 (1947); Pullman, Mayot, and Berthier, J. Chem. Phys. **18**, 257 (1950).
[6] Bergmann, Berthier, Hirshberg, Loewenthal, Pullman, and Pullman, Bull. soc. chim. **18**, 669 (1951).
[7] Pullman, Pullman, Bergmann, Berthier, Hirshberg, and Sprinzak, Bull. soc. chim. **18**, 702 (1951).
[8] See reference **1**, Chap. VII.
[9] The same may be true for some other substituents, too, but probably to a much smaller degree.
[10] For details on the notations see reference **1**, Chap. IV.

Substituted Methanes. XIII. Infrared Spectral Data and Assignments for Dibromodifluoromethane

CHARLOTTE E. DECKER AND FORREST F. CLEVELAND
Spectroscopy Laboratory, Department of Physics, Illinois Institute of Technology, Chicago 16, Illinois
AND
RICHARD B. BERNSTEIN
Department of Chemistry, Illinois Institute of Technology, Chicago 16, Illinois
(Received November 6, 1952)

INFRARED spectral data of CBr_2F_2 have been obtained in one[1] and Raman data in two investigations.[2,3] The present infrared spectral data were obtained for gaseous CBr_2F_2 in the region 400–4000 cm^{-1} using a Perkin-Elmer model 21 double-beam spectrophotometer with NaCl optics, and a Beckman IR-2 spectrophotometer with KBr optics.

The observed wave numbers, estimated relative intensities, and assignments are listed in Table I, together with the infrared data given by Plyler and Acquista.[1] Several new bands have been found, and the others are in good agreement with those reported previously.

TABLE I. Infrared spectral data and assignments for gaseous CBr_2F_2.[a]

Plyler and Acquista ν	I	Present results ν	I[b]	ν_c	Assignment	Type
165[c]	—	165[c]	—	—	ν_4	a_1
282[c]	—	282[c]	—	—	ν_5	a_2
331[d]	*vw*	—	—	—	ν_9	b_2
340[c]	—	340[c]	—	—	ν_3	a_1
367[c]	—	367[c]	—	—	ν_7	b_1
478	*vw*	—	—	*496*	$\nu_4+\nu_9$	B_2
—	—	495	*m*	*496*	$\nu_4+\nu_9$	B_2
—	—	505	*w*	*505*	$\nu_3+\nu_4$	A_1
—	—	564	*m*	*564*	$2\nu_5$	A_1
*P*618 / 621 / *R*624	*vs*	*P*621 / 623[e] / *R*627	*vvs*	—	ν_2	a_1
662	*m*	663	*vs*	*662*	$2\nu_9$	A_1
—	—	667	*s*	*670*	$\nu_3+\nu_9$	B_2
				666	$\nu_8-\nu_4$	B_2
688	*vw*	685	*w*	*680*	$2\nu_8$	A_1
727	*vw*	729	*w*	*734*	$2\nu_7$	A_1
758	*w*	756	*m*	*750*	$\nu_1-\nu_8$	A_1
		764	*m*	*759*	$\nu_1-\nu_9$	B_2
800	*m*	798*sh*	*s*	*788*	$\nu_2+\nu_4$	A_1
*P*829 / *Q*829 / *R*834	*vs*	*P*829 / 831[e] / *R*834	*vvs*	—	ν_8	b_2
*P*870 / *Q*875 / *R*880	*m*	*P*870 / *Q*875 / *R*879	*vs*	*871*	$\nu_6-\nu_5$	B_2
—	—	896	*m*	*895*	[f]$(2\nu_5)+\nu_9$	B_2
912	*vw*	925	*m*	*925*	$\nu_1-\nu_4$	A_1
*P*948 / *Q*952 / *R*957	*m*	*P*948 / *Q*952 / *R*956	*s*	*954*	$\nu_2+\nu_9$	B_2
990	*w*	989	*m*	*990*	$\nu_2+\nu_7$	B_1
				988	$\nu_6-\nu_4$	B_1
				996	$\nu_4+\nu_8$	B_2
—	—	1038	*m*	*1030*	$(2\nu_9)+\nu_7$	B_1
				1036	$\nu_4+\nu_6-\nu_5$	B_2
*P*1086 / 1088 / *R*1093	*vs*	*P*1088 / 1090[e] / *R*1093	*vvs*	—	ν_1	a_1
1122	*w*	1121*sh*	*s*	*1113*	$\nu_5+\nu_8$	B_1
*Q*1150	*vs*	*Q*1153	*vvs*	—	ν_6	b_1
—	—	1184*sh*	*s*	*1187*	$(2\nu_5)+\nu_2$	A_1
1250	*w*	1248	*m*	*1246*	$2\nu_3$	A_1
				1255	$\nu_1+\nu_4$	A_1
—	—	1285	*m*	*1292*	$(\nu_3+\nu_9)+\nu_5$	B_2
				1286	$\nu_4+(\nu_5+\nu_8)$	B_1
—	—	1358	*w*	*1352*	$(2\nu_7)+\nu_2$	A_1
—	—	1404	*w*	*1413*	$(2\nu_5)+\nu_4$	A_1
				1421	$\nu_1+\nu_9$	B_2
1428	*vw*	1429	*m*	*1430*	$\nu_1+\nu_3$	A_1
1449	*vw*	1451	*w*	*1454*	$\nu_2+\nu_8$	B_2
				1457	$\nu_1+\nu_7$	B_1
—	—	(1493)	*vw*	*1493*	$\nu_3+\nu_6$	B_1
1652	*vw*	1653	*m*	*1662*	$2\nu_8$	A_1
1709	*vw*	1710	*w*	*1713*	$\nu_1+\nu_2$	A_1
—	—	1767	*vw*	*1776*	$\nu_2+\nu_6$	B_1
2173	*w*	2178	*m*	*2180*	$2\nu_1$	A_1
2222	*w*	2233	*m*	*2243*	$\nu_1+\nu_6$	B_1
2288	*w*	2303	*m*	*2306*	$2\nu_6$	A_1
—	—	(2767)	*vw*	*2743*	$(2\nu_5)+\nu_1$	A_1
—	—	2989	*vw*	*3009*	$(2\nu_1)+\nu_8$	B_2
—	—	(3226)	*vw*	*3222*	$(\nu_1+\nu_6)+(\nu_2+\nu_7)$	A_1
—	—	3278	*vw*	*3268*	$(2\nu_1)+\nu_1$	A_1
—	—	3347	*vw*	*3331*	$(2\nu_1)+\nu_5$	B_1
—	—	(3477)	*vw*	*3456*	$(2\nu_6)+\nu_6$	B_1

[a] ν = wave number in cm^{-1}; I = estimated relative intensity (*v* = very, *w* = weak, *m* = medium, *s* = strong); ν_c = calculated wave numbers, using 165, 282, 331, 340, 367, 623, 831, 1090, and 1153 as the values of the fundamentals; *sh* = shoulder on strong band; and the parentheses enclose bands whose values are uncertain.
[b] In the present investigation, the intensities I are defined according to the percent transmission of a 10-cm cell at 0.12 atmos pressure as follows: *vw*, 95–100; *w*, 90–95; *m*, 60–90; *s*, 20–60; *vs*, 5–20; *vvs*, 0–5. For a few of the weak bands higher pressures were required.
[c] Raman data (reference 2) for the liquid.
[d] Observed for the liquid. Beyond the range of our spectrometers.
[e] Point of minimum absorption between *P* and *R* branch.
[f] ν_c was obtained using the *observed* value of the overtone or combination band enclosed by the parentheses.

Measurement of Raman displacements, semiquantitative relative intensities, and quantitative depolarization factors, a normal

coordinate treatment, and a calculation of the thermodynamic properties are in progress.

The sample was supplied through the courtesy of Dr. Edmund G. Young, Kinetic Chemicals Division, of the E.I. du Pont de Nemours and Company. The authors appreciate the assistance of the Office of Ordnance Research, the Office of Naval Research, the Atomic Energy Commission, and the American Academy of Arts and Sciences for partial support of this research program.

[1] E. K. Plyler and N. Acquista, J. Research Natl. Bur. Standards **48**, 92 (1952).
[2] G. Glockler and G. R. Leader, J. Chem. Phys. **7**, 553 (1939).
[3] M. L. Delwaulle and F. Francois, Compt. rend. **214**, 828 (1942).

Erratum: Nuclear Magnetic Resonance Experiment on a Four-Proton System in a Single Crystal of $K_2HgCl_4 \cdot H_2O$

[J. Chem. Phys. **20**, 1503–1504 (1952)]

J. Itoh, R. Kusaka, Y. Yamagata, R. Kiriyama, and H. Ibamoto
Department of Physics and Department of Chemistry, Osaka University, Osaka, Japan

THE ordinates of Fig. 2 should be half the values indicated in the figure; i.e., the numbers 20, 10, 0, 10, and 20 should be read as 10, 5, 0, 5, and 10.